USGS
science for a changing world

Prepared in cooperation with the U.S. Department of Defense Task Force for Business and Stability Operations and the Afghanistan Geological Survey

Identification of Mineral Resources in Afghanistan—Detecting and Mapping Resource Anomalies in Prioritized Areas Using Geophysical and Remote Sensing (ASTER and HyMap) Data

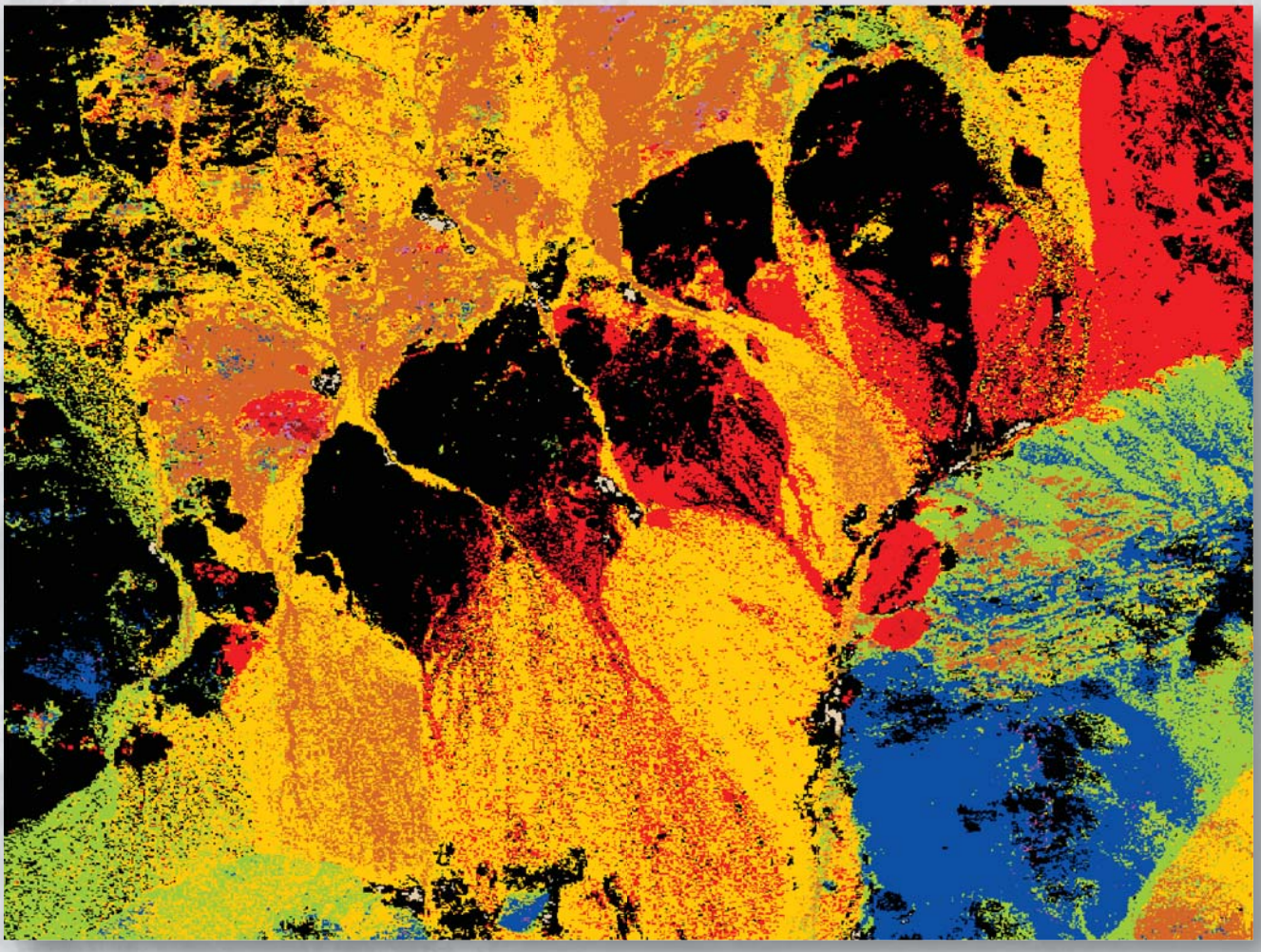

Open-File Report 2011–1229
USGS Afghanistan Project Product No. 201

U.S. Department of the Interior
U.S. Geological Survey

Identification of Mineral Resources in Afghanistan—Detecting and Mapping Resource Anomalies in Prioritized Areas Using Geophysical and Remote Sensing (ASTER and HyMap) Data

Edited by Trude V.V. King, Michaela R. Johnson, Bernard E. Hubbard, and Benjamin J. Drenth

Open-File Report 2011–1229
USGS Afghanistan Project Product No. 201

U.S. Department of the Interior
U.S. Geological Survey

U.S. Department of the Interior
KEN SALAZAR, Secretary

U.S. Geological Survey
Marcia K. McNutt, Director

U.S. Geological Survey, Reston, Virginia: 2011

For product and ordering information:
World Wide Web: http://www.usgs.gov/pubprod
Telephone: 1-888-ASK-USGS

For more information on the USGS—the Federal source for science about the Earth,
its natural and living resources, natural hazards, and the environment:
World Wide Web: http://www.usgs.gov
Telephone: 1-888-ASK-USGS

Suggested citation:
King, T.V.V., Johnson, M.R., Hubbard, B.E., and Drenth, B.J., eds., 2011, Identification of mineral resources in Afghanistan—Detecting and mapping resource anomalies in prioritized areas using geophysical and remote sensing (ASTER and HyMap) data: U.S. Geological Survey Open-File Report 2011–1229, 327 p.

Any use of trade, product, or firm names is for descriptive purposes only and does not imply endorsement by the U.S. Government.

Although this report is in the public domain, permission must be secured from the individual copyright owners to reproduce any copyrighted material contained within this report.

Contents

Chapter 1: Detecting and Mapping Resource Anomalies—Introduction and Background 1
1.1 Introduction 1
1.2 Anomaly Identification and Compilation 1
1.3 Datasets Used for Evaluation 2
1.4 Data Application 3
1.5 References Cited 4
Chapter 2: Description of Structure and Content of Spatial Dataset of Identified Anomalies in Afghanistan 6
2.1 Anomaly Geodatabase Overview 6
2.1.1 Geodatabase Structure and Contents 6
2.1.2 Availability of Anomaly Data 8
2.2 References Cited 9
Chapter 3: Identification of Gravity, Magnetic, and Radiometric Geophysical Anomalies in Afghanistan 10
3.1 Geophysical Anomalies 10
3.1.1 Magnetic Anomalies 10
3.1.2 Gravity Anomalies 10
3.1.3 Radiometric Anomalies 10
3.2 Presentation of Geophysical Anomalies 11
3.3 References Cited 34
Chapter 4: Identification of Mineral Anomalies in Afghanistan Using Advanced Spaceborne Thermal Emission and Reflection Radiometer 36
4.1 Advanced Spaceborne Thermal Emission and Reflection Radiometer Overview 36
4.1.2 ASTER Mapped Minerals 37
4.1.3 ASTER Identified Anomalies 38
4.2 Presentation of ASTER Anomalies 38
4.3 References Cited 156
Chapter 5: Mapping Anomalous Mineral Zones Using HyMap Imaging Spectrometer—Data for Selected Areas of Interest in Afghanistan 158
5.1 Imaging Spectrometer Overview 158
5.2 Imaging Spectrometer Data 158
5.2.1 Iron-Bearing Minerals and Other Materials 158
5.2.2 Carbonates, Phyllosilicates, Sulfates, Altered Minerals, and Other Materials 159
5.3 HyMap Identification of Anomalies 159
5.4 Presentation of HyMap Anomalies 160
5.5 References Cited 319
Chapter 6: Discussion of Anomaly Overlap Areas and Potential for Economic Development 321
6.1 Anomaly Overlap—Conclusions and Discussion 321
6.1.1 Anomaly Overlap Priority 1 322
6.1.2 Anomaly Overlap Priority 2 323
6.1.3 Anomaly Overlap Priority 3 323
6.1.4 Anomaly Overlap Priority 4 324
6.1.5 Anomaly Overlap Priority 5 324
6.2 Potential for Economic Development from Mineral Resources 325
6.3 References Cited 326

Figures

1. Mineral areas of interest identified in Afghanistan 2
3.1.1. Gravity geophysical anomalies located in the Aynak Area of Interest in Afghanistan 12
3.1.2. Reduced-to-pole magnetic geophysical anomalies located in the Aynak Area of Interest in Afghanistan 13
3.2.1. Gravity geophysical anomalies located in the Bakhud Area of Interest in Afghanistan 14
3.2.2. Reduced-to-pole magnetic geophysical anomalies located in the Bakhud Area of Interest in Afghanistan 15
3.3.1. Gravity geophysical anomalies located in the Dusar-Shaida Area of Interest in Afghanistan 16
3.3.2. Reduced-to-pole magnetic geophysical anomalies located in the Dusar-Shaida Area of Interest in Afghanistan 17
3.3.3. Radiometric geophysical anomalies located in the Dusar-Shaida Area of Interest in Afghanistan 18
3.4.1. Reduced-to-pole magnetic geophysical anomalies located in the Ghunday-Achin Area of Interest in Afghanistan 19
3.4.1. Gravity geophysical anomalies located in the Khanneshin Area of Interest in Afghanistan 20
3.4.2. Reduced-to-pole magnetic geophysical anomalies located in the Khanneshin Area of Interest in Afghanistan 21
3.5.1. Reduced-to-pole magnetic geophysical anomalies located in the Kharnak-Kanjar Area of Interest in Afghanistan 22
3.6.1. Gravity geophysical anomalies located in the Kundalan Area of Interest in Afghanistan 23
3.7.1. Reduced-to-pole magnetic geophysical anomalies located in the Nalbandon Area of Interest in Afghanistan 24
3.8.1. Gravity geophysical anomalies located in the North Herat Area of Interest in Afghanistan 25
3.8.2. Reduced-to-pole magnetic geophysical anomalies located in the North Herat Area of Interest in Afghanistan 26
3.8.3. Radiometric geophysical anomalies located in the North Herat Area of Interest in Afghanistan 27
3.9.1. Reduced-to-pole magnetic geophysical anomalies located in the North Takhar Area of Interest in Afghanistan 28
3.10.1.–3.10.2. Reduced-to-pole magnetic geophysical anomalies located in the South Helmand Area of Interest in Afghanistan 29
3.11.1. Reduced-to-pole magnetic geophysical anomalies located in the Tourmaline Area of Interest in Afghanistan 31
3.11.2. Radiometric geophysical anomalies located in the Tourmaline Area of Interest in Afghanistan 32
3.12.1. Reduced-to-pole magnetic geophysical anomalies located in the Zarkashan Area of Interest in Afghanistan 33
4.1.1. Study area map showing extent of ASTER mapped industrial minerals data, mineral areas of interest, cities, and major roads in Afghanistan 37
4.2.1.–4.2.2. ASTER mineral occurrence anomalies located in the Aynak Area of Interest in Afghanistan 40
4.2.3.–4.2.7. ASTER alteration anomalies located in the Aynak Area of Interest in Afghanistan 42
4.3.1. ASTER anomaly located in the Badakhshan Area of Interest in Afghanistan 47
4.3.2.–4.3.4. ASTER color anomalies located in the Badakhshan Area of Interest in Afghanistan 48
4.4.1.–4.4.3. ASTER color anomalies located in the Baghlan Area of Interest in Afghanistan 51
4.4.4.–4.4.12. ASTER alteration anomalies located in the Baghlan Area of Interest in Afghanistan 54
4.5.1.–4.5.2. ASTER color anomalies located in the Dudkash Area of Interest in Afghanistan 63
4.5.3. ASTER alteration anomaly located in the Dudkash Area of Interest in Afghanistan 65
4.5.4.–4.5.6. ASTER color anomalies located in the Dudkash Area of Interest in Afghanistan 66
4.5.7.–4.5.9. ASTER alteration anomalies located in the Dudkash Area of Interest in Afghanistan 69

4.5.10.–4.5.14. ASTER color anomalies located in the Dudkash Area of Interest in Afghanistan 72
4.5.15. ASTER alteration anomaly located in the Dudkash Area of Interest in Afghanistan 77
4.5.16.–4.5.17. ASTER color anomalies located in the Dudkash Area of Interest in Afghanistan 78
4.6.1.–4.6.8. ASTER alteration anomalies located in the Ghunday-Achin Area of Interest in Afghanistan 80
4.6.9.–4.6.10. ASTER mineral occurrence anomalies located in the Ghunday-Achin Area of Interest in Afghanistan 88
4.7.1.–4.7.13. ASTER alteration anomalies located in the Haji-Gak Area of Interest in Afghanistan 90
4.8.1. ASTER alteration anomaly located in the Katawas Area of Interest in Afghanistan 103
4.9.1.–4.9.4. ASTER color anomalies located in the Kunduz Area of Interest in Afghanistan 104
4.10.1.–4.10.15. ASTER color anomalies located in the North Takhar Area of Interest in Afghanistan 108
4.10.16.–4.10.17. ASTER alteration anomalies located in the North Takhar Area of Interest in Afghanistan 123
4.10.18.–4.10.22. ASTER color anomalies located in the North Takhar Area of Interest in Afghanistan 125
4.11.1.–4.11.5. ASTER alteration anomalies located in the Panjsher Valley Area of Interest in Afghanistan 130
4.12.1. ASTER color anomaly located in the Takhar Area of Interest in Afghanistan 135
4.12.2.–4.12.5. ASTER alteration anomalies located in the Takhar Area of Interest in Afghanistan 136
4.12.6.–4.12.8. ASTER color anomalies located in the Takhar Area of Interest in Afghanistan 140
4.13.1.–4.13.8. ASTER alteration anomalies located in the Tourmaline Area of Interest in Afghanistan 143
4.14.1.–4.14.5. ASTER alteration anomalies located in the Zarkashan Area of Interest in Afghanistan 151
5.1.1.–5.1.5. Hyperspectral anomalies located in the Aynak Area of Interest in Afghanistan 161
5.2.1.–5.2.9. Hyperspectral anomalies located in the Badakhshan Area of Interest in Afghanistan 166
5.3.1.–5.3.5. Hyperspectral anomalies located in the Baghlan Area of Interest in Afghanistan 175
5.4.1.–5.4.6. Hyperspectral anomalies located in the Bakhud Area of Interest in Afghanistan 180
5.5.1.–5.5.10. Hyperspectral anomalies located in the Balkhab Area of Interest in Afghanistan 186
5.6.1.–5.6.3. Hyperspectral anomalies located in the Daykundi Area of Interest in Afghanistan 196
5.7.1.–5.7.5. Hyperspectral anomalies located in the Dudkash Area of Interest in Afghanistan 199
5.8.1.–5.8.4. Hyperspectral anomalies located in the Dusar-Shaida Area of Interest in Afghanistan 204
5.9.1. Hyperspectral anomaly located in the Haji-Gak Area of Interest in Afghanistan 208
5.9.2. Hyperspectral anomaly located in the Dusar-Shaida Area of Interest in Afghanistan 209
5.9.3.–5.9.16. Hyperspectral anomalies located in the Haji-Gak Area of Interest in Afghanistan 210
5.10.1.–5.10.2. Hyperspectral anomalies located in the Katawas Area of Interest in Afghanistan 224
5.11.1.–5.11.12. Hyperspectral anomalies located in the Kharnak-Kanjar Area of Interest in Afghanistan 226
5.12.1.–5.12.13. Hyperspectral anomalies located in the Kundalan Area of Interest in Afghanistan 238
5.13.1.–5.13.2. Hyperspectral anomalies located in the Kunduz Area of Interest in Afghanistan 251
5.14.1.–5.14.7. Hyperspectral anomalies located in the Nalbandon Area of Interest in Afghanistan 253
5.15.1.–5.15.10. Hyperspectral anomalies located in the North Herat Area of Interest in Afghanistan 260
5.16.1.–5.16.7. Hyperspectral anomalies located in the Panjsher Valley Area of Interest in Afghanistan 270
5.17.1.–5.17.12. Hyperspectral anomalies located in the South Helmand Area of Interest in Afghanistan 277
5.18.1.–5.18.3. Hyperspectral anomalies located in the Takhar Area of Interest in Afghanistan 289
5.19.1.–5.19.14. Hyperspectral anomalies located in the Tourmaline Area of Interest in Afghanistan 292
5.20.1.–5.20.13. Hyperspectral anomalies located in the Zarkashan Area of Interest in Afghanistan 306
6.1.1. Location map of selected overlapping anomalies defined by the source data (geophysical, GEO; ASTER, AST; or hyperspectral, HSD) within mineral areas of interest in Afghanistan 322

Tables

2.1. Contents and description of anomaly database 6
2.2. Mineral anomaly polygon guide (for HyMap- and ASTER-mapped anomalies only). Criteria based on tables 1 and 2 of Thompson and others (2009) 7

Conversion Factors

SI to Inch/Pound

Multiply	By	To obtain
	Length	
meter (m)	3.281	foot (ft)
kilometer (km)	0.6214	mile (mi)
	Area	
square kilometer (km^2)	247.1	acre
square kilometer (km^2)	0.3861	square mile (mi^2)

Horizontal coordinate information is referenced to the World Geodetic System of 1984 (WGS84).

Chapter 1: Detecting and Mapping Resource Anomalies—Introduction and Background

By Trude V.V. King, Michaela R. Johnson, Bernard E. Hubbard, and Benjamin J. Drenth

1.1 Introduction

As part of the U.S. Geological Survey (USGS) and Department of Defense Task Force for Business and Stability Operations (TFBSO) natural resources revitalization activities in Afghanistan (Peters and others, 2011), three new datasets have been collected, compiled, and analyzed. These data have been used to more fully evaluate the areas of interest (AOIs; fig. 1) where, on the basis of previous U.S.S.R. and Afghanistan studies, the opportunity for early economic development of a number of different mineral, commodity, and deposit types had been identified (Peters and others, 2007; Peters and others, 2011). The new data compilations include (1) regional magnetic and gravity data for use in the characterization of subsurface composition and structure (Sweeney and others, 2006a,b; Ashan and others, 2007; Sweeney and others, 2007; Ashan and others, 2008; Shenwary and others, 2011), (2) Advanced Spaceborne Thermal Emission and Reflection Radiometer (ASTER) data to identify and evaluate surficial alteration patterns related to industrial minerals and other selected targets, and (3) HyMap imaging spectrometer data for characterization and mapping of surficial mineralogy (Cocks and others, 1998; Kokaly and others, 2008; Peters and others, 2011). These datasets have served as fundamental building blocks for the resource evaluation by Peters and others (2011).

During the independent analysis of the geophysical, ASTER, and imaging spectrometer (HyMap) data by USGS scientists, previously unrecognized targets of potential mineralization were identified using evaluation criteria most suitable to the individual dataset. These anomalous zones offer targets of opportunity that warrant additional field verification. This report describes the standards used to define the anomalies, summarizes the results of the evaluations for each type of data, and discusses the importance and implications of regions of anomaly overlap between two or three of the datasets.

1.2 Anomaly Identification and Compilation

A geodatabase of anomalies was created to facilitate the population and sharing of locations of anomalies identified using geophysical (GEO), ASTER (AST), and HyMap imaging spectrometer data (also called hyperspectral data or HSD). The anomaly was identified within an AOI boundary, but in some cases it was extended beyond the AOI to capture the actual extent of the anomaly. The geodatabase was constructed with drop-down lists of categorical classes providing identifying characteristics for each anomaly with an additional text field in the attribute table to provide an extended description. The categorical classes were set up to keep the database consistent and minimize data entry errors. Name and description were the only fields with free text.

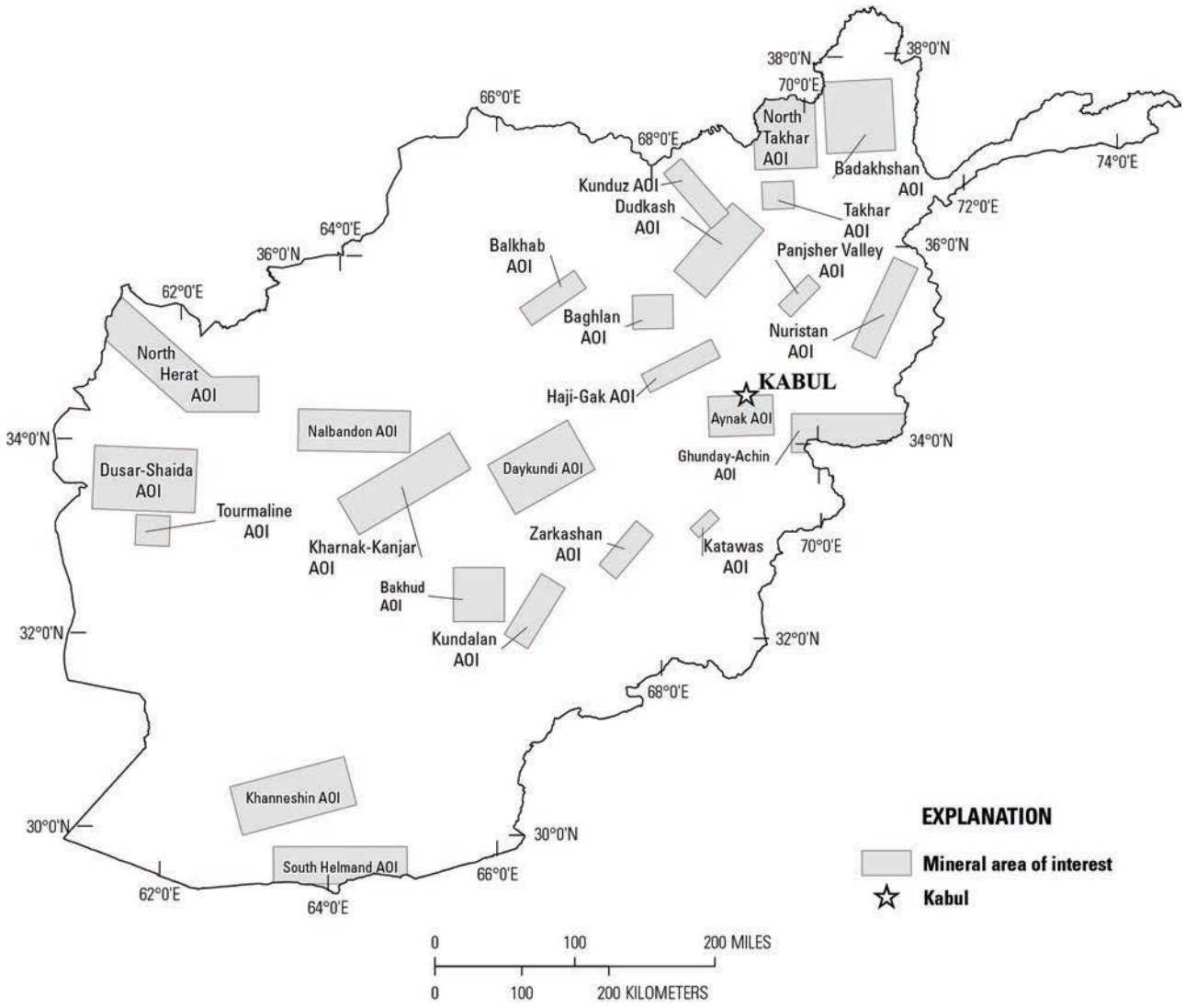

Figure 1. Mineral areas of interest (AOIs) identified in Afghanistan (Peters and others, 2007; Peters and others, 2011).

1.3 Datasets Used for Evaluation

Geophysical data collected during airborne and ground surveys (Sweeney and others, 2006a,b; Sweeney and others, 2007; Ashan and others, 2007; Ashan and others, 2008; Shenwary and others, 2011) were used on a regional scale to assess the subsurface features within the areas of interest, including those features that may be related to anomalies identified by the remotely sensed data (ASTER and HSD). The geophysical data are particularly useful for mapping the extent of rocks with strong physical property contrasts with surrounding rocks, such as strongly magnetized intrusions related to mineral deposits, volcanic rocks, and areas covered by sedimentary rocks.

ASTER is a spaceborne multispectral instrument aboard the Terra satellite, launched in December 1999 (*http://asterweb.jpl.nasa.gov/index.asp*, accessed 8/23/2011). ASTER has three subsystems that operate in a total of 14 spectral bands. The visible near-infrared (VNIR) subsystem measures solar reflectance in three visible and near-infrared bands (0.52–0.86 microns [μm]), the short wavelength infrared (SWIR) subsystem measures solar reflectance in six shortwave infrared bands (1.00–2.43 μm), and the thermal infrared (TIR) subsystem measures thermal infrared emissivity in five

bands (8.125–11.650 μm). The five bands of the TIR subsystem are most useful for mapping primary rock-forming silicate minerals and their related impurities within surficial deposits, including precious- and base-metal mineral deposits and industrial mineral deposits. The nine bands of reflectance data (VNIR and SWIR subsystems) are useful for mapping broad suites of spectrally similar minerals and mineral mixtures such as ferric iron, clays, carbonates, sulfates, and other hydrous phases resulting from alteration of primary rock-forming silicates. Collectively, all 14 wavelength bands of ASTER reflectance and emissivity data can be used to discriminate between minerals that are spectrally similar in certain wavelengths (for example, calcite and chlorite in the SWIR), but spectrally different in other wavelengths (for example, calcite-bearing carbonate rocks and chlorite-bearing ultramafic rocks in the TIR).

HyMap imaging spectrometer data were used to identify the occurrence of selected materials at the surface based on the presence and wavelength position of absorption features in the 0.45- to 2.48-μm-wavelength region (Cocks and others, 1998; Kokaly and others, 2008; Kokaly and others, in press; King and others, in press). Two general categories of minerals are recognized: (1) iron-bearing minerals that have characteristic spectral absorption features that occur at wavelengths near the 1-μm region, and (2) a wide variety of minerals, including carbonates, mica and clay minerals, and sulfates, that have diagnostic spectral absorptions near the 2-μm region. The identified minerals, mineral groups, and suites of minerals were used to define anomalous zones in the data.

1.4 Data Application

Each of the datasets were evaluated independently to define potential zones of anomalous mineralization and subsequently examined as a three-part data compilation to further examine common alteration zones between the three datasets. These areas of commonality show the locations of high-priority targets for future ground-based mineral exploration activities within 16 of the 24 areas already targeted for future economic development. The anomalies identified in this report will support and expand the summarized and interpreted information that were prepared in each of the information packages that are intended to be delivered to the Afghanistan Ministry of Mines for development of bidding packages (Peters and others, 2011). These bidding packages will be designed to attract investors and mining firms to Afghanistan to develop the mineral wealth of the country. This report along with high-resolution images may be accessed at *http://pubs.usgs.gov/of/2011/1229/*.

1.5 References Cited

Ashan, S., Hussain, S., Kohistany, A.H., Shenwary, G.S., Mutty, A.S., Daud, M.A., Abraham, J.D., Anderson, E.D., Drenth, B.J., Finn, C.A., Kucks, R.P., Lindsay, C.R., Phillips, J.D., Sweeney, R.E., Brozena, J.M., Ball, D.C., Childers, V.A., Gardner, J.M., Jarvis, J.L., and Liang, R.T., 2007, Aeromagnetic survey in Afghanistan: A website for distribution of data: U.S. Geological Survey Open-File Report 2007–1247, accessed August 19, 2011, at *http://pubs.usgs.gov/of/2007/1247/*.

Ashan, S., Hussain, S., Kohistany, A.H., Shenwary, G.S., Mutty, A.S., Daud, M.A., Brozena, J.M., Ball, D.C., Childers, V.A., Gardner, J.M., Jarvis, J.L., Liang, R.T., Abraham, J.D., Anderson, E.D., Drenth, B.J., Finn, C.A., Kucks, R.P., Lindsay, C.R., Phillips, J.D., and Sweeney, R.E., 2008, Airborne gravity survey and ground gravity in Afghanistan: A website for distribution of data: U.S. Geological Survey Open-File Report 2008–1089, accessed August 19, 2011, at pubs.usgs.gov/of/2008/1089/.

Cocks T., Jenssen, R., Stewart, A., Wilson, I., and Shields, T., 1998, The HyMap airborne Hymap sensor: The system, calibration and performance, *in* Schaepman, M., Schlapfer, D., and Itten, K.I., eds., Proceedings of the 1st EARSeL Workshop on Imaging Spectroscopy, 6–8 October 1998, Zurich: Paris, EARSeL, p. 37–43, accessed August 19, 2011, at *http://www.neodc.rl.ac.uk/docs/Hymap_specs.pdf*.

King, T.V.V., Kokaly, R.F., Hoefen, T.M., Dudek, K. and Livo, K.E., in press, Surface materials map of Afghanistan: Iron-bearing minerals and other materials: U. S. Geological Survey Scientific Investigations Map 3152-B.

Kokaly, R.F., King, T.V.V., Hoefen, T.M., Dudek, K., and Livo, K.E., in press, Surface materials map of Afghanistan: Carbonates, phyllosilicates, sulfates, altered minerals, and other materials: U. S. Geological Survey Scientific Investigations Map 3152-A.

Kokaly, R.F., King, T.V.V., and Livo, K.E., 2008, Airborne hyperspectral survey of Afghanistan 2007: Flight line planning and HyMap data collection: U.S. Geological Survey Open-File Report 2008–1235, 14 p., accessed August 19, 2011, at *http://pubs.usgs.gov/of/2008/1235/*.

Peters, S.G., Ludington, S.D., Orris, G.J., Sutphin, D.M., Bliss, J.D., and Rytuba, J.J., eds., and the U.S. Geological Survey-Afghanistan Ministry of Mines Joint Mineral Resource Assessment team, 2007, Preliminary non-fuel mineral resource assessment of Afghanistan: U.S. Geological Survey Open-File Report 2007–1214, 810 p., 1 CD-ROM, accessed August 19, 2011, at *http://pubs.usgs.gov/of/2007/1214/*.

Peters, S.G., King, T.V.V, Mack, T.J., Chornack, M.P., eds., and the U.S. Geological Survey Afghanistan Mineral Assessment Team, 2011, Summaries of important areas for mineral investment and production opportunities of nonfuel minerals in Afghanistan: U.S. Geological Survey Open-File Report 2011–1204, 1,810 p. plus appendixes on DVD. (Also available at *http://pubs.usgs.gov/of/2011/1204/.)*

Shenwary, G.S.; Kohistany, A.H.; Hussain, Sardar; Ashan, Said; Mutty, A.S.; Daud, M.A.; Wussow, M.W.; Sweeney, R.E.; Phillips, J.D.; Lindsay, C.R.; Kucks, R.P.; Finn, C.A.; Drenth, B.A.; Anderson, E.D.; Abraham, J.D.; Liang, R.T.; Jarvis, J.L.; Gardner, J.M.; Childers, V.A.; Ball, D.C.; and Brozena, J.M., 2011, Aeromagnetic surveys in Afghanistan—An updated website for distribution of data: U.S. Geological Survey Open-File Report 2011–1055, 8 p., accessed August 19, 2011, at *http://pubs.usgs.gov/of/2011/1055/*.

Sweeney, R.E., Kucks, R.P, Hill, P.L., and Finn, C.A., 2006a, Aeromagnetic and gravity surveys in Afghanistan: A website for distribution of data: U.S. Geological Survey Open-File Report 2006–1204, accessed August 19, 2011, at *http://pubs.usgs.gov/of/2006/1204/*.

Sweeney, R.E., Kucks, R.P, Hill, P.L., and Finn, C.A., 2006b, Aeromagnetic survey in western Afghanistan: A web site for distribution of data: U.S. Geological Survey Open-File Report 2006–1325, accessed August 19, 2011, at *http://pubs.usgs.gov/of/2006/1325/*.

Sweeney, R.E., Kucks, R.P., Hill, P.L., and Finn, C.A., 2007, Radiometric survey in western Afghanistan: A website for distribution of data: U.S. Geological Survey Open-File Report 2007–1042, accessed August 19, 2011, at *http://pubs.usgs.gov/of/2007/1042/*.

Chapter 2: Description of Structure and Content of Spatial Dataset of Identified Anomalies in Afghanistan

By Michaela R. Johnson

2.1 Anomaly Geodatabase Overview

An Environmental Systems Research Institute geodatabase (Zeiler, 2010) of anomalies was created to facilitate the population and sharing of anomaly geographic locations and anomaly source-data types. Data types were identified using GEO for geophysical data, AST for ASTER data, and HSD for imaging spectrometer (HyMap) data. The anomaly was identified within an area of interest (AOI) boundary (Peters and others, 2007) but, in some cases, extended beyond to capture the actual extent of the anomaly. The geodatabase was constructed with drop-down lists of categorical classes providing identifying characteristics for each anomaly with an additional text field in the attribute table to provide an extended text description (table 2.1). The categorical classes were set up to keep the database consistent and minimize data entry errors. Area name and description were the only fields with free text.

Table 2.1. Contents and description of anomaly database.

Field name	Field type	Description
Source_data	pick-list	Pick-list by data type, ex. Geophysics, hymap, aster
Anomaly_type	pick-list	Pick-list by anomaly type name
HSD_mineral_type	pick-list	HyMap mineral type
Geophys_mineral_type	pick-list	Geophysical anomaly type
Aster_mineral_class	pick-list	Pick-list by ASTER mineral class
Aster_mineral_subclass	pick-list	Pick-list by ASTER mineral subclass
HSD_aster_mineral_deposit_type	pick-list	Pick-list by categories in table 2.2
Area_name	text	Unique name for mapped anomaly
Size	pick-list	Pick-list (local or regional)
Size_description	pick-list	Pick-list (description of local/regional size)
Description	text	Descriptive text about the anomaly

2.1.1 Geodatabase Structure and Contents

The geodatabase houses an anomaly polygon-feature class, Afghan_anomaly, and an anomaly point-feature class, Afghan_anomaly_point. Polygon features approximating the geographical extent of the anomaly were delineated for each anomaly type (GEO, AST, and HSD). The anomaly point features were generated as another option to identify the anomalies. Using the same structure as the anomaly polygon attribute table, the point features were created from the polygon features using the ArcToolBox

geoprocessing tool, Feature_To_Point, which creates a point inside each of the polygon features and retains all of the attributes (Environmental Systems Research Institute, 2010).

Attributes were set up to be populated by pick-list to be consistent across the anomaly data source types and to reduce data entry errors. The anomaly was described by its source-data type (GEO, AST, or HSD) and further classified by anomaly type: mineral occurrence, alteration assemblage, color, and geophysical method (gravity, magnetic, or radiometric). The mineral occurrence type of anomaly was determined based on the occurrence of a high concentration of a single mineral. A typical situation would be a high concentration of hematite, kaolinite, or dolomite that appears anomalous in comparison to the dominant mineral concentration in a given area. The color type of anomaly was defined by anomalous areas of color from imagery—iron-stained (typically red or green in color) or bleached areas. Both colors (red and green) can be attributed to iron-staining depending on the wavelength bands used to produce the color composite image. Landsat natural- and false-color composites were ancillary data used with AST and HSD data to verify the identification of the color anomalies (Davis, 2006). These may not be associated with a single mineral and commonly are not related to the geology. Alteration assemblage types of anomalies were based on categorical deposit types containing key minerals given in table 2.2 (Thompson and others, 2009).

Table 2.2. Mineral anomaly polygon guide (for HyMap- and ASTER-mapped anomalies only). Criteria based on tables 1 and 2 of Thompson and others (2009).

Deposit types	Mineral assemblages	Comments
Propylitic (chloritic/ albitic)	calcite, epidote, chlorite (wairakite, mg-chlorites, chlinochlore), illite/smectite, montmorillonite, actinolite	Includes porphyry zones, massive sulfides and sedex (mg/fe-chlorites), and linear epithermal veins and polymetallic zones.
Phyllic (sericitic)	sericite (muscovite, illite, paragonite, phengite, celedanite), apatite, biotite	Includes sericitic zones of massive sulfide and sedex deposits.
Argillic	kaolinite, dickite, montmorillonite, illite/smectite, chlorite, calcite and epidote	Mostly well exposed in porphyry (intrusive) mineral deposits (usually too small to see or map in linear-dominated epithermal and polymetallic vein systems).
Advanced argillic	kaolinite, dickite, alunite, diaspore, pyrophyllite, zunyite, cristobalite (opal/chalcedony), jarosite, topaz, tourmaline	Includes all types ranging from sulfide bodies with supergene jarosite, and high- to low-sulfidation. Typically small or isolated pixels in linear vein systems.
Greisen	topaz and tourmaline	Mostly in tin-bearing areas and the largest granitic and pegmatite exposures.
Ferric/laterite/bauxite	kaolinite, gibbsite, goethite, quartz	Lumped class that includes strong goethite, mineral gossanized areas, unusual ferricrete-indistinguishable deposits, and paleo-bauxite and laterite deposits rich in Al.

Each anomaly was identified by a unique name and a description of the defining anomaly features. The anomaly name was determined from the data source type, from the priority area name, and numbered sequentially when there was more than a single anomaly. For example, HSD_(priority_area)_(seq_no) would result in HSD_Balkab_1. The description was populated with a short description of the anomaly.

Additional categorical data were defined for the anomaly. The geophysical anomalies were divided into subclasses for the magnetic and gravity anomalies: magnetic high, magnetic low, gravity high, and gravity low. ASTER (AST) anomalies were divided into mineral classes and subclasses. The primary ASTER mineral class was broken into carbonates, clays and micas, and other minerals of interest. These classes were divided into subclasses of minerals: calcite, dolomite, calcite-dolomite and clays, illite and (or) muscovite, smectite, kaolinite, ferric iron and (or) gossanized zones, gypsum, gibbsite, sulfur, and magnesite. The HyMap (HSD) anomalies were classified into mineral types of iron-bearing minerals, alteration minerals, or both. Additionally, the AST and HSD alteration assemblage anomalies were categorized by criteria described by Thompson and others (2009) (table 2.2). The size of the anomaly was also described categorically as a primary size class (local or regional) and further subdivided by size and (or) whether it had structural control: 0–1 km across (broadest expanse), 1–5 km across, greater than 5 km across, not structurally controlled (based on mapped faults), or structural control (based on mapped faults).

2.1.2 Availability of Anomaly Data

The anomaly polygon and point feature classes in the geodatabase were exported to non-proprietary formats to facilitate sharing across various software platforms: shapefile (Environmental Systems Research Institute, 1998) and a compressed (zipped) Keyhole Markup Language (KMZ) (*http://code.google.com/apis/kml/documentation/kml_tut.html*, accessed 8/23/2011). The drop-down lists and values in the anomaly tables in the geodatabase were coded domains. For example, in the field Source_data, the actual value was a 1, 2, or 3, which corresponded to a coded domain of Hyperspectral, Geophysical, or ASTER. The value shown in the geodatabase table was the coded domain value, but the value exported to the shapefile was the raw value: 1, 2, or 3. The coded domains within the geodatabase were saved as tables and used to populate the shapefile attribute table. Federal Geographic Data Committee (FGDC) compliant metadata were provided with the shapefiles of anomaly polygon and point locations. The data were provided with this report as shapefiles and KMZ files.

Afghanistan anomaly polygon
- *shapefile*
- *KMZ*

Afghanistan anomaly point
- *shapefile*
- *KMZ*

2.2 References Cited

Davis, P.A., 2006, Calibrated Landsat ETM+ nonthermal-band image mosaics of Afghanistan: U.S. Geological Survey Open-File Report 2006–1345, 16 p., accessed August 19, 2011, at *http://pubs.usgs.gov/of/2006/1345/*.

Environmental Systems Research Institute, 1998, ESRI Shapefile technical description: Redlands, Calif., Environmental Systems Research Institute, accessed August 19, 2011, at *http://www.esri.com/library/whitepapers/pdfs/shapefile.pdf*.

Environmental Systems Research Institute, 2010, ArcGIS desktop 9.3 help: Feature to point (data management) (ArcInfo only): Redlands, Calif., Environmental Systems Research Institute, accessed August 19, 2011, at *http://webhelp.esri.com/arcgisdesktop/9.3/index.cfm?id=1798&pid=1790&topicname=Feature_To_Point* (Data_Management).

Peters, S.G., Ludington, S.D., Orris, G.J., Sutphin, D.M., Bliss, J.D., and Rytuba, J.J., eds., and the U.S. Geological Survey-Afghanistan Ministry of Mines Joint Mineral Resource Assessment team, 2007, Preliminary non-fuel mineral resource assessment of Afghanistan: U.S. Geological Survey Open-File Report 2007–1214, 810 p., 1 CD-ROM, accessed August 19, 2011, at *http://pubs.usgs.gov/of/2007/1214/*.

Thompson, A.J.B, Hauff, P.L., and Robitaille, A.J., 2009, Alteration mapping in exploration: Application of short-wave infrared (SWIR) spectroscopy: Society of Economic Geologists (SEG) Reviews in Economic Geology, v. 16, p. 12–23.

Zeiler, M., 2010, Modeling our world, 2nd ed.: The ESRI guide to geodatabase concepts: Redlands, Calif., ESRI Press, 308p.

Chapter 3: Identification of Gravity, Magnetic, and Radiometric Geophysical Anomalies in Afghanistan

By Benjamin J. Drenth

3.1 Geophysical Anomalies

Two major types of regional geophysical data are available for Afghanistan: magnetic and gravity. The significance of each for anomaly mapping in Afghanistan is summarized here. Radiometric anomalies are also presented here.

3.1.1 Magnetic Anomalies

Magnetic anomalies reflect spatial variations of total magnetization—the vector sum of induced and remnant magnetizations (Blakely, 1995). Induced magnetization, an instantaneous property, is proportional to magnetic susceptibility and has the same direction as the present-day ambient field. Remnant magnetization is permanent, is related to the formation of a rock and geologic history, and may be directed in a different direction than the induced magnetization. Large-magnitude components of remnant magnetization are common in volcanic rocks but rare in nonmafic/ultramafic plutons (Clark, 1999). At a regional scale, magnetic data are useful for mapping granitoid plutons related to arc tectonic environments, which commonly produce magnetic highs (Clark, 1999). This is important in Afghanistan where many mineral deposits are associated with arc-related plutons. The current magnetic map of Afghanistan (Shenwary and others, 2011) is merged from several different data sources, including vintage airborne surveys from the 1960s (Sweeney and others, 2006a) and 1970s (Sweeney and others, 2006b), as well as airborne and ground data collected between 2006-2008 (Ashan and others, 2007; Shenwary and others, 2011).

3.1.2 Gravity Anomalies

Gravity anomalies reflect lateral variations of density, with gravity highs occurring over regions of relatively high densities, such as crustal blocks that include dense basement, and gravity lows occurring over large volumes of low-density materials, such as sedimentary basins and silicic intrusions. The current gravity map of Afghanistan (Ashan and others, 2008) is merged from ground data collected in the mid-20th century (McGinnis, 1971) and around 2006 (Ashan and others, 2008).

3.1.3 Radiometric Anomalies

Radiometric data are also available for a portion of western Afghanistan (Sweeney and others, 2007). Major anomalies and anomaly patterns are mentioned in the anomaly database, but these data have not been interpreted in detail.

3.2 Presentation of Geophysical Anomalies

This chapter and series of maps summarize existing geologic interpretations of anomalies in several different areas of interest (AOI) for mineral exploration (figs. 3.1.1–3.11.1). For example, magnetic anomalies in several areas are interpreted to reflect plutons that may be parts of systems that host porphyry copper deposits.

The maps display the geophysical dataset (gravity, magnetic, or radiometric) within the corresponding AOI as an image with the mapped values scaled in a color range from dark blue to pink. Solid black lines define the approximate shape and extent of the identified anomaly polygons. Point features shown on the map are color-coded categorical representations of the type of anomaly and subtype. For example, a magnetic-high geophysical anomaly is shown as a small red square (Type of anomaly: Magnetic) overlain on a larger burgundy circle (Geophysical anomaly subclass: Magnetic high). The point features on the maps are displaying some of the additional categorical descriptions about the anomalies that are contained in the attribute table of the shapefile and contained in the KMZ file provided in chapter 2 of this report.

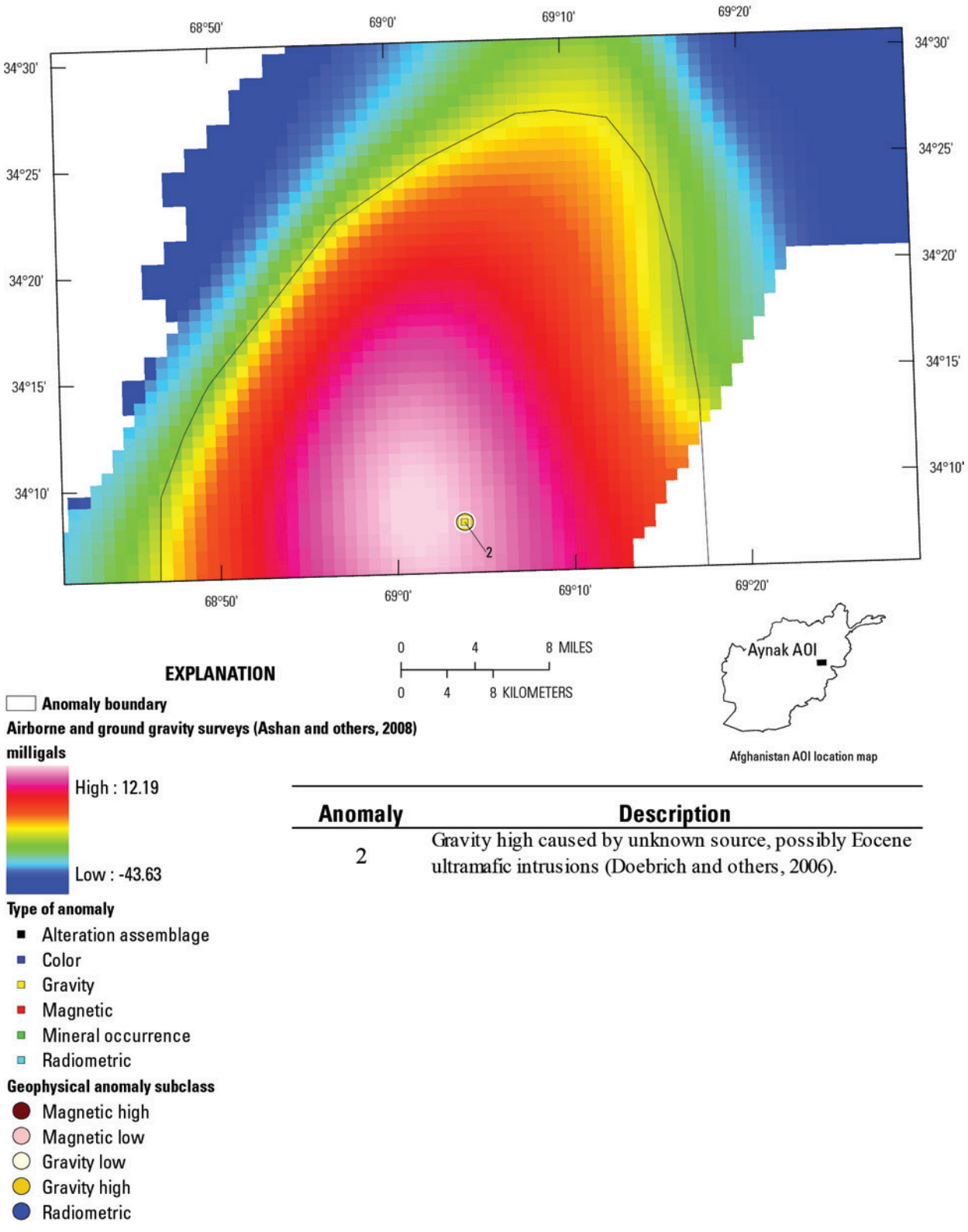

Anomaly	Description
2	Gravity high caused by unknown source, possibly Eocene ultramafic intrusions (Doebrich and others, 2006).

Figure 3.1.1. Gravity geophysical anomalies located in the Aynak Area of Interest (AOI) in Afghanistan.

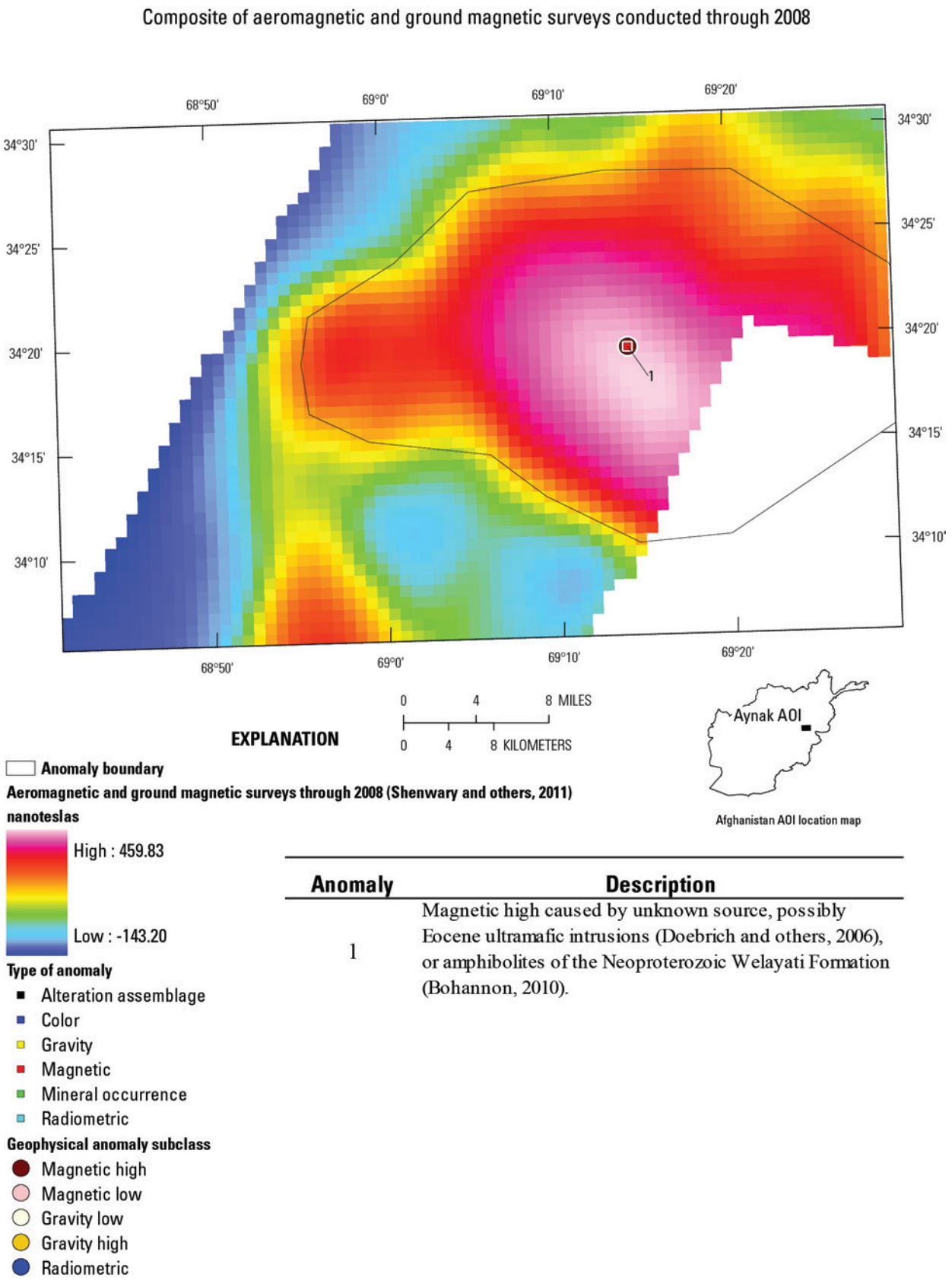

Anomaly	Description
1	Magnetic high caused by unknown source, possibly Eocene ultramafic intrusions (Doebrich and others, 2006), or amphibolites of the Neoproterozoic Welayati Formation (Bohannon, 2010).

Figure 3.1.2. Reduced-to-pole magnetic geophysical anomalies located in the Aynak Area of Interest (AOI) in Afghanistan.

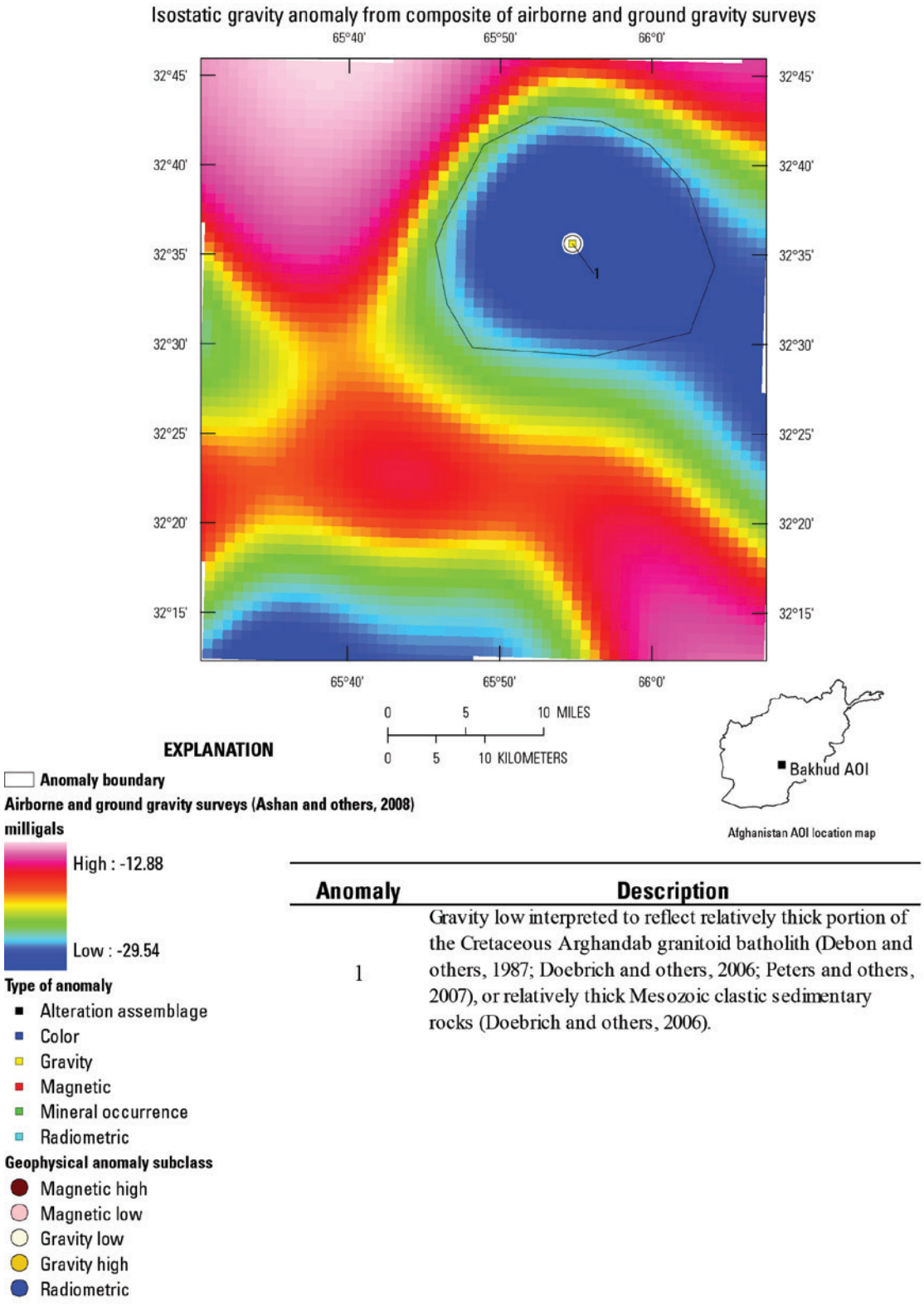

Anomaly	Description
1	Gravity low interpreted to reflect relatively thick portion of the Cretaceous Arghandab granitoid batholith (Debon and others, 1987; Doebrich and others, 2006; Peters and others, 2007), or relatively thick Mesozoic clastic sedimentary rocks (Doebrich and others, 2006).

Figure 3.2.1. Gravity geophysical anomalies located in the Bakhud Area of Interest (AOI) in Afghanistan.

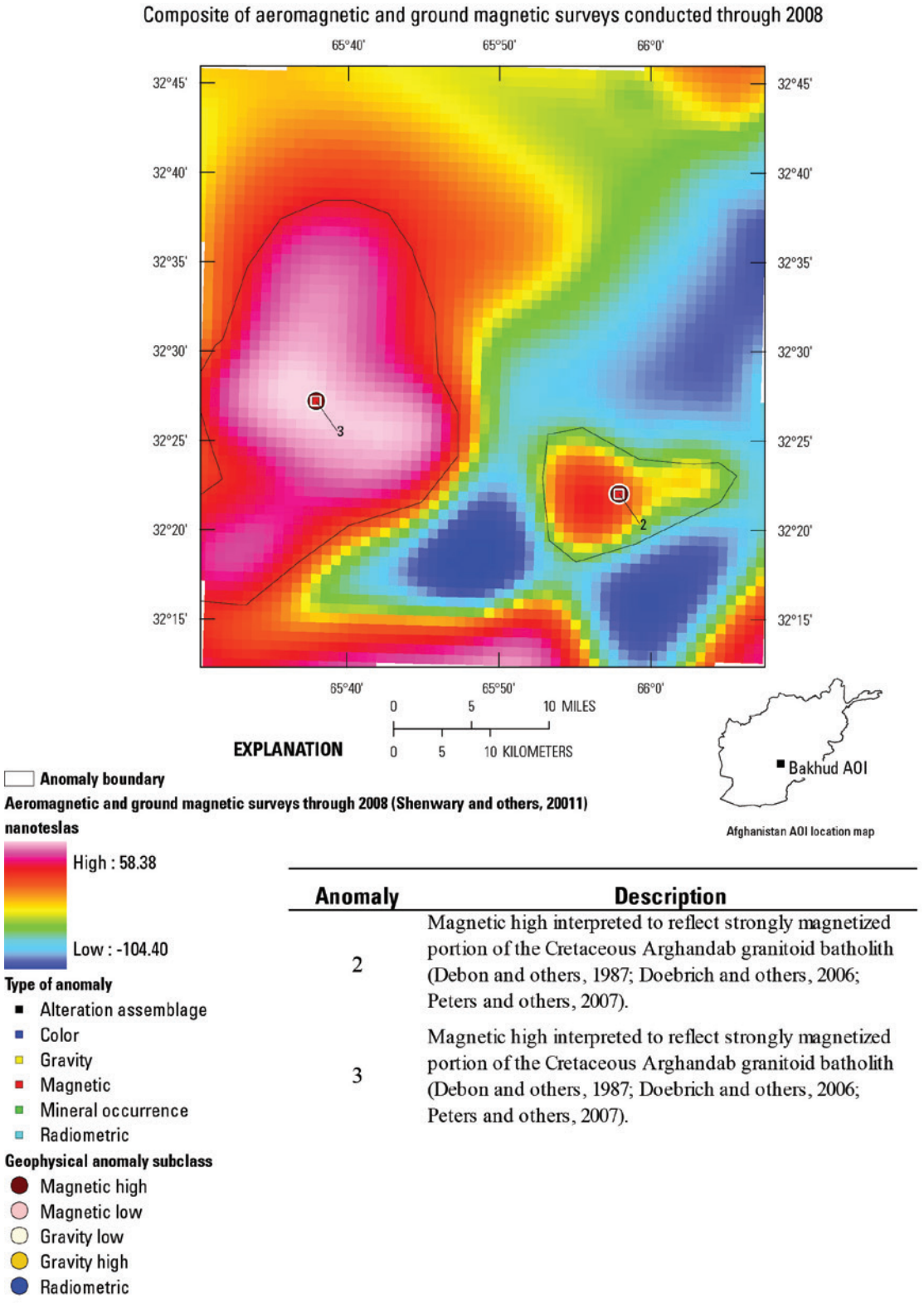

Anomaly	Description
2	Magnetic high interpreted to reflect strongly magnetized portion of the Cretaceous Arghandab granitoid batholith (Debon and others, 1987; Doebrich and others, 2006; Peters and others, 2007).
3	Magnetic high interpreted to reflect strongly magnetized portion of the Cretaceous Arghandab granitoid batholith (Debon and others, 1987; Doebrich and others, 2006; Peters and others, 2007).

Figure 3.2.2. Reduced-to-pole magnetic geophysical anomalies located in the Bakhud Area of Interest (AOI) in Afghanistan.

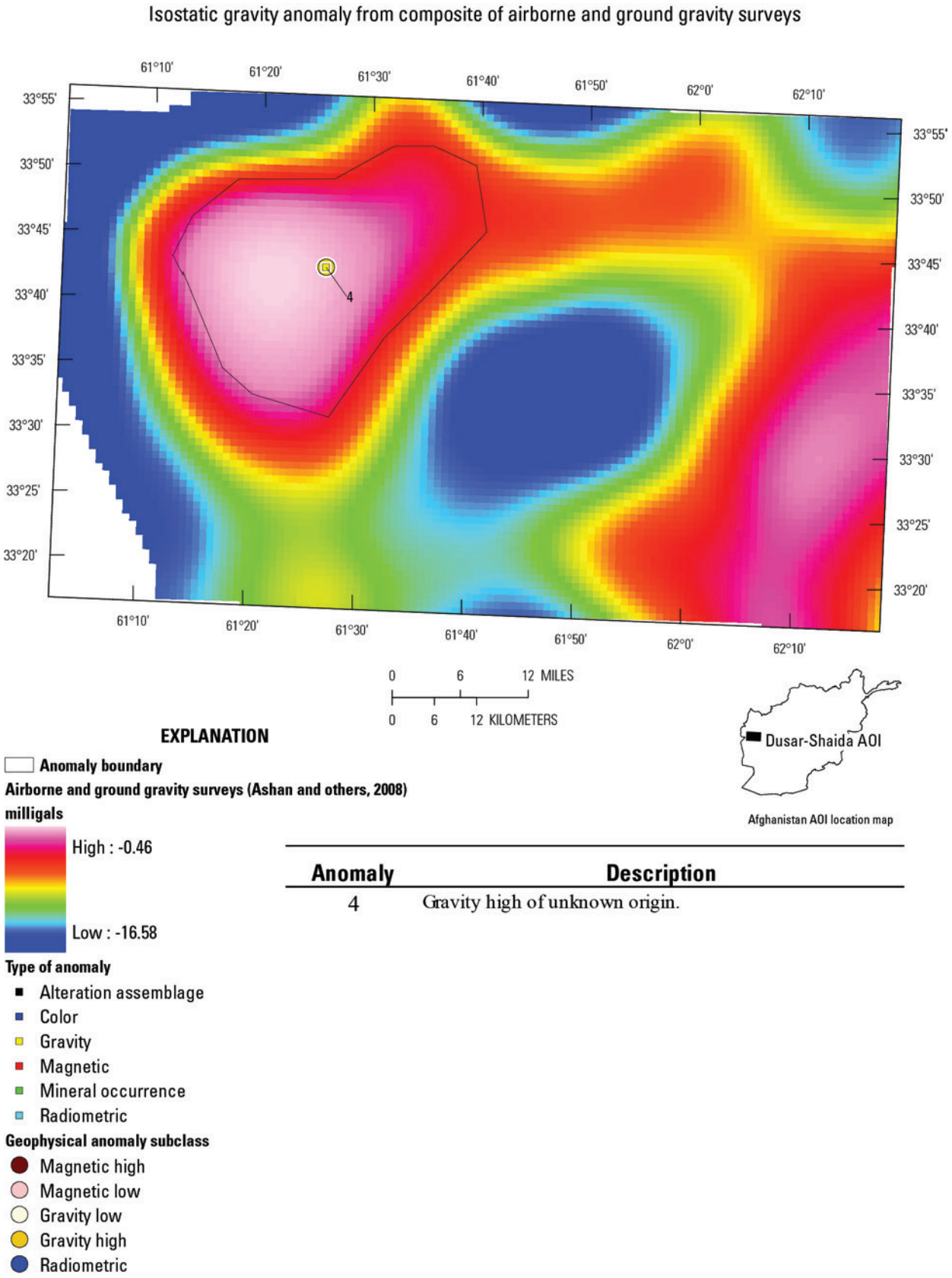

Figure 3.3.1. Gravity geophysical anomalies located in the Dusar-Shaida Area of Interest (AOI) in Afghanistan.

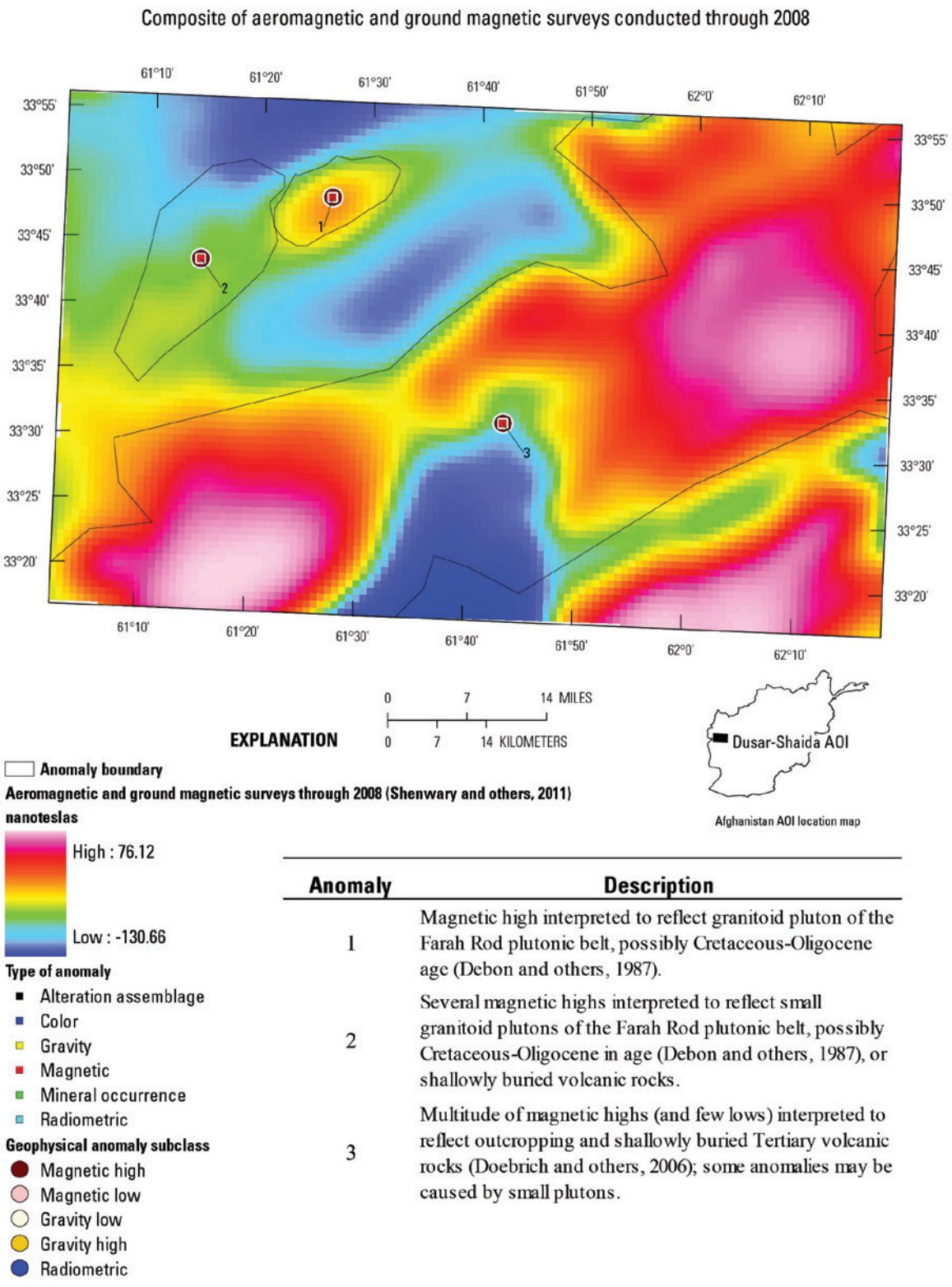

Anomaly	Description
1	Magnetic high interpreted to reflect granitoid pluton of the Farah Rod plutonic belt, possibly Cretaceous-Oligocene age (Debon and others, 1987).
2	Several magnetic highs interpreted to reflect small granitoid plutons of the Farah Rod plutonic belt, possibly Cretaceous-Oligocene in age (Debon and others, 1987), or shallowly buried volcanic rocks.
3	Multitude of magnetic highs (and few lows) interpreted to reflect outcropping and shallowly buried Tertiary volcanic rocks (Doebrich and others, 2006); some anomalies may be caused by small plutons.

Figure 3.3.2. Reduced-to-pole magnetic geophysical anomalies located in the Dusar-Shaida Area of Interest (AOI) in Afghanistan.

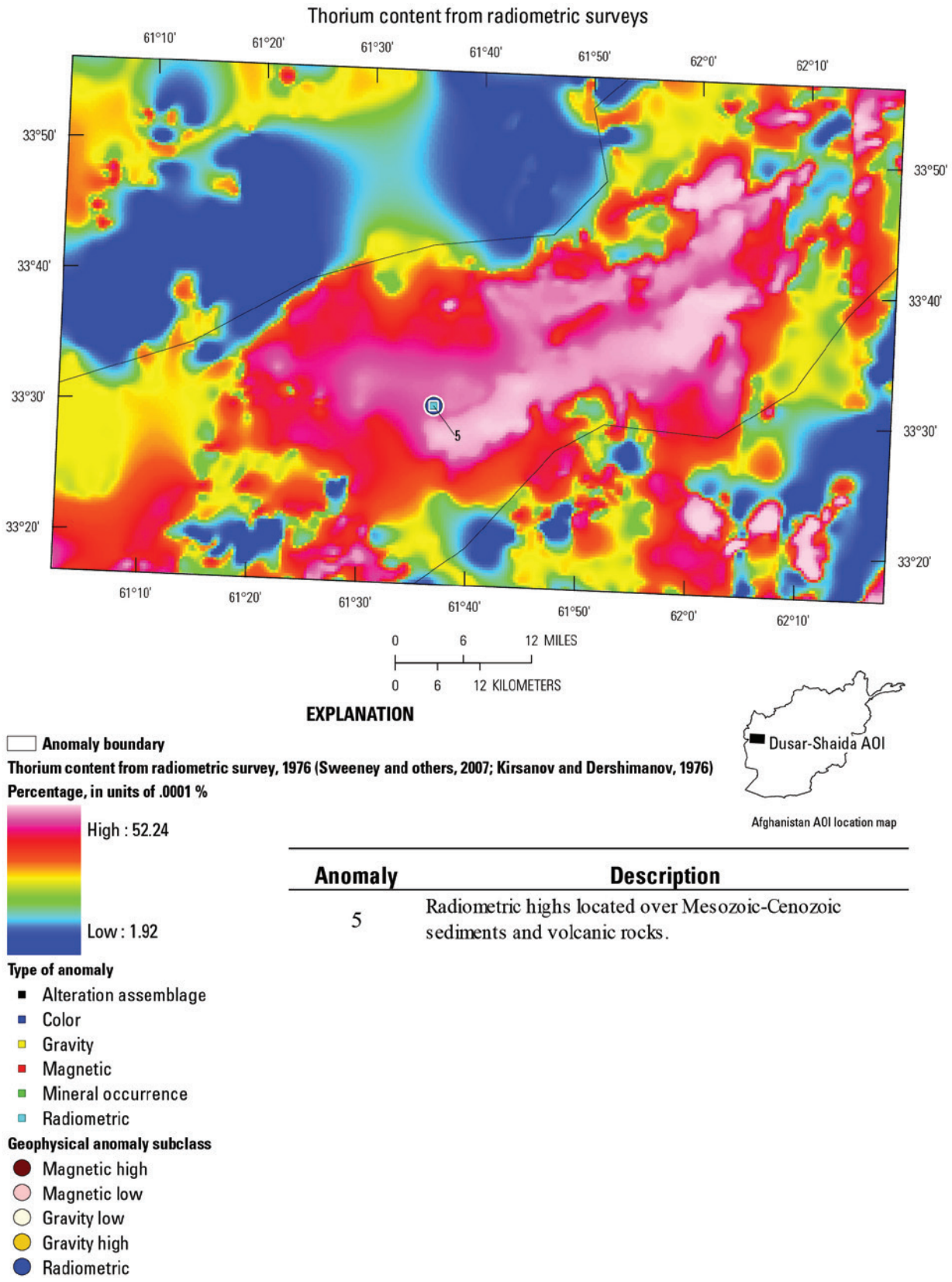

Figure 3.3.3. Radiometric geophysical anomalies located in the Dusar-Shaida Area of Interest (AOI) in Afghanistan.

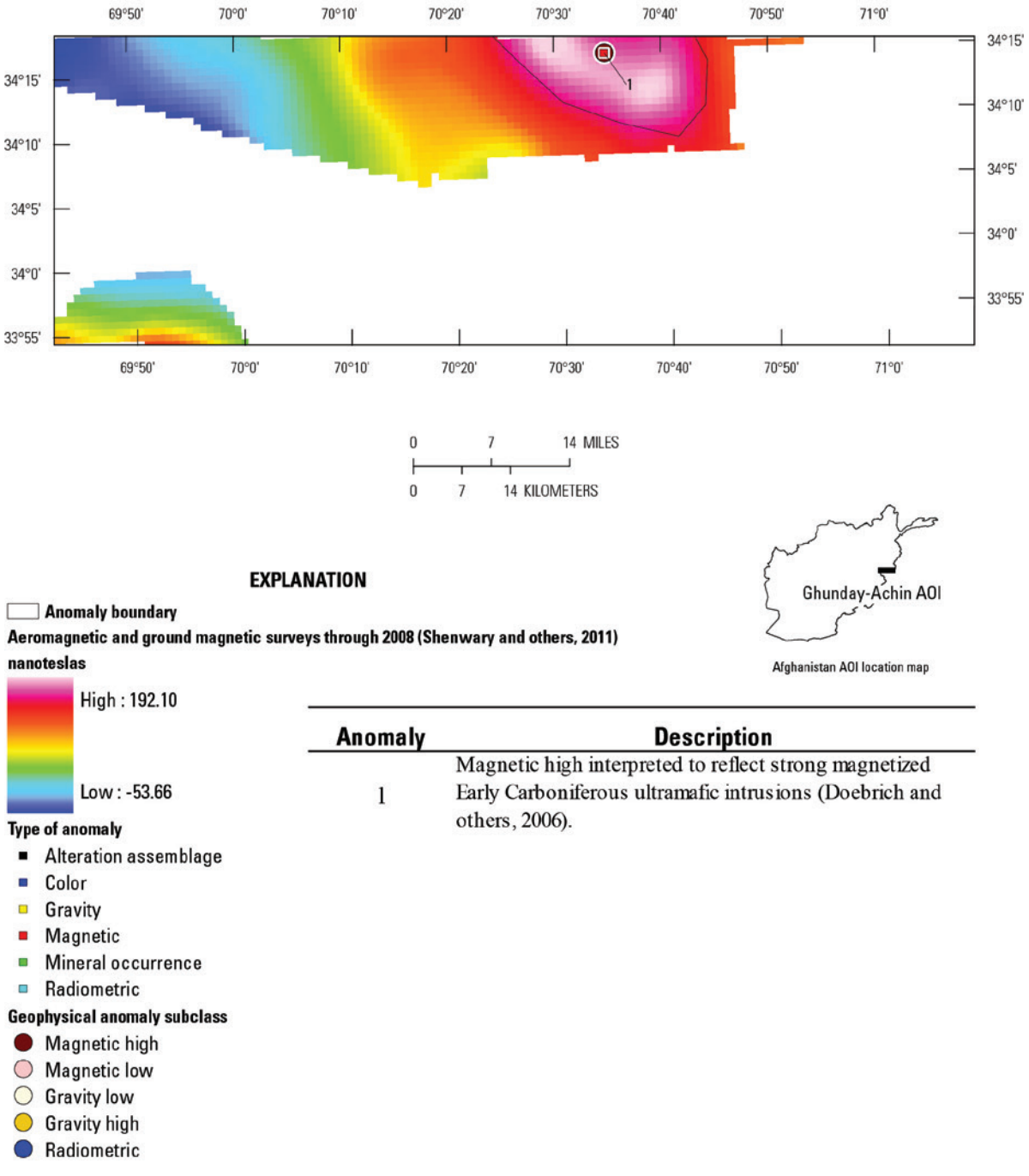

Figure 3.4.1. Reduced-to-pole magnetic geophysical anomalies located in the Ghunday-Achin Area of Interest (AOI) in Afghanistan.

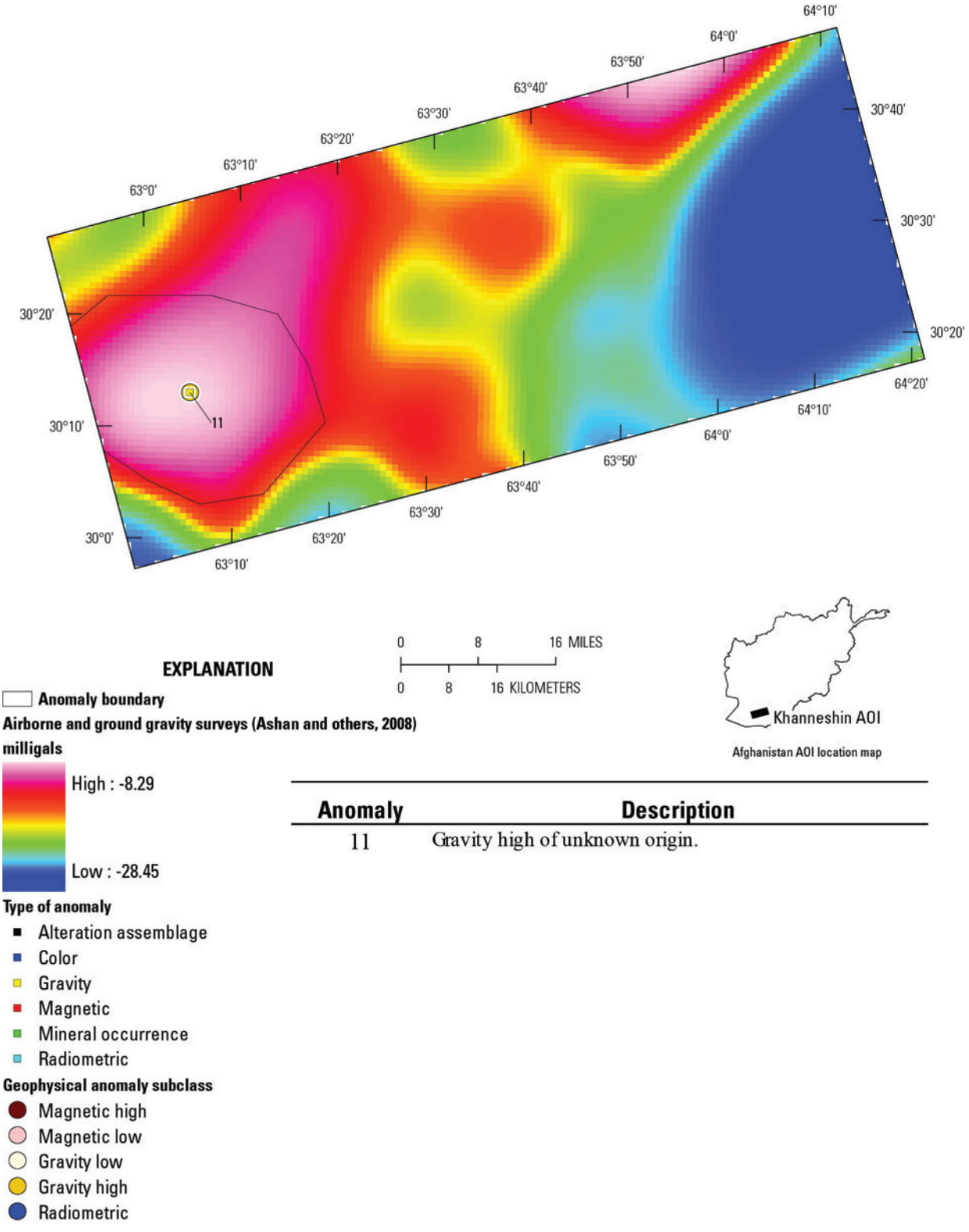

Figure 3.4.1. Gravity geophysical anomalies located in the Khanneshin Area of Interest (AOI) in Afghanistan.

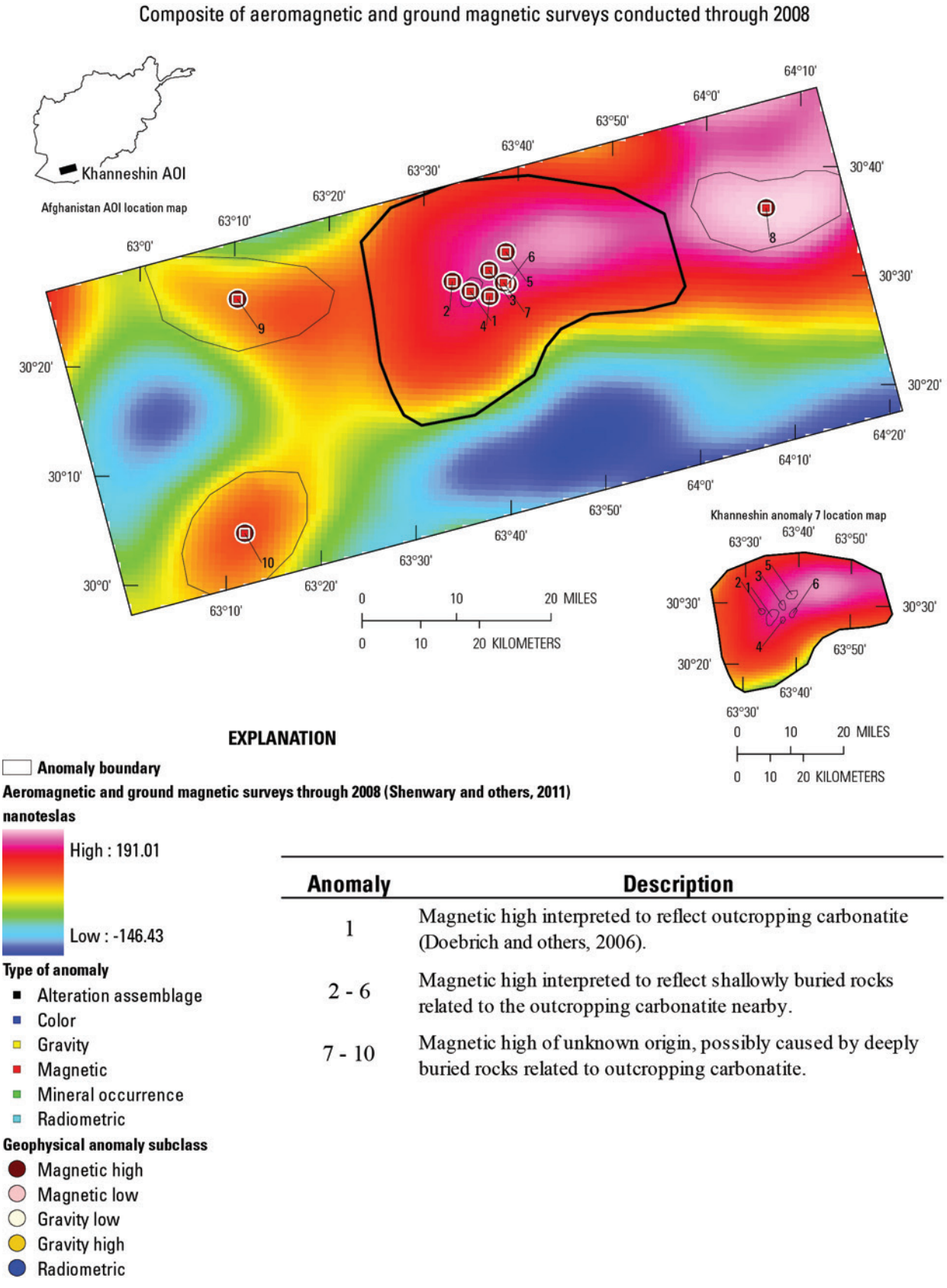

Anomaly	Description
1	Magnetic high interpreted to reflect outcropping carbonatite (Doebrich and others, 2006).
2 - 6	Magnetic high interpreted to reflect shallowly buried rocks related to the outcropping carbonatite nearby.
7 - 10	Magnetic high of unknown origin, possibly caused by deeply buried rocks related to outcropping carbonatite.

Figure 3.4.2. Reduced-to-pole magnetic geophysical anomalies located in the Khanneshin Area of Interest (AOI) in Afghanistan.

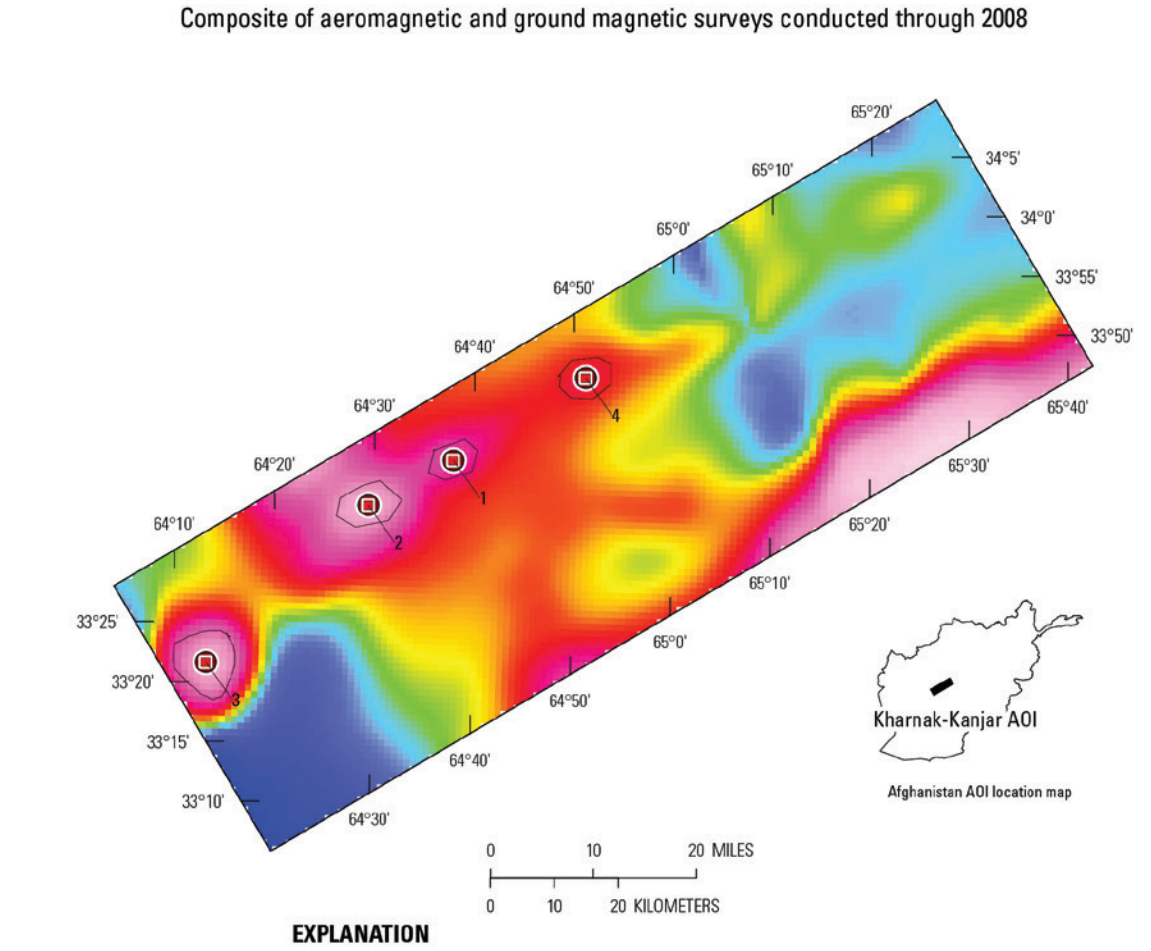

EXPLANATION

Anomaly boundary

Aeromagnetic and ground magnetic surveys through 2008 (Shenwary and others, 2011)

nanoteslas

High : 20.57

Low : -71.41

Type of anomaly

- Alteration assemblage
- Color
- Gravity
- Magnetic
- Mineral occurrence
- Radiometric

Geophysical anomaly subclass

- Magnetic high
- Magnetic low
- Gravity low
- Gravity high
- Radiometric

Anomaly	Description
1	Magnetic high interpreted to reflect granitoid pluton of the Farah Rod plutonic belt, possibly Cretaceous-Oligocene age (Debon and others, 1987).
2	Magnetic high interpreted to reflect granitoid pluton of the Farah Rod plutonic belt, possibly Cretaceous-Oligocene age (Debon and others, 1987).
3	Magnetic high interpreted to reflect granitoid pluton of the Farah Rod plutonic belt, possibly Cretaceous-Oligocene age (Debon and others, 1987).
4	Magnetic high interpreted to reflect granitoid pluton of the Farah Rod plutonic belt, possibly Cretaceous-Oligocene age (Debon and others, 1987).

Figure 3.5.1 Reduced-to-pole magnetic geophysical anomalies located in the Kharnak-Kanjar Area of Interest (AOI) in Afghanistan.

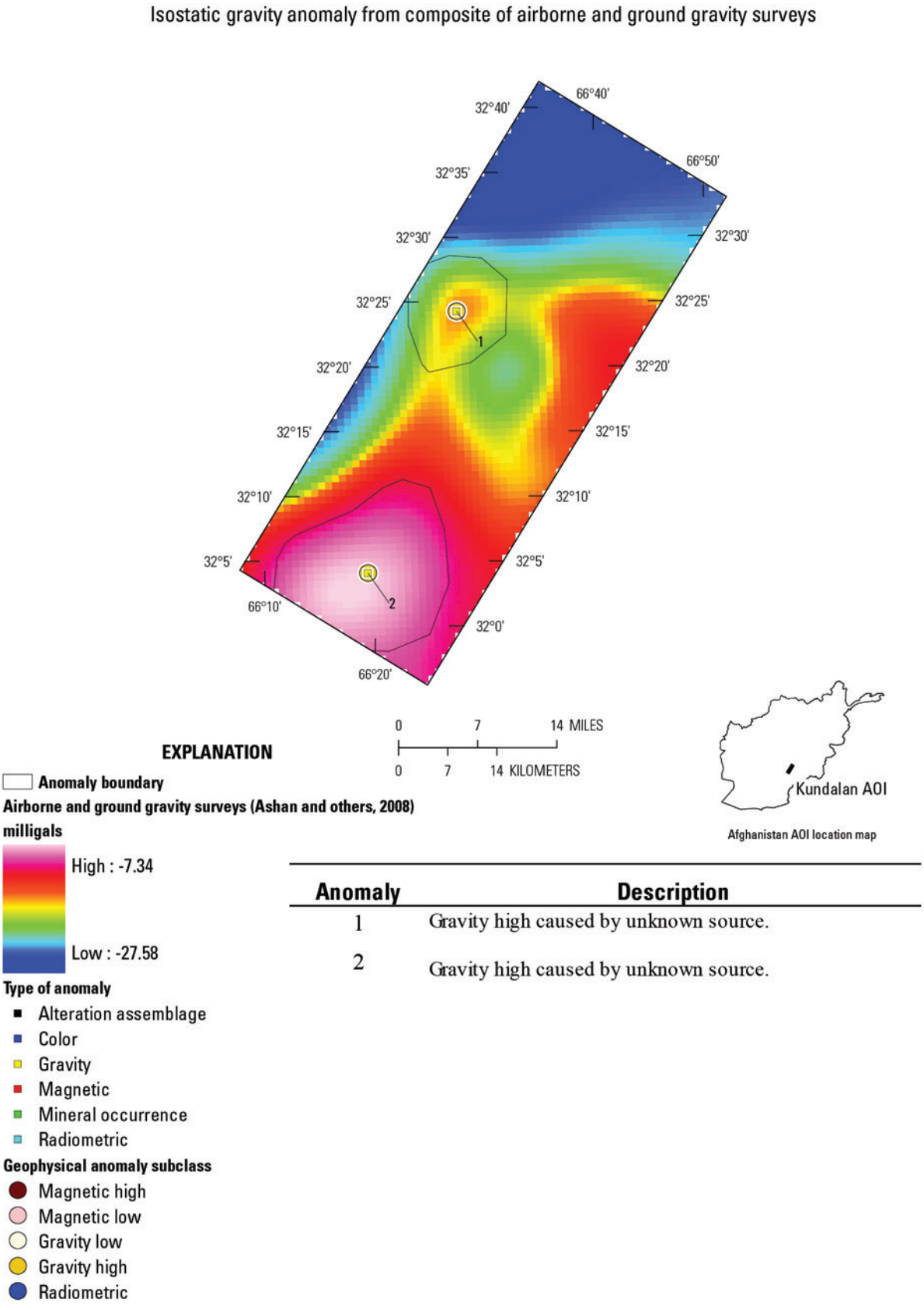

Figure 3.6.1. Gravity geophysical anomalies located in the Kundalan Area of Interest (AOI) in Afghanistan.

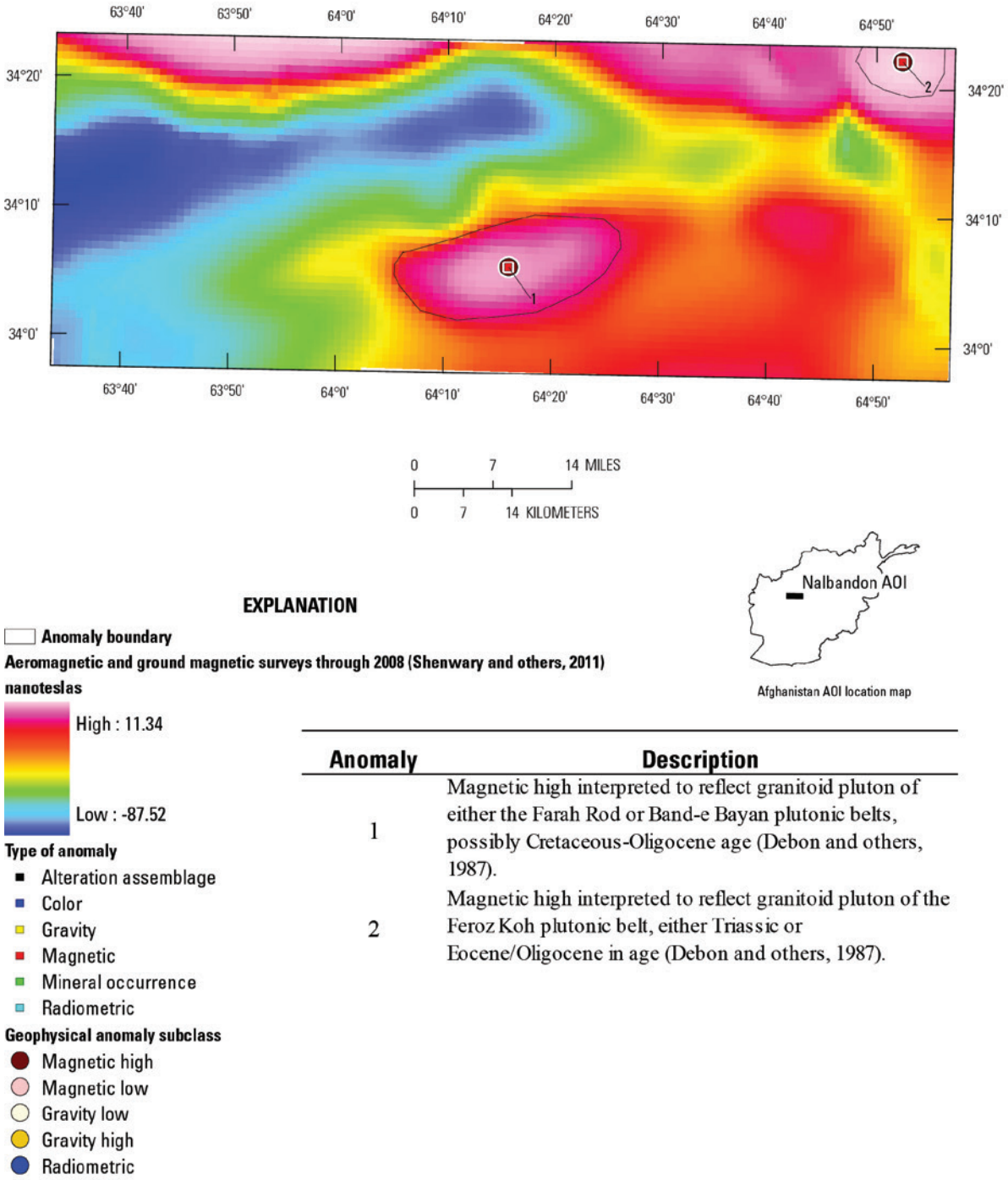

Anomaly	Description
1	Magnetic high interpreted to reflect granitoid pluton of either the Farah Rod or Band-e Bayan plutonic belts, possibly Cretaceous-Oligocene age (Debon and others, 1987).
2	Magnetic high interpreted to reflect granitoid pluton of the Feroz Koh plutonic belt, either Triassic or Eocene/Oligocene in age (Debon and others, 1987).

Figure 3.7.1. Reduced-to-pole magnetic geophysical anomalies located in the Nalbandon Area of Interest (AOI) in Afghanistan.

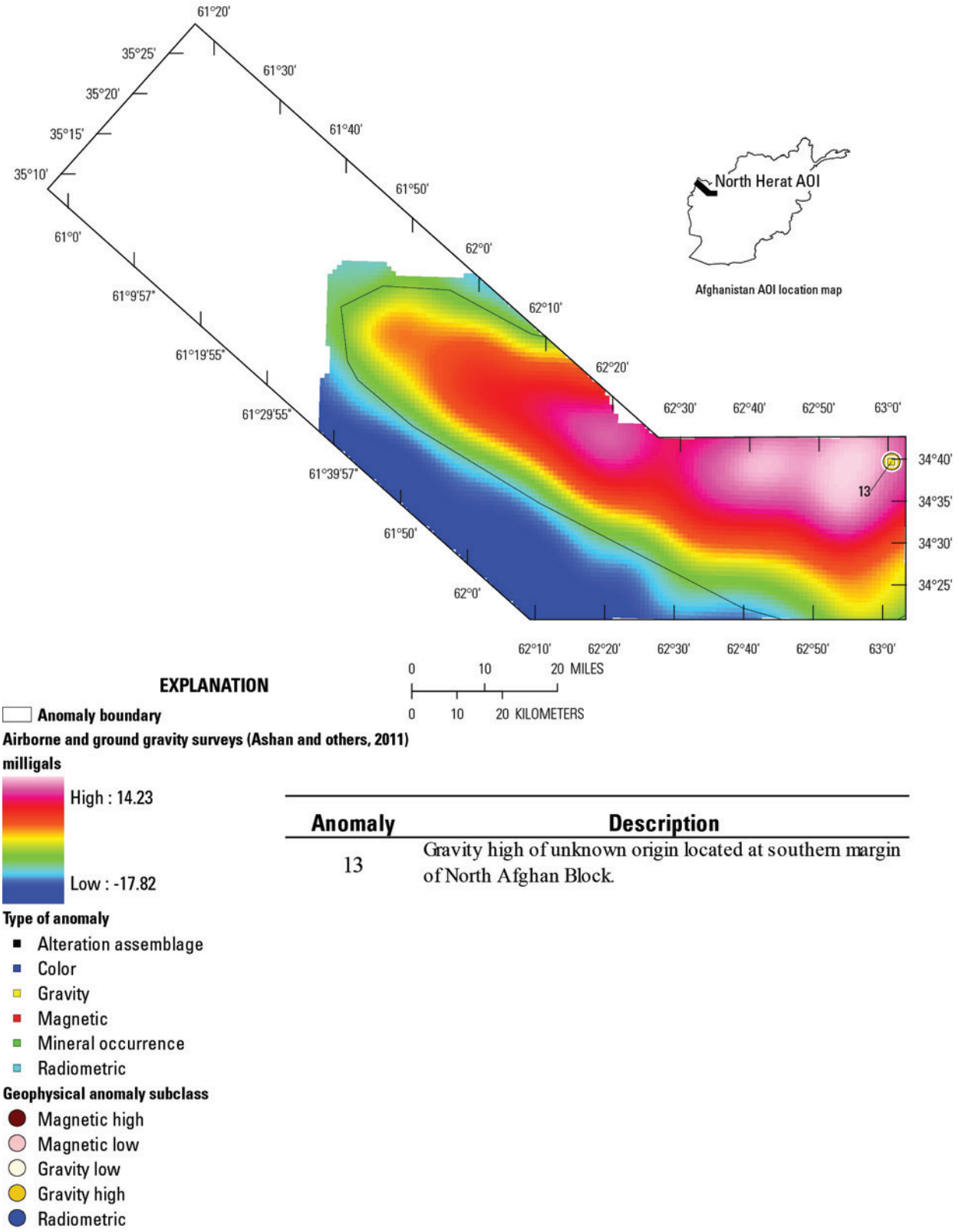

Anomaly	Description
13	Gravity high of unknown origin located at southern margin of North Afghan Block.

Figure 3.8.1. Gravity geophysical anomalies located in the North Herat Area of Interest (AOI) in Afghanistan.

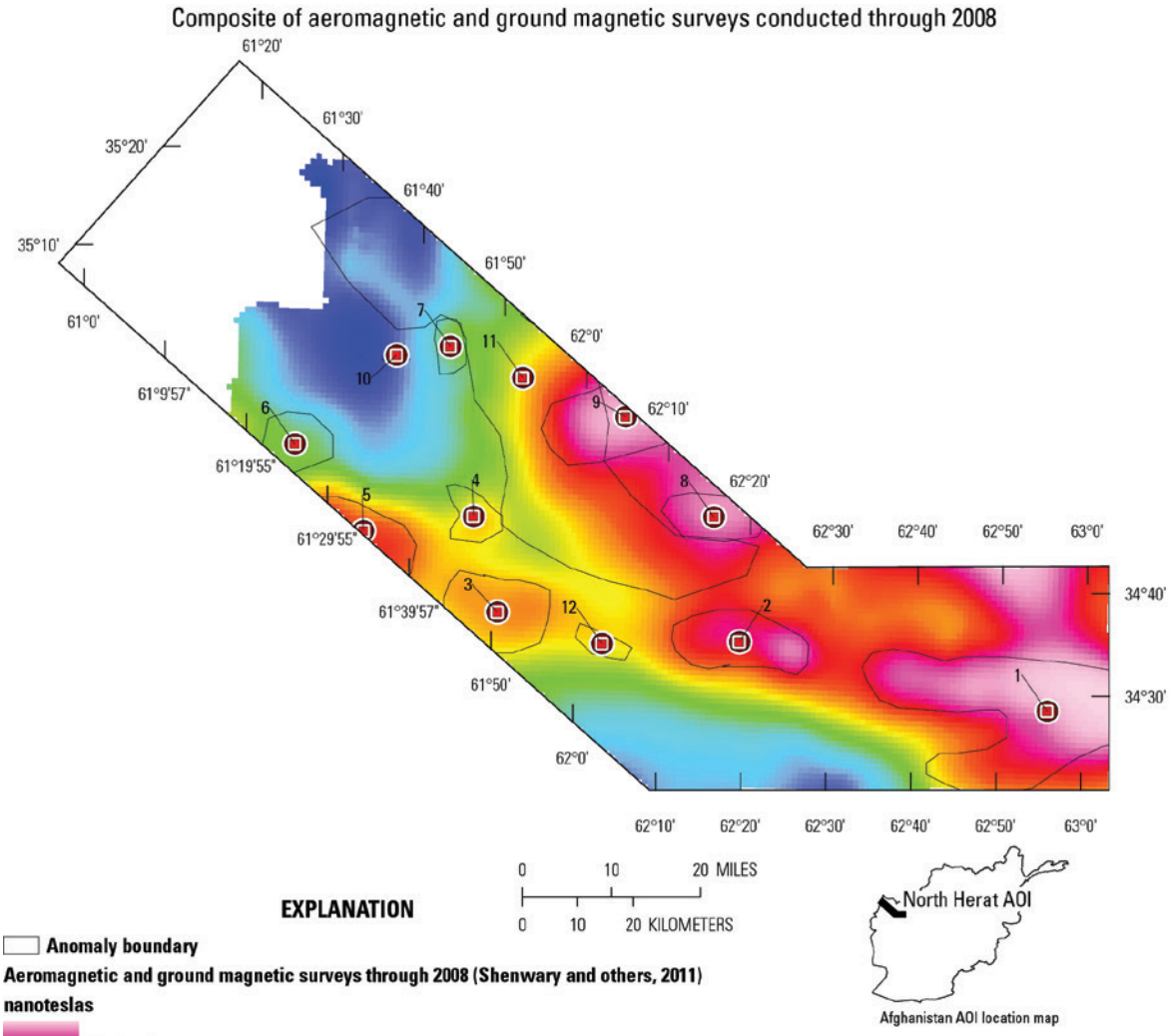

Anomaly	Description
1 - 10	Magnetic high interpreted to reflect granitoid pluton of the Feroz Koh plutonic belt, either Triassic or Eocene/Oligocene in age (Debon and others, 1987).
11	Region of several magnetic highs and lows, interpreted to reflect volcanic rocks and plutons related to Feroz Koh plutonic belt, either Triassic or Eocene/Oligocene in age (Debon and others, 1987).
12	Magnetic high interpreted to reflect granitoid pluton of the Feroz Koh plutonic belt, either Triassic or Eocene/Oligocene in age (Debon and others, 1987).

Figure 3.8.2. Reduced-to-pole magnetic geophysical anomalies located in the North Herat Area of Interest (AOI) in Afghanistan.

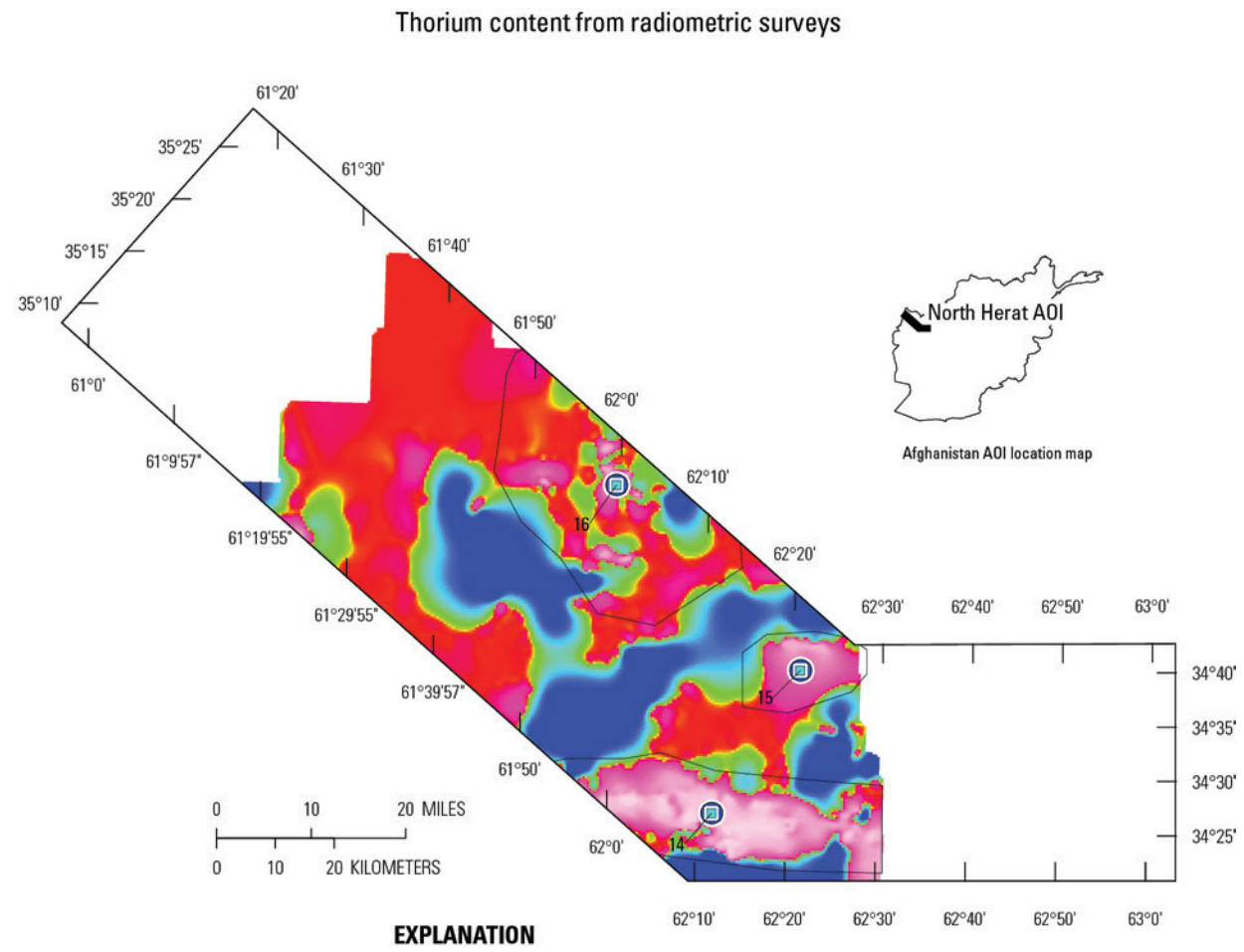

Anomaly boundary

Thorium content from radiometric survey, 1976 (Sweeney and others, 2007; Kirsanov and Dershimanov, 1976)

Percentage, in units of .0001 %

High : 20.29

Low : 3.00

Type of anomaly

- Alteration assemblage
- Color
- Gravity
- Magnetic
- Mineral occurrence
- Radiometric

Geophysical anomaly subclass

- Magnetic high
- Magnetic low
- Gravity low
- Gravity high
- Radiometric

Anomaly	Description
14	Radiometric highs located over Tertiary sediments.
15	Radiometric highs located over Paleozoic, Mesozoic, and Cenozoic sediments.
16	Radiometric highs located over Cenozoic sediments and volcanic rocks.

Figure 3.8.3. Radiometric geophysical anomalies located in the North Herat Area of Interest (AOI) in Afghanistan.

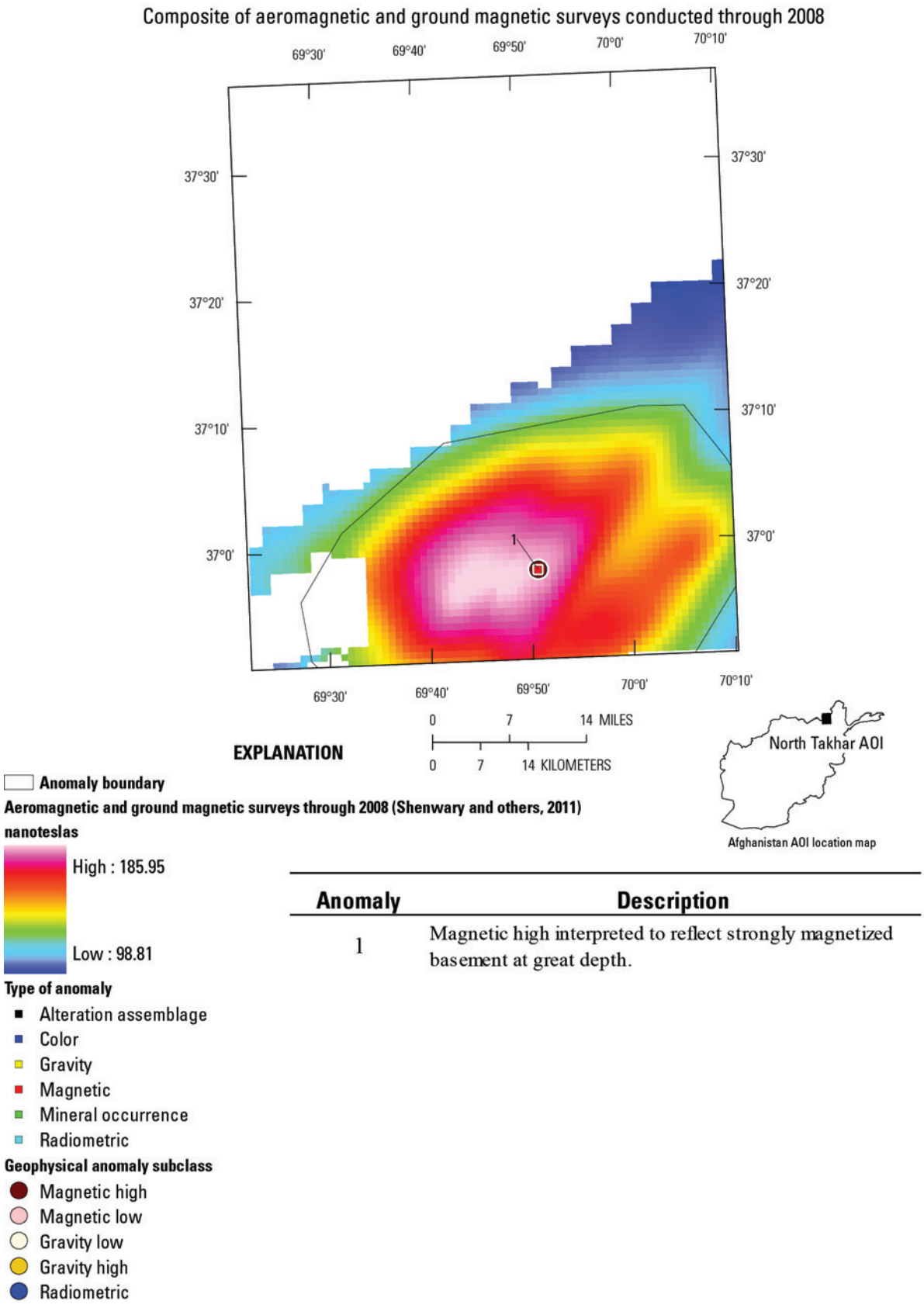

Anomaly	Description
1	Magnetic high interpreted to reflect strongly magnetized basement at great depth.

Figure 3.9.1. Reduced-to-pole magnetic geophysical anomalies located in the North Takhar Area of Interest (AOI) in Afghanistan.

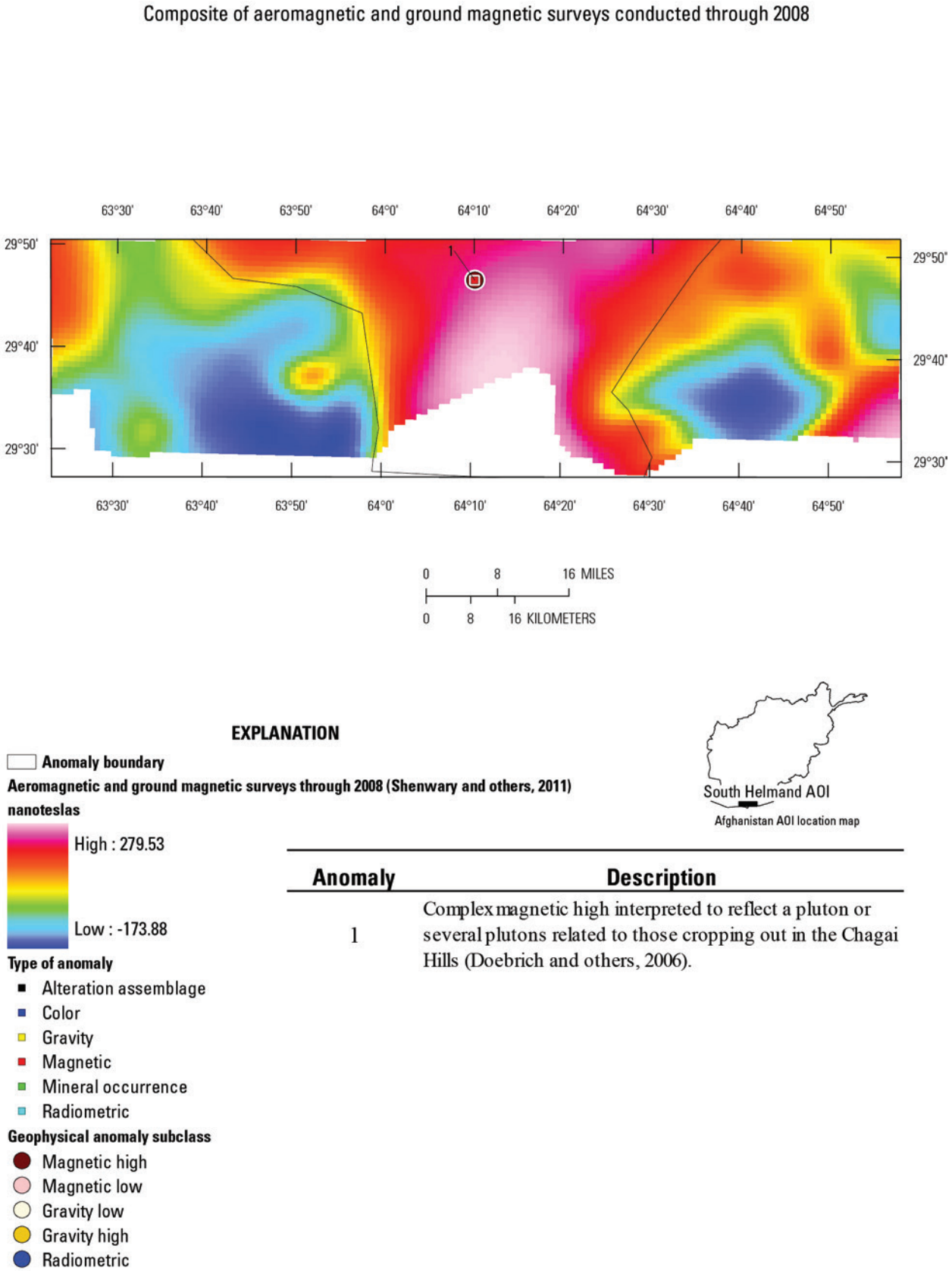

Figure 3.10.1. Reduced-to-pole magnetic geophysical anomalies located in the South Helmand Area of Interest (AOI) in Afghanistan.

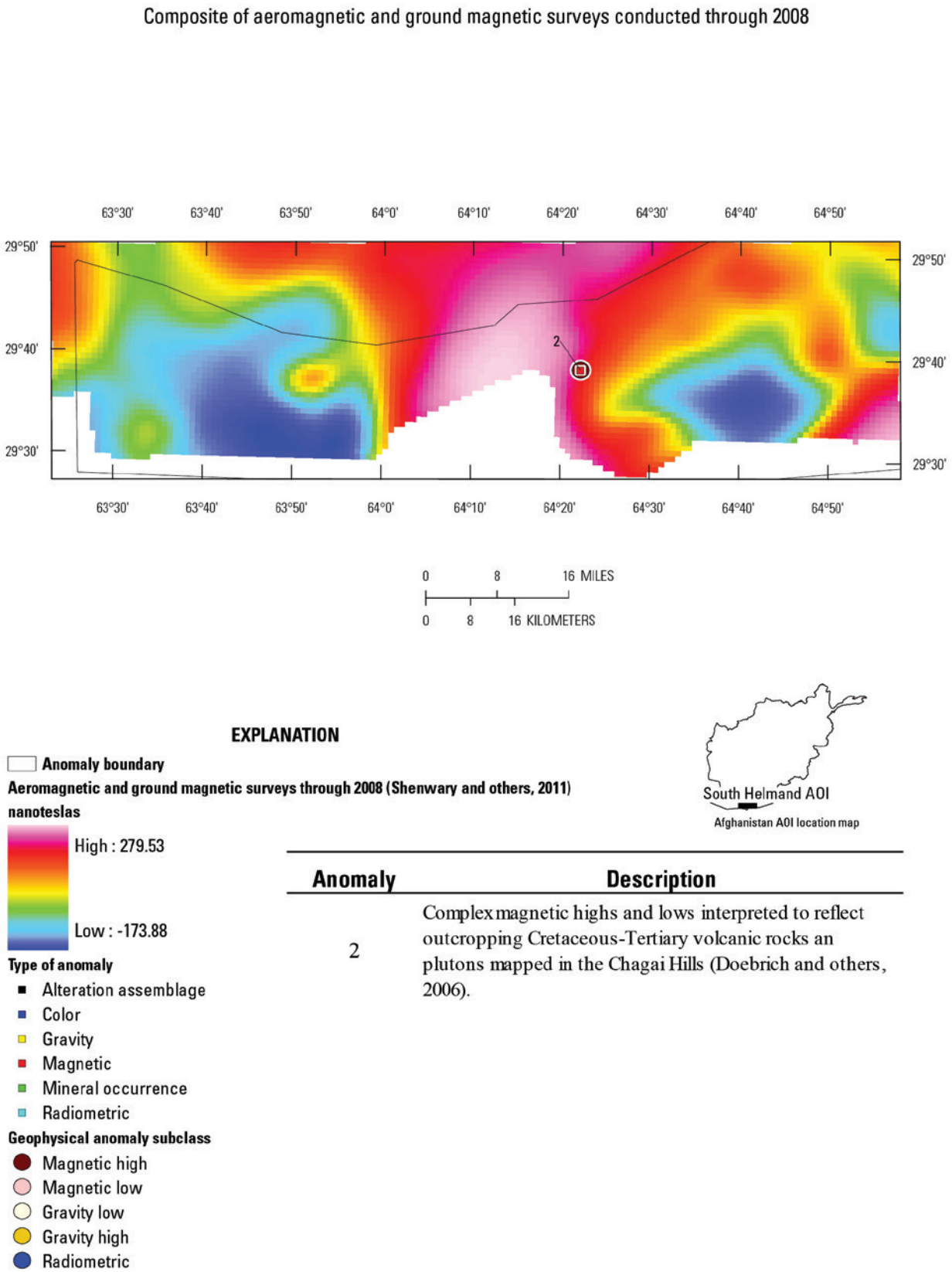

Figure 3.10.2. Reduced-to-pole magnetic geophysical anomalies located in the South Helmand Area of Interest (AOI) in Afghanistan.

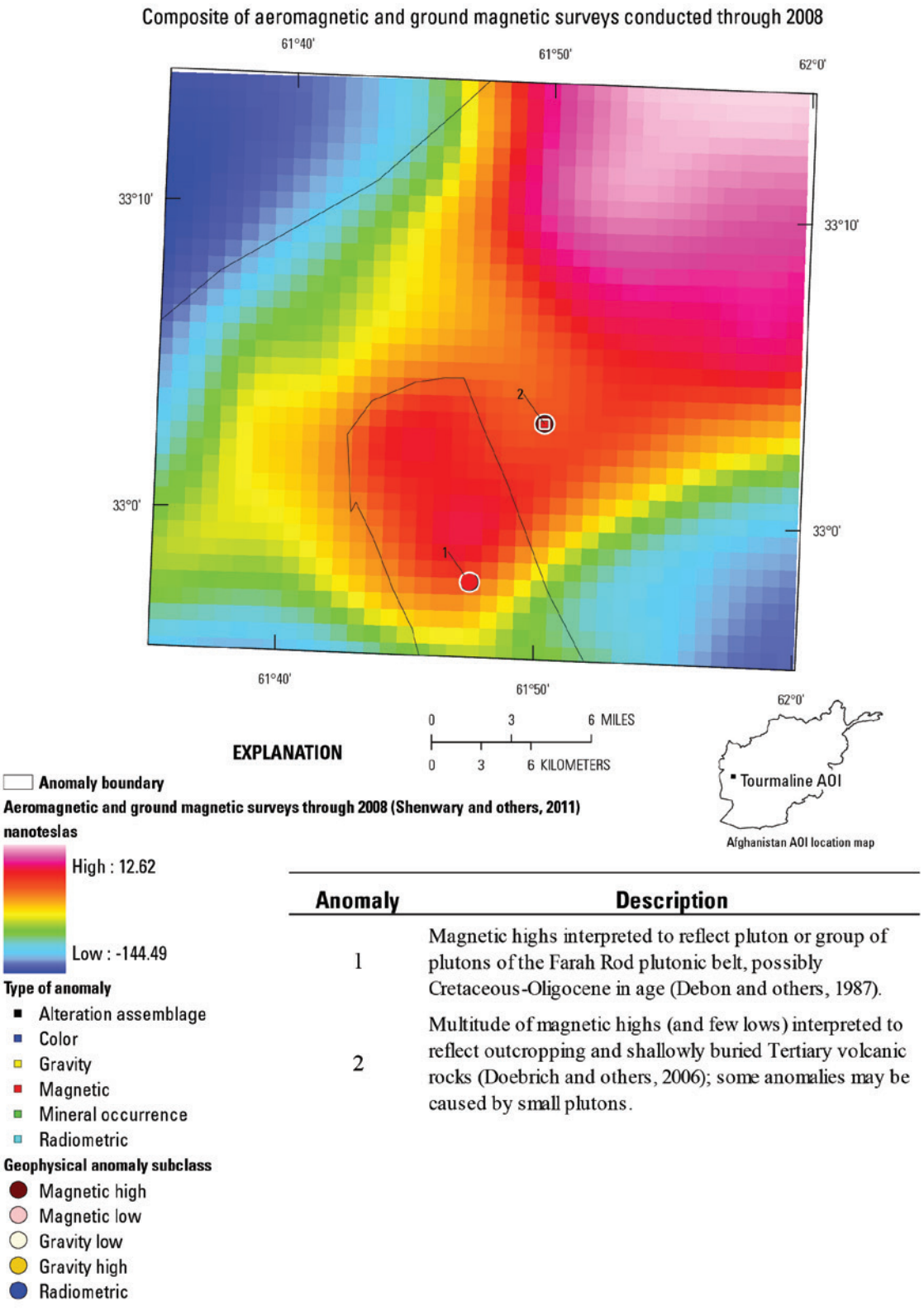

Anomaly	Description
1	Magnetic highs interpreted to reflect pluton or group of plutons of the Farah Rod plutonic belt, possibly Cretaceous-Oligocene in age (Debon and others, 1987).
2	Multitude of magnetic highs (and few lows) interpreted to reflect outcropping and shallowly buried Tertiary volcanic rocks (Doebrich and others, 2006); some anomalies may be caused by small plutons.

Figure 3.11.1. Reduced-to-pole magnetic geophysical anomalies located in the Tourmaline Area of Interest (AOI) in Afghanistan.

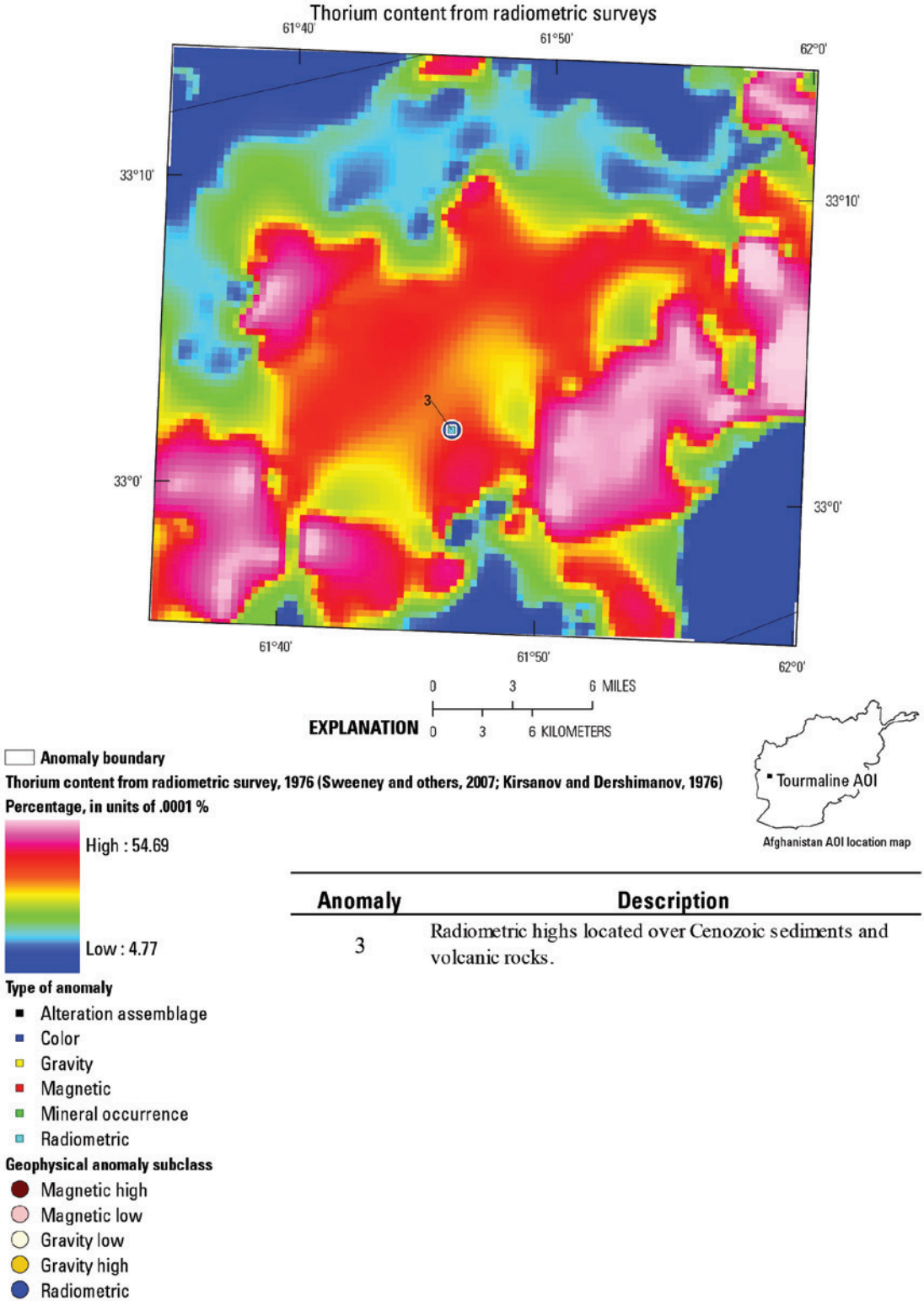

Anomaly	Description
3	Radiometric highs located over Cenozoic sediments and volcanic rocks.

Figure 3.11.2. Radiometric geophysical anomalies located in the Tourmaline Area of Interest (AOI) in Afghanistan.

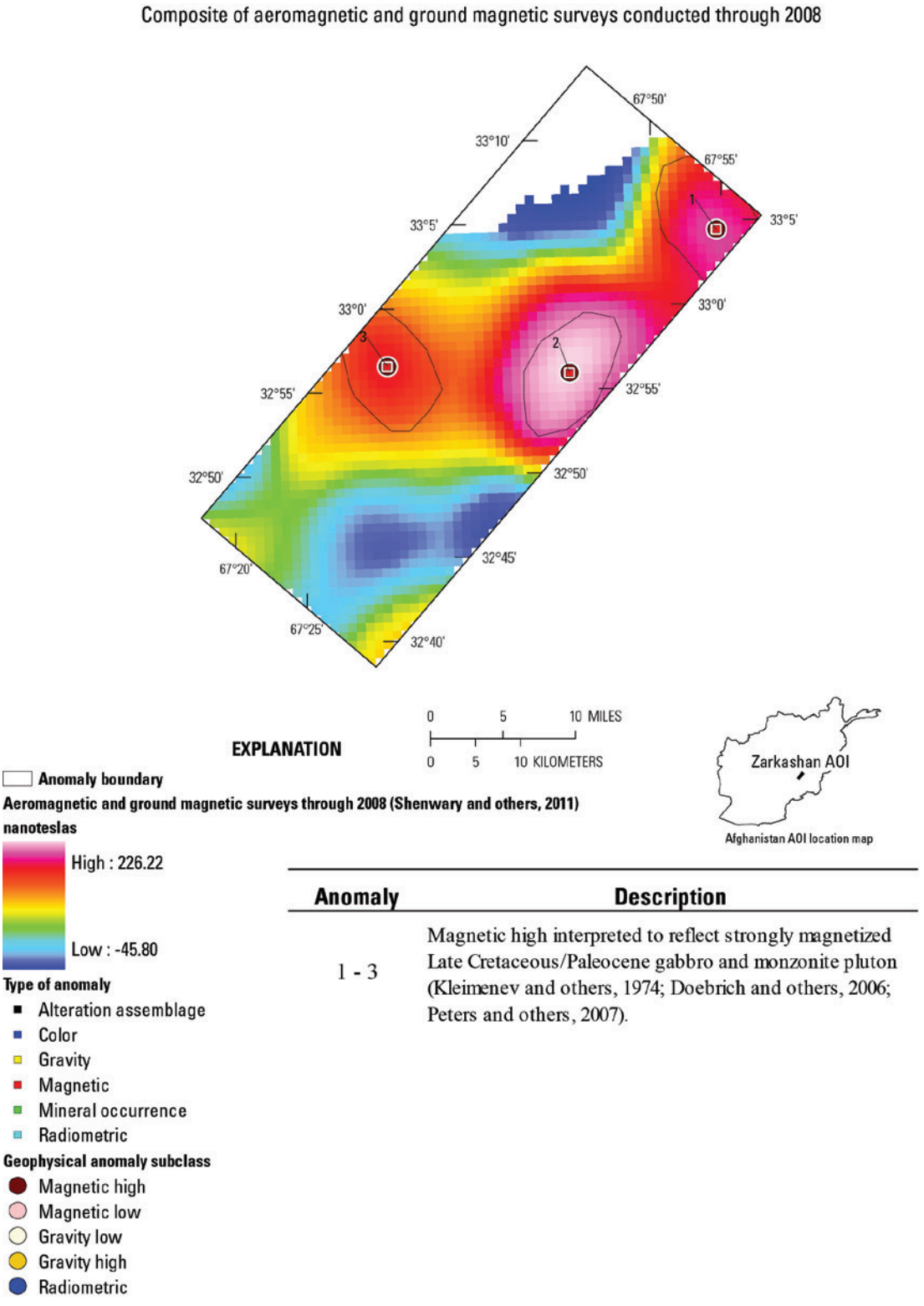

Figure 3.12.1. Reduced-to-pole magnetic geophysical anomalies located in the Zarkashan Area of Interest (AOI) in Afghanistan.

3.3 References Cited

Ashan, S., Hussain, S., Kohistany, A.H., Shenwary, G.S., Mutty, A.S., Daud, M.A., Abraham, J.D., Anderson, E.D., Drenth, B.J., Finn, C.A., Kucks, R.P., Lindsay, C.R., Phillips, J.D., Sweeney, R.E., Brozena, J.M., Ball, D.C., Childers, V.A., Gardner, J.M., Jarvis, J.L., and Liang, R.T., 2007, Aeromagnetic survey in Afghanistan: A website for distribution of data: U.S. Geological Survey Open-File Report 2007–1247, accessed August 19, 2011, at *http://pubs.usgs.gov/of/2007/1247/*.

Ashan, S., Hussain, S., Kohistany, A.H., Shenwary, G.S., Mutty, A.S., Daud, M.A., Brozena, J.M., Ball, D.C., Childers, V.A., Gardner, J.M., Jarvis, J.L., Liang, R.T., Abraham, J.D., Anderson, E.D., Drenth, B.J., Finn, C.A., Kucks, R.P., Lindsay, C.R., Phillips, J.D., and Sweeney, R.E., 2008, Airborne gravity survey and ground gravity in Afghanistan: A website for distribution of data: U.S. Geological Survey Open-File Report 2008–1089, accessed August 19, 2011, at *http://pubs.usgs.gov/of/2008/1089/*.

Blakely, R.J., 1995, Potential theory in gravity and magnetic applications: Cambridge, United Kingdom, Cambridge University Press, 441 p.

Clark, D.A., 1999, Magnetic petrology of igneous intrusions: Implications for exploration and magnetic interpretation: Exploration Geophysics, v. 30, p. 5–26.

Debon, F., Afzali, H., Le-Fort, P., and Sonet, J., 1987, Major intrusive stages in Afghanistan; typology, age and geodynamic setting: Geologische Rundschau, vol. 76, no. 1, p. 245–264.

Doebrich, J.L., and Wahl, R.R., 2006, Geologic and mineral resource map of Afghanistan: U.S. Geological Survey Open-File Report 2006–1038, 1 sheet, scale 1:850,000, available at *http://pubs.usgs.gov/of/2006/1038*.

Kirsanov, V.N., and Derzhimanov, R.S., 1976, Map of thorium contents of Afghanistan (western area), scale 1:100,000.

Kleimenev, M.A., Kamaev, S.V., and Kelesnichenke, V.A., 1974, Report on the results of geophysical investigations carried out in 1973–beginning of 1974 for solid minerals: Part 1: Republic of Afghanistan Ministry of Mines and Industries Department of Geology and Mineral Survey, 74 p.

McGinnis, L.D., 1971, Gravity fields and tectonics of the Hindu Kush: Journal of Geophysical Research, v. 76, p. 1894–1904.

Peters, S.G., Ludington, S.D., Orris, G.J., Sutphin, D.M., Bliss, J.D., and Rytuba, J.J., eds., and the U.S. Geological Survey-Afghanistan Ministry of Mines Joint Mineral Resource Assessment team, 2007, Preliminary non-fuel mineral resource assessment of Afghanistan: U.S. Geological Survey Open-File Report 2007–1214, 810 p., 1 CD-ROM, accessed August 19, 2011, at *http://pubs.usgs.gov/of/2007/1214/*.

Shenwary, G.S.; Kohistany, A.H.; Hussain, Sardar; Ashan, Said; Mutty, A.S.; Daud, M.A.; Wussow, M.W.; Sweeney, R.E.; Phillips, J.D.; Lindsay, C.R.; Kucks, R.P.; Finn, C.A.; Drenth, B.A.; Anderson, E.D.; Abraham, J.D.; Liang, R.T.; Jarvis, J.L.; Gardner, J.M.; Childers, V.A.; Ball, D.C.; and Brozena, J.M., 2011, Aeromagnetic surveys in Afghanistan—An updated website for distribution of data: U.S. Geological Survey Open-File Report 2011–1055, 8 p., accessed August 19, 2011, at *http://pubs.usgs.gov/of/2011/1055/*.

Sweeney, R.E., Kucks, R.P, Hill, P.L., and Finn, C.A., 2006a, Aeromagnetic and gravity surveys in Afghanistan: A web site for distribution of data: U.S. Geological Survey Open-File Report 2006–1204, accessed August 19, 2011, at *http://pubs.usgs.gov/of/2006/1204/*.

Sweeney, R.E., Kucks, R.P, Hill, P.L., and Finn, C.A., 2006b, Aeromagnetic survey in western Afghanistan: A web site for distribution of data: U.S. Geological Survey Open-File Report 2006–1325 accessed August 19, 2011, at *http://pubs.usgs.gov/of/2006/1325/*.

Sweeney, R.E., Kucks, R.P, Hill, P.L., and Finn, C.A., 2007, Radiometric survey in western Afghanistan: A website for distribution of data: U.S. Geological Survey Open-File Report 2007–1042, accessed August 19, 2011, at *http://pubs.usgs.gov/of/2007/1042/*.

Chapter 4: Identification of Mineral Anomalies in Afghanistan Using Advanced Spaceborne Thermal Emission and Reflection Radiometer

By Bernard E. Hubbard

4.1 Advanced Spaceborne Thermal Emission and Reflection Radiometer Overview

Advanced Spaceborne Thermal Emission and Reflection Radiometer (ASTER) data were initially used to map key industrial rocks and minerals for building and construction throughout the major population and transportation corridor of east-central Afghanistan, which is centered on Kabul, the capital and largest city (fig 4.1.1). ASTER is a spaceborne multispectral instrument aboard the Terra satellite, which was launched in December 1999 and has been operational since February 2000. The ASTER instrument consists of three subsystems, each operating in a different spectral region (*http://asterweb.jpl.nasa.gov/index.asp,* accessed 8/23/2011). The subsystems measure reflected and emitted radiation in 14 spectral bands, with an additional measurement in Band 3 for generating stereo digital elevation models (DEMs). The VNIR subsystem measures reflected radiation in three bands in the Visible and Near-InfraRed wavelengths (0.52–0.86 microns [μm]); the SWIR subsystem measures reflected radiation in six bands in the ShortWave InfraRed wavelengths (1.00–2.43 μm); and the TIR subsystem measures emitted radiation in five bands in the Thermal InfraRed wavelengths (8.125–11.650 μm). Ground resolution is 15, 30, and 90 meters for the VNIR, SWIR, and TIR subsystems, respectively.

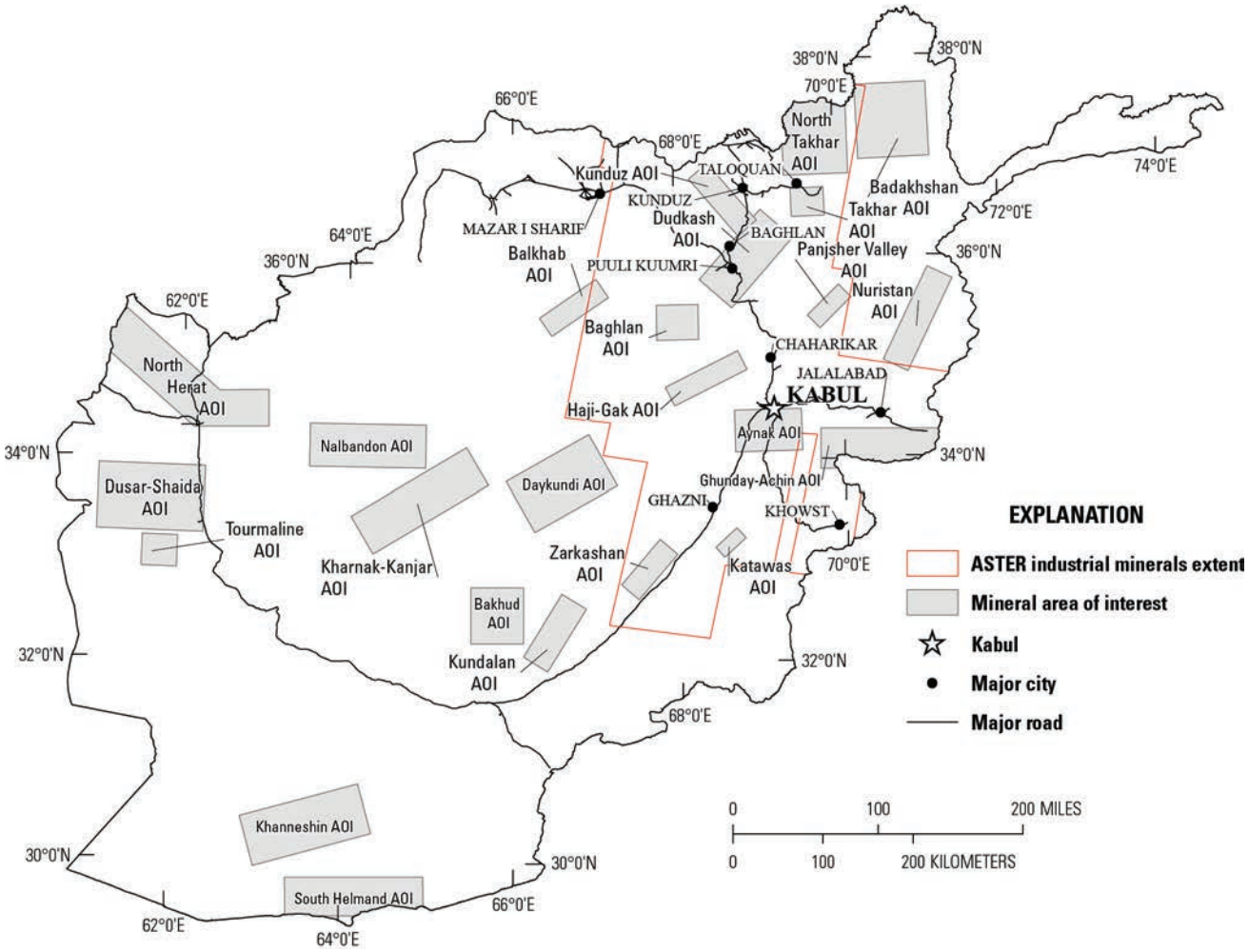

Figure 4.1.1. Study area map showing extent of ASTER mapped industrial minerals data, mineral areas of interest, cities, and major roads in Afghanistan.

4.1.2 ASTER Mapped Minerals

Four classes of industrial rocks and minerals were mapped over an approximately 146,000-km^2 region (shown on fig. 4.1.1 as a red outline representing 22.5 percent of the country and containing over 60 percent of the total population) using nine-band ASTER level-1B radiance data calibrated to reflectance (VNIR and SWIR image data with radiometric and geometric coefficients applied) (Mars and Rowan, 2010) which will be discussed in a forth coming report, "Regional mapping of industrial rock and mineral resources in east-central Afghanistan using spaceborne ASTER imagery" (B.E. Hubbard, USGS, written commun., 2011). Ancillary compositional information was provided using ASTER spectral emissivity derived from the five atmospherically corrected TIR bands of "radiance at surface" data (Gillespie and others, 1998; Ninomiya and others, 2005; Rockwell and Hofstra, 2008).

Targeted industrial rocks and minerals include (1) carbonate rocks containing either abundant calcite, dolomite mixtures, argillaceous and (or) weathered carbonate rocks containing residual clay minerals; (2) clay mineral deposits of a variety of origins containing either mixtures of or abundant amounts of kaolinite, montmorillonite, illite and (or) muscovite; (3) gypsum and other sulfate minerals as detectable (Oztan and Suzen, 2011); and (4) ferricrete, gossan, laterite, bauxite, magnesite, sulfur, and other materials that are either abundant enough and (or) have uniquely strong spectral signatures that can be detected easily using two or more ASTER bands (using band ratios, relative band-depth

images, and spectral matched-filtering [Rowan and others, 2003; Rowan and Mars, 2003; Rowan and others, 2005]). The TIR emissivity data were also used to distinguish carbonate rocks from nearby ultramafic rocks containing chlorite and (or) epidote (for example, Rowan and Mars, 2003; Dalton and others, 2004; Ninomiya and others, 2005).

4.1.3 ASTER Identified Anomalies

Several of these ASTER-mapped industrial minerals, such as kaolinite, ferric iron, and sericite, also are associated with hydrothermally altered rocks that contain either precious- and (or) base-metal ore deposits (Crowley, 1994). In total, 108 anomalies were identified based on ASTER regional mapping of industrial rocks and minerals throughout all or part of 12 mineralized areas of interest (AOI) defined by Peters and others (2007). Most of the anomalies were discovered as a coincidence, since the main goal was not targeted hydrothermal alteration mineral mapping over igneous and volcanic rocks (see for example, Mars and Rowan, 2007).

Mineral anomalies include areas identified as possible hydrothermal alteration of igneous, sedimentary, and metamorphic rocks, including supergene alteration potentially related to bedded massive sulfide deposits, epithermal and (or) polymetallic veins. Also identified were areas of ferric-iron dominant gossan, laterite (possible bauxite resource), high-value industrial minerals, such as magnesite, and sulfur- and phosphate-bearing minerals of evaporitic and (or) biogenic origin.

In addition to mineral assemblages, such as unusual spatial and spectral mixing patterns between the most abundant clay- and ferric-iron mineral types, other criteria used to facilitate the identification of mineral anomalies included (1) color, using false-color Landsat 7-4-2 and ASTER 6-3-1 composite images to enhance “bleached” and “iron-stained” rocks; (2) geometric shape, such as circular features indicative of an igneous intrusion with associated hydrothermal circulation or linear features suggesting structural control of hydrothermal fluids; (3) large size of feature and (or) large strength of related mineral absorption feature; (4) topographic features suggesting widespread erosion and removal of often “clay-rich” altered rocks in areas of high concentration of bedrocks; and (5) correlation of mapped features with geochemical stream-sediment halos (for example, Peters and others, 2007), including those representing downstream areas of sediment accumulation. Hydrothermally altered areas were also categorized by deposit type, including argillic, phyllic, and propylitic as defined by Thompson and others (2009) for a variety of hypogene and supergene mineral assemblages including those typical of porphyry, vein, stockwork, and bedded sulfide deposits.

Using a single ASTER scene that was processed differently from those in the ASTER industrial minerals area shown in fig. 4.1.1, an additional eight mineral anomalies were identified in the Tourmaline AOI (Peters and others, 2007). In this case, all potential hydrothermal-alteration-related minerals, including chlorite, epidote, and other phyllosilicates (Thompson and others, 2009) not found in this AOI, were targeted using image end members extracted from Eocene to Oligocene volcanic and intrusive rocks (Doebrich and Wahl, 2006) exposed throughout the Tourmaline AOI. Image end-member extraction, n-dimensional spectral-band analysis, and partial spectral unmixing were applied following the more detailed methods presented by Hubbard and others (2007) for mapping volcanic-hosted massive sulfide and porphyry deposits in the Alaska Range and Talkeetna Mountains of Alaska.

4.2 Presentation of ASTER Anomalies

A total of 116 ASTER anomalies were identified throughout 13 mineralized AOIs (Peters and others, 2007), some of which have commonality with anomalies identified through HyMap image analysis, geophysical data, and (or) both (figs. 4.2.1–4.14.5). The maps display the ASTER-mapped industrial minerals dataset as an image color-coded by mineral class and described in the map explanation under the heading: ASTER mineral classes. Solid black lines with a white outline define the approximate shape and extent of the identified anomaly polygons. Point features shown on the maps are a three-layer color-coded categorical representation of the ASTER mineral class and subclass, mineral deposit type (Thompson and others, 2009), and type of anomaly. For example, an

"Alteration assemblage" type of anomaly, categorized as a "Phyllic (Sericitic)" mineral deposit type and further identified by mineral class and subclass as a "Clays & Micas: Illite and/or Muscovite" anomaly is shown as a large green square (Type of anomaly: Alteration assemblage) overlain by a smaller dark blue circle (Mineral deposit type [Thompson and others, 2009]: Phyllic [Sericitic]) and again overlain by a smaller bright green square (ASTER mineral class and subclass: Clays & Micas: Illite and/or Muscovite). The point features on the maps are displaying some of the additional categorical descriptions about the anomalies that are contained in the attribute table of the shapefile and contained in the KMZ file provided in chapter 2 of this report.

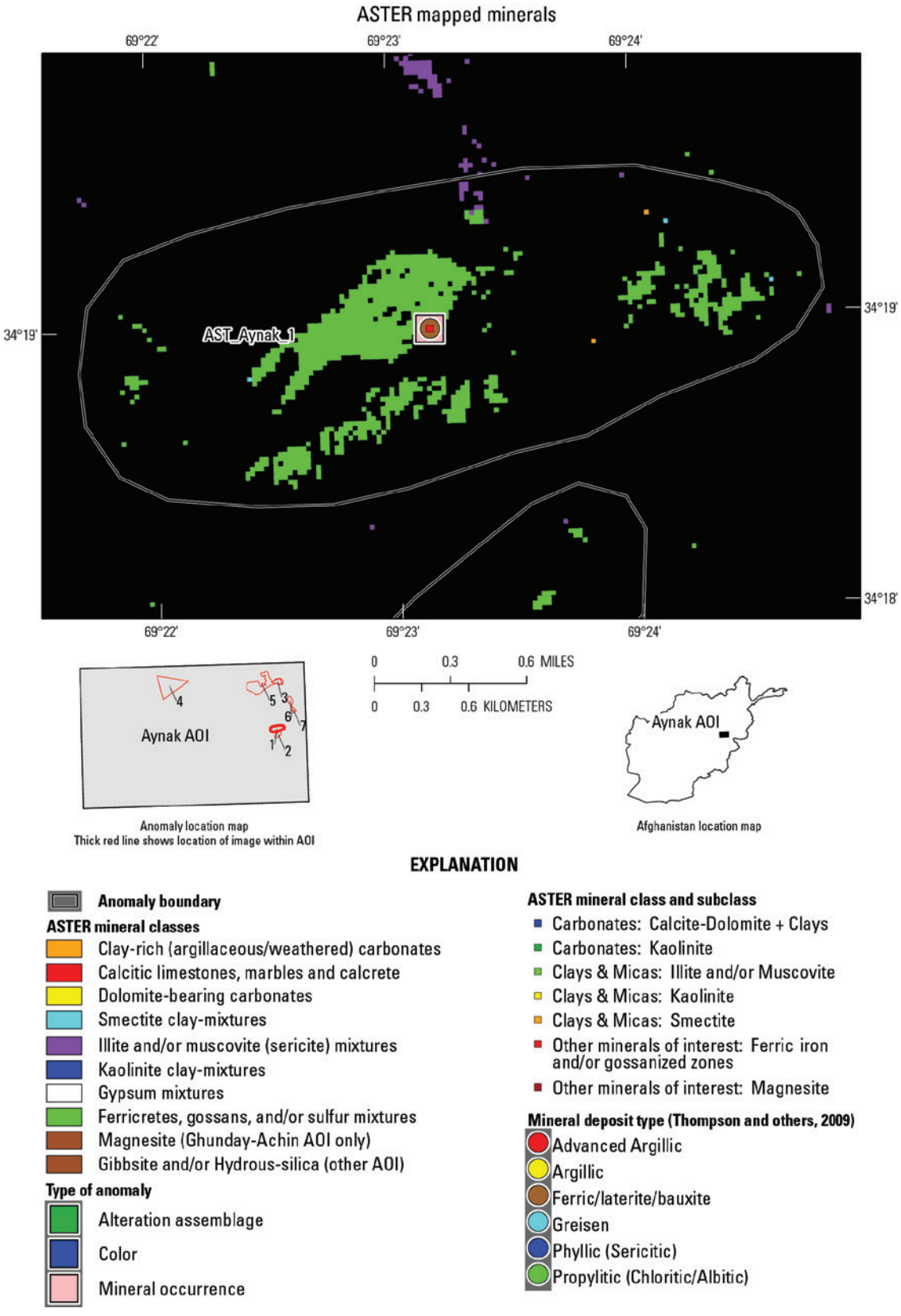

Figure 4.2.1. ASTER mineral occurrence anomaly located in the Aynak Area of Interest (AOI) in Afghanistan. Ferric iron-bearing gossan discovered above Aynak sedimentary exhalative deposits associated with Gezghay Copper occurrence (Orris and Bliss, 2002).

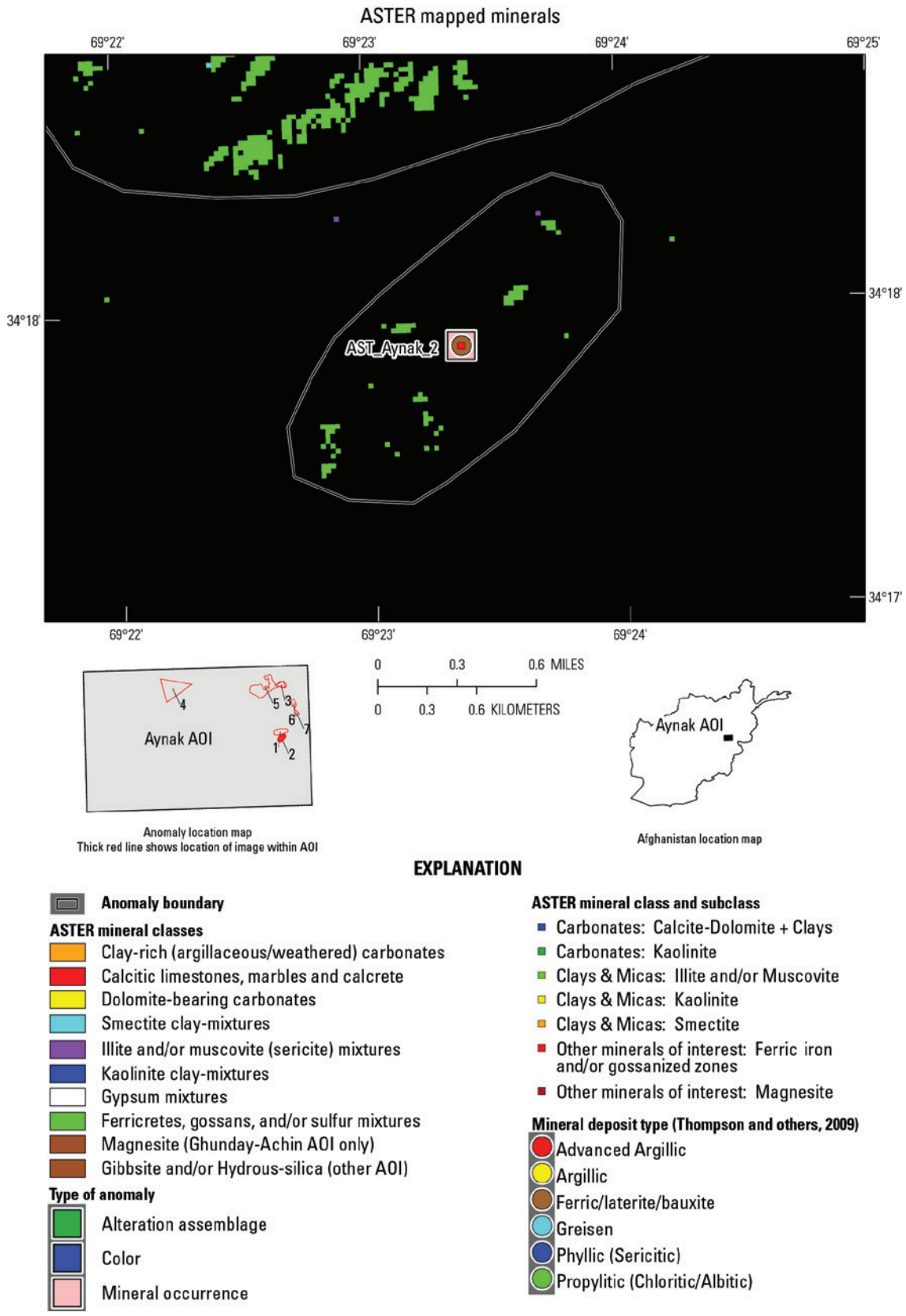

Figure 4.2.2. ASTER mineral occurrence anomaly located in the Aynak Area of Interest (AOI) in Afghanistan. Ferric iron-bearing gossan discovered above Aynak sedimentary exhalative deposits associated with Gezghay Copper occurrence (Orris and Bliss, 2002).

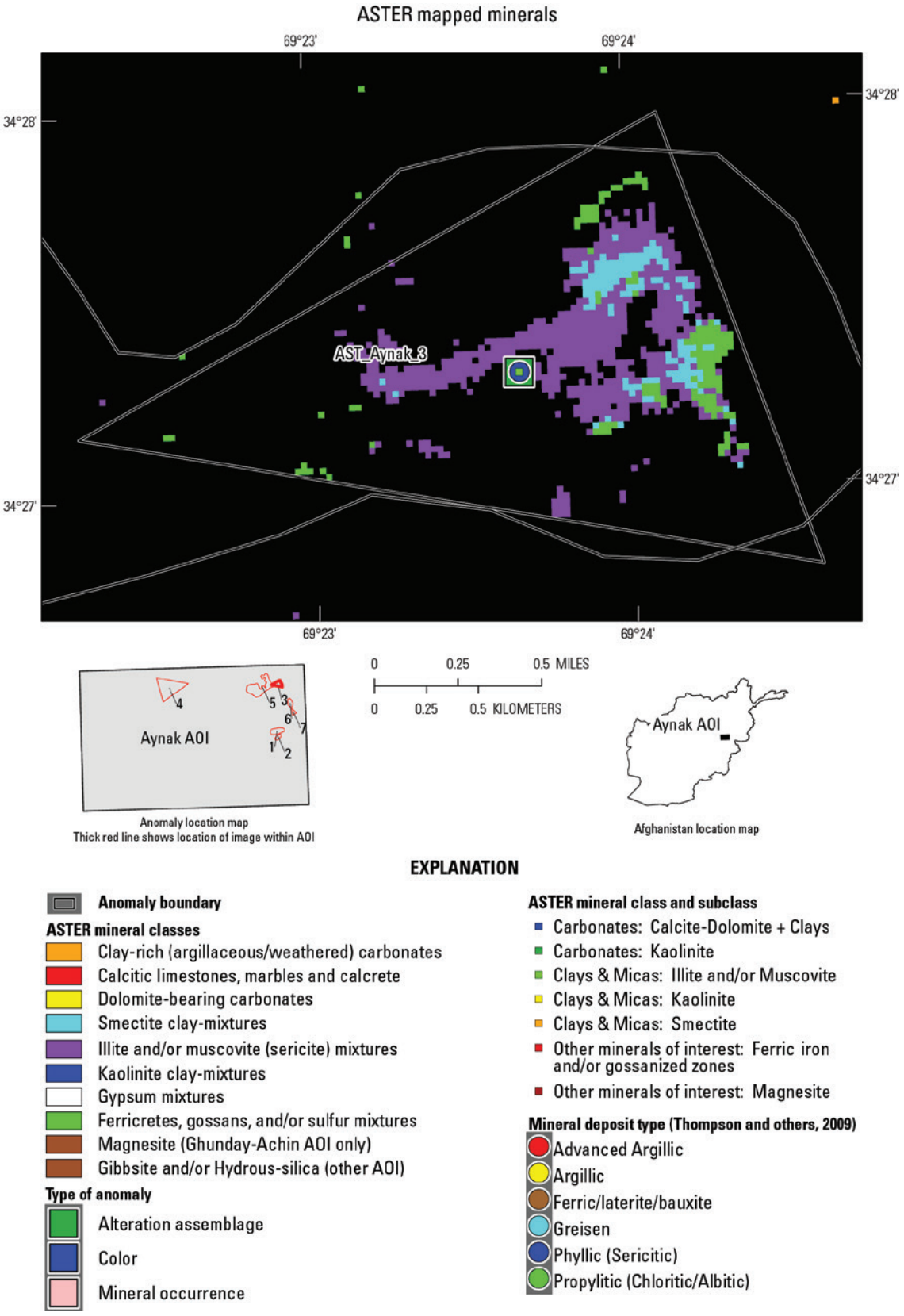

Figure 4.2.3. ASTER alteration anomaly located in the Aynak Area of Interest (AOI) in Afghanistan. Bleached and/or iron-stained areas containing mixtures of carbonates, ferric iron, illite and/or muscovite with smectite-rich cores.

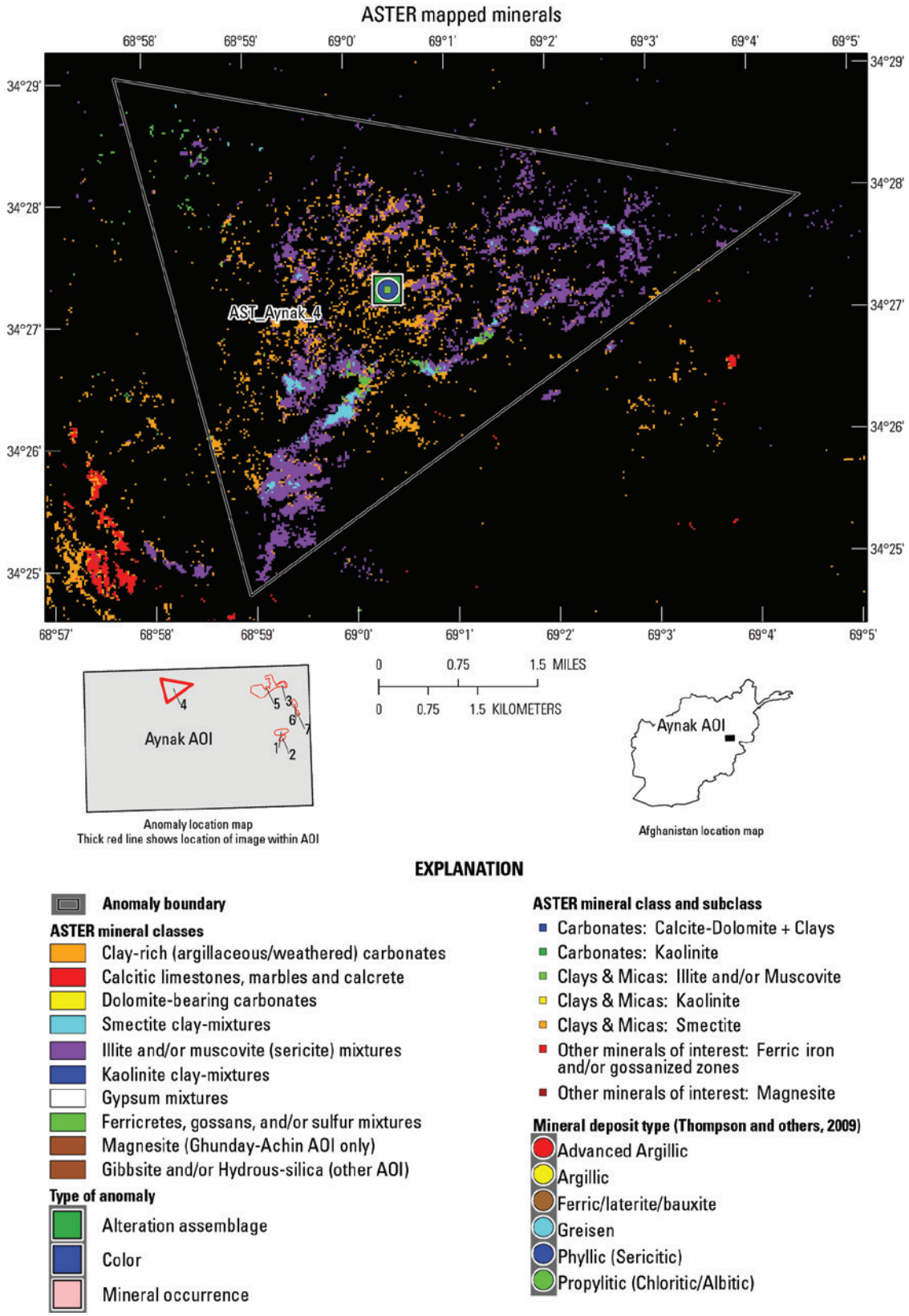

Figure 4.2.4. ASTER alteration anomaly located in the Aynak Area of Interest (AOI) in Afghanistan. Bleached and/or iron-stained areas containing mixtures of carbonates, ferric iron, illite and/or muscovite with smectite-rich cores.

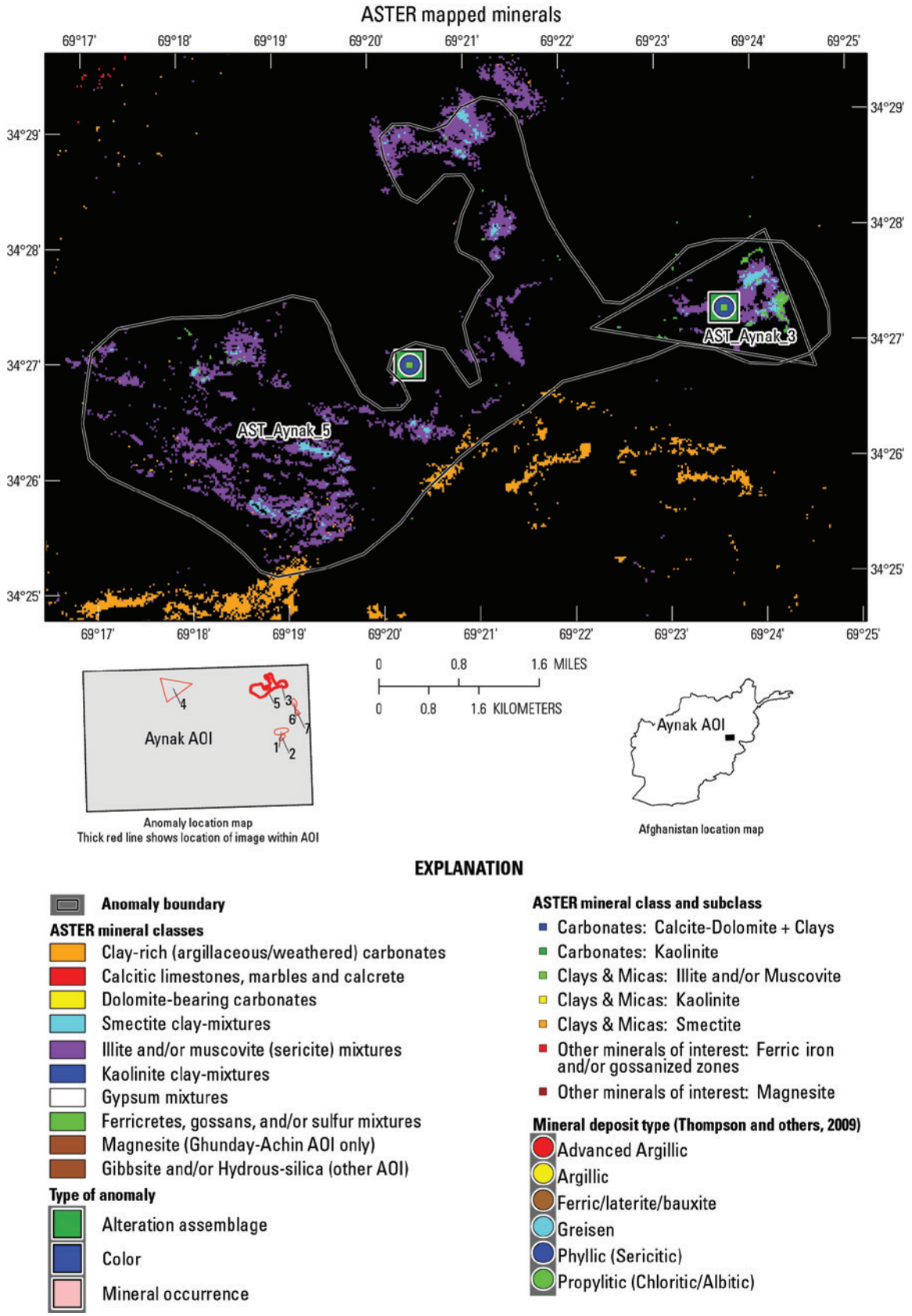

Figure 4.2.5. ASTER alteration anomaly located in the Aynak Area of Interest (AOI) in Afghanistan. Bleached and/or iron-stained areas containing mixtures of carbonates, ferric iron, illite and/or muscovite with smectite-rich cores. Anomaly is a larger and regionally more extensive mapped area that encompasses the smaller local-scale anomaly, AST_Aynak_3.

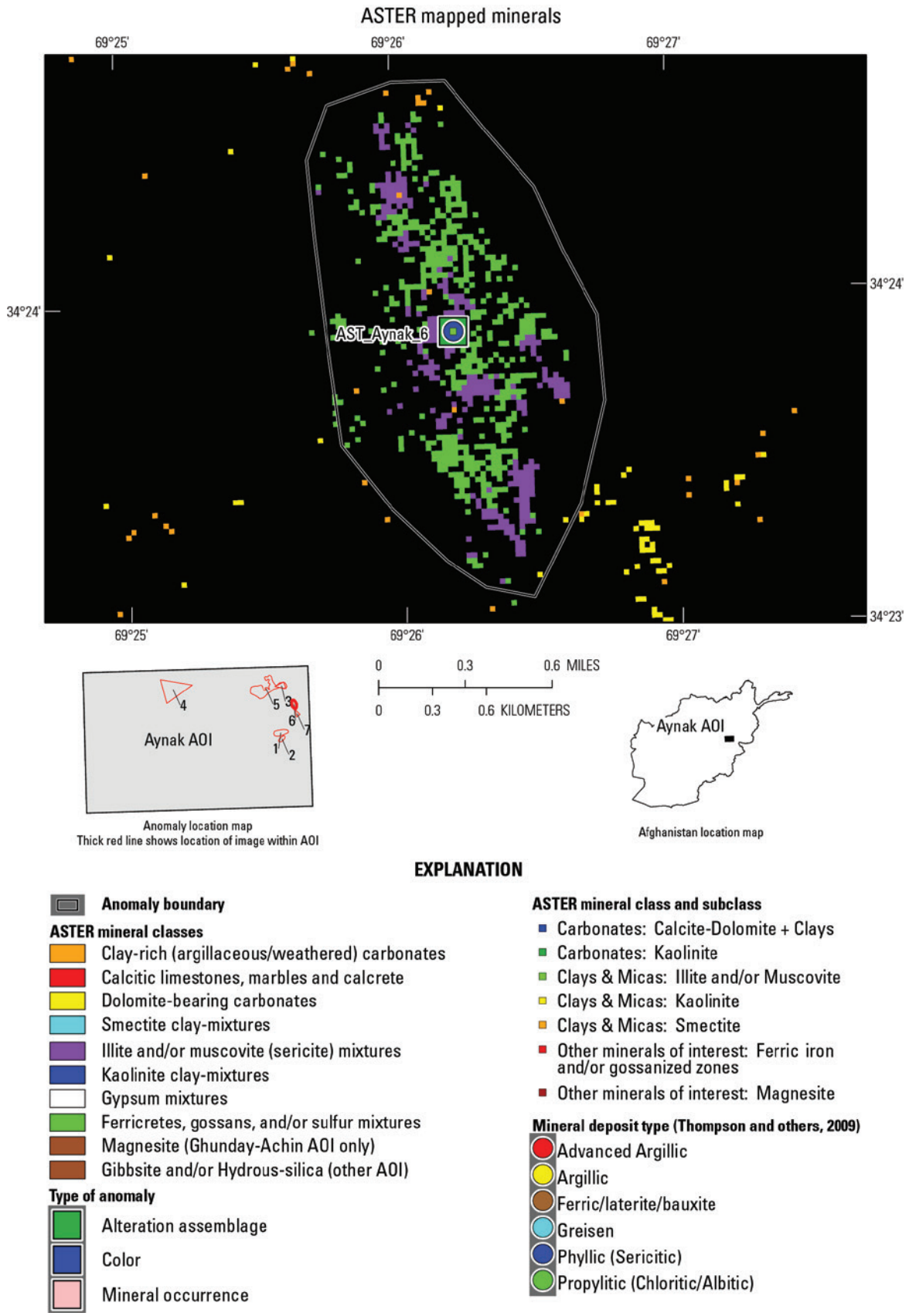

Figure 4.2.6. ASTER alteration anomaly located in the Aynak Area of Interest (AOI) in Afghanistan. Visual appearance of anomaly area shows dark rocks lacking the bleaching/iron-staining as displayed by anomalies AST_Aynak_3 and AST_Aynak_4, although mineralogy is same. Anomaly area contains mixtures of carbonates, ferric iron, illite and/or muscovite with smectite-rich cores.

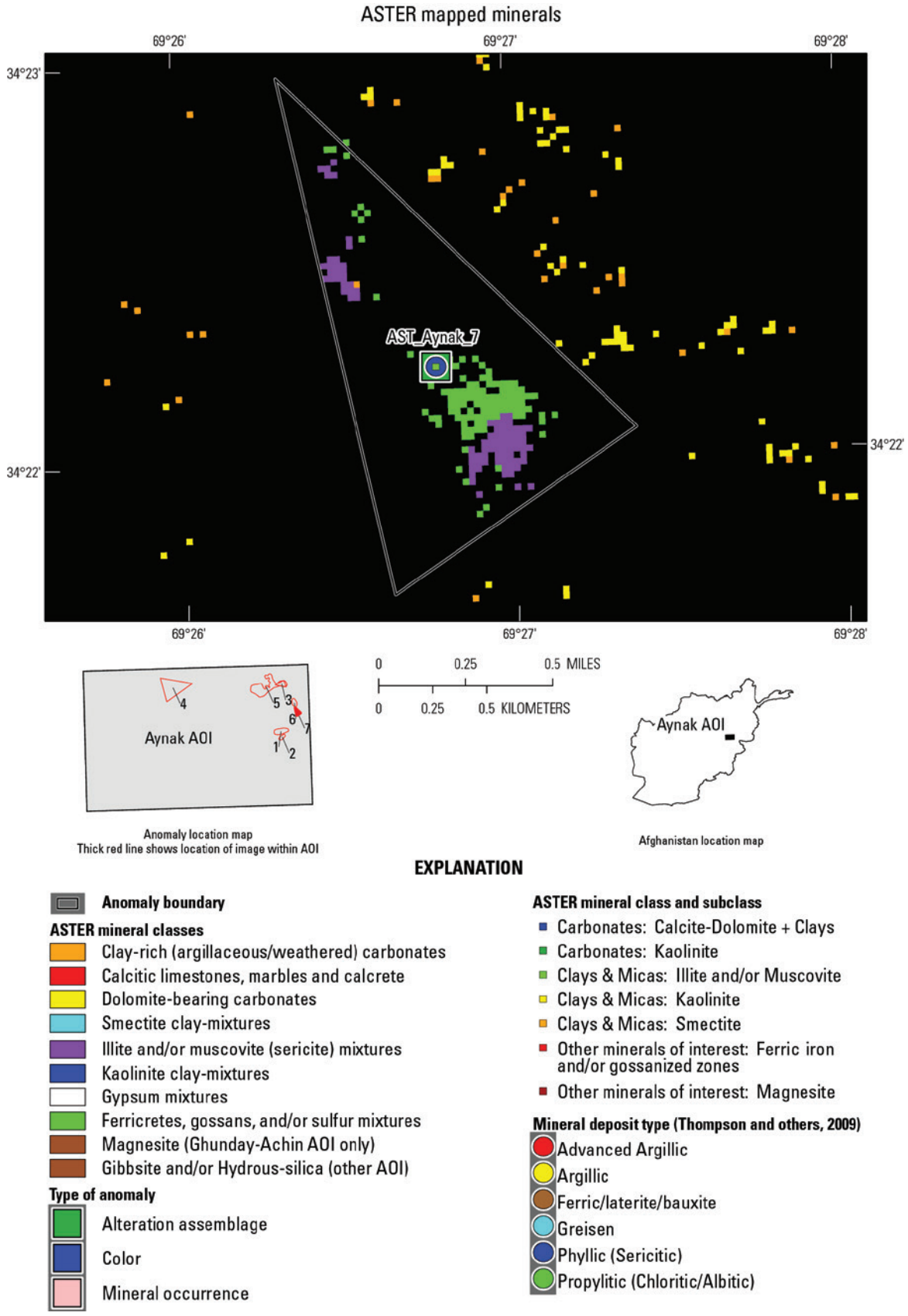

Figure 4.2.7. ASTER alteration anomaly located in the Aynak Area of Interest (AOI) in Afghanistan. Visual appearance of anomaly area shows dark rocks lacking the bleaching/iron-staining as displayed by anomalies AST_Aynak_3 and AST_Aynak_4, although mineralogy is same. Anomaly area contains mixtures of carbonates, ferric iron, illite and/or muscovite with smectite-rich cores.

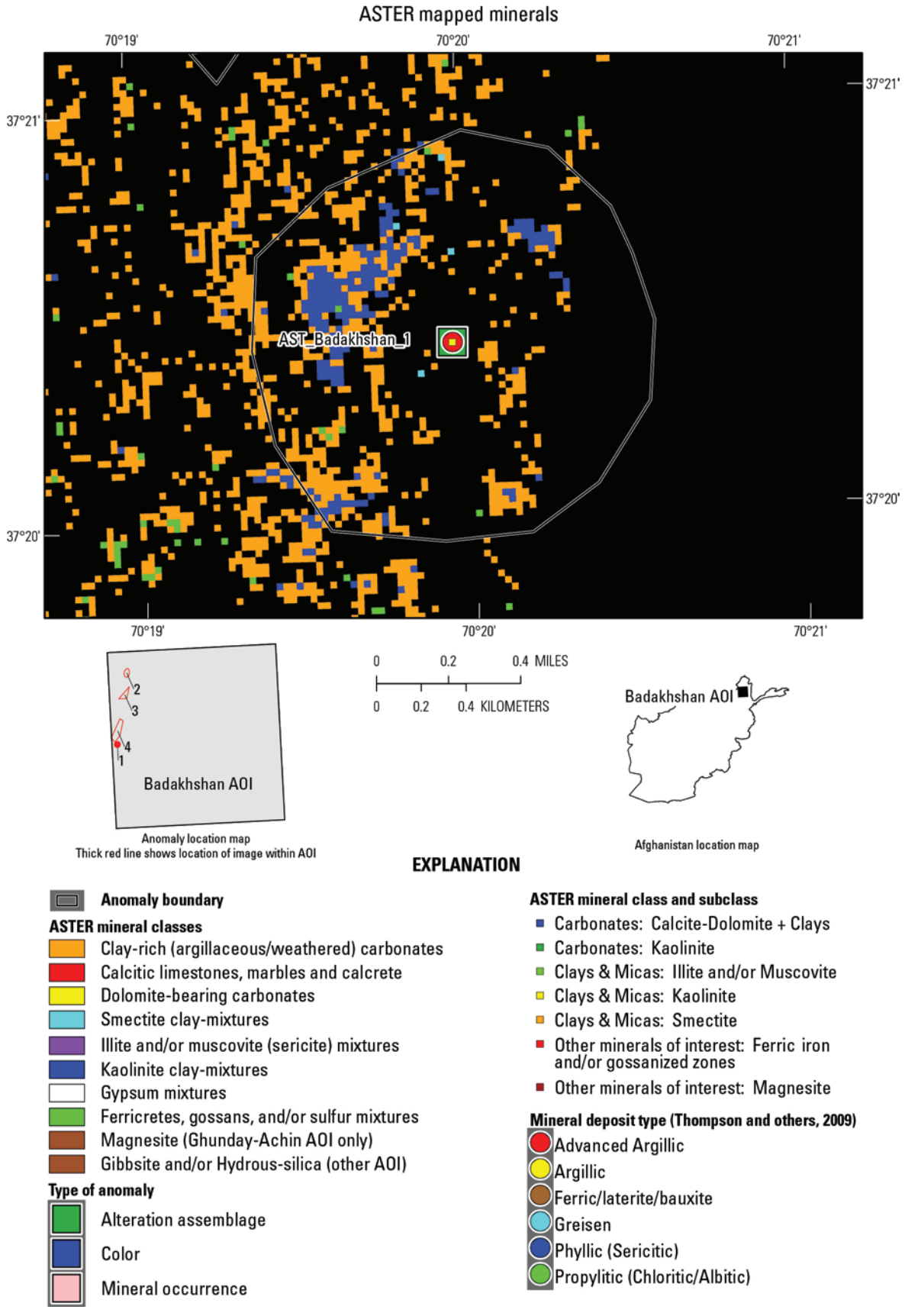

Figure 4.3.1. ASTER alteration assemblage anomaly located in the Badakhshan Area of Interest (AOI) in Afghanistan. Kaolinite-, calcrete- and ferricrete-bearing area that may be related either to an "in place" sulfide lode deposit or to sulfide weathering within "paleo" placer Au deposits.

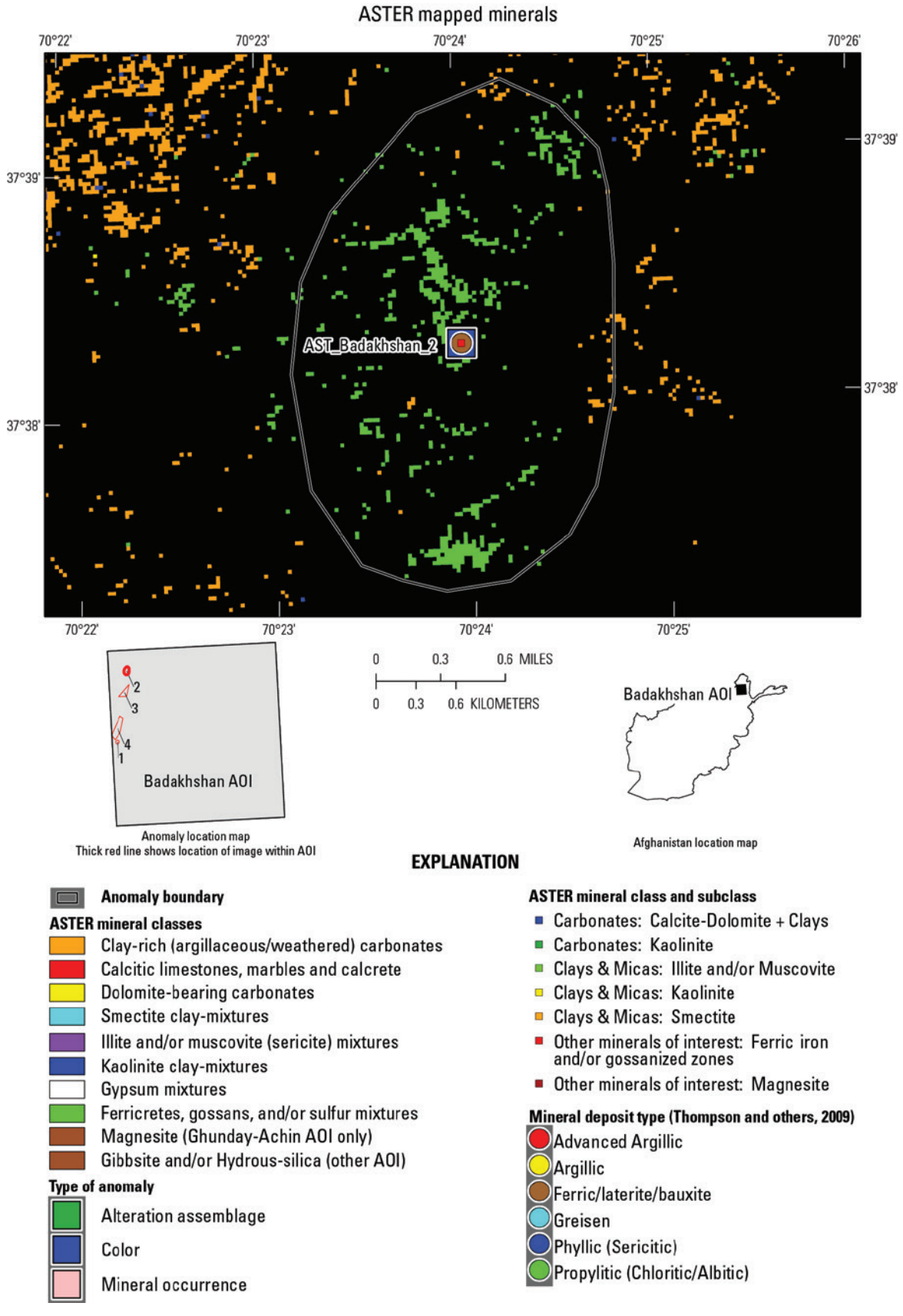

Figure 4.3.2. ASTER color anomaly located in the Badakhshan Area of Interest (AOI) in Afghanistan based on presence of Carboniferous age mafic volcanic rocks with unusual bright red color in ASTER RGB=631 and mapping high in ferric iron abundance (volcanic-hosted massive sulfide potential, though additional mapping of possible chlorite/epidote needed).

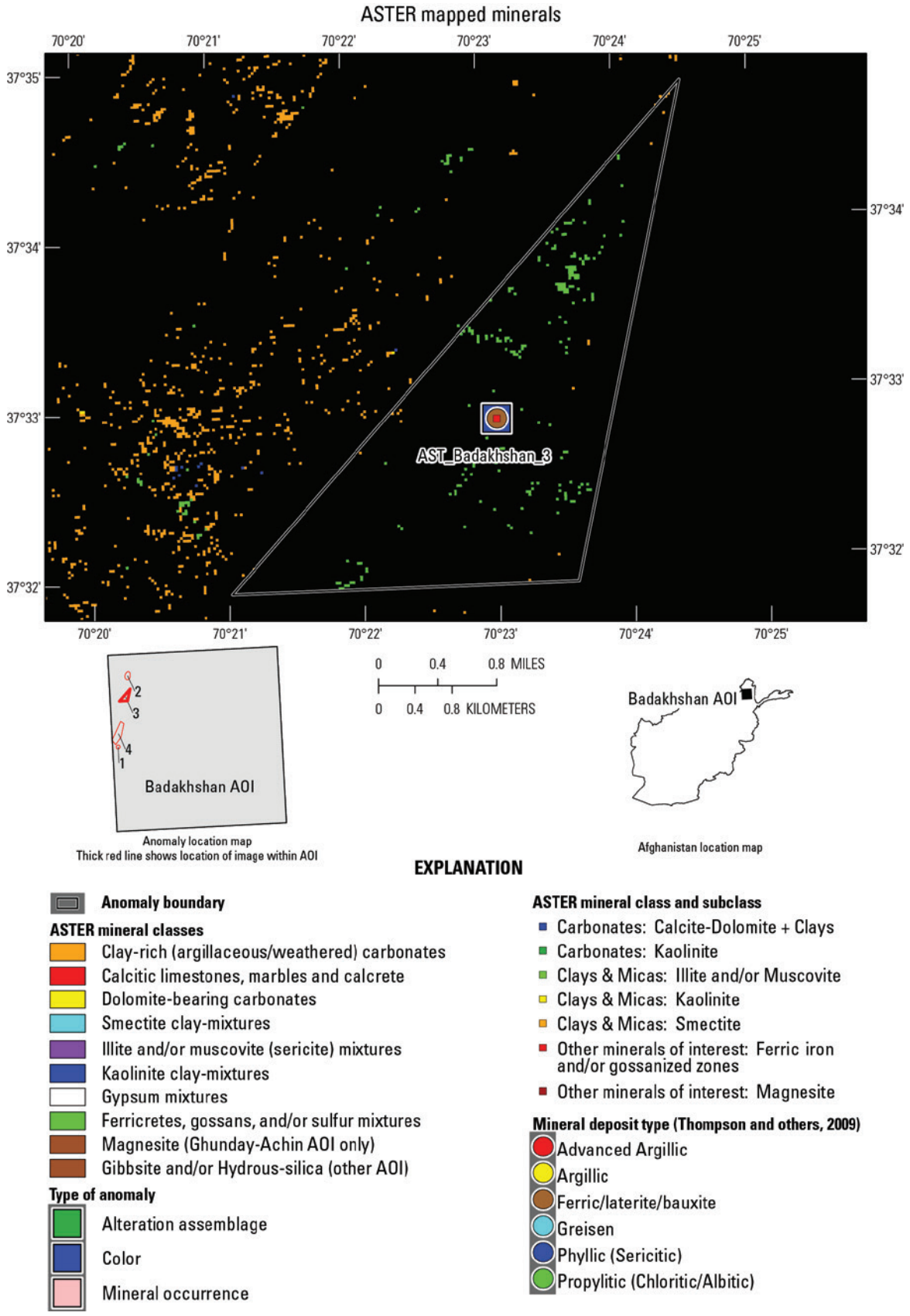

Figure 4.3.3. ASTER color anomaly located in the Badakhshan Area of Interest (AOI) in Afghanistan. Carboniferous age mafic volcanic rocks with unusual dark-red color in ASTER RGB=631 and mapped as being high in ferric iron abundance (volcanic-hosted massive sulfide potential, though additional mapping of possible chlorite/epidote needed).

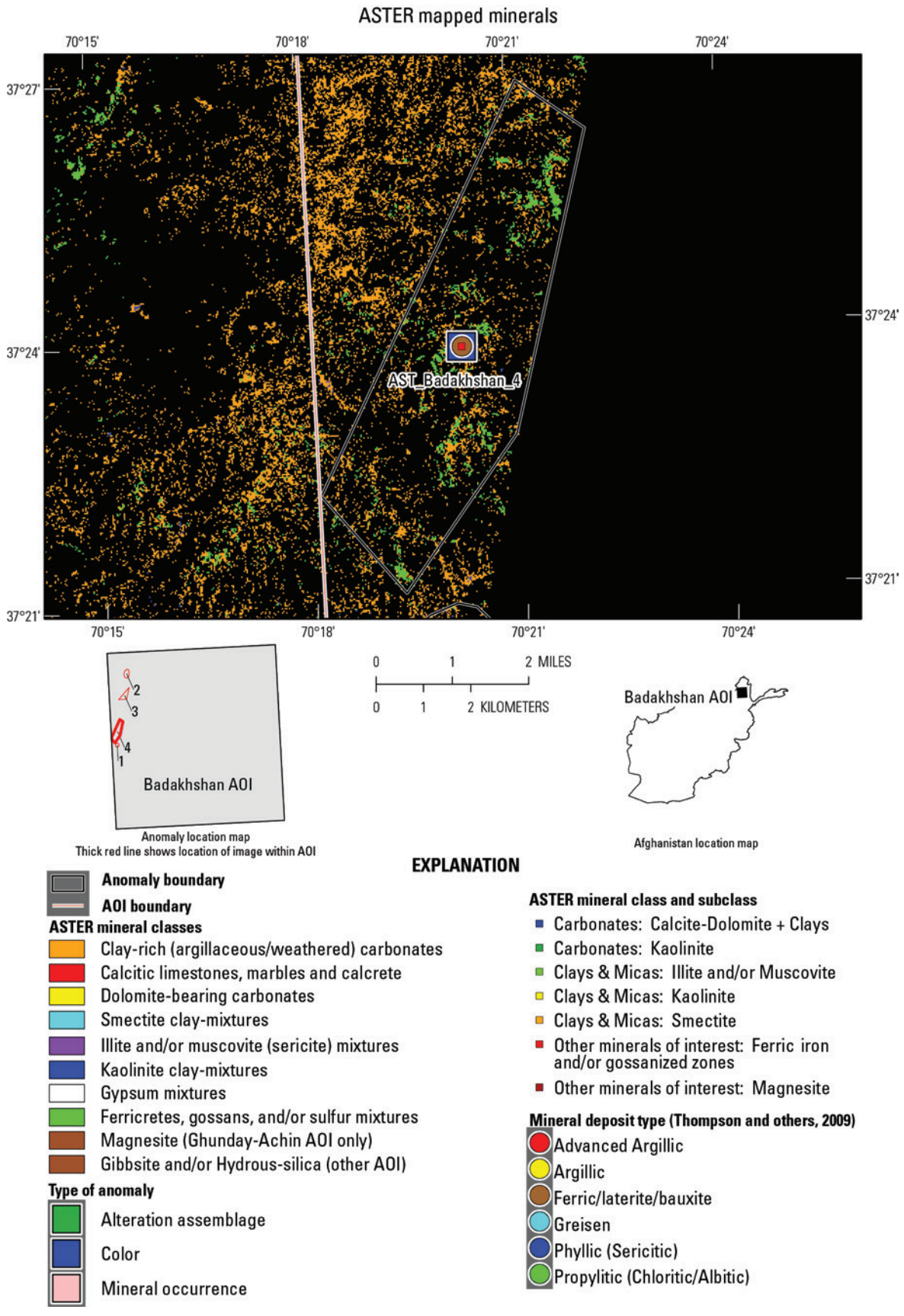

Figure 4.3.4. ASTER color anomaly located in the Badakhshan Area of Interest (AOI) in Afghanistan. Possible ferricrete-cemented surficial deposits related to placer sulfide weathering and spatially correlated with Au stream geochemistry anomaly.

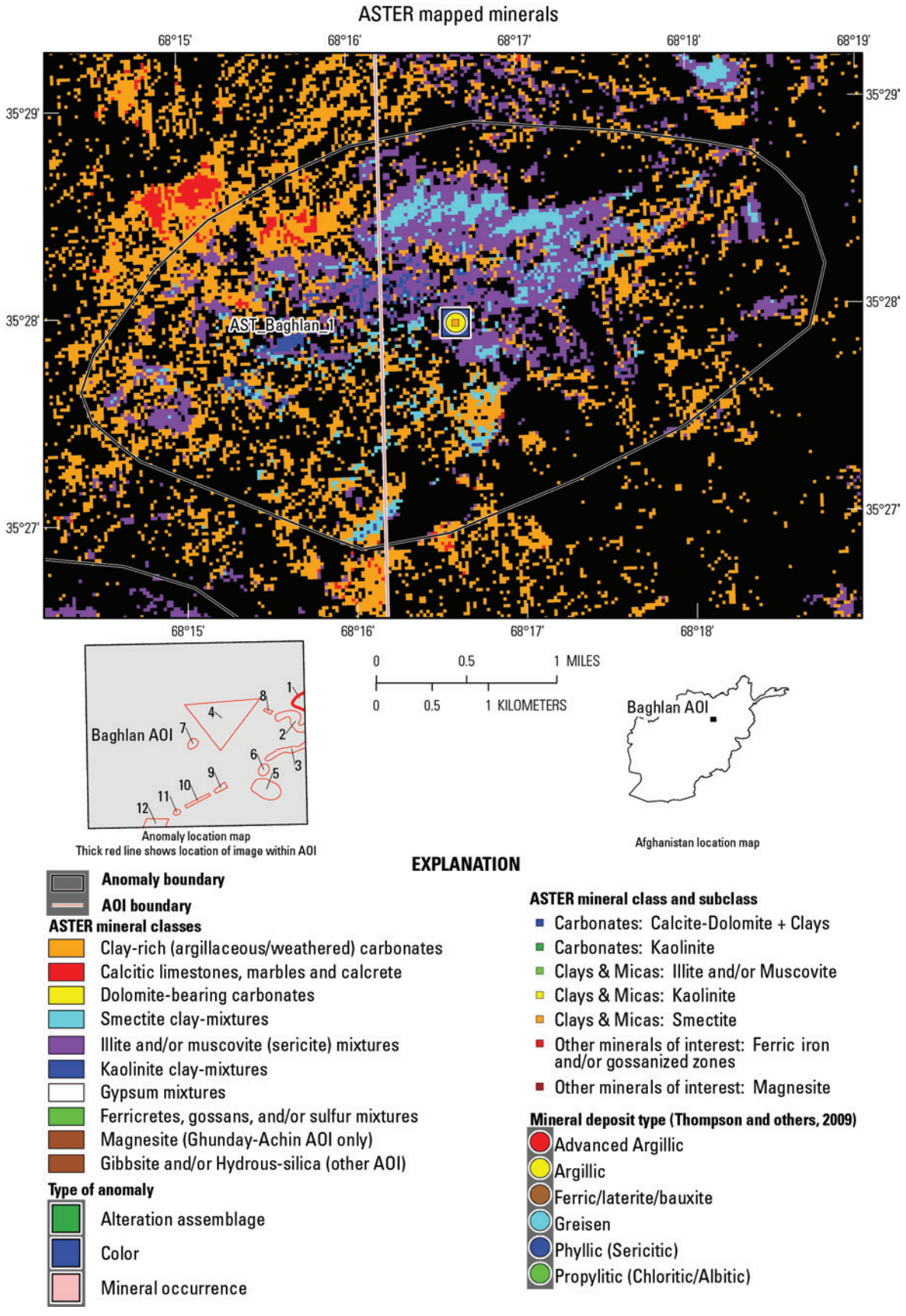

Figure 4.4.1. ASTER color anomaly located in the Baghlan Area of Interest (AOI) in Afghanistan. Montmorillonite-dominated areas appear as bleached areas within darker rocks.

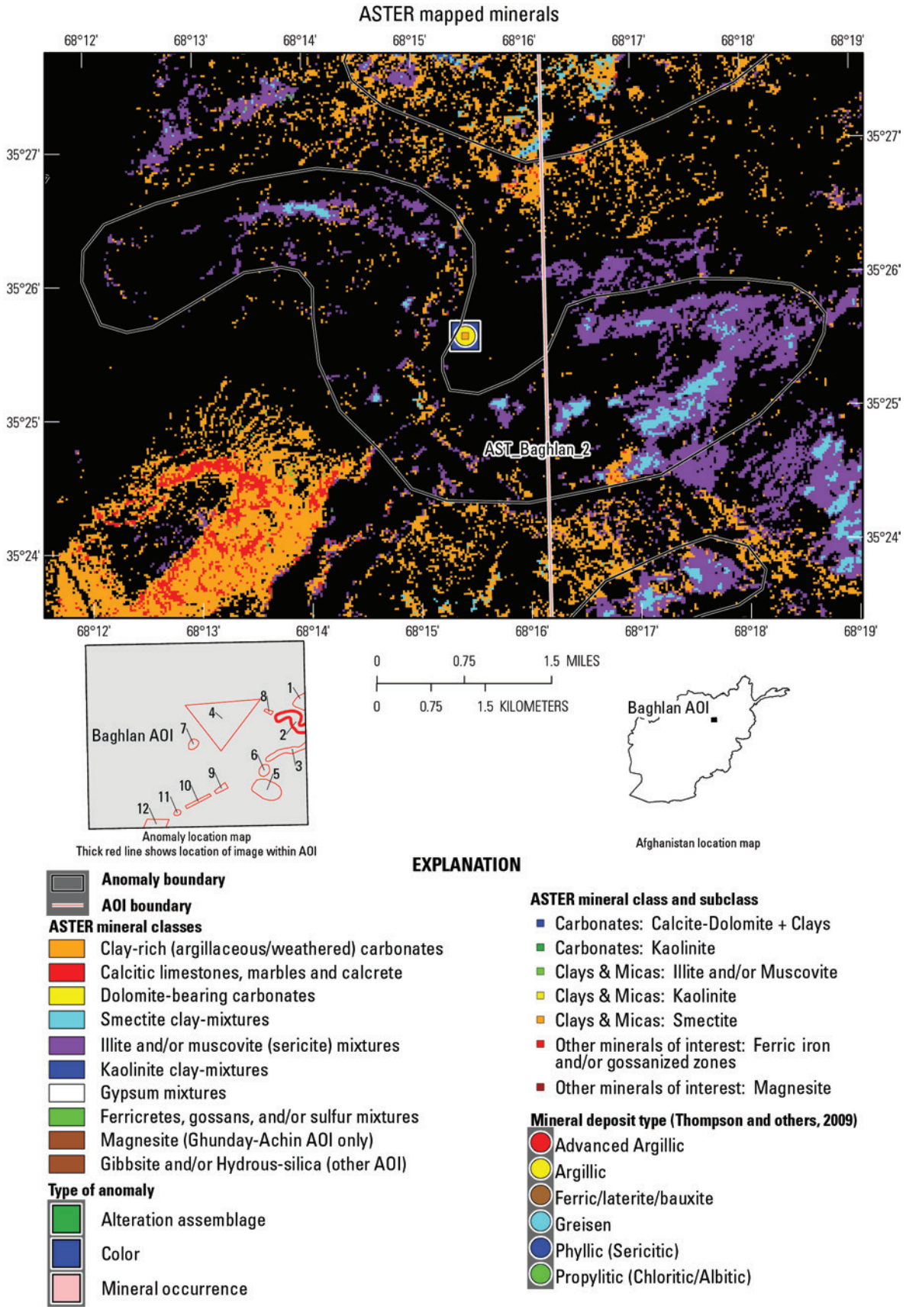

Figure 4.4.2. ASTER color anomaly located in the Baghlan Area of Interest (AOI) in Afghanistan. Montmorillonite-dominated areas appear as bleached areas within darker tightly folded rocks.

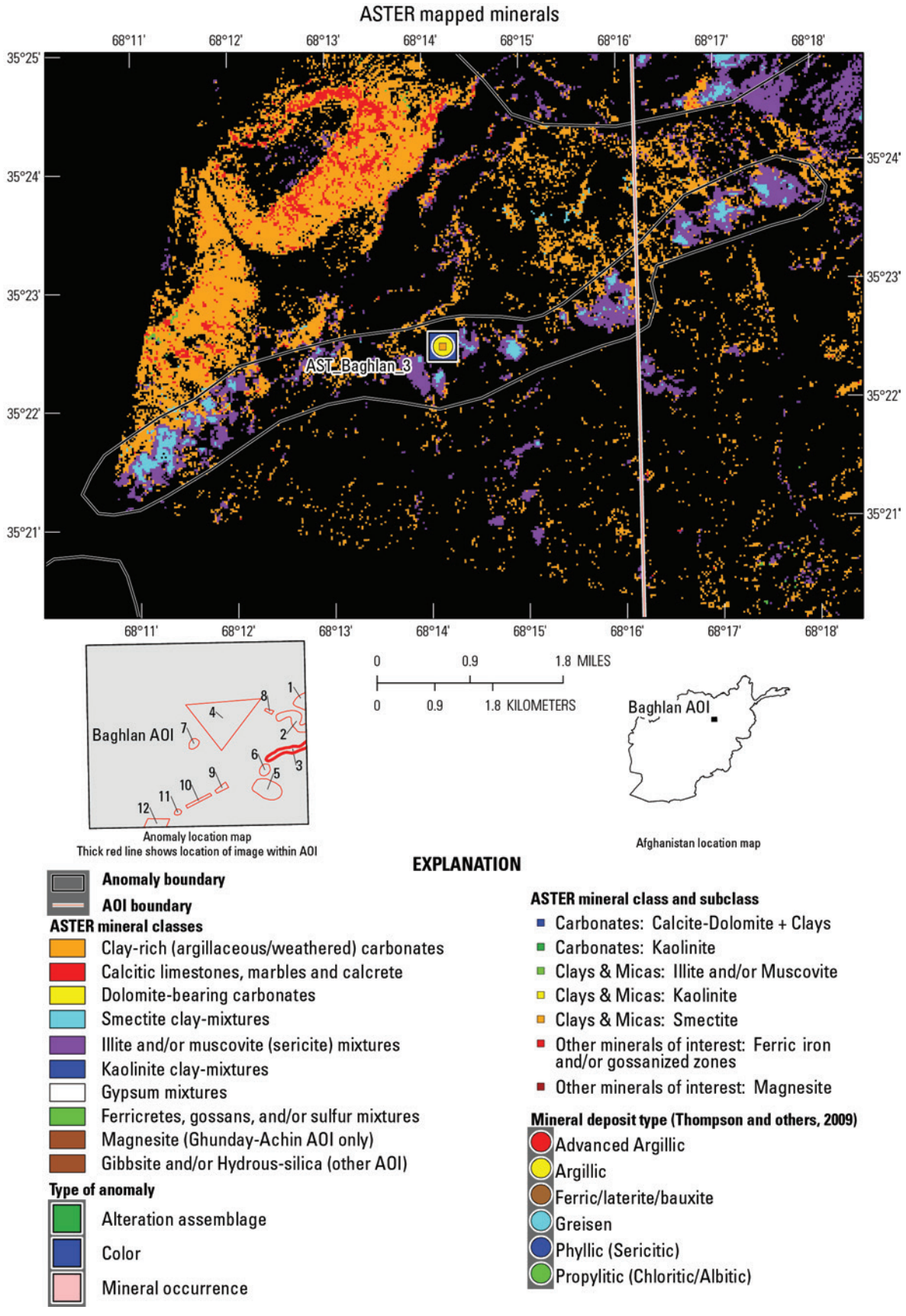

Figure 4.4.3. ASTER color anomaly located in the Baghlan Area of Interest (AOI) in Afghanistan. Montmorillonite-dominated areas appear as bleached areas within darker fault-controlled rocks.

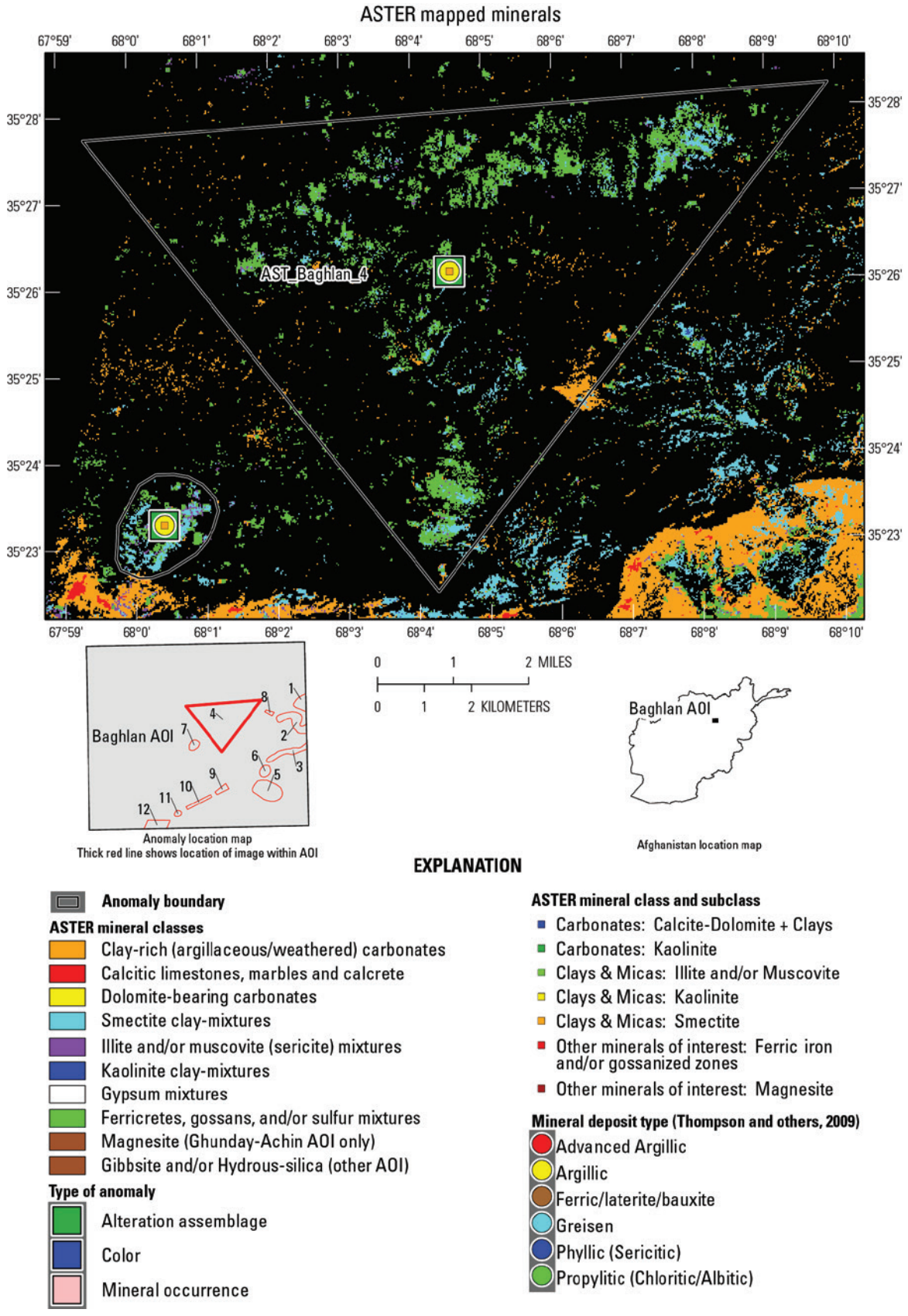

Figure 4.4.4. ASTER alteration anomaly located in the Baghlan Area of Interest (AOI) in Afghanistan. Contains a mixture of smectite and ferric iron gossans associated with Late Triassic intrusive rocks, primarily granodiorite (Doebrich and Wahl, 2006), and is upstream source of a lead and copper stream-geochemistry anomaly.

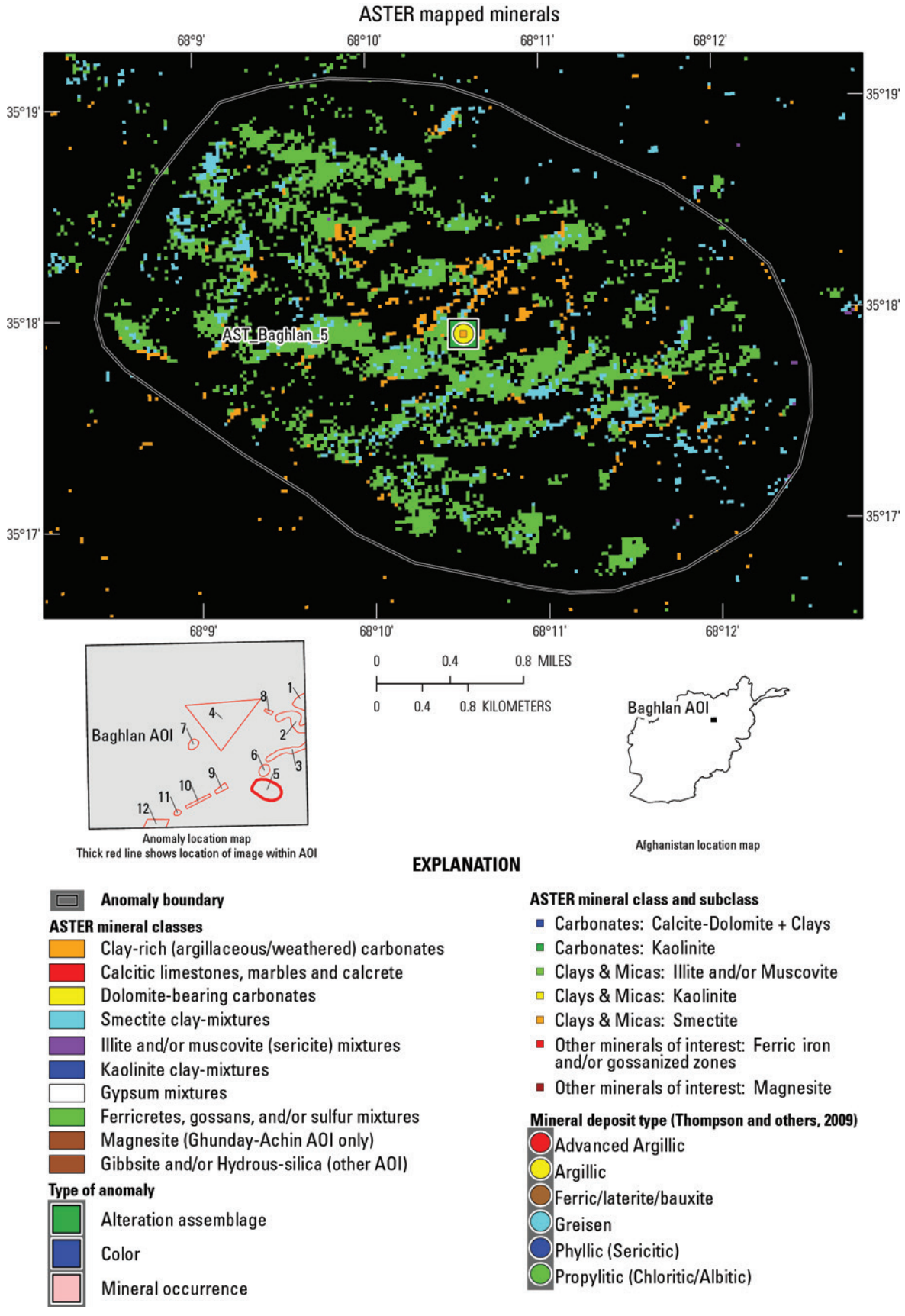

Figure 4.4.5. ASTER alteration anomaly located in the Baghlan Area of Interest (AOI) in Afghanistan. Contains a mixture of smectite and ferric iron gossans associated with Late Triassic intrusive rocks, primarily granodiorite (Doebrich and Wahl, 2006), and is co-extensive with a mercury stream-geochemistry anomaly.

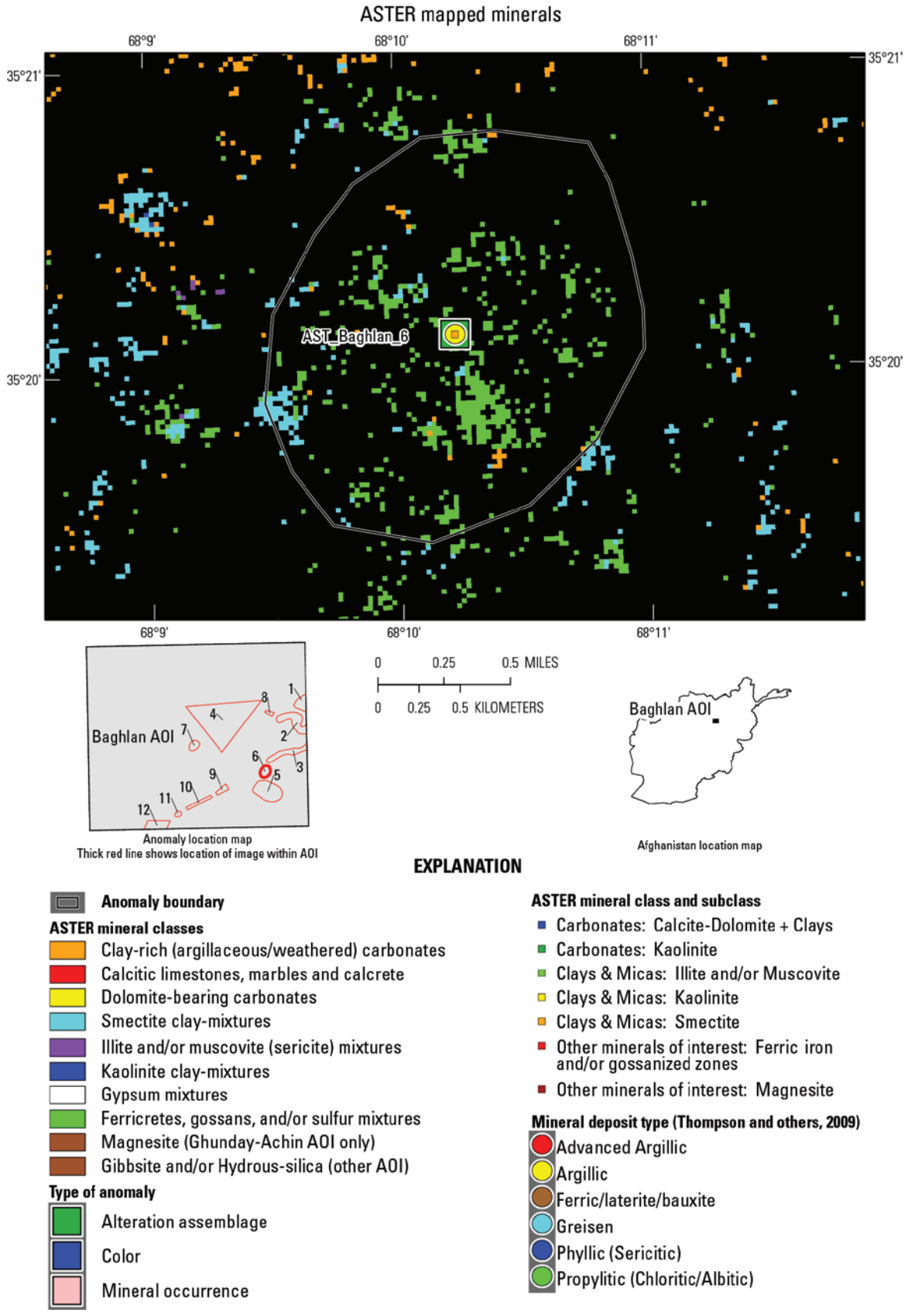

Figure 4.4.6. ASTER alteration anomaly located in the Baghlan Area of Interest (AOI) in Afghanistan in latest Triassic (Rhaetian) age volcanic rocks dominated by smectite and/or strong ferric iron alteration (potentially volcanic-hosted massive sulfides) near an unnamed polymetallic vein occurrence (Orris and Bliss, 2002).

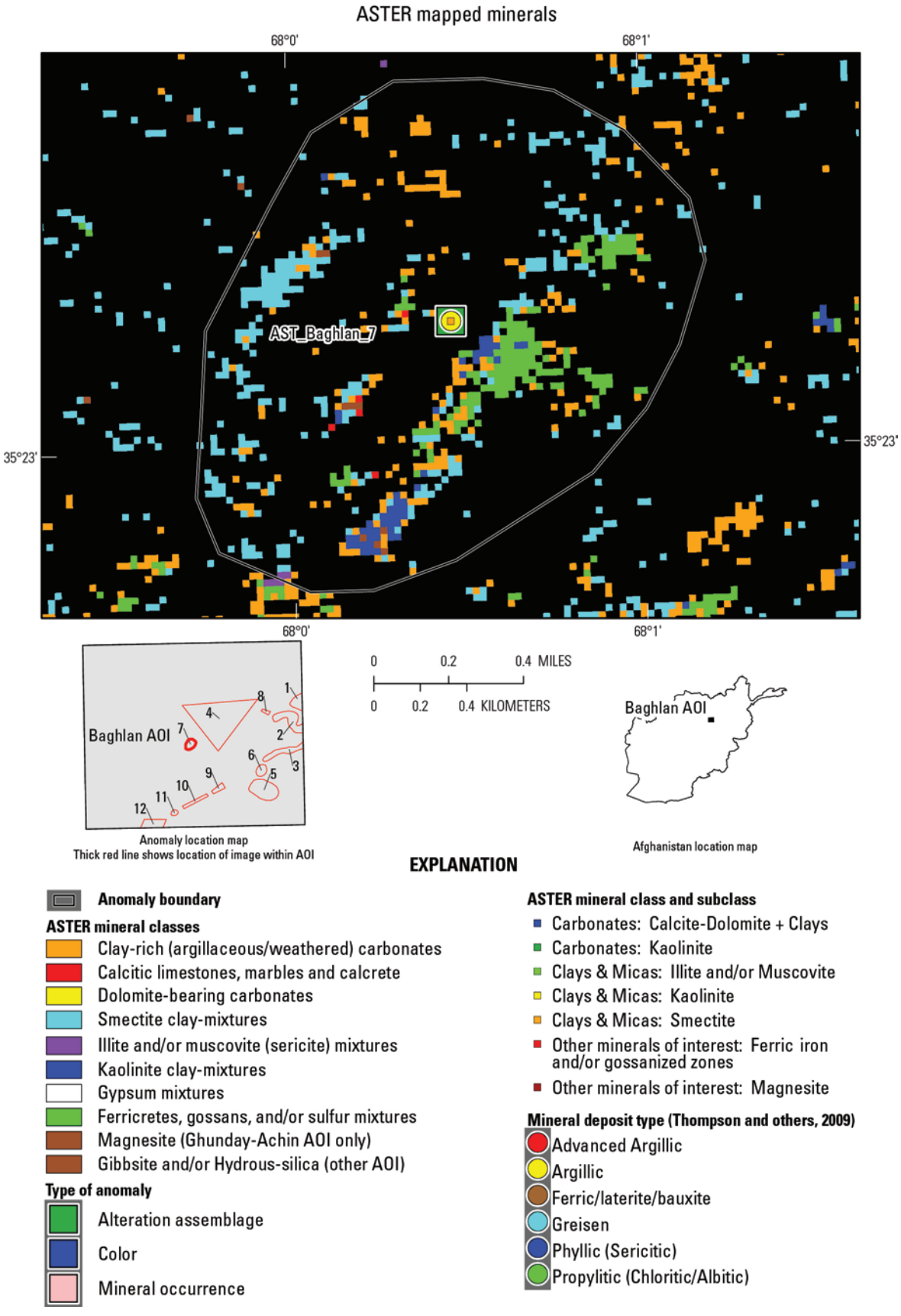

Figure 4.4.7. ASTER alteration anomaly located in the Baghlan Area of Interest (AOI) in Afghanistan in latest Triassic (Rhaetian) age volcanic rocks dominated by smectite and/or strong ferric iron alteration (potentially volcanic-hosted massive sulfides).

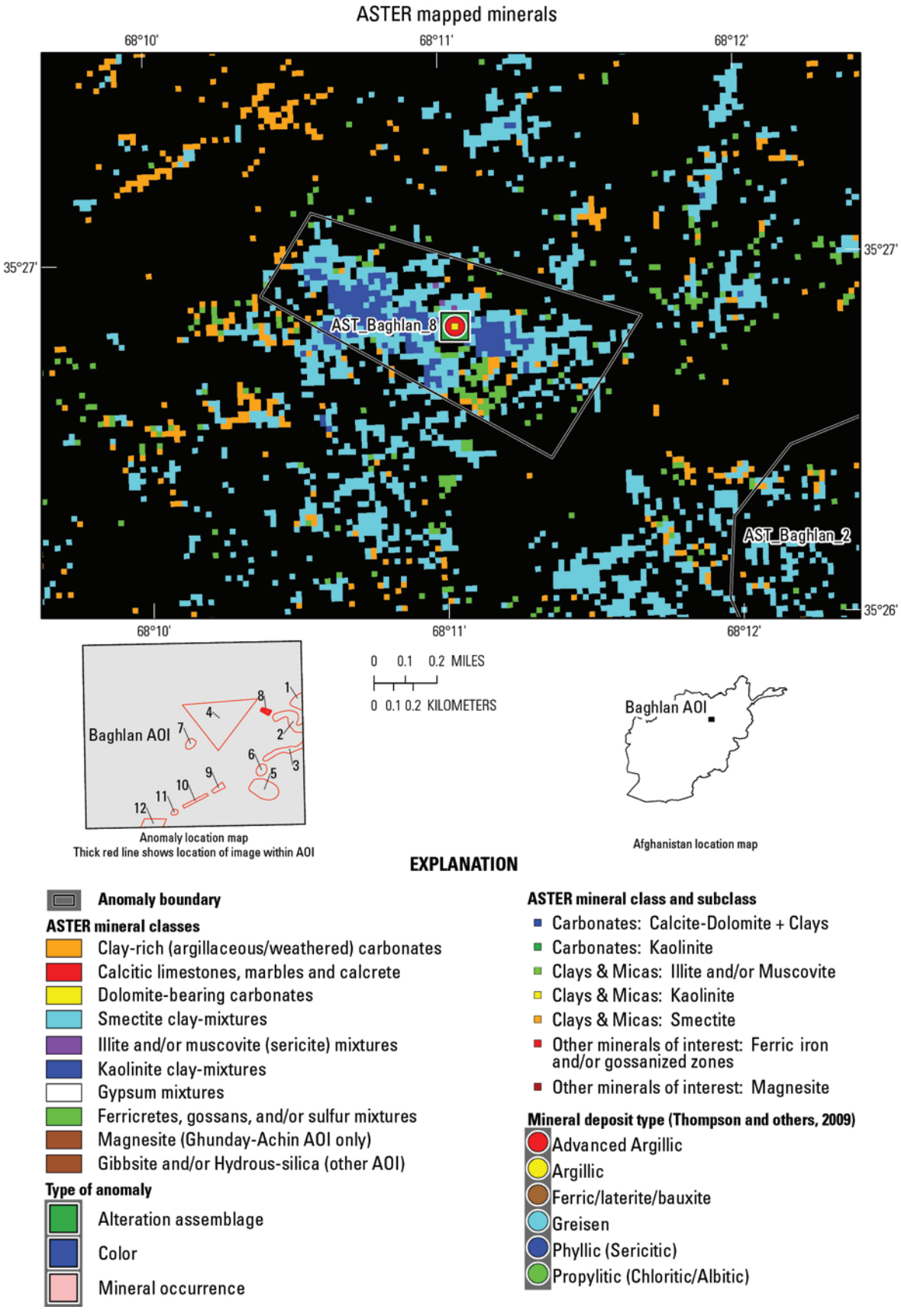

Figure 4.4.8. ASTER alteration anomaly located in the Baghlan Area of Interest (AOI) in Afghanistan. Kaolinite-bearing possible continuation of anomaly, AST_Baghlan_2, with mineral areas appearing as bleached areas within darker tightly folded rocks.

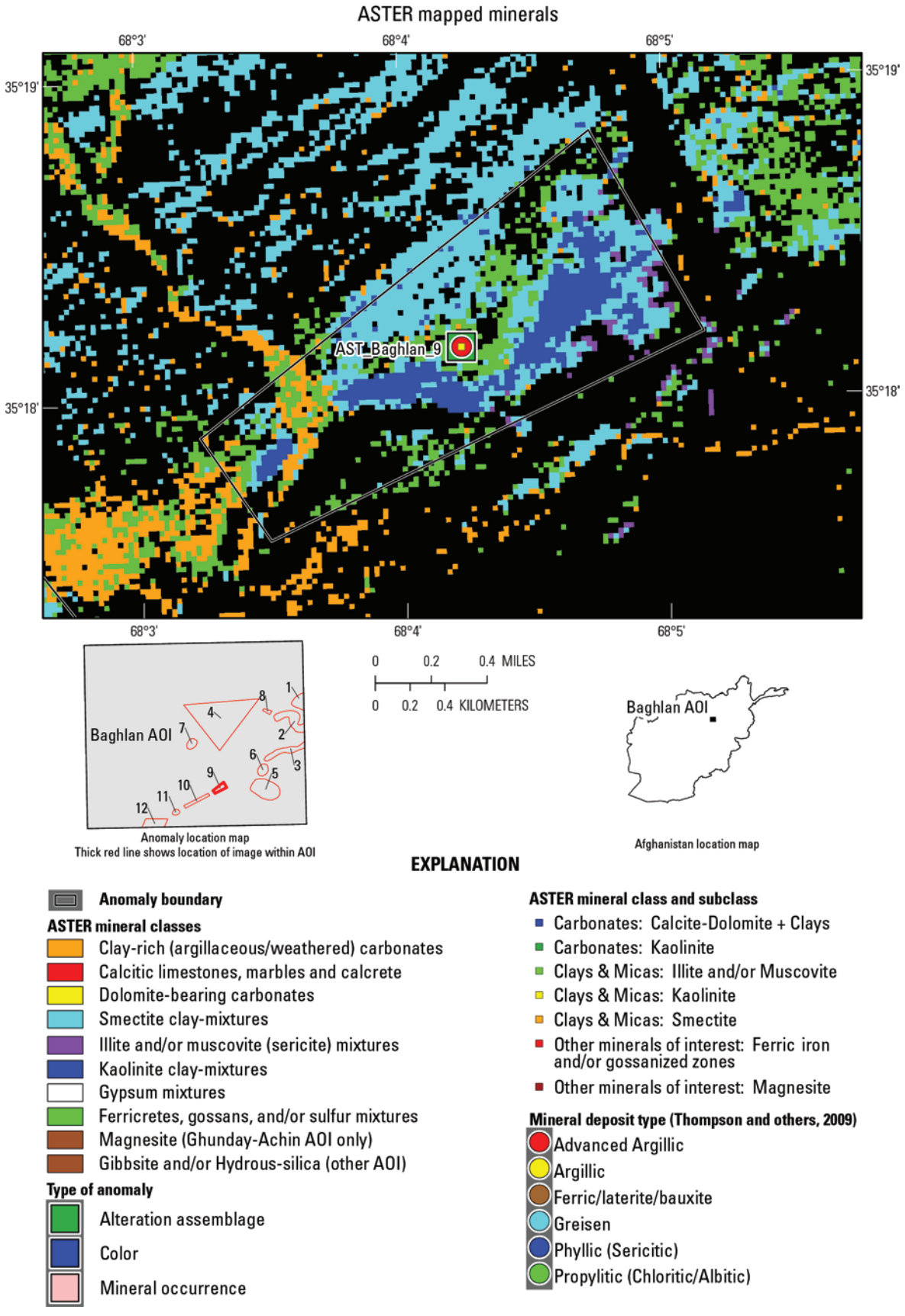

Figure 4.4.9. ASTER alteration anomaly located in the Baghlan Area of Interest (AOI) in Afghanistan. Kaolinite-dominated area with numerous nearby associated mineral occurrences (Orris and Bliss, 2002). The origin of the kaolinite may be hydrothermally altered rhyolitic-tuff deposits.

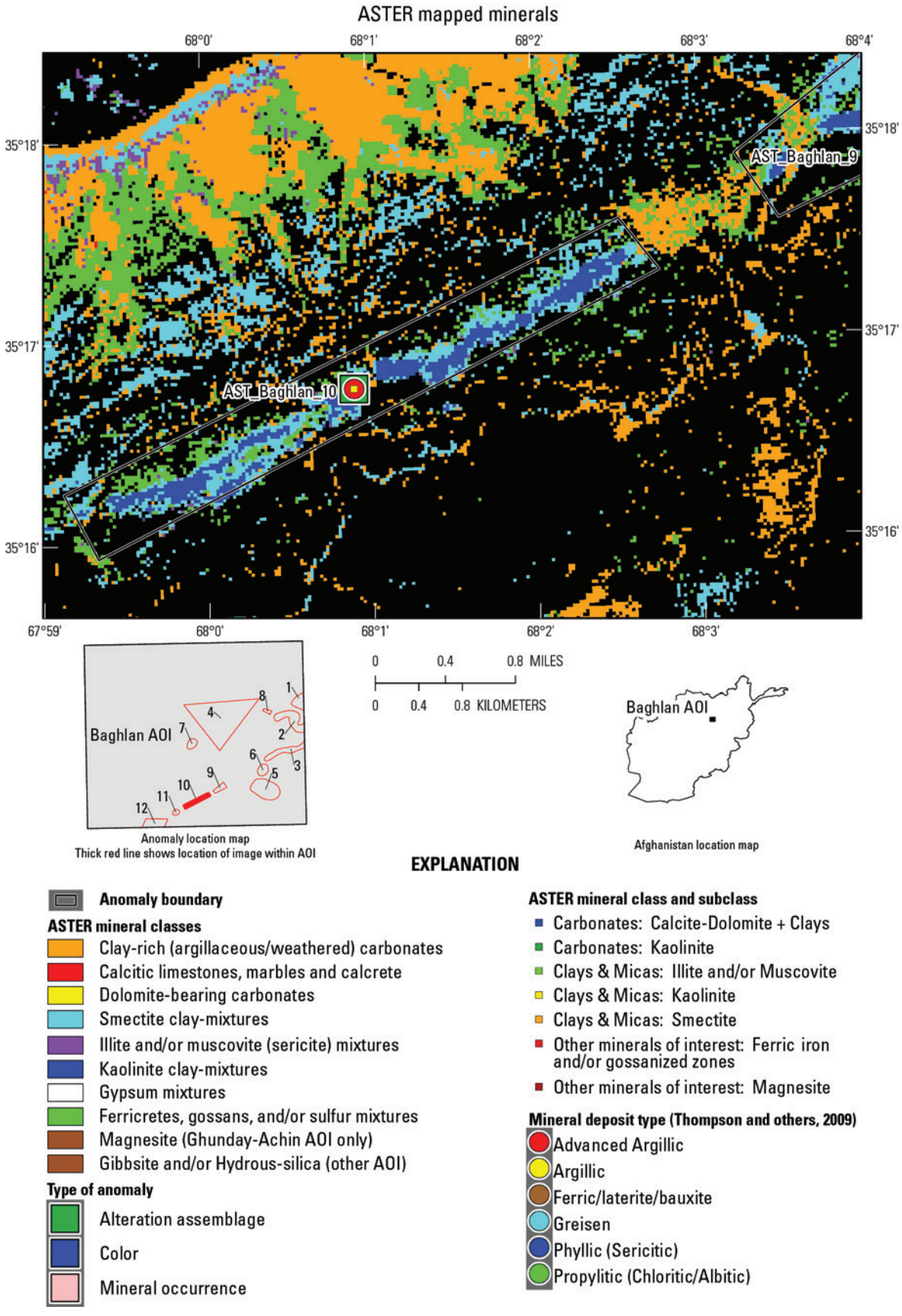

Figure 4.4.10. ASTER alteration anomaly located in the Baghlan Area of Interest (AOI) in Afghanistan. Kaolinite-dominated area that appears to be westward continuation of anomaly, AST_Baghlan_9. The origin of the kaolinite may be hydrothermally altered rhyolitic-tuff deposits.

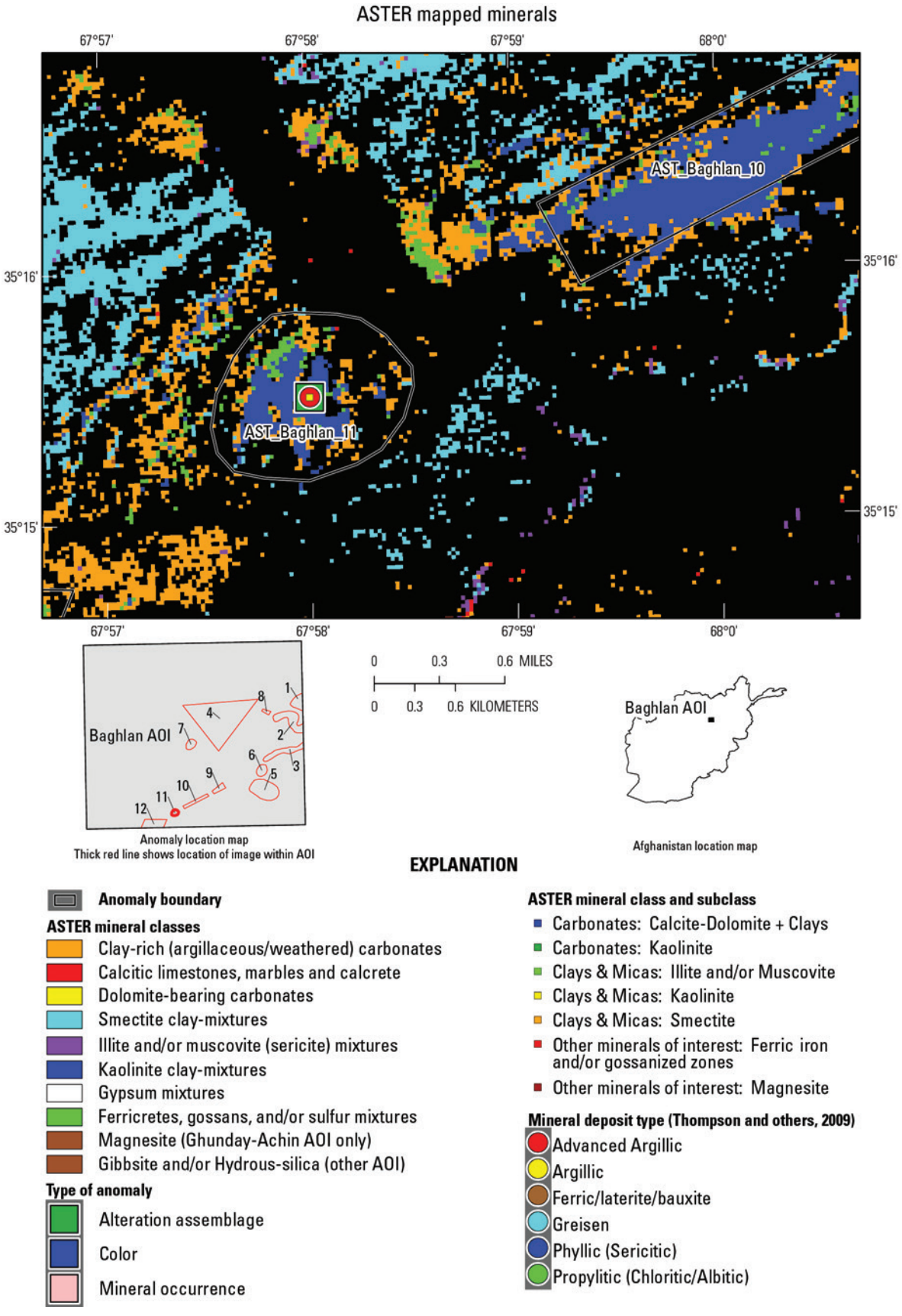

Figure 4.4.11. ASTER alteration anomaly located in the Baghlan Area of Interest (AOI) in Afghanistan. Kaolinite-dominated area that appears to be westward continuation of the anomalies, AST_Baghlan_9 and AST_Baghlan_10. The origin of the kaolinite may be hydrothermally altered rhyolitic-tuff deposits.

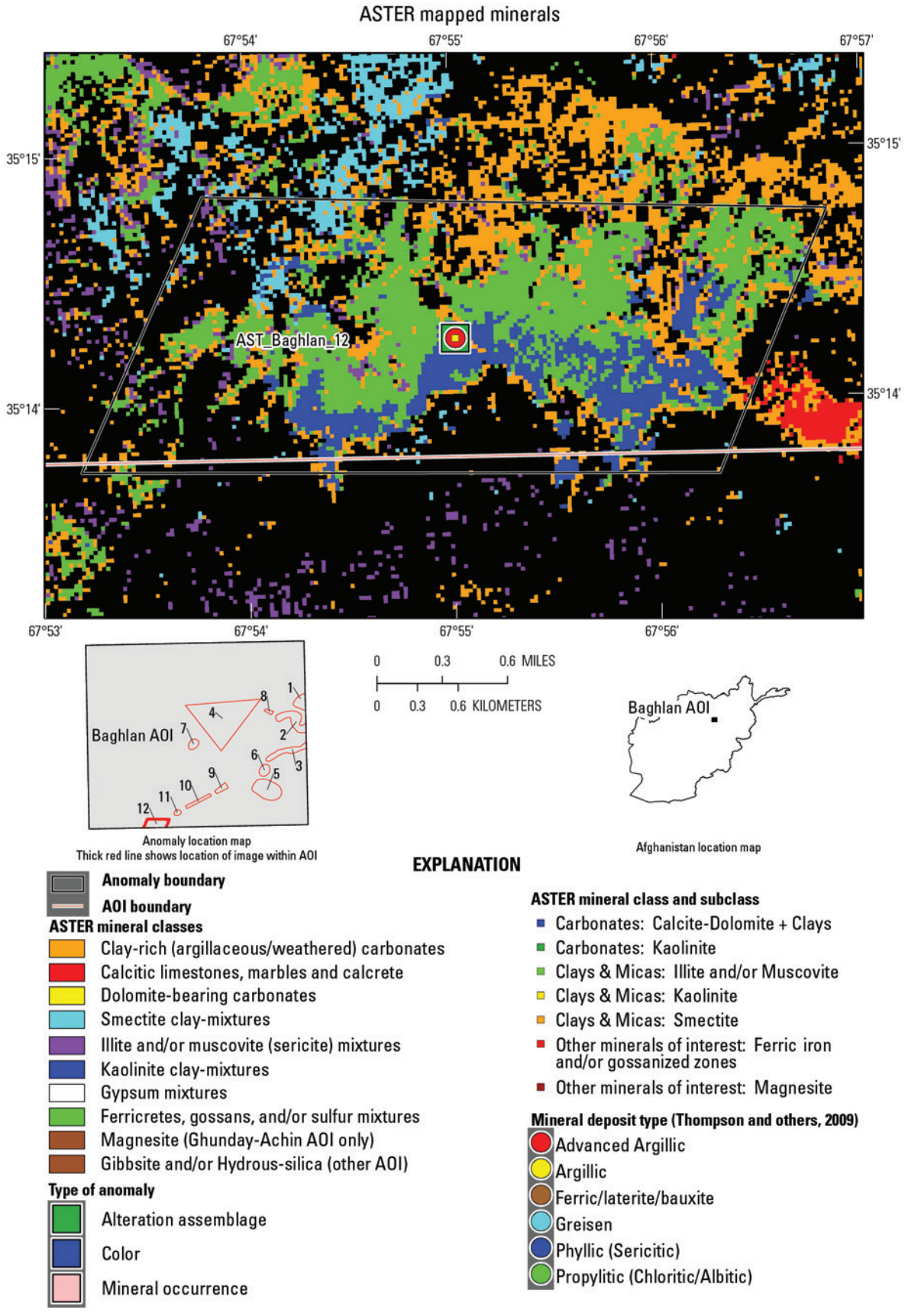

Figure 4.4.12. ASTER alteration anomaly located in the Baghlan Area of Interest (AOI) in Afghanistan. Kaolinite-dominated area that displays an iron-staining coloration, which is mapped in green as a ferric iron abundant zone.

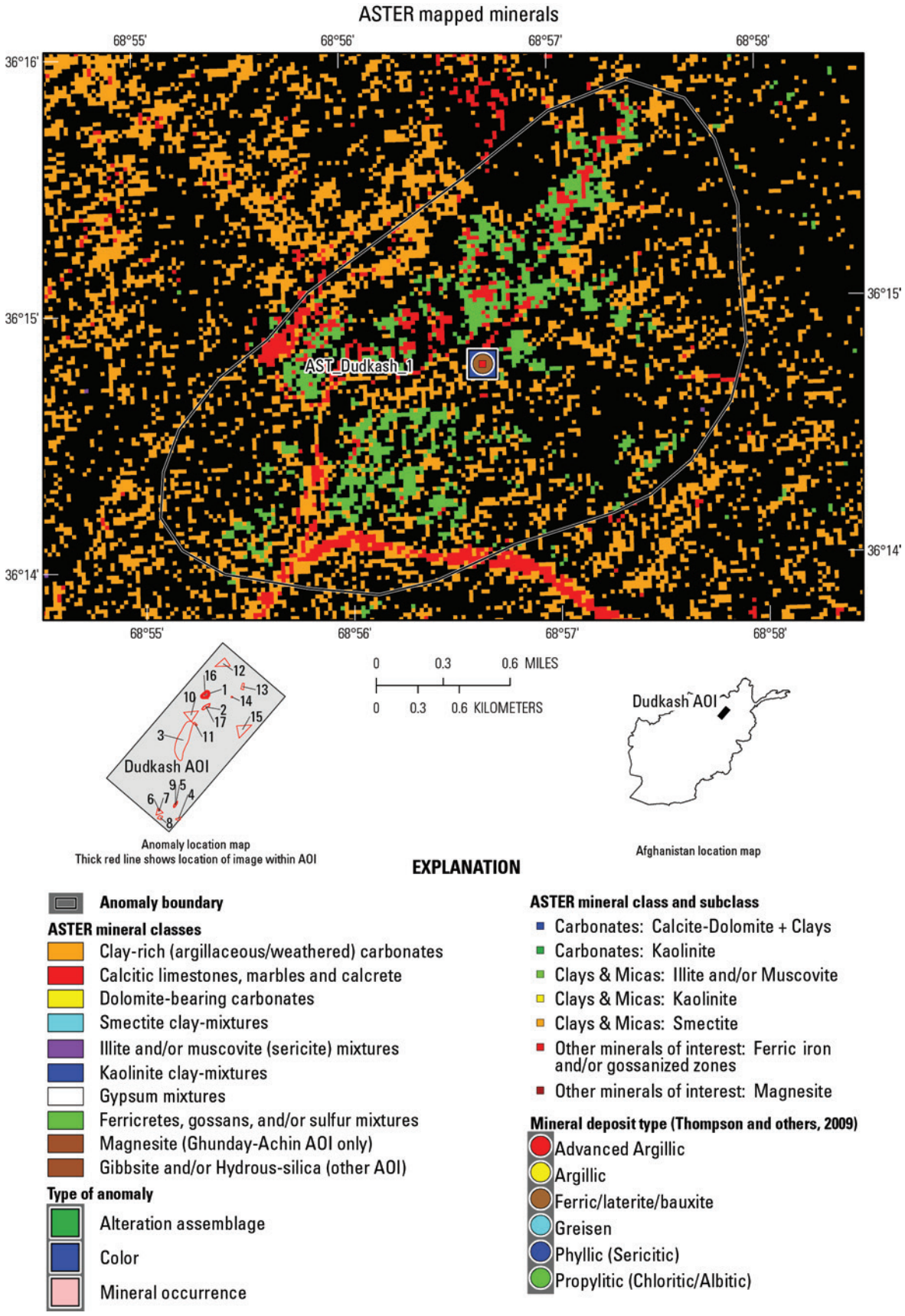

Figure 4.5.1. ASTER color anomaly located in the Dudkash Area of Interest (AOI) in Afghanistan. Anomaly is a possible sulfur- and/or phosphate-bearing area. Further spectral analysis is needed to distinguish sulfur from strong ferric iron.

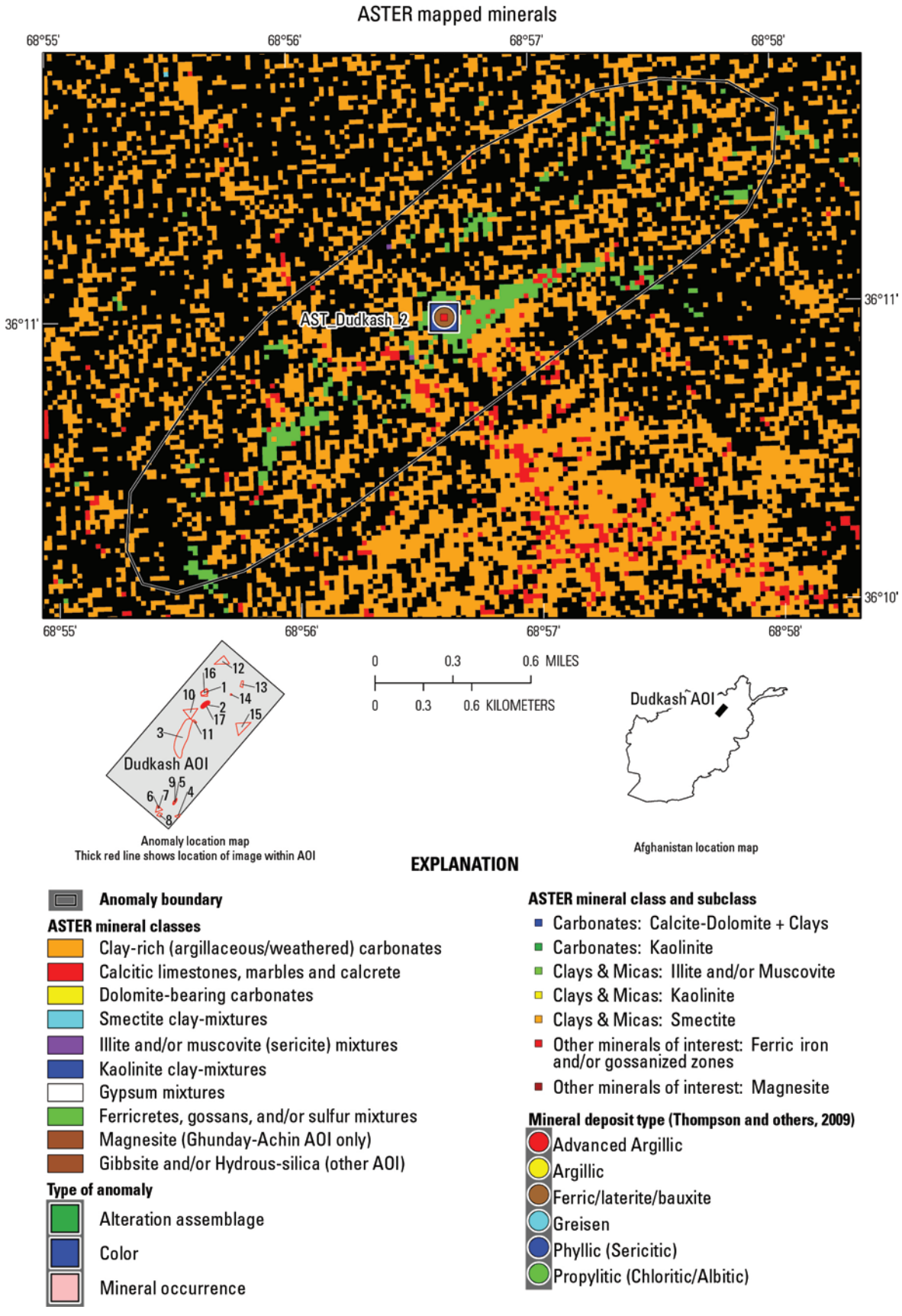

Figure 4.5.2. ASTER color anomaly located in the Dudkash Area of Interest (AOI) in Afghanistan. Anomaly is a possible sulfur- and/or phosphate-bearing area. Further spectral analysis is needed to distinguish sulfur from strong ferric iron.

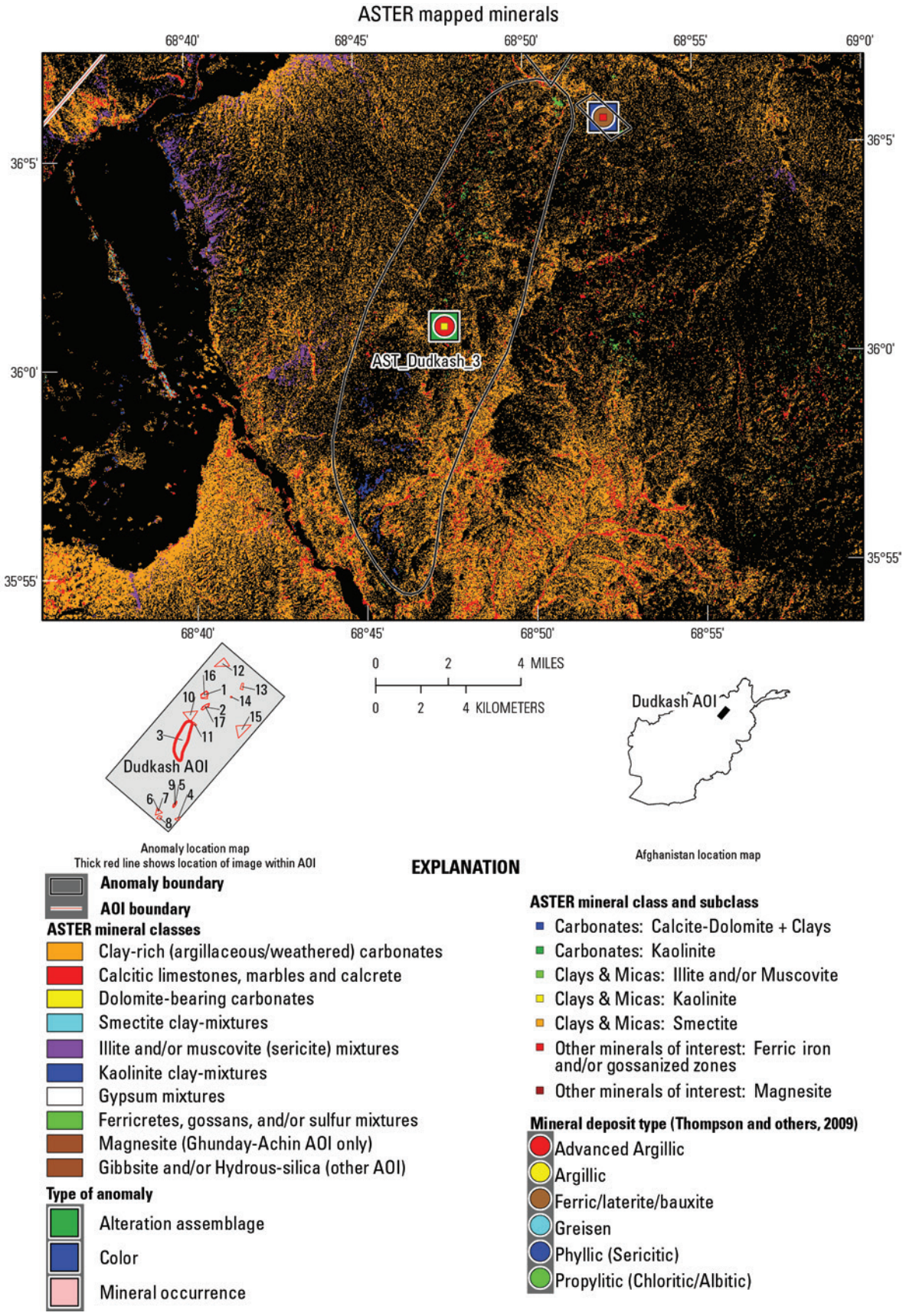

Figure 4.5.3. ASTER alteration anomaly located in the Dudkash Area of Interest (AOI) in Afghanistan. Anomaly has kaolinite zones associated with lead and copper stream-geochemistry anomaly, which is either coal or mineral-alteration related.

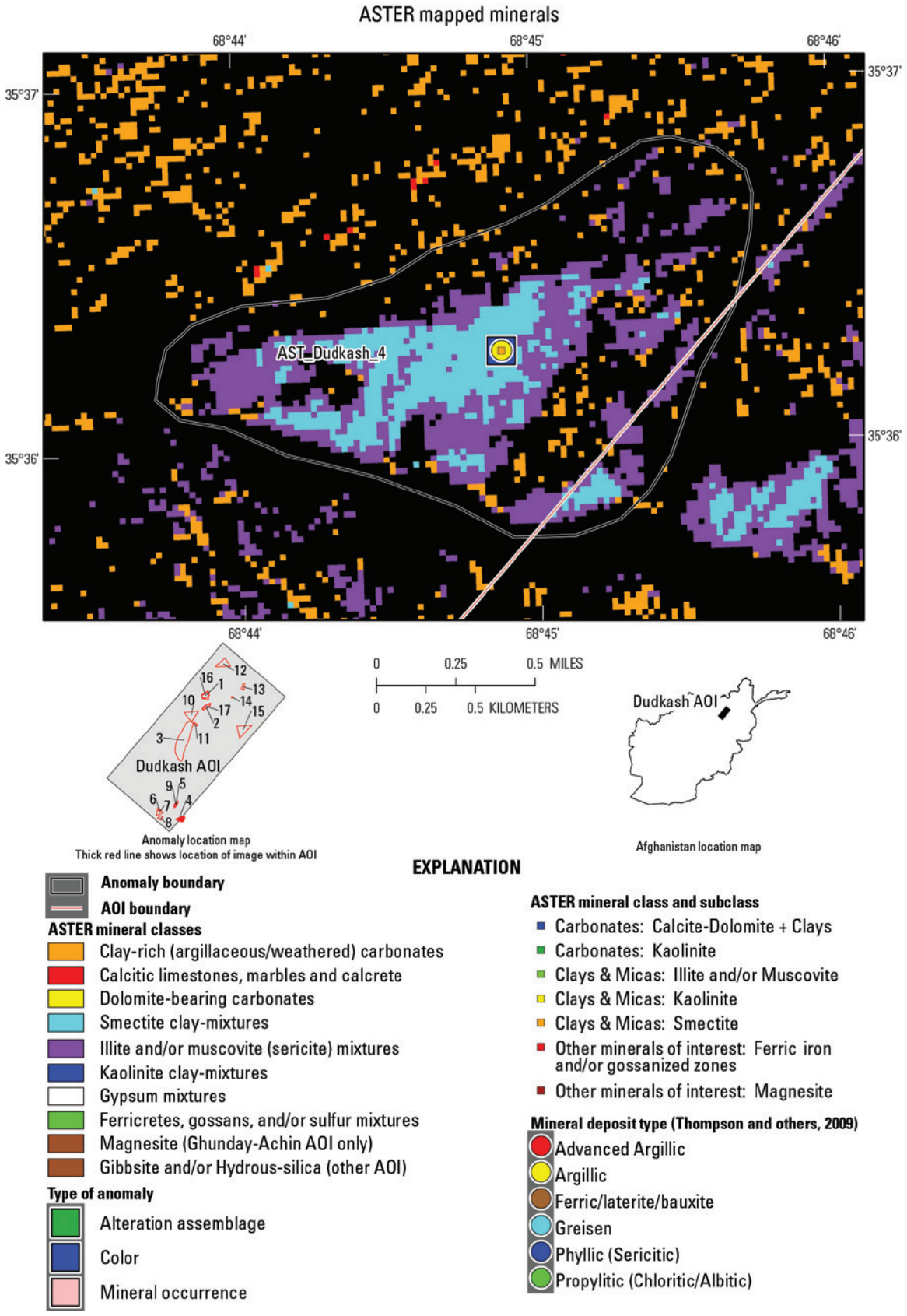

Figure 4.5.4. ASTER color anomaly located in the Dudkash Area of Interest (AOI) in Afghanistan. Anomaly is a montmorillonite-dominated area, which appears as bleached areas within darker rocks.

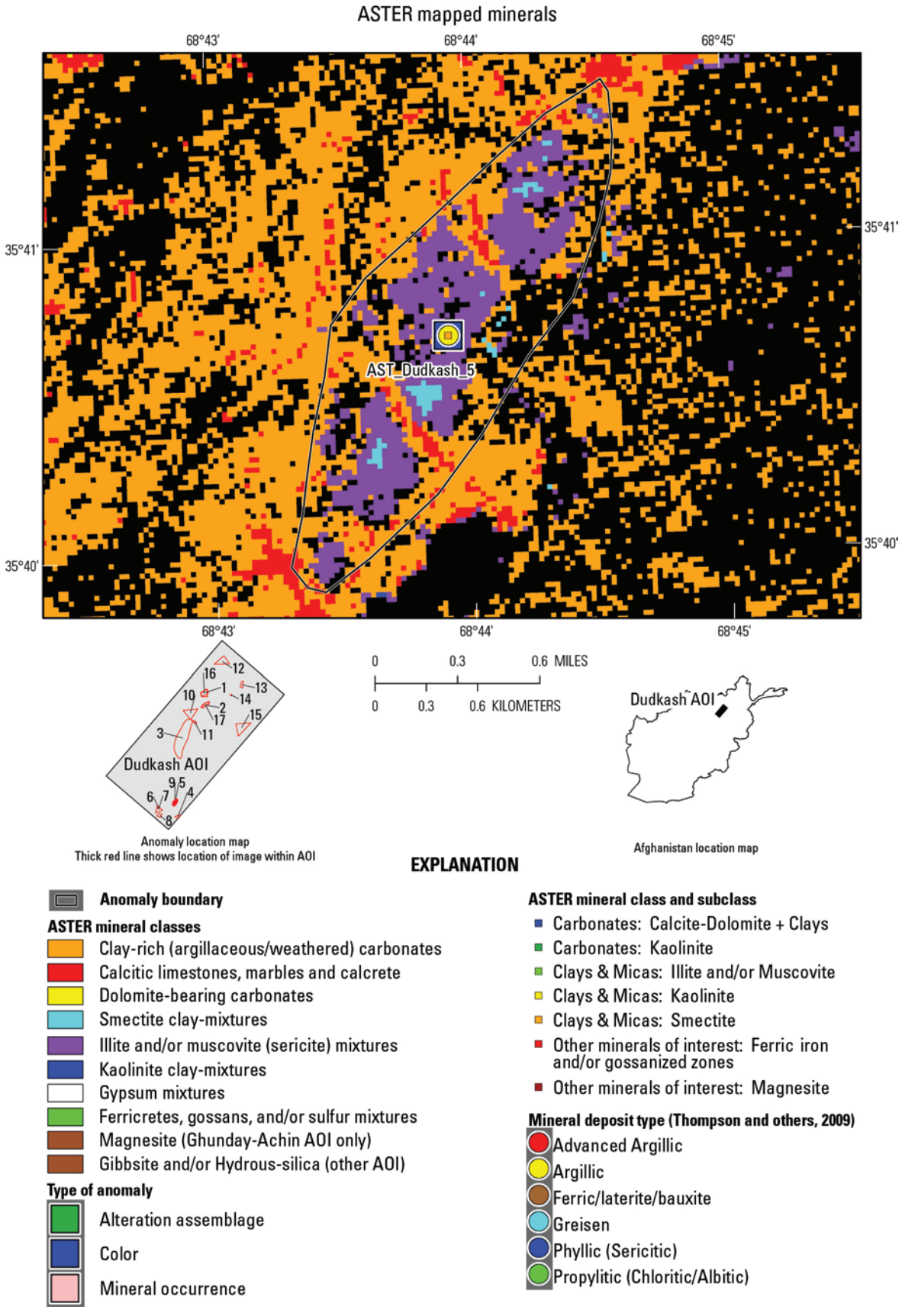

Figure 4.5.5. ASTER color anomaly located in the Dudkash Area of Interest (AOI) in Afghanistan. Anomaly is a montmorillonite-dominated area, which appears as bleached areas within darker rocks.

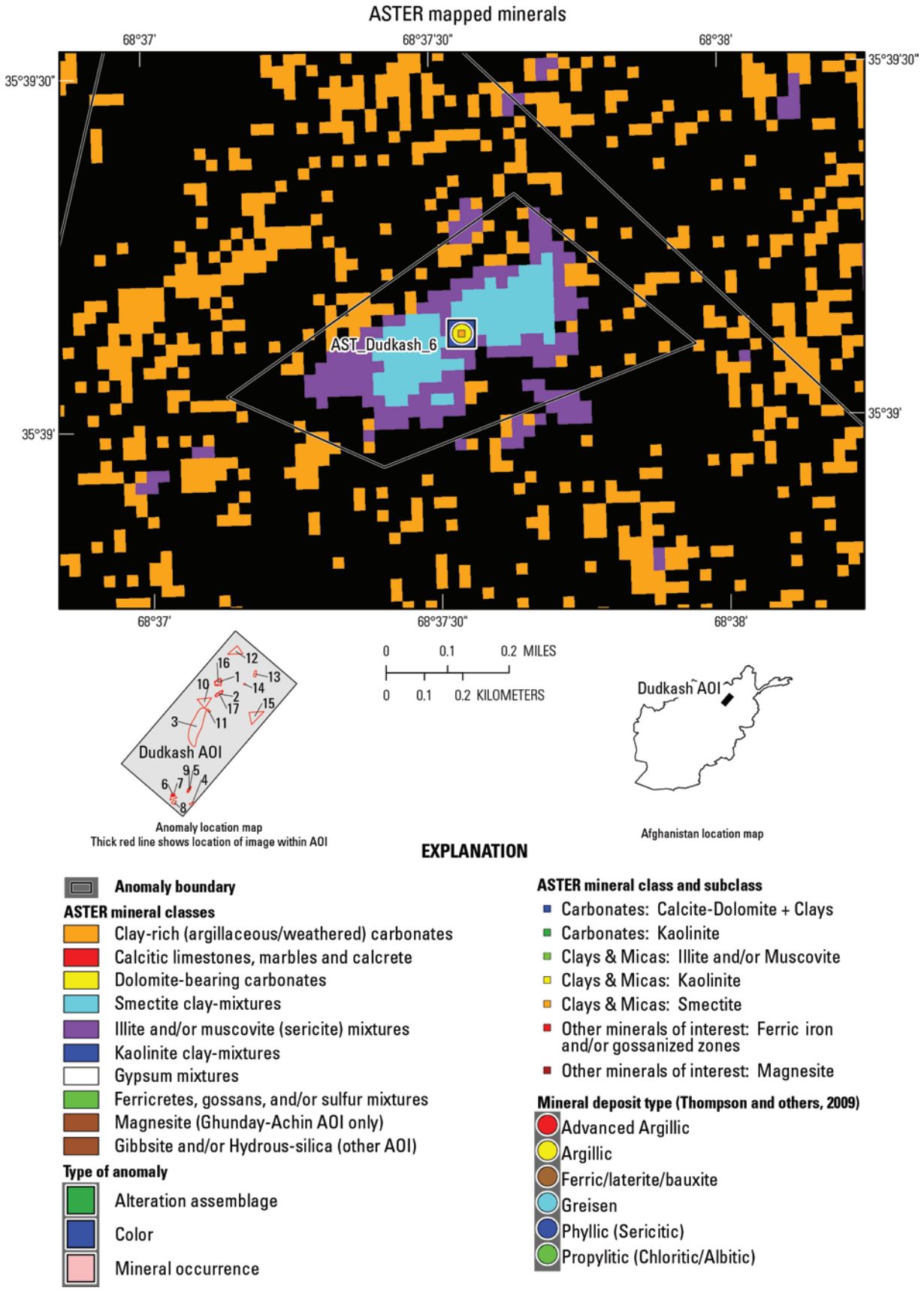

Figure 4.5.6. ASTER color anomaly located in the Dudkash Area of Interest (AOI) in Afghanistan. Anomaly is a montmorillonite-dominated area, which appears as bleached areas within darker rocks.

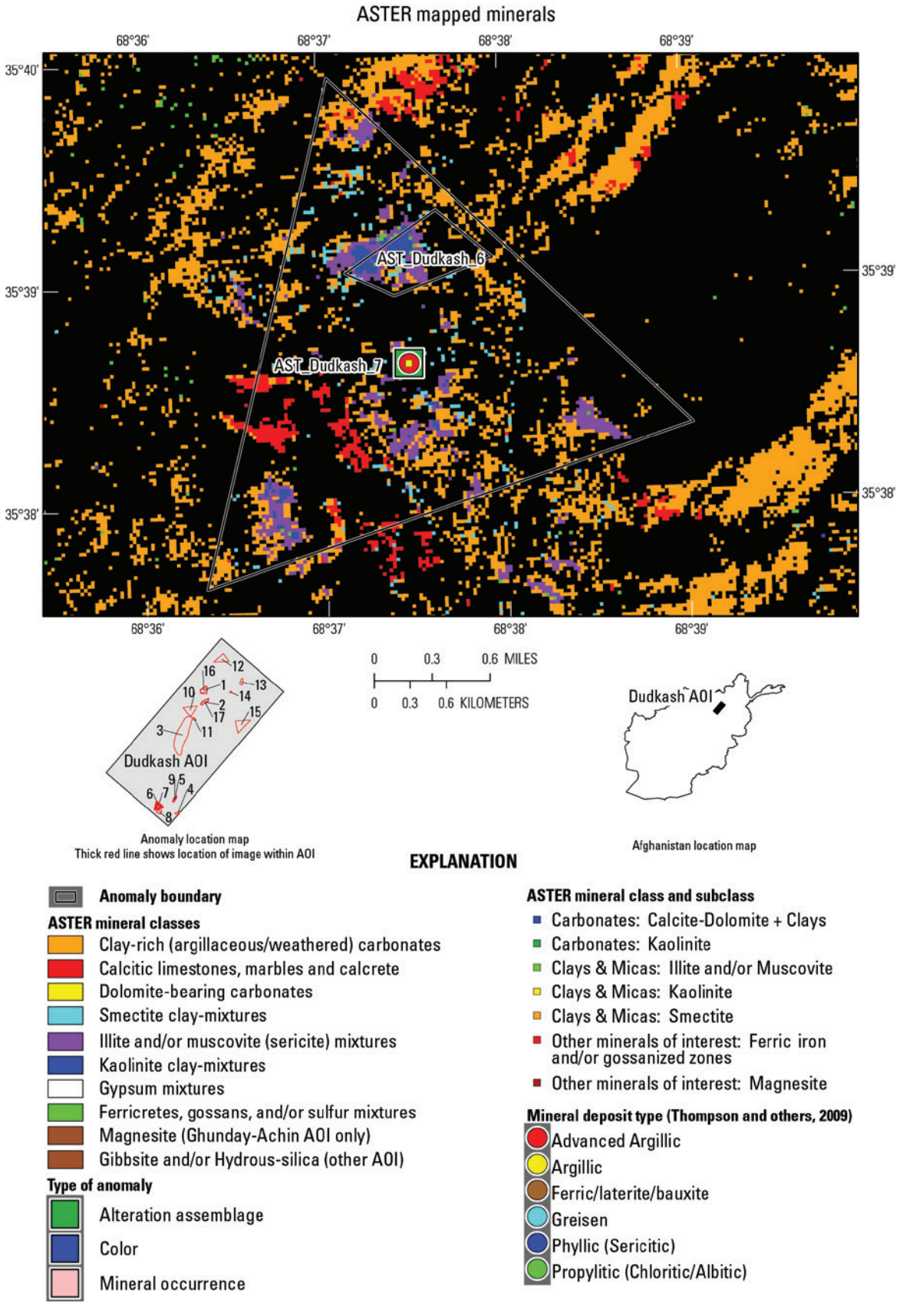

Figure 4.5.7. ASTER alteration anomaly located in the Dudkash Area of Interest (AOI) in Afghanistan. Anomaly contains locally bleached kaolinite/smectite-bearing areas within otherwise dark rocks, although illite/muscovite/smectite appears to be more widespread. Anomaly encompasses smaller AST_Dudkash_6 anomaly.

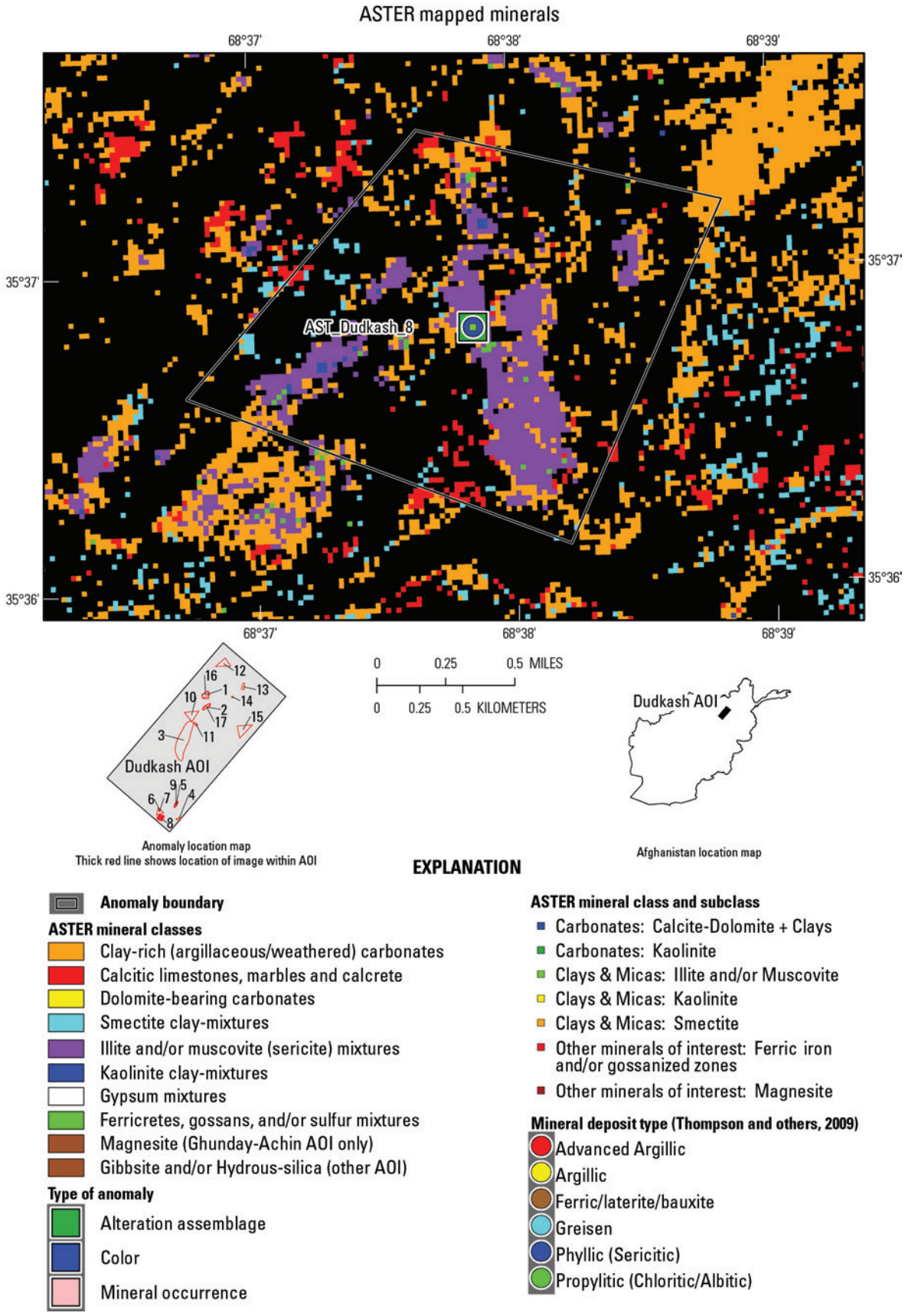

Figure 4.5.8. ASTER alteration anomaly located in the Dudkash Area of Interest (AOI) in Afghanistan. Anomaly is dominated by sericitic alteration minerals and contains locally bleached patches of kaolinite.

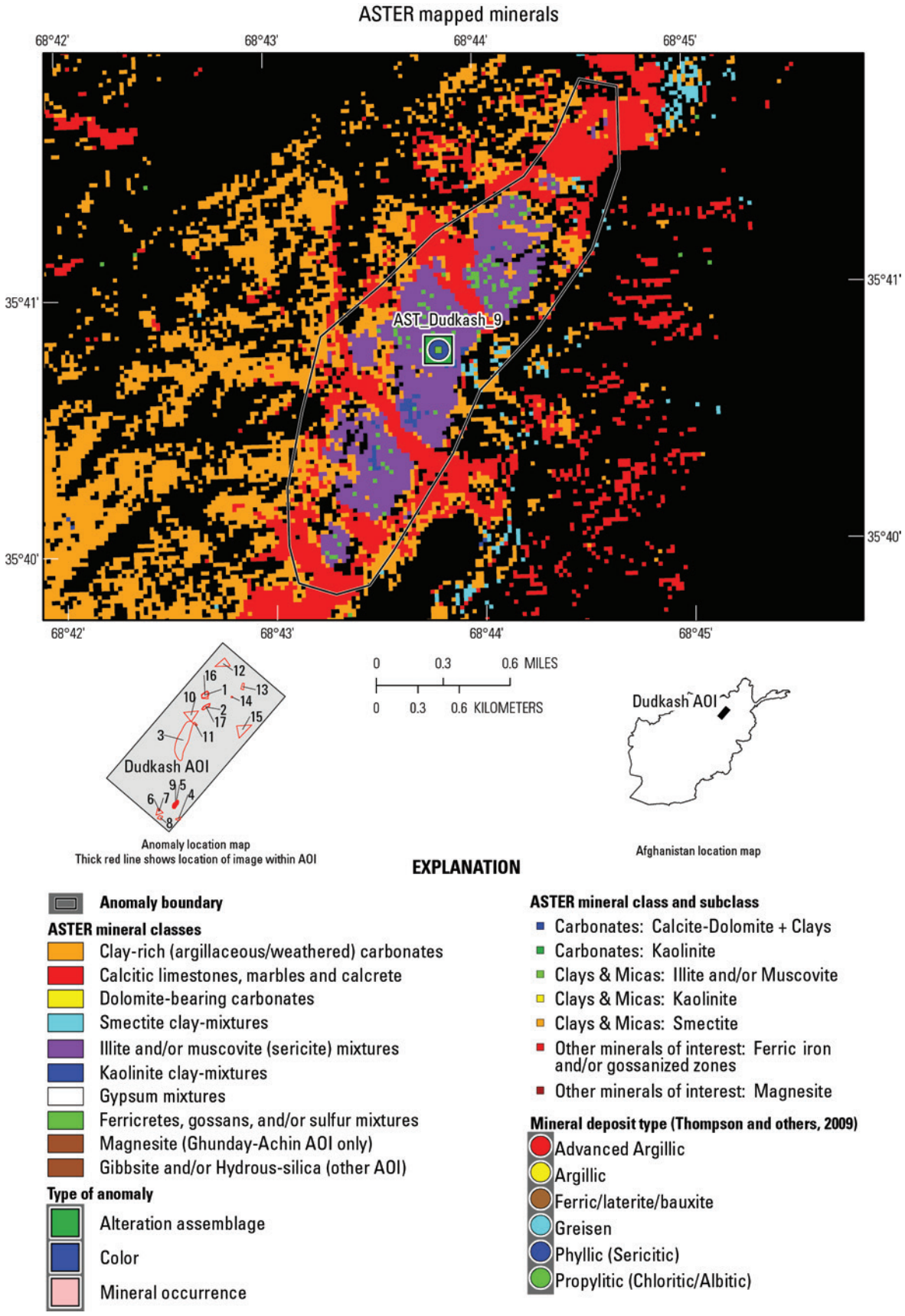

Figure 4.5.9. ASTER alteration anomaly located in the Dudkash Area of Interest (AOI) in Afghanistan. Anomaly is dominated by illite/muscovite/smectite with a few small pixels containing some kaolinite, appears darker than surrounding carbonate rocks, and shares a similar extent with the AST_Dudkash_5 anomaly.

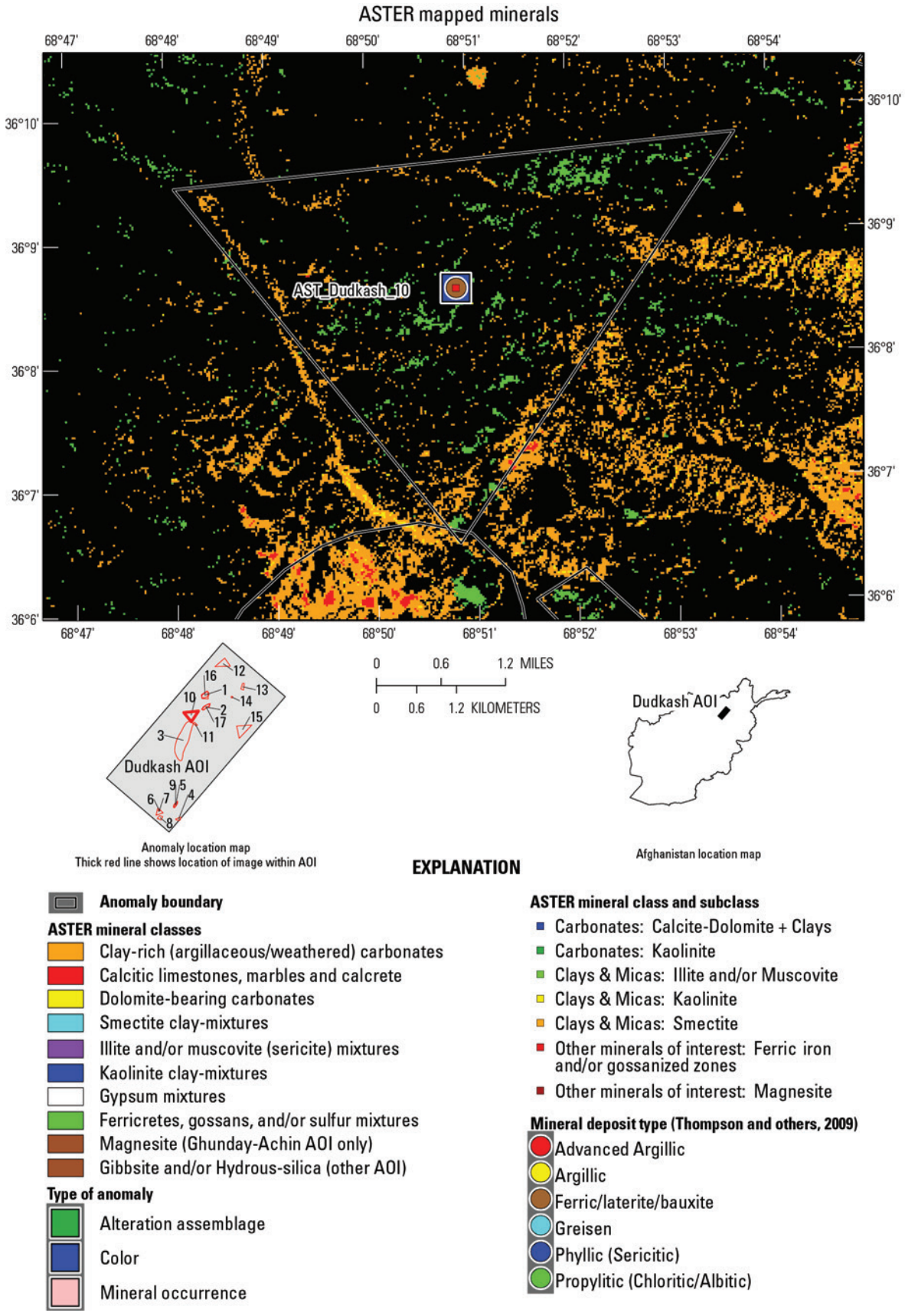

Figure 4.5.10. ASTER color anomaly located in the Dudkash Area of Interest (AOI) in Afghanistan. Anomaly is a possible sulfur- and/or phosphate-bearing area excluding downstream alluvial fan areas. Further spectral analysis is needed to distinguish sulfur from strong ferric iron.

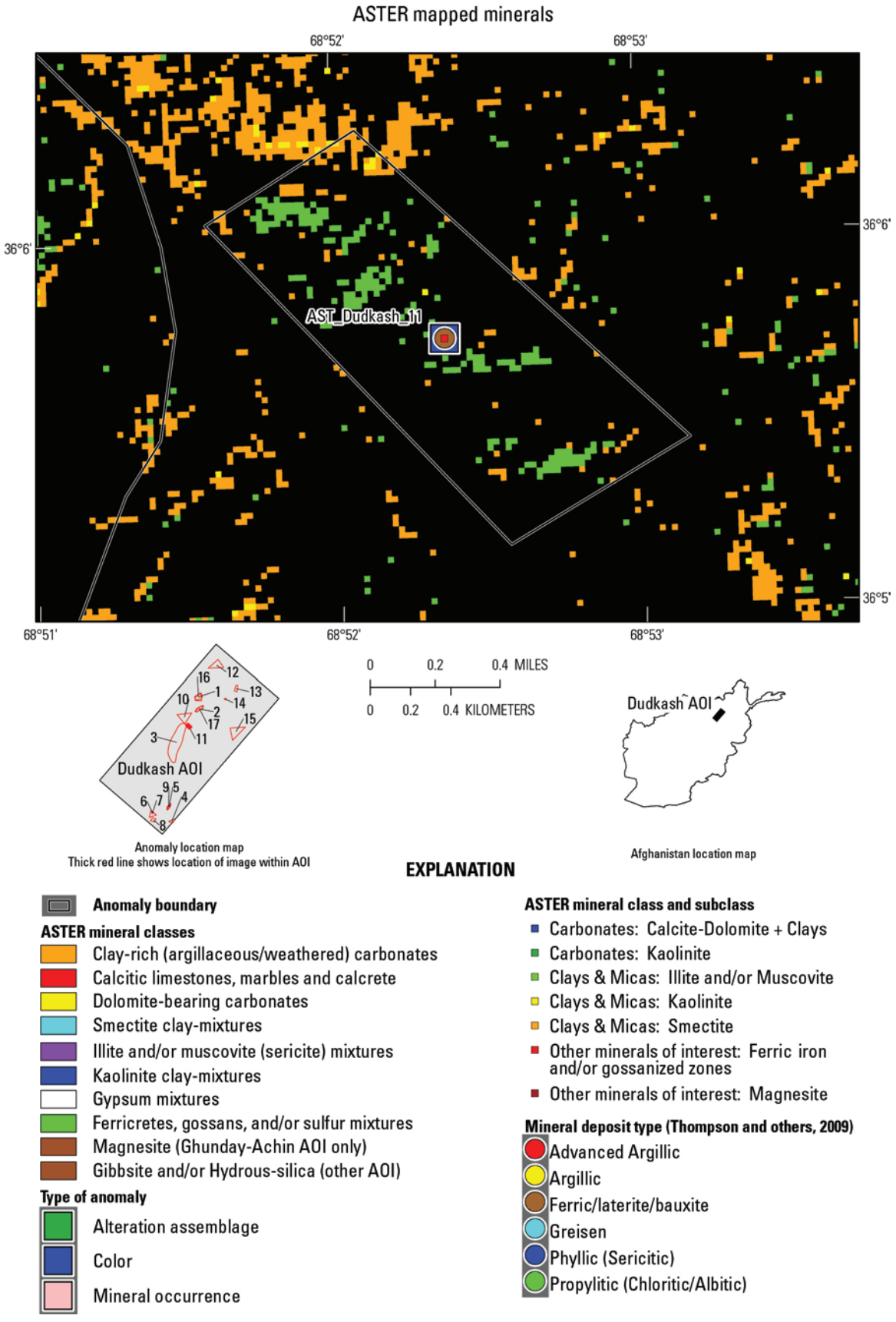

Figure 4.5.11. ASTER color anomaly located in the Dudkash Area of Interest (AOI) in Afghanistan. Anomaly is a possible sulfur- and/or phosphate-bearing area. Further spectral analysis is needed to distinguish sulfur from strong ferric iron.

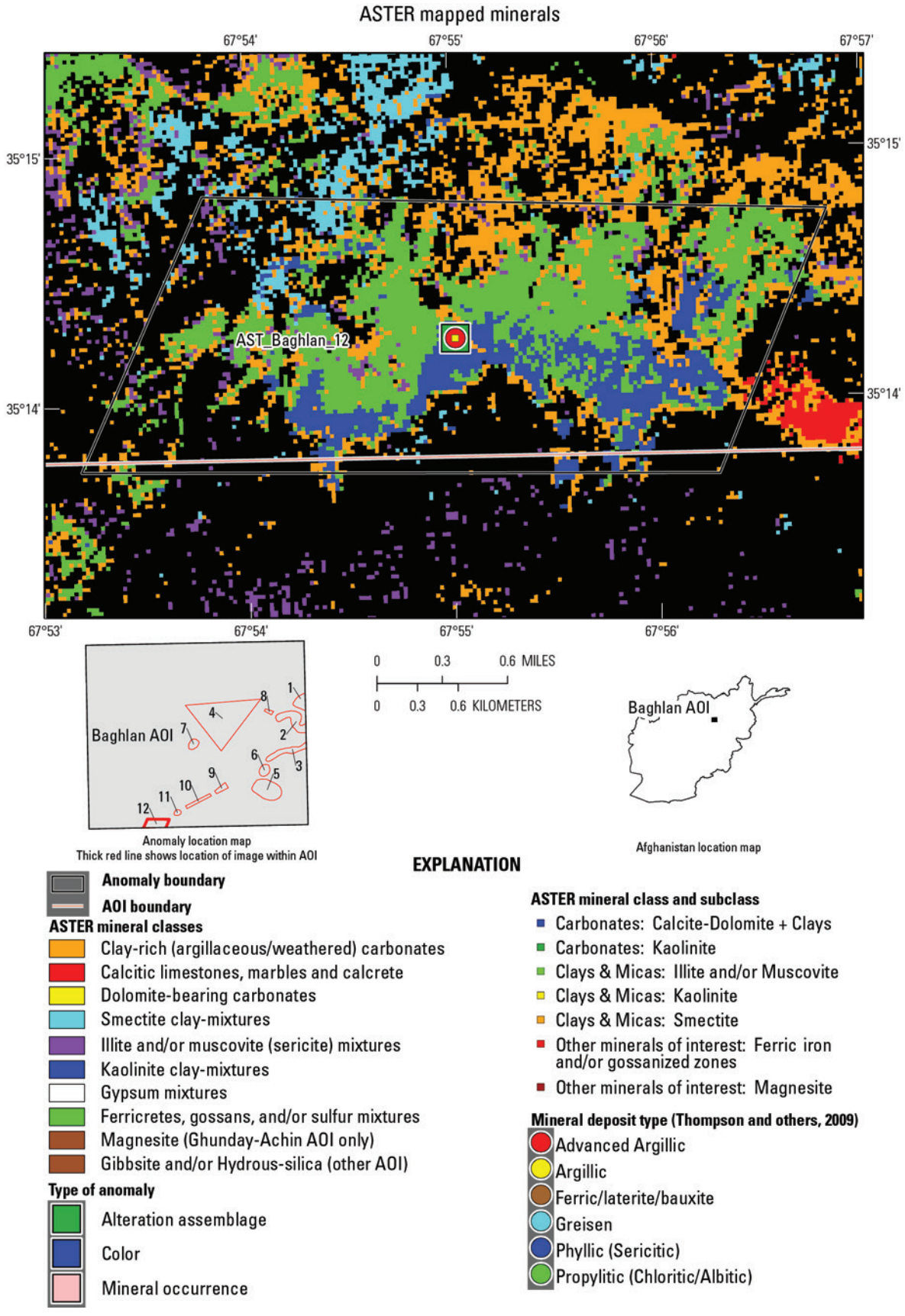

Figure 4.5.12. ASTER color anomaly located in the Dudkash Area of Interest (AOI) in Afghanistan. Anomaly is a possible sulfur- and/or phosphate-bearing area. Further spectral analysis is needed to distinguish sulfur from strong ferric iron.

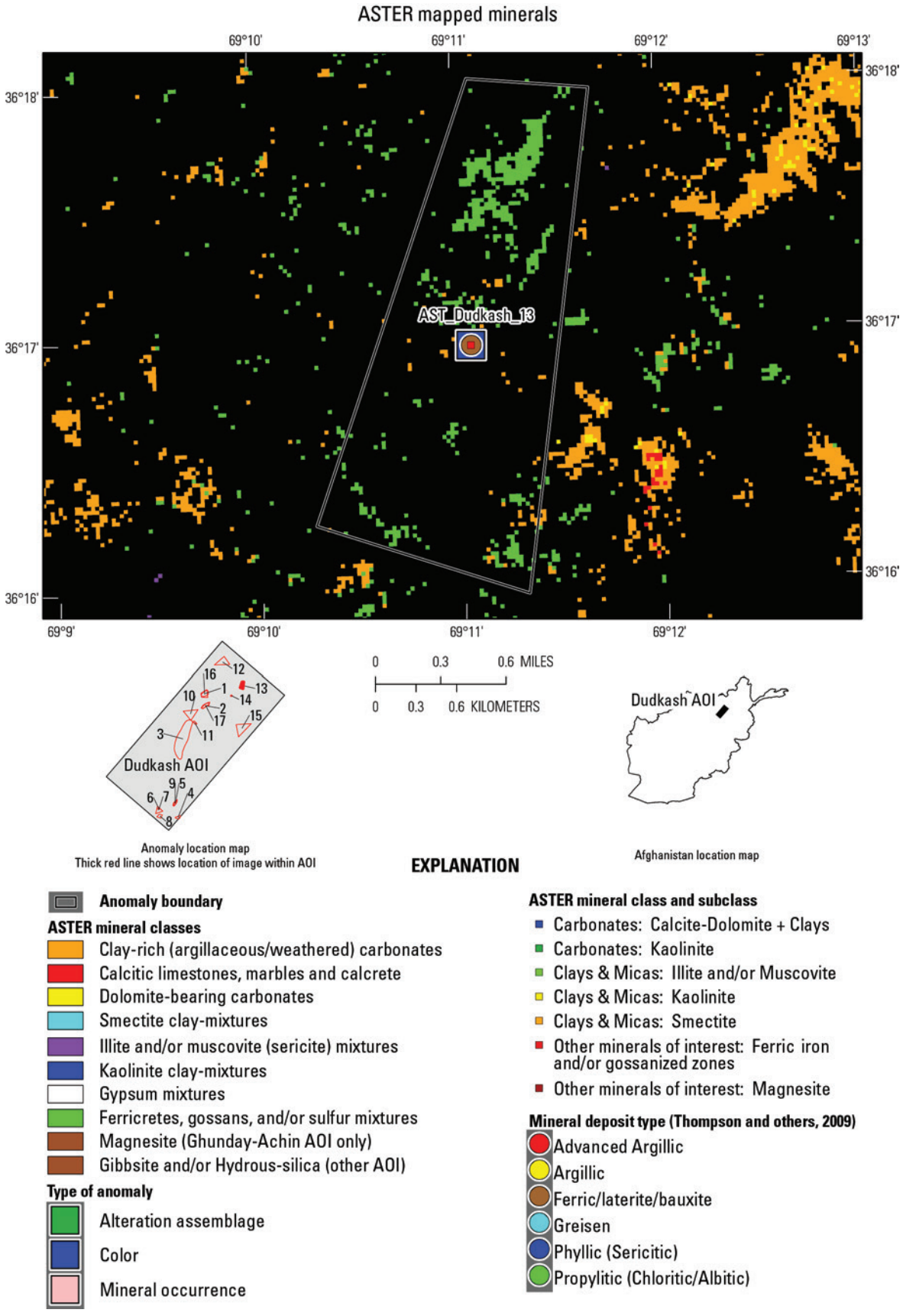

Figure 4.5.13. ASTER color anomaly located in the Dudkash Area of Interest (AOI) in Afghanistan. Anomaly is a possible sulfur- and/or phosphate-bearing area. Further spectral analysis is needed to distinguish sulfur from strong ferric iron.

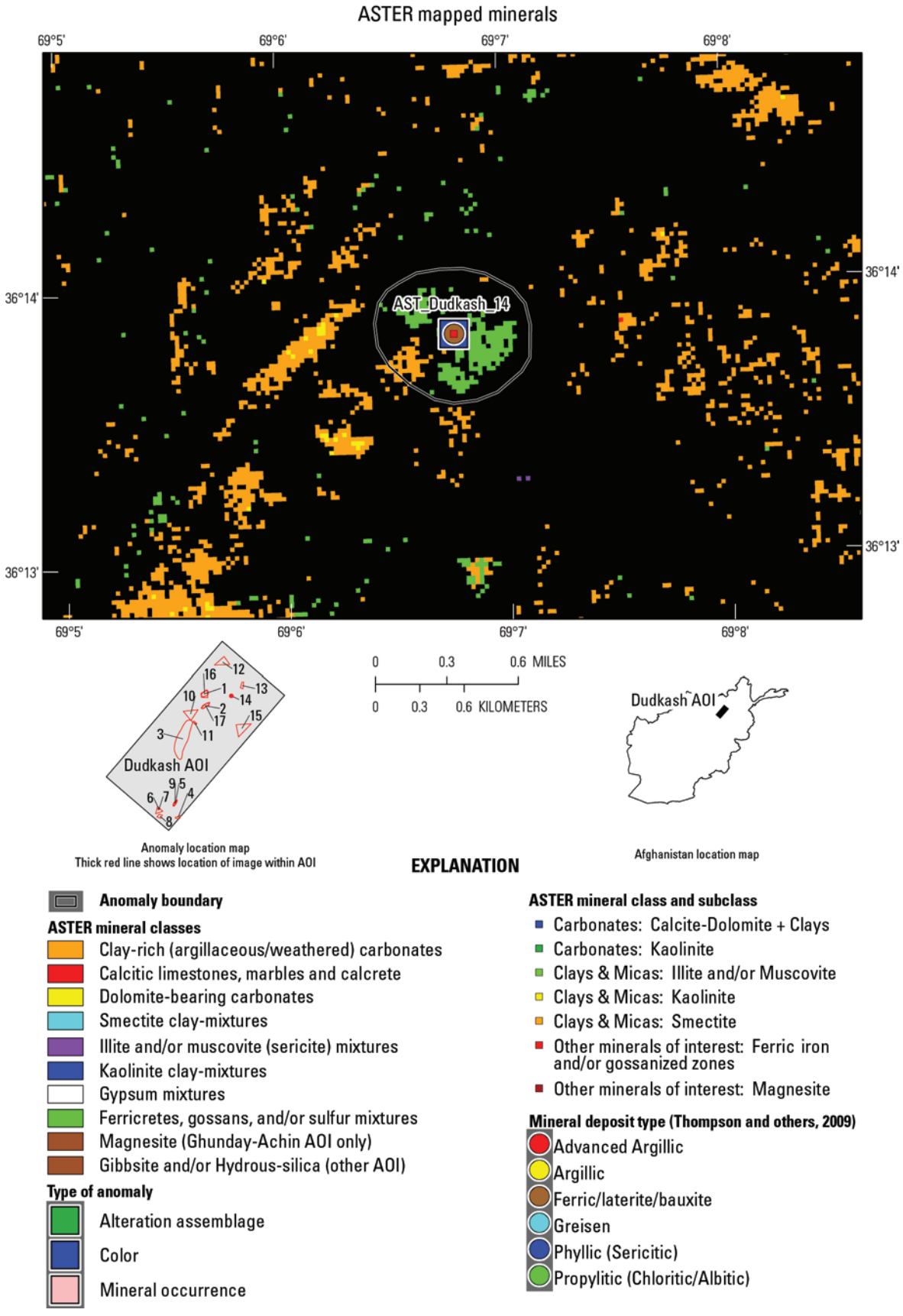

Figure 4.5.14. ASTER color anomaly located in the Dudkash Area of Interest (AOI) in Afghanistan. Anomaly is a possible sulfur and/or phosphate-bearing area. Further spectral analysis is needed to distinguish sulfur from strong ferric iron.

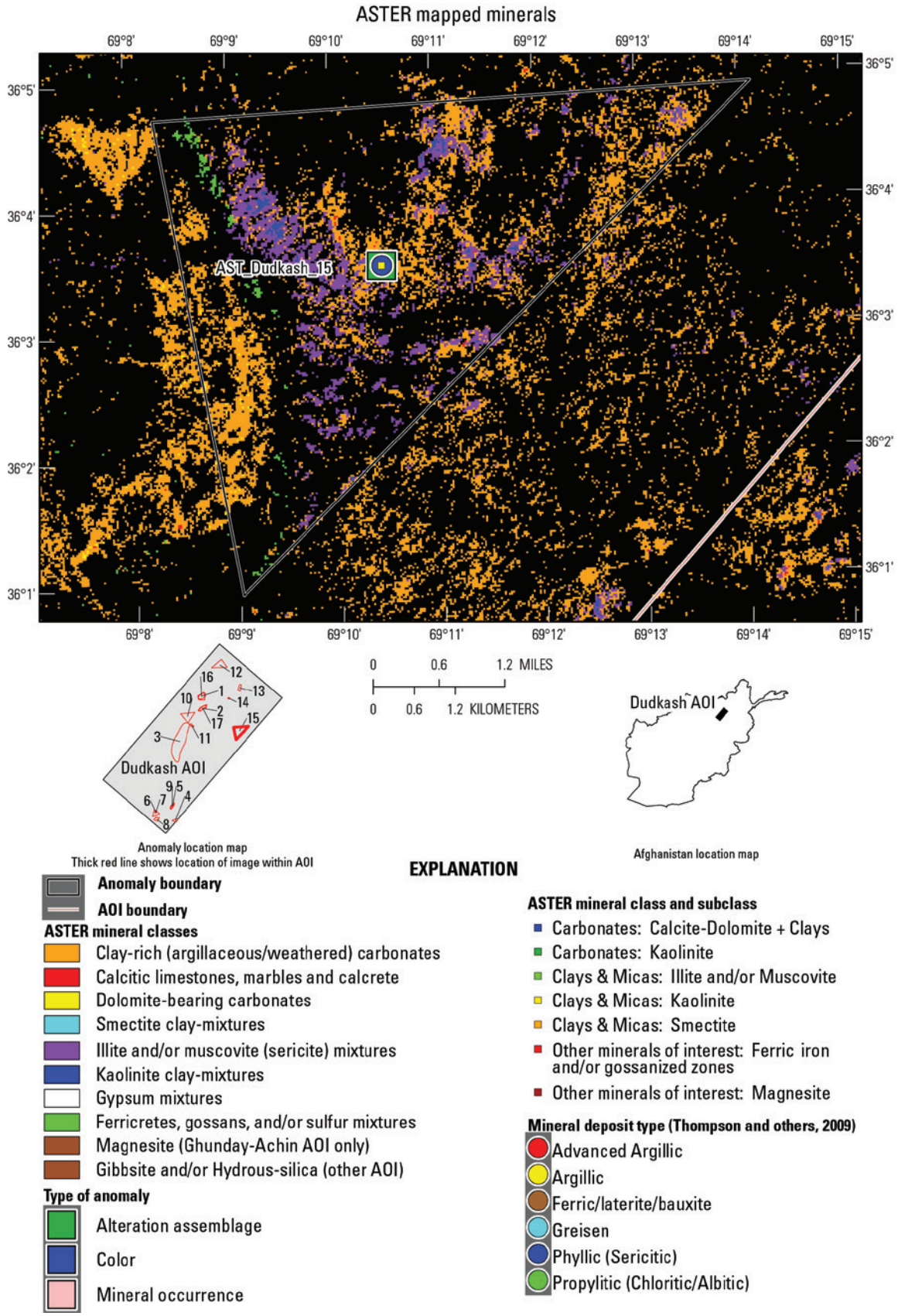

Figure 4.5.15. ASTER alteration anomaly located in the Dudkash Area of Interest (AOI) in Afghanistan. Anomaly is near a copper-sulfide occurrence (Orris and Bliss, 2002) and is an area of localized kaolinite in bleached rocks, dominated by sericitic/phyllic alteration minerals, which could be related to Triassic granodiorite intrusions (Doebrich and Wahl, 2006).

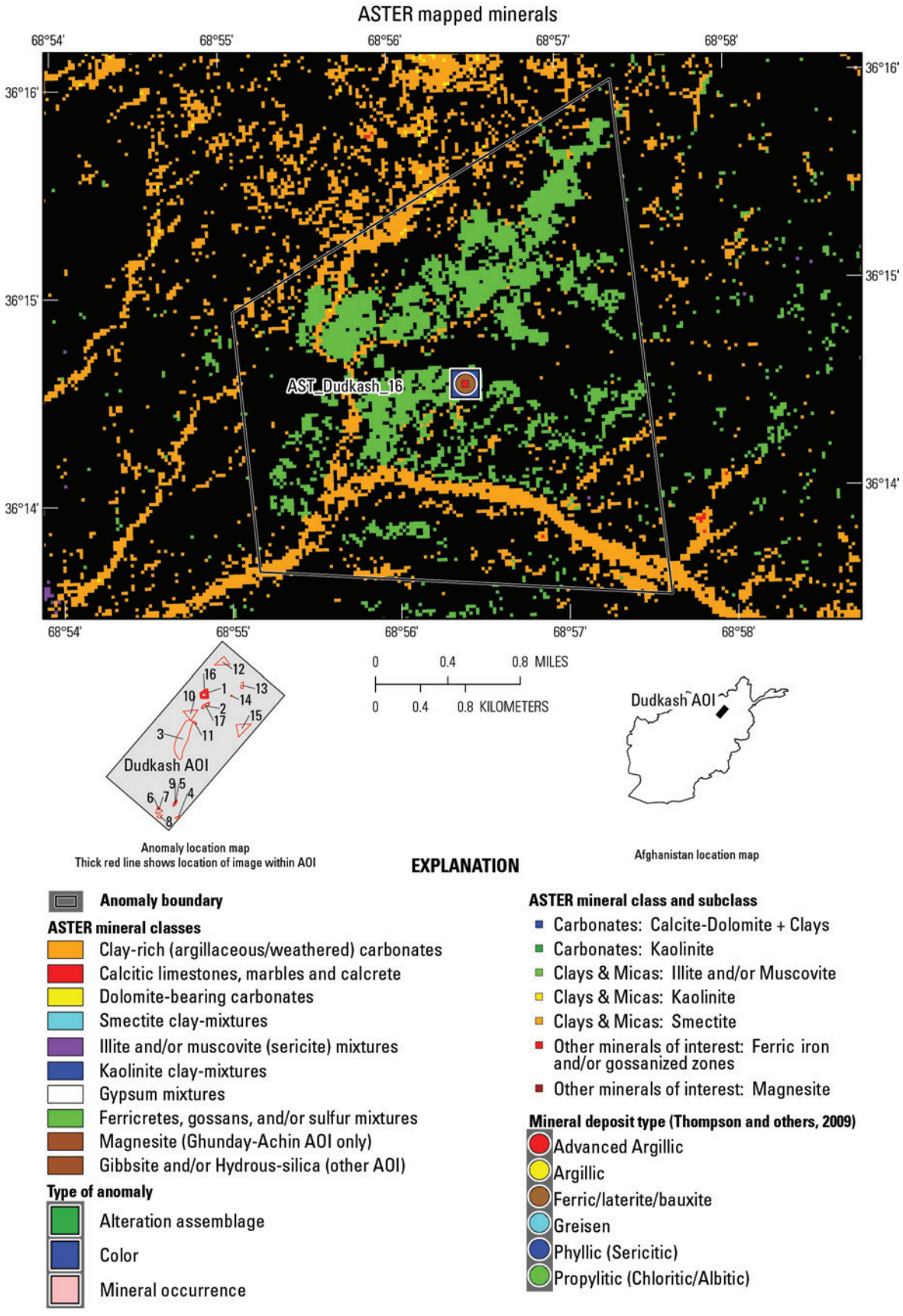

Figure 4.5.16. ASTER color anomaly located in the Dudkash Area of Interest (AOI) in Afghanistan. Anomaly sharing a similar extent as anomaly, AST_Dudkash_1, is a possible sulfur- and/or phosphate-bearing area. Further spectral analysis is needed to distinguish sulfur from strong ferric iron.

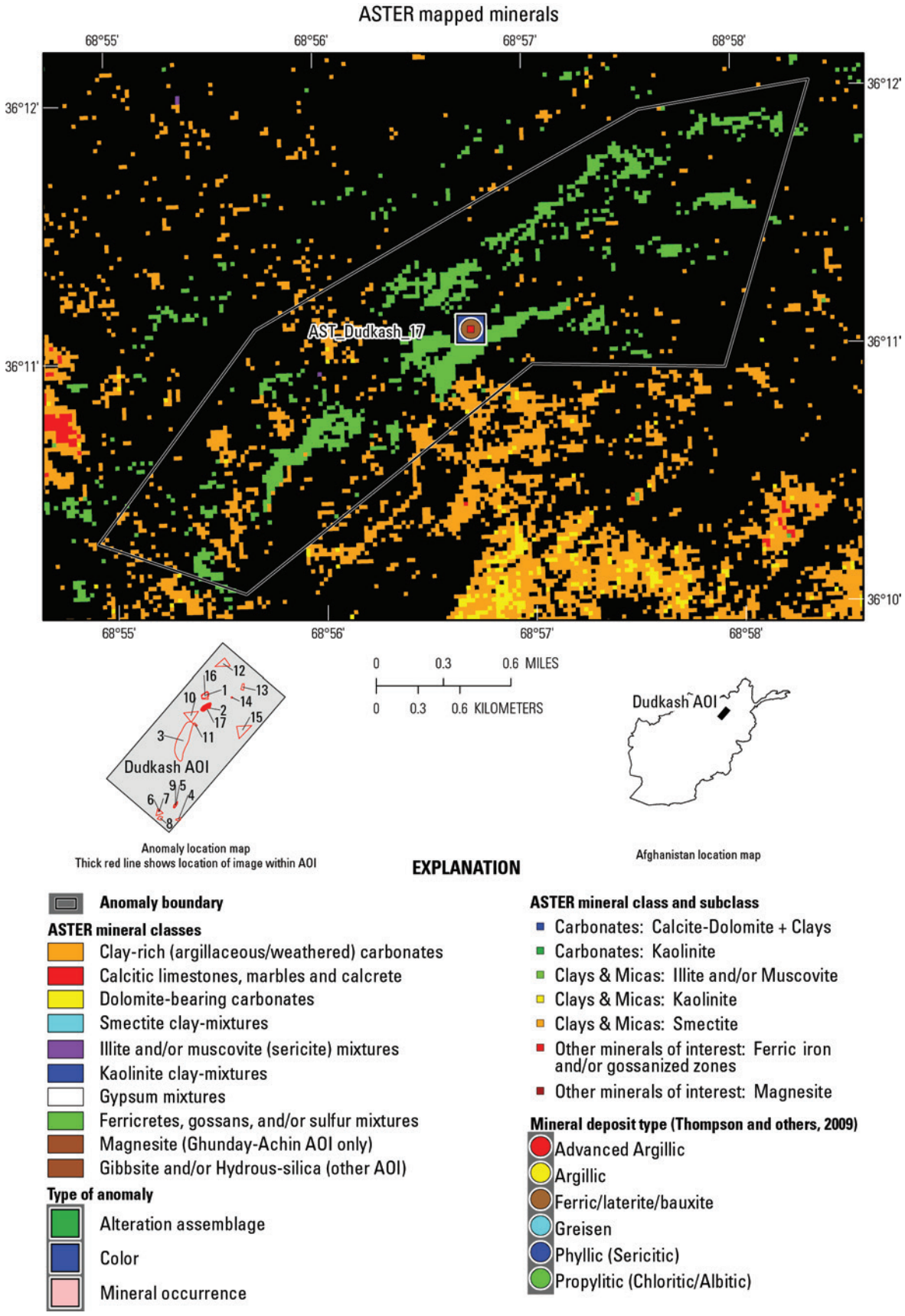

Figure 4.5.17. ASTER color anomaly located in the Dudkash Area of Interest (AOI) in Afghanistan. Anomaly shares a similar extent with another anomaly, AST_Dudkash_2, and is a possible sulfur- and/or phosphate-bearing area. Further spectral analysis is needed to distinguish sulfur from strong ferric iron.

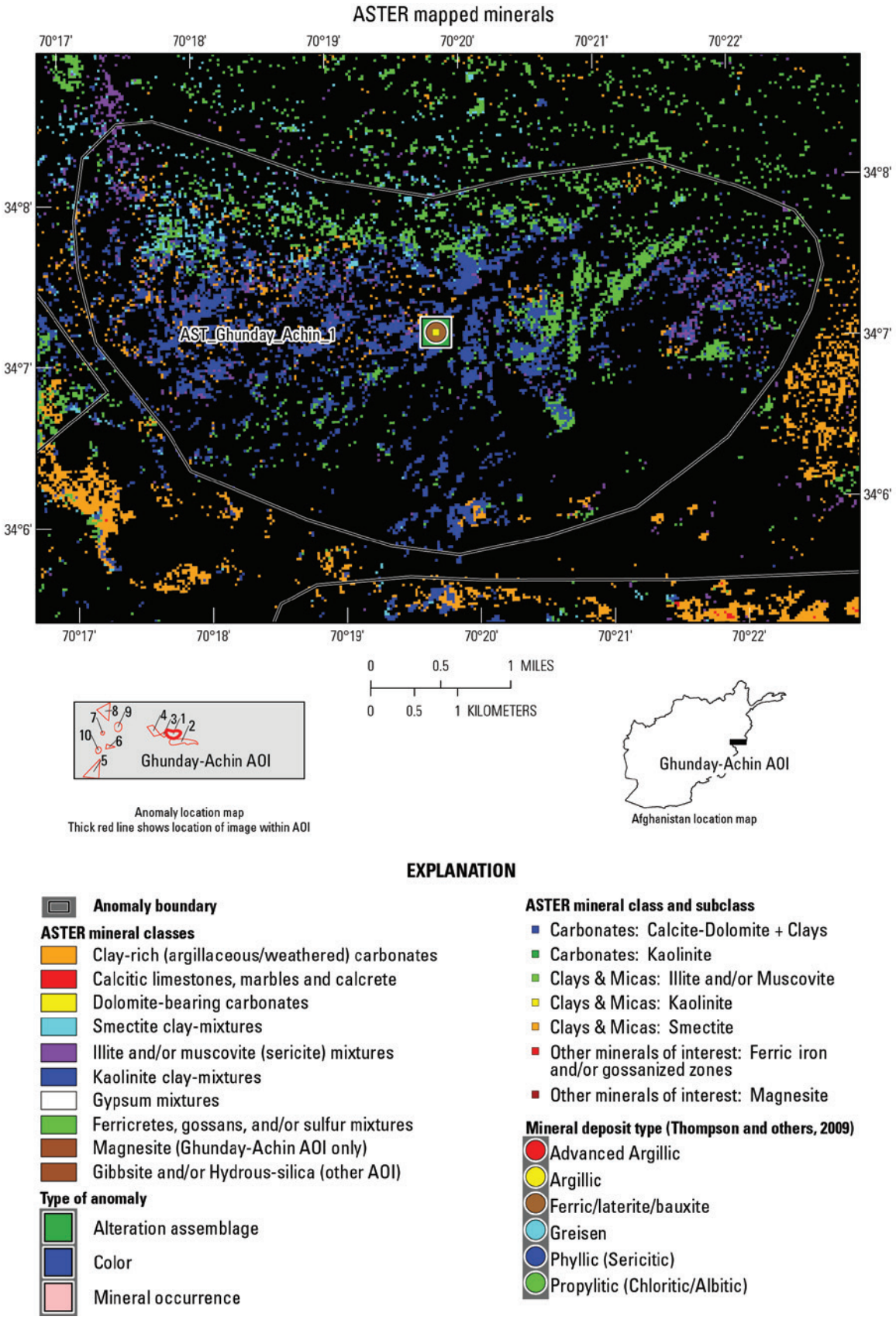

Figure 4.6.1. ASTER alteration anomaly located in the Ghunday-Achin Area of Interest (AOI) in Afghanistan. Anomaly is defined by large areas of kaolinite and ferric iron in the foothills of the Tora Bora Mountains and cave complex. The origin of the anomaly is most likely from intense weathering, although hydrothermal alteration is also possible.

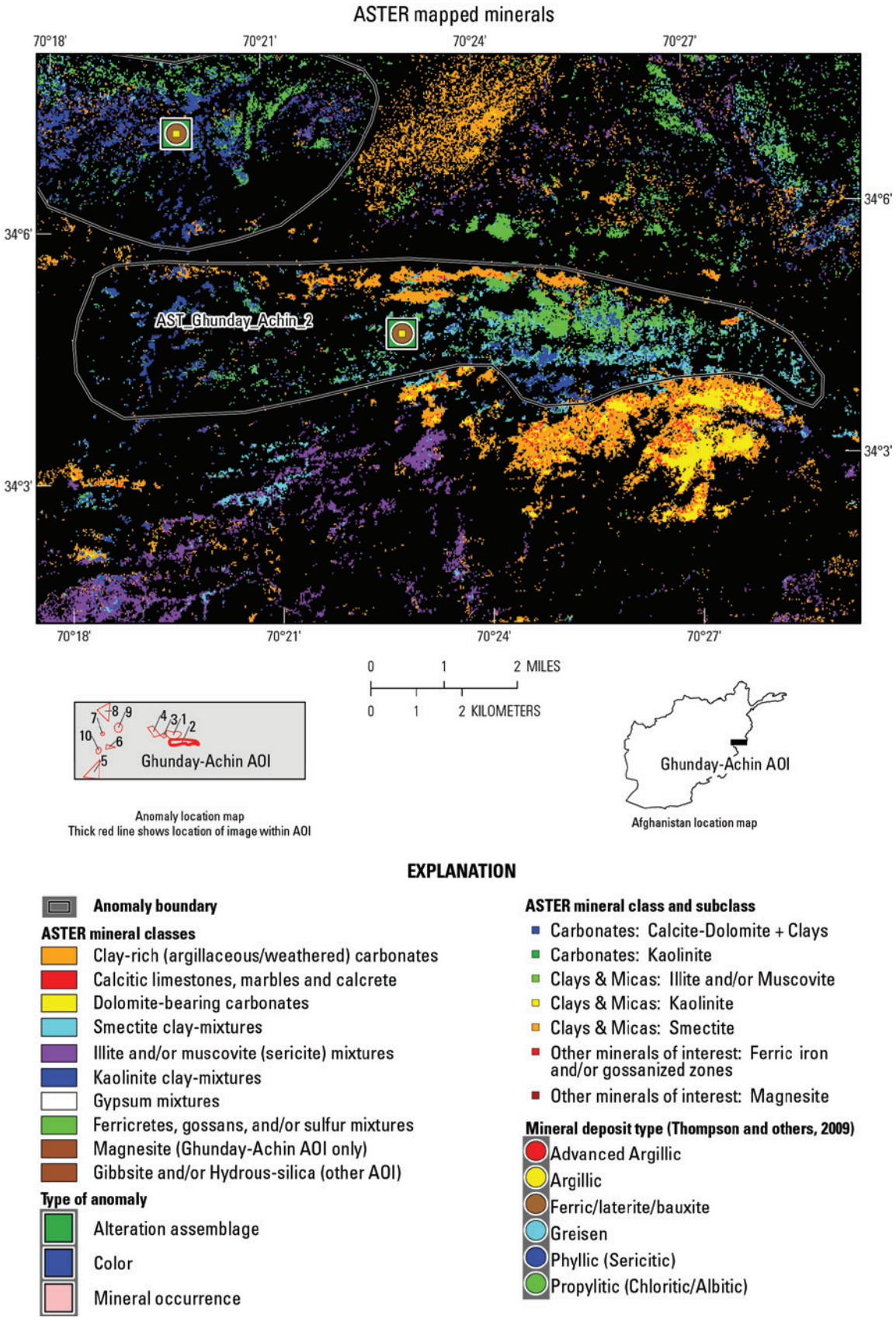

Figure 4.6.2. ASTER alteration anomaly located in the Ghunday-Achin Area of Interest (AOI) in Afghanistan. Anomaly is defined by large areas of kaolinite and ferric iron in the foothills of the Tora Bora Mountains and cave complex. The origin of the anomaly is most likely from intense weathering, although hydrothermal alteration is also possible.

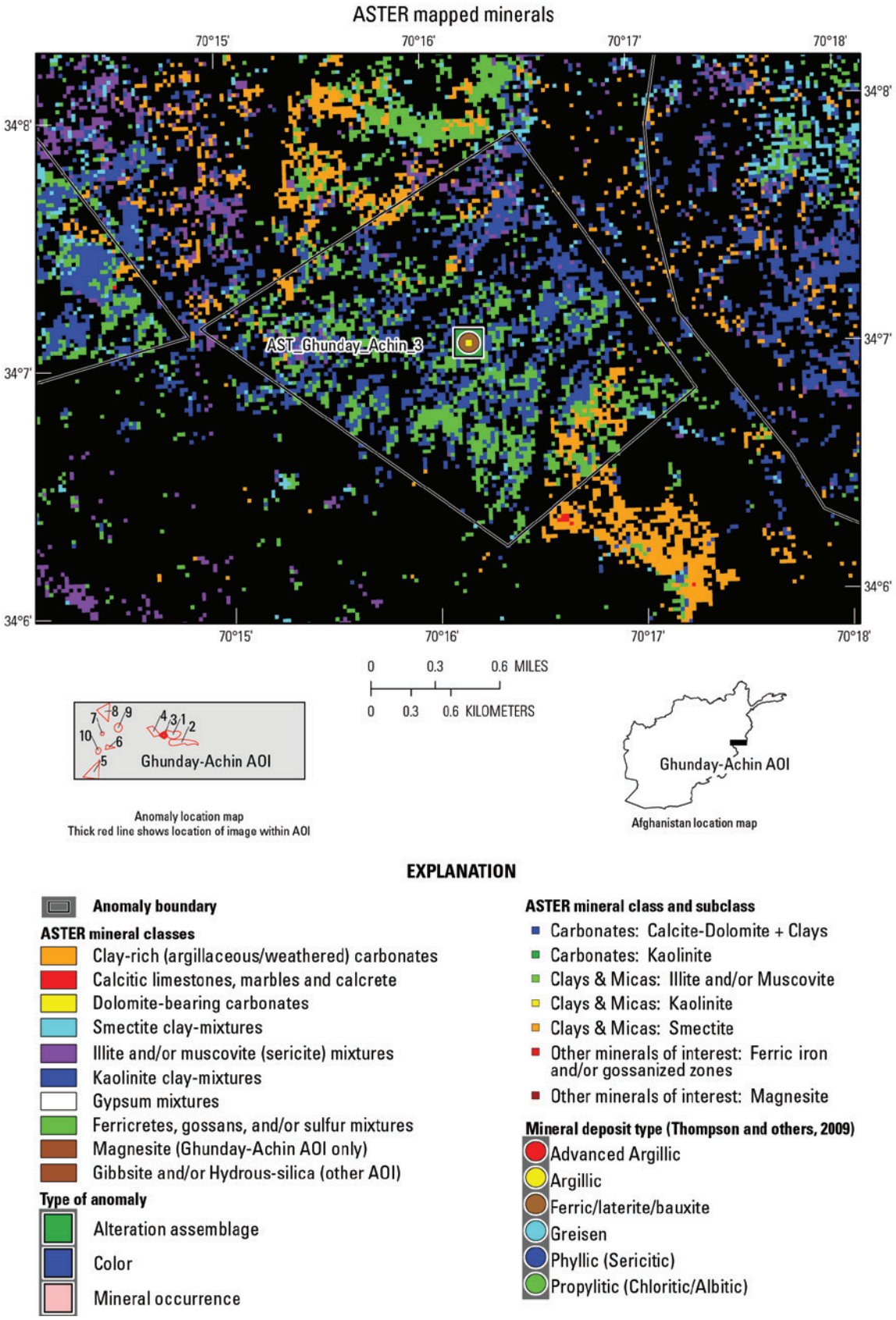

Figure 4.6.3. ASTER alteration anomaly located in the Ghunday-Achin Area of Interest (AOI) in Afghanistan. Anomaly is defined by large areas of kaolinite and ferric iron in the foothills of the Tora Bora Mountains and cave complex. The origin of the anomaly is most likely from intense weathering, although hydrothermal alteration is also possible.

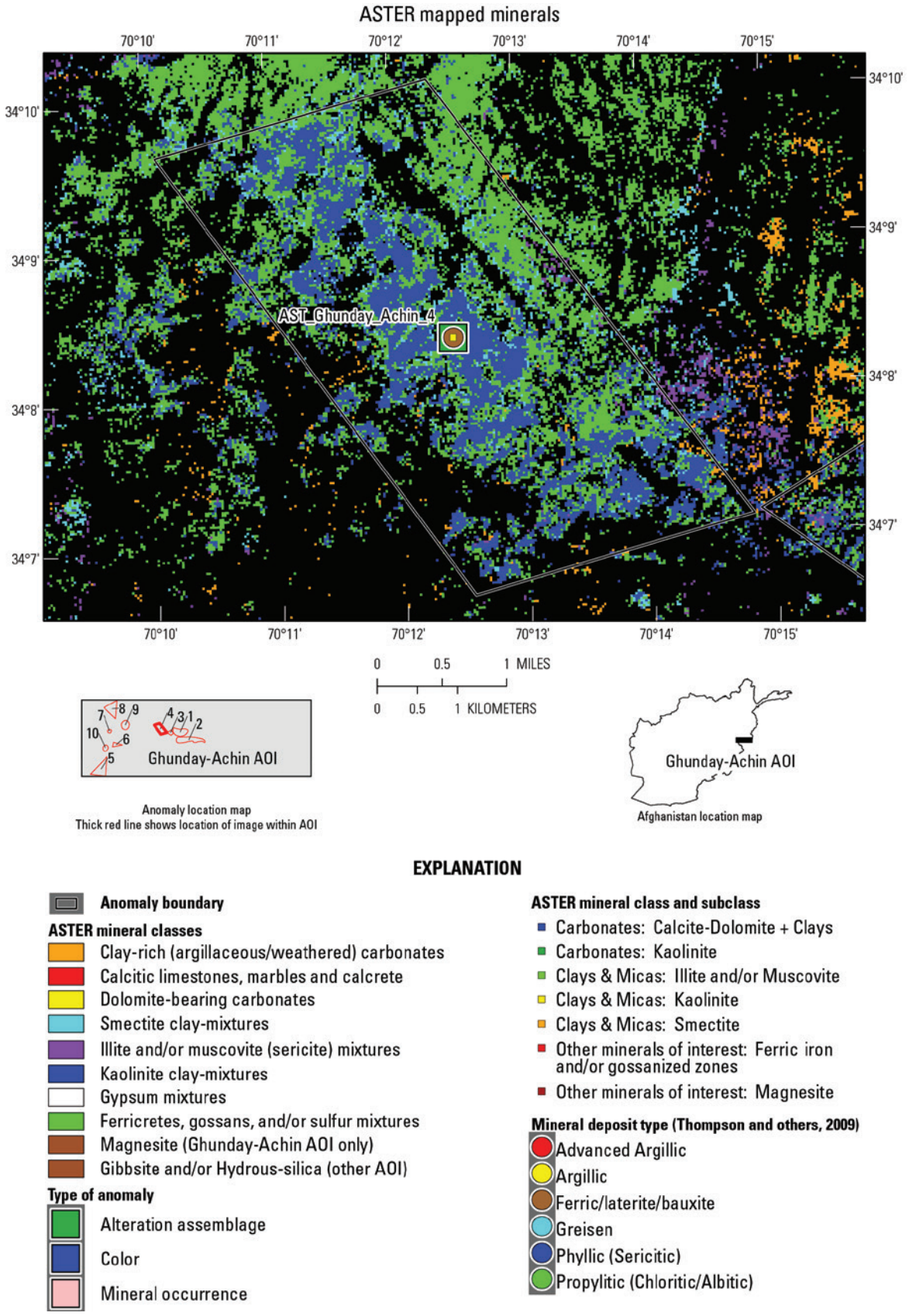

Figure 4.6.4. ASTER alteration anomaly located in the Ghunday-Achin Area of Interest (AOI) in Afghanistan. Anomaly is defined by large areas of kaolinite and ferric iron in the foothills of the Tora Bora Mountains and cave complex. The origin of the anomaly is most likely from intense weathering, although hydrothermal alteration is also possible.

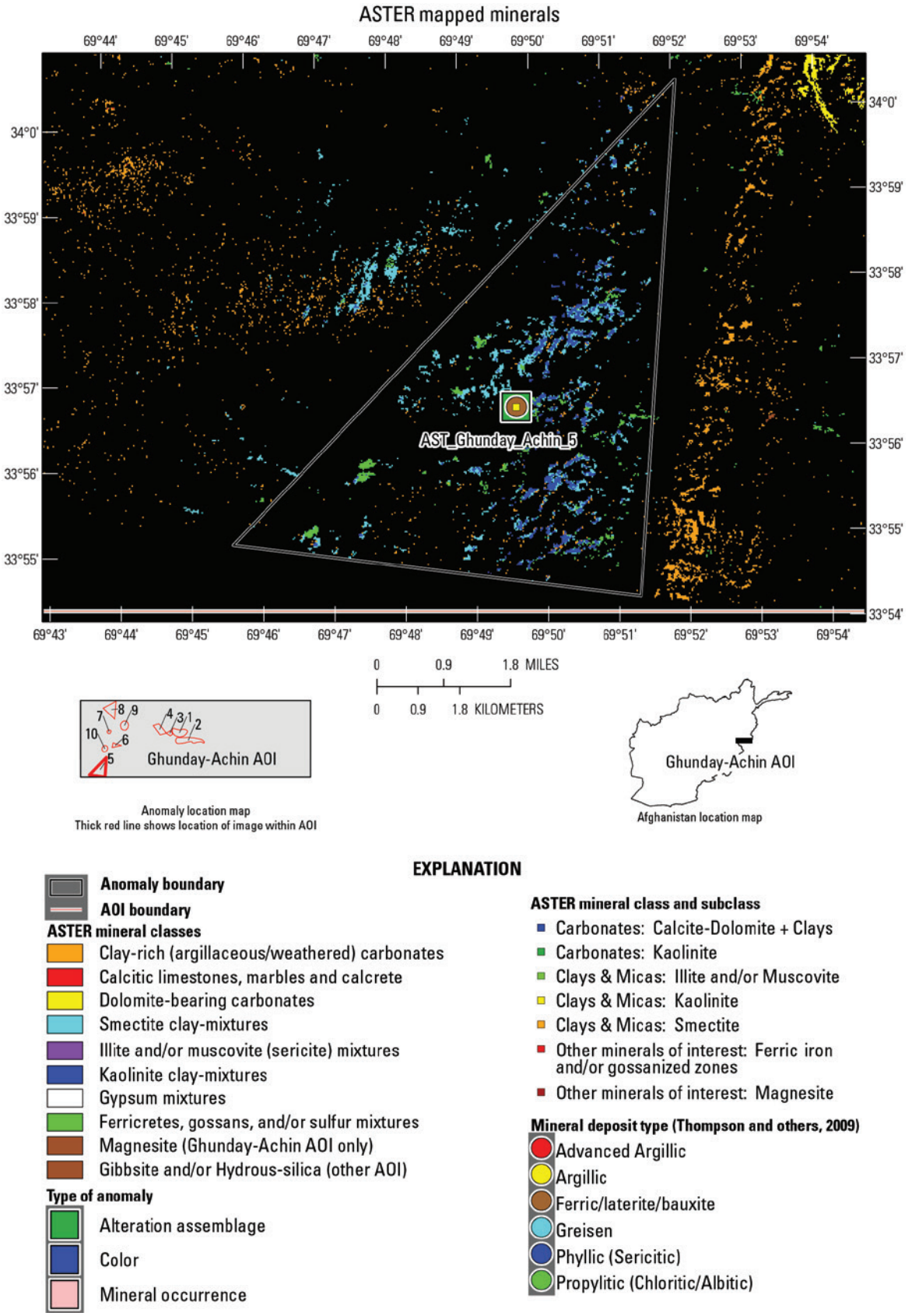

Figure 4.6.5. ASTER alteration anomaly located in the Ghunday-Achin Area of Interest (AOI) in Afghanistan. Anomaly is defined by large areas of kaolinite and ferric iron in the foothills of the Tora Bora Mountains and cave complex. The origin of the anomaly is most likely from intense weathering, although hydrothermal alteration is also possible.

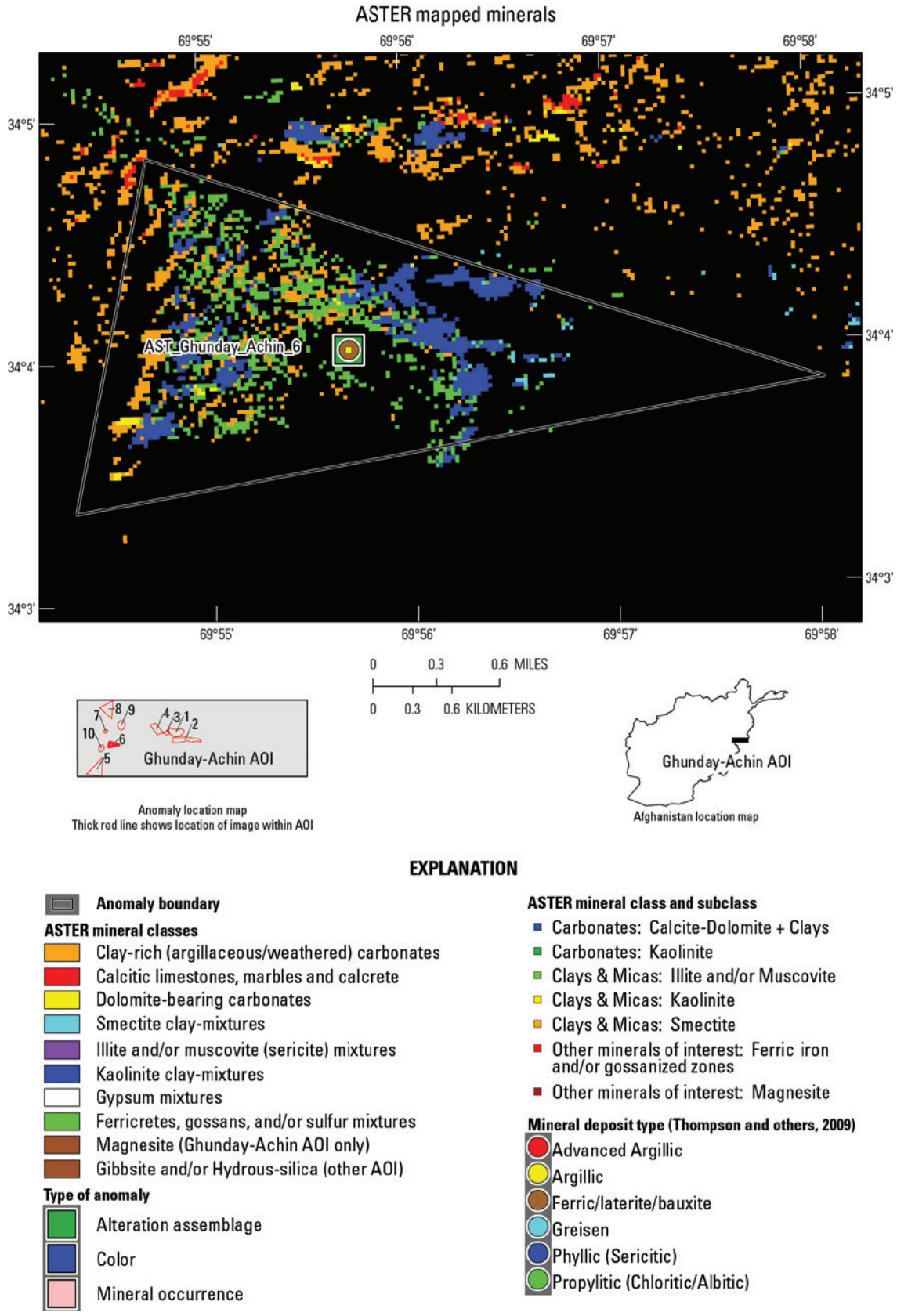

Figure 4.6.6. ASTER alteration anomaly located in the Ghunday-Achin Area of Interest (AOI) in Afghanistan. Anomaly is an area of kaolinite and ferric iron in the upper/alpine and often snow-covered slopes of the Tora Bora Mountains. The origin of the anomaly is more likely to be from hydrothermal alteration than from weathering.

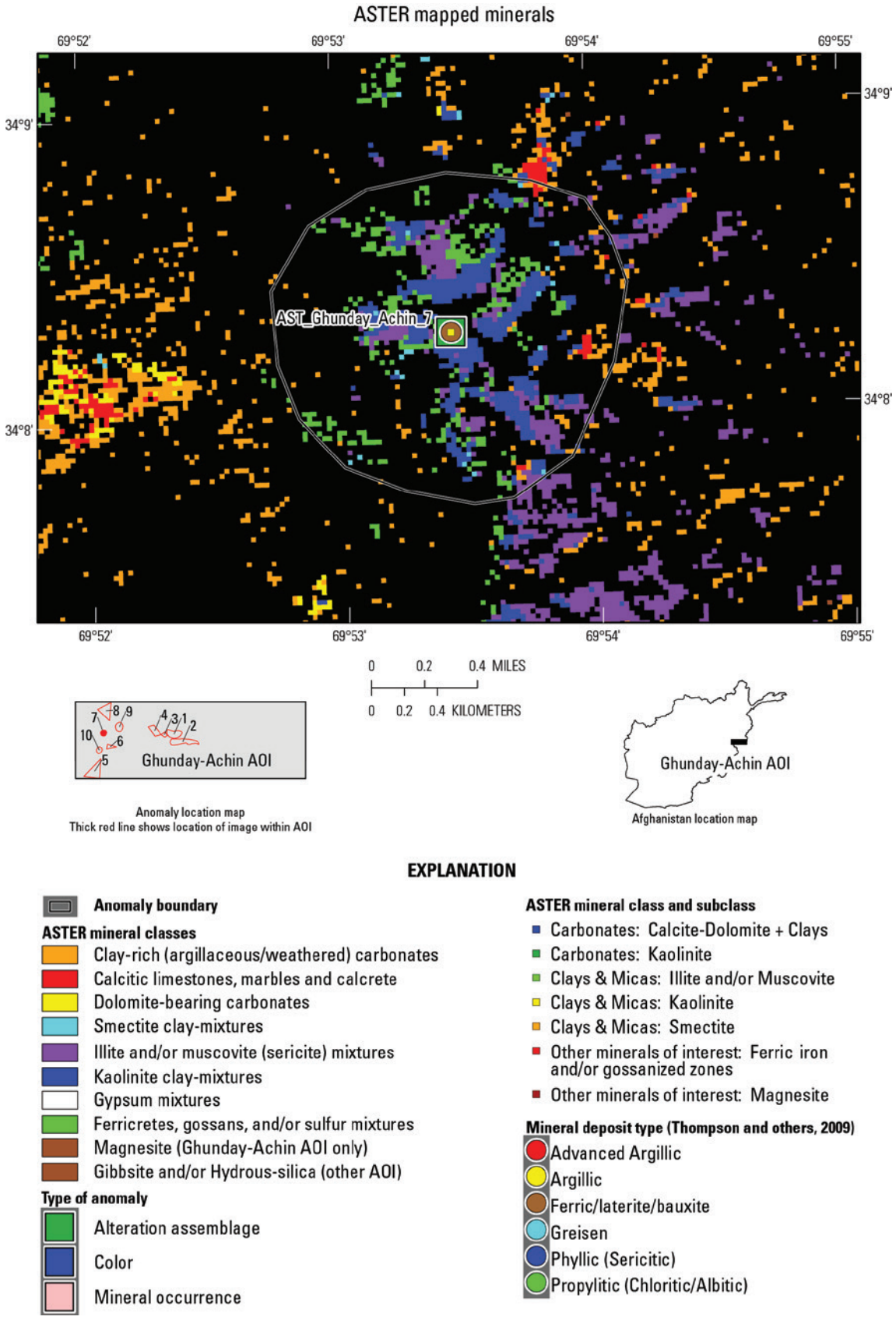

Figure 4.6.7. ASTER alteration anomaly located in the Ghunday-Achin Area of Interest (AOI) in Afghanistan. Anomaly is an area of kaolinite and ferric iron in the upper/alpine and often snow-covered slopes of the Tora Bora Mountains. The origin of the anomaly is more likely to be from hydrothermal alteration origin than from weathering.

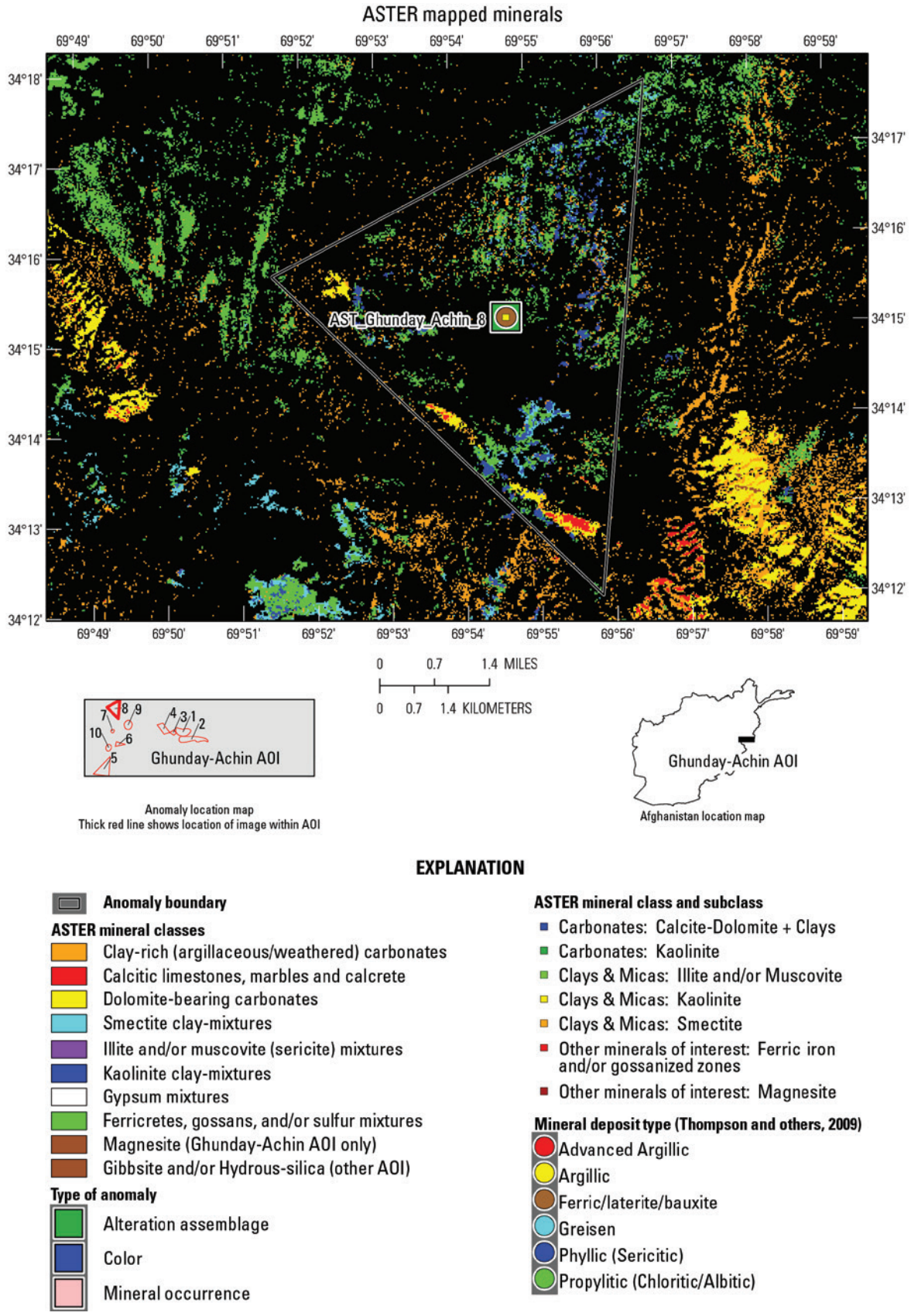

Figure 4.6.8. ASTER alteration anomaly located in the Ghunday-Achin Area of Interest (AOI) in Afghanistan. Anomaly is defined by large areas of kaolinite and ferric iron in the foothills of the Tora Bora Mountains and cave complex. The origin of the anomaly is most likely from intense weathering, although hydrothermal alteration is also possible.

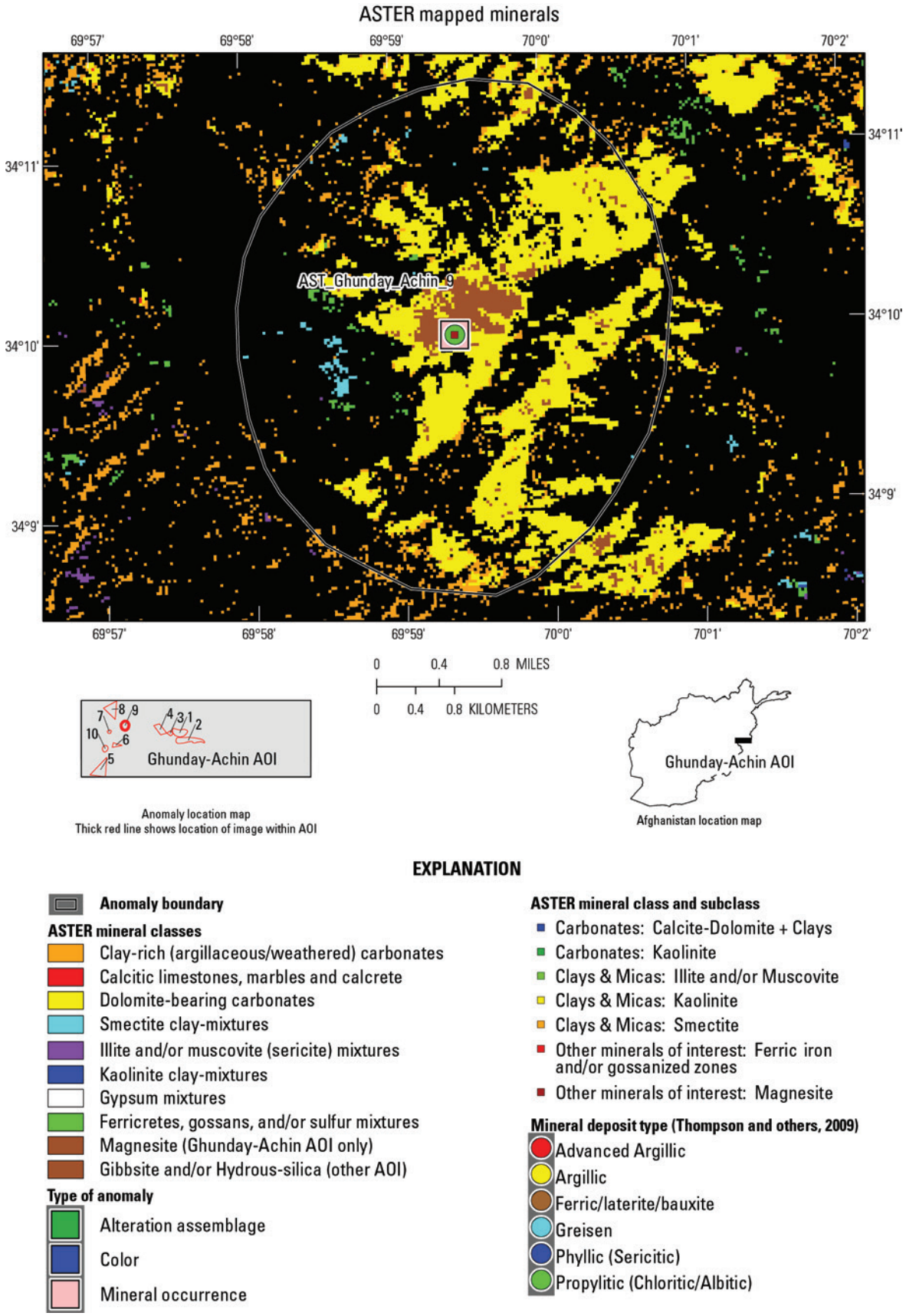

Figure 4.6.9. ASTER mineral occurrence anomaly located in the Ghunday-Achin Area of Interest (AOI) in Afghanistan. Anomaly is defined by a large dolomite-hosted magnesite deposit and was catalogued as an ultramafic-hosted talc occurrence (Orris and Bliss, 2002).

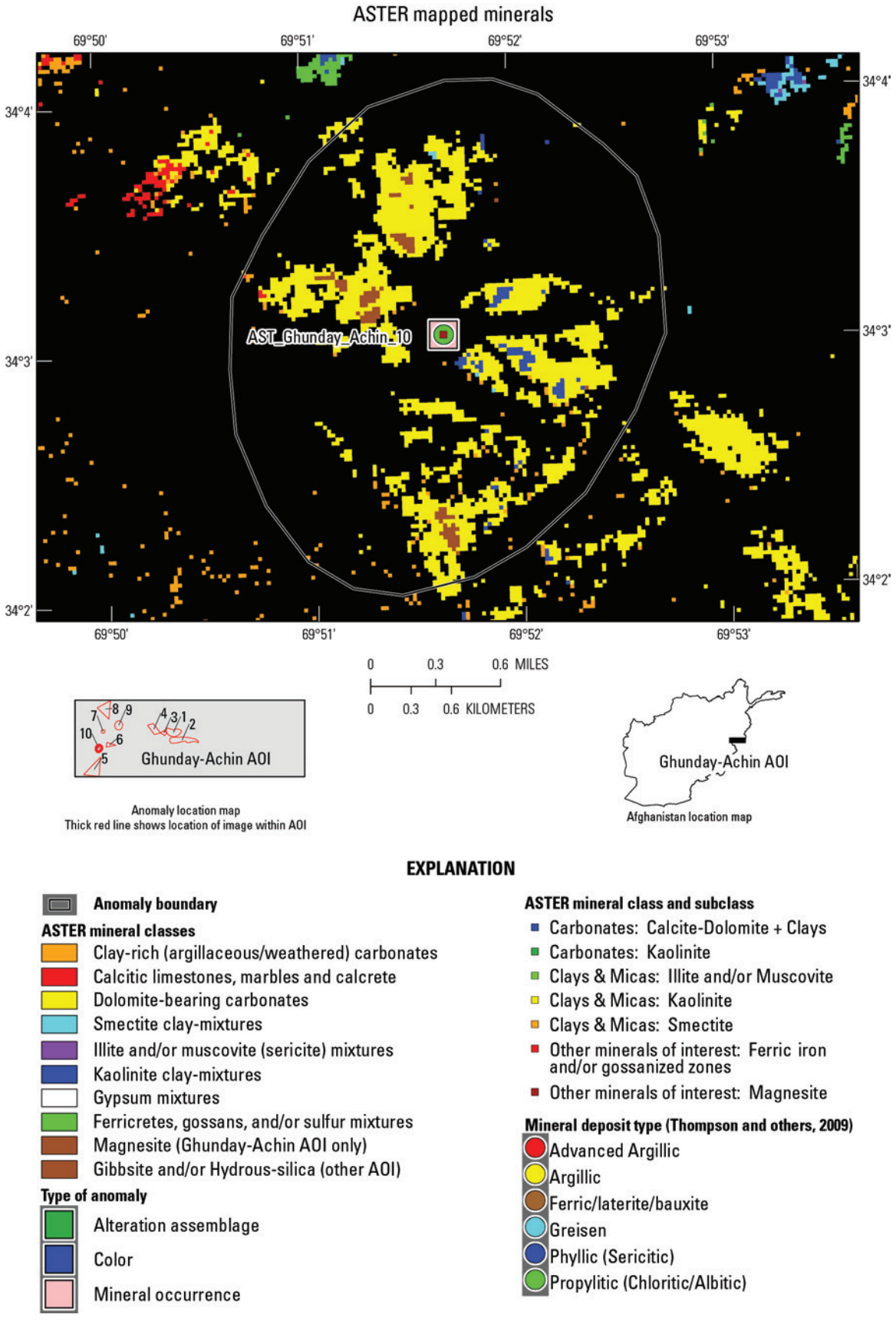

Figure 4.6.10. ASTER mineral occurrence anomaly located in the Ghunday-Achin Area of Interest (AOI) in Afghanistan. Anomaly is defined by smaller dolomite-hosted magnesite deposits.

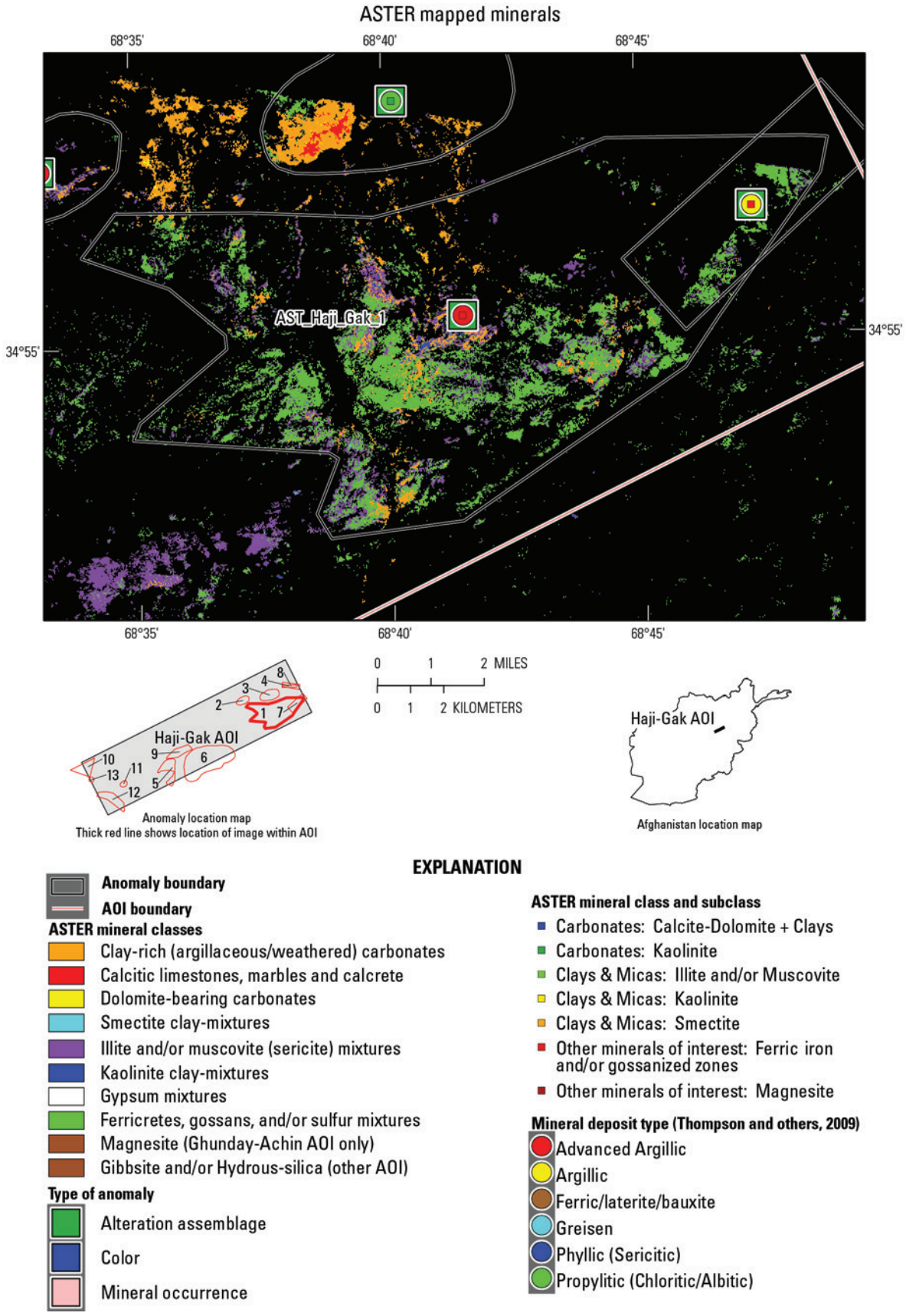

Figure 4.7.1. ASTER alteration anomaly located in the Haji-Gak Area of Interest (AOI) in Afghanistan. Anomaly is defined by kaolinite cores surrounded by illite/muscovite and carbonate mixtures with ferric iron most abundant.

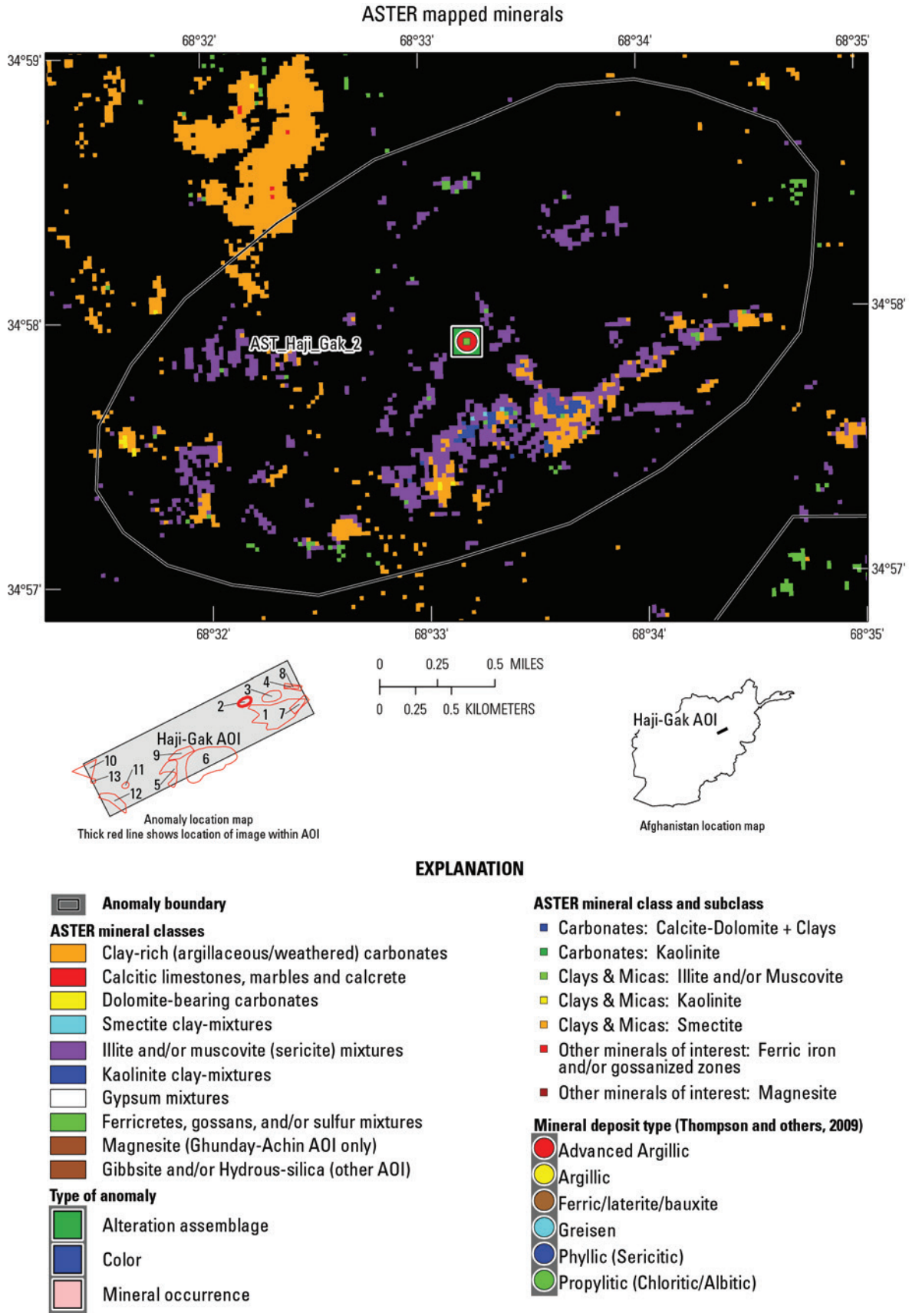

Figure 4.7.2. ASTER alteration anomaly located in the Haji-Gak Area of Interest (AOI) in Afghanistan. Anomaly is defined by kaolinite cores surrounded by illite/muscovite and carbonate mixtures with little or no ferric iron present.

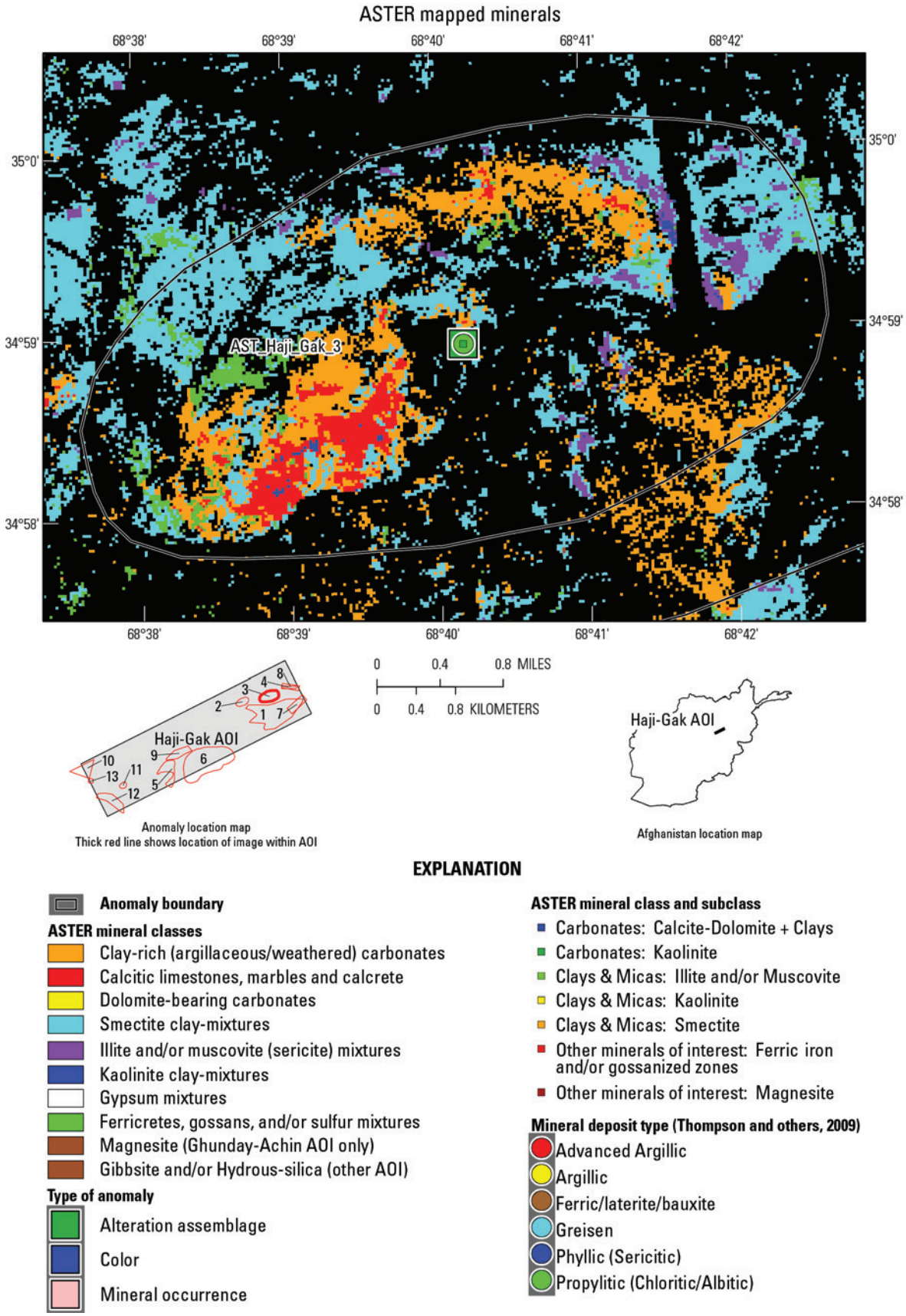

Figure 4.7.3. ASTER alteration anomaly located in the Haji-Gak Area of Interest (AOI) in Afghanistan. Anomaly is defined by small (less than 200 m) zones of kaolinite surrounded by larger circular patterns of argillaceous carbonates and illite/smectite clays.

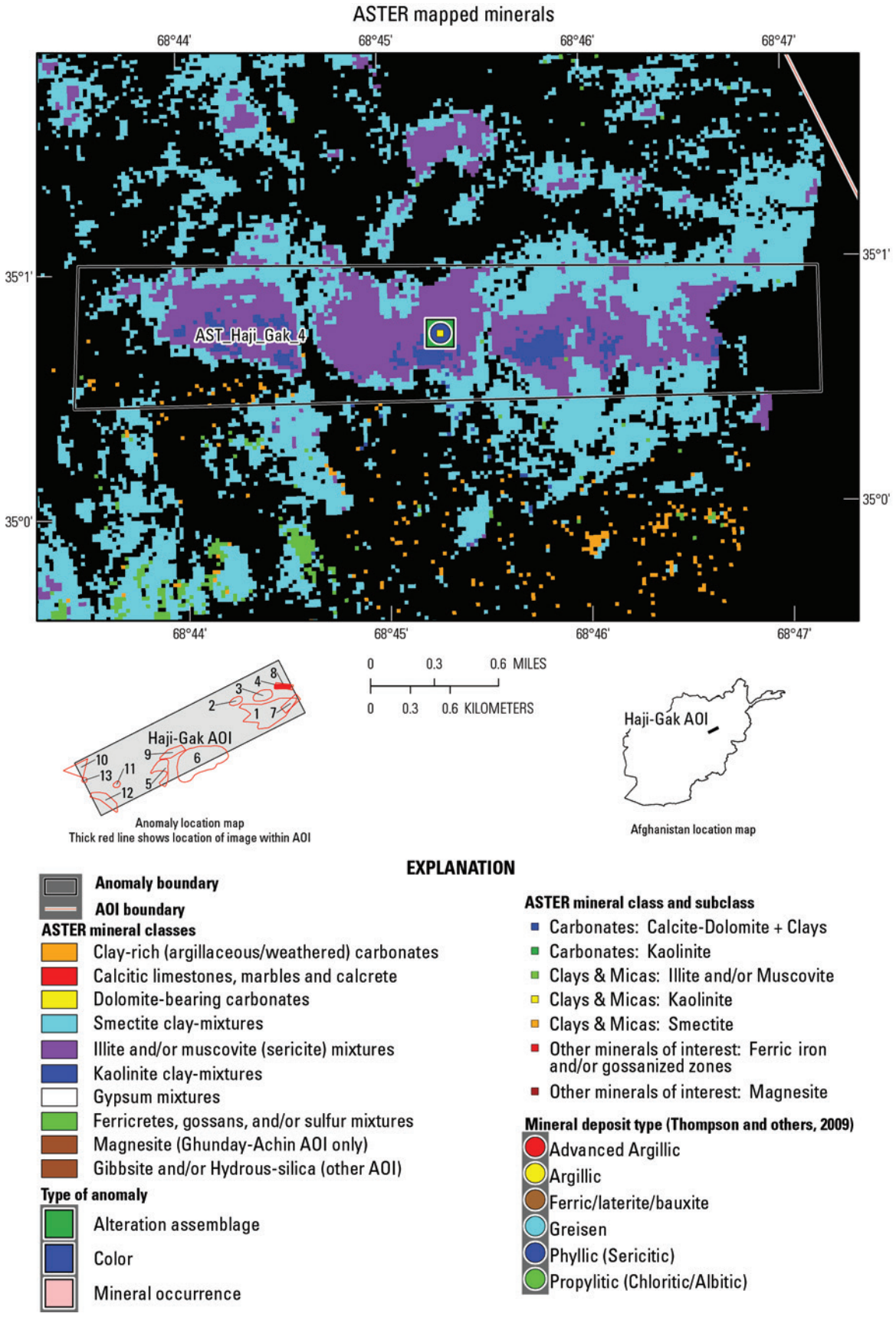

Figure 4.7.4. ASTER alteration anomaly located in the Haji-Gak Area of Interest (AOI) in Afghanistan. Anomaly is defined by linearly trending zones of illite and/or muscovite with embedded pixels dominated by kaolinite showing a possible epithermal or polymetallic vein.

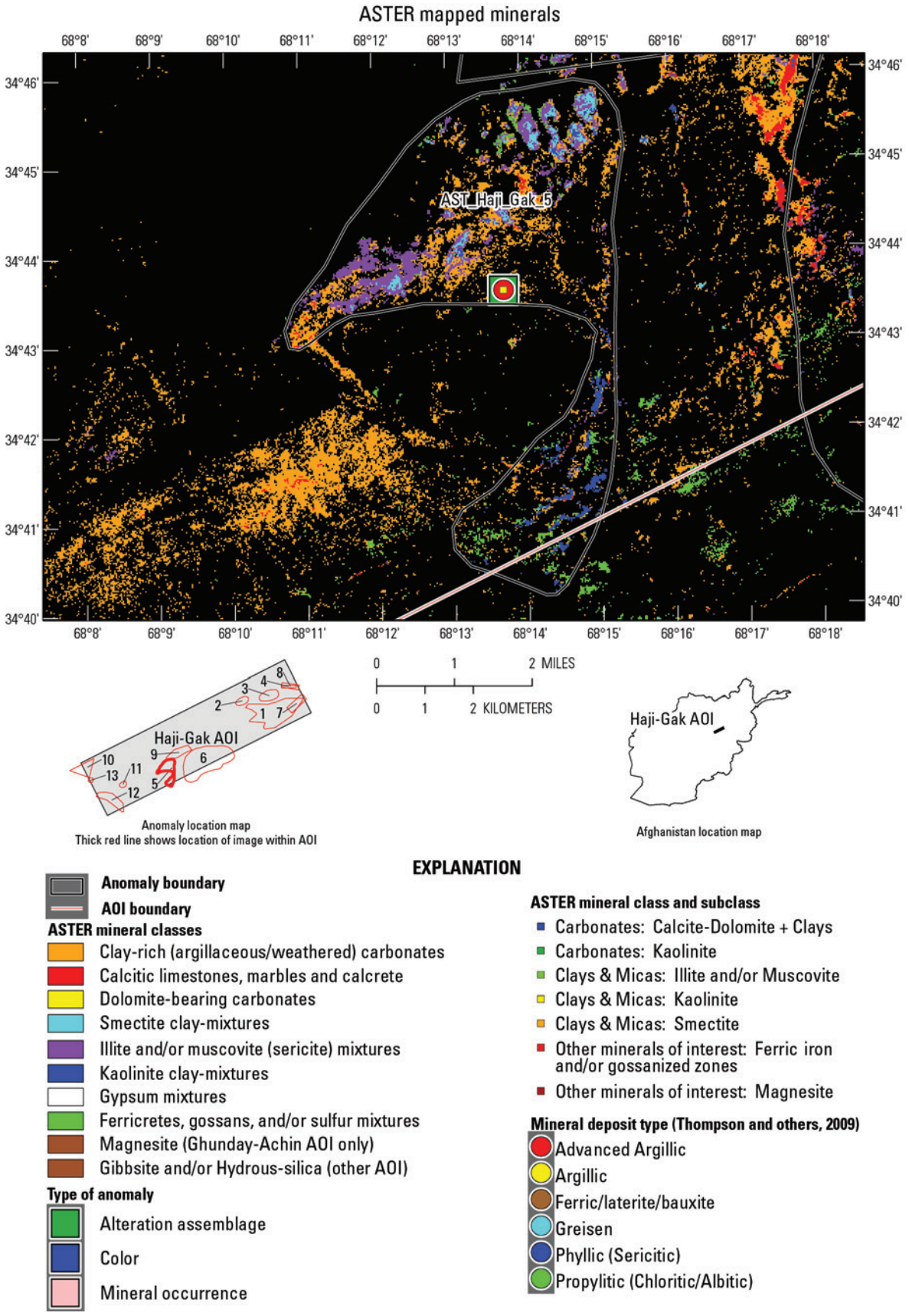

Figure 4.7.5. ASTER alteration anomaly located in the Haji-Gak Area of Interest (AOI) in Afghanistan. Anomaly is defined by eroded ridge-forming bedrock and downstream talus/alluvial deposits enriched in kaolinite and strong ferric iron.

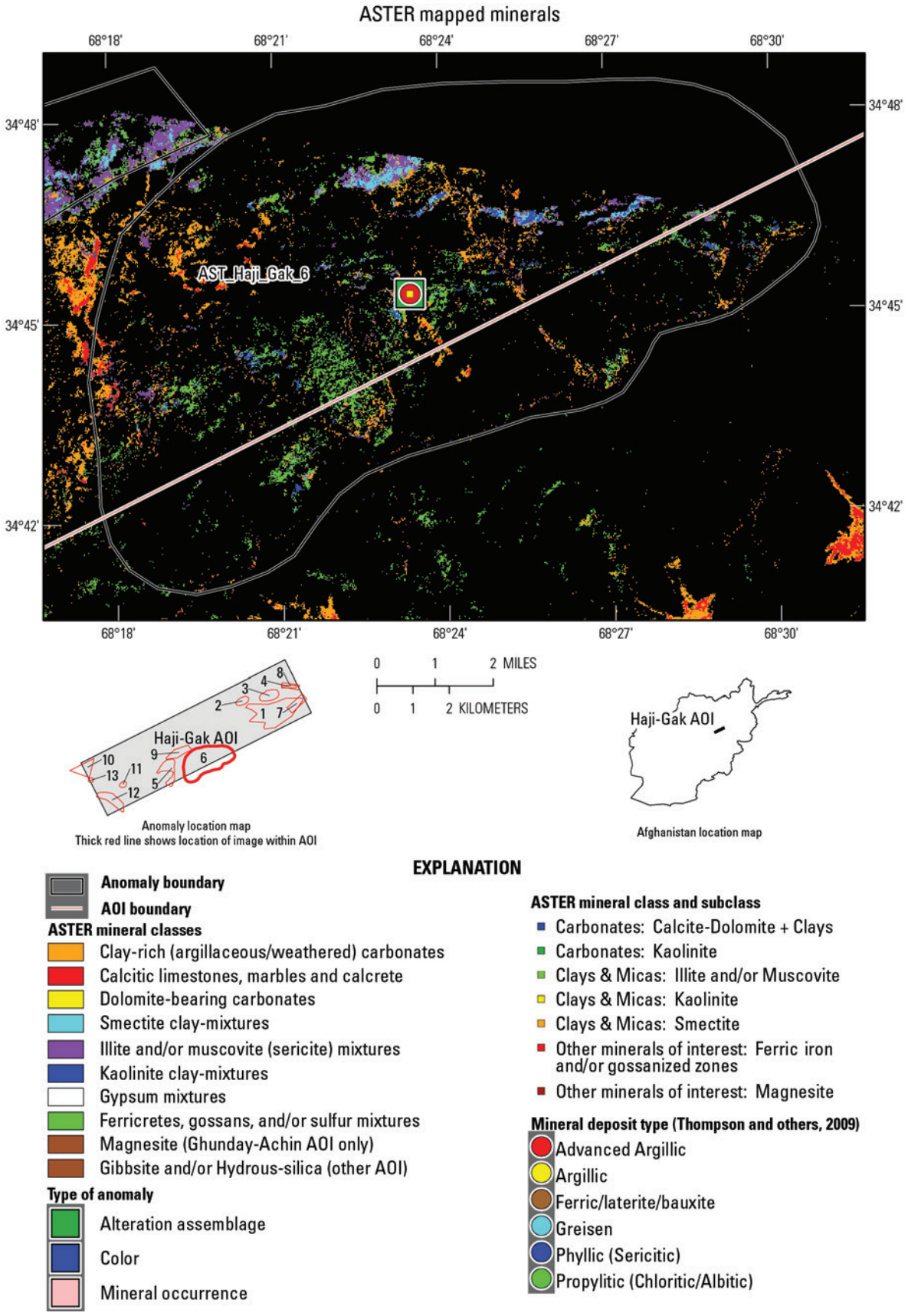

Figure 4.7.6. ASTER alteration anomaly located in the Haji-Gak Area of Interest (AOI) in Afghanistan. Anomaly is defined by eroded ridge-forming bedrock and downstream talus/alluvial deposits enriched in kaolinite and strong ferric iron.

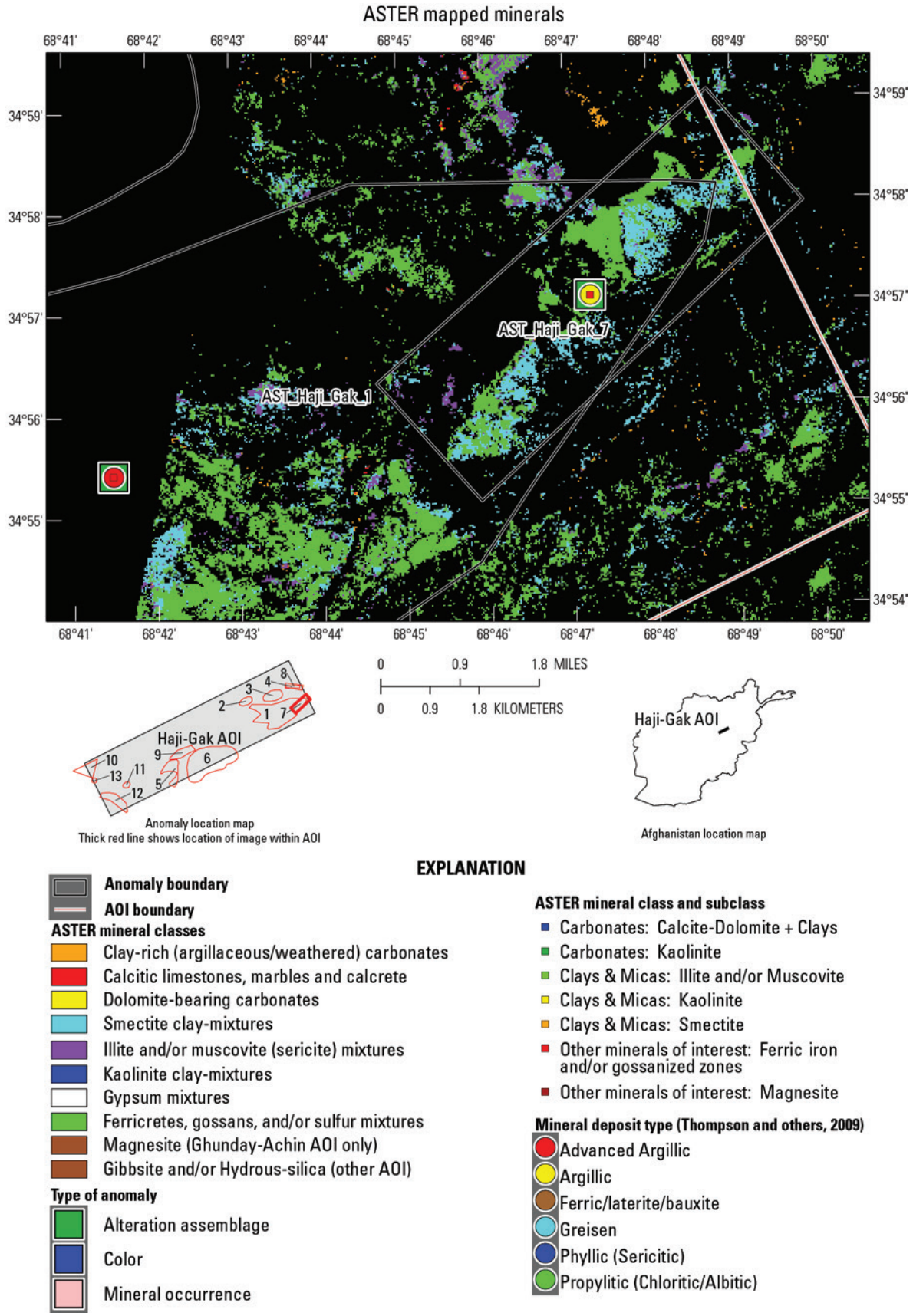

Figure 4.7.7. ASTER alteration anomaly located in the Haji-Gak Area of Interest (AOI) in Afghanistan. Anomaly is linearly controlled, dominated by smectite and ferric iron, and overlaps eastern extent of anomaly AST_Haji_Gak_1.

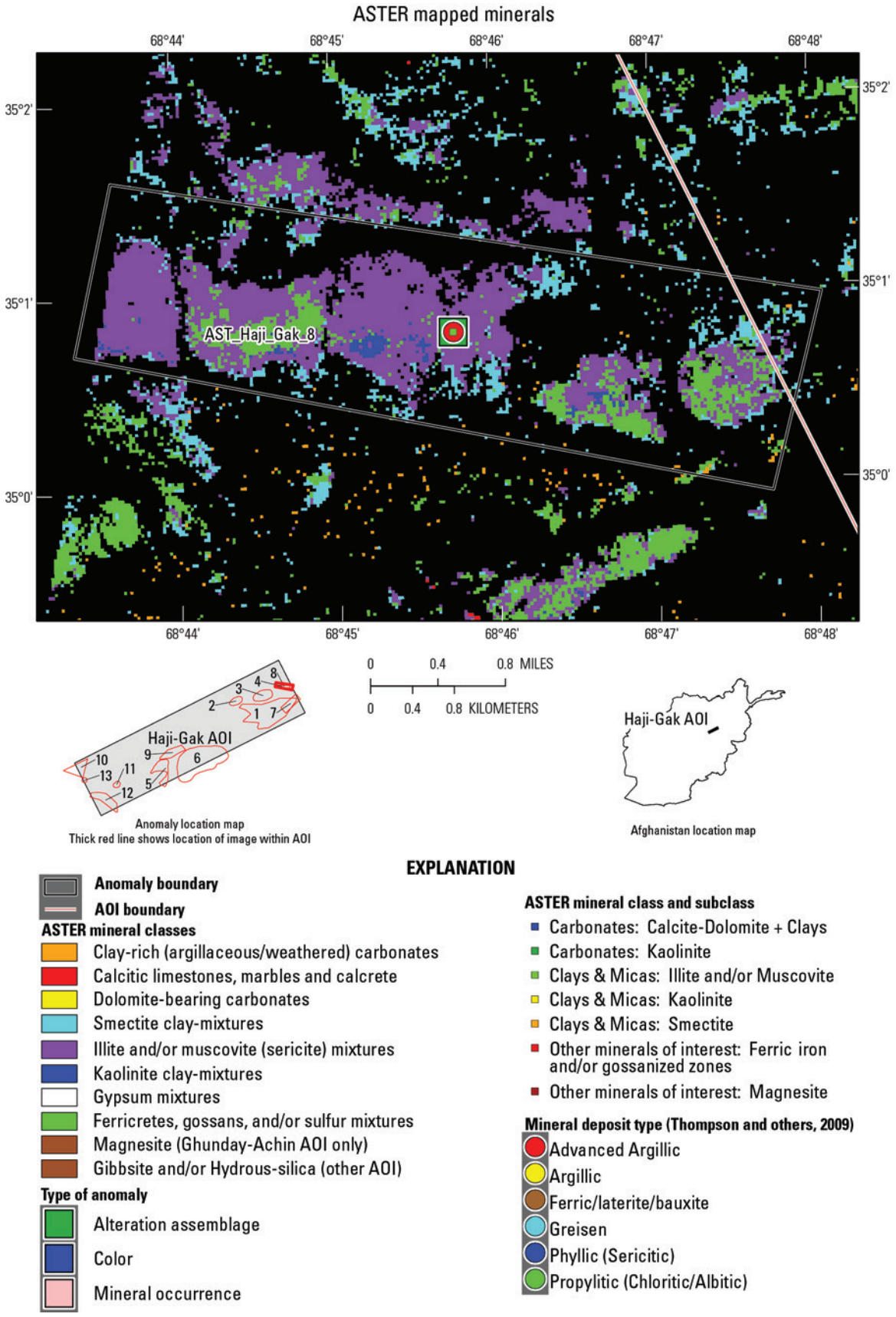

Figure 4.7.8. ASTER alteration anomaly located in the Haji-Gak Area of Interest (AOI) in Afghanistan. Anomaly is defined by kaolinite cores surrounded by illite/muscovite with strong ferric iron signatures. Anomaly is linearly trending and shares a similar extent with another anomaly, AST_Haji_Gak_4.

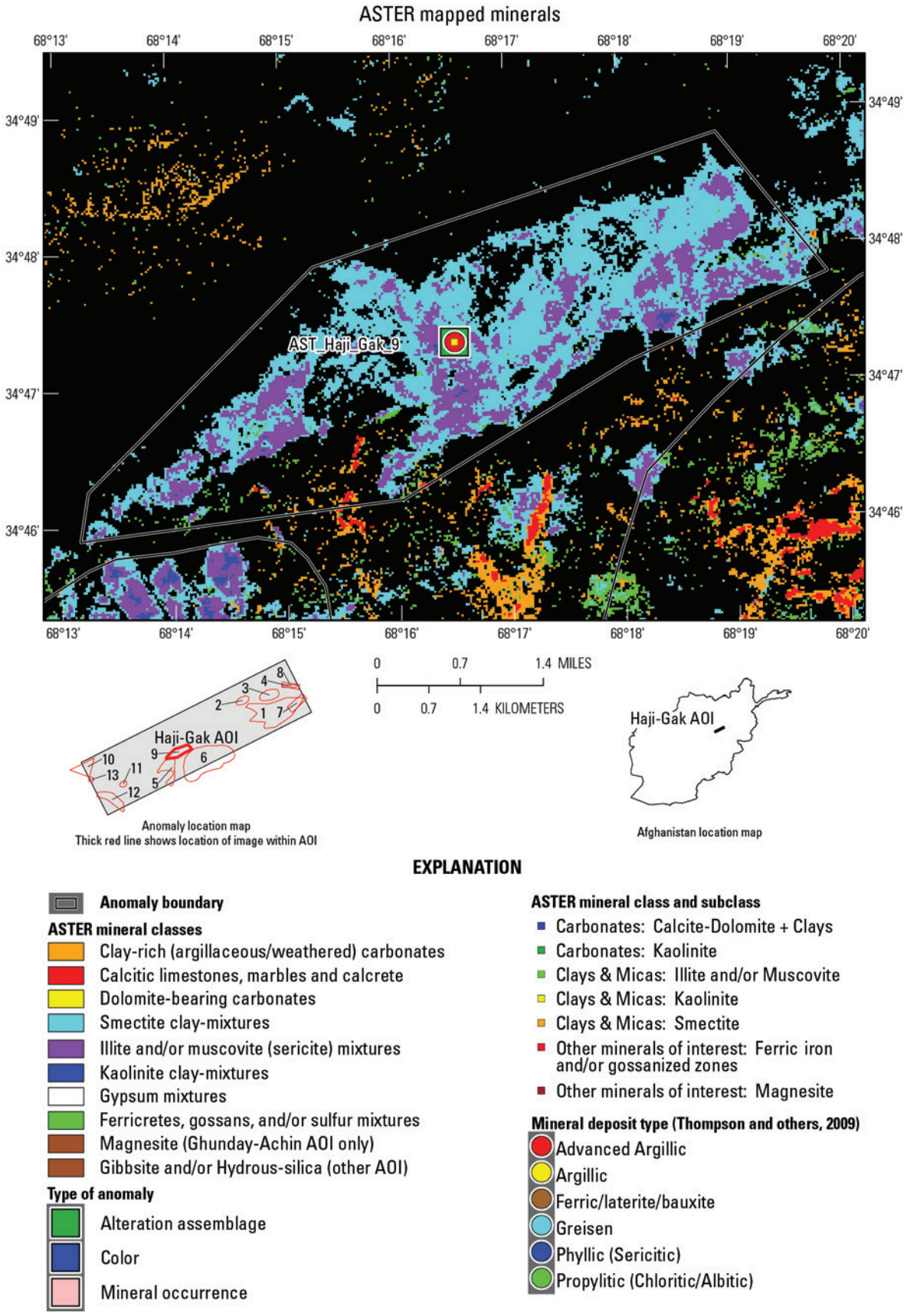

Figure 4.7.9. ASTER alteration anomaly located in the Haji-Gak Area of Interest (AOI) in Afghanistan. Anomaly is defined by ridge-forming bedrock, locally enriched with kaolinite, and strong ferric iron with illite/muscovite/smectite all dominant.

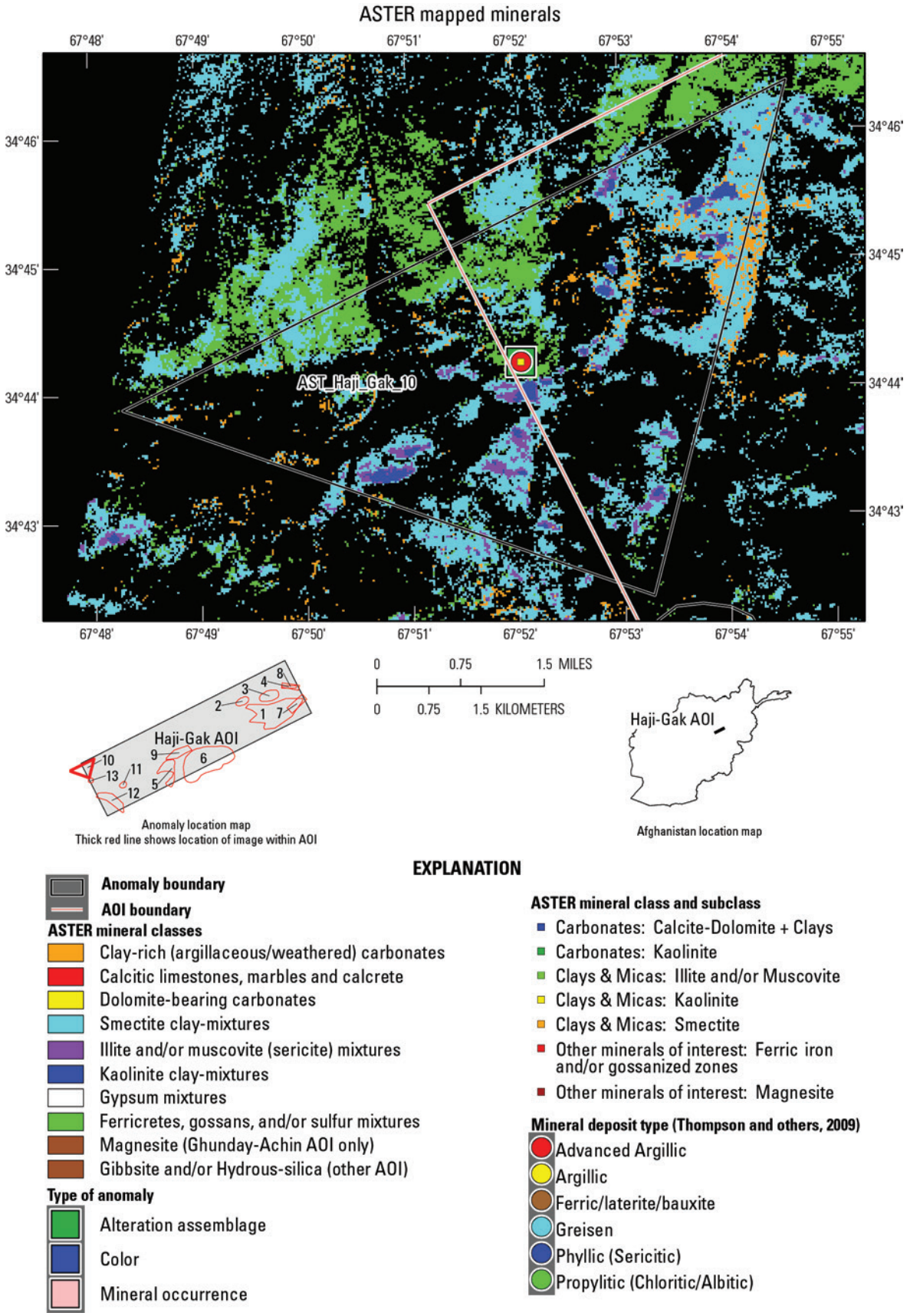

Figure 4.7.10. ASTER alteration anomaly located in the Haji-Gak Area of Interest (AOI) in Afghanistan. Anomaly is defined by localized kaolinite- and sericite-bearing zones within a massive complex dominated by smectite and strong ferric iron alteration.

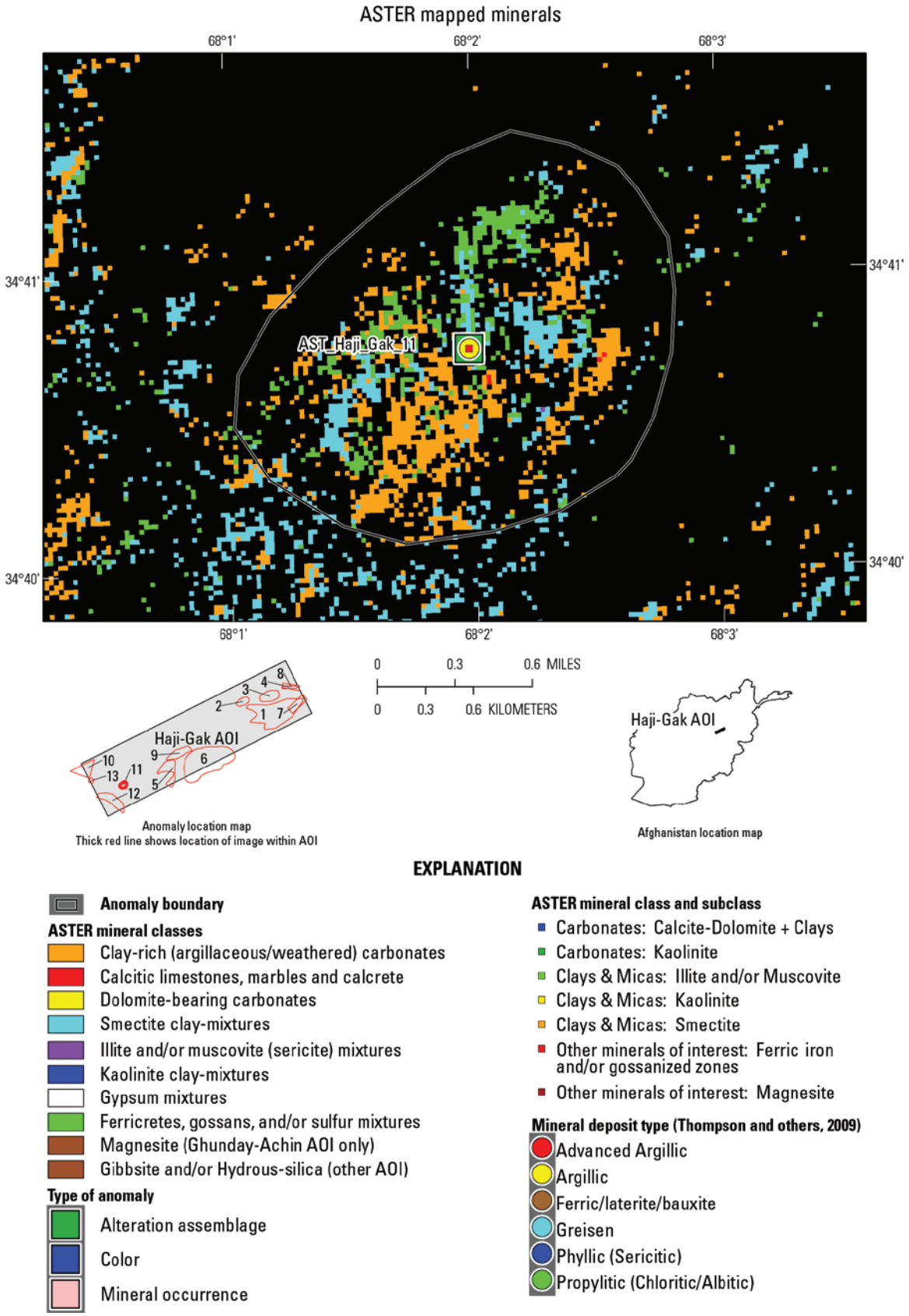

Figure 4.7.11. ASTER alteration anomaly located in the Haji-Gak Area of Interest (AOI) in Afghanistan. Anomaly is a potential volcanic-hosted massive sulfide zone defined by strong ferric iron and smectite forming a circular zone with clay-carbonate mixtures within greenschist facies metavolcanic rocks (Doebrich and Wahl, 2006).

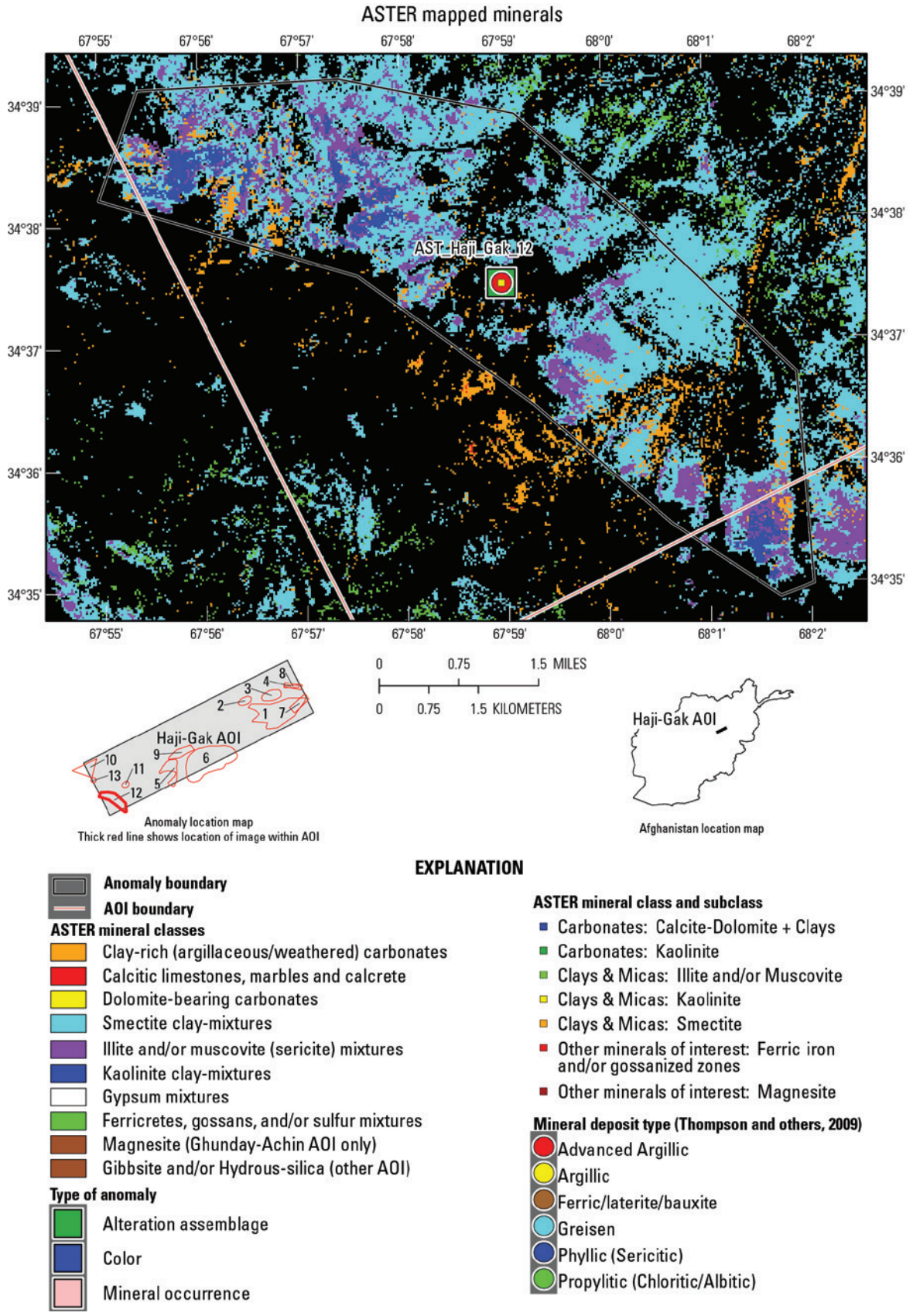

Figure 4.7.12. ASTER alteration anomaly located in the Haji-Gak Area of Interest (AOI) in Afghanistan. Anomaly is defined by abundant argillic cores (kaolinite-bearing) surrounded by argillic and phyllic zones in areas mapped as predominantly Oligocene age granite intrusive rocks (Doebrich and Wahl, 2006).

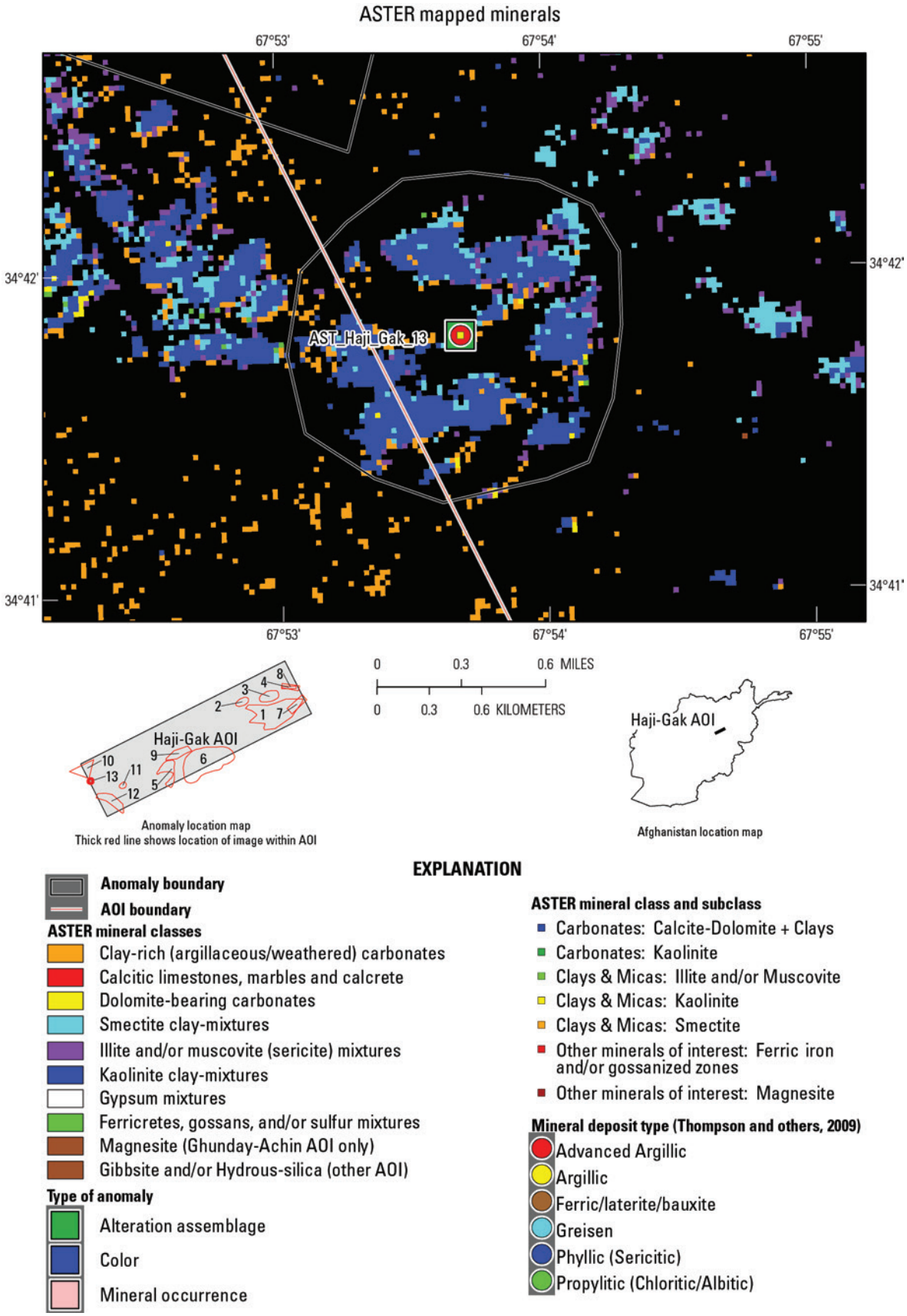

Figure 4.7.13. ASTER alteration anomaly located in the Haji-Gak Area of Interest (AOI) in Afghanistan. Anomaly is a kaolinite-dominated alteration zone.

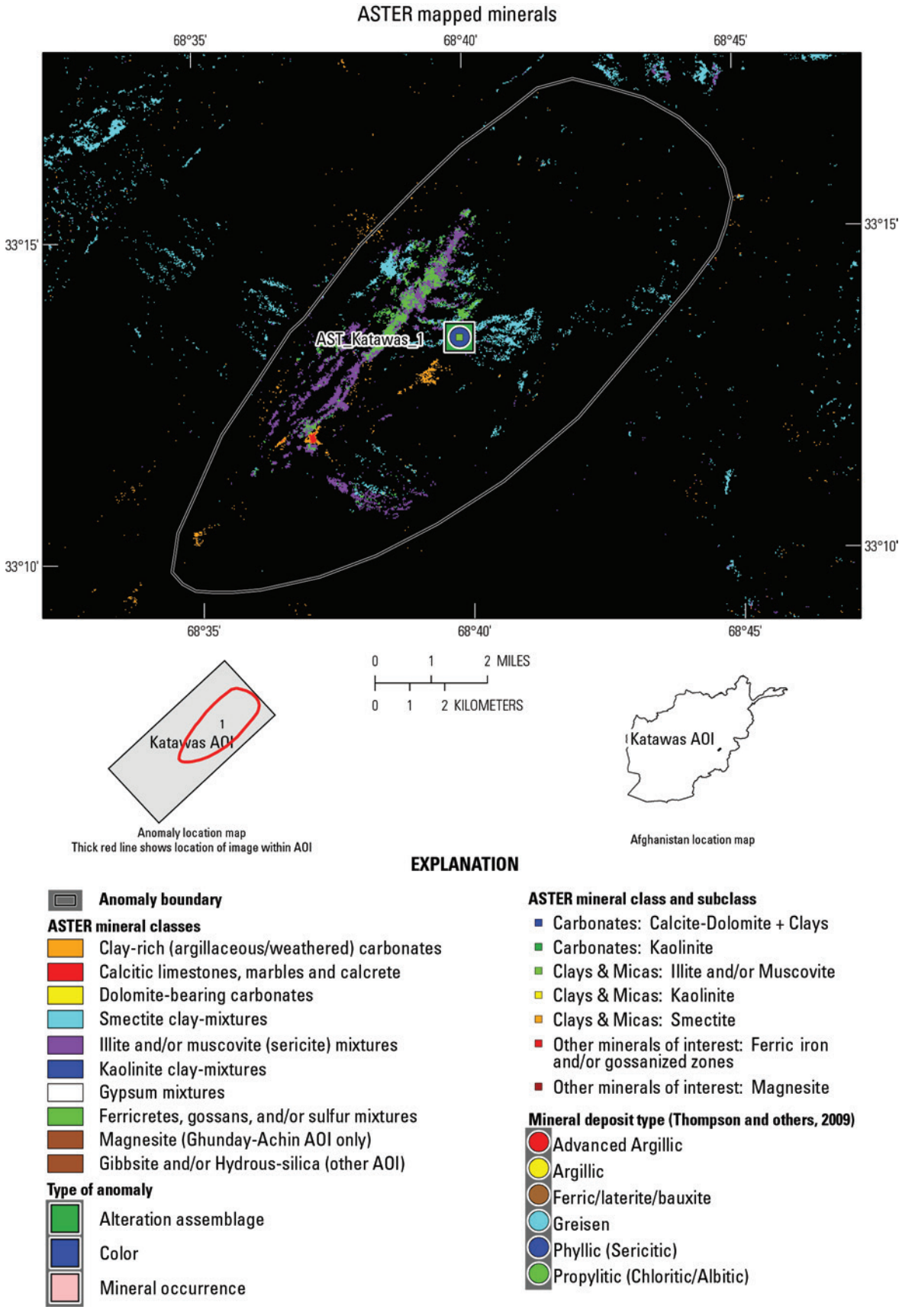

Figure 4.8.1. ASTER alteration anomaly located in the Katawas Area of Interest (AOI) in Afghanistan. Linear splay along the Chaman fault zone with possible epithermal gold and mercury based on stream-geochemistry-anomalies data.

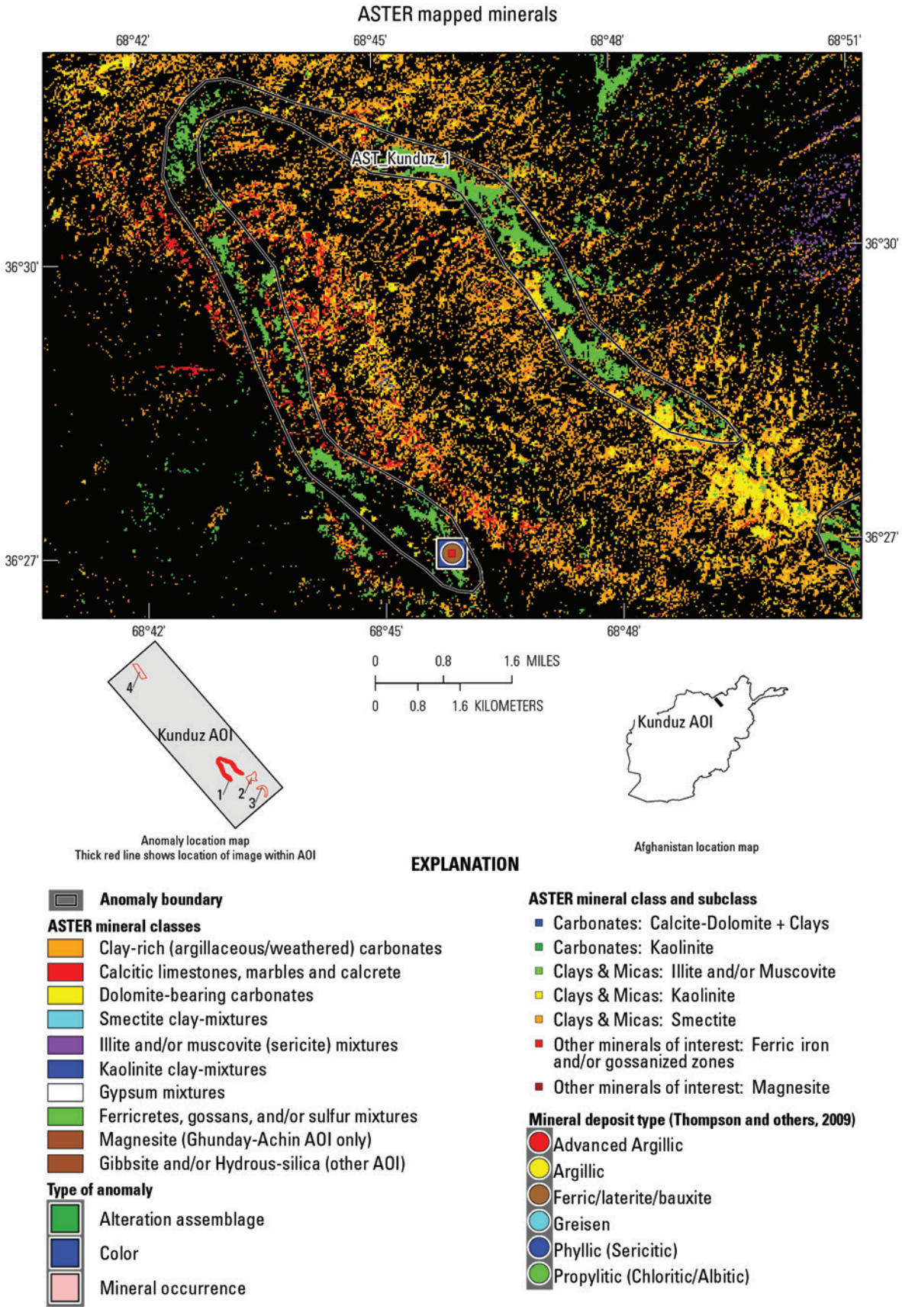

Figure 4.9.1. ASTER color anomaly located in the Kunduz Area of Interest (AOI) in Afghanistan. Possible sulfur- and/or phosphate-bearing area in tightly folded dolomitic rocks with downstream alluvium. Further spectral analysis needed to distinguish sulfur from strong ferric iron.

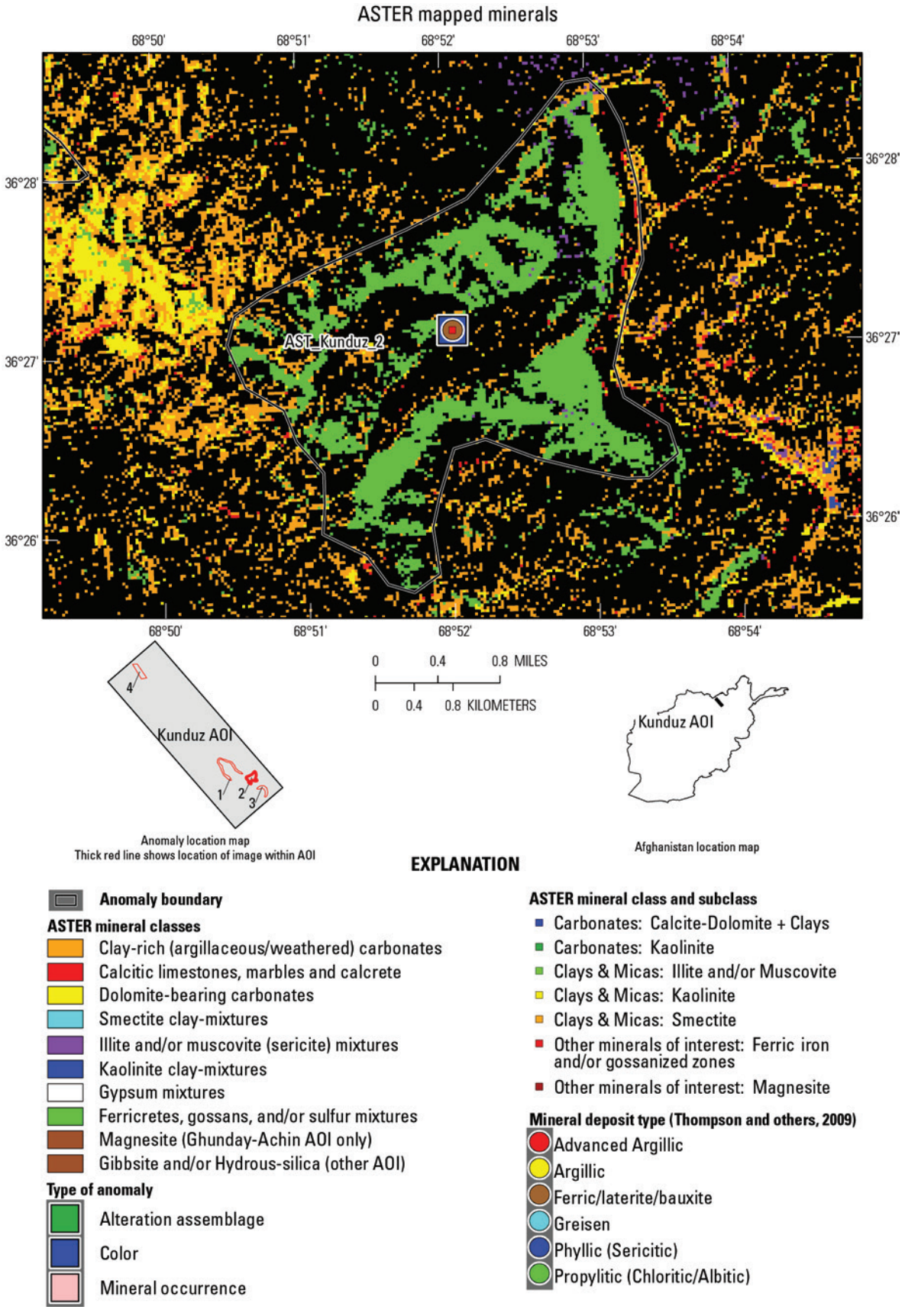

Figure 4.9.2. ASTER color anomaly located in the Kunduz Area of Interest (AOI) in Afghanistan. Possible sulfur- and/or phosphate-bearing area in tightly folded dolomitic rocks. Further spectral analysis needed to distinguish sulfur from strong ferric iron.

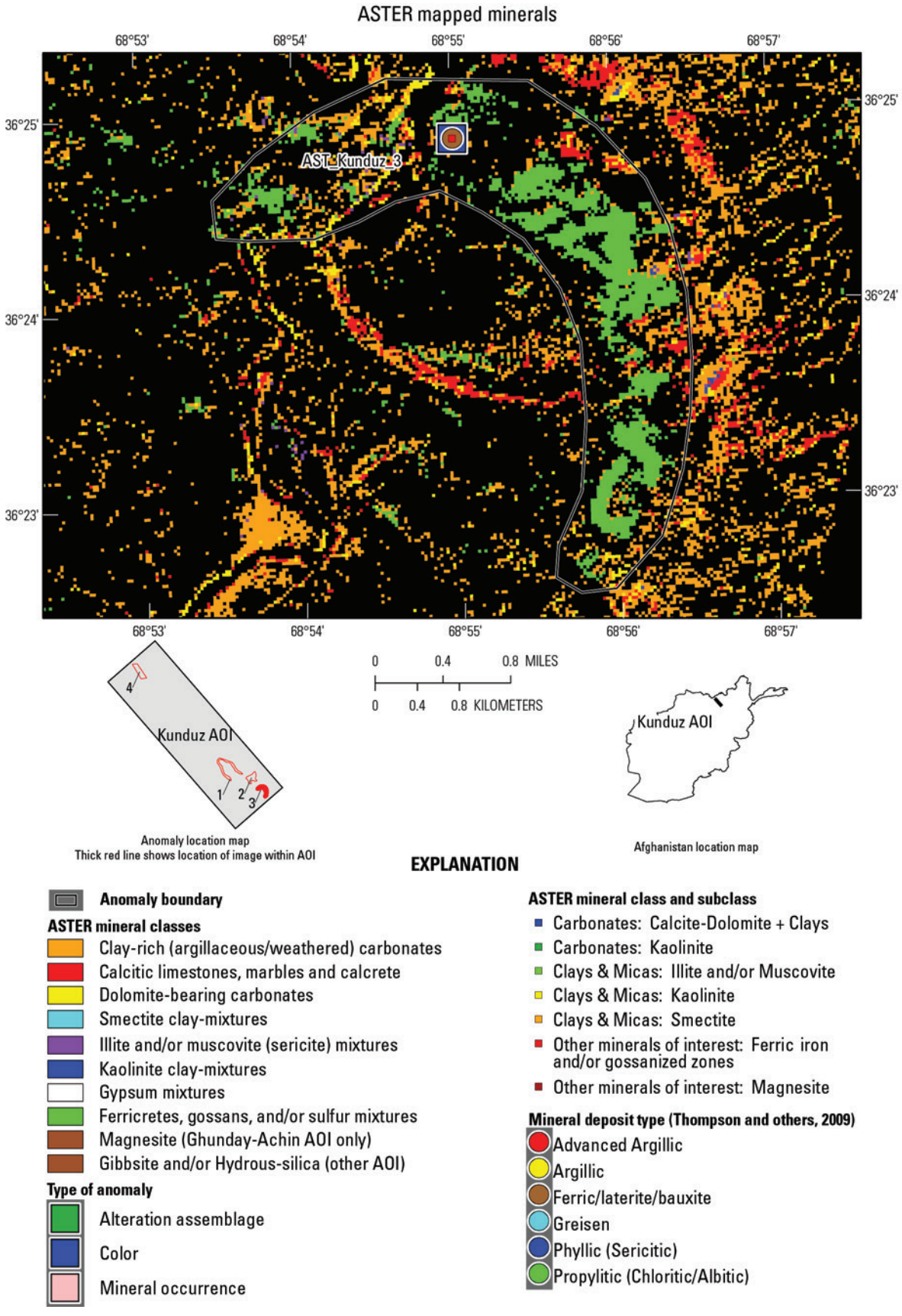

Figure 4.9.3. ASTER color anomaly located in the Kunduz Area of Interest (AOI) in Afghanistan. Possible sulfur- and/or phosphate-bearing area in tightly folded dolomitic-rocks. Further spectral analysis needed to distinguish sulfur from strong ferric iron.

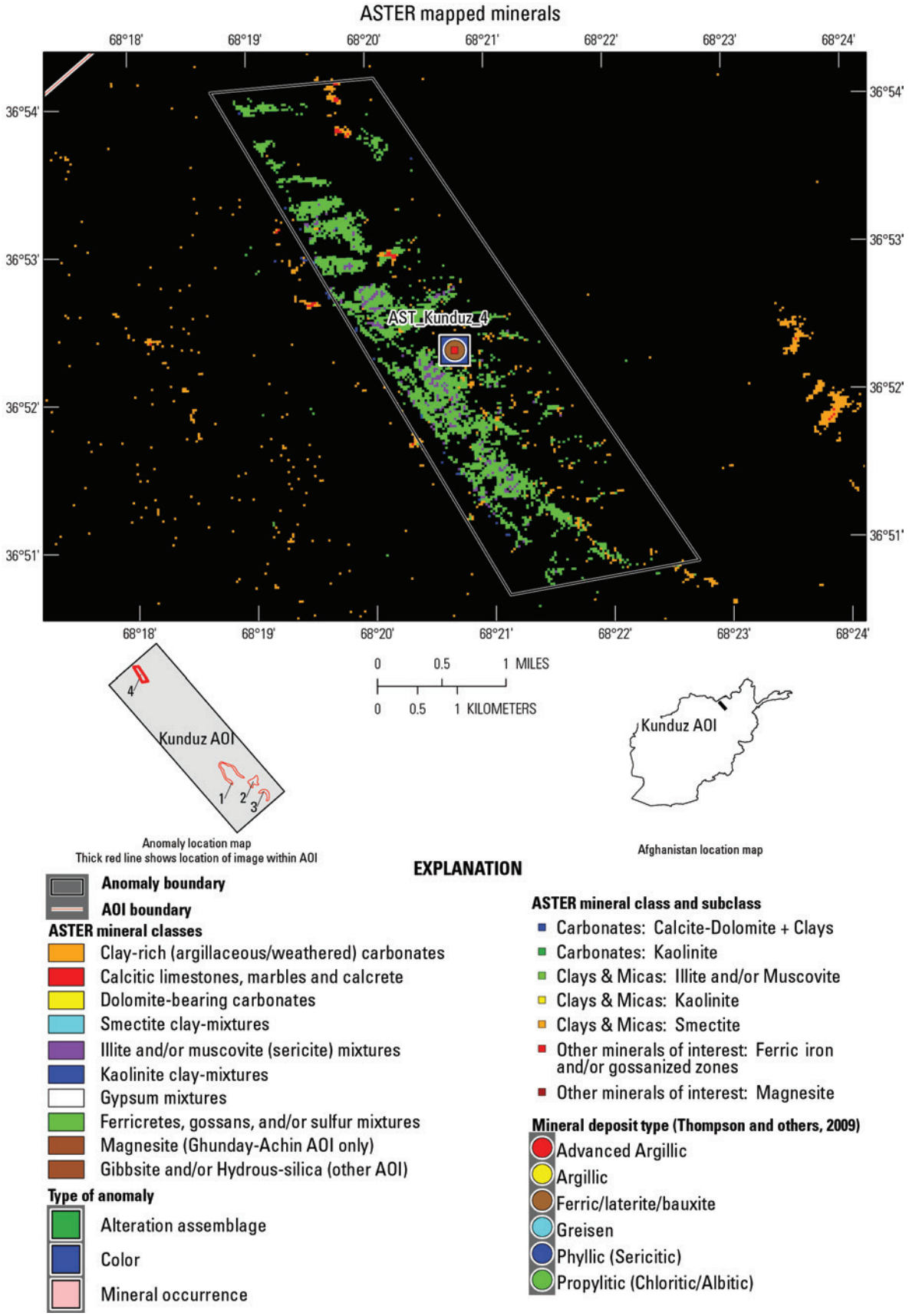

Figure 4.9.4. ASTER color anomaly located in the Kunduz Area of Interest (AOI) in Afghanistan. Possible sulfur- and/or phosphate-bearing area within argillaceous/dolomitic carbonates. Further spectral analysis needed to distinguish sulfur from strong ferric iron.

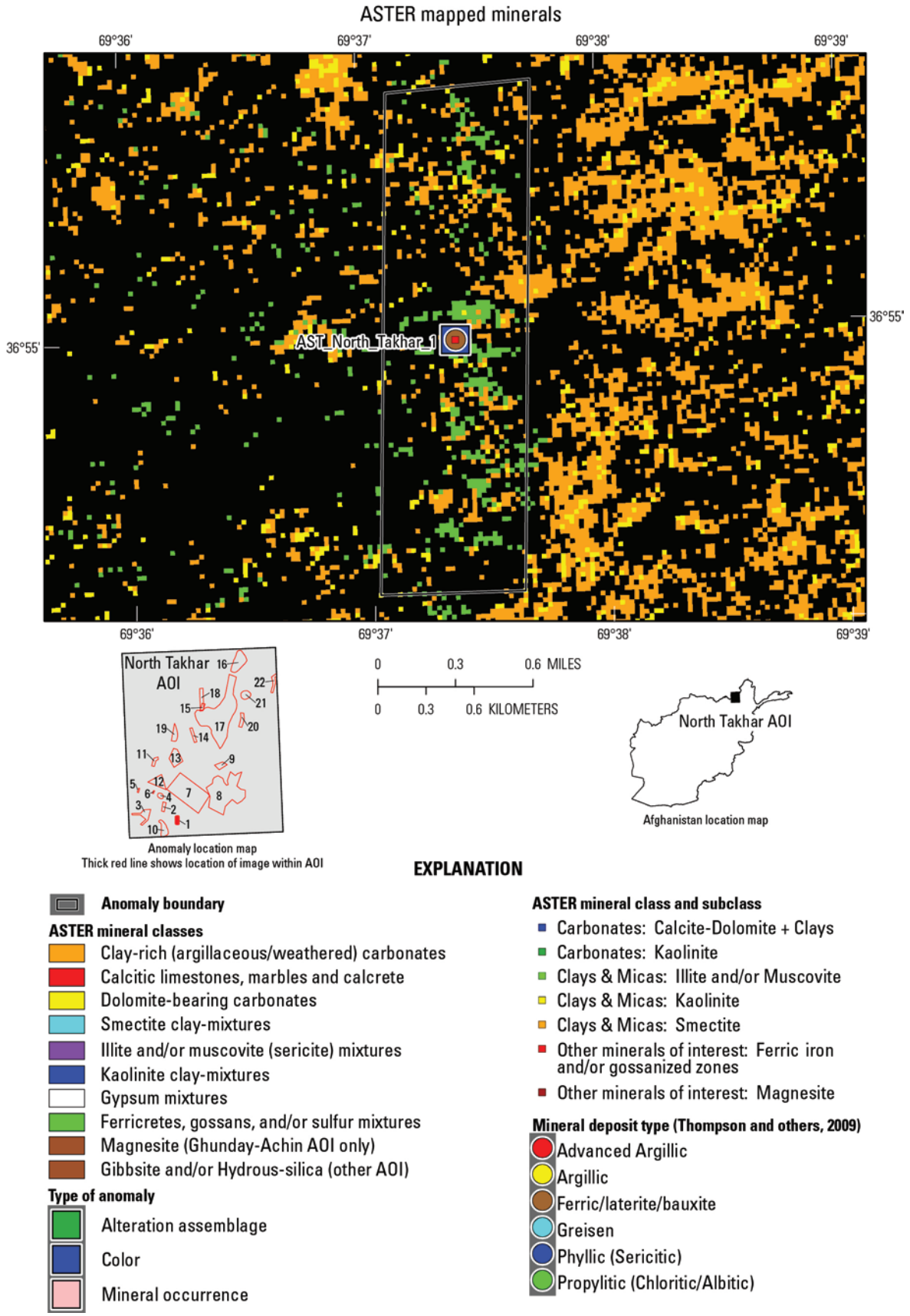

Figure 4.10.1. ASTER color anomaly located in the North Takhar Area of Interest (AOI) in Afghanistan. Possible sulfur- and/or phosphate-bearing area hosted within weathered dolomitic carbonates. Further spectral analysis needed to distinguish sulfur from strong ferric iron.

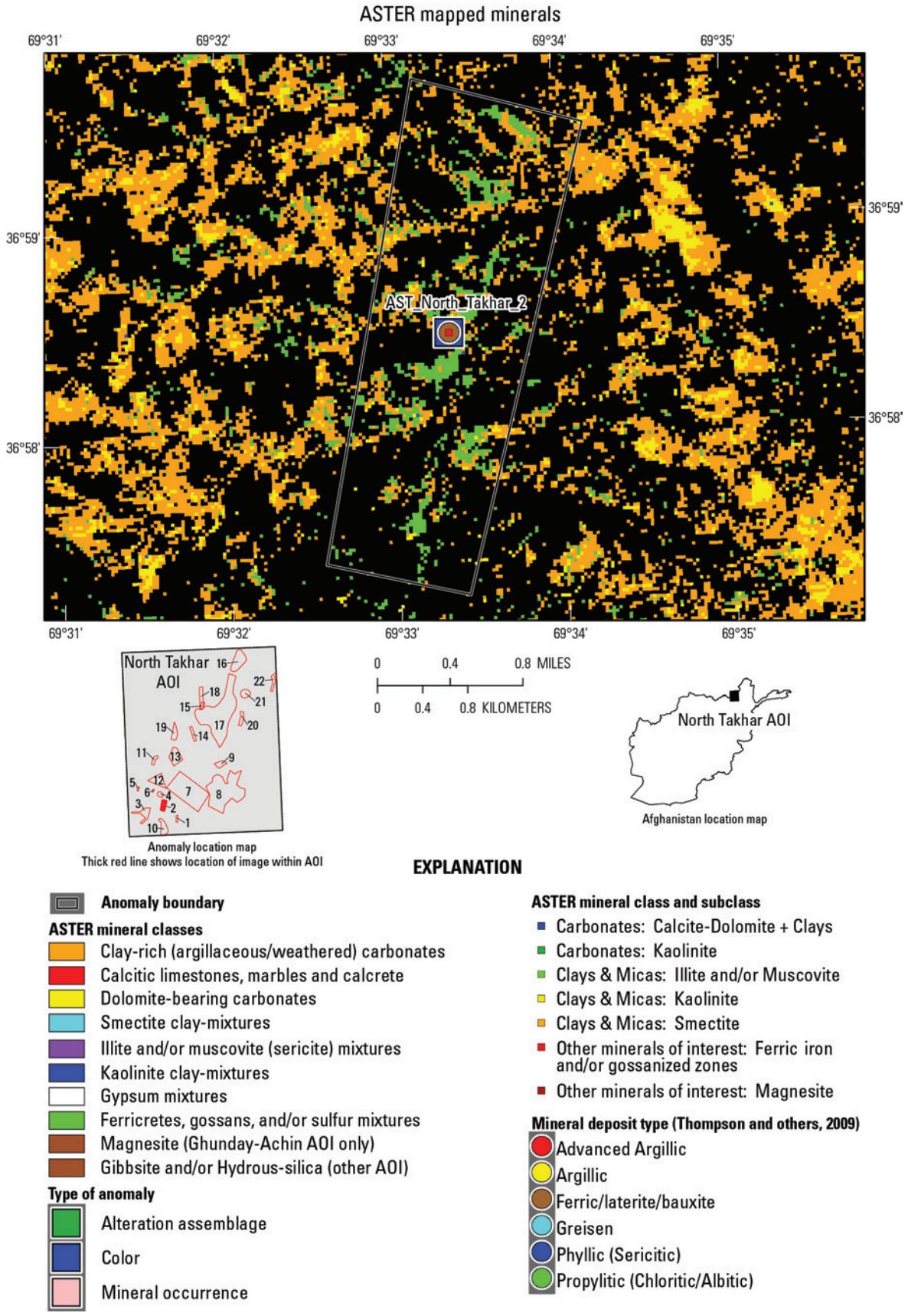

Figure 4.10.2. ASTER color anomaly located in the North Takhar Area of Interest (AOI) in Afghanistan. Possible sulfur- and/or phosphate-bearing area hosted within weathered dolomitic carbonates. Further spectral analysis needed to distinguish sulfur from strong ferric iron.

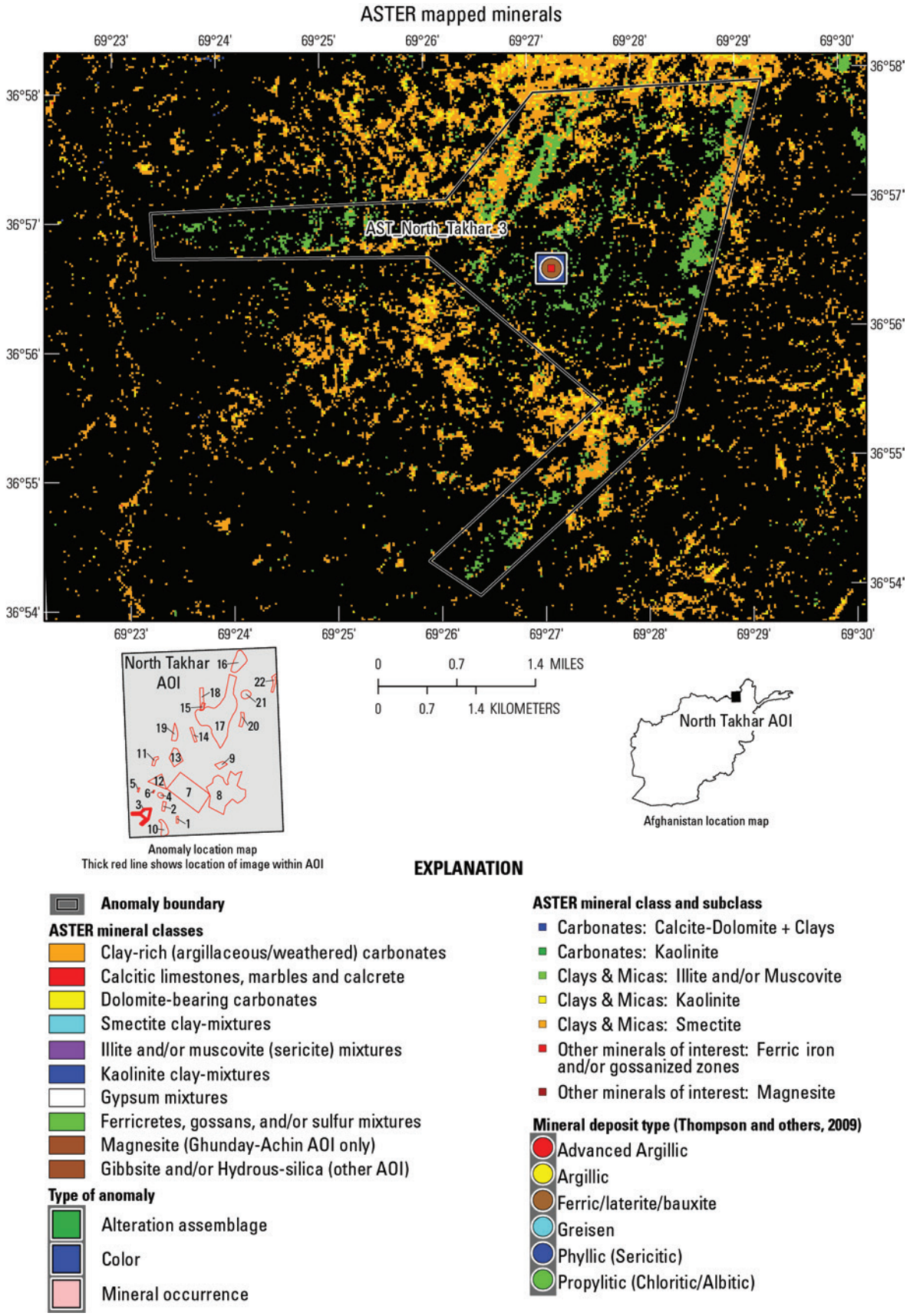

Figure 4.10.3. ASTER color anomaly located in the North Takhar Area of Interest (AOI) in Afghanistan. Possible sulfur- and/or phosphate-bearing area hosted within weathered dolomitic carbonates. Further spectral analysis needed to distinguish sulfur from strong ferric iron.

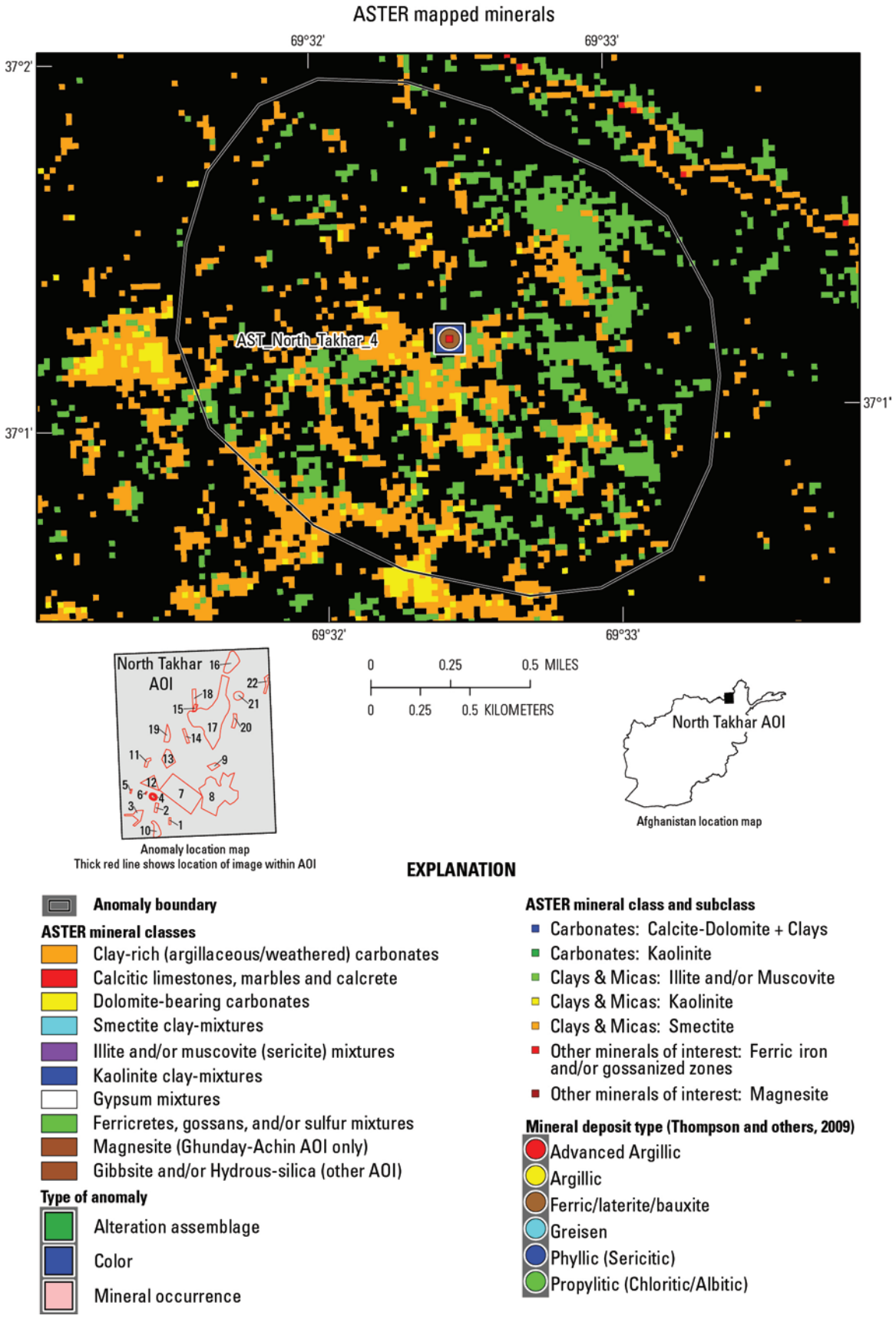

Figure 4.10.4. ASTER color anomaly located in the North Takhar Area of Interest (AOI) in Afghanistan. Possible sulfur- and/or phosphate-bearing area hosted within weathered dolomitic carbonates. Further spectral analysis needed to distinguish sulfur from strong ferric iron.

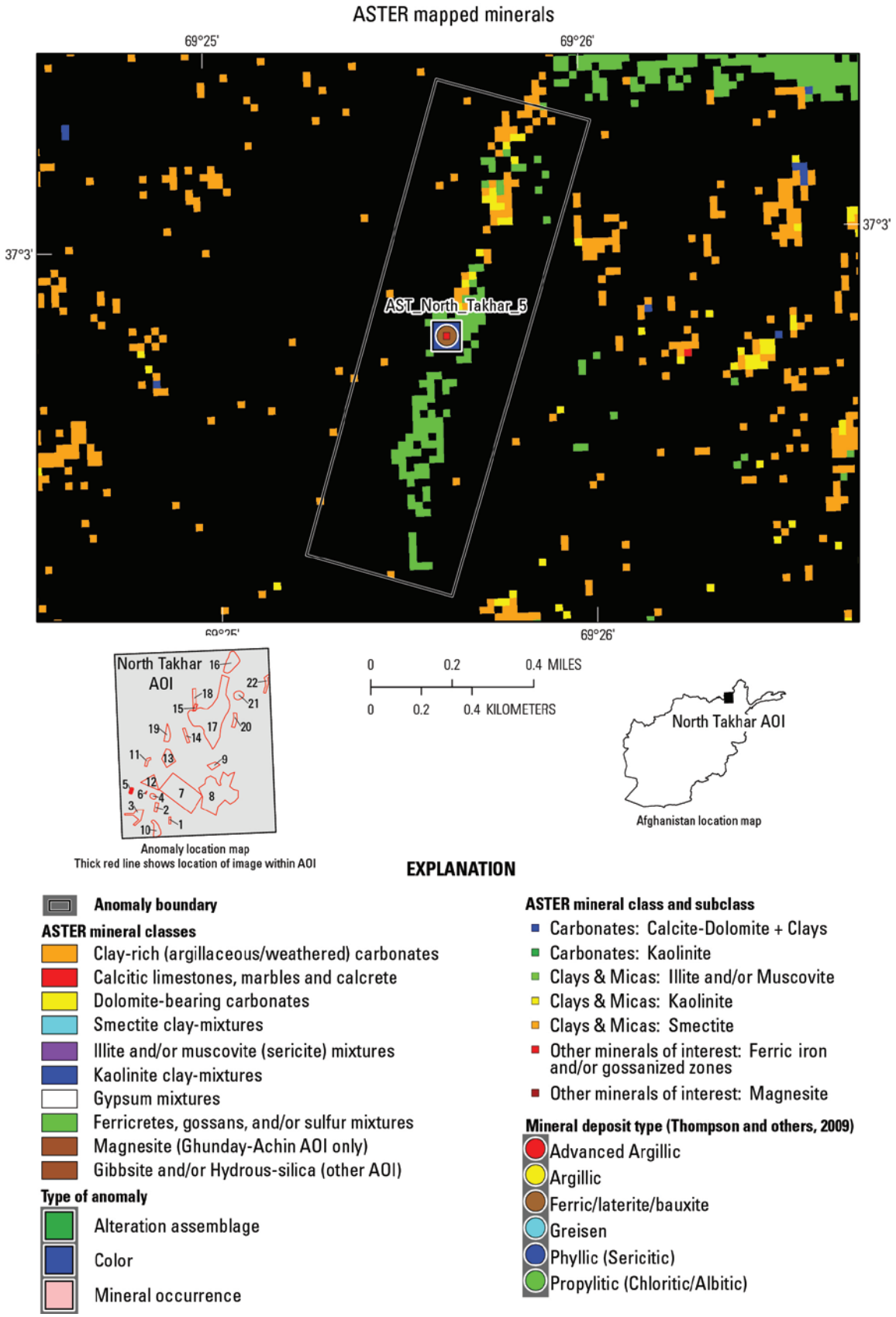

Figure 4.10.5. ASTER color anomaly located in the North Takhar Area of Interest (AOI) in Afghanistan. Possible sulfur- and/or phosphate-bearing area hosted within weathered dolomitic carbonates, excluding downstream alluvial fan areas. Further spectral analysis is needed to distinguish sulfur from strong ferric iron.

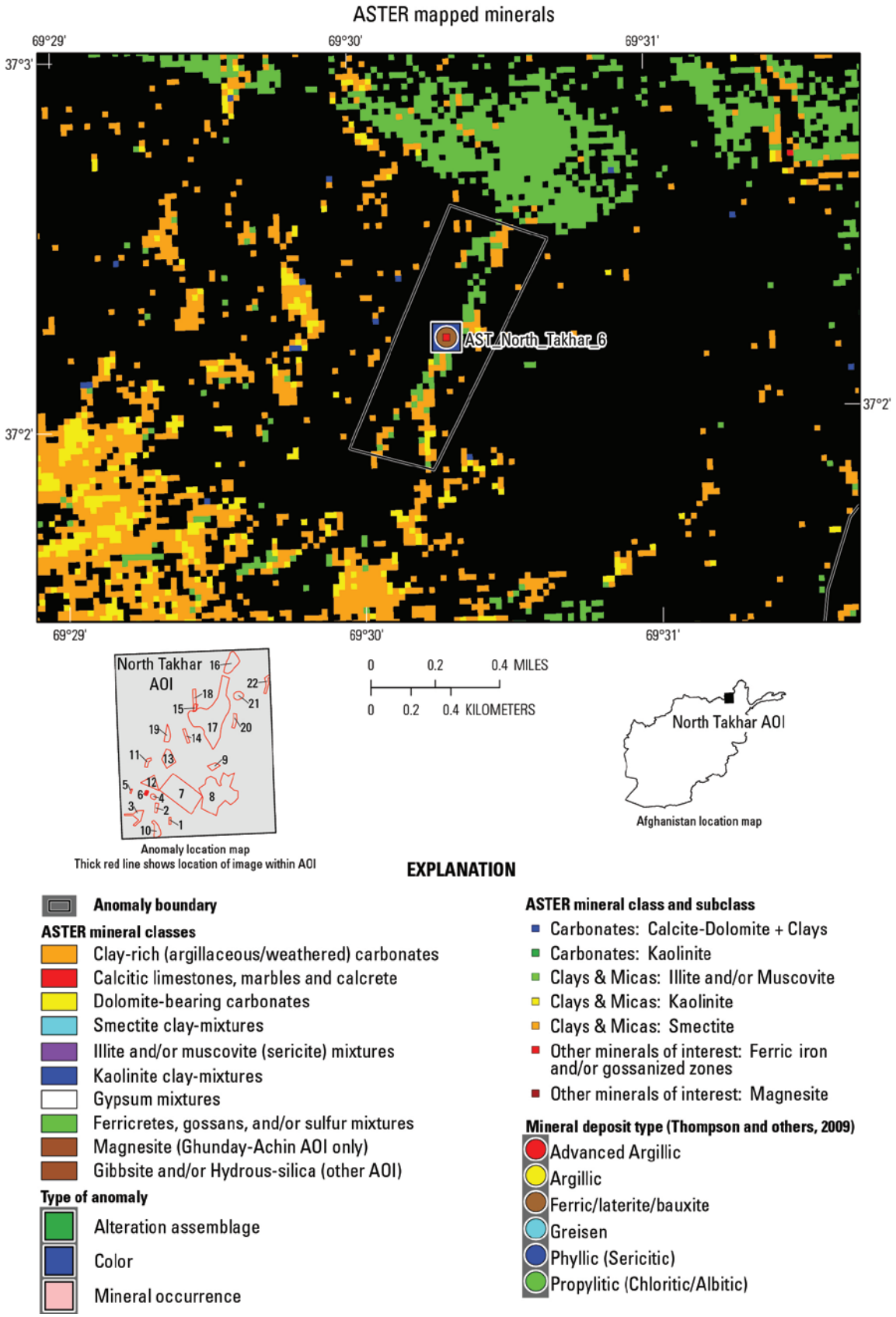

Figure 4.10.6. ASTER color anomaly located in the North Takhar Area of Interest (AOI) in Afghanistan. Possible sulfur- and/or phosphate-bearing area hosted within weathered dolomitic carbonates, excluding downstream alluvial fan areas. Further spectral analysis is needed to distinguish sulfur from strong ferric iron.

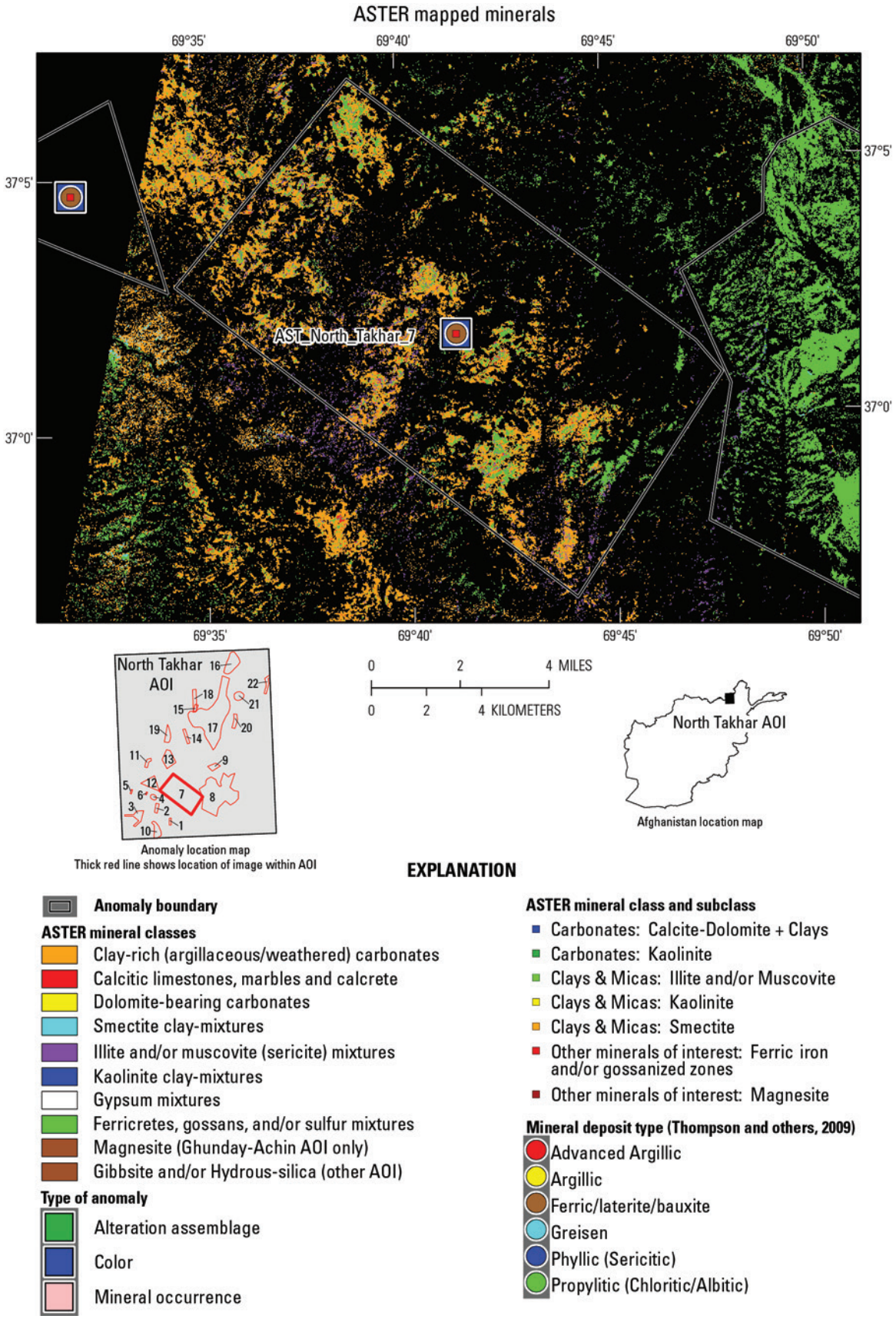

Figure 4.10.7. ASTER color anomaly located in the North Takhar Area of Interest (AOI) in Afghanistan. Extensive areas of ferricrete-bearing bedrock, excluding alluvial areas related to placer sulfide weathering.

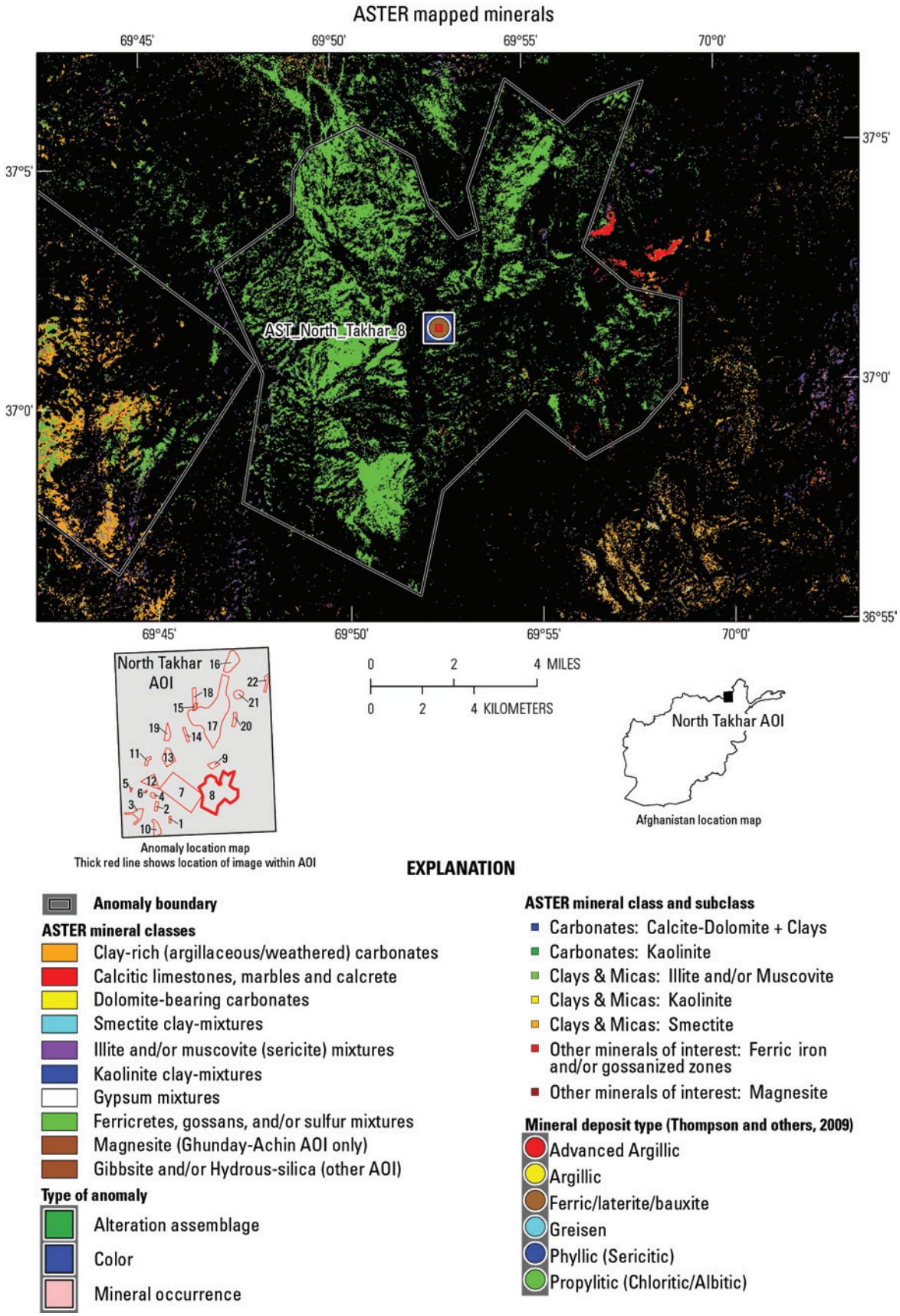

Figure 4.10.8. ASTER color anomaly located in the North Takhar Area of Interest (AOI) in Afghanistan. Extensive areas of ferricrete-bearing bedrock, excluding alluvial areas related to placer sulfide weathering.

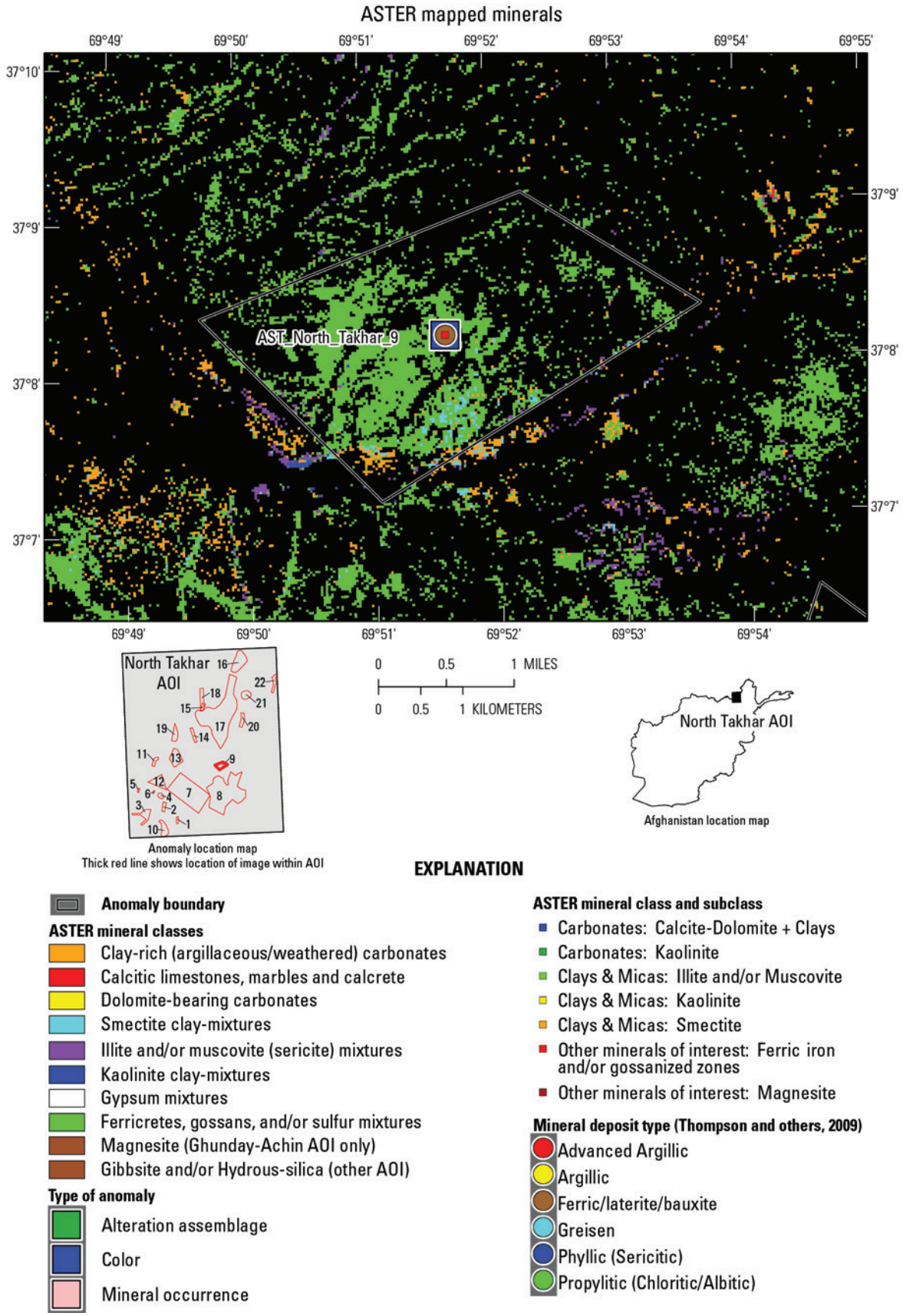

Figure 4.10.9. ASTER color anomaly located in the North Takhar Area of Interest (AOI) in Afghanistan. Extensive areas of ferricrete-bearing bedrock, excluding alluvial areas related to placer sulfide weathering.

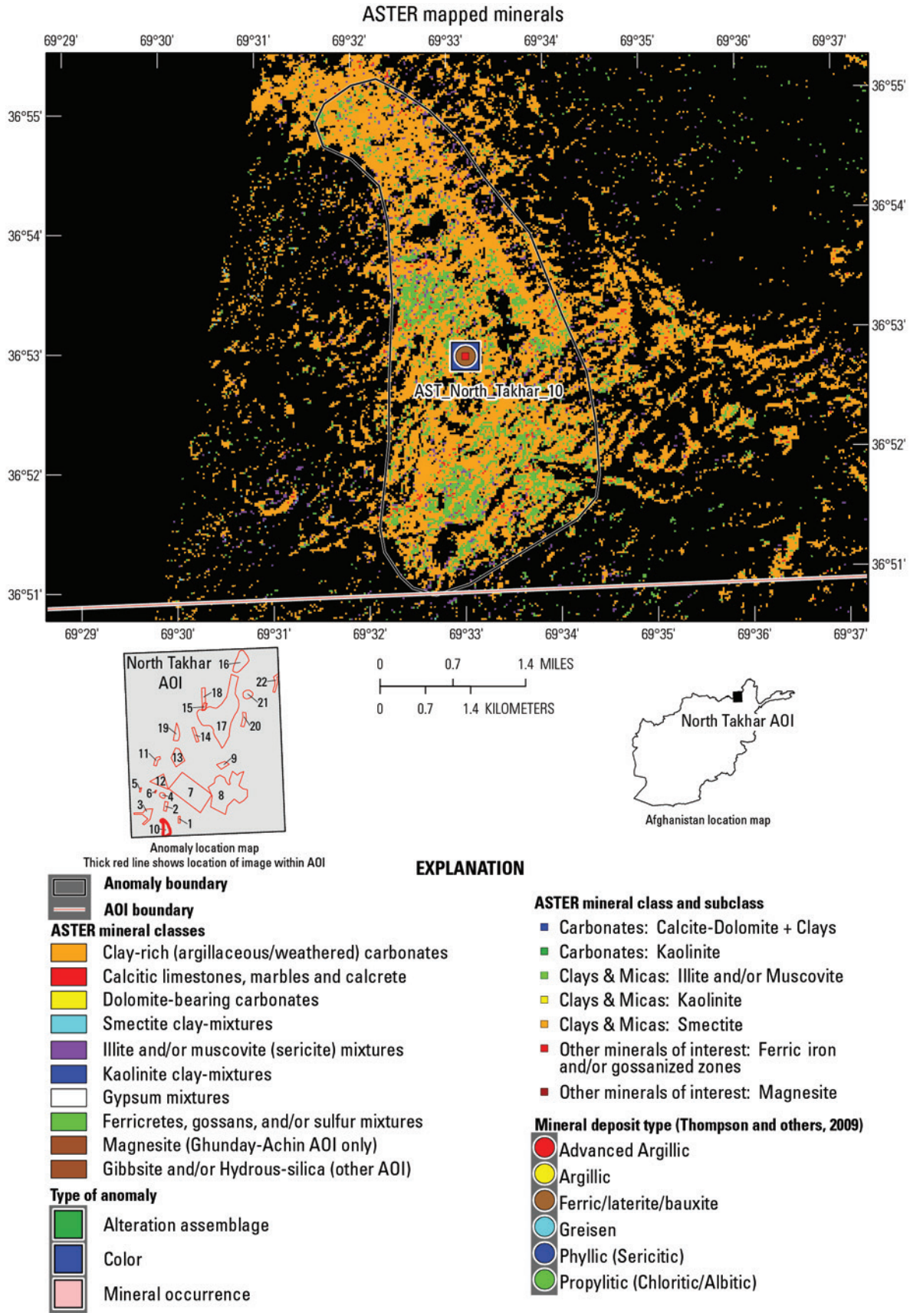

Figure 4.10.10. ASTER color anomaly located in the North Takhar Area of Interest (AOI) in Afghanistan. Possible sulfur- and/or phosphate-bearing area hosted within weathered carbonates and/or bedrock units containing clay and/or carbonate cements.

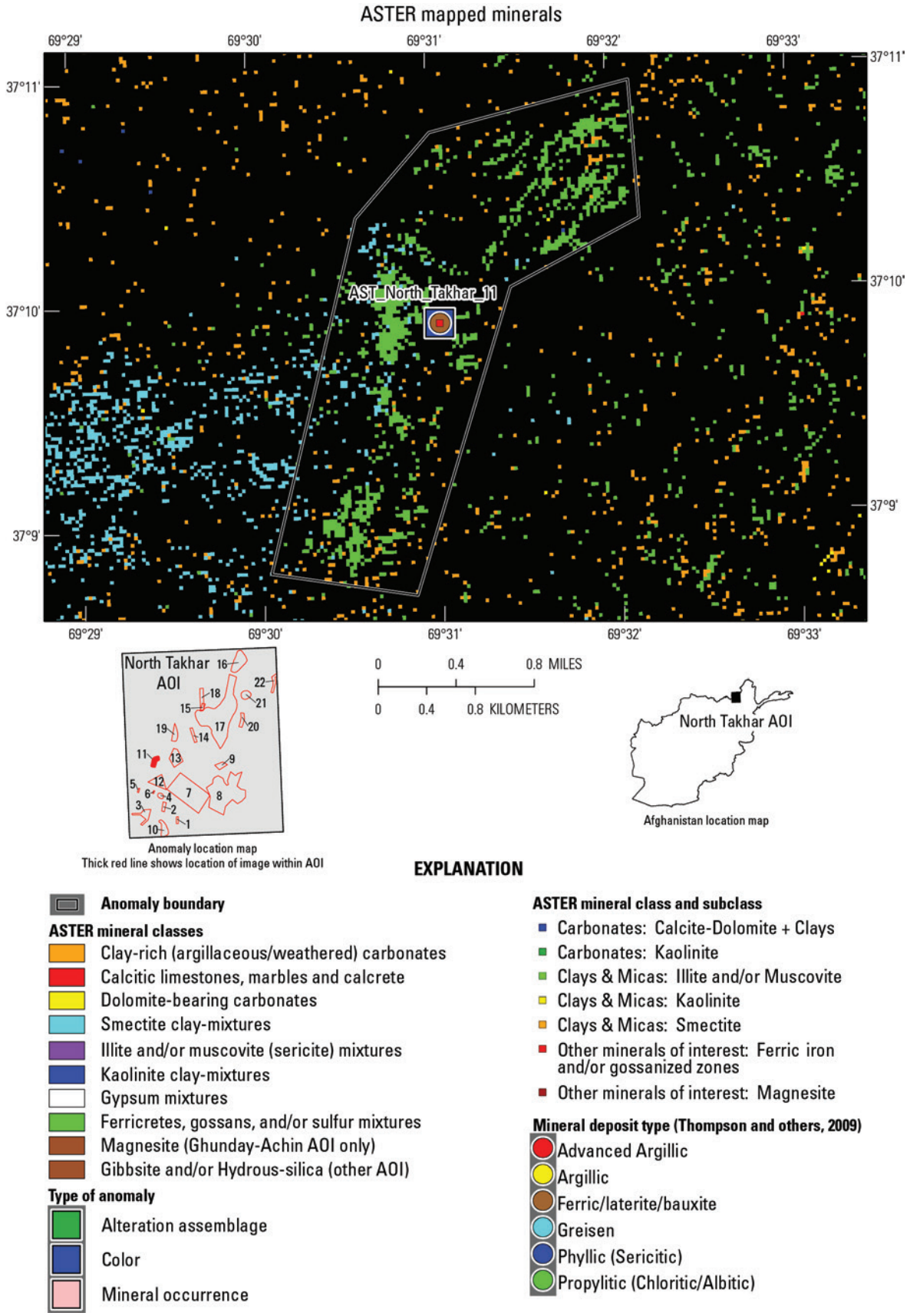

Figure 4.10.11. ASTER color anomaly located in the North Takhar Area of Interest (AOI) in Afghanistan. Possible sulfur- and/or phosphate-bearing area within weathered and/or argillaceous dolomitic carbonate rocks. Further spectral analysis is needed to distinguish sulfur from strong ferric iron.

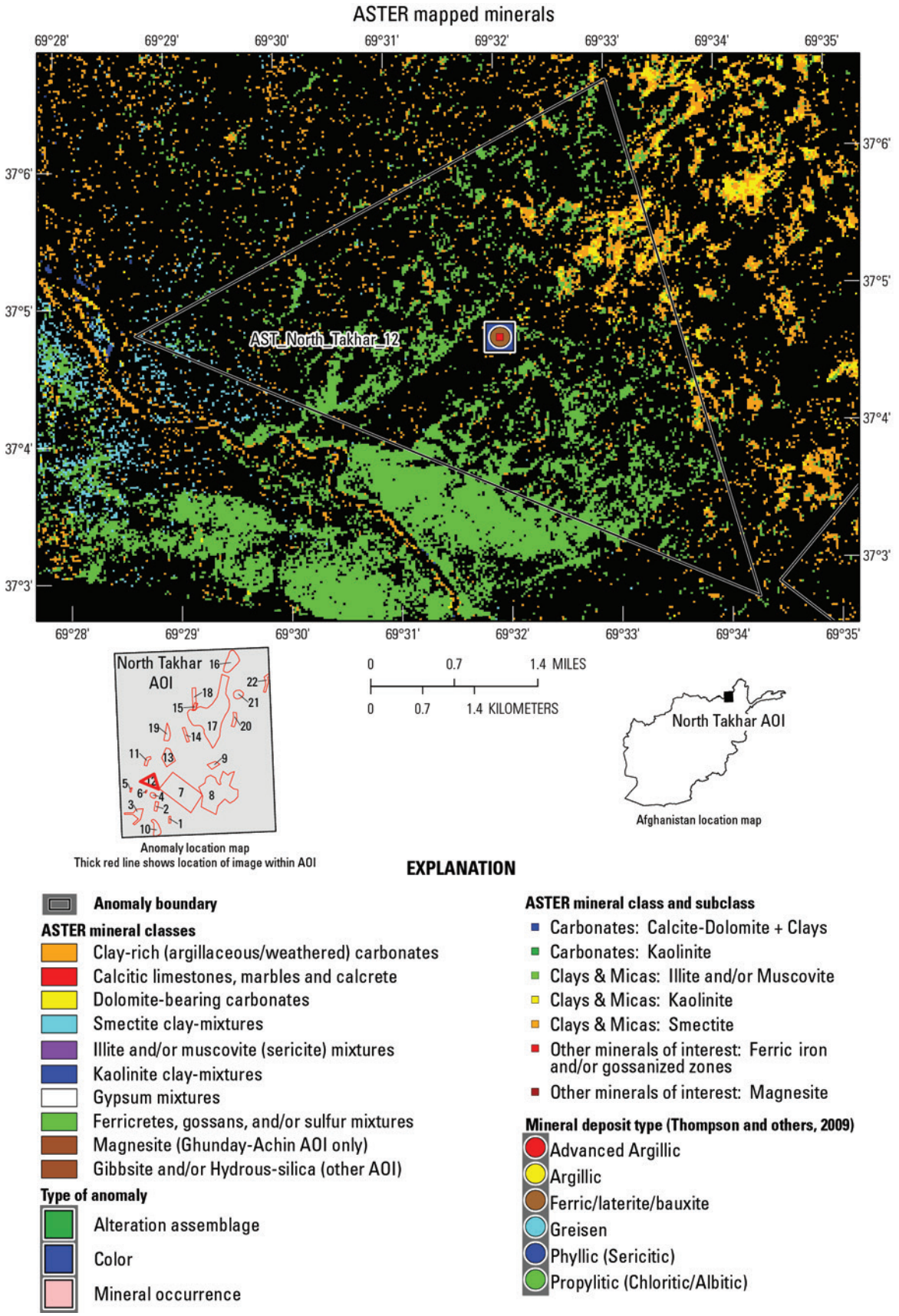

Figure 4.10.12. ASTER color anomaly located in the North Takhar Area of Interest (AOI) in Afghanistan. Possible sulfur- and/or phosphate-bearing area within weathered and/or argillaceous dolomitic carbonate rocks. Further spectral analysis is needed to distinguish sulfur from strong ferric iron.

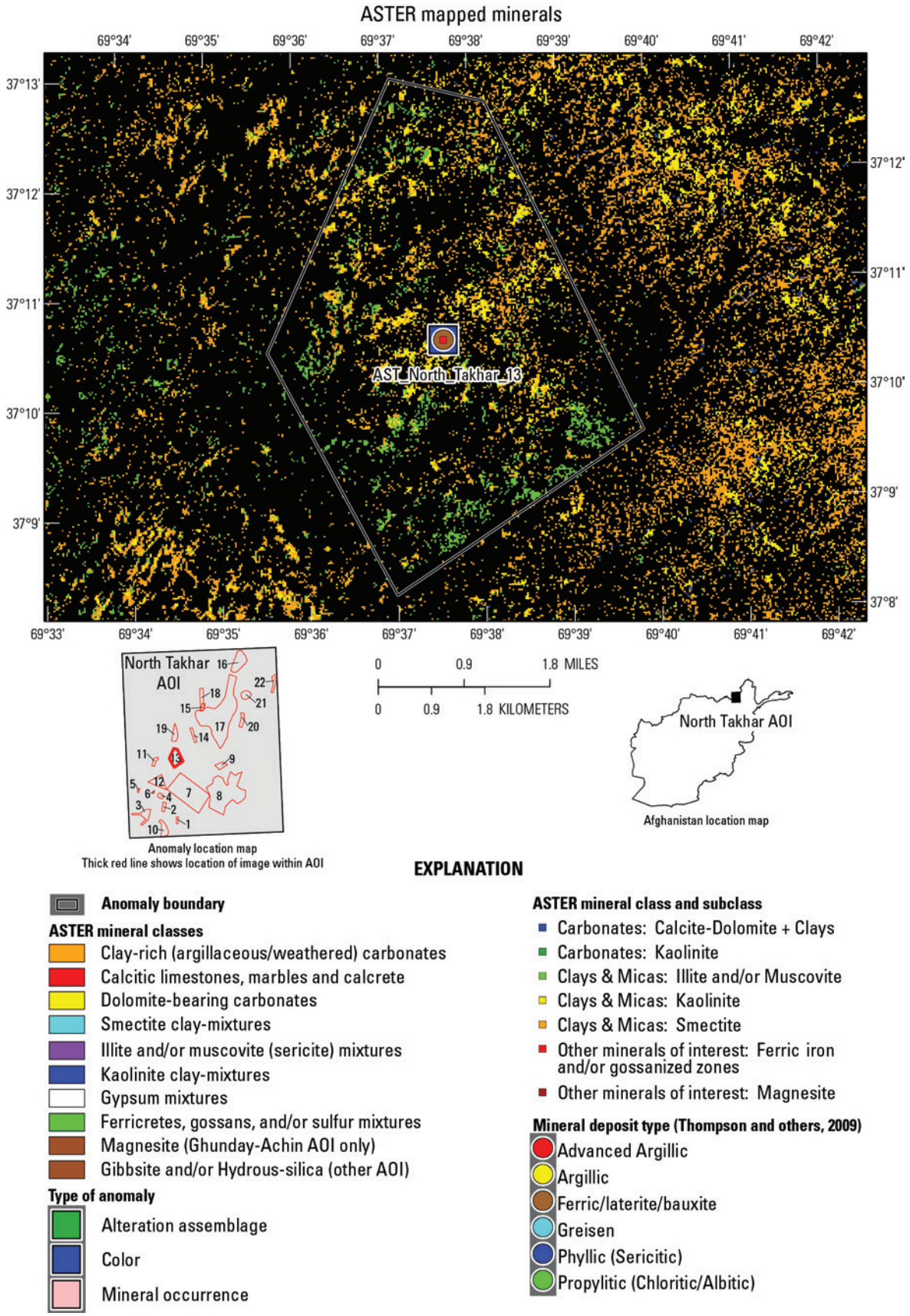

Figure 4.10.13. ASTER color anomaly located in the North Takhar Area of Interest (AOI) in Afghanistan. Possible sulfur- and/or phosphate-bearing area within weathered and/or argillaceous dolomitic carbonate rocks. Further spectral analysis is needed to distinguish sulfur from strong ferric iron.

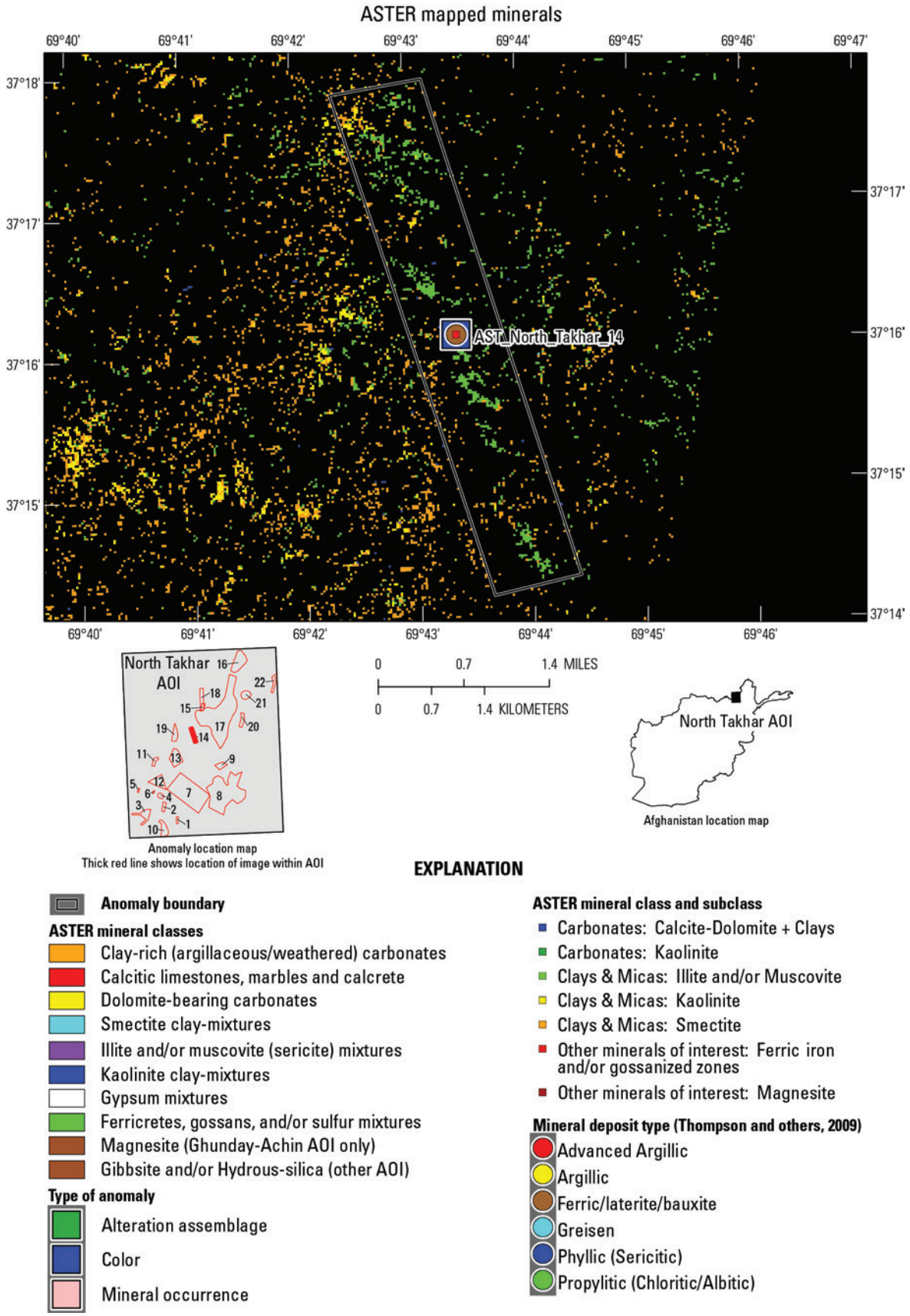

Figure 4.10.14. ASTER color anomaly located in the North Takhar Area of Interest (AOI) in Afghanistan. Possible sulfur- and/or phosphate-bearing area within weathered and/or argillaceous dolomitic carbonate rocks. Further spectral analysis is needed to distinguish sulfur from strong ferric iron.

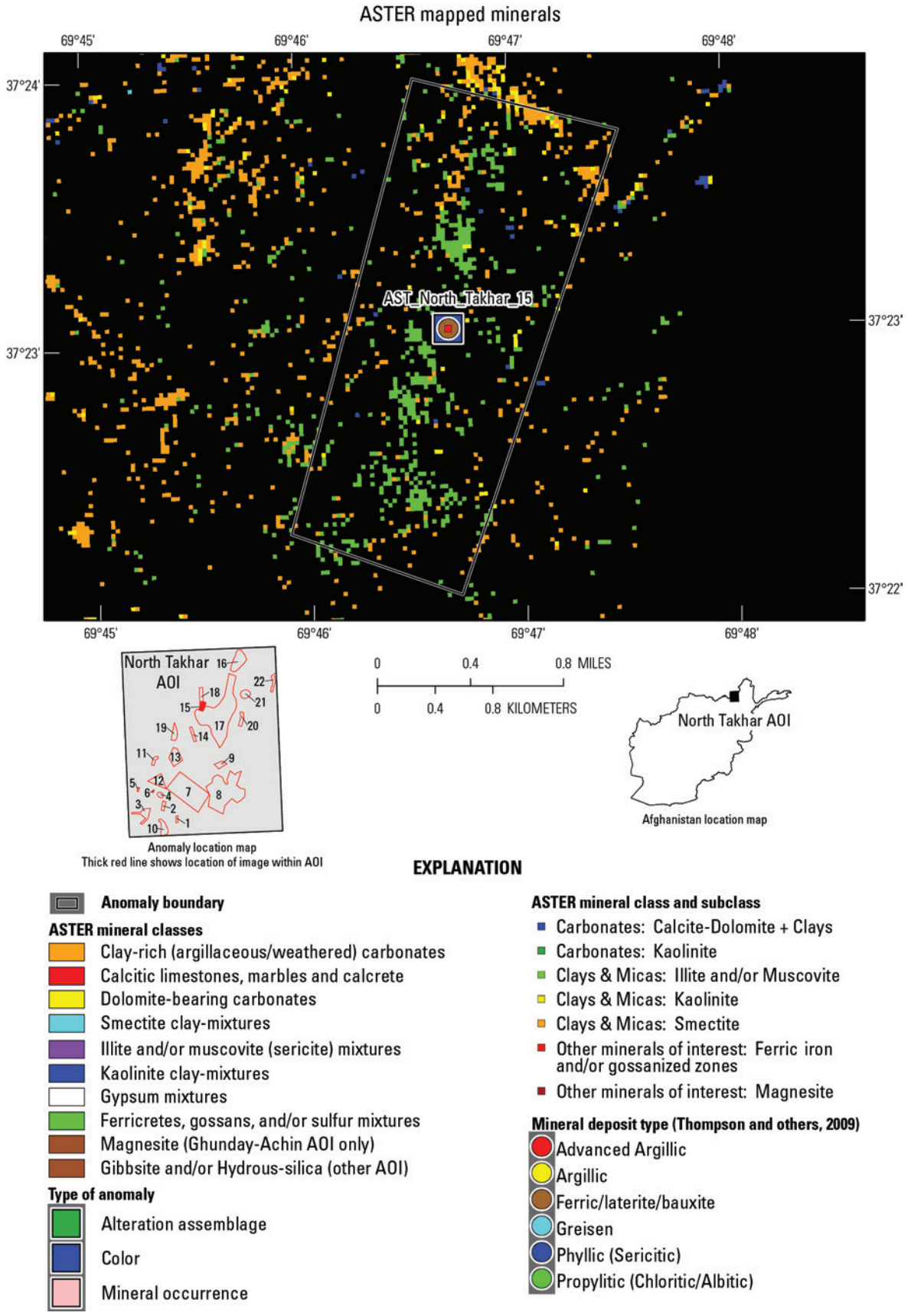

Figure 4.10.15. ASTER color anomaly located in the North Takhar Area of Interest (AOI) in Afghanistan. Possible sulfur- and/or phosphate-bearing area within weathered and/or argillaceous dolomitic carbonate rocks. Further spectral analysis is needed to distinguish sulfur from strong ferric iron.

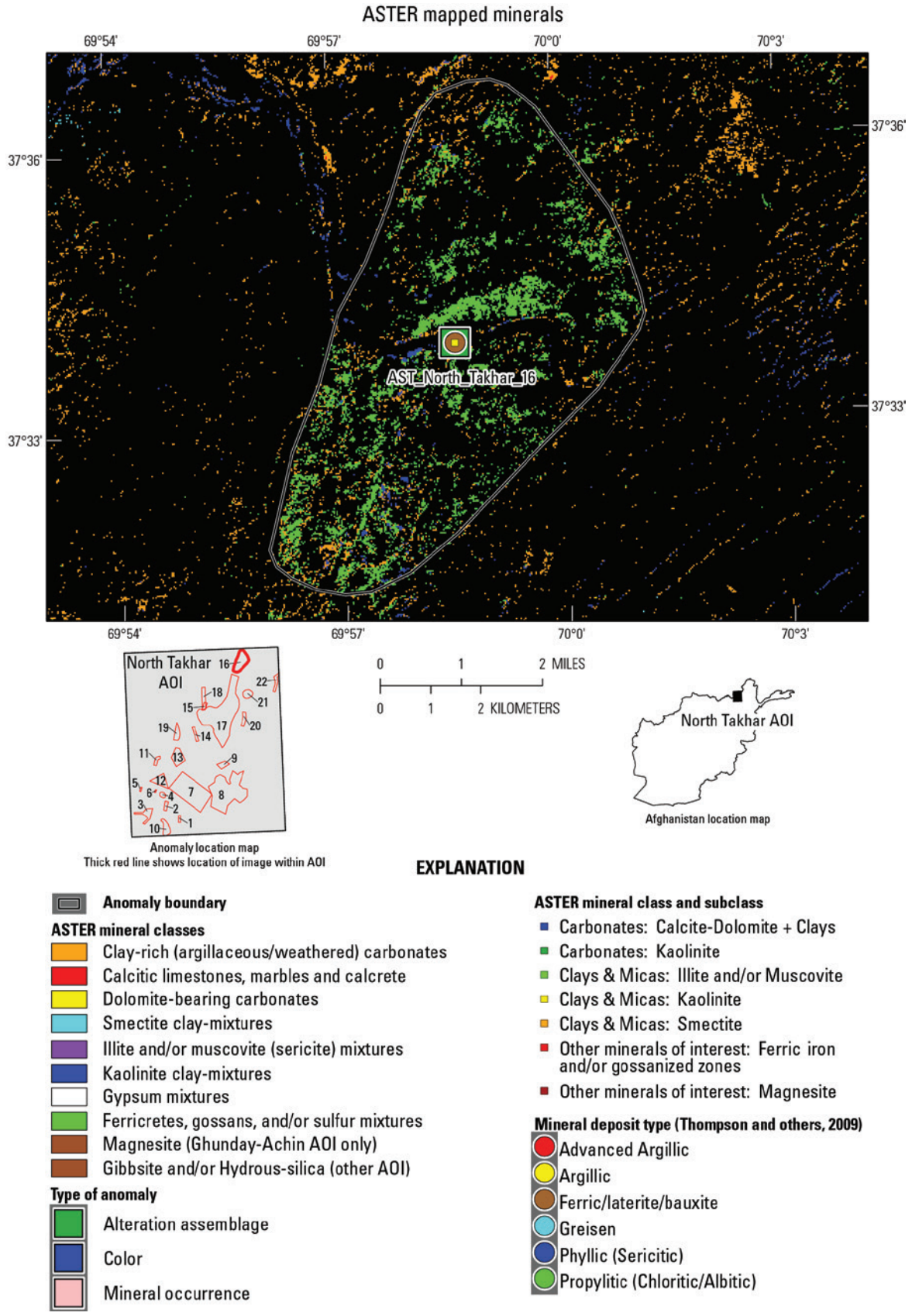

Figure 4.10.16. ASTER alteration anomaly located in the North Takhar Area of Interest (AOI) in Afghanistan. Anomaly located along the border between Afghanistan and Tajikistan within mapped Miocene stratified clay deposits (Doebrich and Wahl, 2006) with kaolinite locally dominant along Amu Darya floodplain (paleo-laterite/ferricrete deposits).

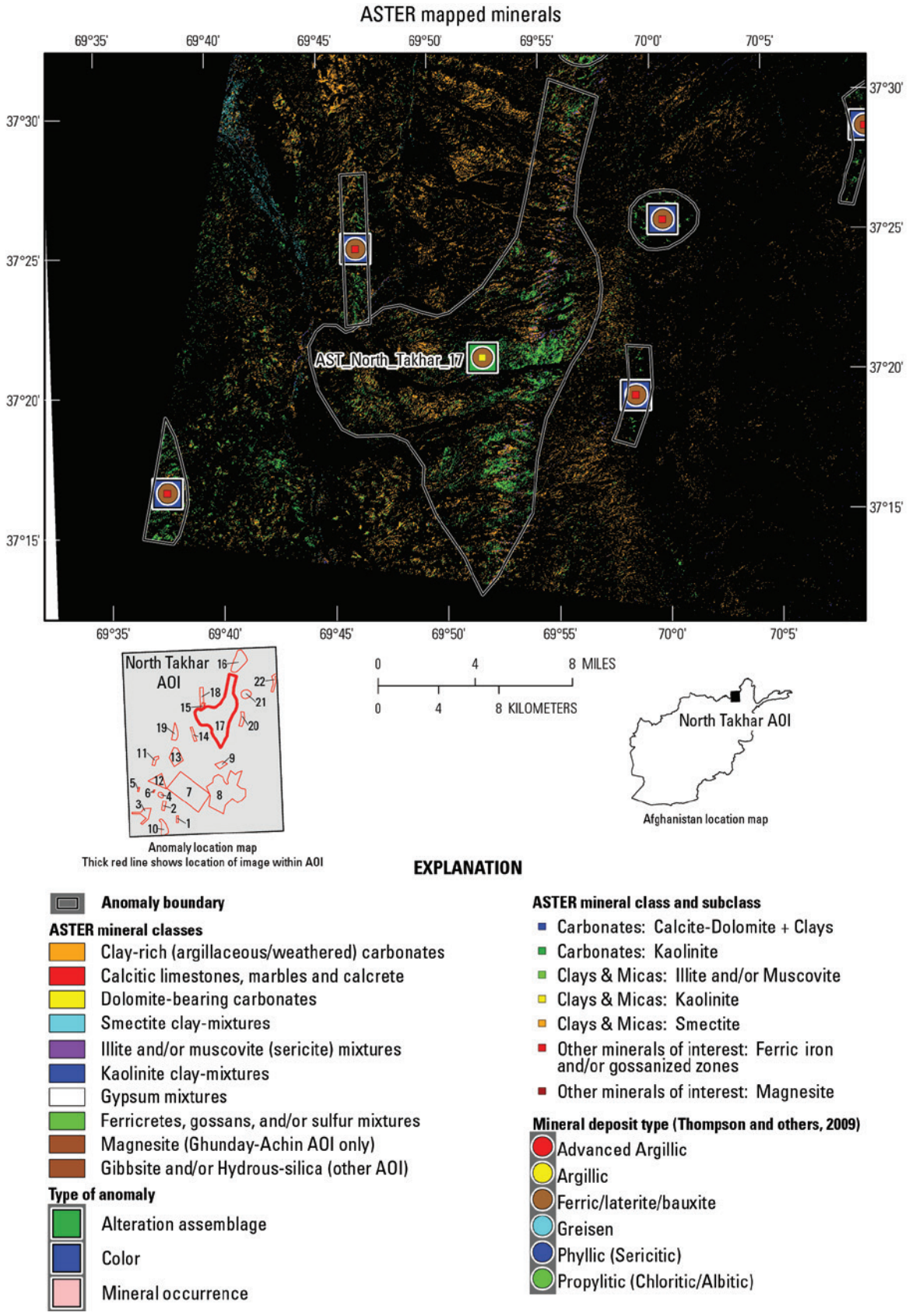

Figure 4.10.17. ASTER alteration anomaly located in the North Takhar Area of Interest (AOI) in Afghanistan. Anomaly located along the border between Afghanistan and Tajikistan within mapped Miocene stratified clay deposits (Doebrich and Wahl, 2006) with kaolinite locally dominant along Amu Darya floodplain (paleo-laterite/ferricrete deposits).

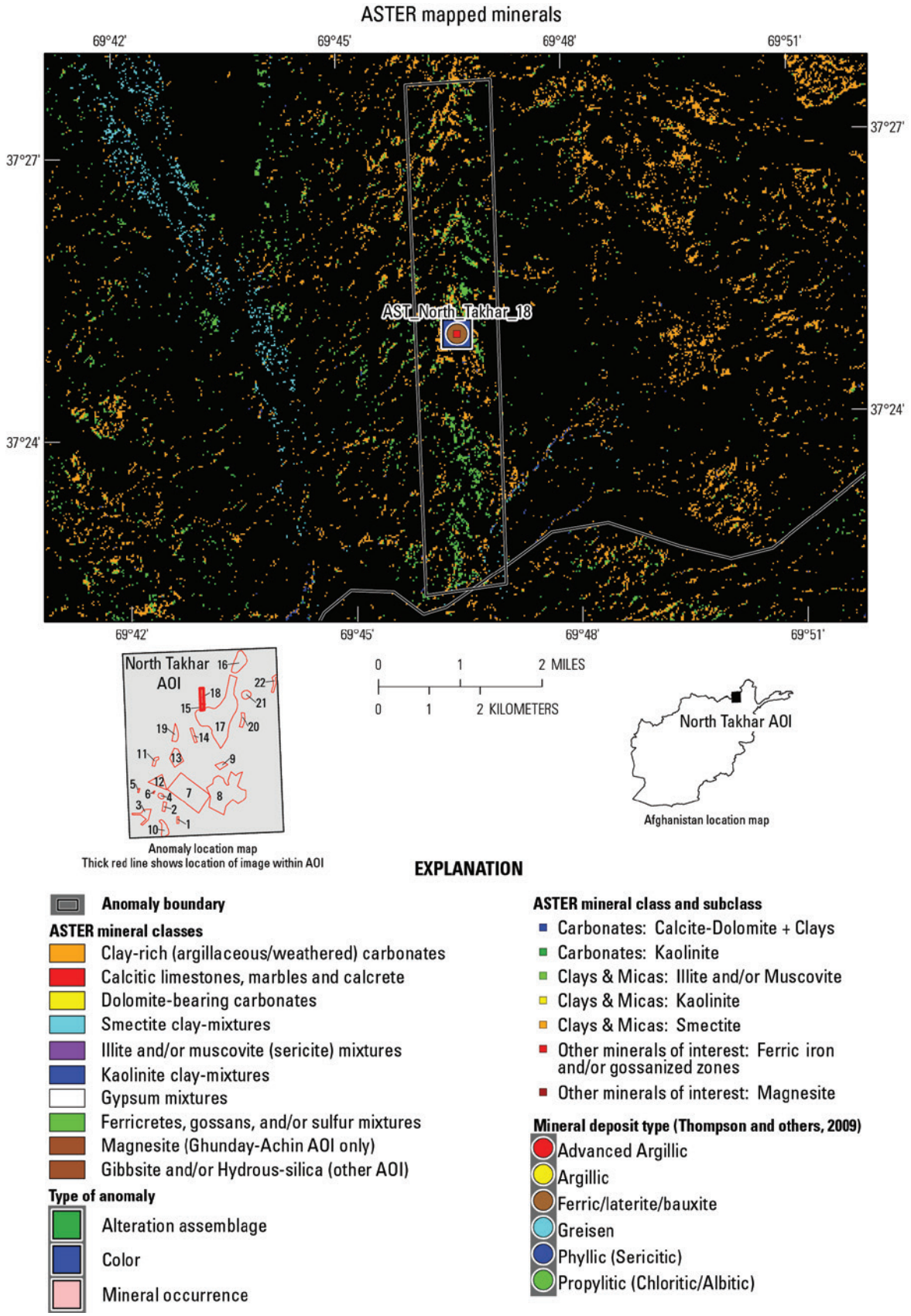

Figure 4.10.18. ASTER color anomaly located in the North Takhar Area of Interest (AOI) in Afghanistan. Extensive areas of ferricrete-bearing bedrock (alluvial fan and terrace areas intentionally excluded) perhaps related to placer sulfide weathering (abundant kaolinite zones locally throughout) and associated with downstream mercury geochemistry anomaly.

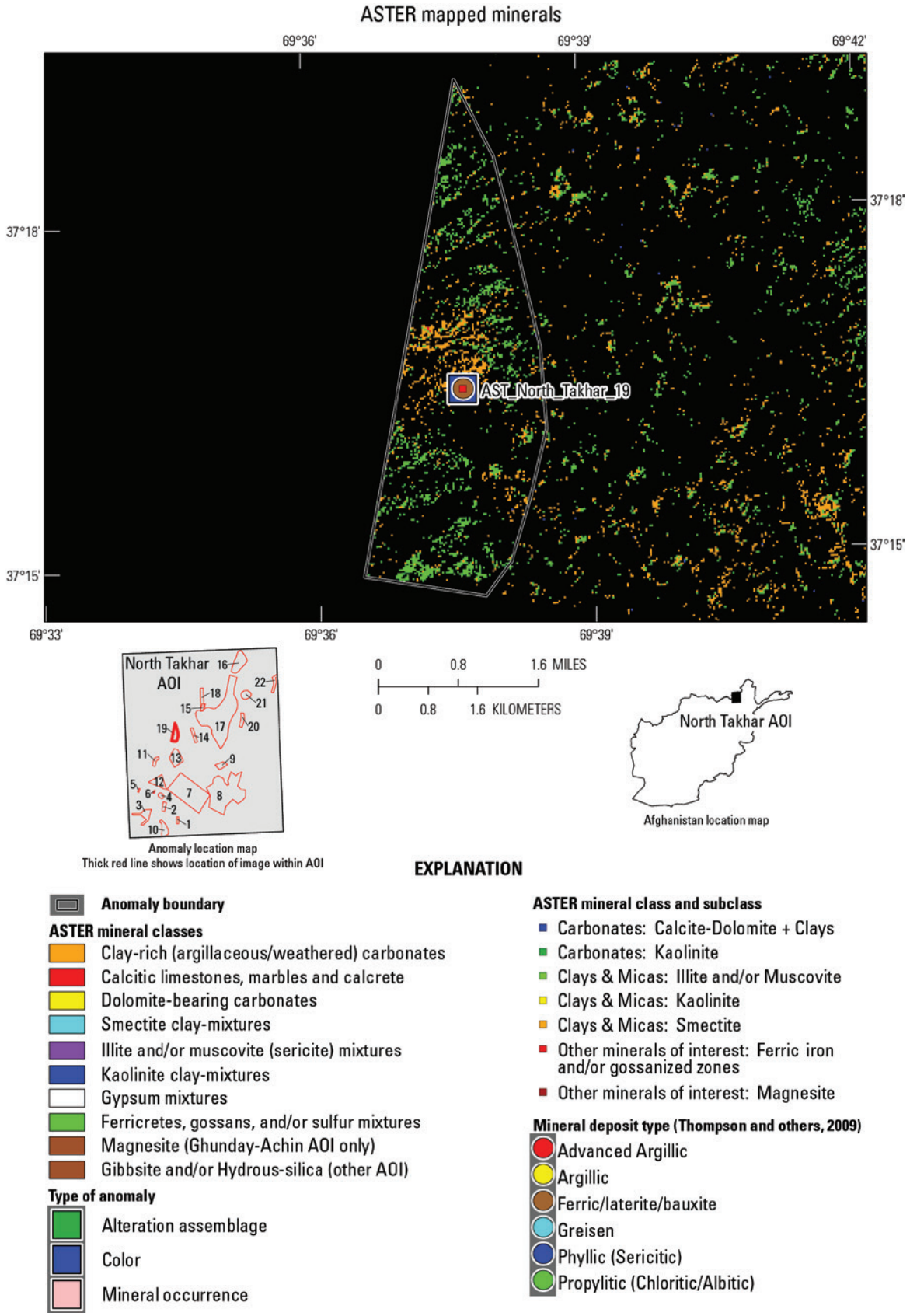

Figure 4.10.19. ASTER color anomaly located in the North Takhar Area of Interest (AOI) in Afghanistan. Possible sulfur- and/or phosphate-bearing area within weathered and/or argillaceous, or clay-rich, carbonate and carbonate-cemented clastic rocks. Further spectral analysis needed to distinguish sulfur from strong ferric iron.

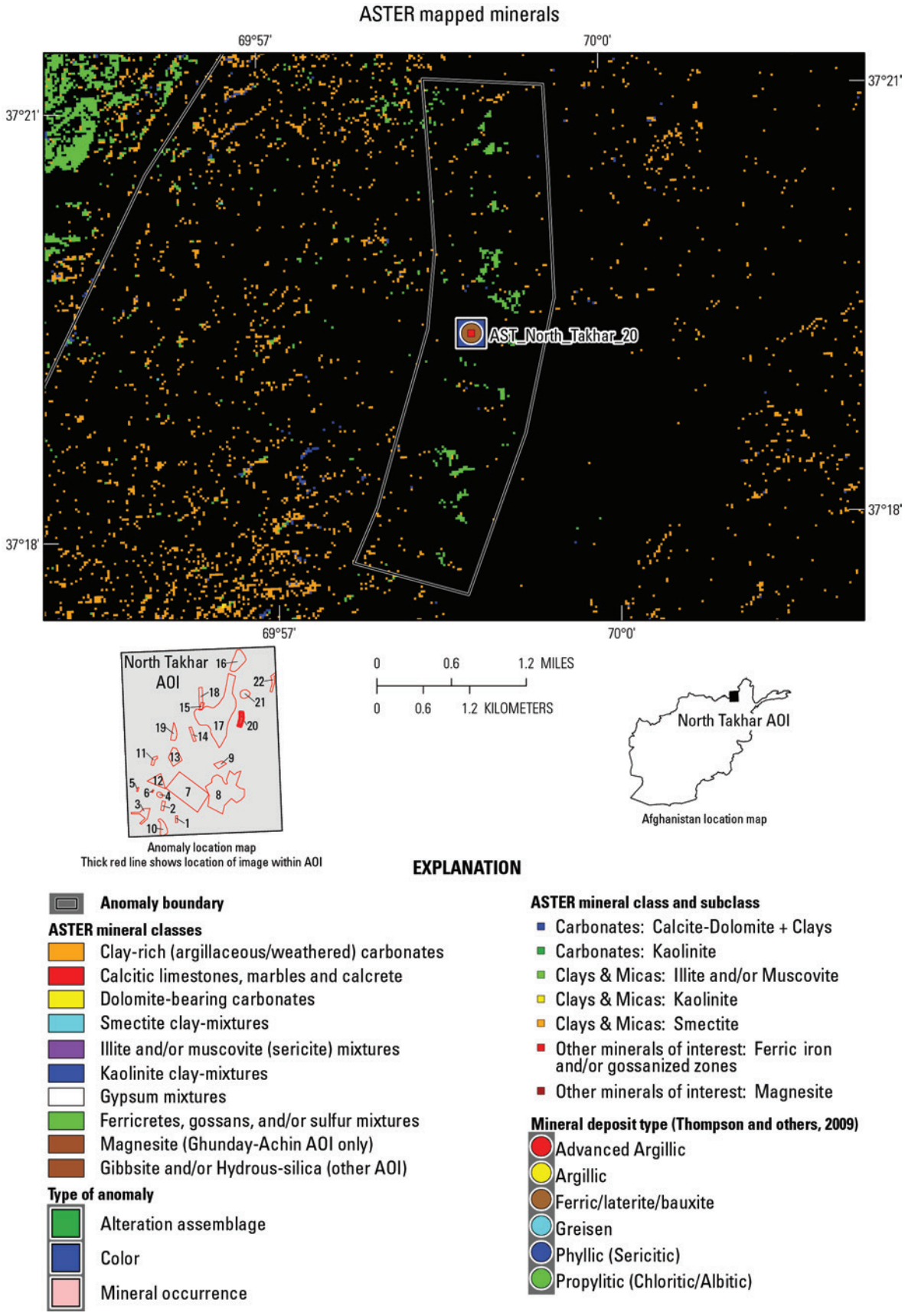

Figure 4.10.20. ASTER color anomaly located in the North Takhar Area of Interest (AOI) in Afghanistan. Possible ferricrete-cemented surficial deposits related to placer sulfide weathering.

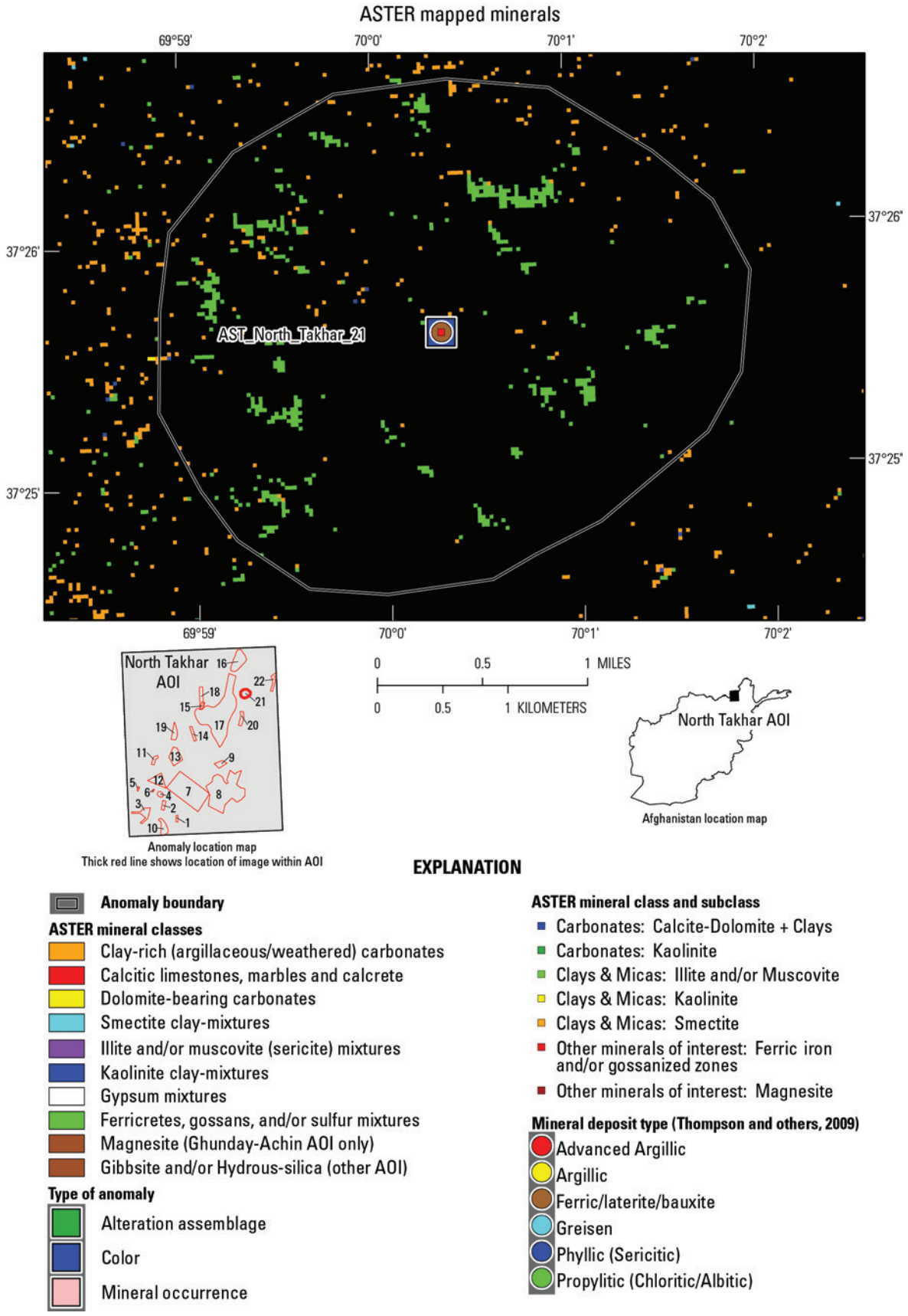

Figure 4.10.21. ASTER color anomaly located in the North Takhar Area of Interest (AOI) in Afghanistan. Possible ferricrete-cemented surficial deposits related to placer sulfide weathering.

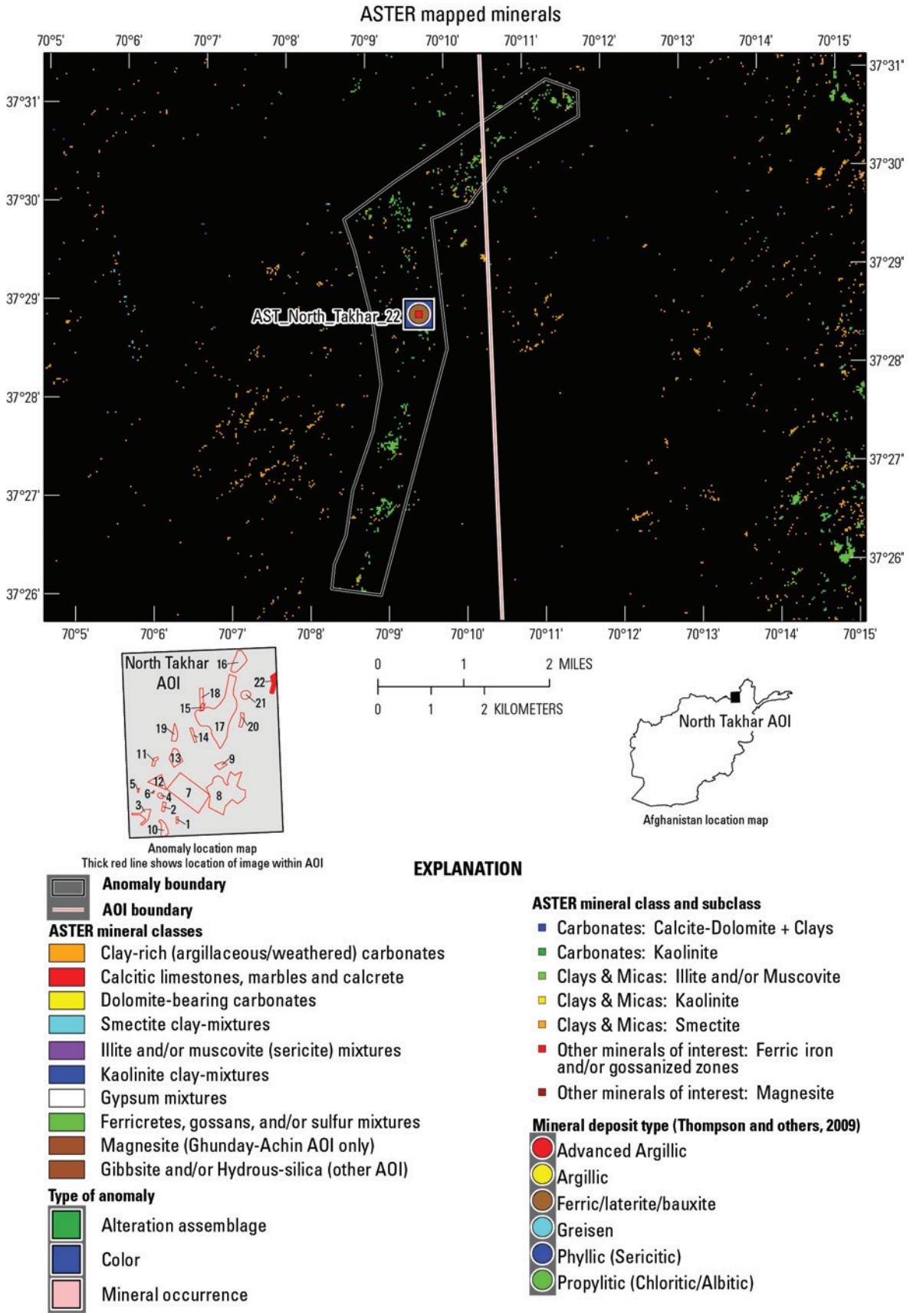

Figure 4.10.22. ASTER color anomaly located in the North Takhar Area of Interest (AOI) in Afghanistan. Possible ferricrete-cemented surficial deposits related to placer sulfide weathering.

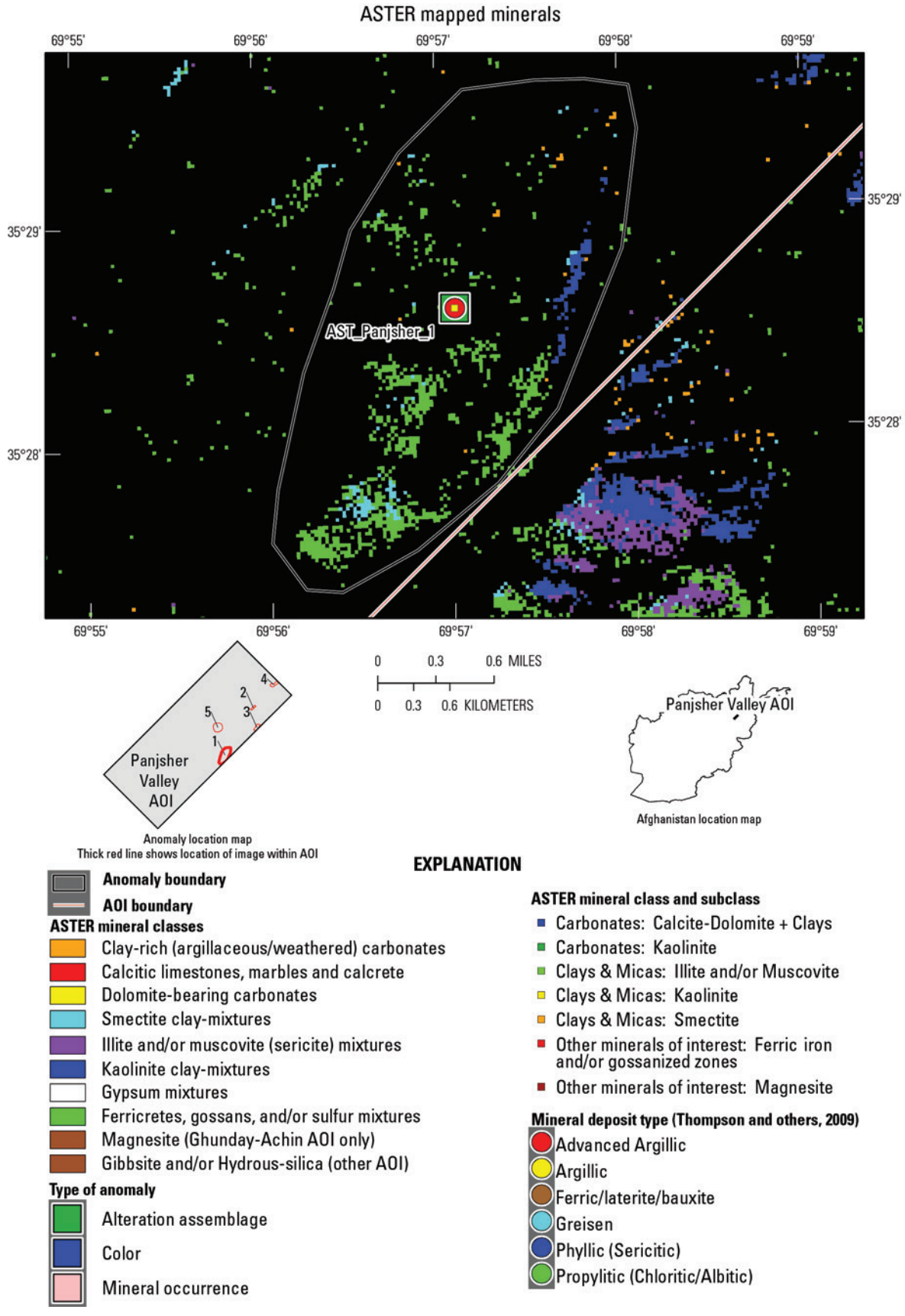

Figure 4.11.1. ASTER alteration anomaly located in the Panjsher Valley Area of Interest (AOI) in Afghanistan. Anomaly defined by ferric iron-staining with localized, linear kaolinite-rich bleach zones based on spectral mapping results.

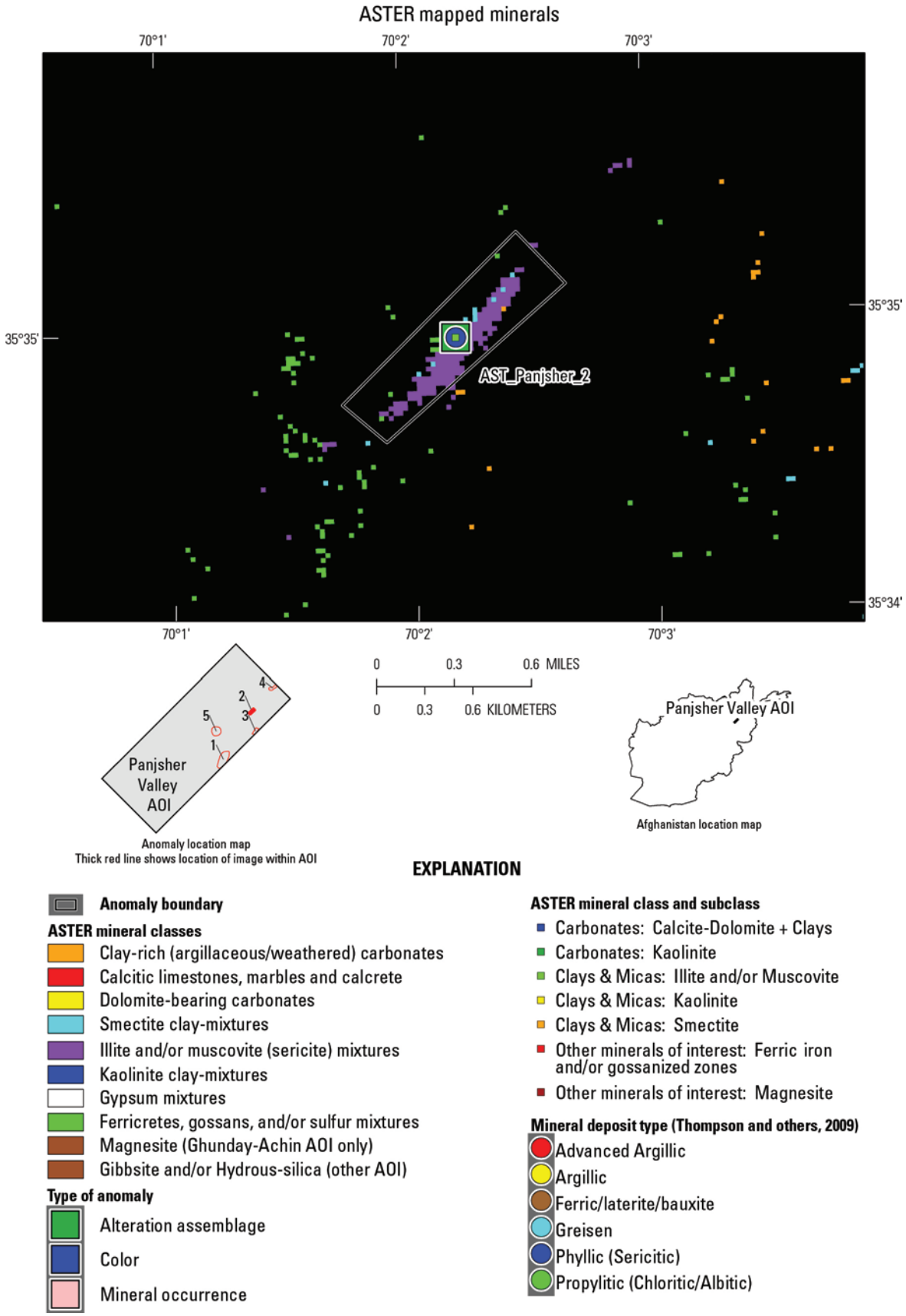

Figure 4.11.2. ASTER alteration anomaly located in the Panjsher Valley Area of Interest (AOI) in Afghanistan. Anomaly is defined as a linear zone with abundant illite/muscovite, which is red in color differing from the surrounding darker rocks.

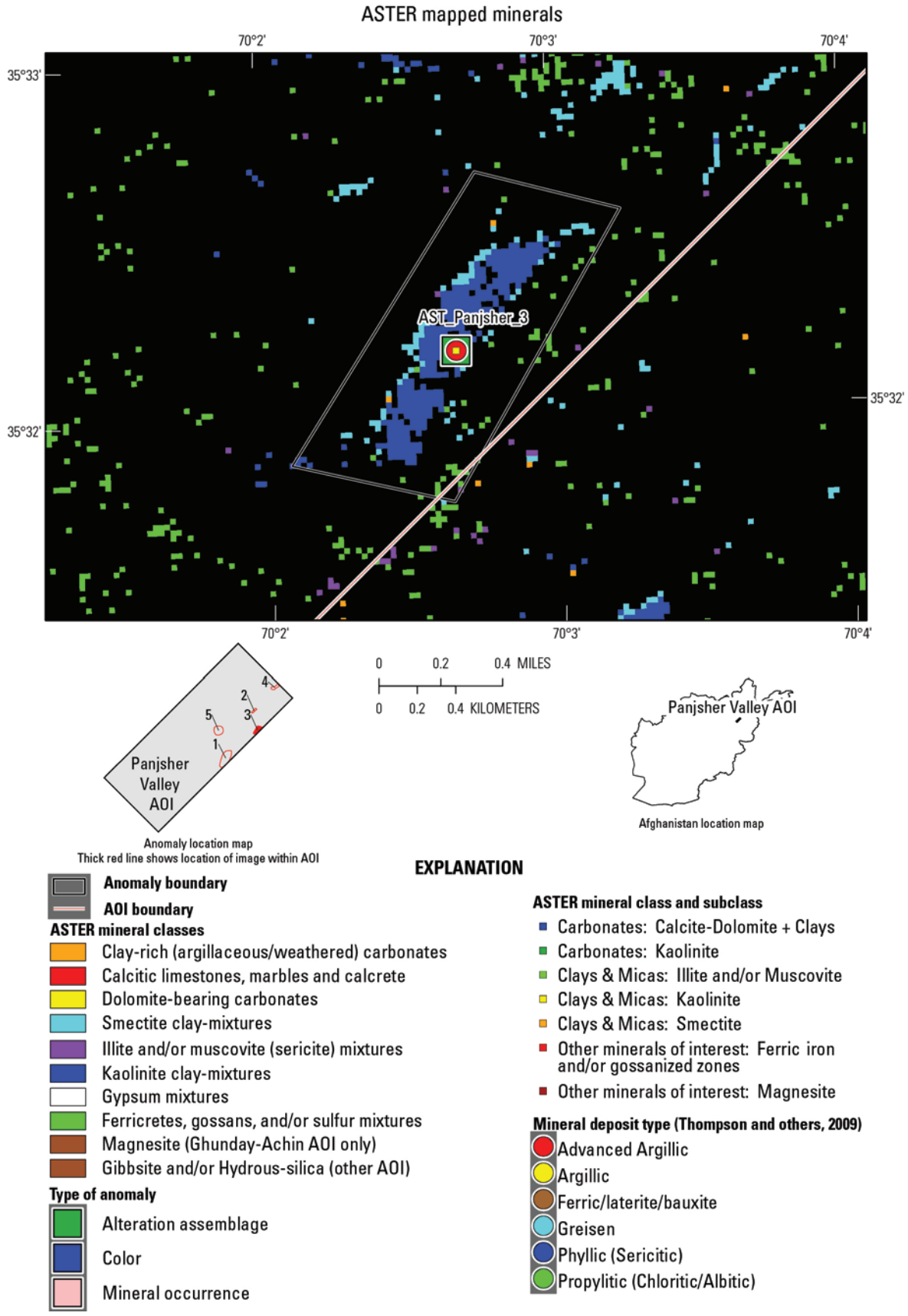

Figure 4.11.3. ASTER alteration anomaly located in the Panjsher Valley Area of Interest (AOI) in Afghanistan. Anomaly defined by intensely bleached, kaolinite-abundant, bright rocks within alpine-glaciated rocks.

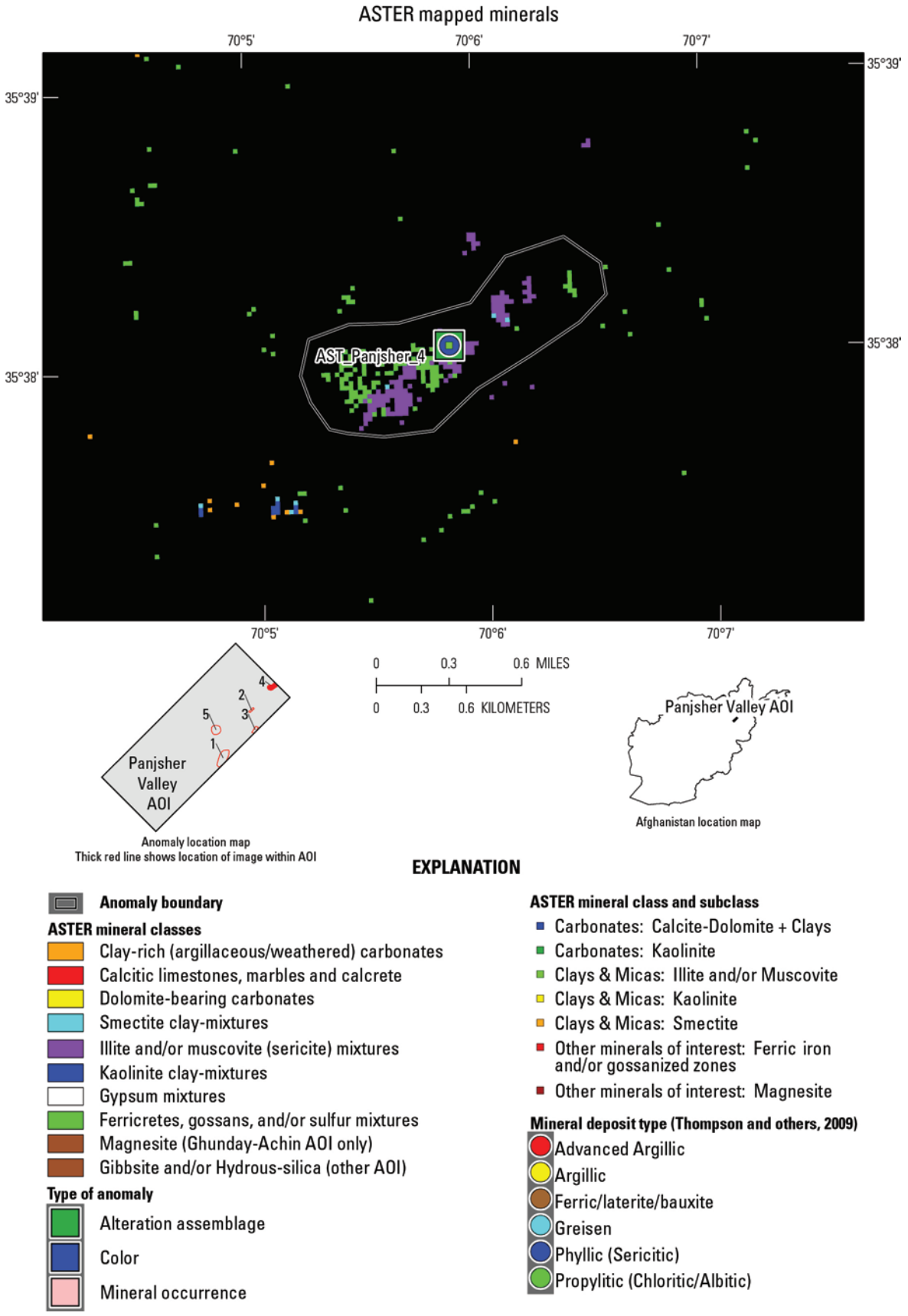

Figure 4.11.4. ASTER alteration anomaly located in the Panjsher Valley Area of Interest (AOI) in Afghanistan. Anomaly contains ferric iron and illite/muscovite abundant rocks, which are red in color differing from the surrounding darker rocks.

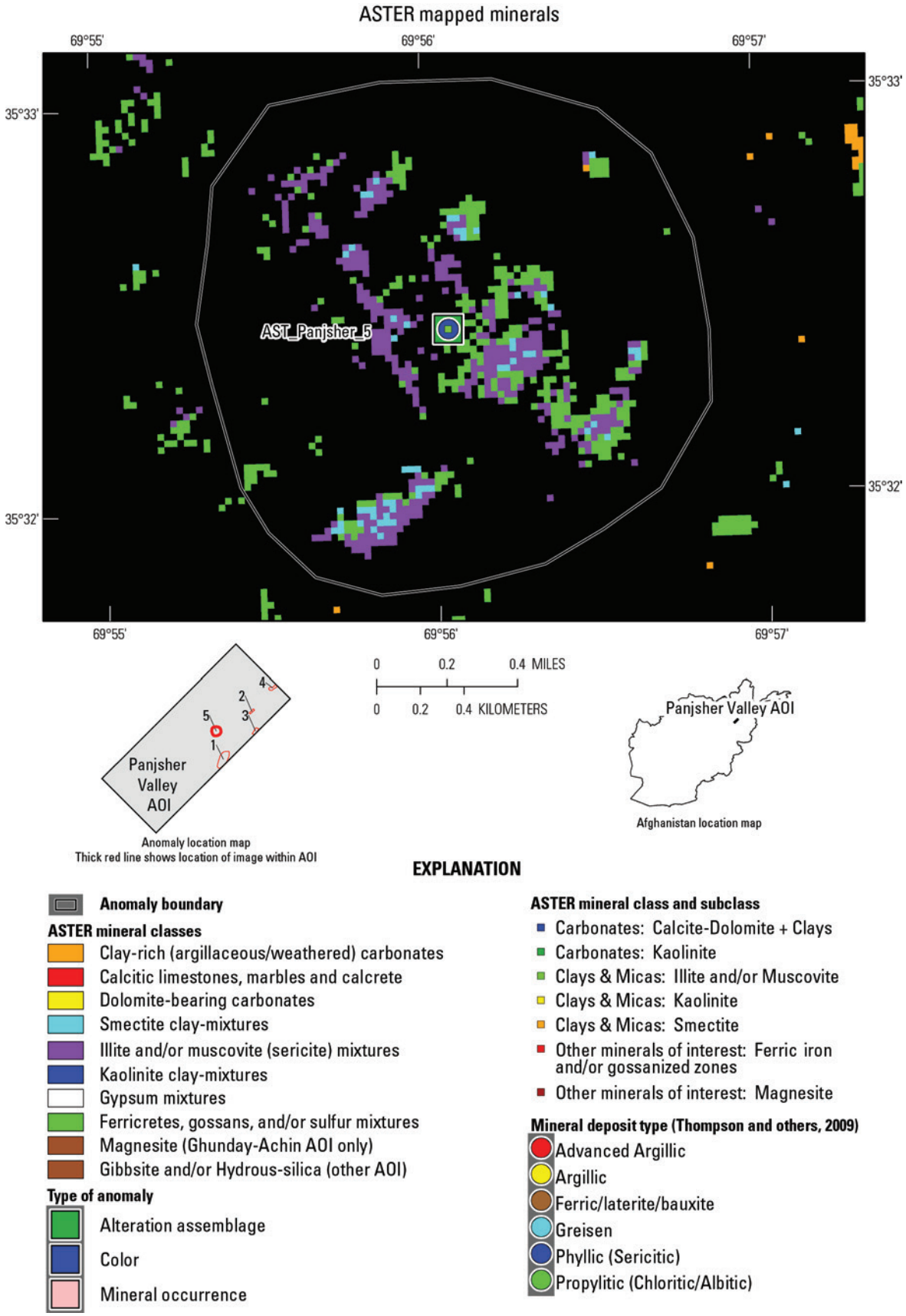

Figure 4.11.5. ASTER alteration anomaly located in the Panjsher Valley Area of Interest (AOI) in Afghanistan. Anomaly based on intensely iron-stained rocks with abundant illite/muscovite.

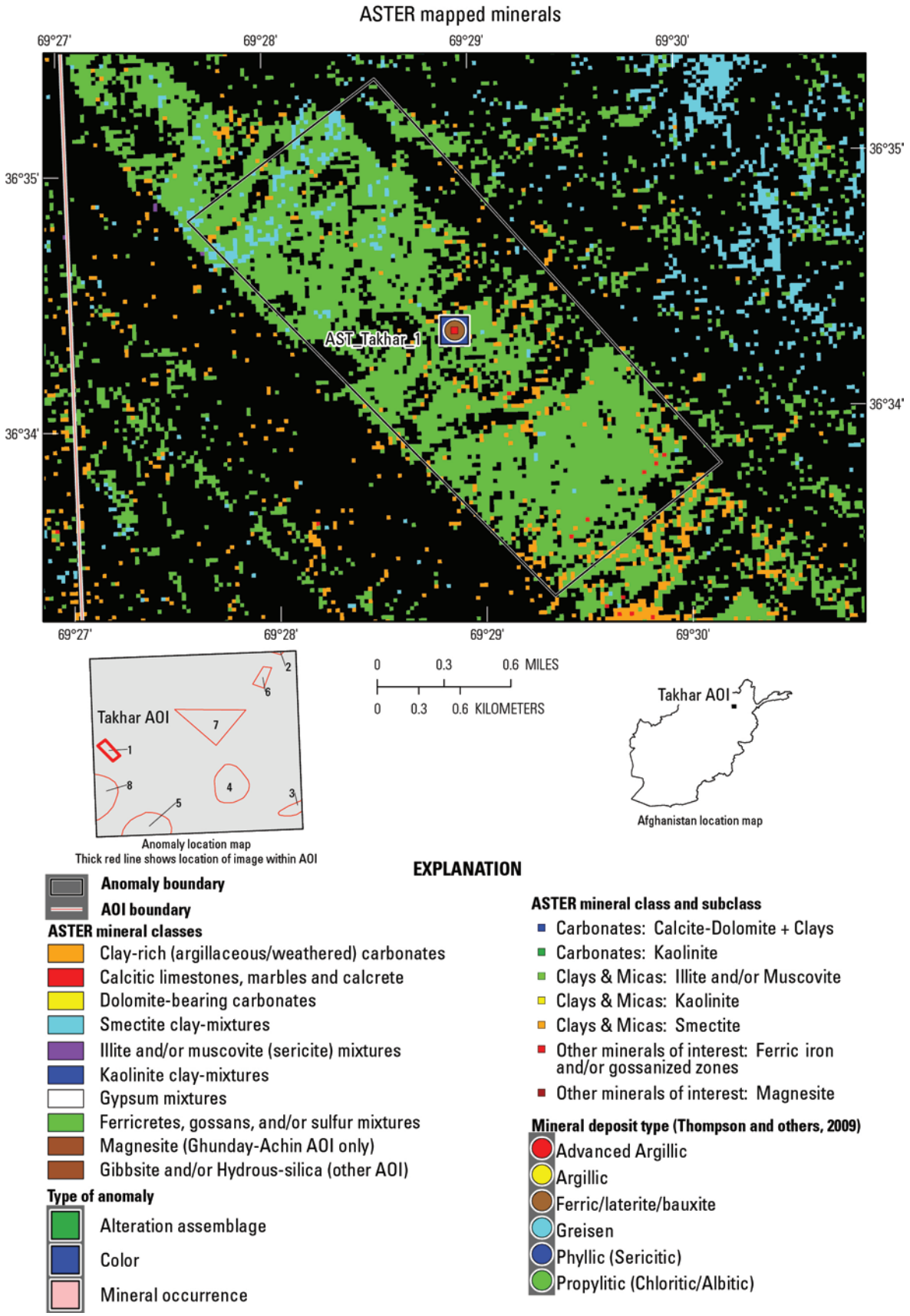

Figure 4.12.1. ASTER color anomaly located in the Takhar Area of Interest (AOI) in Afghanistan. Possible sulfur- and/or phosphate-bearing area within weathered and/or argillaceous dolomitic carbonate rocks. Further spectral analysis is needed to distinguish sulfur from strong ferric iron.

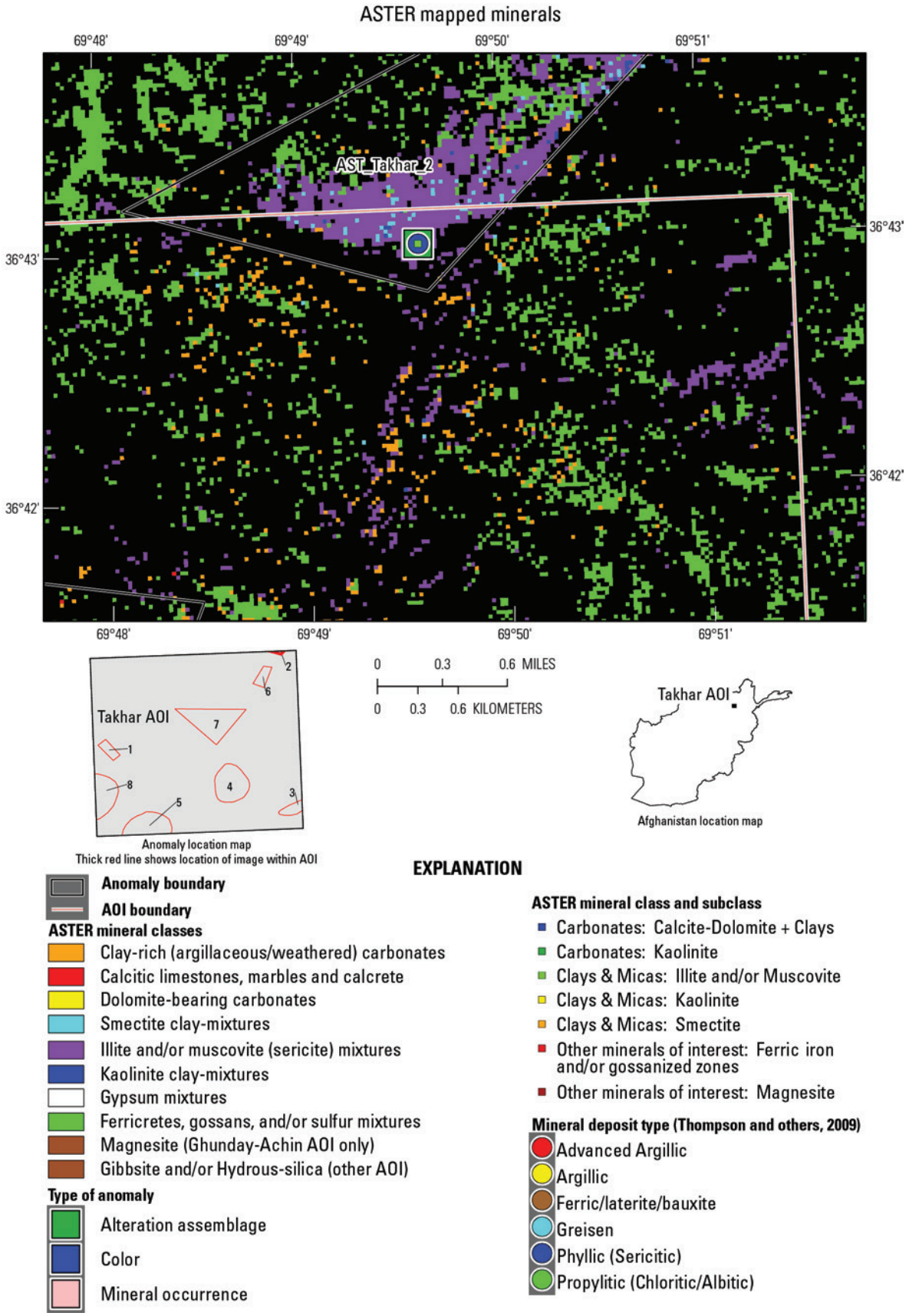

Figure 4.12.2. ASTER alteration anomaly located in the Takhar Area of Interest (AOI) in Afghanistan. Bleached area displayed indication of hydrothermal alteration origin with strong ferric iron mixing with sericitic clays and micas.

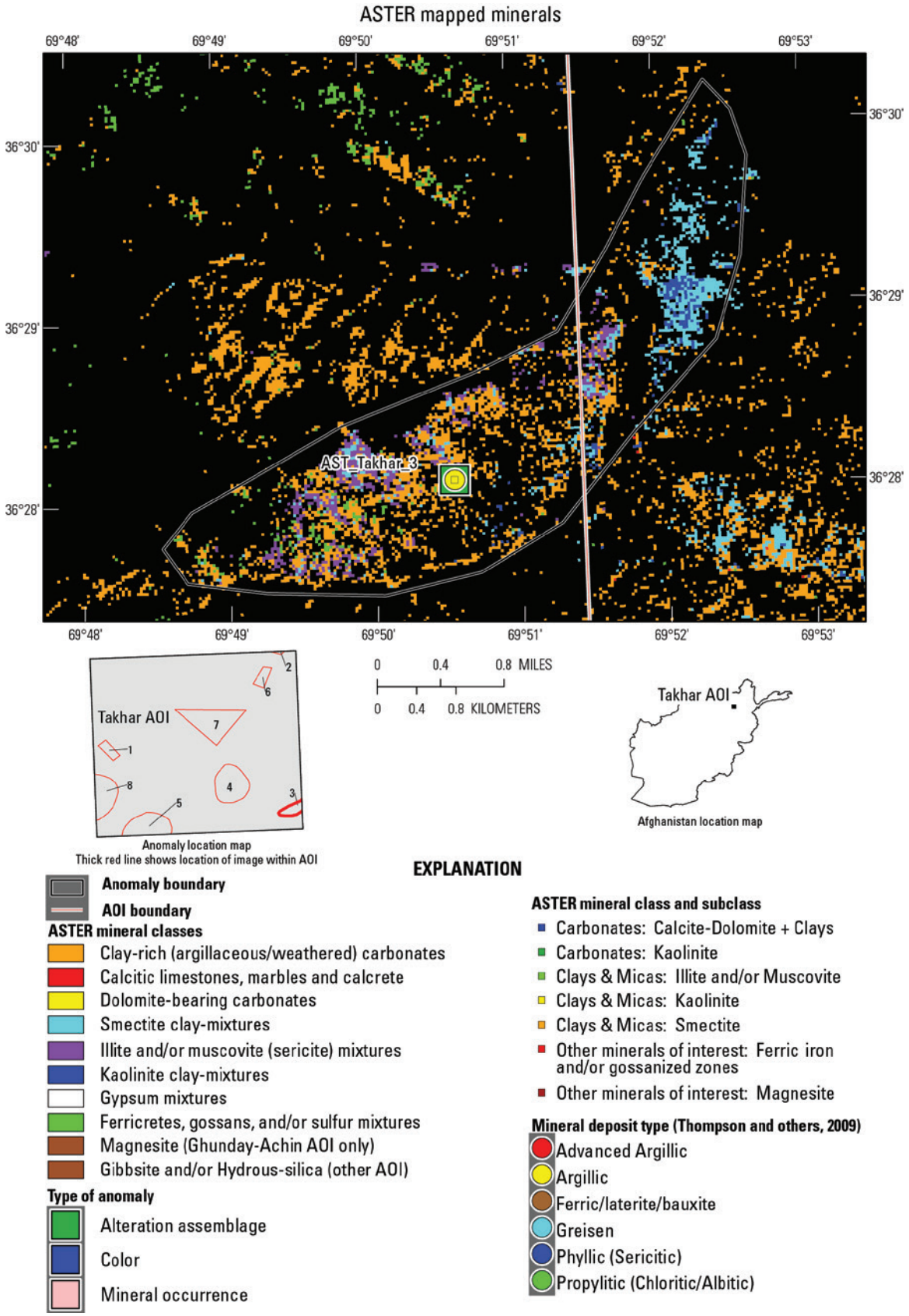

Figure 4.12.3. ASTER alteration anomaly located in the Takhar Area of Interest (AOI) in Afghanistan. Iron-stained and bleached area displayed rocks exhibiting mixtures of clays, carbonates, ferric iron, illite/muscovite, kaolinite, and smectite, with the latter being the most dominant. Argillic zones were the most spatially extensive.

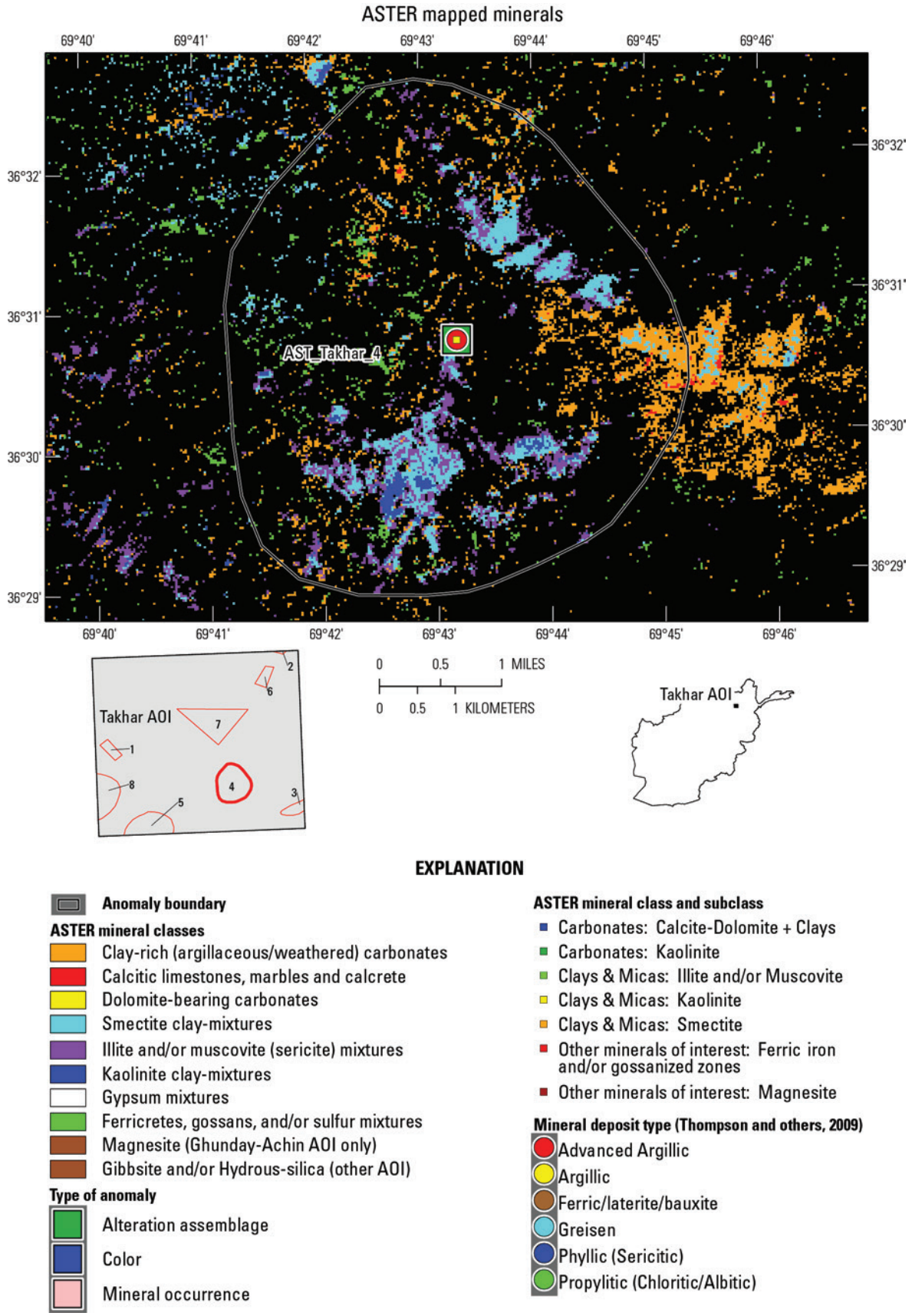

Figure 4.12.4. ASTER alteration anomaly located in the Takhar Area of Interest (AOI) in Afghanistan. Advanced argillic, argillic, and phyllic/sericitic zones form the center of overlapping lead and mercury stream-geochemistry anomalies hosted by rocks mapped as Late Triassic intrusive rocks.

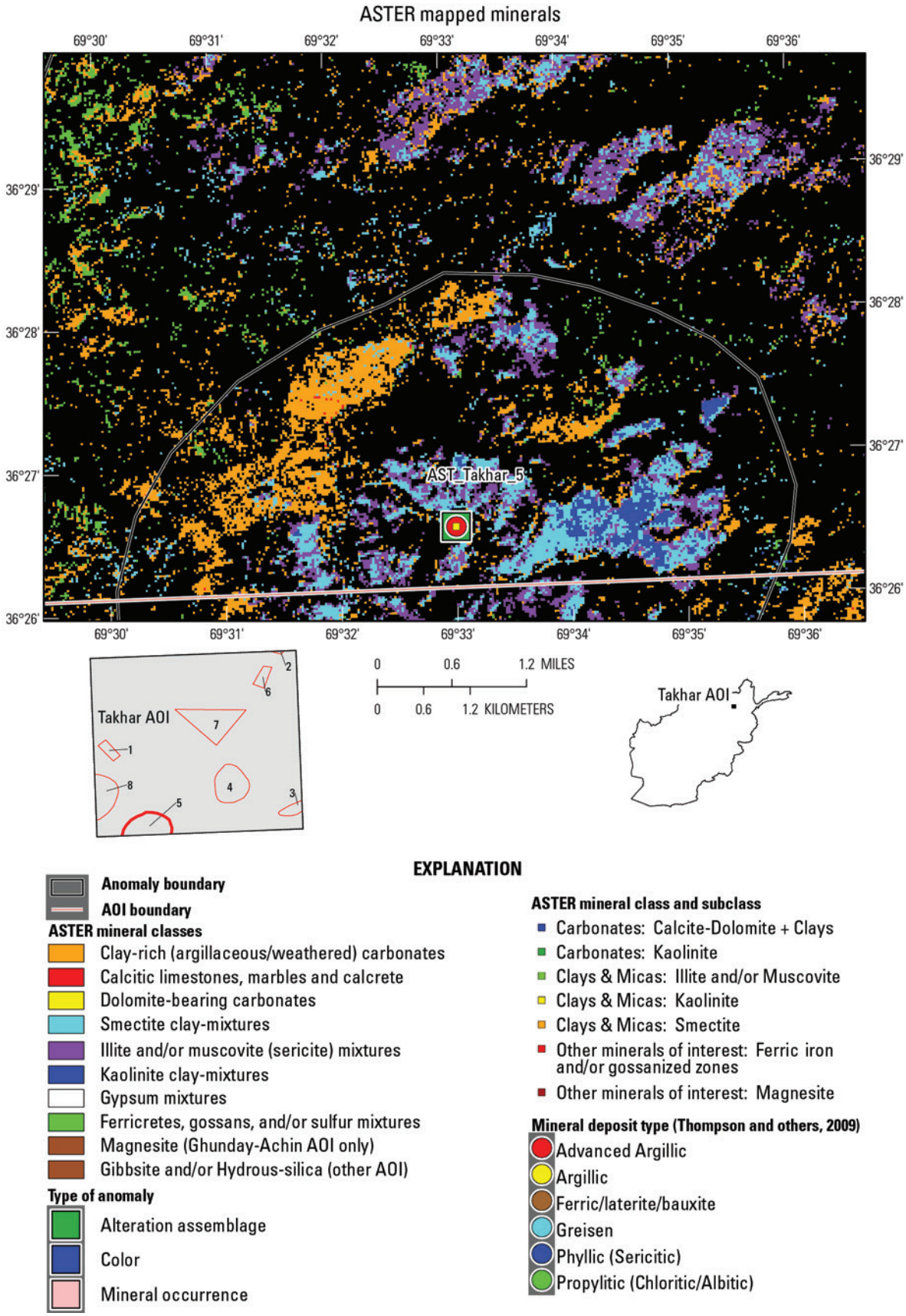

Figure 4.12.5. ASTER alteration anomaly located in the Takhar Area of Interest (AOI) in Afghanistan. Mostly bleached appearing rocks dominated by mixtures of kaolinite, smectite, illite, and/or muscovite.

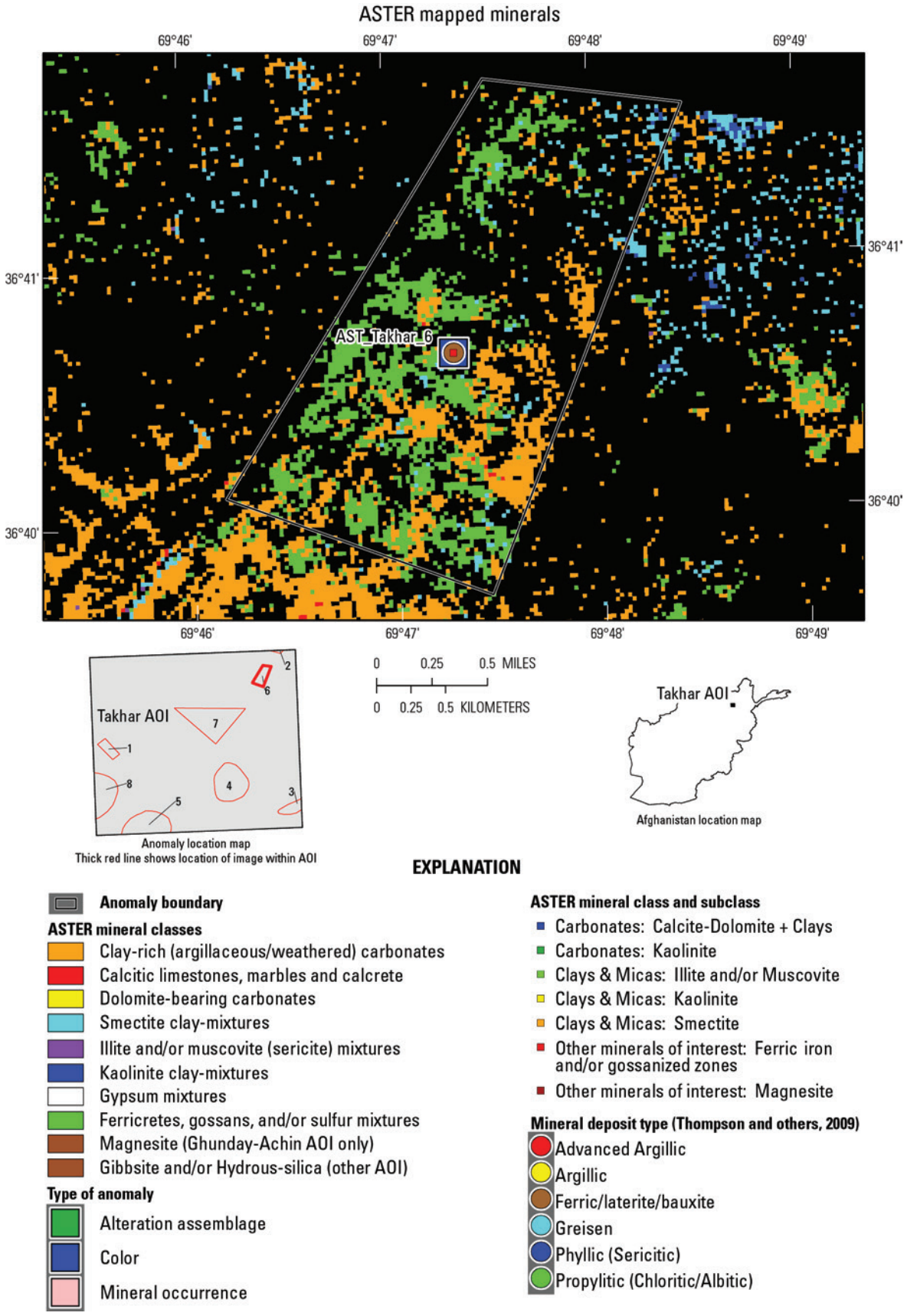

Figure 4.12.6. ASTER color anomaly located in the Takhar Area of Interest (AOI) in Afghanistan. Possible sulfur- and/or phosphate-bearing area within weathered and/or argillaceous carbonate rocks. Further spectral analysis needed to distinguish sulfur from strong ferric iron.

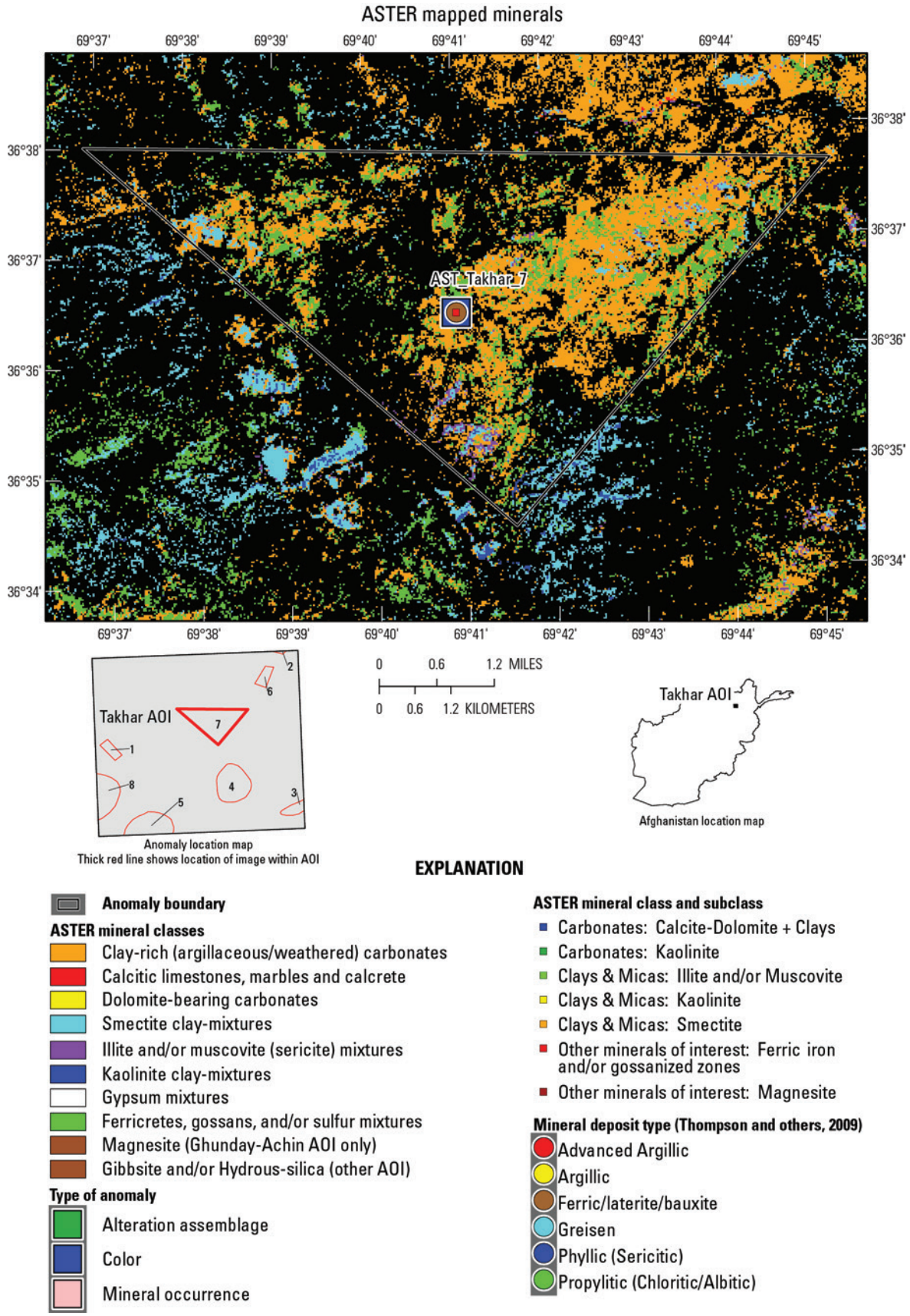

Figure 4.12.7. ASTER color anomaly located in the Takhar Area of Interest (AOI) in Afghanistan. Possible sulfur- and/or phosphate-bearing area within weathered and/or argillaceous carbonate rocks. Further spectral analysis needed to distinguish sulfur from strong ferric iron.

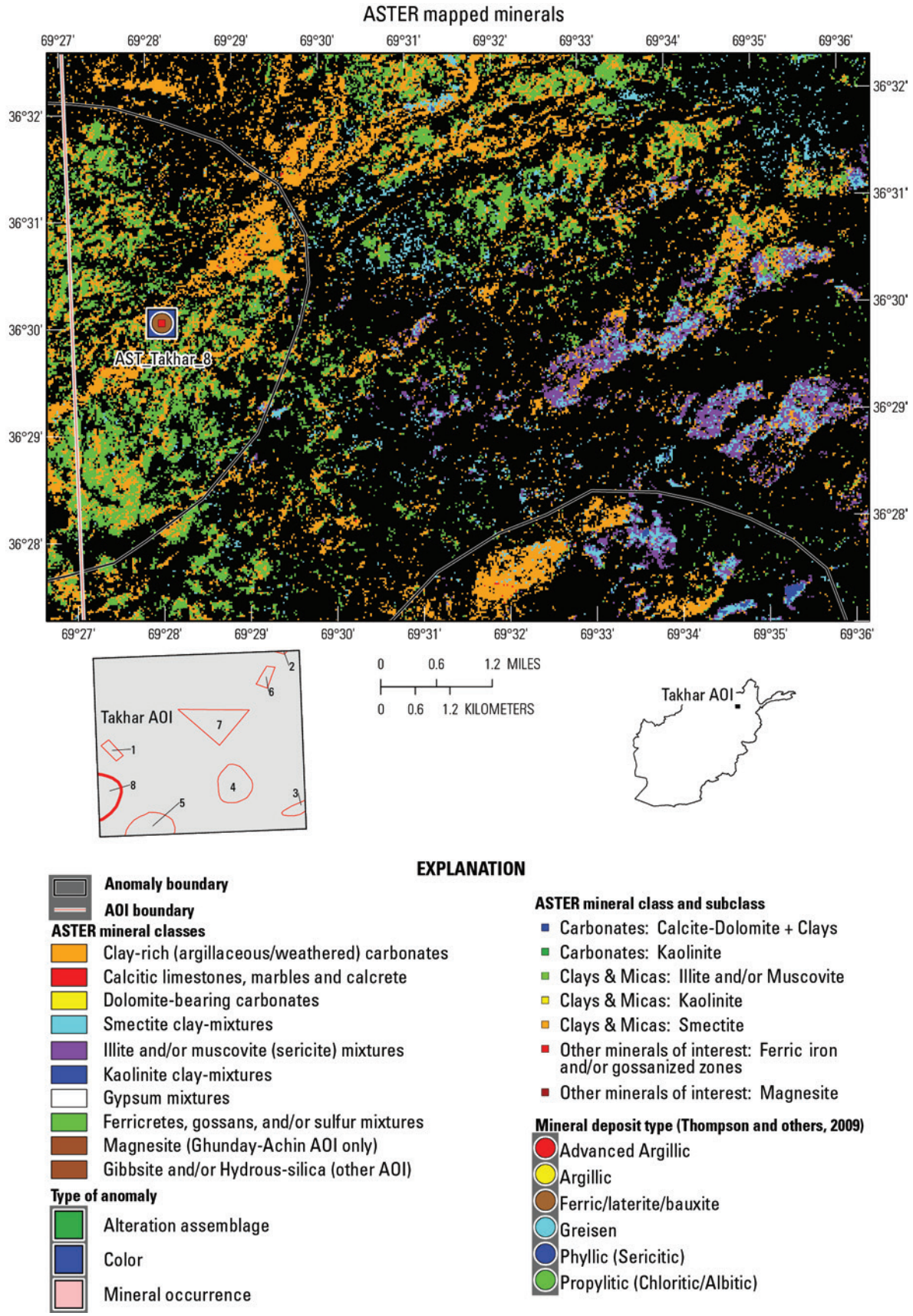

Figure 4.12.8. ASTER color anomaly located in the Takhar Area of Interest (AOI) in Afghanistan. Possible sulfur- and/or phosphate-bearing area within weathered and/or argillaceous carbonate rocks. Further spectral analysis needed to distinguish sulfur from strong ferric iron.

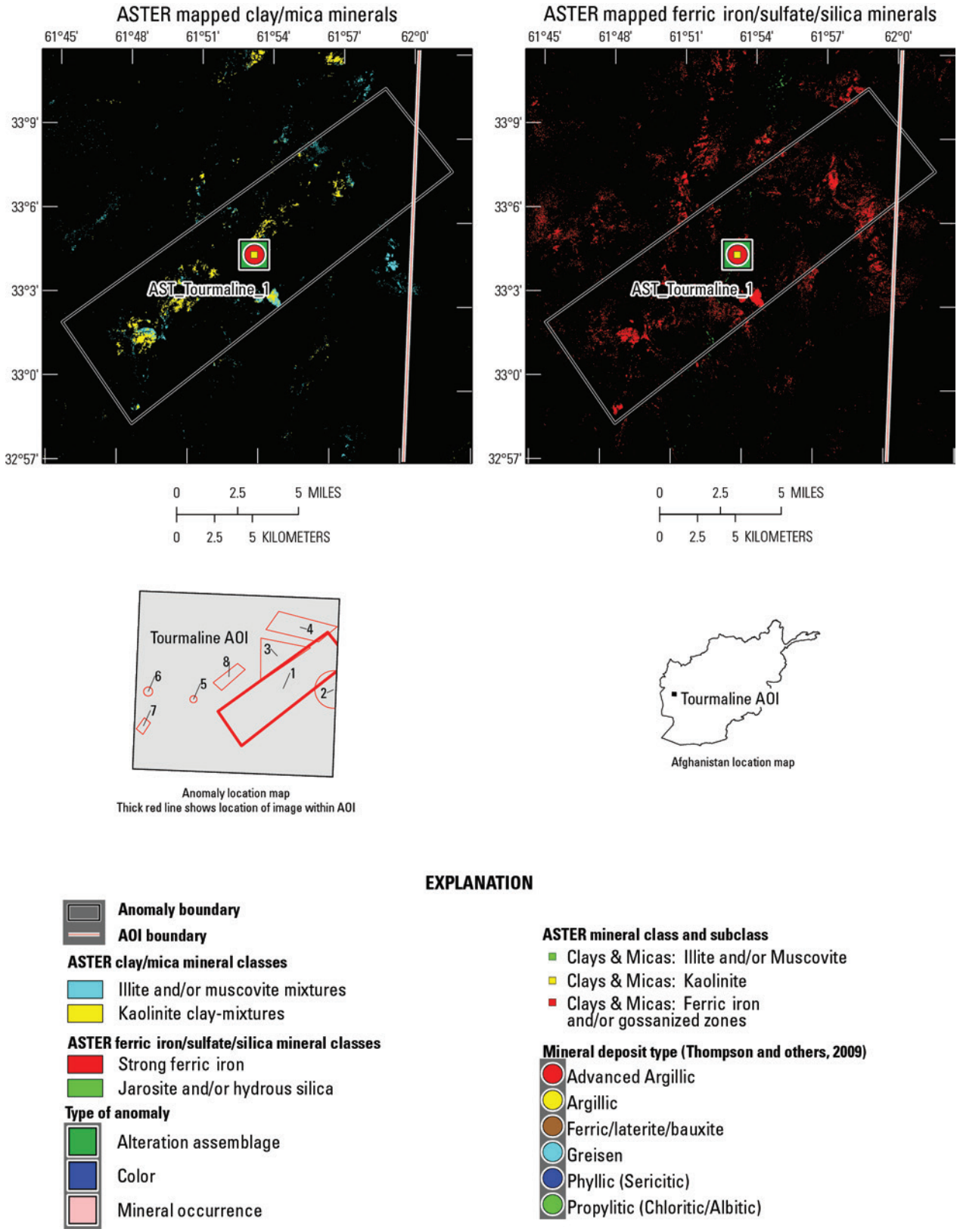

Figure 4.13.1. ASTER alteration anomaly located in the Tourmaline Area of Interest (AOI) in Afghanistan. Regionally extensive and linearly trending zone of mostly kaolinite, sericite, strong ferric iron, and localized areas containing either jarosite-sulfate and/or hydrous-silica minerals.

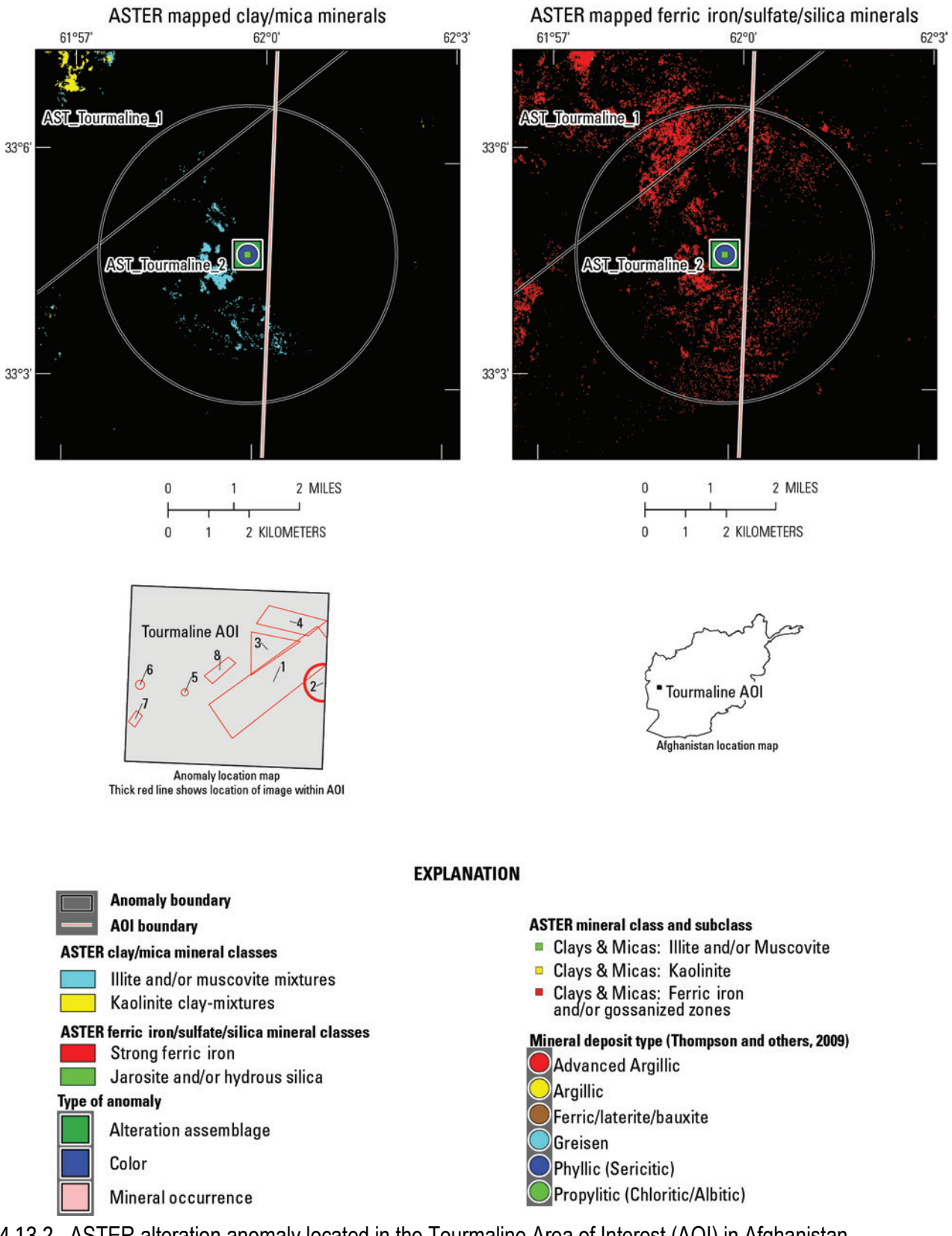

Figure 4.13.2. ASTER alteration anomaly located in the Tourmaline Area of Interest (AOI) in Afghanistan. Broadly circular-shaped region dominated by strong ferric iron and phyllic alteration minerals, overlapping with anomaly AST_Tourmaline_1.

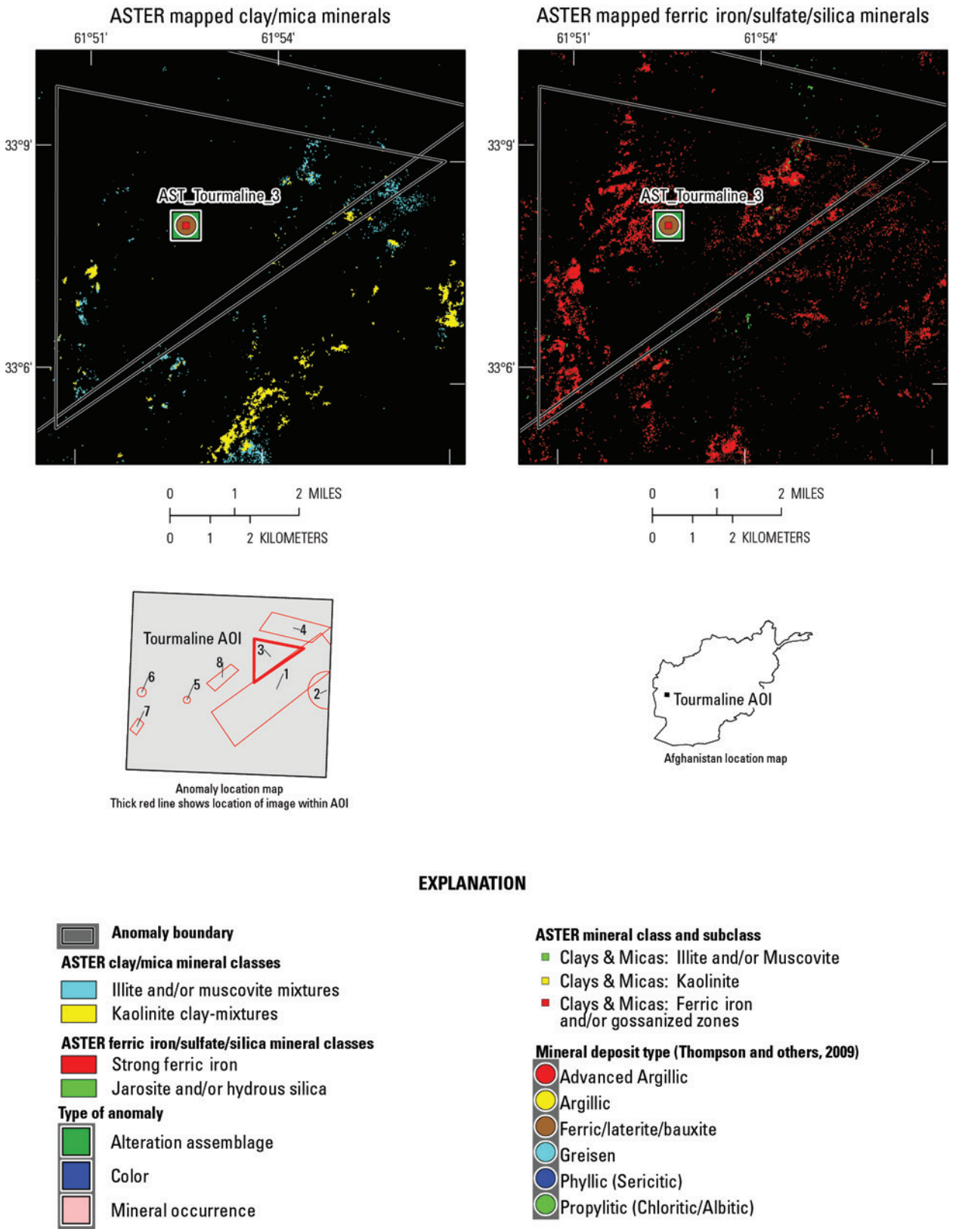

Figure 4.13.3. ASTER alteration anomaly located in the Tourmaline Area of Interest (AOI) in Afghanistan. Regionally extensive area of strong ferric iron staining, with localized areas of argillic/advanced-argillic alteration (larger kaolinite-dominated areas) and phyllic alteration (smaller illite- and/or muscovite-dominated areas).

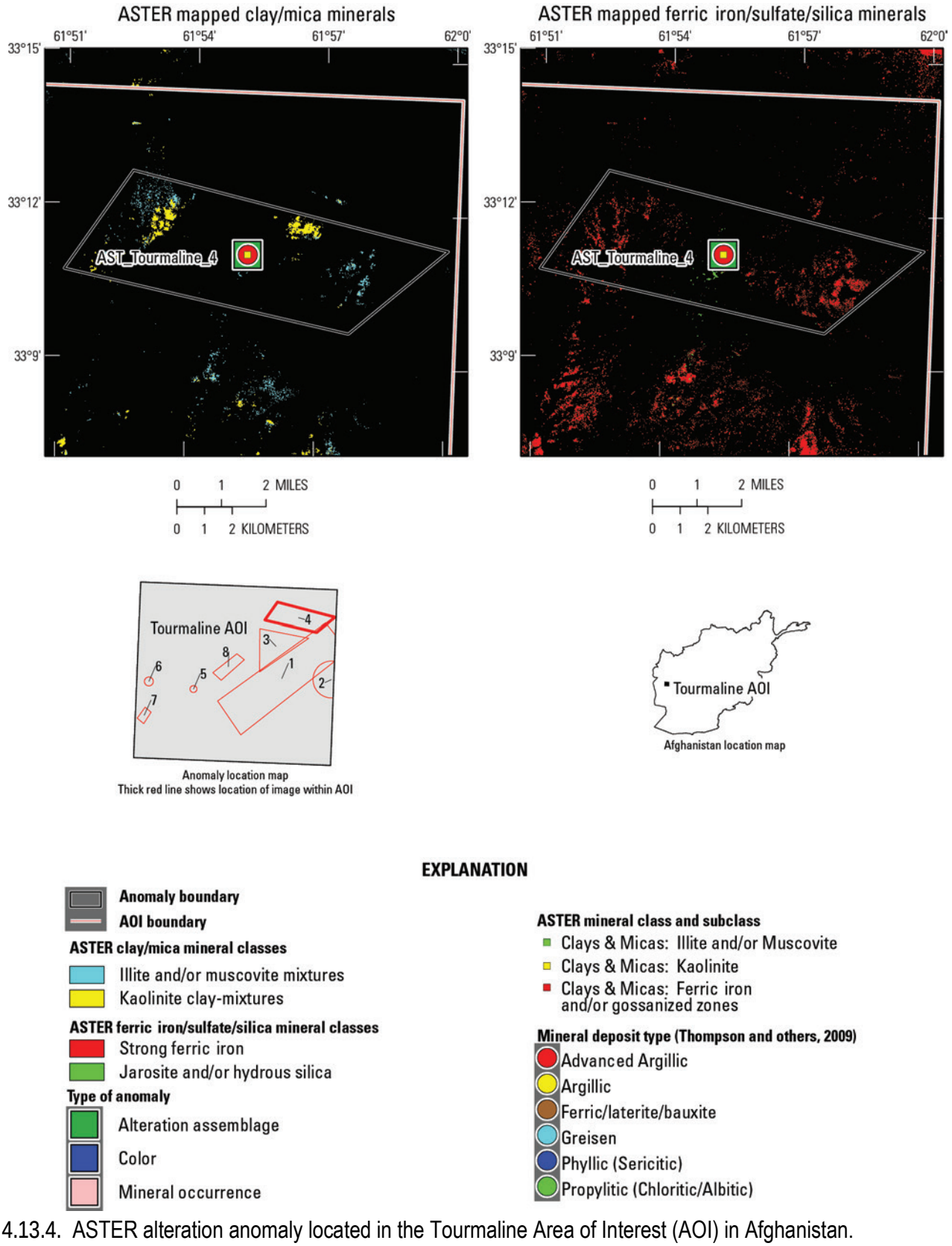

Figure 4.13.4. ASTER alteration anomaly located in the Tourmaline Area of Interest (AOI) in Afghanistan. Regionally extensive area of mostly clay/mica alteration with large areas of overlapping ferric iron staining with argillic/advanced-argillic alteration mineral areas surpassing phyllic/sericitic alteration mineral areas.

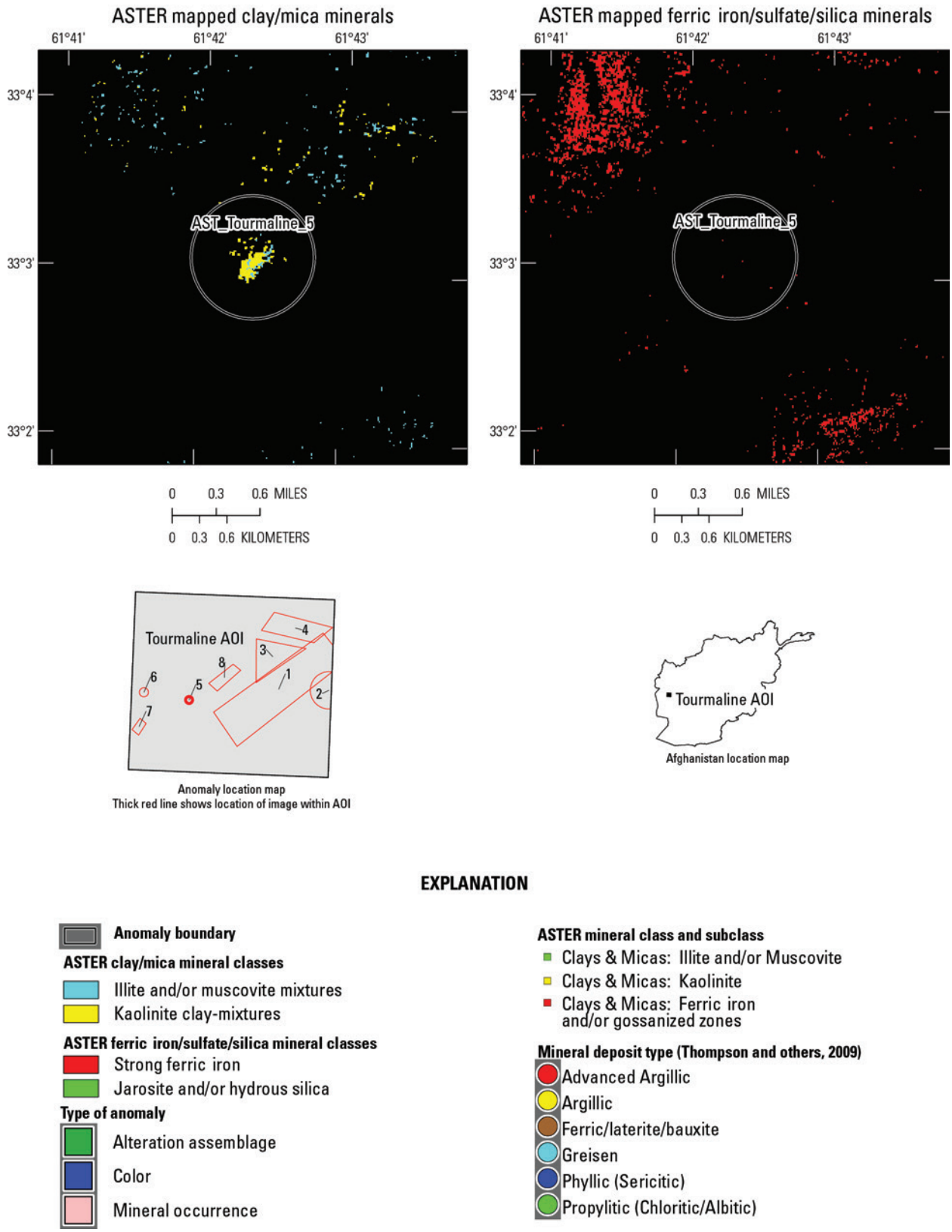

Figure 4.13.5. ASTER alteration anomaly located in the Tourmaline Area of Interest (AOI) in Afghanistan. Localized area of mixed argillic/advanced-argillic alteration and phyllic/sericitic alteration, perhaps epithermal vein or volcanic-hosted sulfide-related.

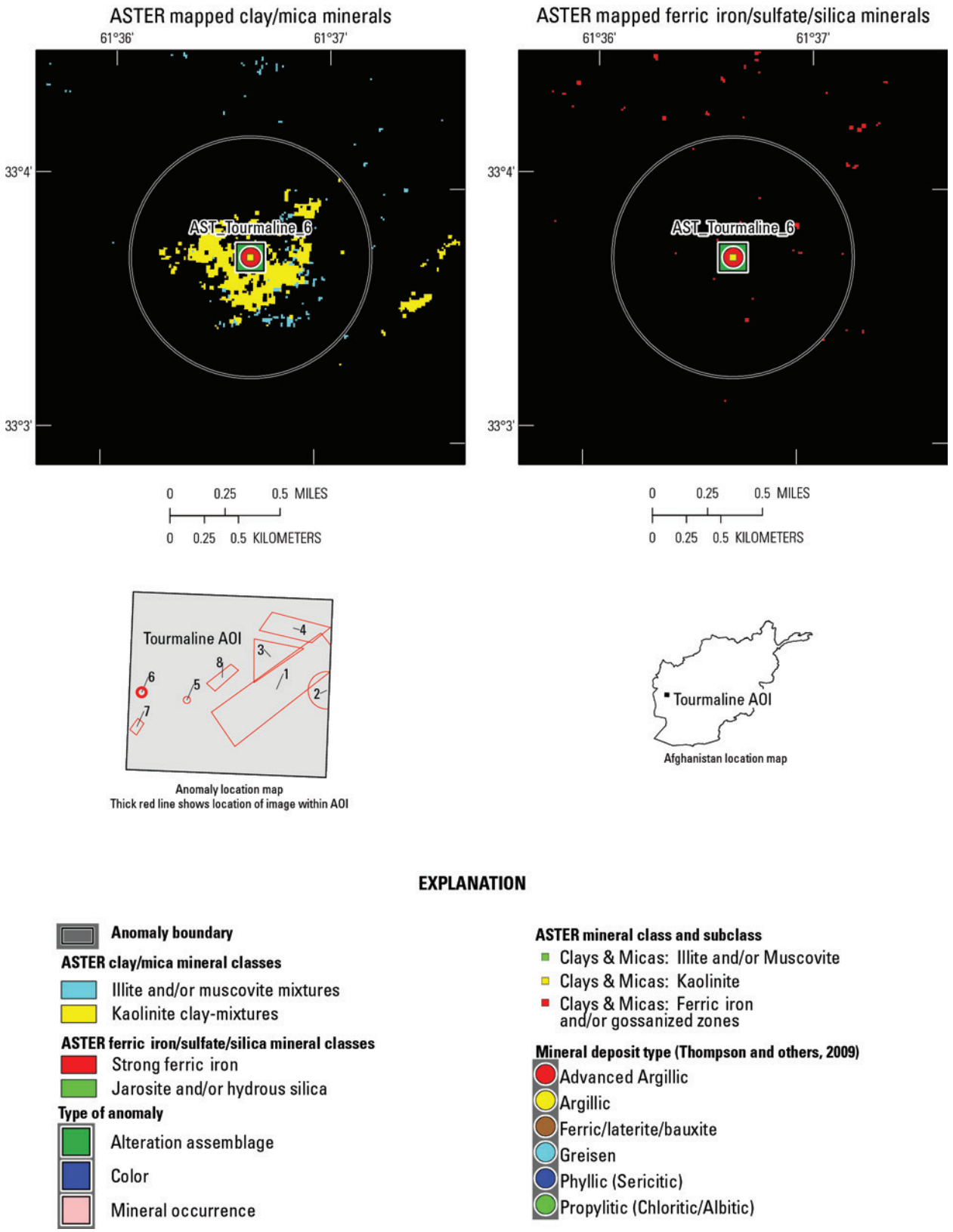

Figure 4.13.6. ASTER alteration anomaly located in the Tourmaline Area of Interest (AOI) in Afghanistan. Localized area of mostly argillic/advanced-argillic alteration assemblage dominated by kaolinite.

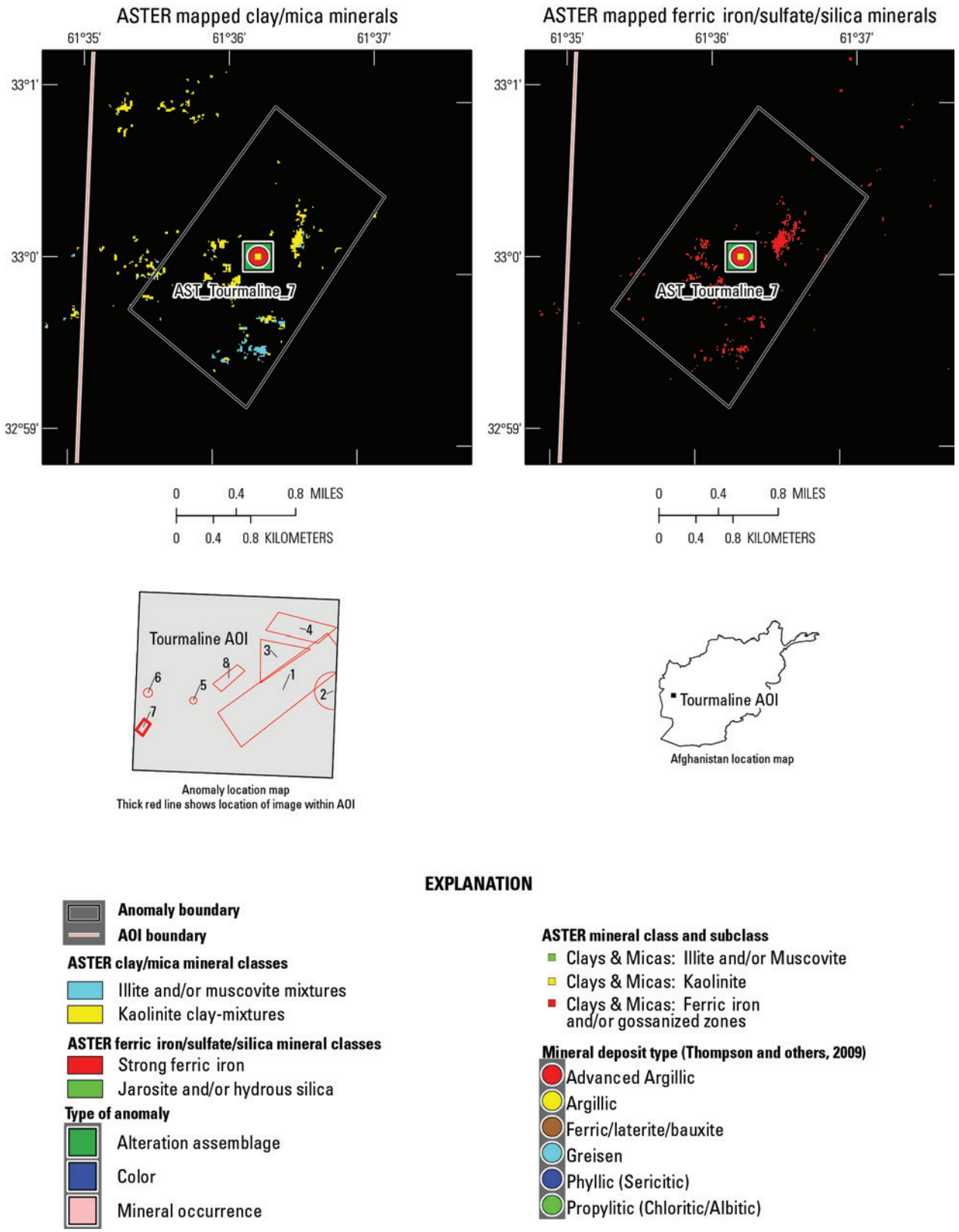

Figure 4.13.7. ASTER alteration anomaly located in the Tourmaline Area of Interest (AOI) in Afghanistan. Localized area of mostly argillic/advanced-argillic alteration with lesser amounts of phyllic/sericitic alteration and ferric iron-staining. Anomaly has potential for linearly trending vein alteration with volcanic-hosted sulfide sources.

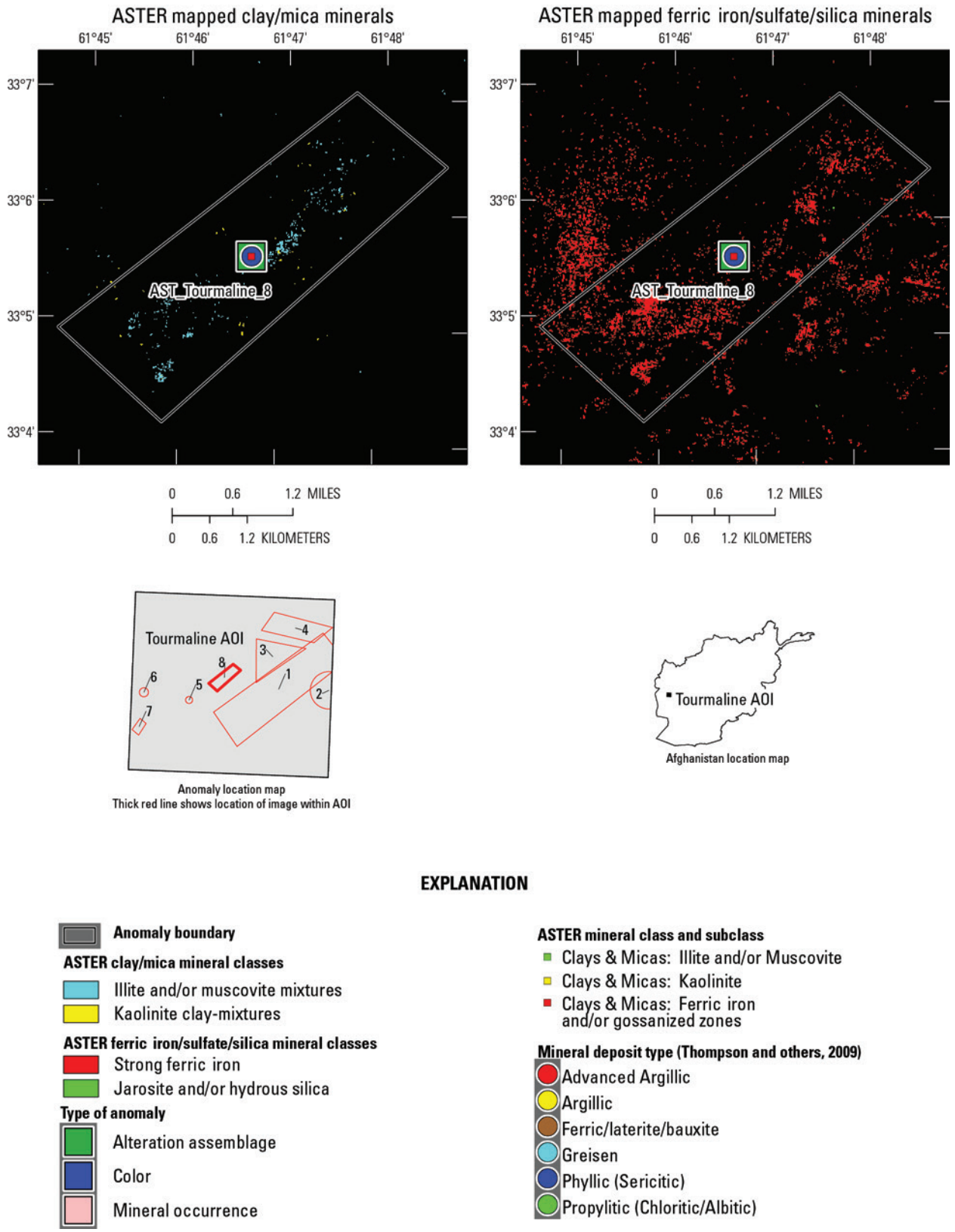

Figure 4.13.8. ASTER alteration anomaly located in the Tourmaline Area of Interest (AOI) in Afghanistan. Regionally extensive and linearly trending zone of strong ferric iron mixed with localized phyllic/sericitic alteration minerals and could be structurally related to the AST_Tourmaline_1 anomaly.

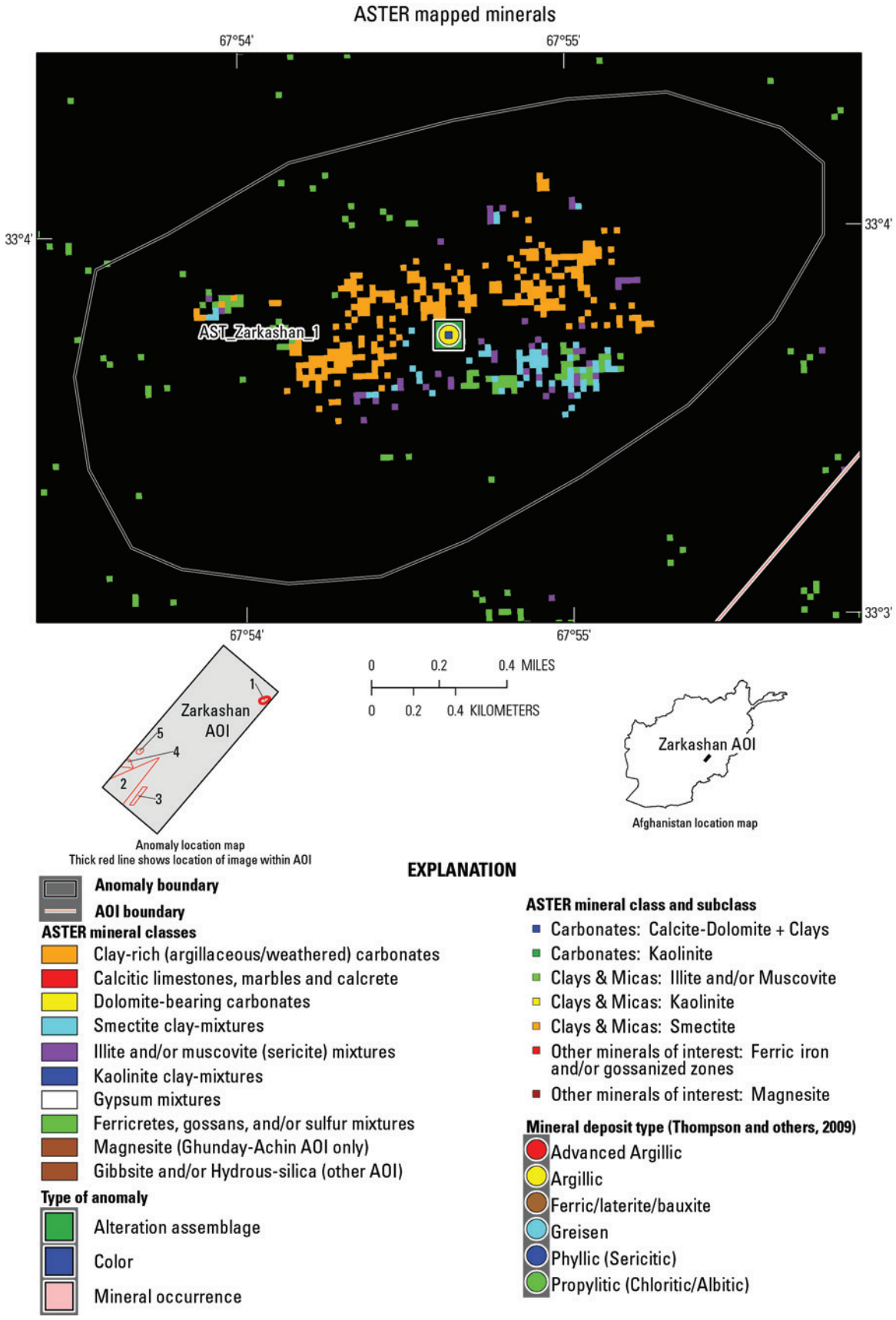

Figure 4.14.1. ASTER alteration anomaly located in the Zarkashan Area of Interest (AOI) in Afghanistan. Anomaly is a circular-shaped upstream source area from a mercury stream-geochemistry anomaly.

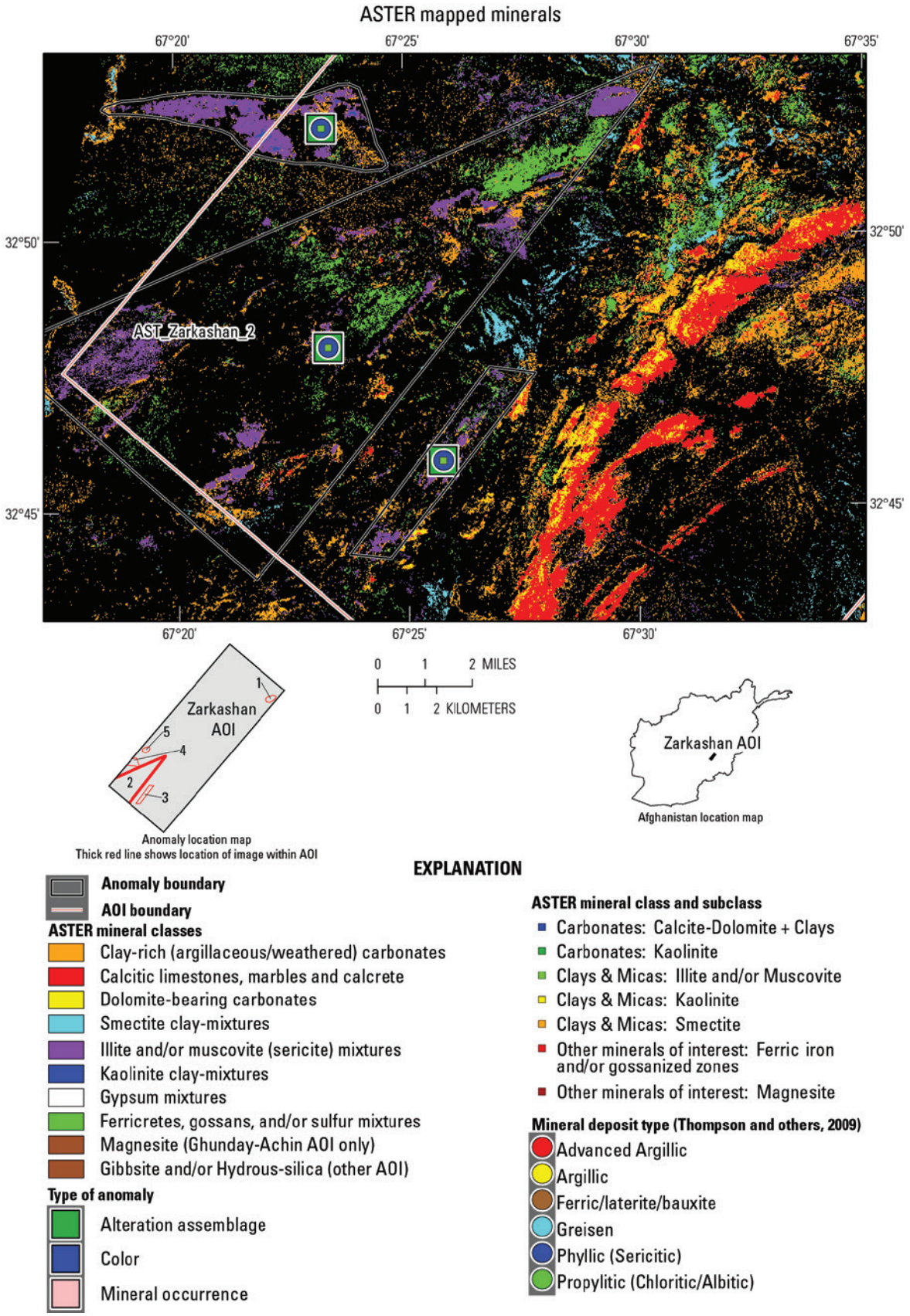

Figure 4.14.2. ASTER alteration anomaly located in the Zarkashan Area of Interest (AOI) in Afghanistan. Phyllic/sericitic and strong ferric iron-alteration associated with a Zarkashan skarn mineralized zone. Further ASTER mapping needed to map extent of noncarbonate-related propylitic minerals such as chlorite and/or epidote.

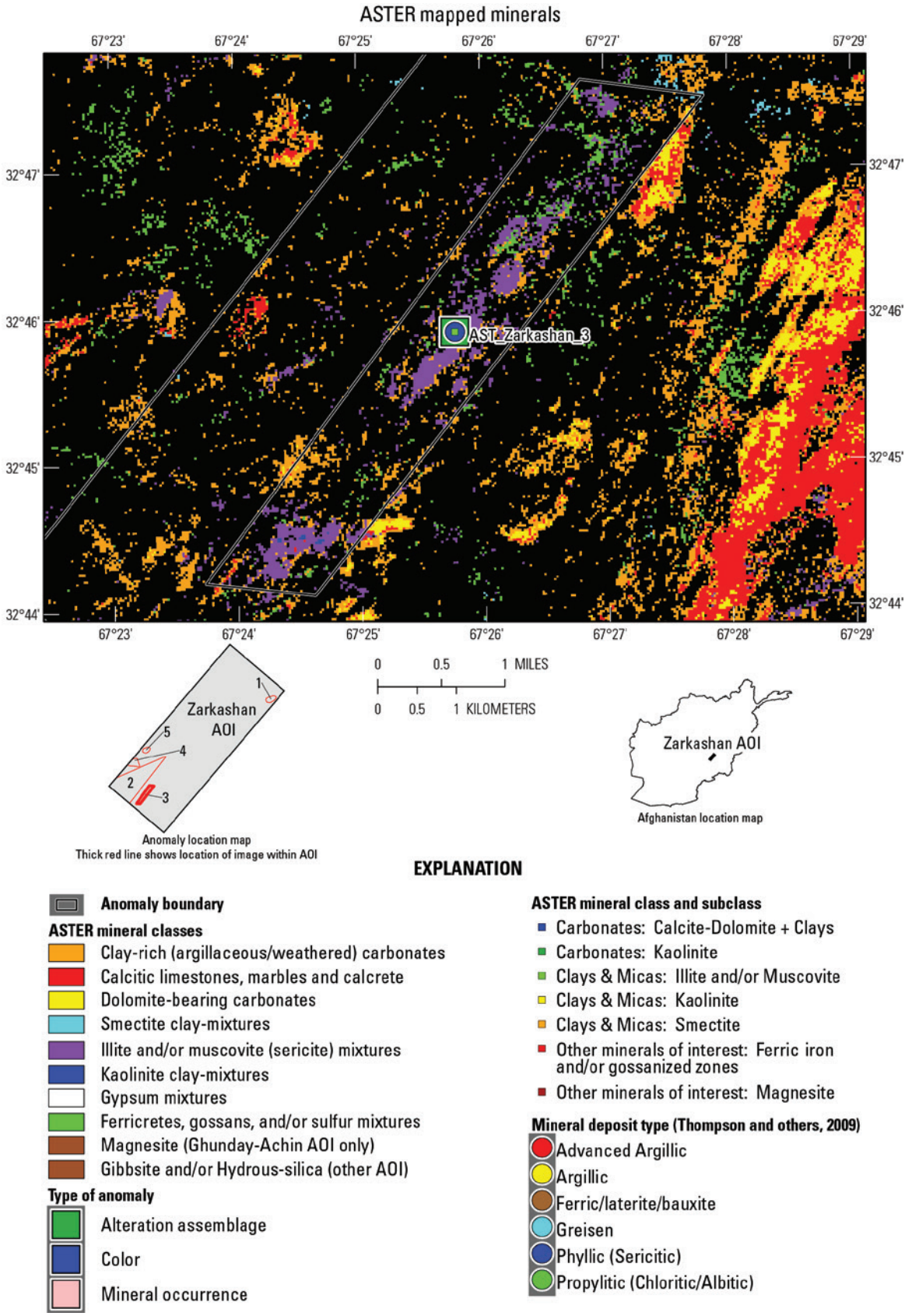

Figure 4.14.3. ASTER alteration anomaly located in the Zarkashan Area of Interest (AOI) in Afghanistan. Phyllic/sericitic alteration along a linear zone associated with Zarkashan skarn mineralized zone. Further ASTER mapping needed to map extent of noncarbonate-related propylitic minerals such as chlorite and/or epidote.

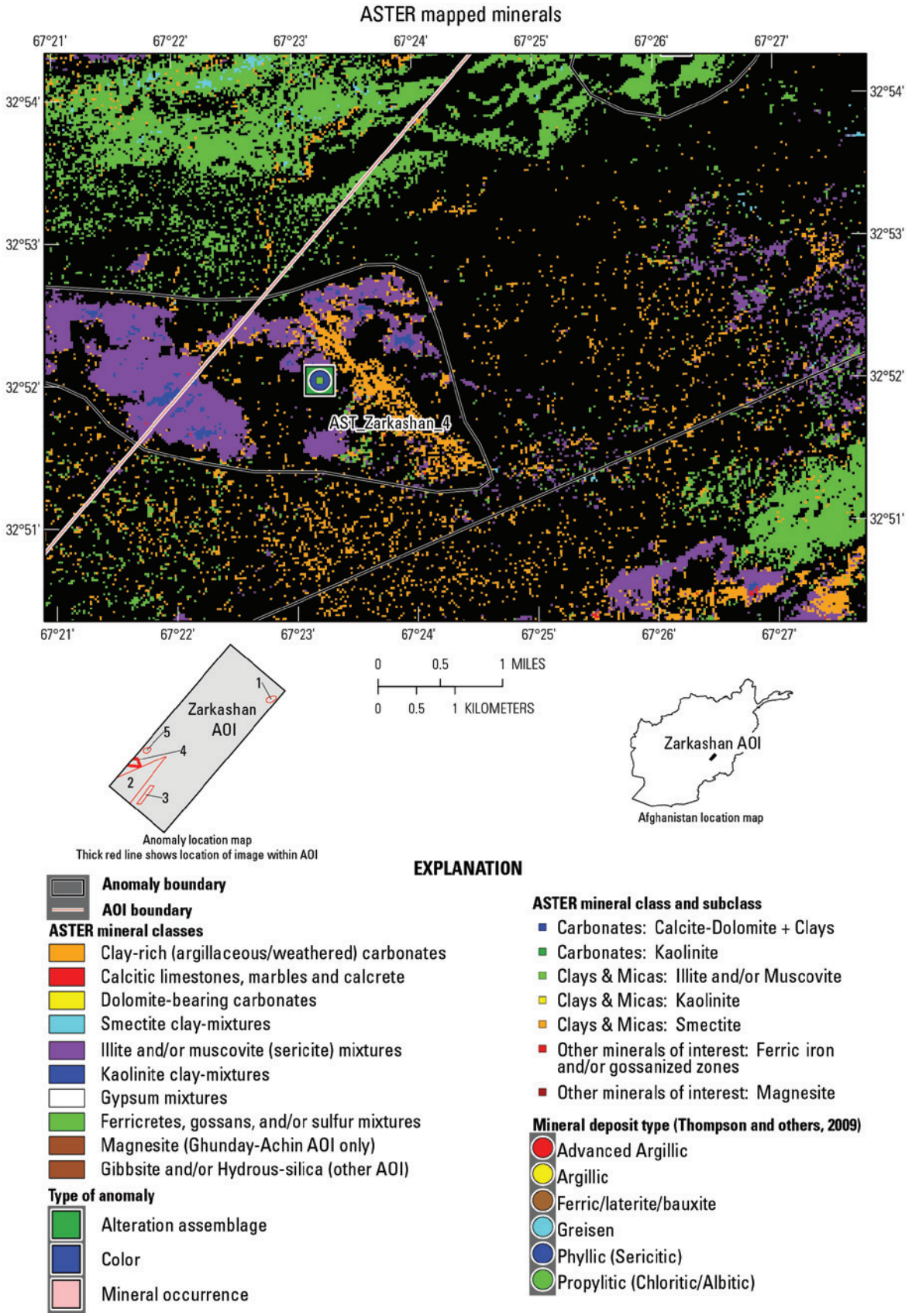

Figure 4.14.4. ASTER alteration anomaly located in the Zarkashan Area of Interest (AOI) in Afghanistan. Phyllic/sericitic alteration containing small kaolinite-abundant zones possibly the result of acid-sulphate leach processes in acid-neutralizing carbonate host rocks. Further processing of ASTER needed to show chlorite/epidote.

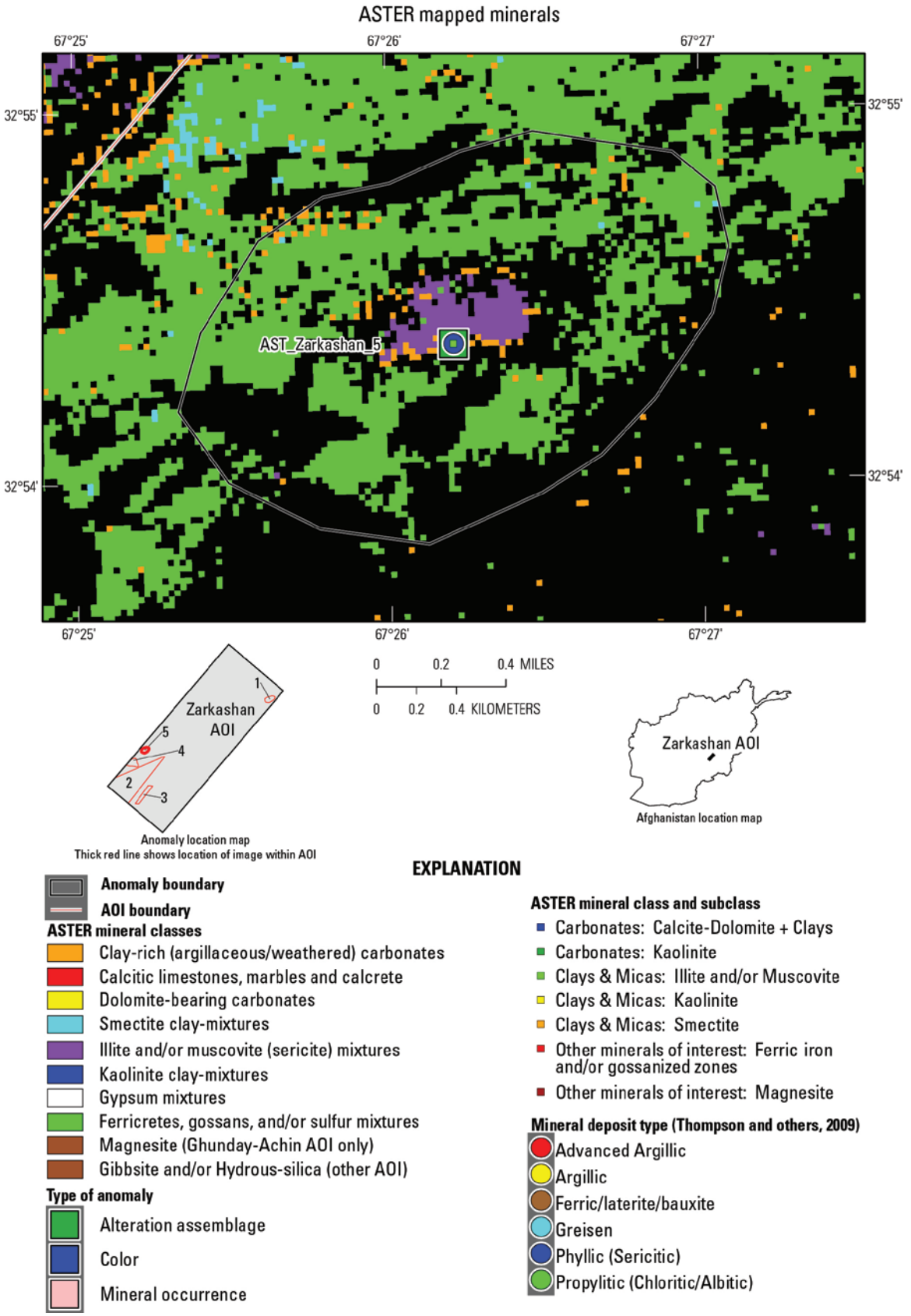

Figure 4.14.5. ASTER alteration anomaly located in the Zarkashan Area of Interest (AOI) in Afghanistan. Phyllic/sericitic alteration surrounded by strong ferric iron along a regional structural trend. Further ASTER mapping needed to map extent of noncarbonate related propylitic minerals such as chlorite and/or epidote.

4.3 References Cited

Crowley, J.K., 1994, Remote-sensing spectral properties of selected industrial minerals and ores, chap. F *of* Advances in research on mineral resources, 1994: U.S. Geological Survey Bulletin 2081, p. 43–51.

Dalton, J.B., Bove, D.J., Mladinich, C.S., and Rockwell, B.W., 2004, Identification of spectrally similar materials using the USGS Tetracorder algorithm: The calcite-epidote-chlorite problem: Remote Sensing of Environment, v. 89, p. 455–466.

Doebrich, J.L., and Wahl, R.R., 2006, Geologic and mineral resource map of Afghanistan: U.S. Geological Survey Open-File Report 2006–1038, 1 sheet, scale 1:850,000, available at *http://pubs.usgs.gov/of/2006/1038.*

Gillespie, A.R., Matsunaga, T., Rokugawa, S., and Hook, S.J., 1998, Temperature and emissivity separation from Advanced Spaceborne Thermal Emission and Reflection Radiometer (ASTER) images: IEEE Transactions on Geoscience and Remote Sensing, v. 36, p. 1113–1126.

Hubbard, B.E., Rowan, L.C., Dusel-Bacon, C., and Eppinger, R.G., 2007, Geologic mapping and mineral resource assessment of the Healy and Talkeetna Mountains quadrangles, Alaska, using minimal cloud- and snow-cover ASTER data: U.S. Geological Survey Open-File Report 2007–1046, accessed August 19, 2011, at *http://pubs.usgs.gov/of/2007/1046.*

Mars, J.C., and Rowan, L.C., 2007, Mapping phyllic and argillic-altered rocks in southeastern Afghanistan using Advanced Spaceborne Thermal Emission and Reflection Radiometer (ASTER) data: U.S. Geological Survey Open-File Report 2007-1006, Poster format, accessed August 19, 2011, at *http://pubs.usgs.gov/of/2007/1006.*

Mars, J.C., and Rowan, L.C., 2010, Spectral assessment of new ASTER SWIR surface reflectance data products for spectroscopic mapping of rocks and minerals: Remote Sensing of Environment, v. 114, p. 2011–2025.

Ninomiya, Y., Fu, B., and Cudahy, T.J., 2005, Detecting lithology with Advanced Spaceborne Thermal Emission and Reflection Radiometer (ASTER) multispectral thermal infrared "radiance-at-sensor" data: Remote Sensing of Environment, v. 99, p. 127–139.

Oztan, N.S., and Suzen, M.L., 2011, Mapping evaporite minerals by ASTER: International Journal of Remote Sensing, v. 32, no. 6, p. 1651–1673.

Peters, S.G., Ludington, S.D., Orris, G.J., Sutphin, D.M., Bliss, J.D., and Rytuba, J.J., eds., and the U.S. Geological Survey-Afghanistan Ministry of Mines Joint Mineral Resource Assessment team, 2007, Preliminary non-fuel mineral resource assessment of Afghanistan: U.S. Geological Survey Open-File Report 2007–1214, 810 p., 1 CD-ROM, accessed August 19, 2011, at *http://pubs.usgs.gov/of/2007/1214/.*

Rockwell, B.W., and Hofstra, A.H., 2008, Identification of quartz and carbonate minerals across northern Nevada using ASTER thermal infrared emissivity data—Implications for geologic mapping and mineral resource investigations in well-studied and frontier areas: Geosphere, v. 4, no. 1, p. 218–246.

Rowan, L.C., and Mars, J.C., 2003, Lithologic mapping in the Mountain Pass, California area using Advanced Spaceborne Thermal Emission and Reflection Radiometer (ASTER) data: Remote Sensing of Environment, v. 84, p. 350–366.

Rowan, L.C., Hook, S.J., Abrams, M.J., and Mars, J.C., 2003, Mapping hydrothermally altered rocks at Cuprite, Nevada, using the Advanced Spaceborne Thermal Emission and Reflection Radiometer (ASTER), A new satellite-imaging system: Economic Geology, v. 98, p. 1019–1027.

Rowan, L.C., Mars, J.C., and Simpson, C.J., 2005, Lithologic mapping of the Mordor, NT, Australia ultramafic complex by using the Advanced Spaceborne Thermal Emission and Reflection Radiometer (ASTER): Remote Sensing of Environment, v. 99, p. 105–126.

Thompson, A.J.B, Hauff, P.L., and Robitaille, A.J., 2009, Alteration mapping in exploration: Application of Short-Wave Infrared (SWIR) spectroscopy, *in* Bendell, R., Crosta, A.P., and Grunsky, E., eds., Remote sensing and spectral geology: Society of Economic Geologists (SEG) Reviews in Economic Geology, v. 16, p. 12–23.

Chapter 5: Mapping Anomalous Mineral Zones Using HyMap Imaging Spectrometer—Data for Selected Areas of Interest in Afghanistan

By T.V.V. King, T.M Hoefen, M.R. Johnson., R.F. Kokaly, and K.E. Livo

5.1 Imaging Spectrometer Overview

The HyMap imaging spectrometer measures the reflected visible and near-infrared light from the Earth's surface in many narrow data channels, producing a reflectance spectrum for each pixel in the image. Calibrated HyMap reflectance spectra can be interpreted and used to identify surface materials and their composition. As part of a collaborative effort between the U.S. Geological Survey (USGS), National Aeronautics and Space Administration (NASA), U.S. Department of State, Afghan Geological Survey, and Afghanistan Ministry of Mines, an airborne hyperspectral survey using the HyMap sensor (Cocks and others, 1998) was conducted in Afghanistan from August 22 to October 2, 2007.

The HyMap imaging spectrometer has 512 cross-track pixels and covers the wavelength range 0.43 to 2.48 microns (μm) in 128 channels. HyMap was flown on a WB-57 high-altitude aircraft at approximately 50,000 ft and collected 218 flight lines covering a total surface area of 438,012 km^2 (Kokaly and others, 2008). The resulting dataset includes more than 800,000,000 pixels of imaging spectrometer data. After conversion to reflectance and georegistration, these data were analyzed by comparing each pixel's reflectance spectrum against entries in a library of reference spectra (97 spectral standards) of various surface materials (Kokaly, 2011). The results were then used to create maps of minerals, vegetation, and other materials (Peters and others, 2011).

5.2 Imaging Spectrometer Data

The results of the spectroscopic analysis are presented in two maps. One map shows the distribution of iron-bearing minerals, with absorption features in the visible and near-infrared wavelength region; this map is referred to as the iron-bearing minerals and other materials map or, alternatively, as the 1-μm map (King and others, in press). The second map shows the distribution of carbonates, phyllosilicates, sulfates, altered minerals, and other minerals that have their primary absorption features in the shortwave infrared wavelength region; this map is referred to as the carbonates, phyllosilicates, sulfates, altered minerals, and other materials map or, alternatively, as the 2-μm map (Kokaly and others, in press). Some mineral classes in the two maps are composites of results of multiple reference spectra with similar composition (for example, the kaolinite class is a combination of results for two reference spectra—well-crystalline kaolinite and poorly crystalline kaolinite). The compositing of results reduced the number of mineral classes for clarity of presentation.

5.2.1 Iron-Bearing Minerals and Other Materials

The results of the 1-μm analysis—the iron-bearing minerals and other materials map—were grouped into 28 mineral classes. Iron-bearing minerals with different mineral compositions but similar, broad spectral features are difficult to classify as specific minerals. Thus, generic spectral mineral

classes, including several minerals with similar absorption features, such as Fe^{3+} Type 1 and Fe^{3+} Type 2, are depicted on the map.

5.2.2 Carbonates, Phyllosilicates, Sulfates, Altered Minerals, and Other Materials

The results of the 2-μm analysis, the carbonates, phyllosilicates, sulfates, altered minerals, and other materials map, were grouped into 32 classes. Minerals with slightly different mineral compositions but similar spectral features are less easily distinguished; thus, some identified mineral classes consist of several minerals with similar spectra, such as the chlorite or epidote class. In both analyses, when a comparison with reference spectra produced no viable match, a designation of "not classified" was assigned to a pixel.

5.3 HyMap Identification of Anomalies

In collaboration with the Department of Defense Task Force for Business and Stability Operations (TFBSO), the HyMap imaging spectrometer data and Landsat broad-band sensor data of 21 Areas of Interest (AOI; fig. 1) were analyzed to better define the magnitude and extent of previously known mineral occurrences and to identify potential areas of mineralization (Peters and others, 2011). During the analysis of these AOIs, 158 anomalies were observed in the HyMap mineral maps (figs. 5.1.1–5.20.13). Criteria used to identify the anomalies included (1) spatially coherent distinct mineral occurrences that differed from the composition of surrounding material, (2) mineral assemblage anomalies based on the composition of coherently mapped groups of pixels, (3) shape of anomalous zone, and (4) color of physical features using HyMap data. When color variations were observed in the HyMap data, the Landsat Enhanced Thematic Mapper (ETM) data (Davis, 2006) were used as a secondary reference for comparison.

Mineral assemblage anomalies included areas of potential hydrothermal alteration of sedimentary, igneous, and metamorphic rocks. For areas that were defined by a specific variety of mineral assemblages, hydrothermally altered rocks were further categorized by mineral alteration types (for example, argillic, phyllic, and propylitic) as defined by Thompson and others (2009).

Color anomalies were generally related to areas of intense alteration that commonly resulted in light-colored or bleached patterns: red coloring of rocks related to iron-oxidation and green coloring of host rocks related to clay content. The most common geometric anomalies consist of rounded features, associated with surficial expressions of intrusions or buried intrusions, and linear expressions of alteration, generally associated with faults or fractures that act as conduits for fluids associated with mineral alteration.

Although the occurrence of certain minerals, such as pyrophyllite, buddingtonite, dickite, and jarosite, suggest that mineralization processes may have operated in the area, these minerals can occur through common rock-forming processes. Consequently, the distribution patterns of the identified minerals are extremely important in understanding the geologic framework of mapped anomalous zones and are also important in evaluating the potential for mineral deposits in these zones. Further field verification and geochemical sampling of these anomalous zones are recommended to corroborate the imaging spectroscopy data and to understand the geologic framework of the area.

No anomalies were identified in areas of previously known mineral prospects, although correlations between the minerals mapped in the HyMap data and reported mineral alteration of the prospects was common (Abdullah and others,1977; Peters and others, 2007; Peters and others, 2011).

In some instances anomalies identified in the HyMap data are congruous with anomalies in the geophysical data (Drenth and others, chap. 3, this volume; Sweeney and others, 2006; Shenwary and others, 2011) and ASTER data (Hubbard, chap. 4, this volume). Such areas should be considered prime targets for detailed site characterization because each of the anomalous areas were identified independently in the respective dataset.

5.4 Presentation of HyMap Anomalies

All HyMap identified anomalies are displayed in a series of maps showing both the 1-μm and 2-μm data (figs. 5.1.1–5.20.13). The maps display the imaging spectrometer (HyMap) datasets in separate map windows as images color-coded by mineral class names and described in the map explanation under the headings, “Mineral class name–Iron-bearing minerals” and “Mineral class name–Alteration minerals.” Solid black lines with a white outline define the approximate shape and extent of the identified anomaly polygons. Point features shown on the map are color-coded categorical representations of the type of anomaly and when applicable, alteration assemblage deposit type (Thompson and others, 2009). For example, an anomaly with an "Advanced argillic" alteration assemblage deposit type and "Alteration assemblage" type of anomaly is shown as a small black square (Type of anomaly: Alteration assemblage) overlain on a larger red circle (Alteration assemblage deposit type: Advanced argillic). The point features on the maps are displaying some of the additional categorical descriptions about the anomalies that are contained in the attribute table of the shapefile and contained in the KMZ file provided in chapter 2 of this report.

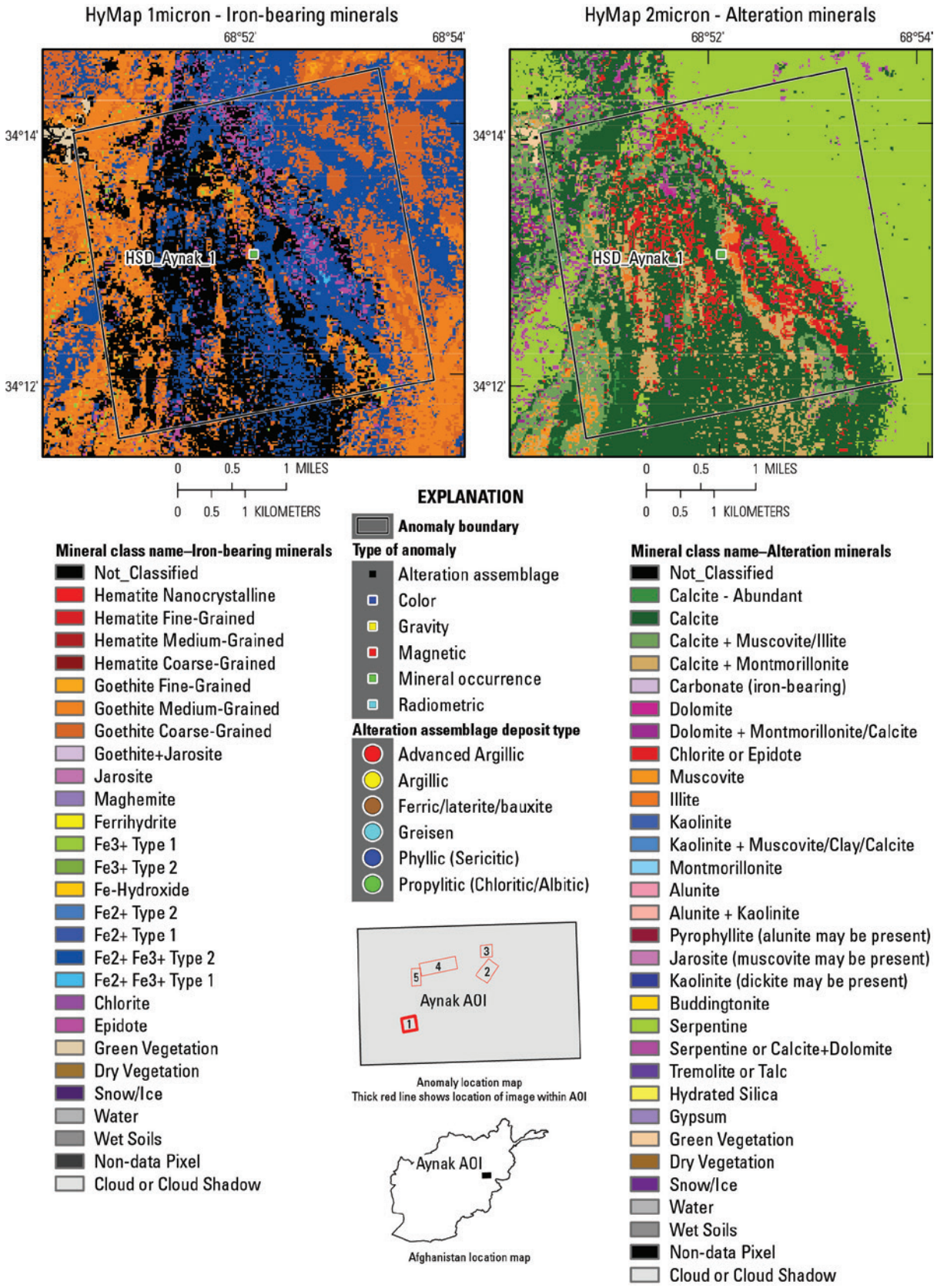

Figure 5.1.1. Hyperspectral anomaly located in the Aynak Area of Interest (AOI) in Afghanistan based on presence of Chlorite or Epidote, Serpentine, Illite, Dolomite minerals, Fe^{3+} Type 1, and Goethite minerals.

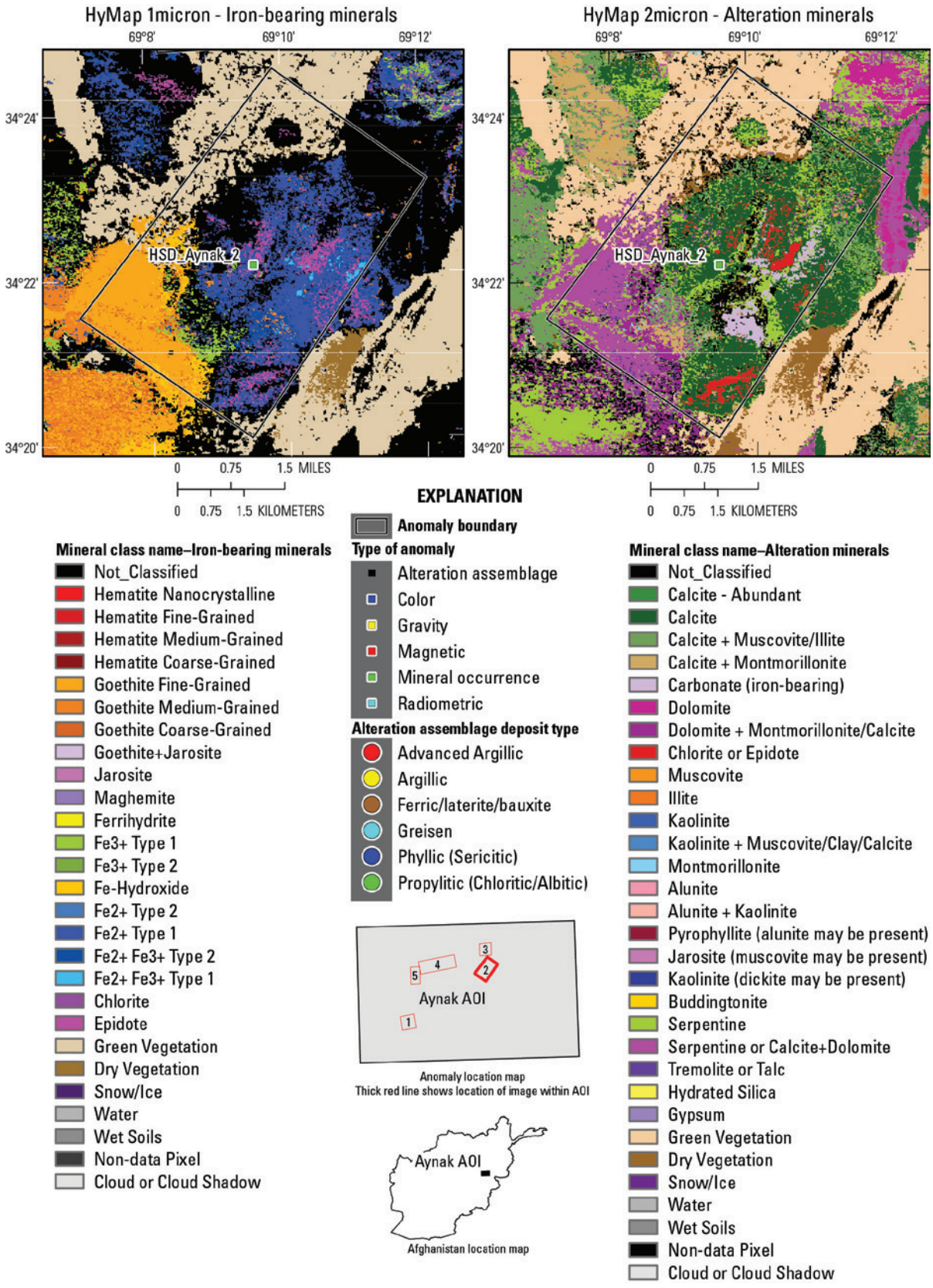

Figure 5.1.2. Hyperspectral anomaly located in the Aynak Area of Interest (AOI) in Afghanistan based on presence of Chlorite or Epidote, Carbonate (iron-bearing), Serpentine, Dolomite minerals, and Fe^{3+} Type 1.

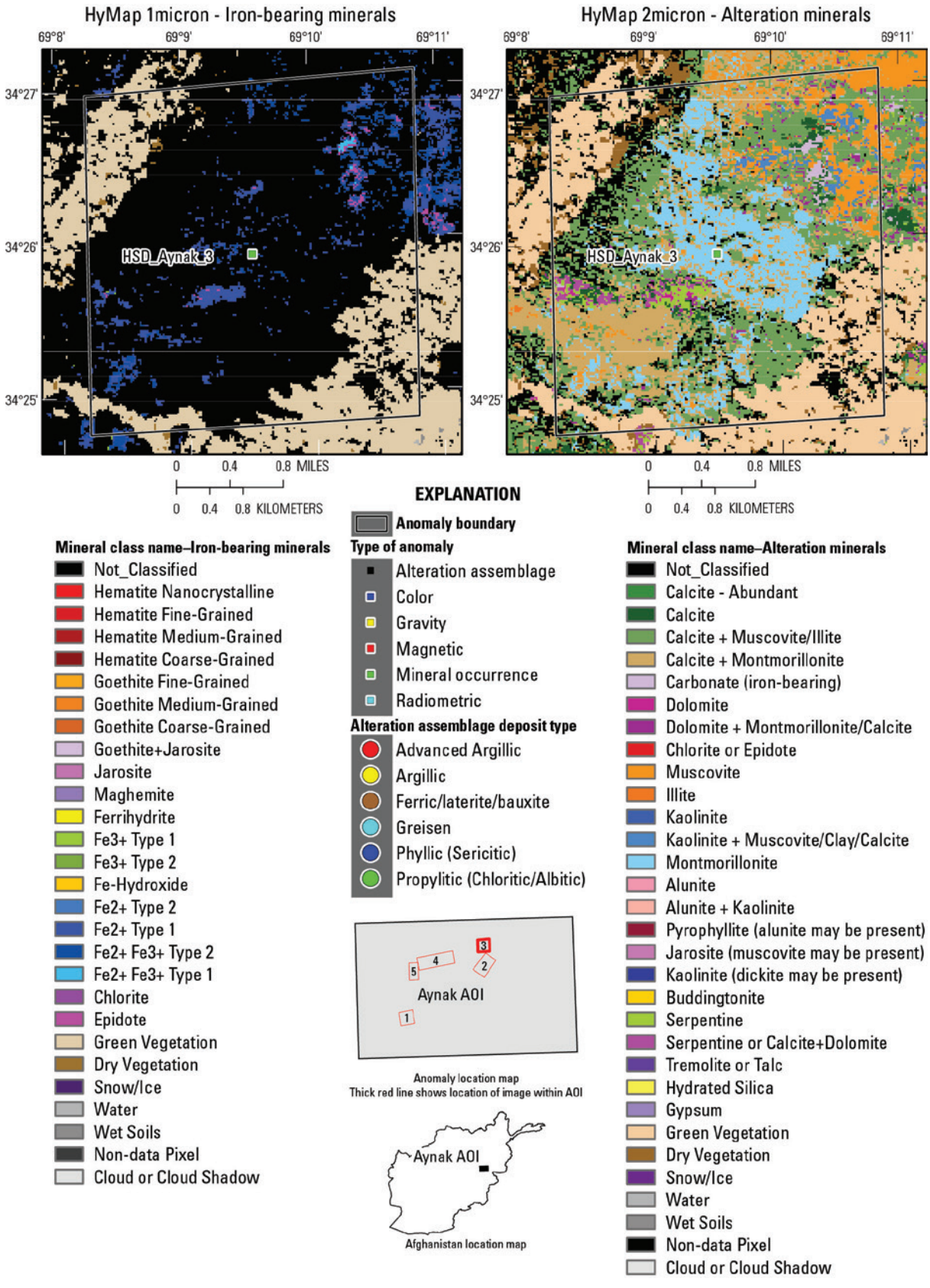

Figure 5.1.3. Hyperspectral anomaly located in the Aynak Area of Interest (AOI) in Afghanistan based on presence of Chlorite or Epidote, Carbonate (iron-bearing), Serpentine, Dolomite minerals, and Fe^{3+} Type 1.

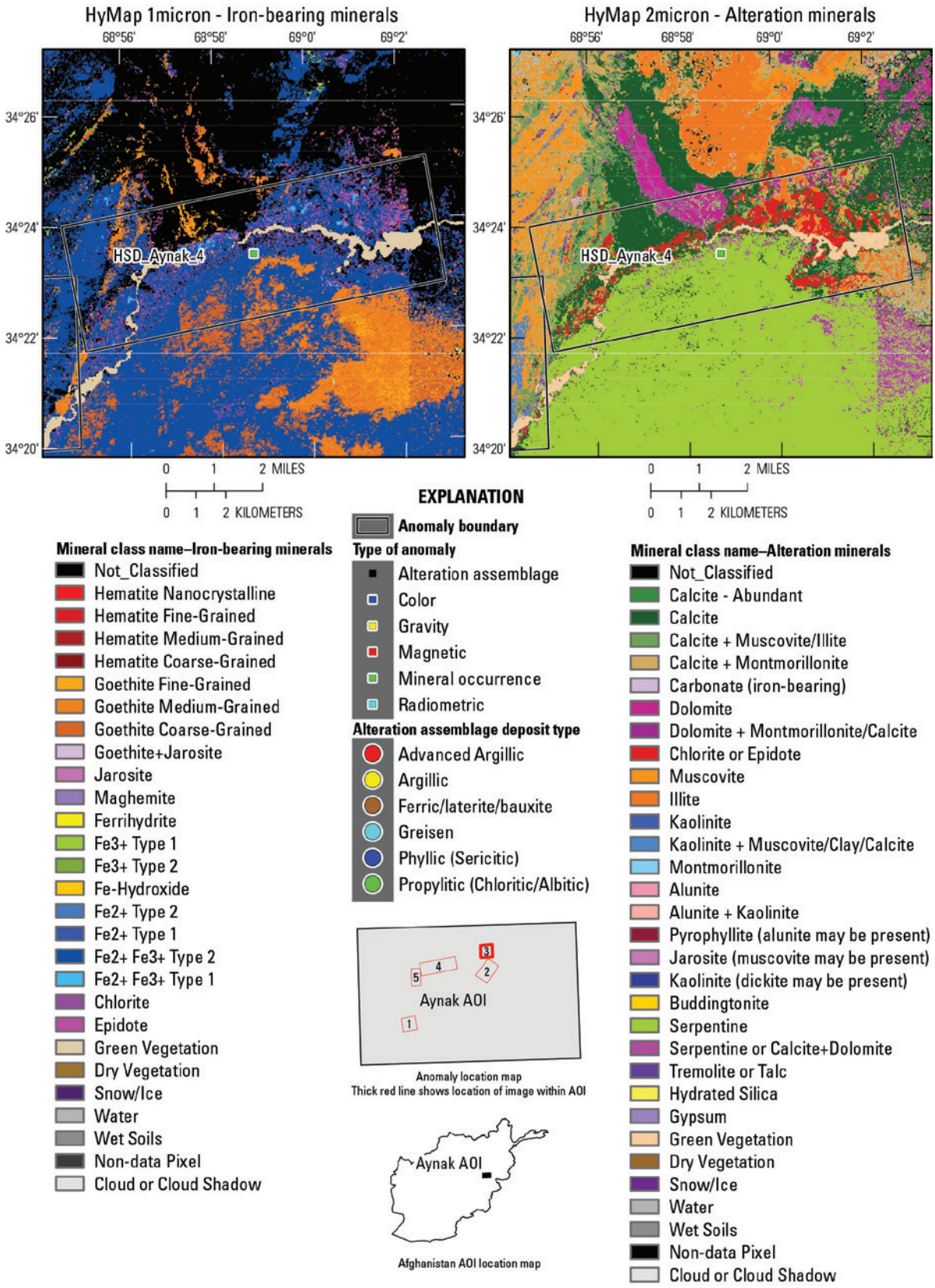

Figure 5.1.4. Hyperspectral anomaly located in the Aynak Area of Interest (AOI) in Afghanistan based on presence of Chlorite or Epidote, Serpentine, and Fe^{2+} Fe^{3+} Type 1.

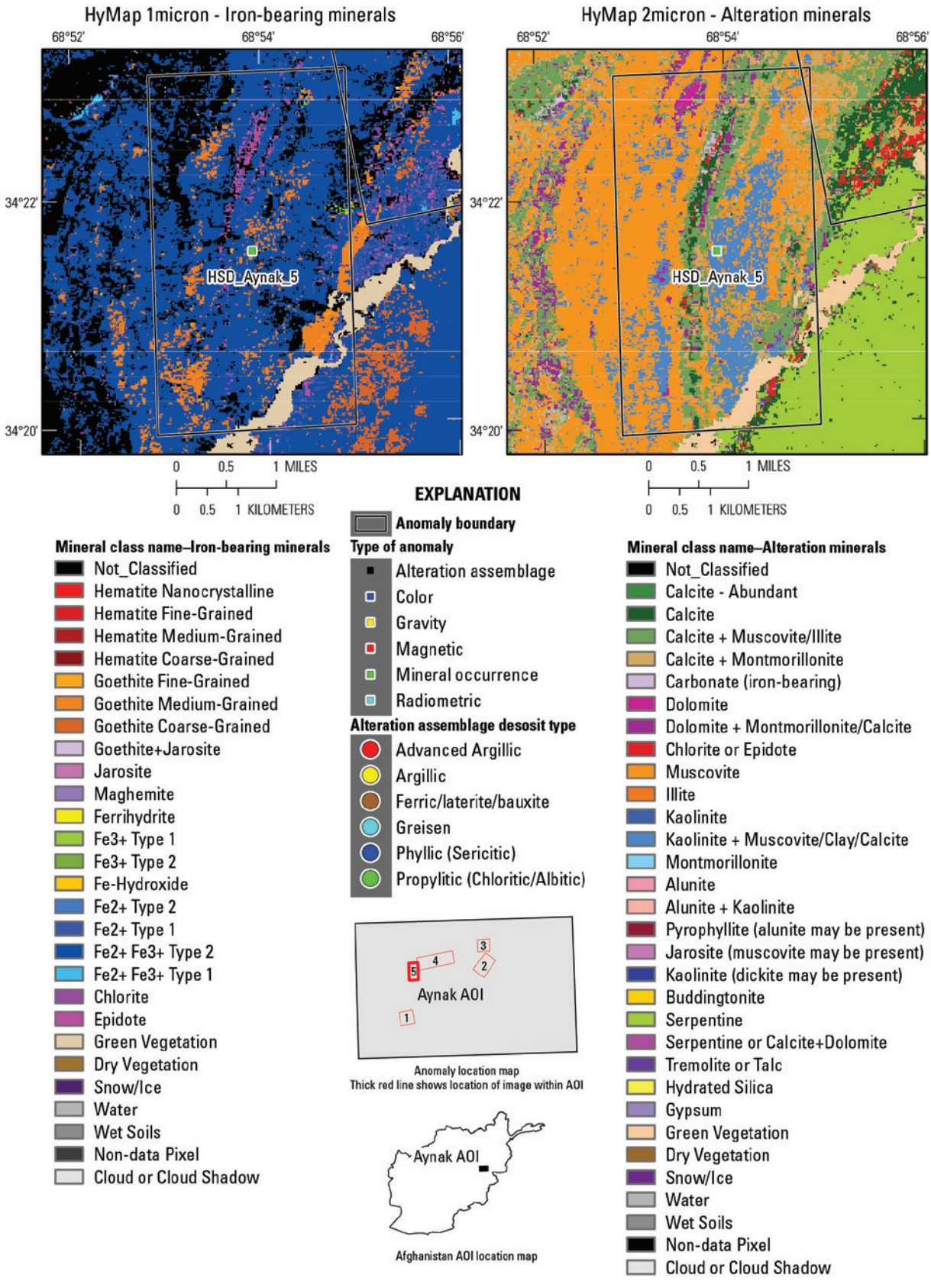

Figure 5.1.5. Hyperspectral anomaly located in the Aynak Area of Interest (AOI) in Afghanistan based on presence of Kaolinite minerals, Dolomite minerals, Carbonate (iron-bearing), and Chlorite or Epidote.

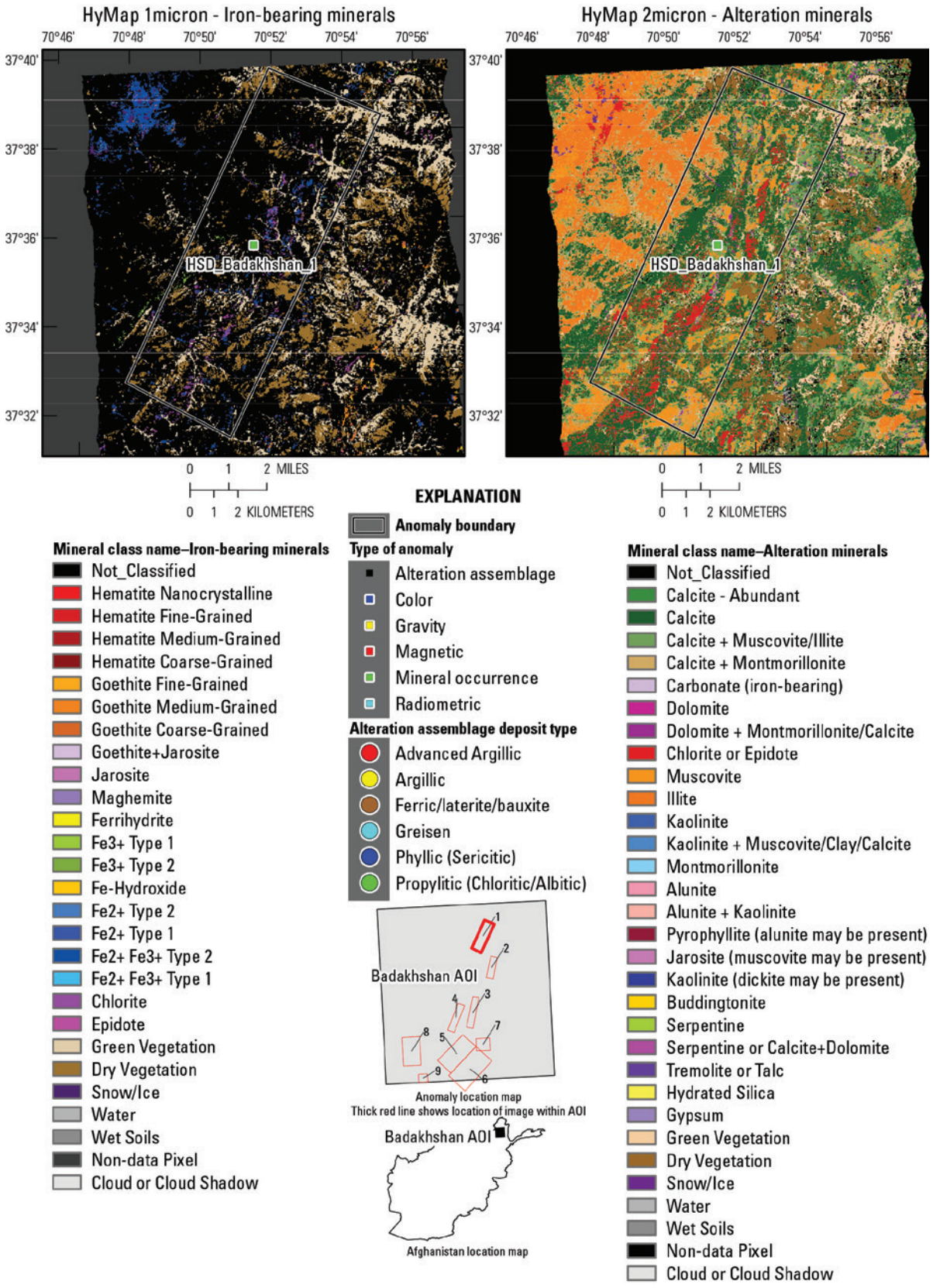

Figure 5.2.1. Hyperspectral anomaly located in the Badakhshan Area of Interest (AOI) in Afghanistan based on presence of Chlorite or Epidote, Serpentine, Dolomite minerals, Tremolite or Talc, and Ferrihydrite.

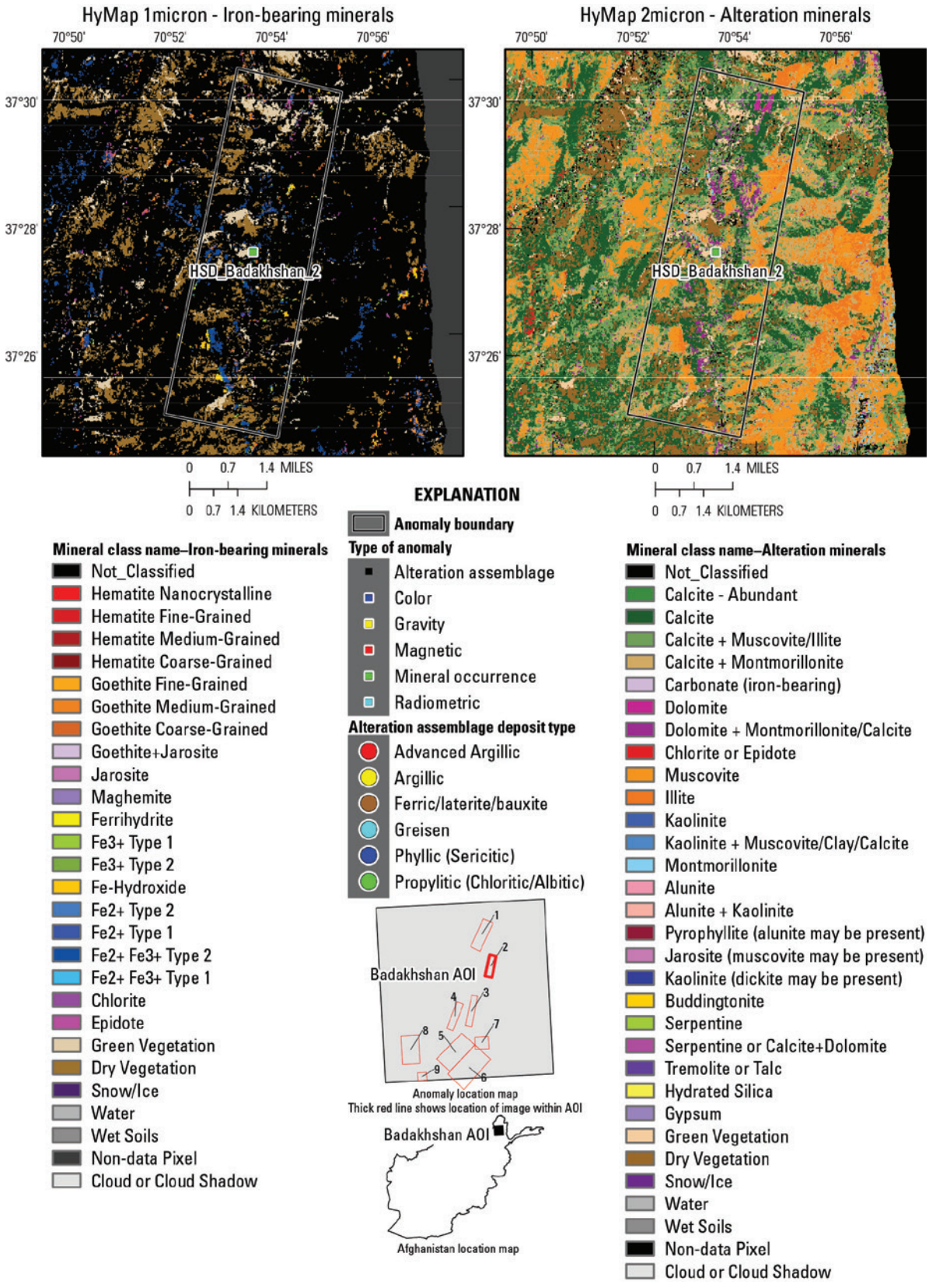

Figure 5.2.2. Hyperspectral anomaly located in the Badakhshan Area of Interest (AOI) in Afghanistan based on presence of Dolomite minerals, Serpentine, Montmorillonite, Fe-Hydroxide, and Goethite minerals.

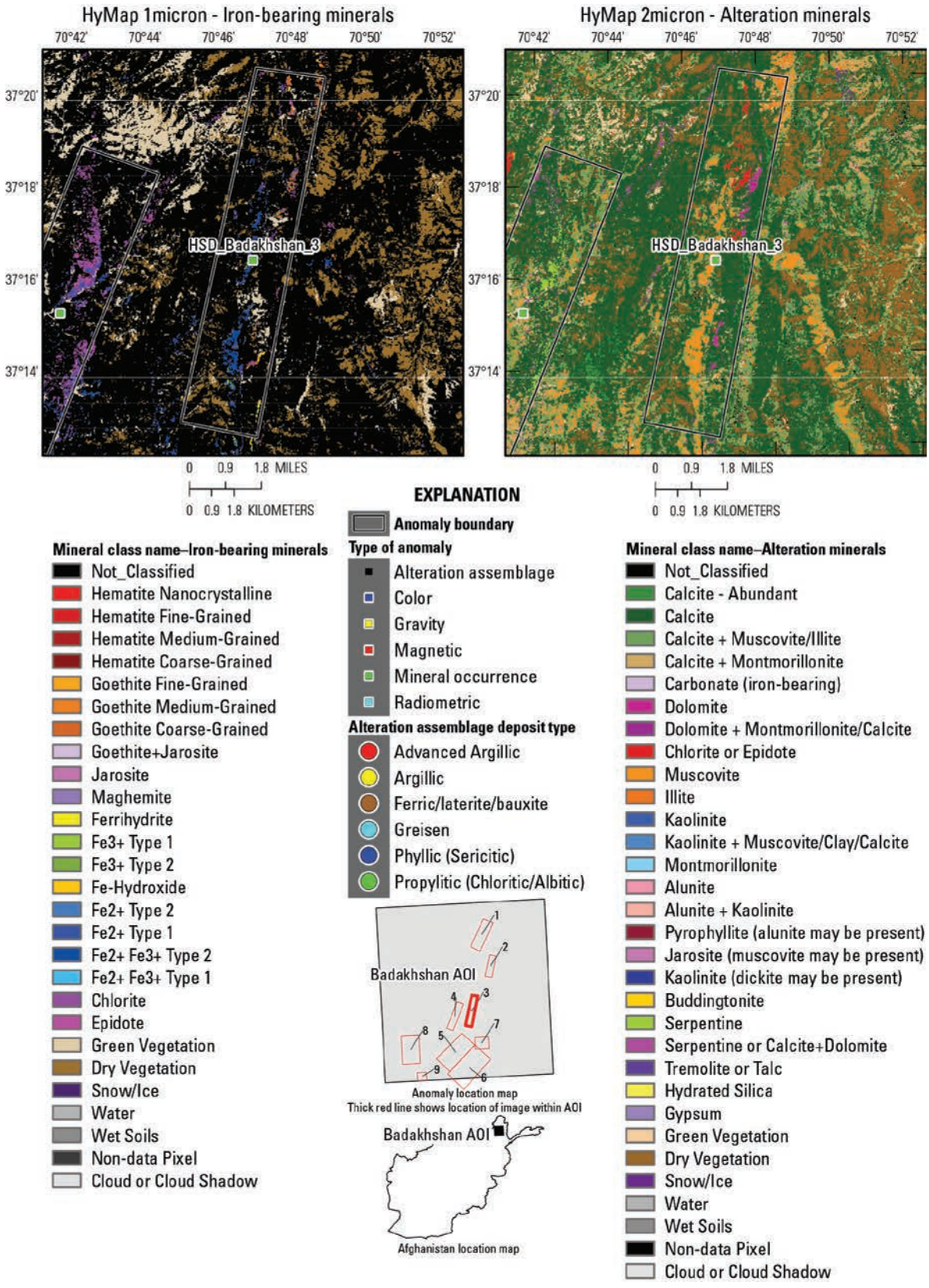

Figure 5.2.3. Hyperspectral anomaly located in the Badakhshan Area of Interest (AOI) in Afghanistan based on presence of Muscovite minerals, Dolomite minerals, Chlorite or Epidote, Serpentine, Illite, Goethite minerals, and Fe^{3+}.

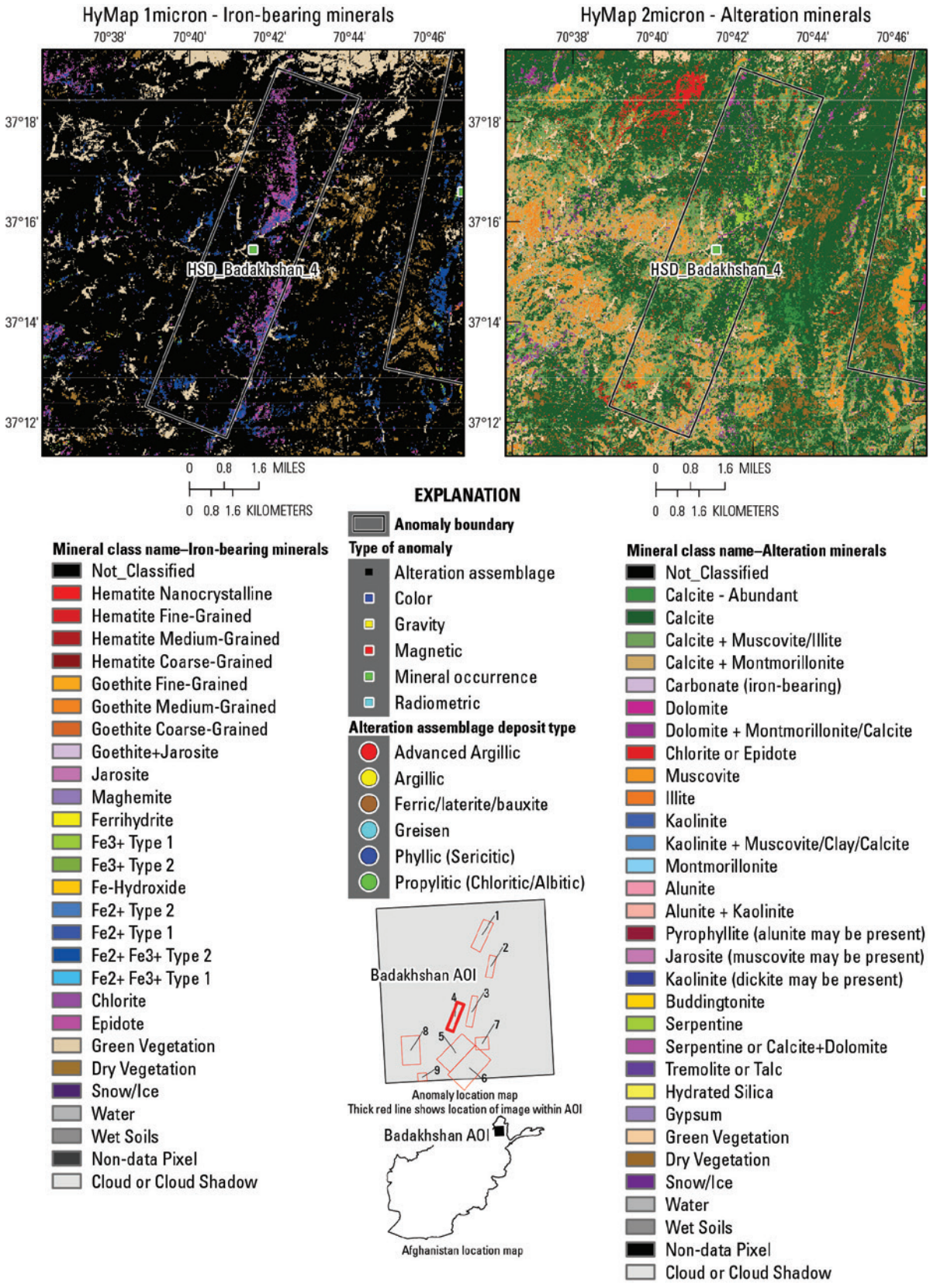

Figure 5.2.4. Hyperspectral anomaly located in the Badakhshan Area of Interest (AOI) in Afghanistan based on presence of Serpentine, Dolomite minerals, Epidote, and Fe^{2+} Type 1.

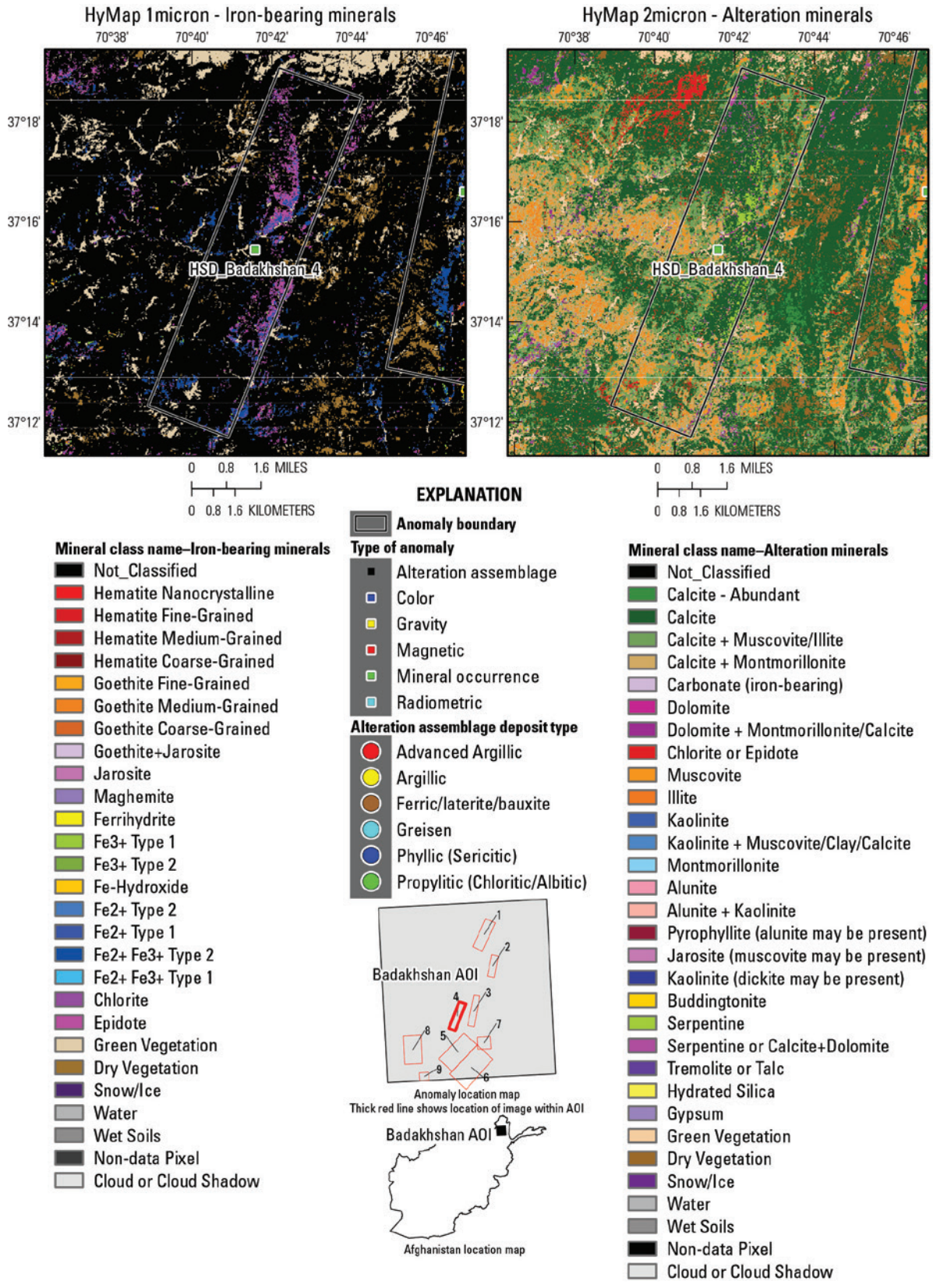

Figure 5.2.5. Hyperspectral anomaly located in the Badakhshan Area of Interest (AOI) in Afghanistan based on presence of Chlorite or Epidote, Serpentine, Carbonate (iron-bearing), Goethite minerals, Fe^{2+} Fe^{3+} Type 2, and Muscovite.

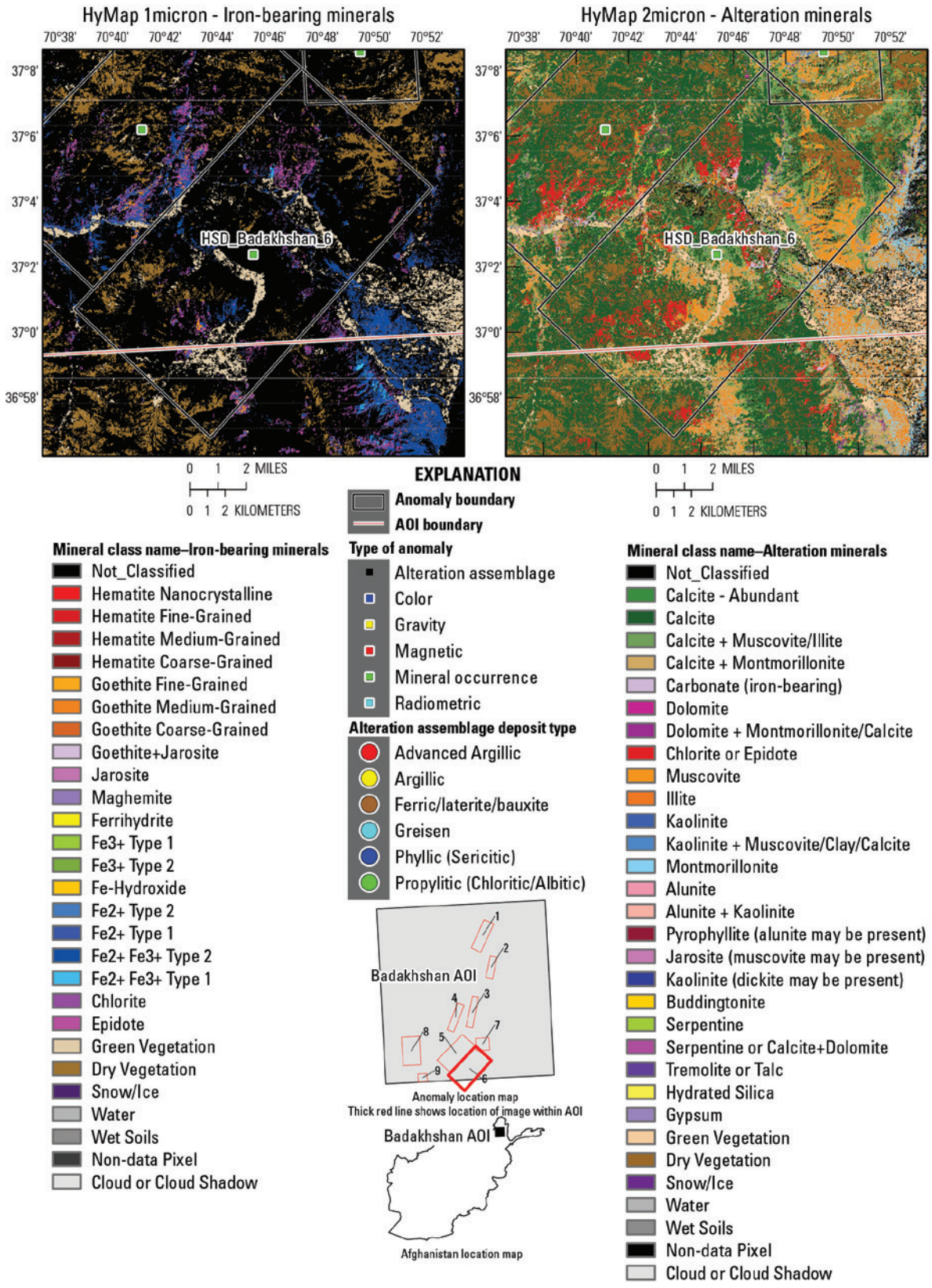

Figure 5.2.6. Hyperspectral anomaly located in the Badakhshan Area of Interest (AOI) in Afghanistan based on presence of Chlorite or Epidote, Carbonate (iron-bearing), Serpentine, Dolomite minerals, and Fe^{2+} Fe^{3+} Type 1.

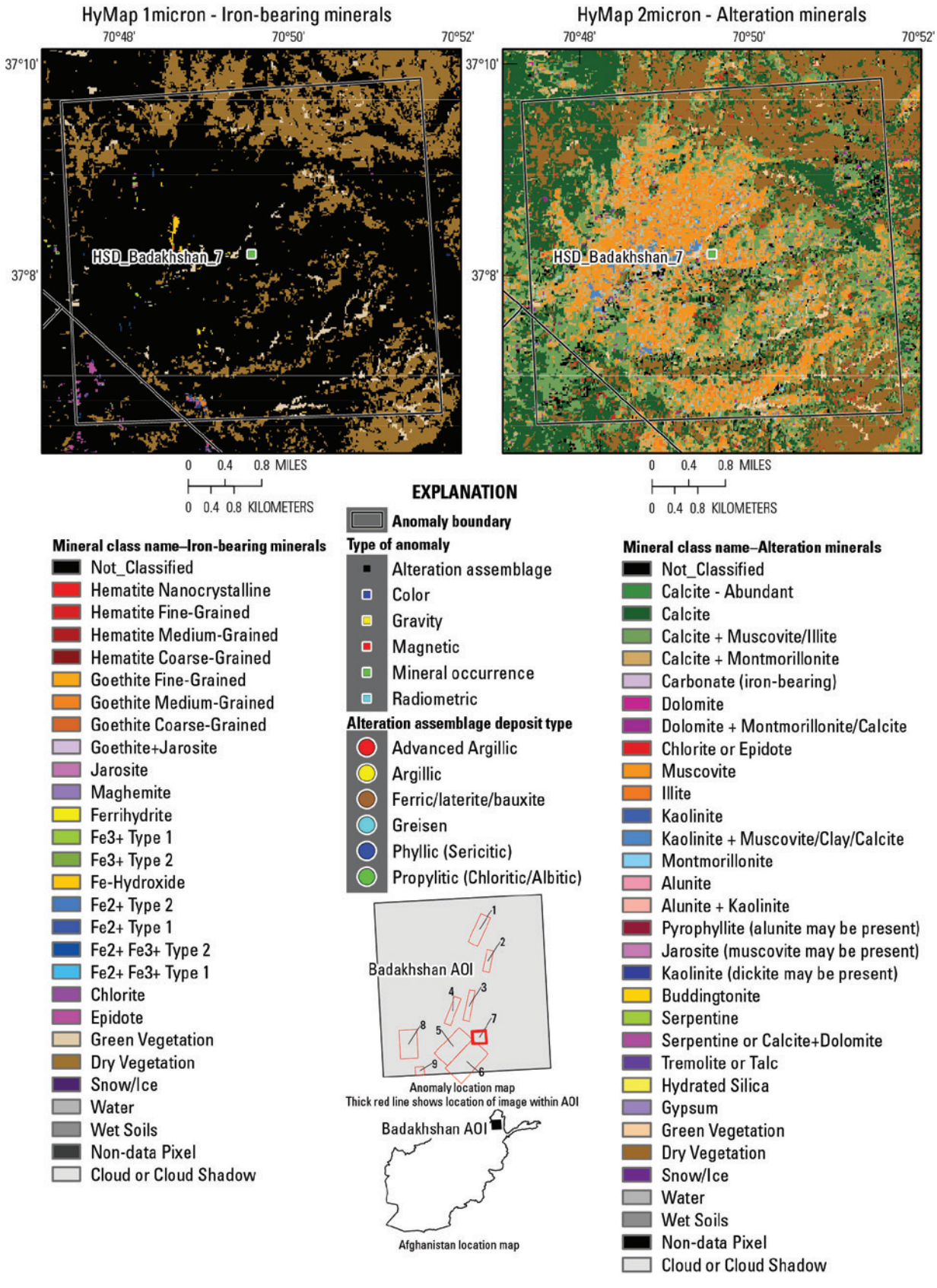

Figure 5.2.7. Hyperspectral anomaly located in the Badakhshan Area of Interest (AOI) in Afghanistan based on presence of Muscovite, Kaolinite minerals, and Fe-Hydroxide.

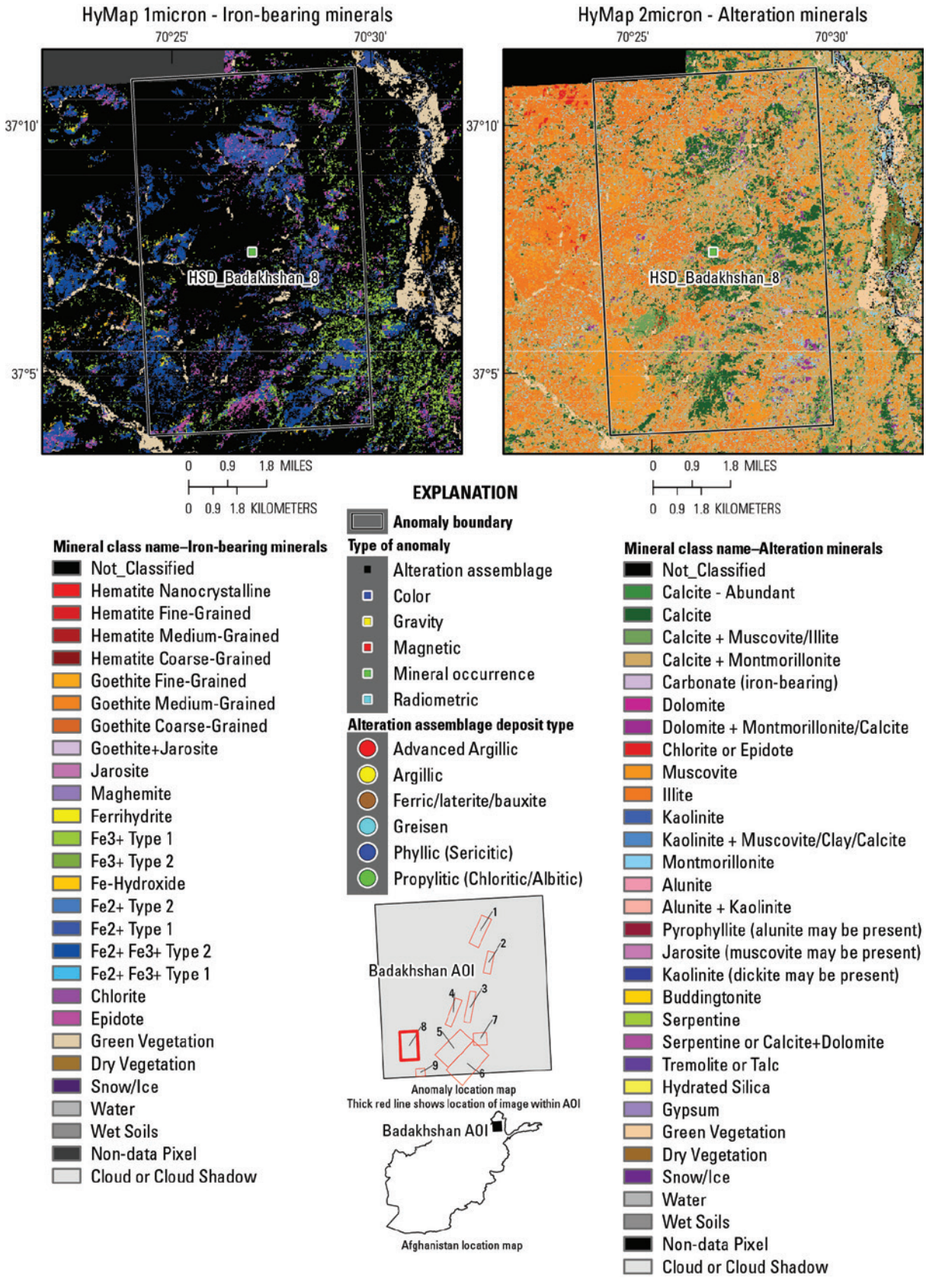

Figure 5.2.8. Hyperspectral anomaly located in the Badakhshan Area of Interest (AOI) in Afghanistan based on presence of Carbonate (iron-bearing) and Dolomite minerals.

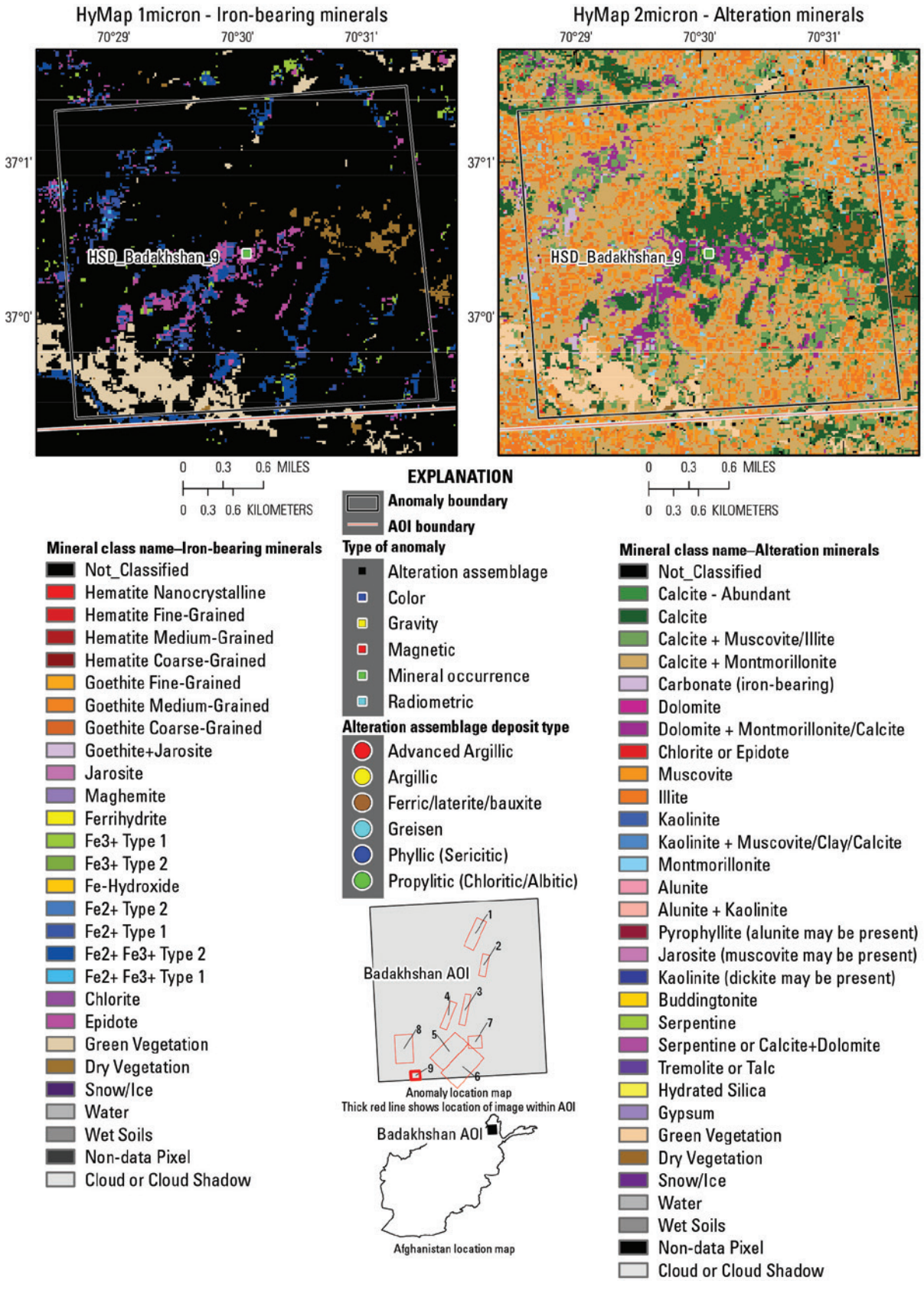

Figure 5.2.9. Hyperspectral anomaly located in the Badakhshan Area of Interest (AOI) in Afghanistan based on presence of Dolomite minerals, Carbonate (iron-bearing), Serpentine, and Epidote.

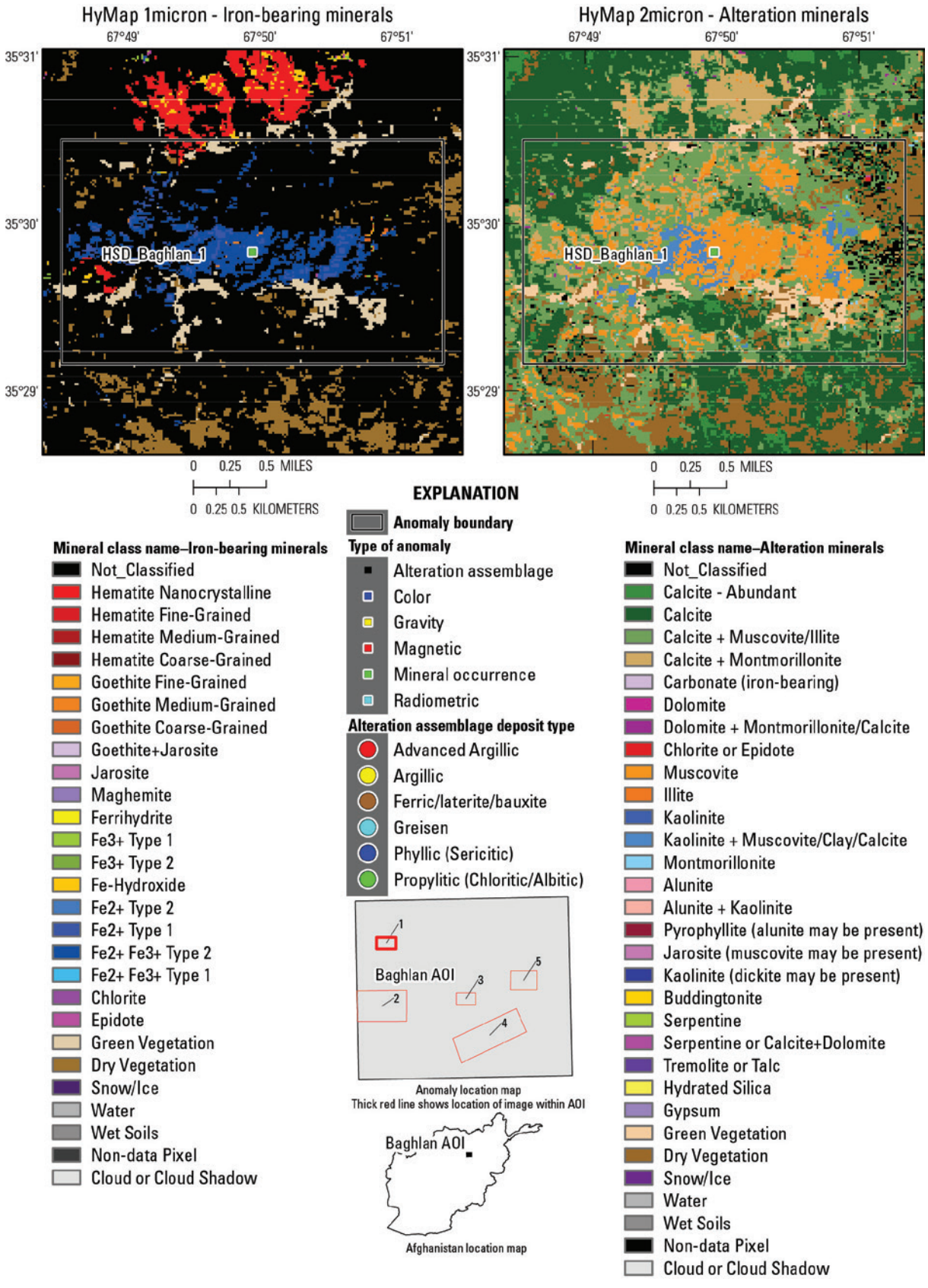

Figure 5.3.1. Hyperspectral anomaly located in the Baghlan Area of Interest (AOI) in Afghanistan based on presence of Muscovite, Kaolinite minerals, Fe^{2+} Fe^{3+} Type2 and Fe^{2+} Type1.

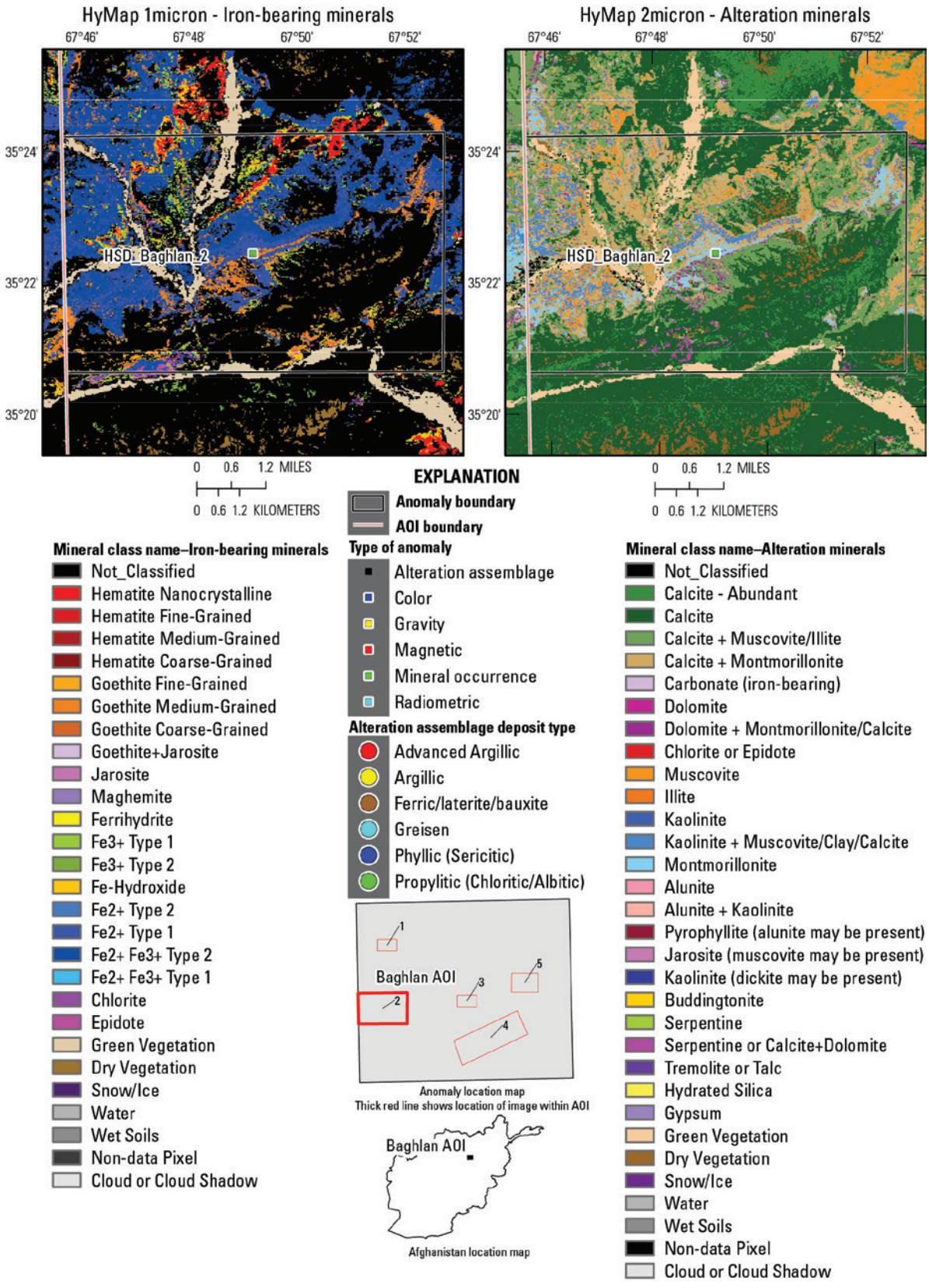

Figure 5.3.2. Hyperspectral anomaly located in the Baghlan Area of Interest (AOI) in Afghanistan based on presence of Kaolinite minerals, Montmorillonite, Dolomite minerals, Serpentine minerals, Fe^{2+} Fe^{3+} Type2, Hematite minerals, Fe^{3+} Type 1, Goethite minerals, and Epidote.

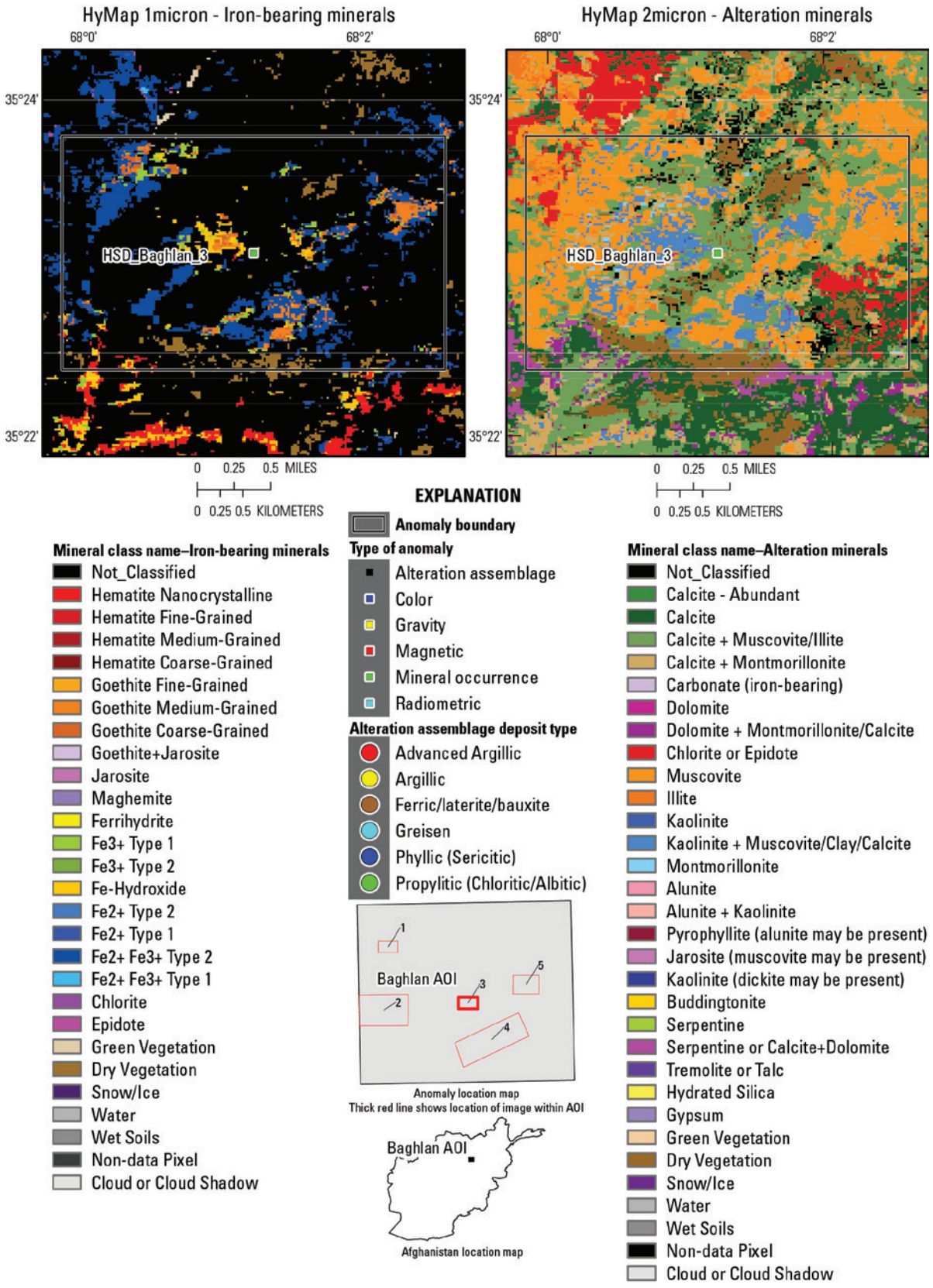

Figure 5.3.3. Hyperspectral anomaly located in the Baghlan Area of Interest (AOI) in Afghanistan based on presence of Kaolinite minerals, Muscovite, Montmorillonite, Fe-Hydroxide, and Goethite minerals.

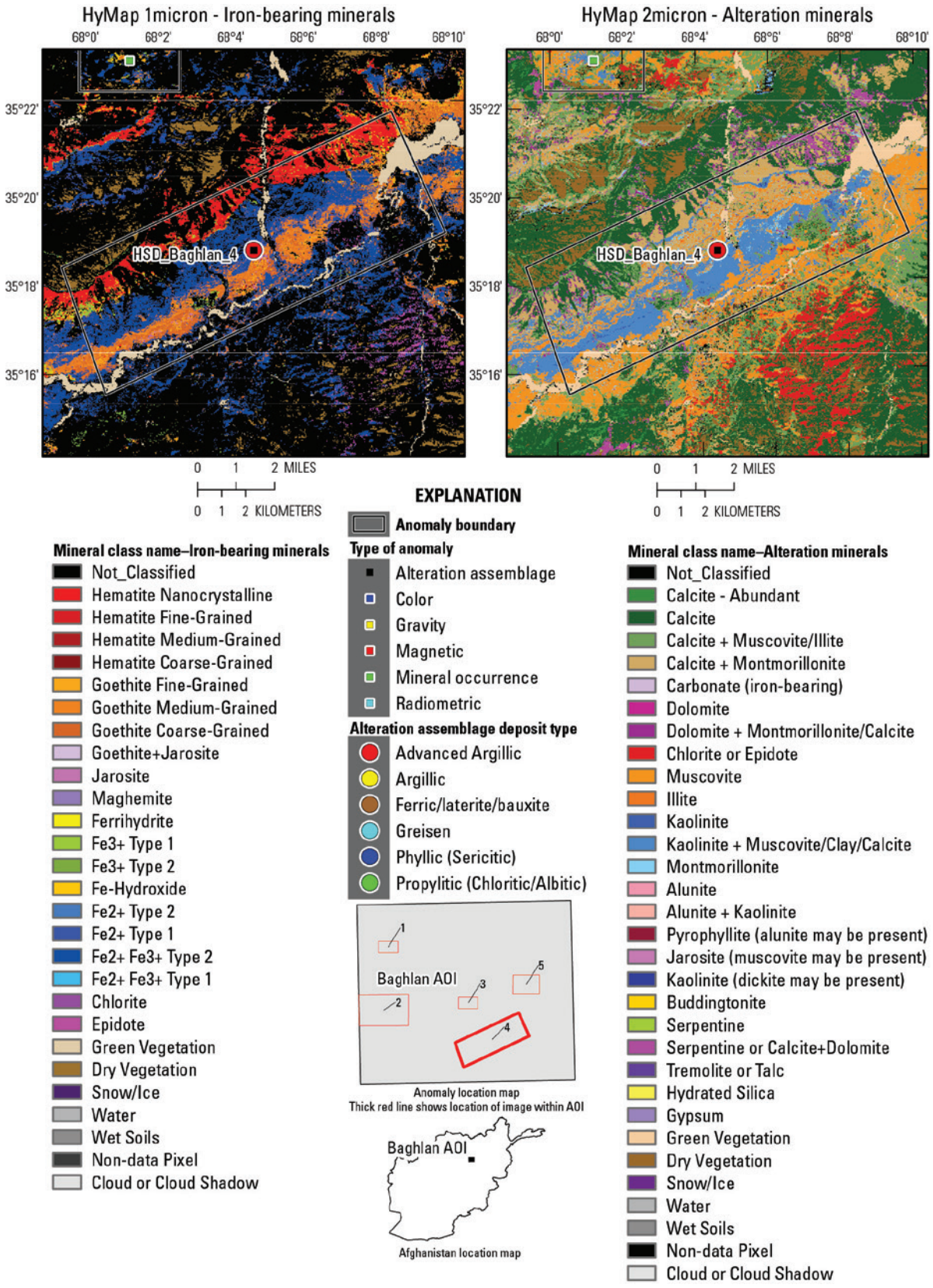

Figure 5.3.4. Hyperspectral anomaly located in the Baghlan Area of Interest (AOI) in Afghanistan based on presence of Kaolinite minerals, Muscovite, Dolomite minerals, Dickite, Montmorillonite, Goethite minerals, Hematite minerals, and Jarosite.

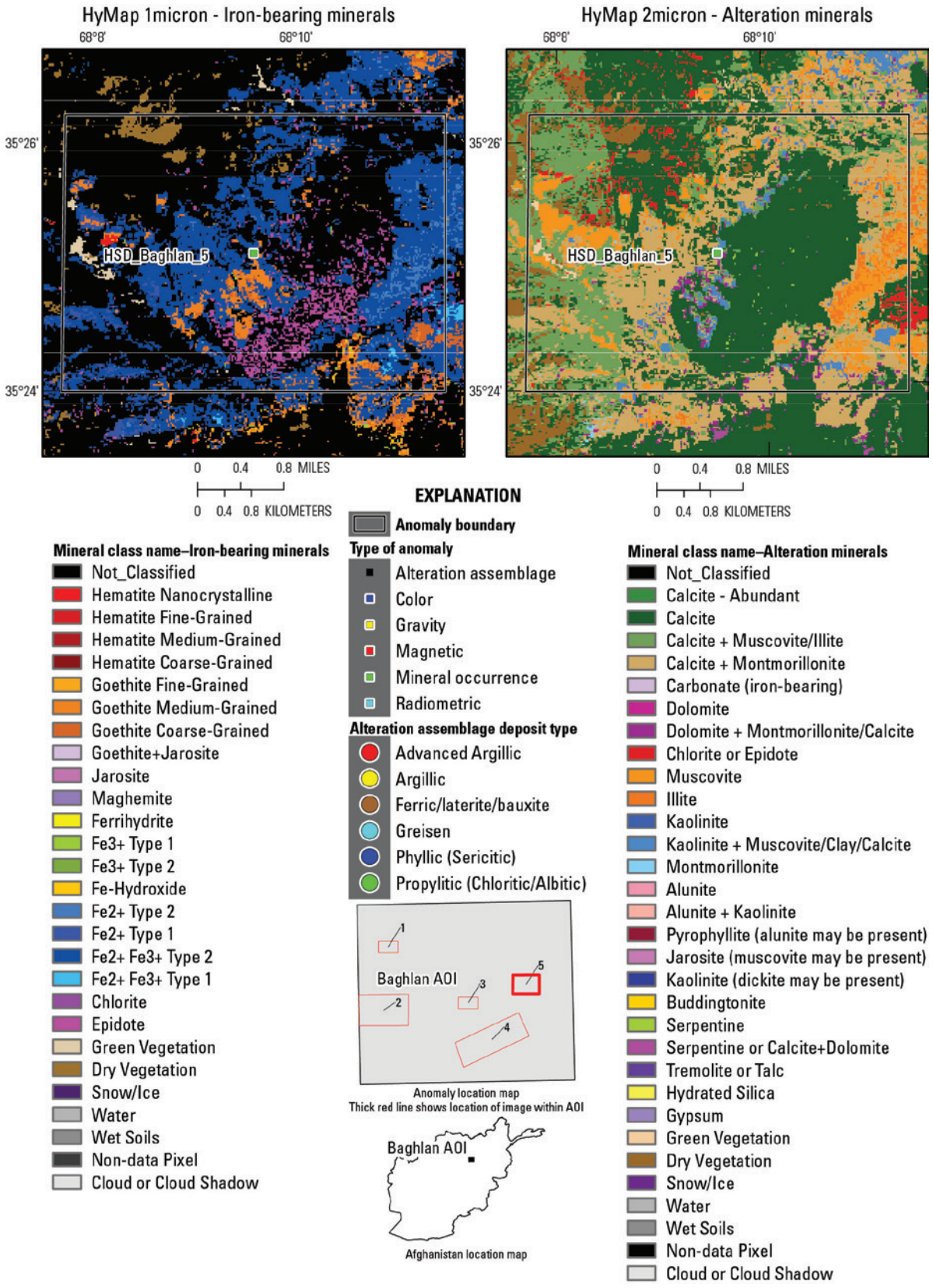

Figure 5.3.5. Hyperspectral anomaly located in the Baghlan Area of Interest (AOI) in Afghanistan based on presence of Calcite, Kaolinite minerals, Dolomite minerals, Epidote, Goethite minerals, and Hematite minerals.

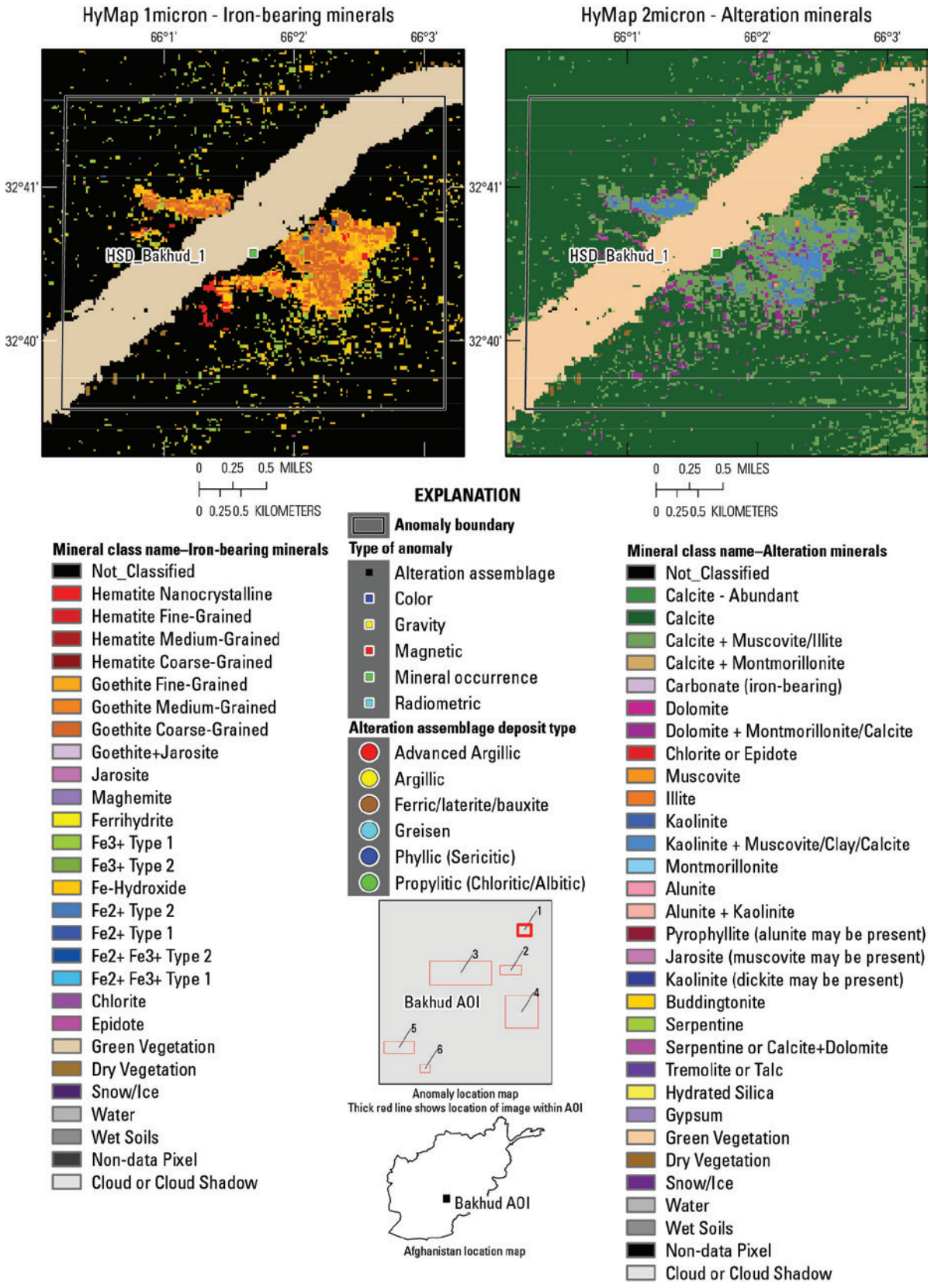

Figure 5.4.1. Hyperspectral anomaly located in the Bakhud Area of Interest (AOI) in Afghanistan based on presence of Kaolinite minerals, Goethite minerals, Hematite minerals, and Fe-Hydroxide.

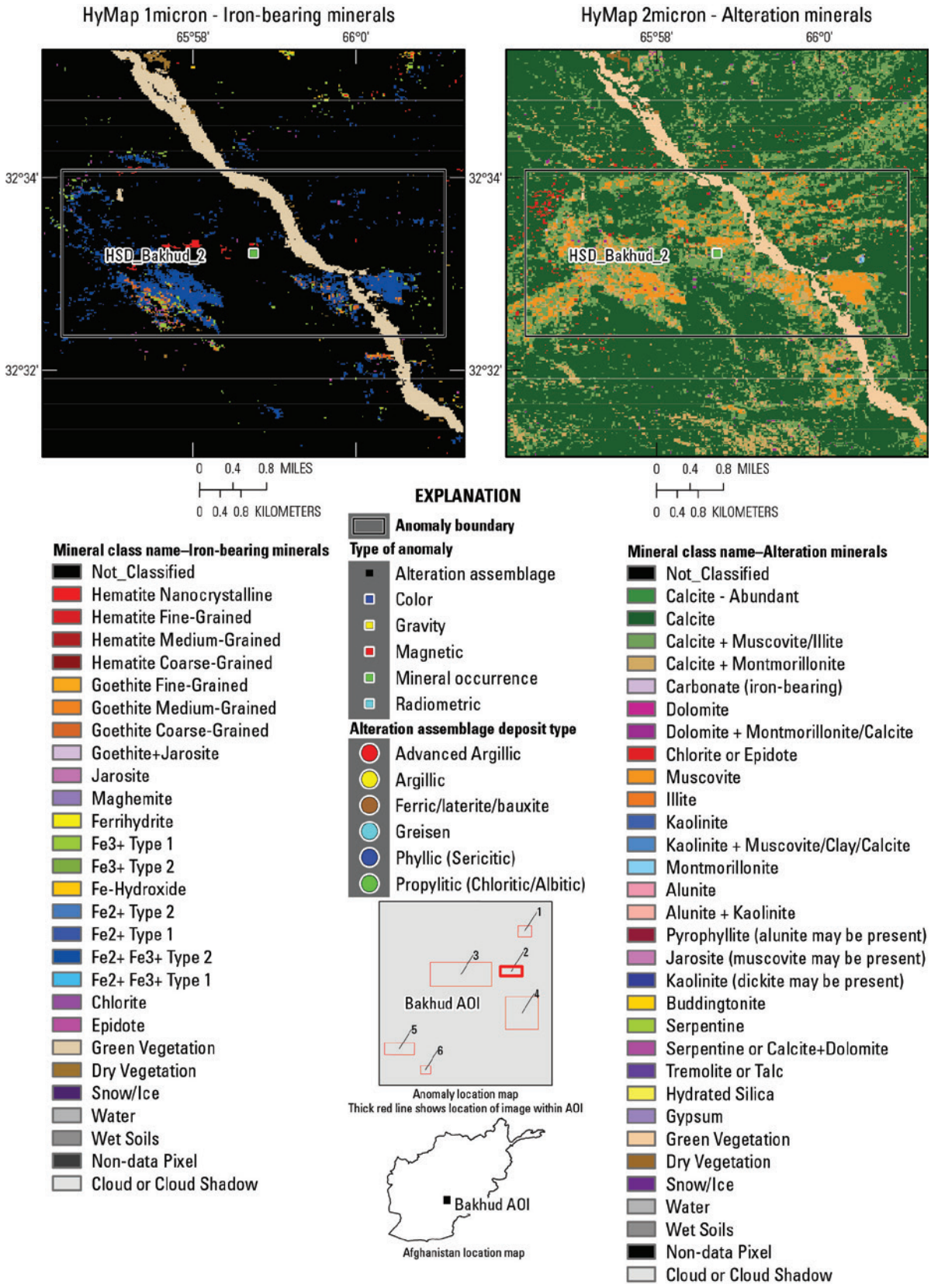

Figure 5.4.2. Hyperspectral anomaly located in the Bakhud Area of Interest (AOI) in Afghanistan based on presence of Muscovite, Montmorillonite, Kaolinite minerals, Goethite minerals, Fe^{3+} Type 1, Epidote, and Hematite.

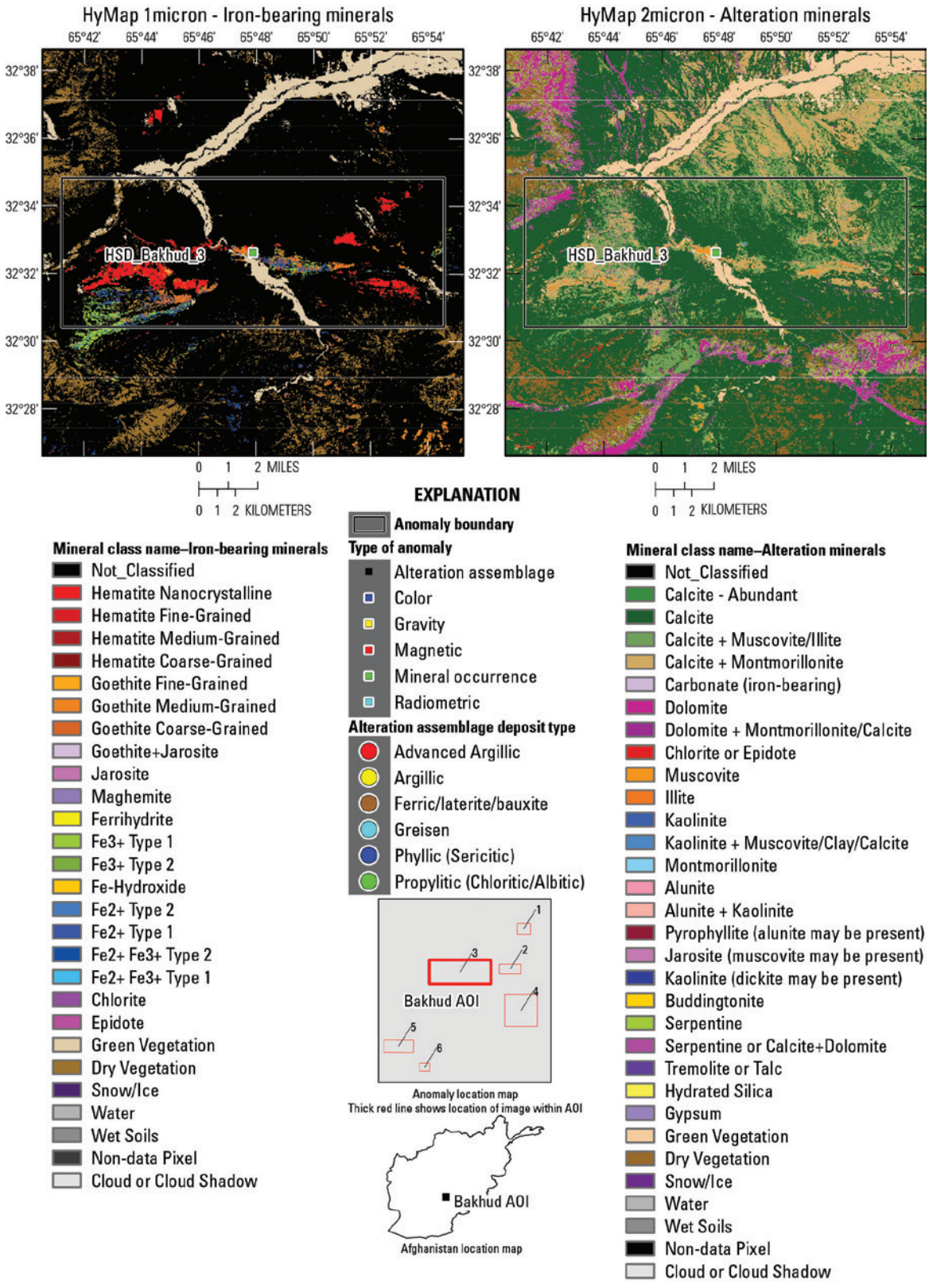

Figure 5.4.3. Hyperspectral anomaly located in the Bakhud Area of Interest (AOI) in Afghanistan based on presence of Hematite minerals, Fe^{3+} Type 1, Goethite minerals, and Muscovite.

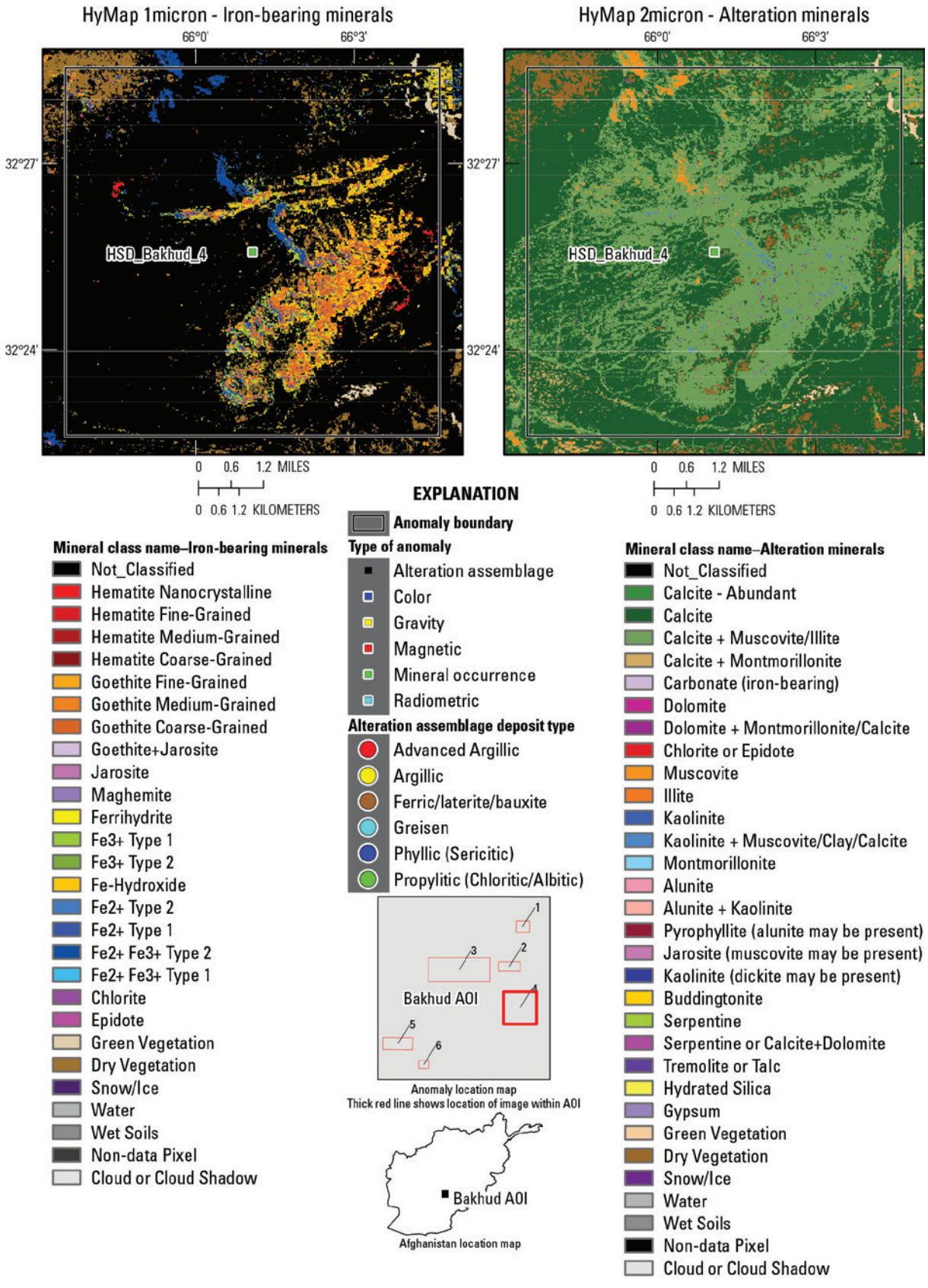

Figure 5.4.4. Hyperspectral anomaly located in the Bakhud Area of Interest (AOI) in Afghanistan based on presence of Kaolinite minerals, Goethite minerals, Fe^{3+} Type 1, Hematite minerals, Fe-Hydroxide.

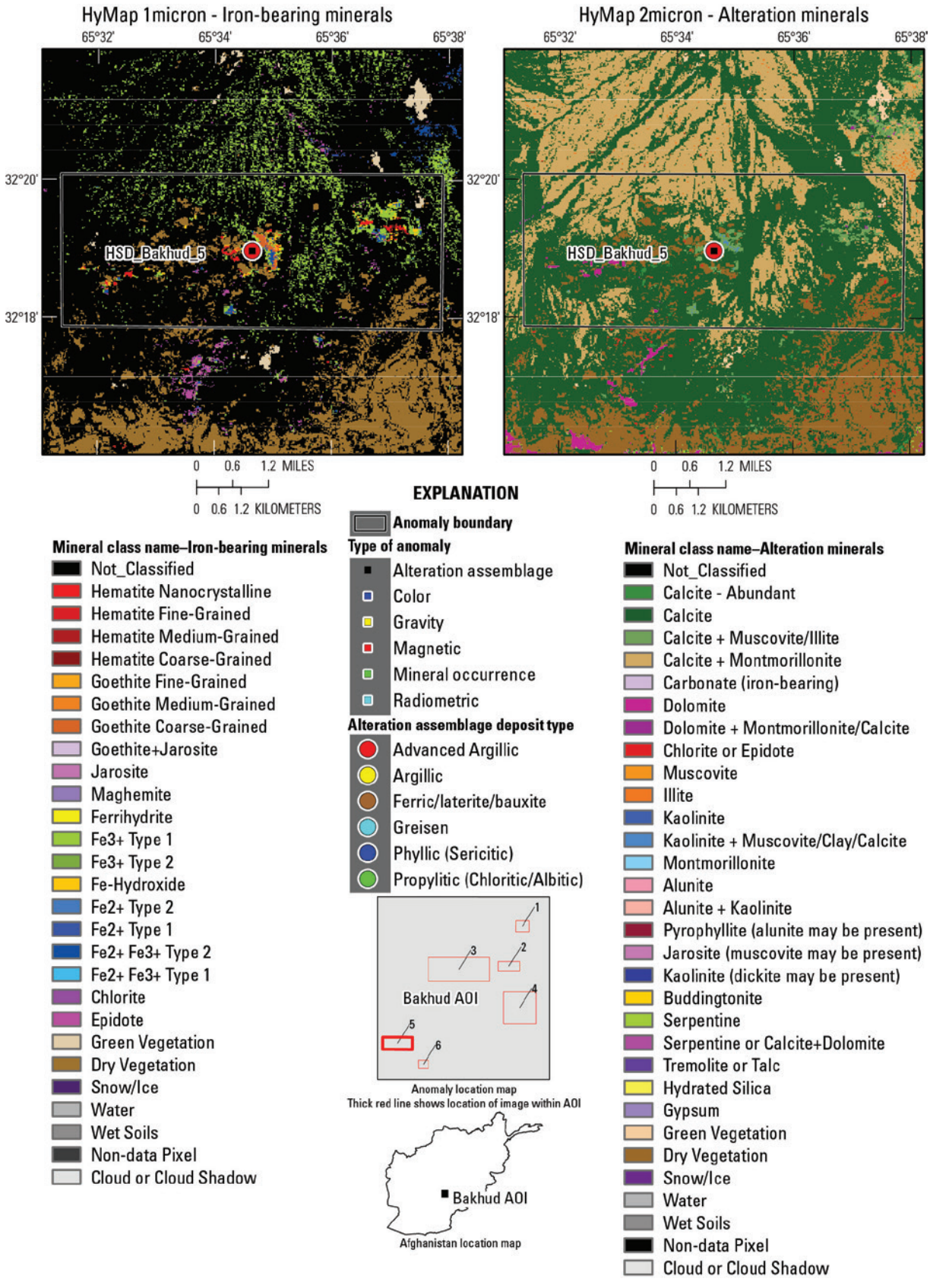

Figure 5.4.5. Hyperspectral anomaly located in the Bakhud Area of Interest (AOI) in Afghanistan based on presence of Kaolinite minerals, Hematite minerals, Goethite minerals, Fe^{3+} Type 1, Epidote, and Jarosite.

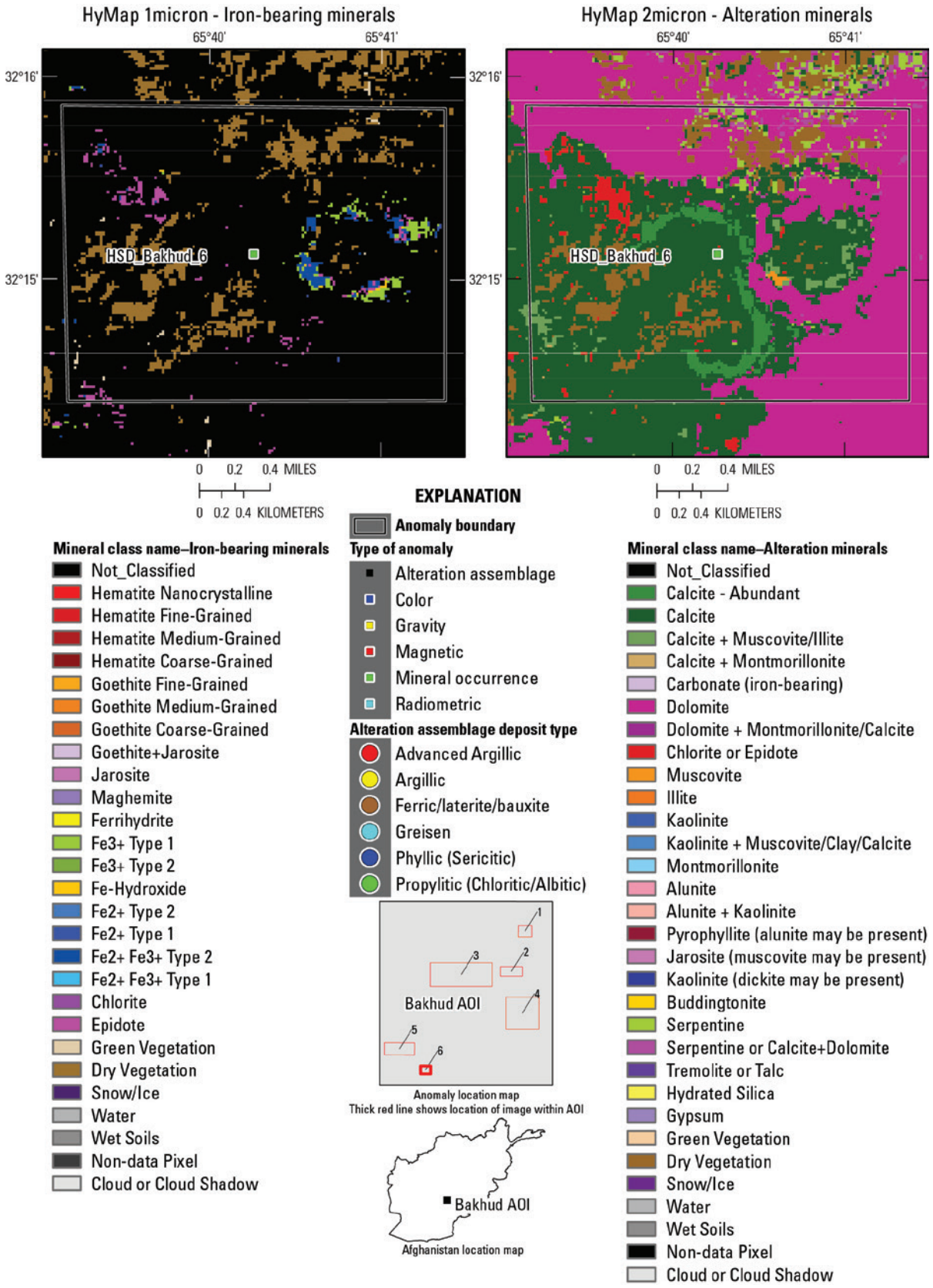

Figure 5.4.6. Hyperspectral anomaly located in the Bakhud Area of Interest (AOI) in Afghanistan based on presence of Calcite, Muscovite, Chlorite or Epidote, Fe^{3+} Type 1, Fe-Hydroxide, and Fe^{2+} Fe^{3+} Type 2.

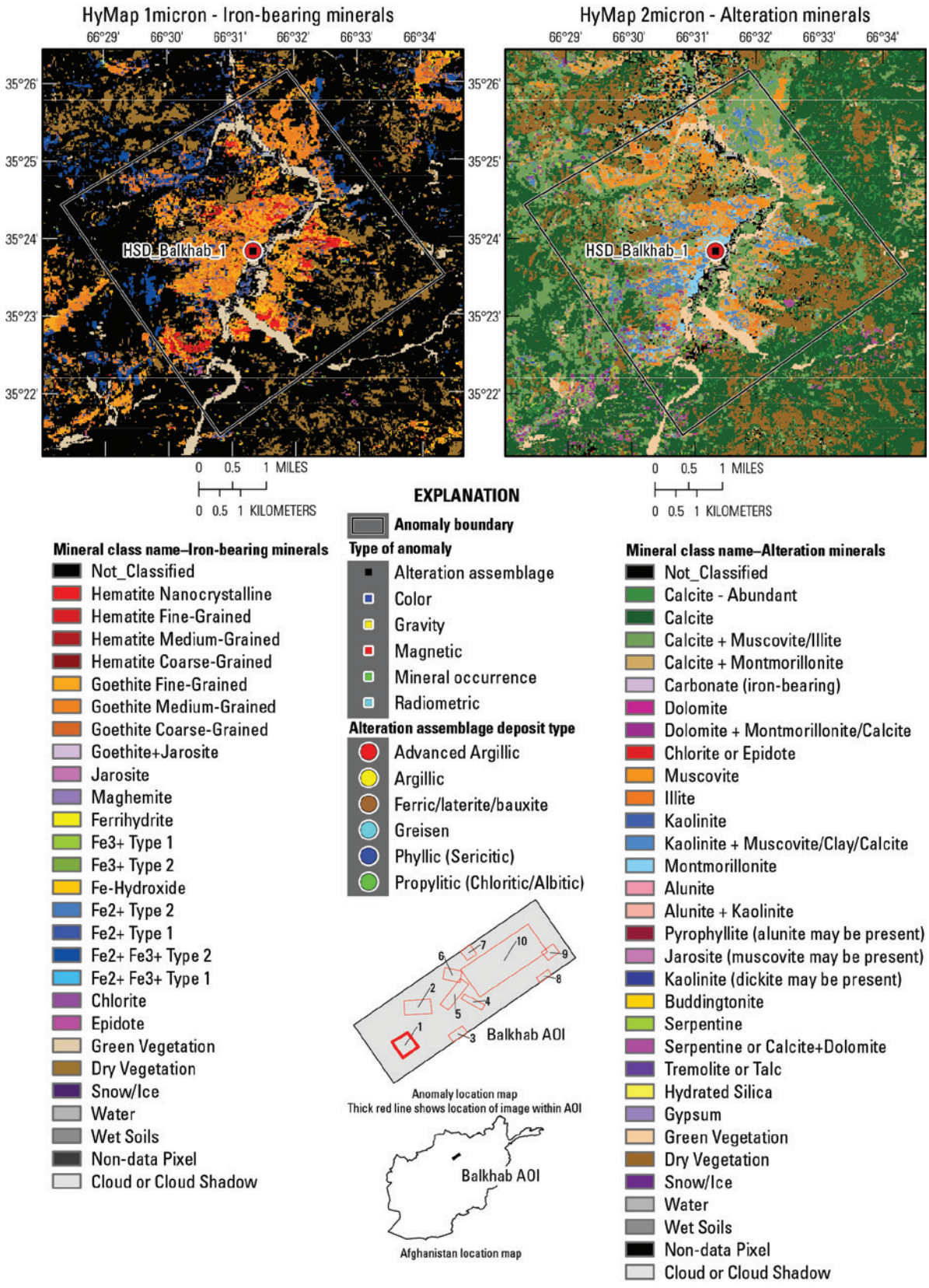

Figure 5.5.1. Hyperspectral anomaly located in the Balkhab Area of Interest (AOI) in Afghanistan based on presence of Kaolinite minerals, Montmorillonite, Dolomite minerals, Goethite minerals, Hematite minerals, Jarosite, Maghemite, and Fe^{3+} Type 1.

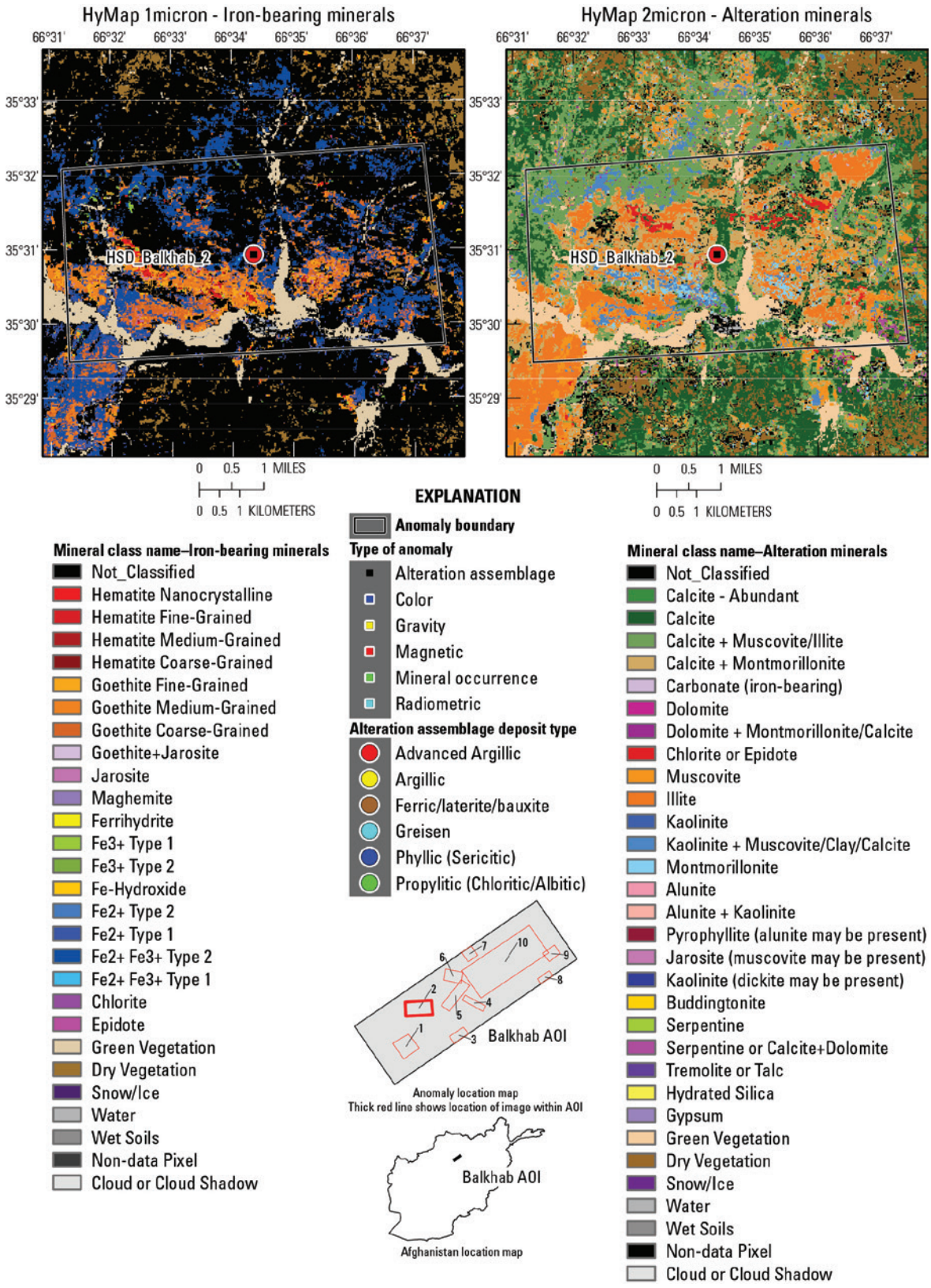

Figure 5.5.2. Hyperspectral anomaly located in the Balkhab Area of Interest (AOI) in Afghanistan based on presence of Chlorite or Epidote, Kaolinite minerals, Montmorillonite, Serpentine minerals, Goethite minerals, Hematite minerals, Jarosite, and Fe^{3+} Type 1.

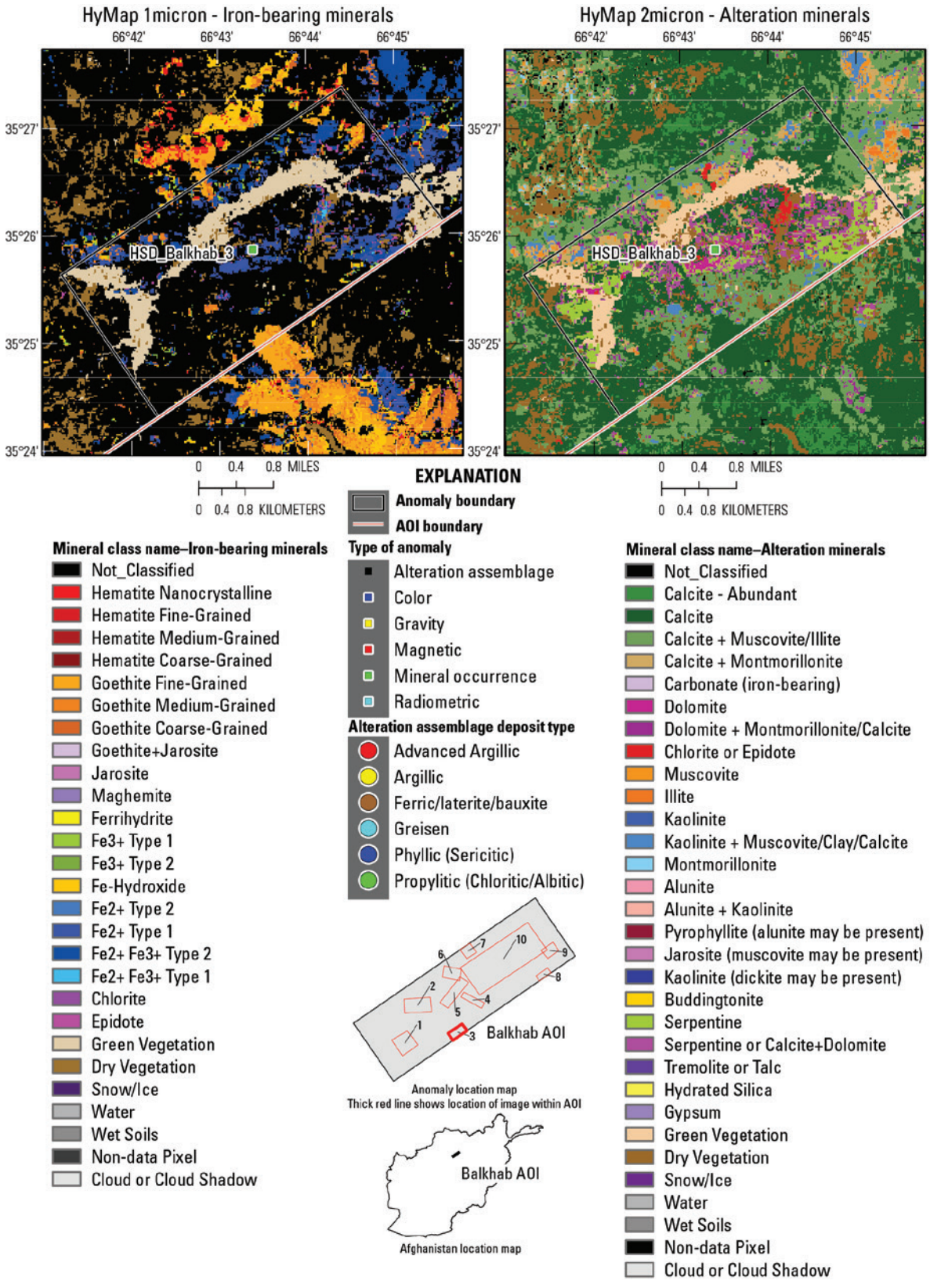

Figure 5.5.3. Hyperspectral anomaly located in the Balkhab Area of Interest (AOI) in Afghanistan based on presence of Serpentine minerals, Chlorite or Epidote, Dolomite minerals, Goethite minerals, Fe-Hydroxide, and Fe^{3+} Type 1.

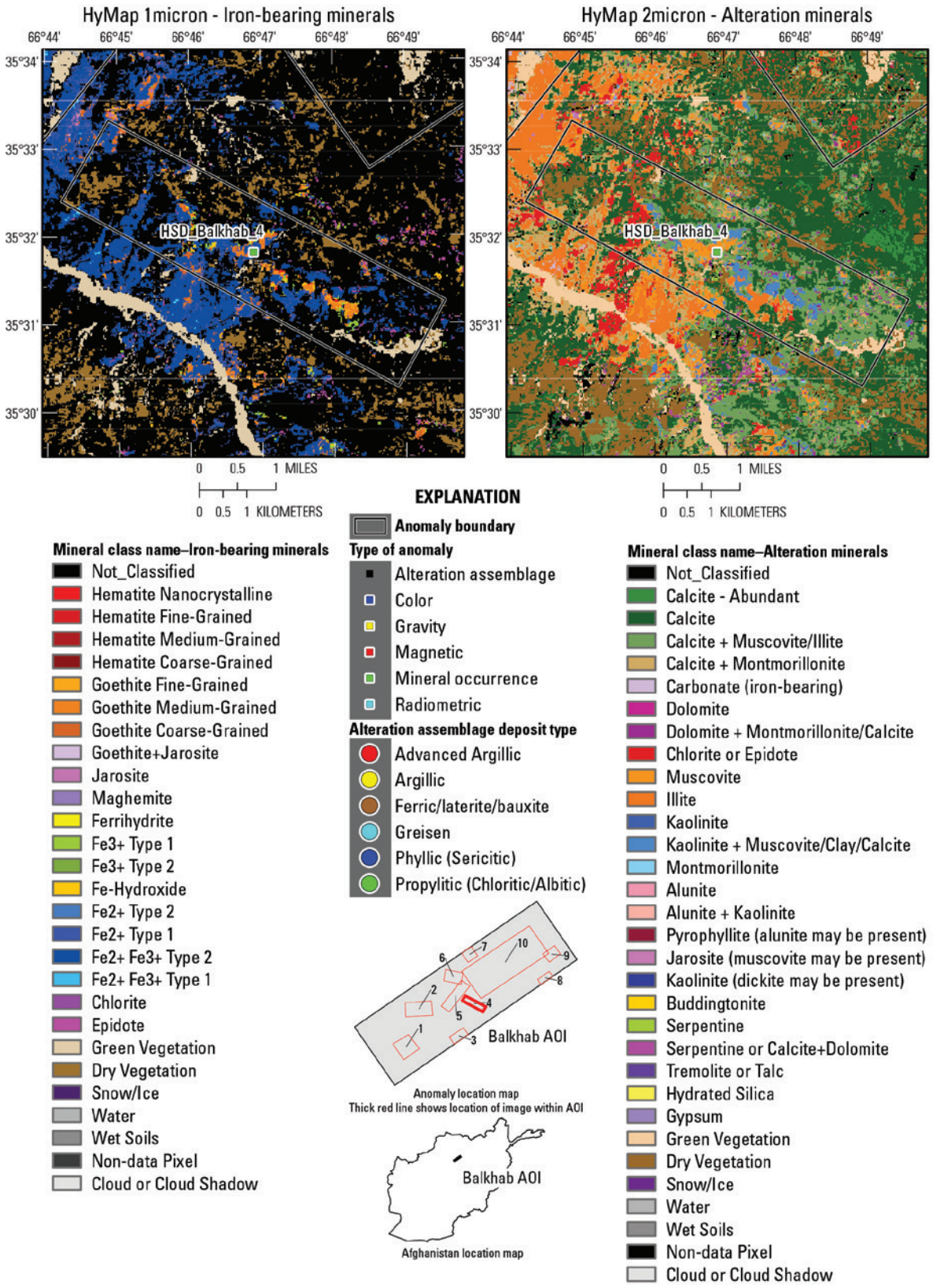

Figure 5.5.4. Hyperspectral anomaly located in the Balkhab Area of Interest (AOI) in Afghanistan based on presence of Kaolinite minerals, Illite, Muscovite, Chlorite or Epidote, Goethite minerals, and Hematite minerals.

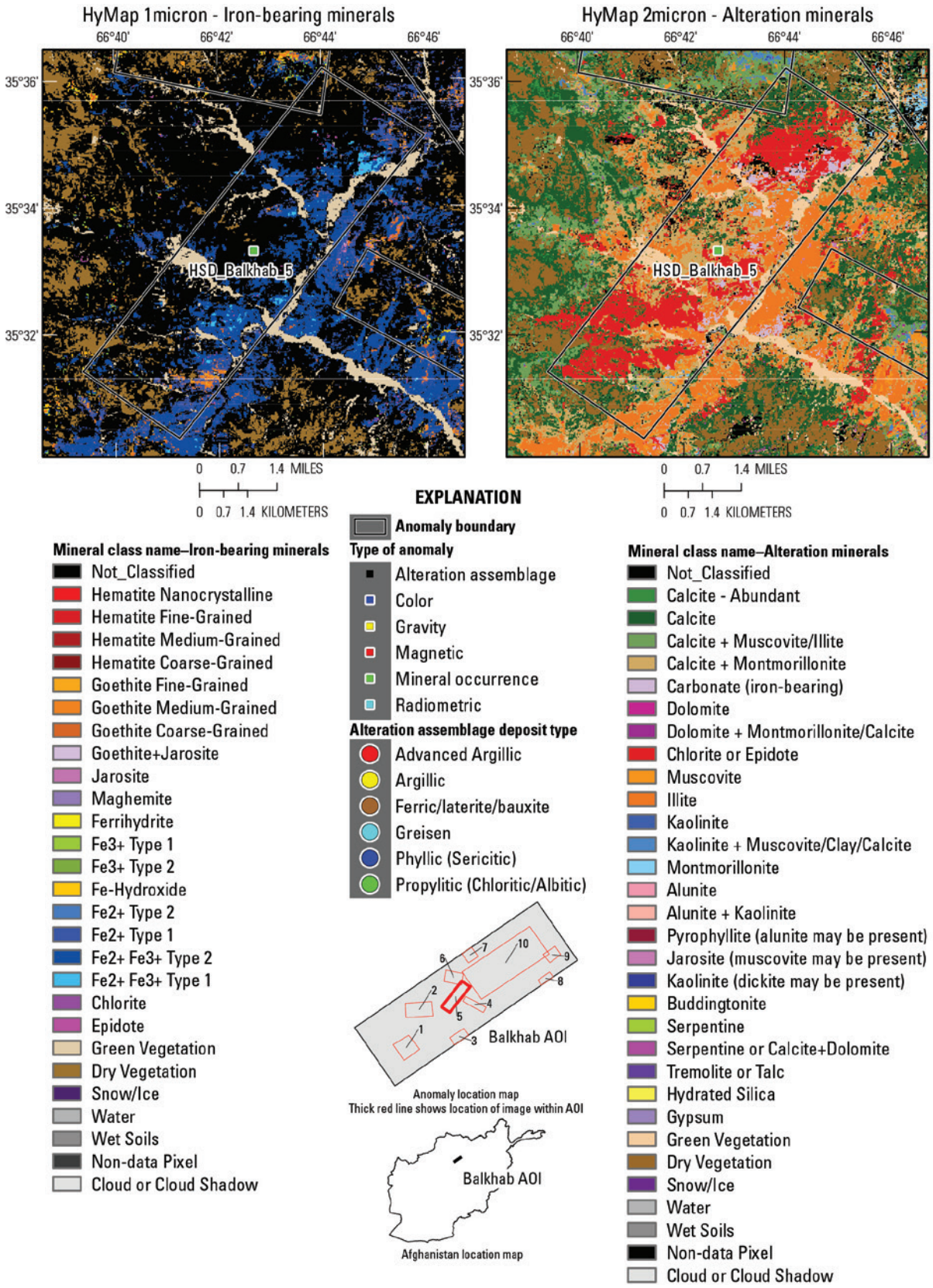

Figure 5.5.5. Hyperspectral anomaly located in the Balkhab Area of Interest (AOI) in Afghanistan based on presence of Chlorite or Epidote, Carbonate (iron-bearing), and Goethite minerals.

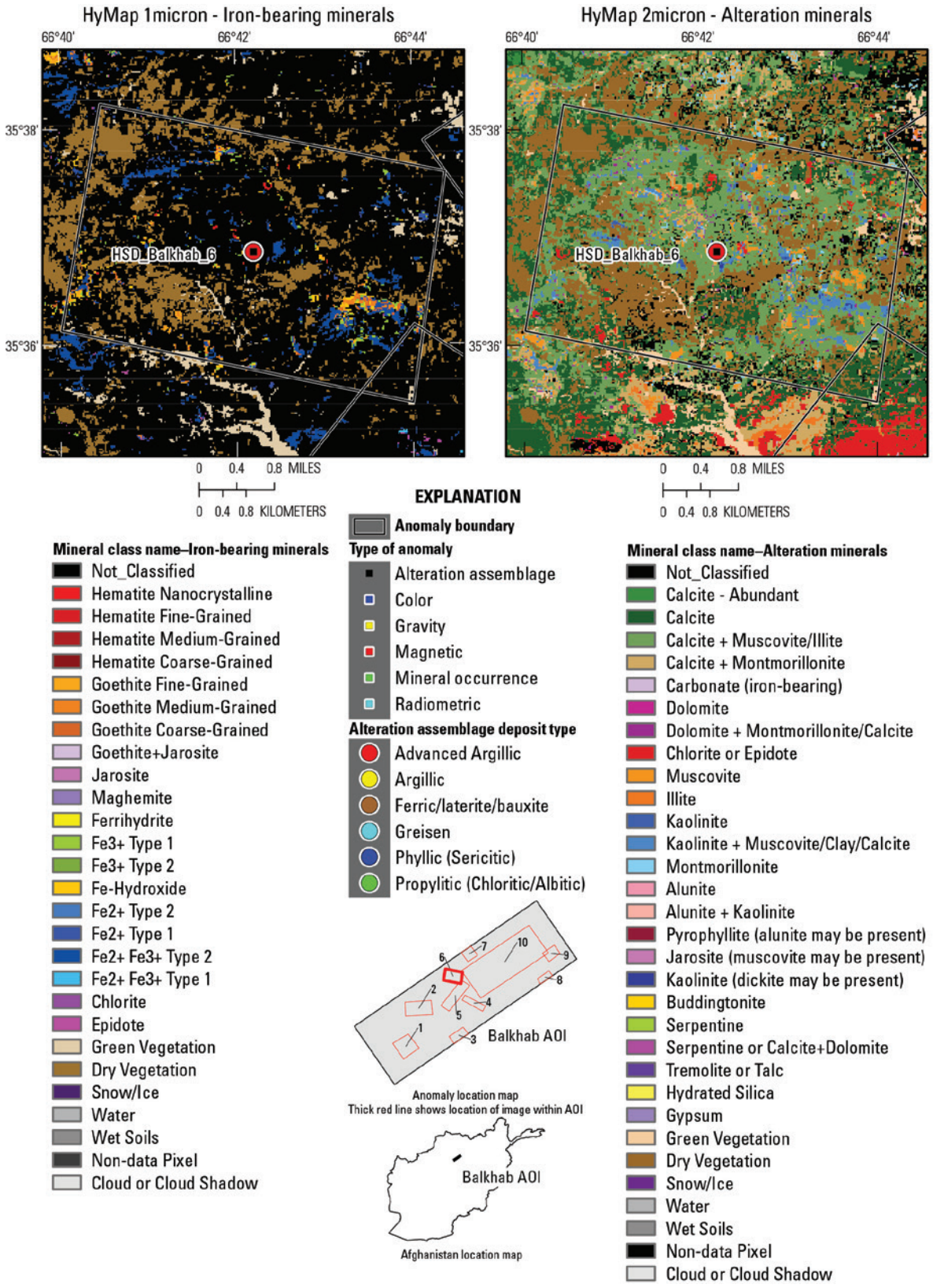

Figure 5.5.6. Hyperspectral anomaly located in the Balkhab Area of Interest (AOI) in Afghanistan based on presence of Kaolinite minerals, Dickite, Chlorite or Epidote, Pyrophyllite, Alunite minerals, Goethite minerals, Fe-Hydroxide, and Fe^{3+} Type 1.

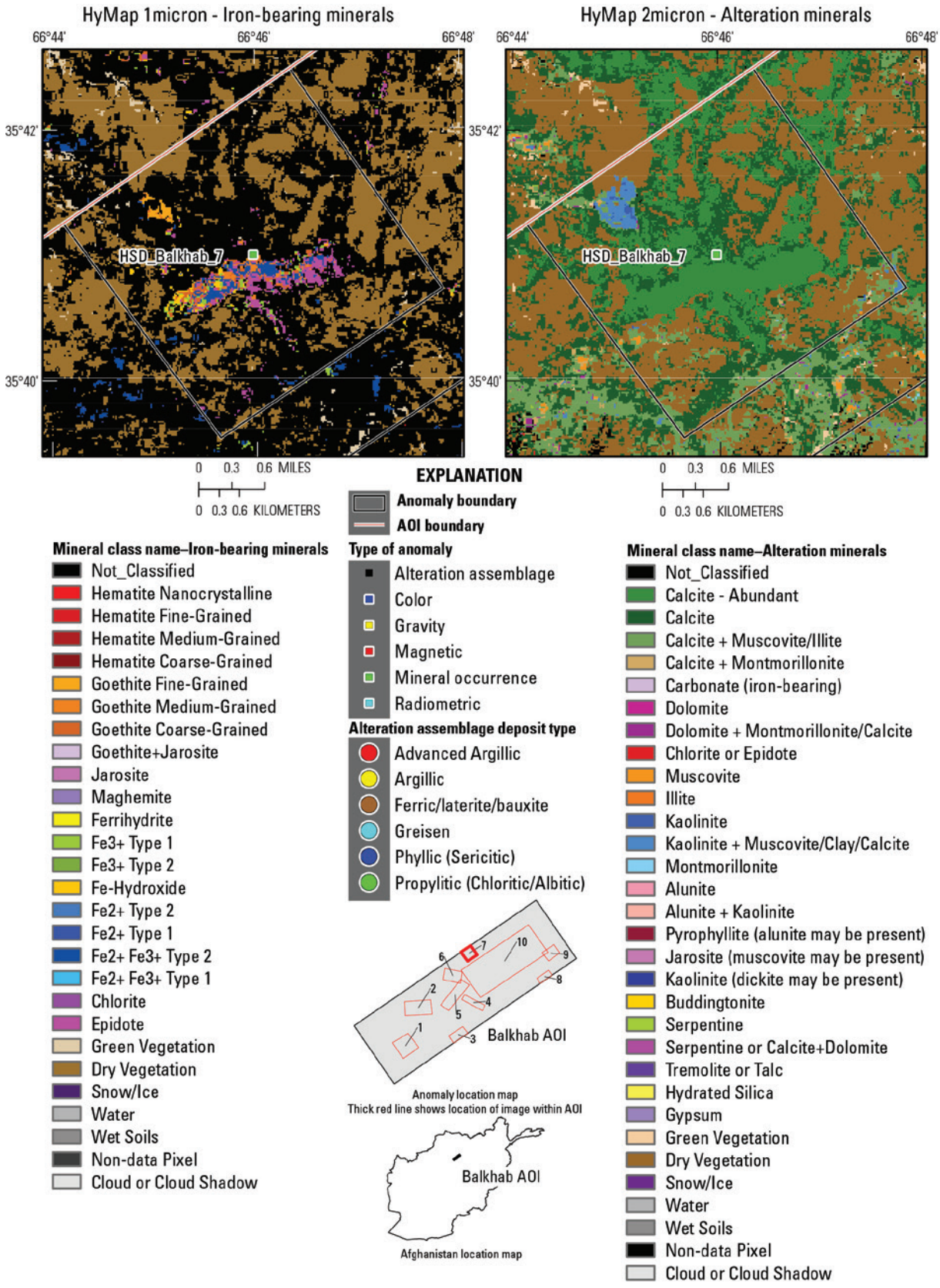

Figure 5.5.7. Hyperspectral anomaly located in the Balkhab Area of Interest (AOI) in Afghanistan based on presence of Kaolinite minerals, Calcite, Goethite minerals, Fe^{3+} Type 1, and Fe-Hydroxide.

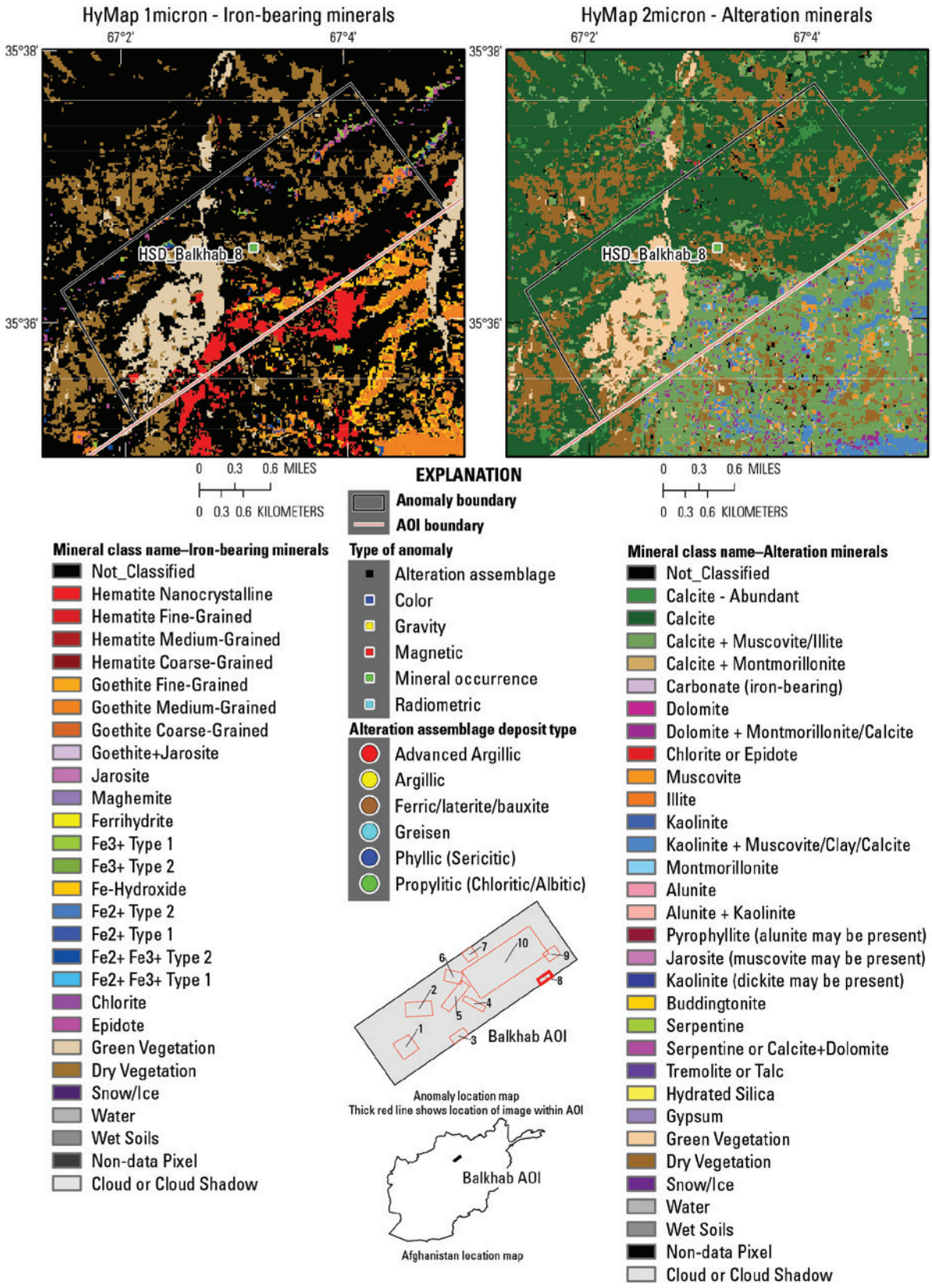

Figure 5.5.8. Hyperspectral anomaly located in the Balkhab Area of Interest (AOI) in Afghanistan based on presence of Hematite minerals and Goethite minerals.

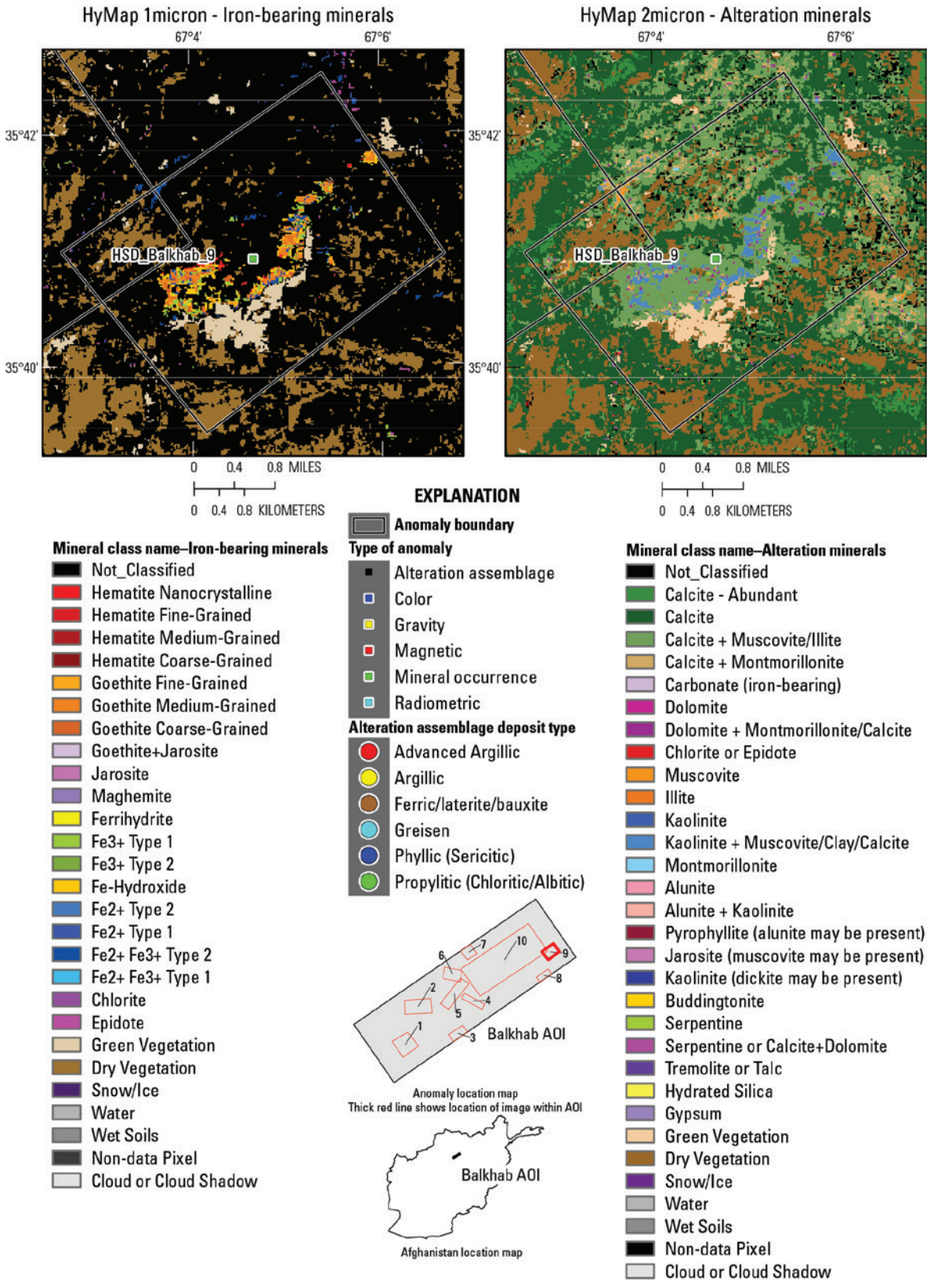

Figure 5.5.9. Hyperspectral anomaly located in the Balkhab Area of Interest (AOI) in Afghanistan based on presence of Kaolinite minerals, Dolomite minerals, Serpentine, Hematite minerals, Goethite minerals, Fe-Hydroxide, and Fe^{3+} Type 1.

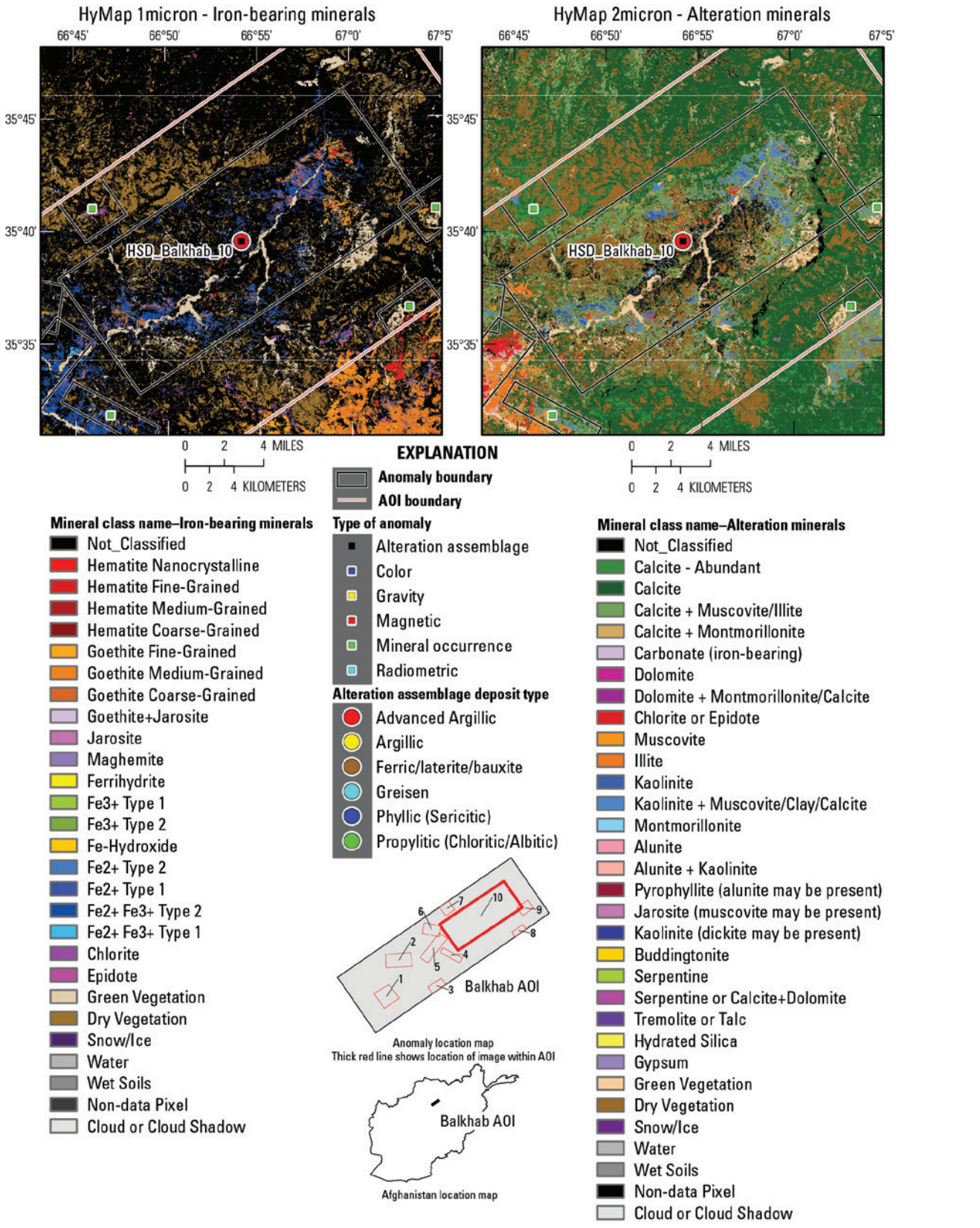

Figure 5.5.10. Hyperspectral anomaly located in the Balkhab Area of Interest (AOI) in Afghanistan based on presence of Kaolinite minerals, Dickite, Pyrophyllite, Dolomite minerals, Montmorillonite, Chlorite or Epidote, Muscovite, Goethite minerals, and Hematite minerals.

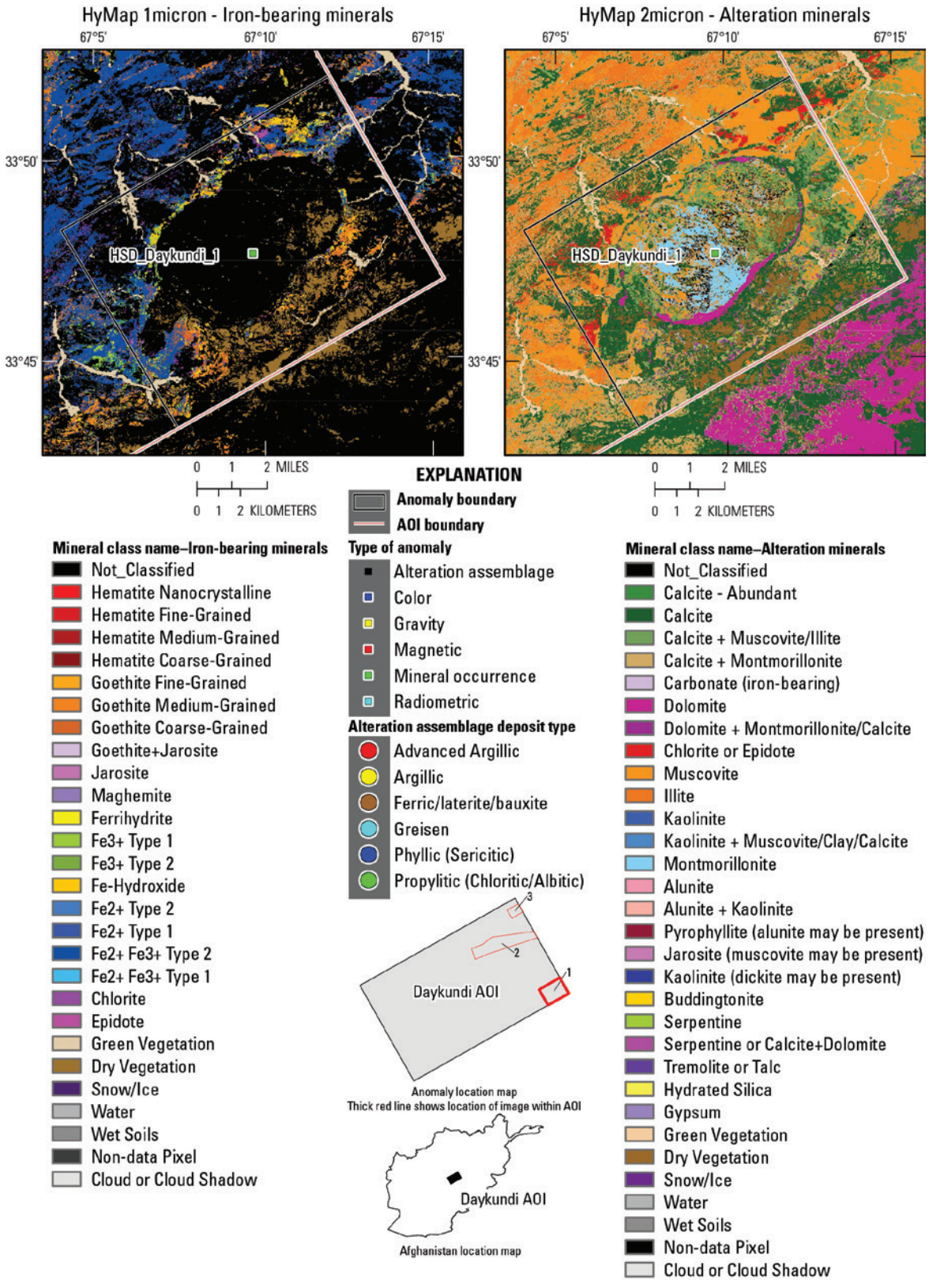

Figure 5.6.1. Hyperspectral anomaly located in the Daykundi Area of Interest (AOI) in Afghanistan based on presence of Montmorillonite, Dolomite Minerals, Goethite minerals, Fe^{3+} Type1, and Fe-Hydroxide.

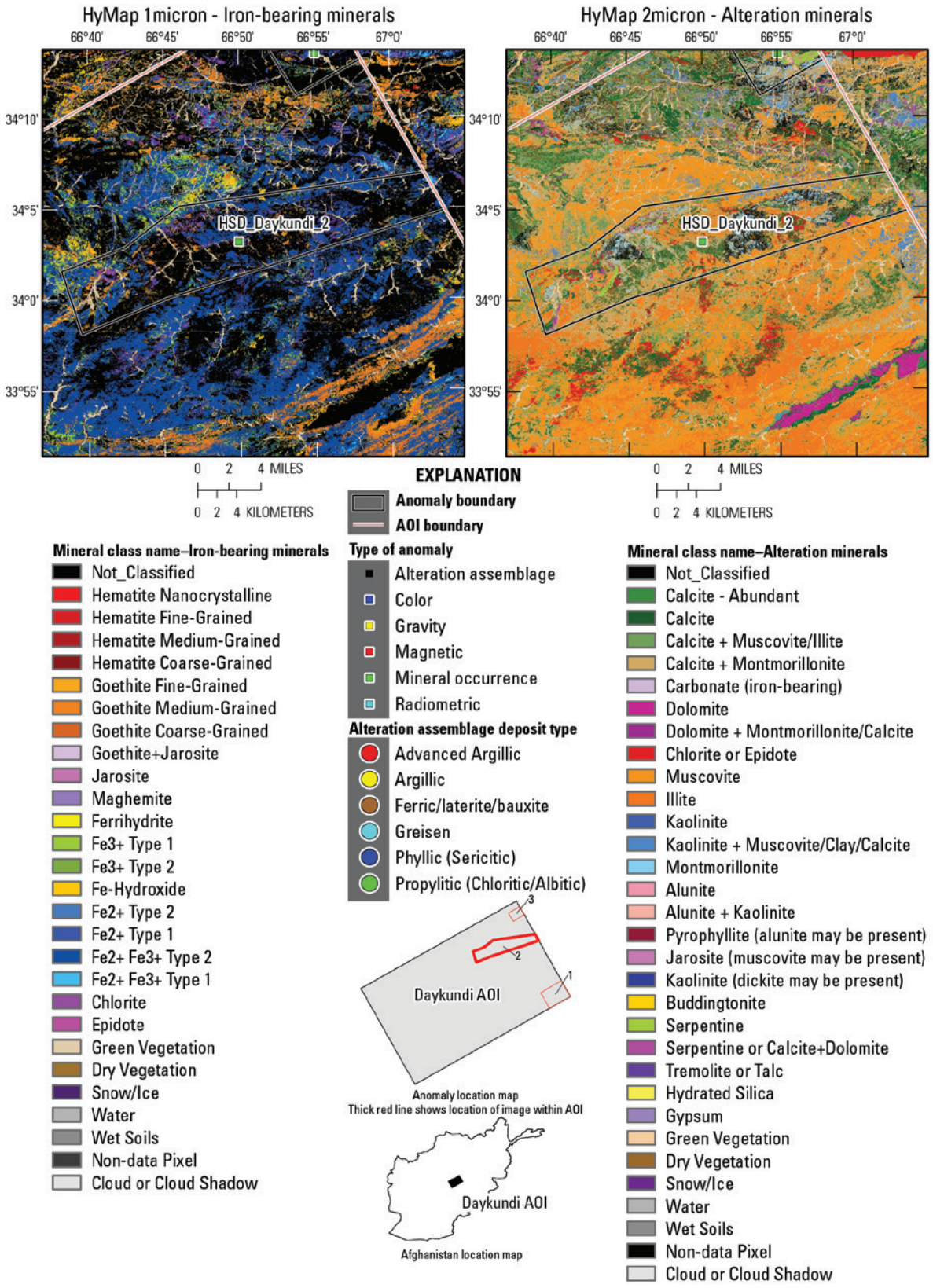

Figure 5.6.2. Hyperspectral anomaly located in the Daykundi Area of Interest (AOI) in Afghanistan based on presence of Serpentine minerals, Montmorillonite, Chlorite or Epidote, Dolomite minerals, Tremolite or Talc, and Goethite minerals.

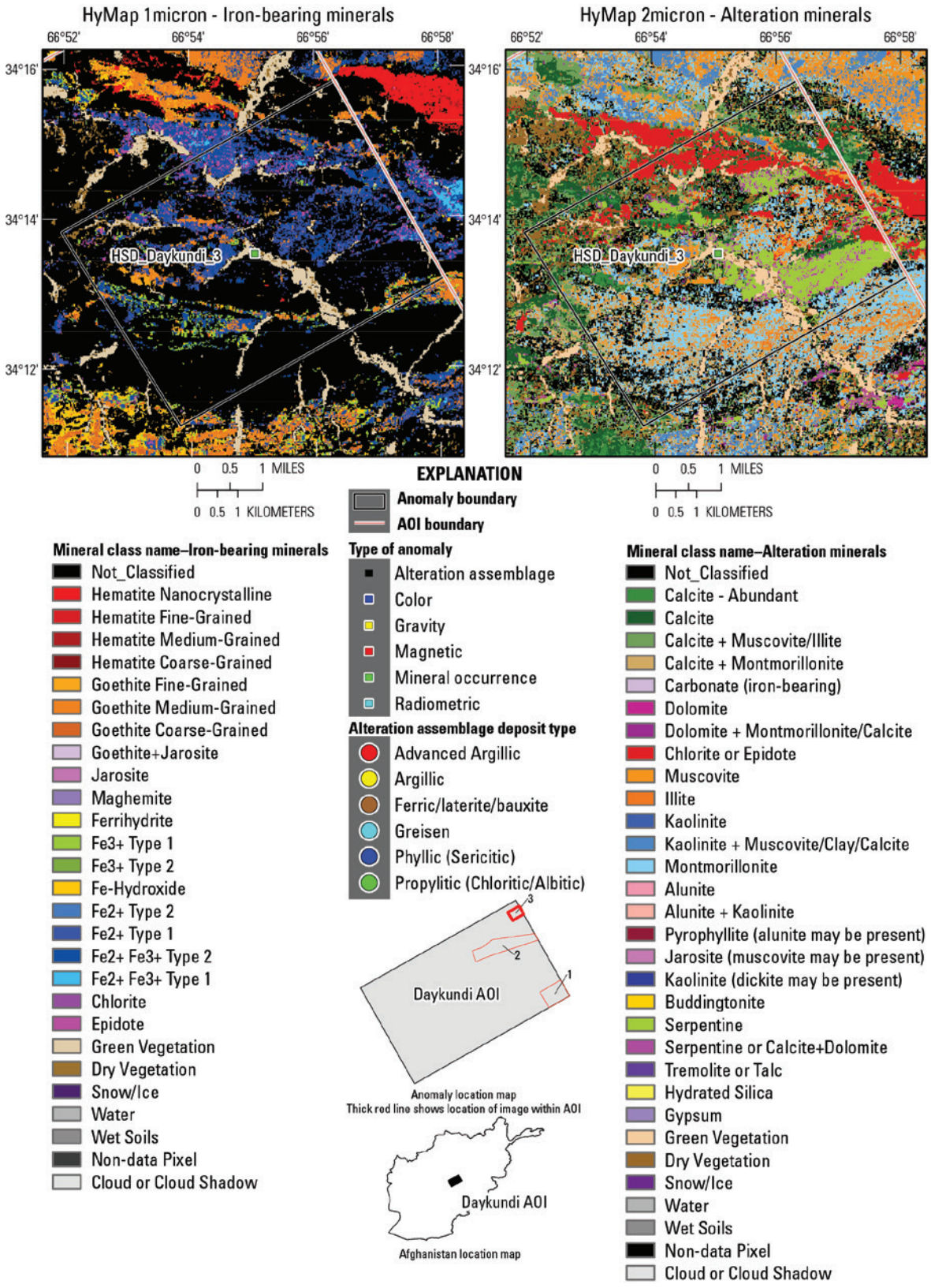

Figure 5.6.3. Hyperspectral anomaly located in the Daykundi Area of Interest (AOI) in Afghanistan based on presence of Serpentine minerals, Montmorillonite, and Chlorite or Epidote.

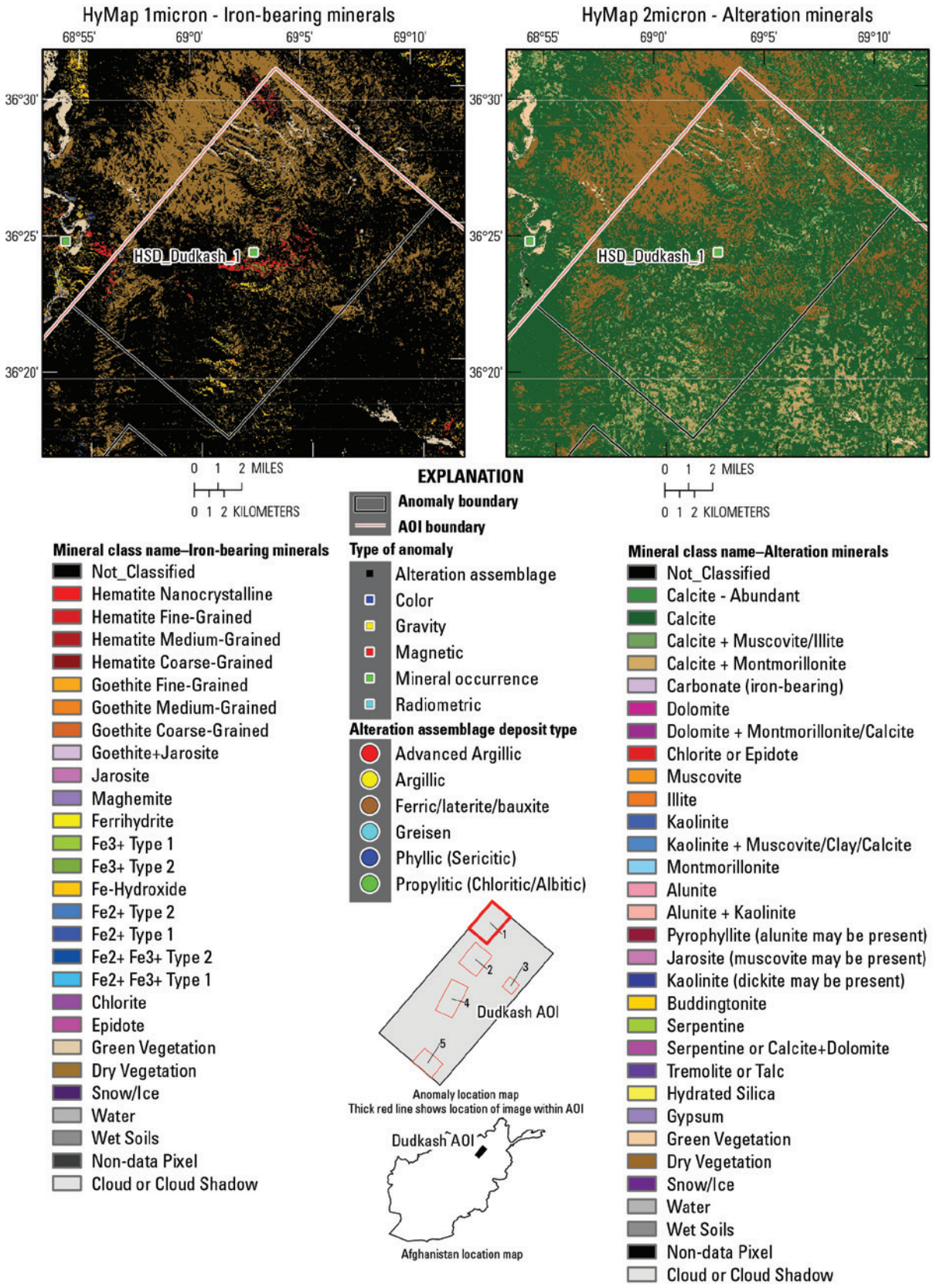

Figure 5.7.1. Hyperspectral anomaly located in the Dudkash Area of Interest (AOI) in Afghanistan based on presence of Hematite and Fe-Hydroxide.

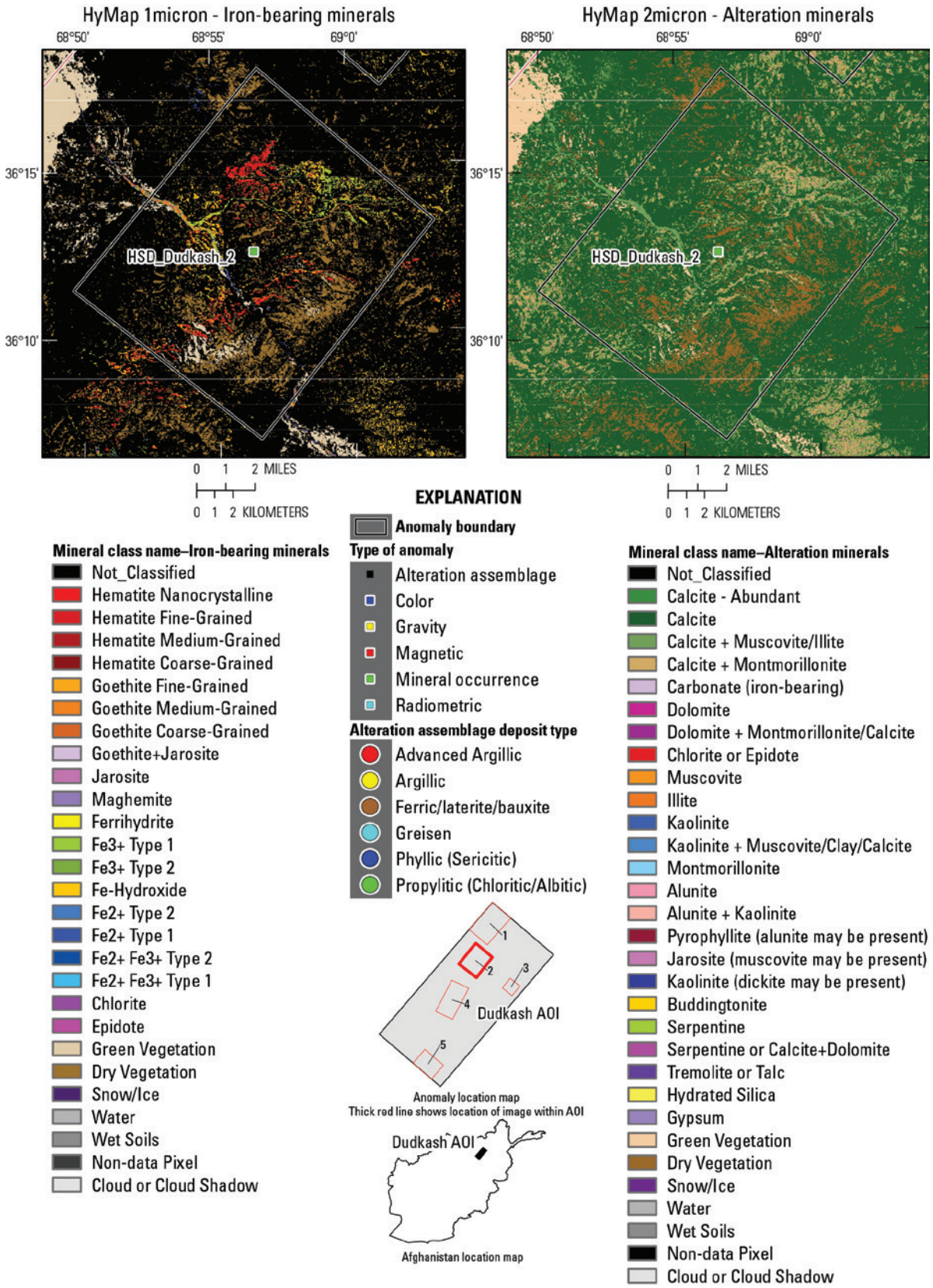

Figure 5.7.2. Hyperspectral anomaly located in the Dudkash Area of Interest (AOI) in Afghanistan based on presence of Hematite, Fe3+ Type 1, and Fe-Hydroxide.

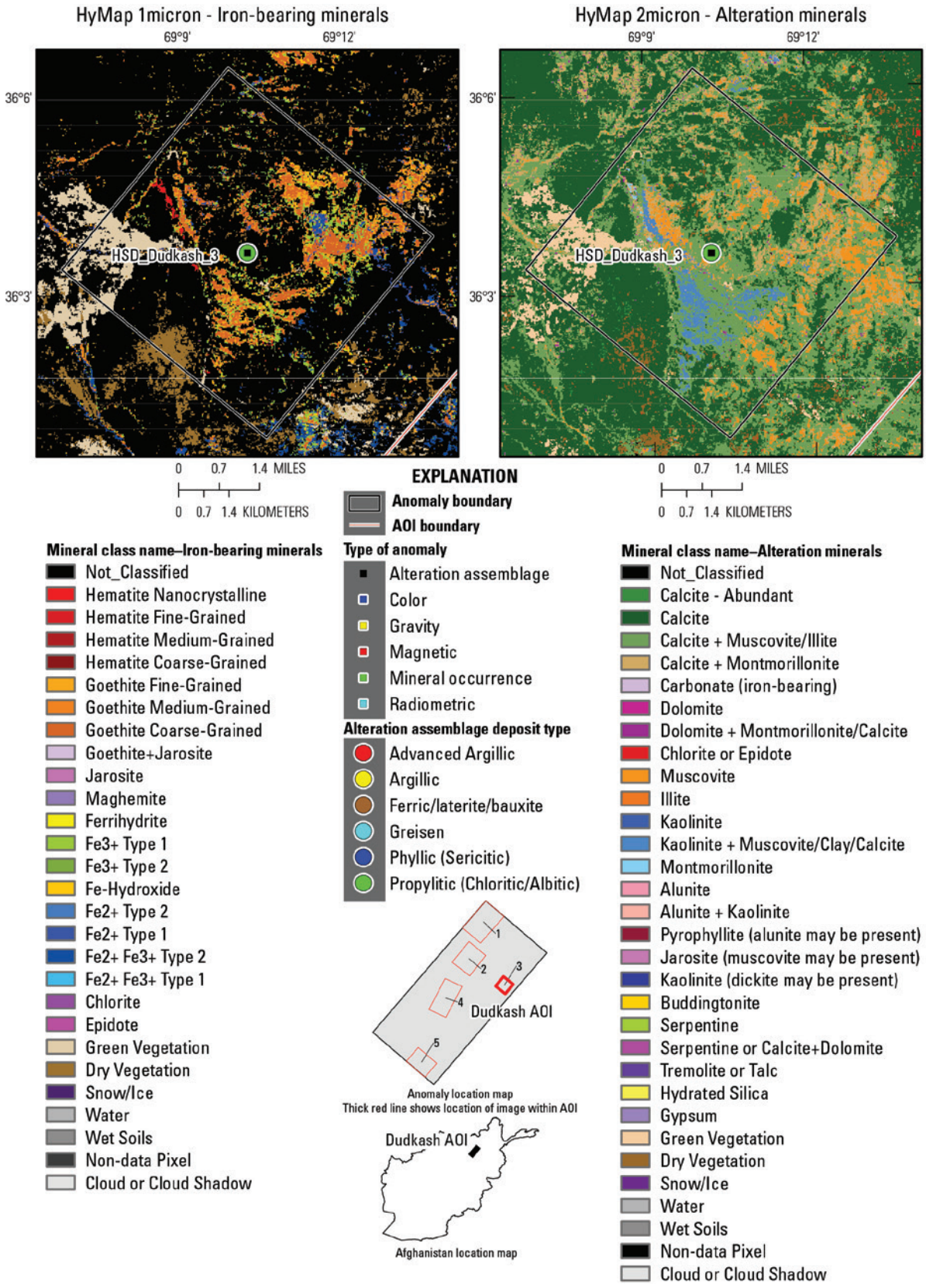

Figure 5.7.3. Hyperspectral anomaly located in the Dudkash Area of Interest (AOI) in Afghanistan based on presence of Kaolinite minerals, Muscovite, Montmorillonite, Hematite, Goethite minerals, Fe^{3+} Type 1, and Epidote.

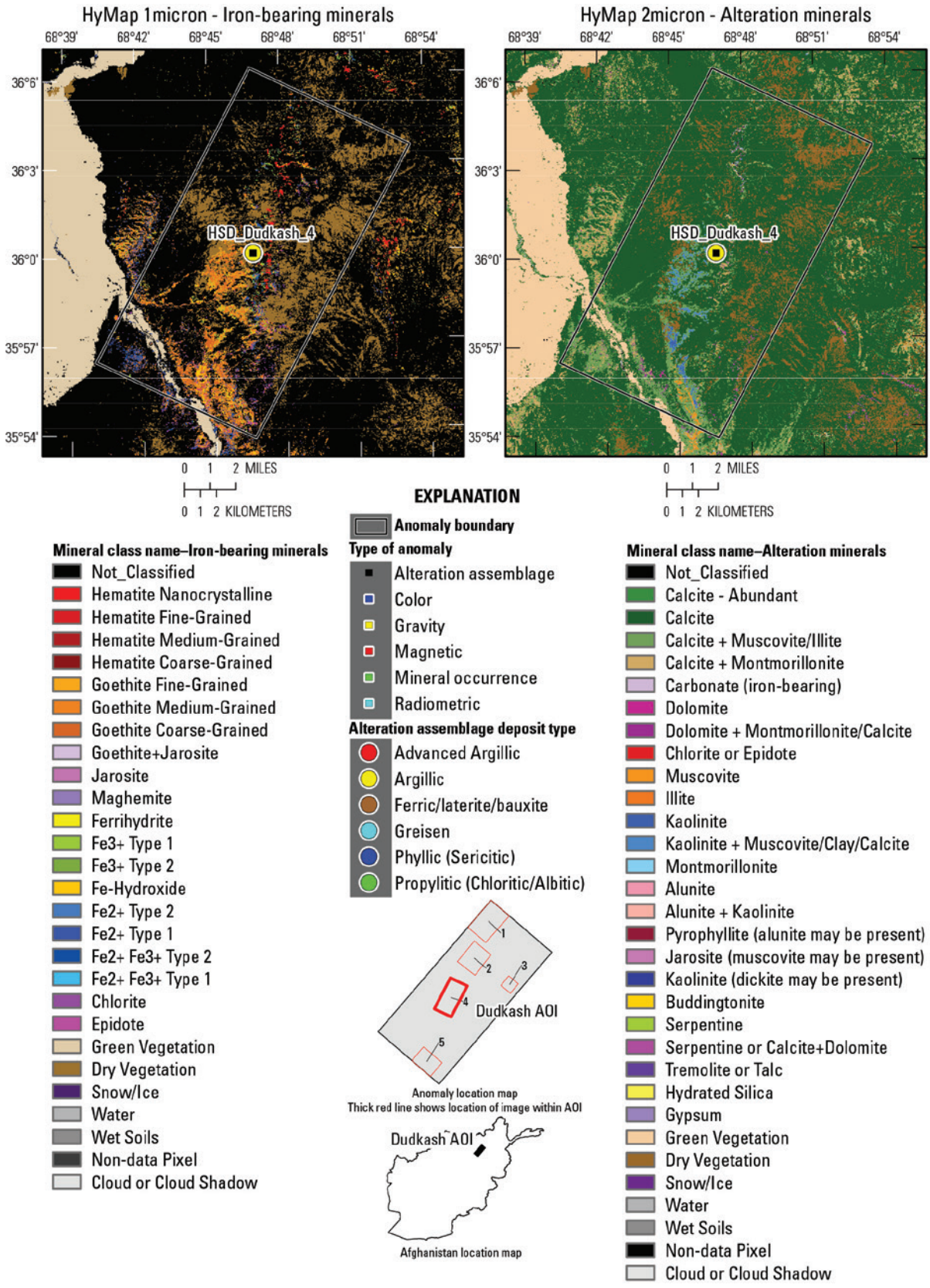

Figure 5.7.4. Hyperspectral anomaly located in the Dudkash Area of Interest (AOI) in Afghanistan based on presence of Goethite minerals, Hematite, Fe-Hydroxide, Epidote, Kaolinite minerals, Dolomite minerals, Muscovite, and Alunite.

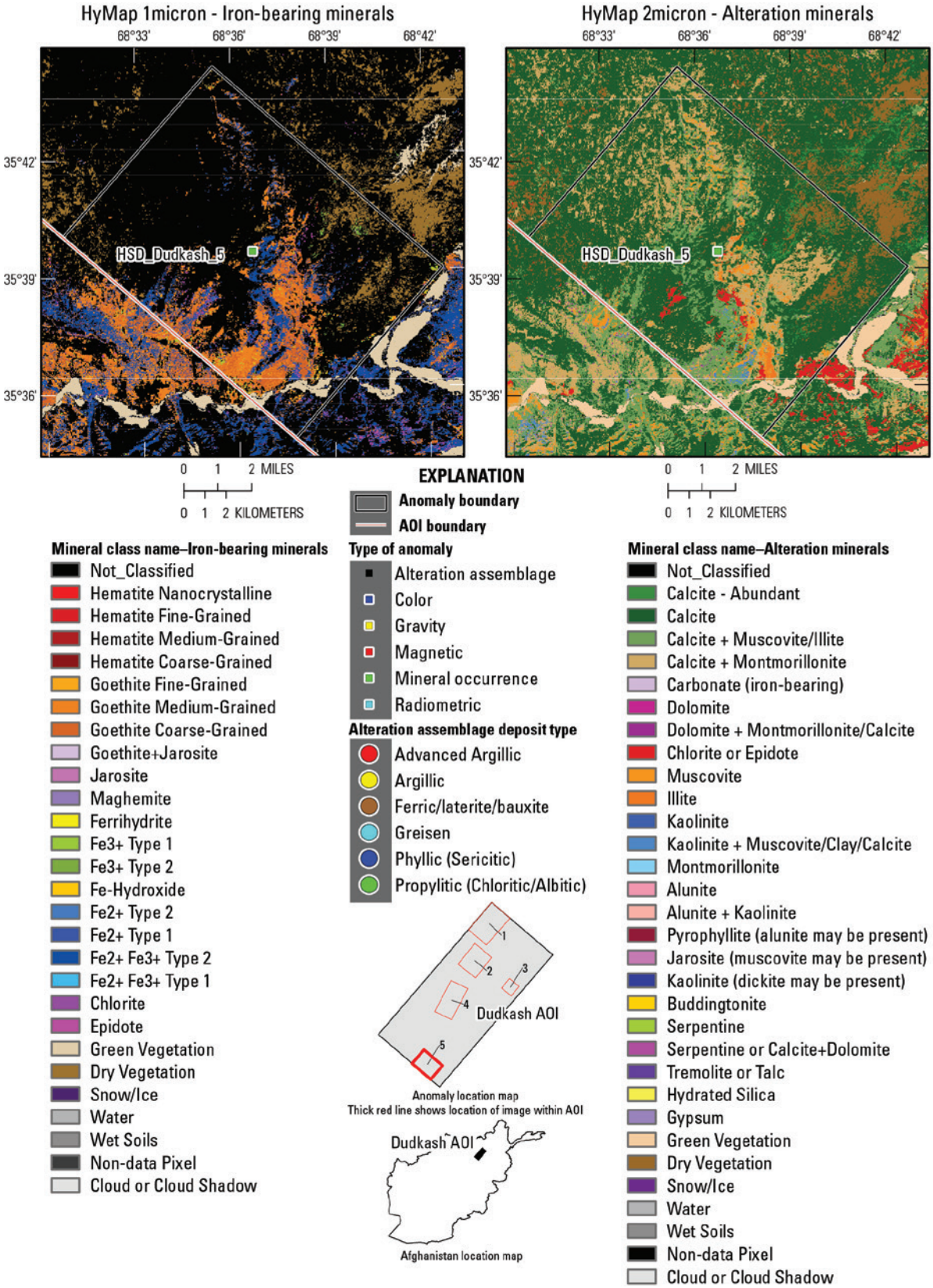

Figure 5.7.5. Hyperspectral anomaly located in the Dudkash Area of Interest (AOI) in Afghanistan based on presence of Chlorite or Epidote, Muscovite, Kaolinite minerals, Illite, Goethite minerals, Fe^{3+} Type 1, and Fe-Hydroxide.

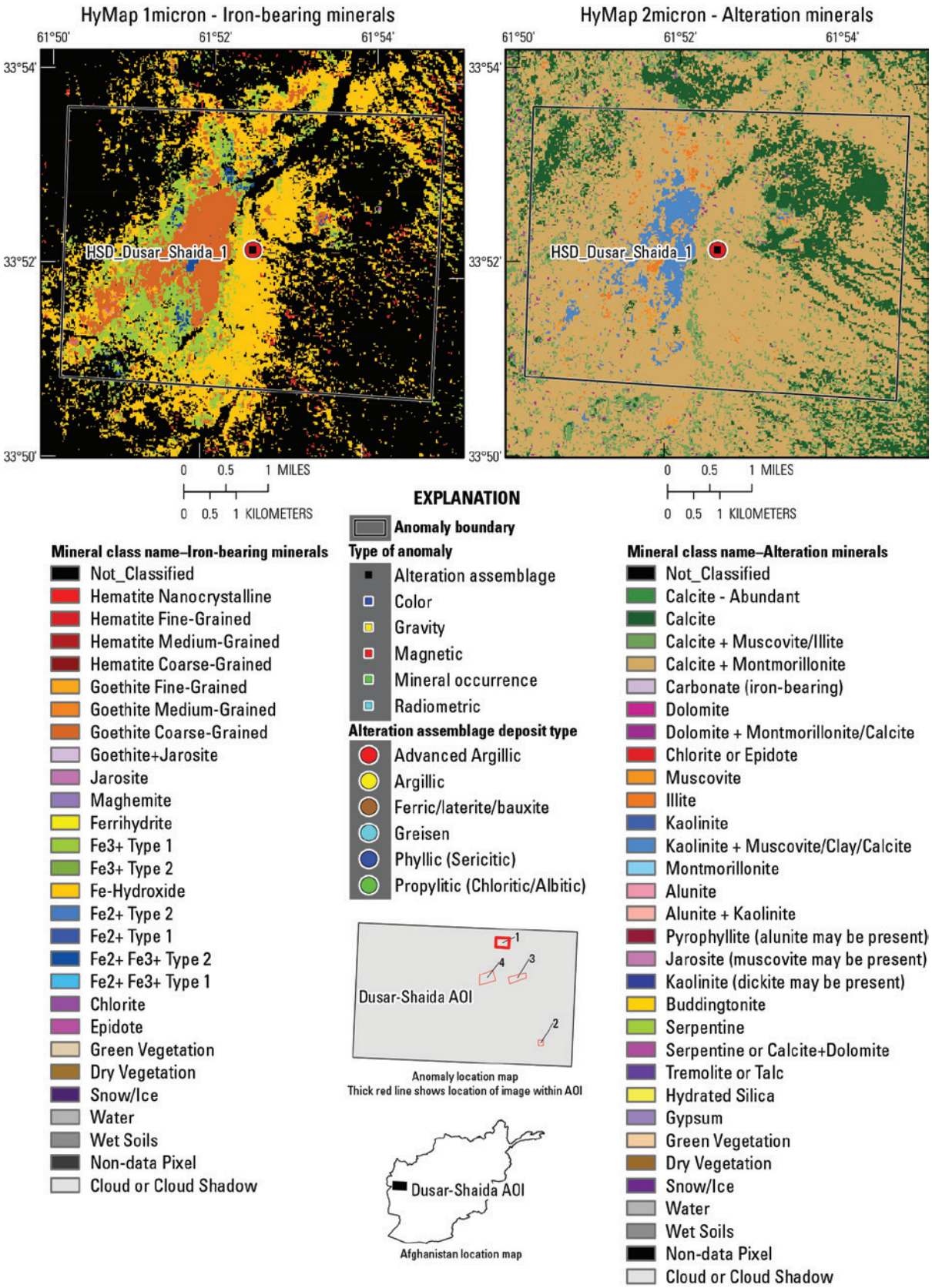

Figure 5.8.1. Hyperspectral anomaly located in the Dusar-Shaida Area of Interest (AOI) in Afghanistan based on presence of Muscovite, Kaolinite minerals, Illite, Goethite minerals, Fe^{3+} Type1, Fe-Hydroxide, and Jarosite.

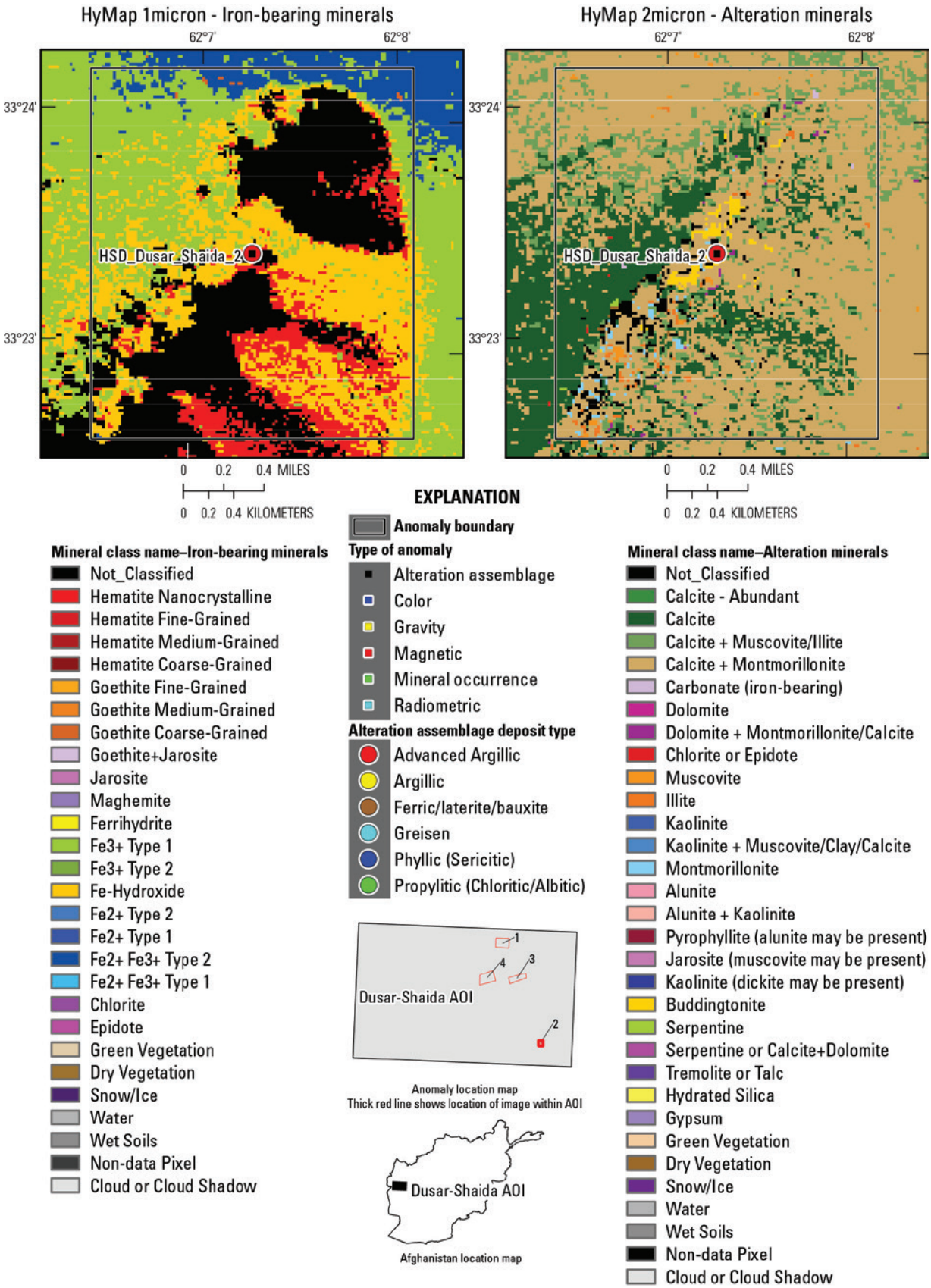

Figure 5.8.2. Hyperspectral anomaly located in the Dusar-Shaida Area of Interest (AOI) in Afghanistan based on presence of Buddingtonite.

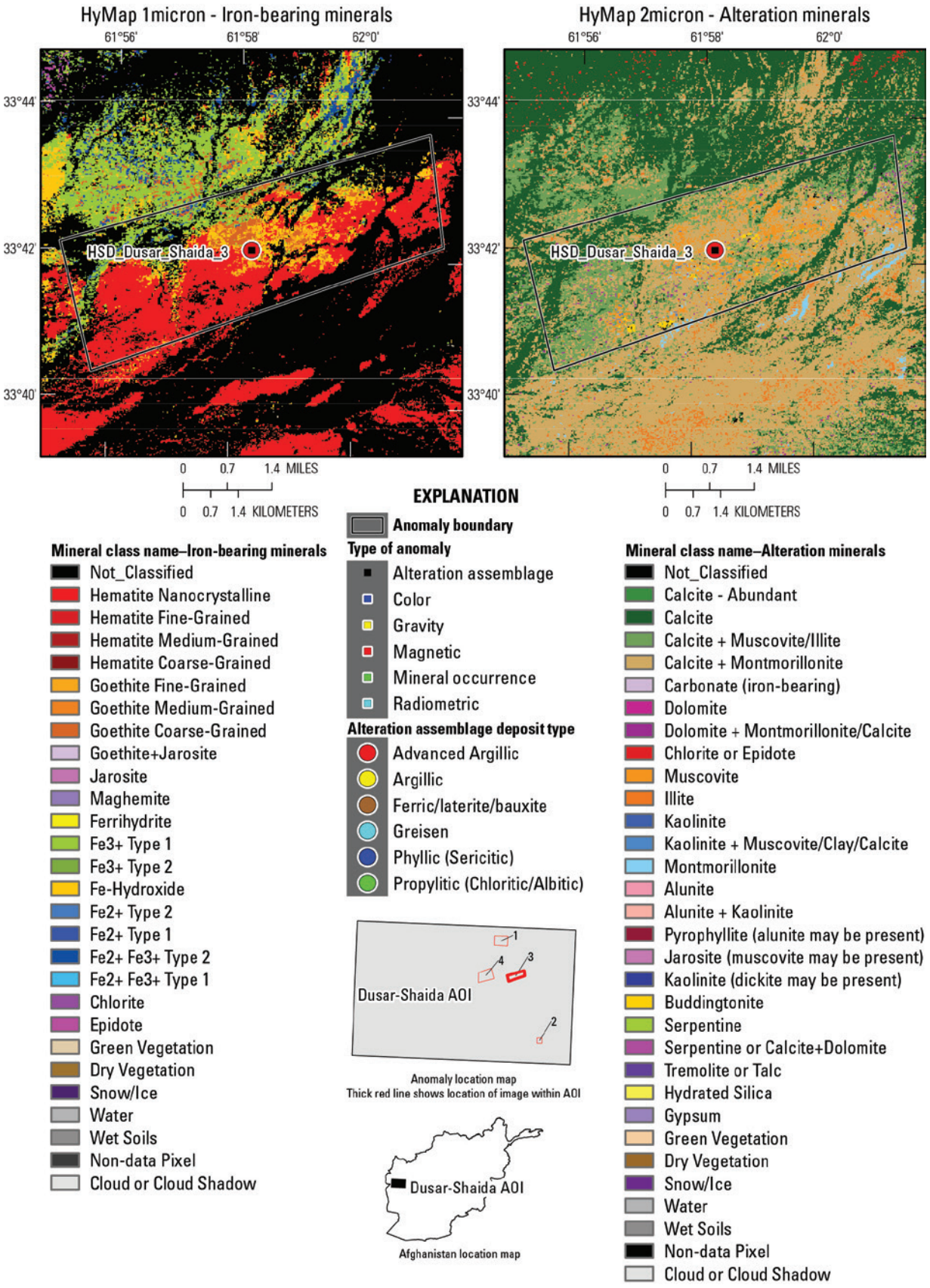

Figure 5.8.3. Hyperspectral anomaly located in the Dusar-Shaida Area of Interest (AOI) in Afghanistan based on presence of Buddingtonite.

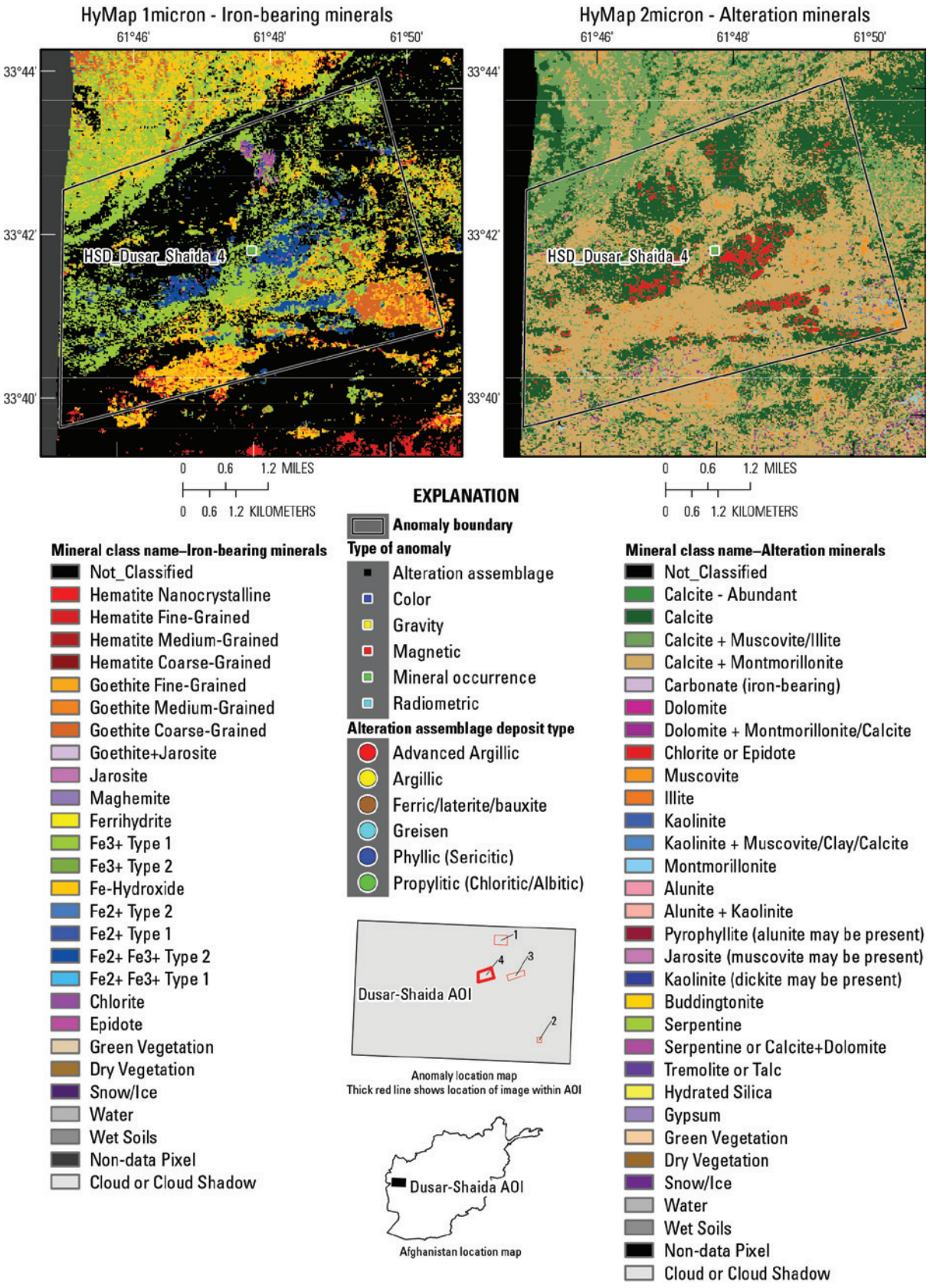

Figure 5.8.4. Hyperspectral anomaly located in the Dusar-Shaida Area of Interest (AOI) in Afghanistan based on presence of Calcite, Chlorite or Epidote, Fe^{3+} Type1, Hematite minerals, Fe^{2+} Fe^{3+} Type2, and Goethite minerals.

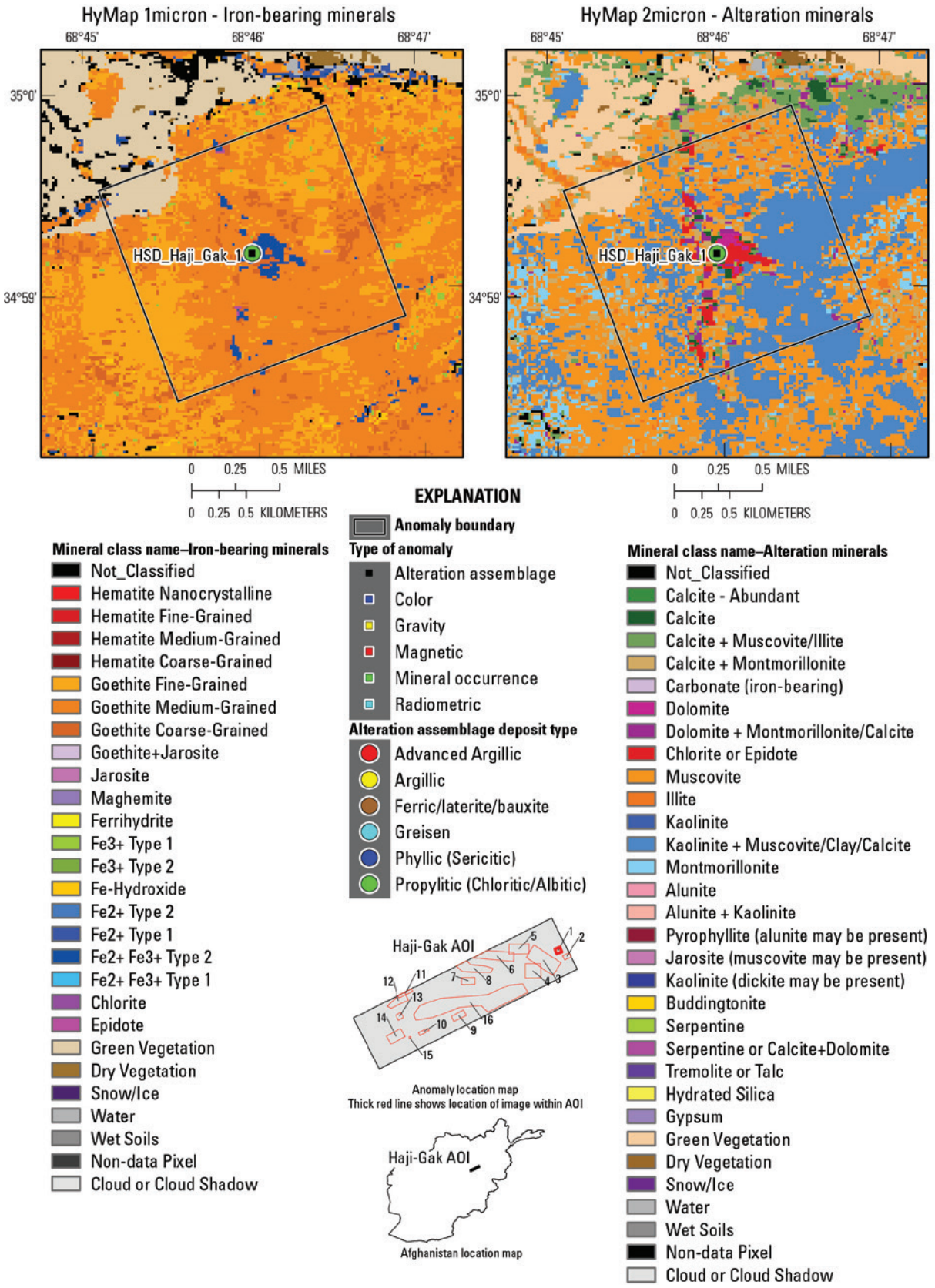

Figure 5.9.1. Hyperspectral anomaly located in the Haji-Gak Area of Interest (AOI) in Afghanistan based on presence of Calcite, Chlorite or Epidote, Dolomite minerals, Kaolinite minerals, Montmorillonite, Fe3+ Type1, Fe2+ Fe3+ Type2, and Goethite minerals.

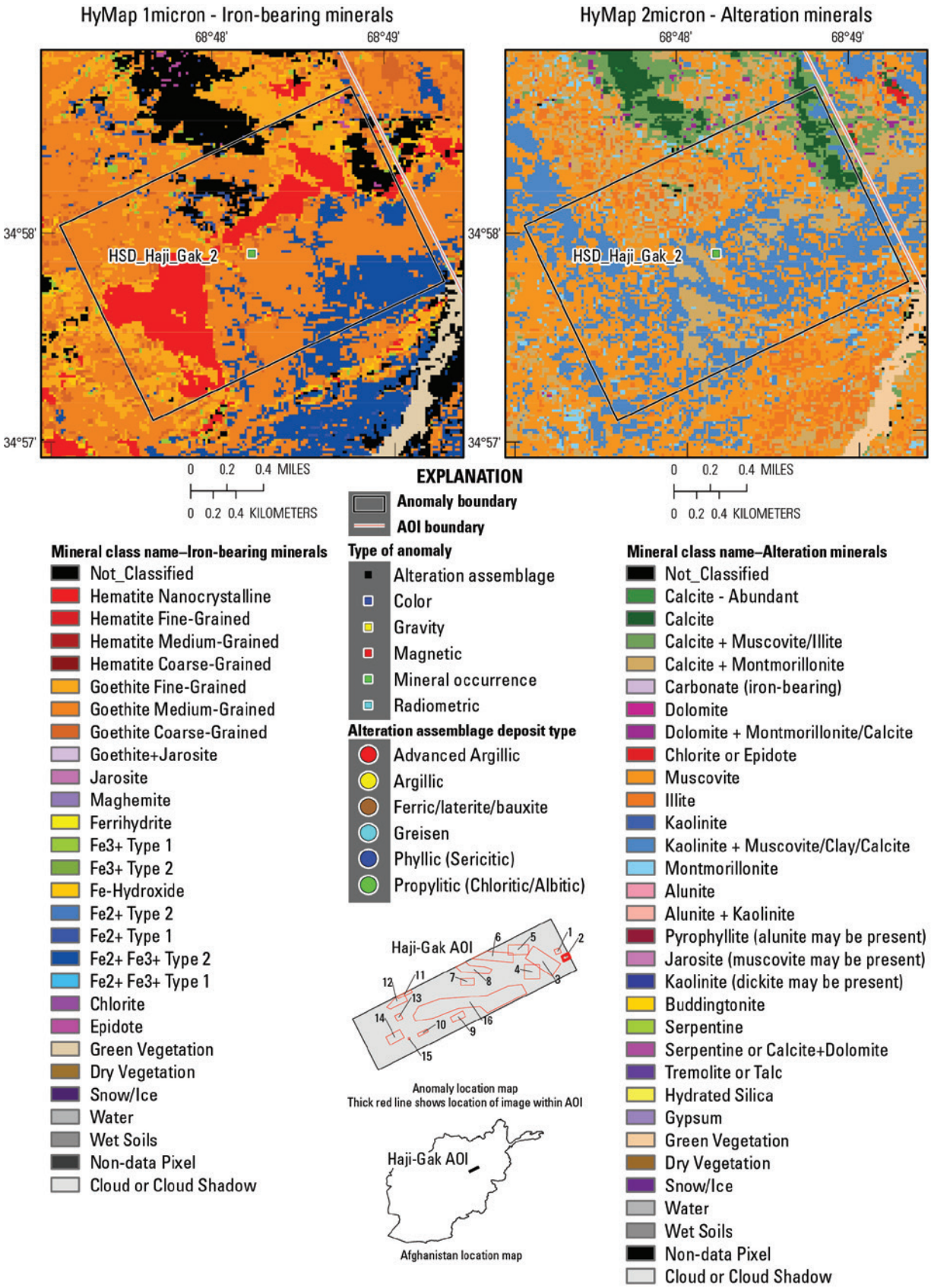

Figure 5.9.2. Hyperspectral anomaly located in the Dusar-Shaida Area of Interest (AOI) in Afghanistan based on presence of Hematite minerals and Goethite minerals.

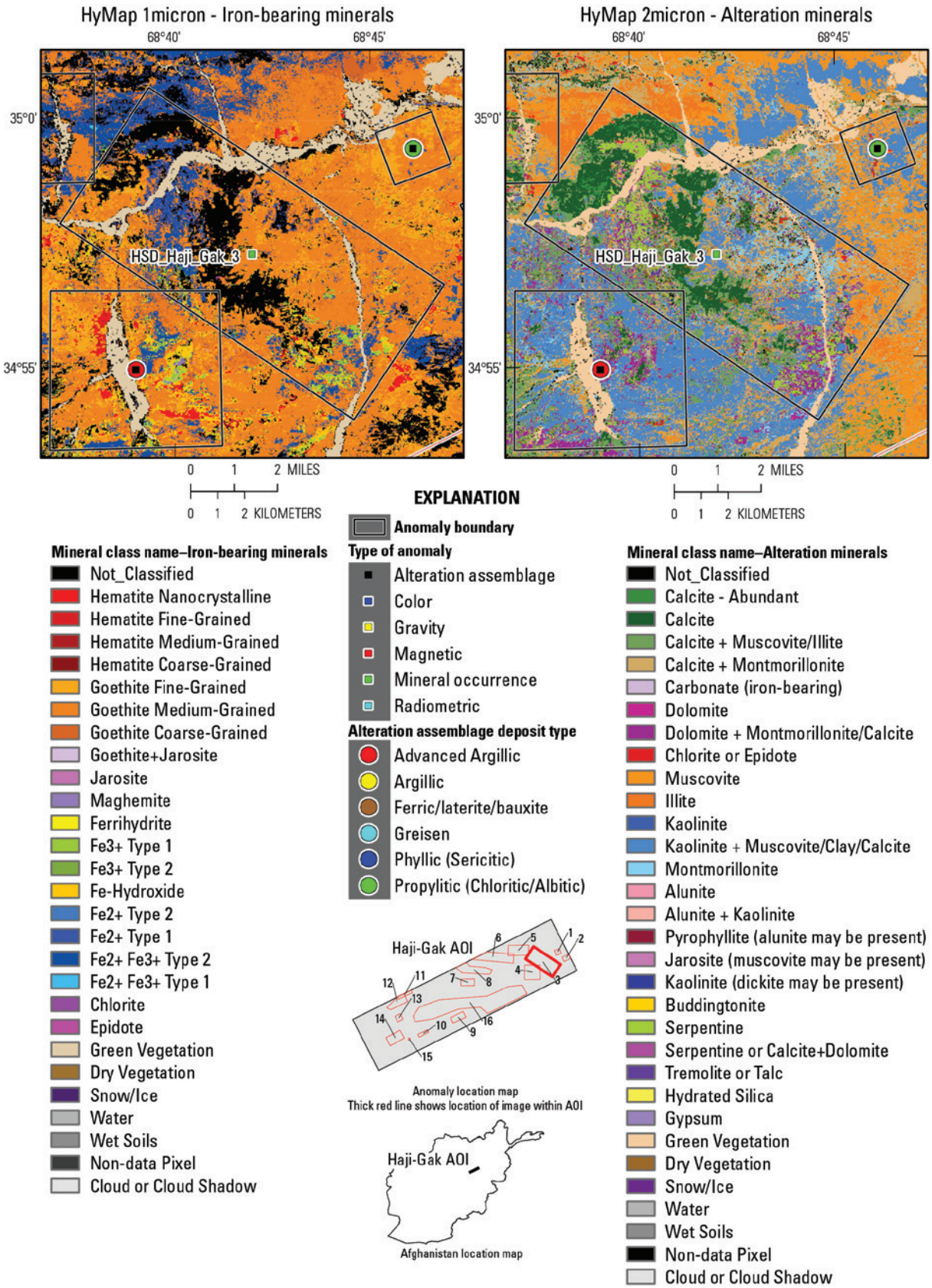

Figure 5.9.3. Hyperspectral anomaly located in the Haji-Gak Area of Interest (AOI) in Afghanistan based on presence of Calcite, Serpentine minerals, Dolomite minerals, Tremolite or Talc, Hematite minerals and Goethite minerals.

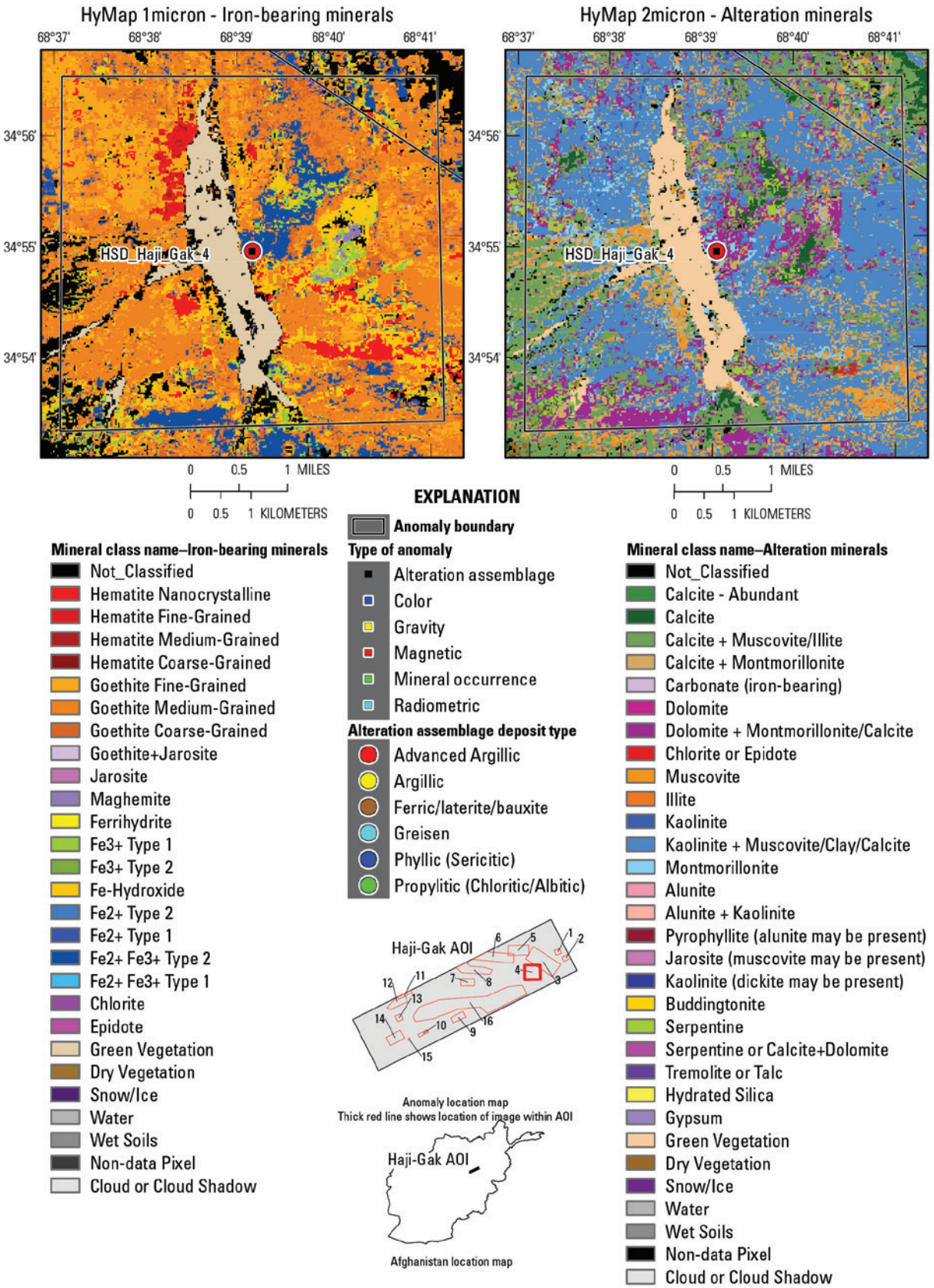

Figure 5.9.4. Hyperspectral anomaly located in the Haji-Gak Area of Interest (AOI) in Afghanistan based on presence of Calcite, Serpentine minerals, Dolomite minerals, Kaolinite minerals, Montmorillonite, Muscovite, Maghemite, Jarosite, Goethite minerals, Ferrihydrite, and Hematite minerals.

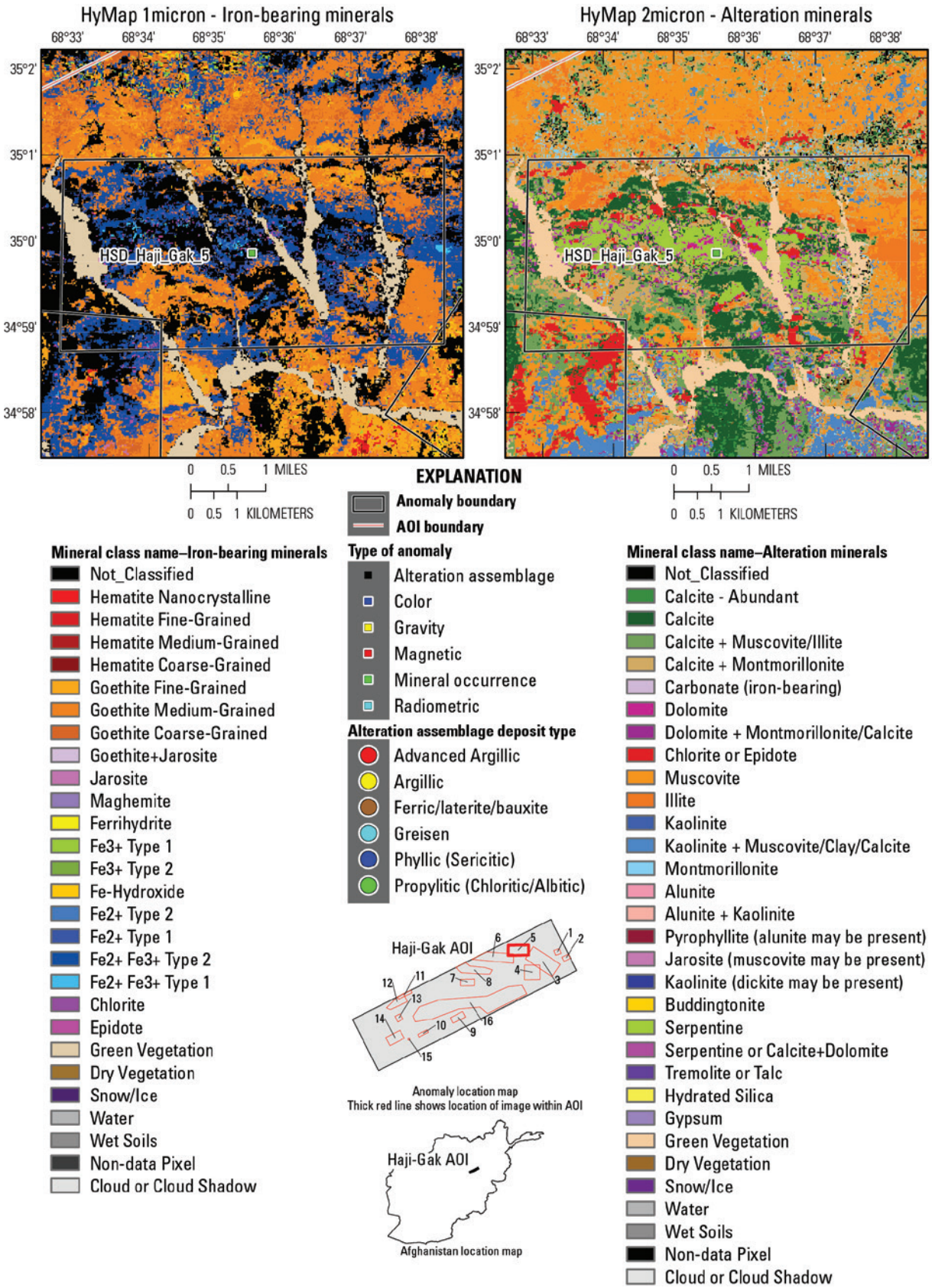

Figure 5.9.5. Hyperspectral anomaly located in the Haji-Gak Area of Interest (AOI) in Afghanistan based on presence of Serpentine minerals, Chlorite or Epidote, and Dolomite minerals.

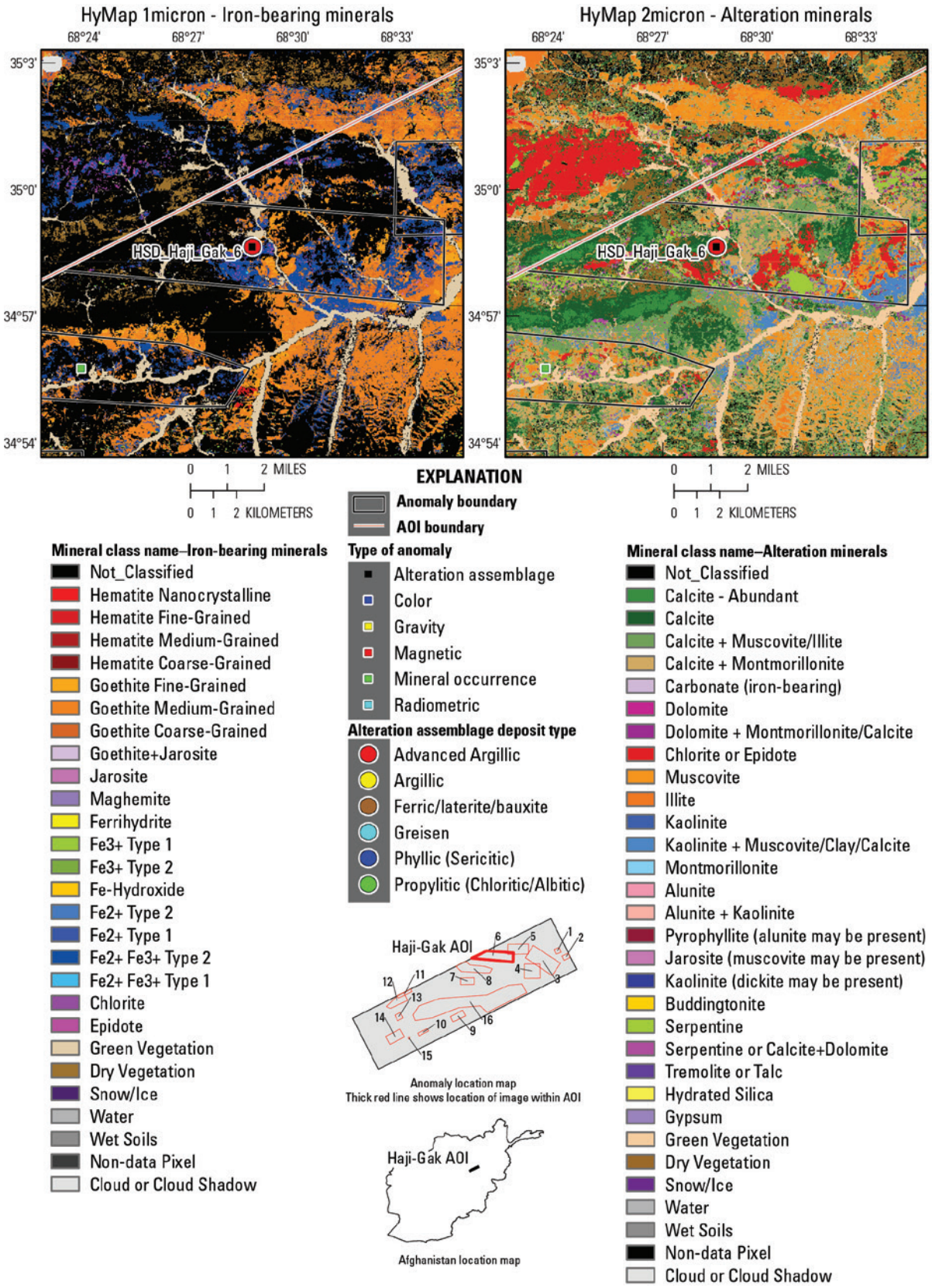

Figure 5.9.6. Hyperspectral anomaly located in the Haji-Gak Area of Interest (AOI) in Afghanistan based on presence of Chlorite or Epidote, Serpentine minerals, Dolomite minerals, Kaolinite minerals, Tremolite or Talc, Goethite minerals, and Jarosite.

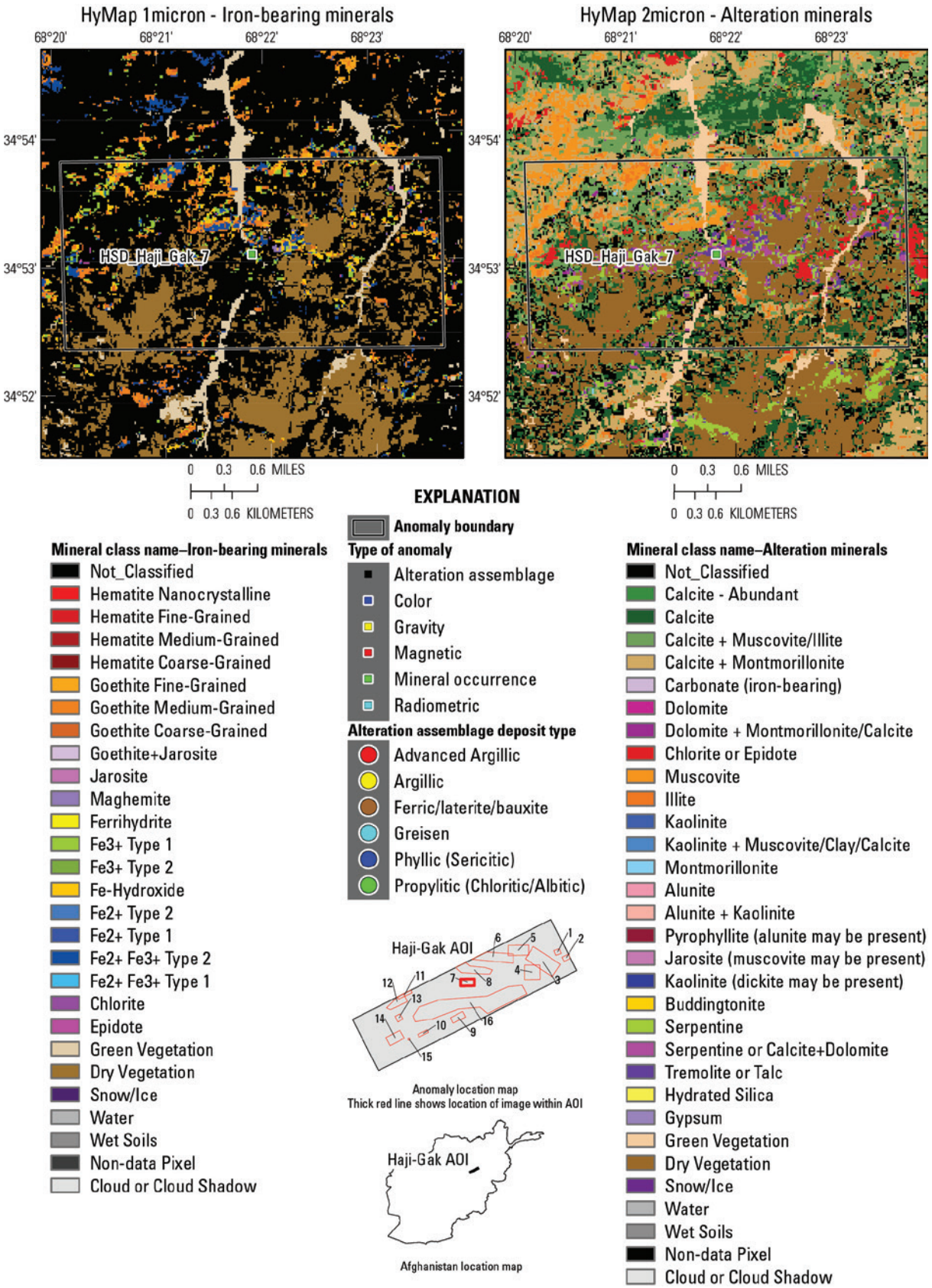

Figure 5.9.7. Hyperspectral anomaly located in the Haji-Gak Area of Interest (AOI) in Afghanistan based on presence of Tremolite or Talc, Serpentine minerals, Chlorite or Epidote, Maghemite, Fe^{3+} Type 1, and Goethite minerals.

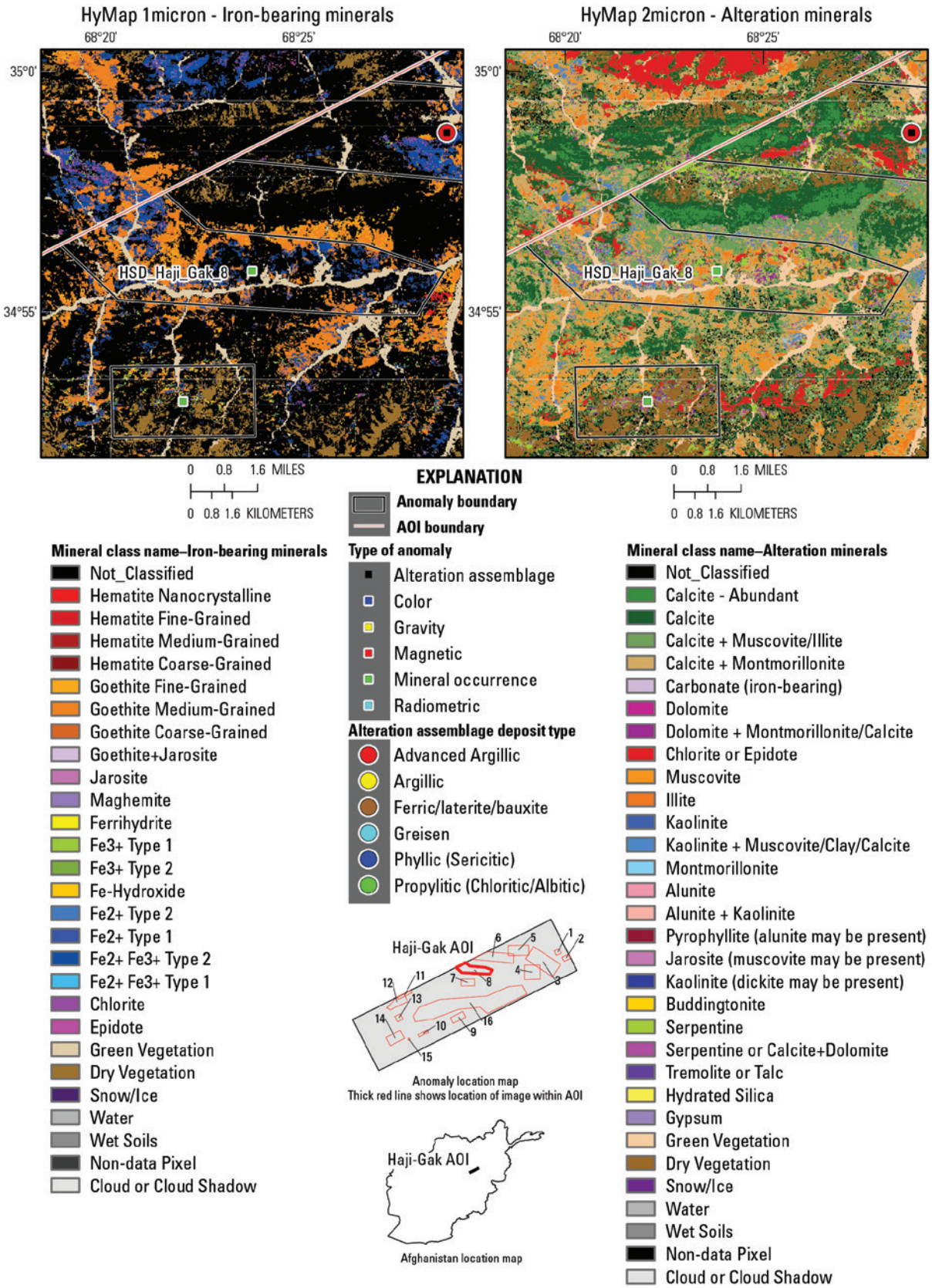

Figure 5.9.8. Hyperspectral anomaly located in the Haji-Gak Area of Interest (AOI) in Afghanistan based on presence of Serpentine minerals, Alunite minerals, Chlorite or Epidote, Dolomite minerals, Goethite minerals, and Fe-Hydroxide.

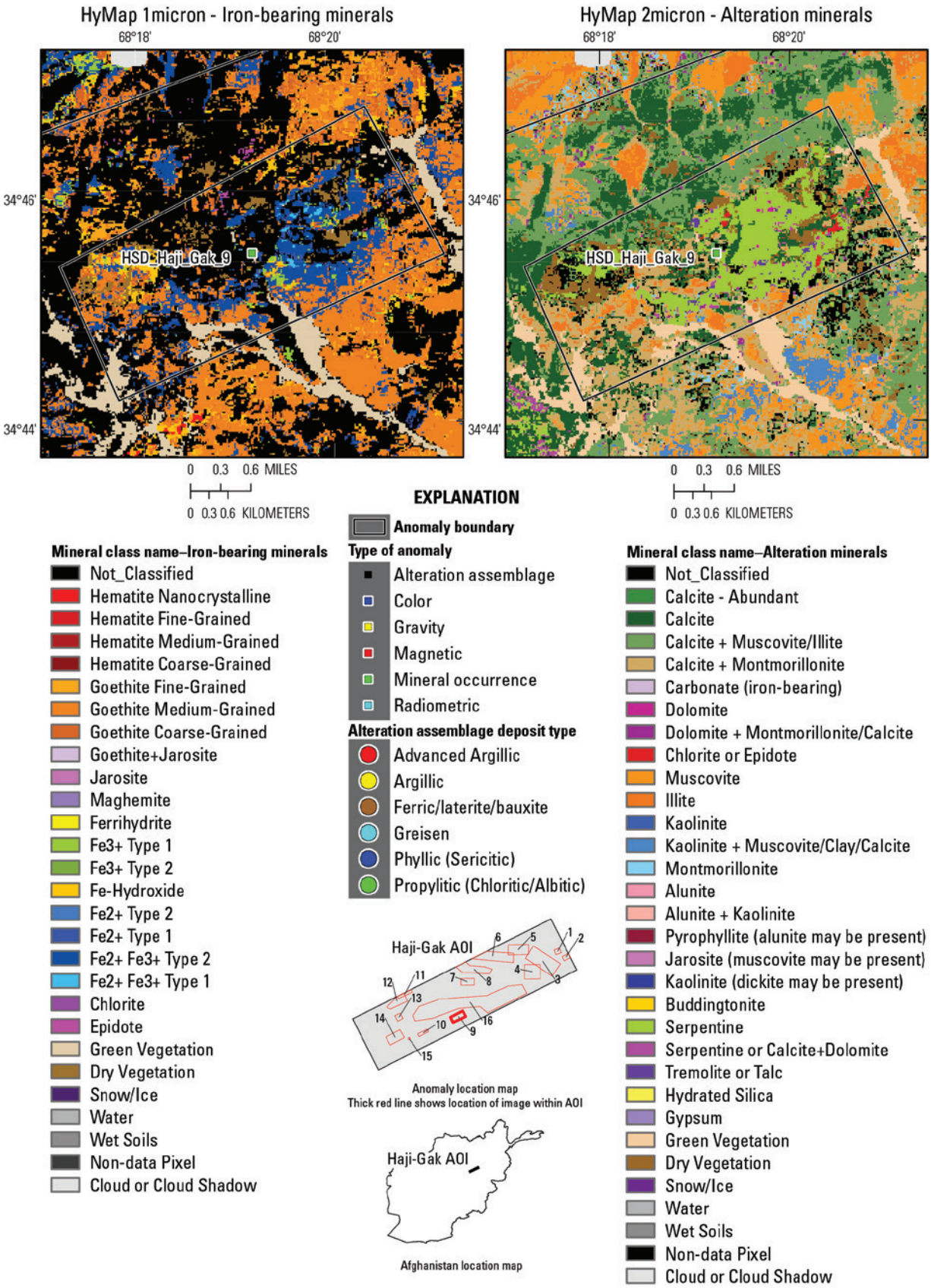

Figure 5.9.9. Hyperspectral anomaly located in the Haji-Gak Area of Interest (AOI) in Afghanistan based on presence of Serpentine, Tremolite or Talc, Goethite minerals, Fe^{3+} Type 1, and Fe-Hydroxide.

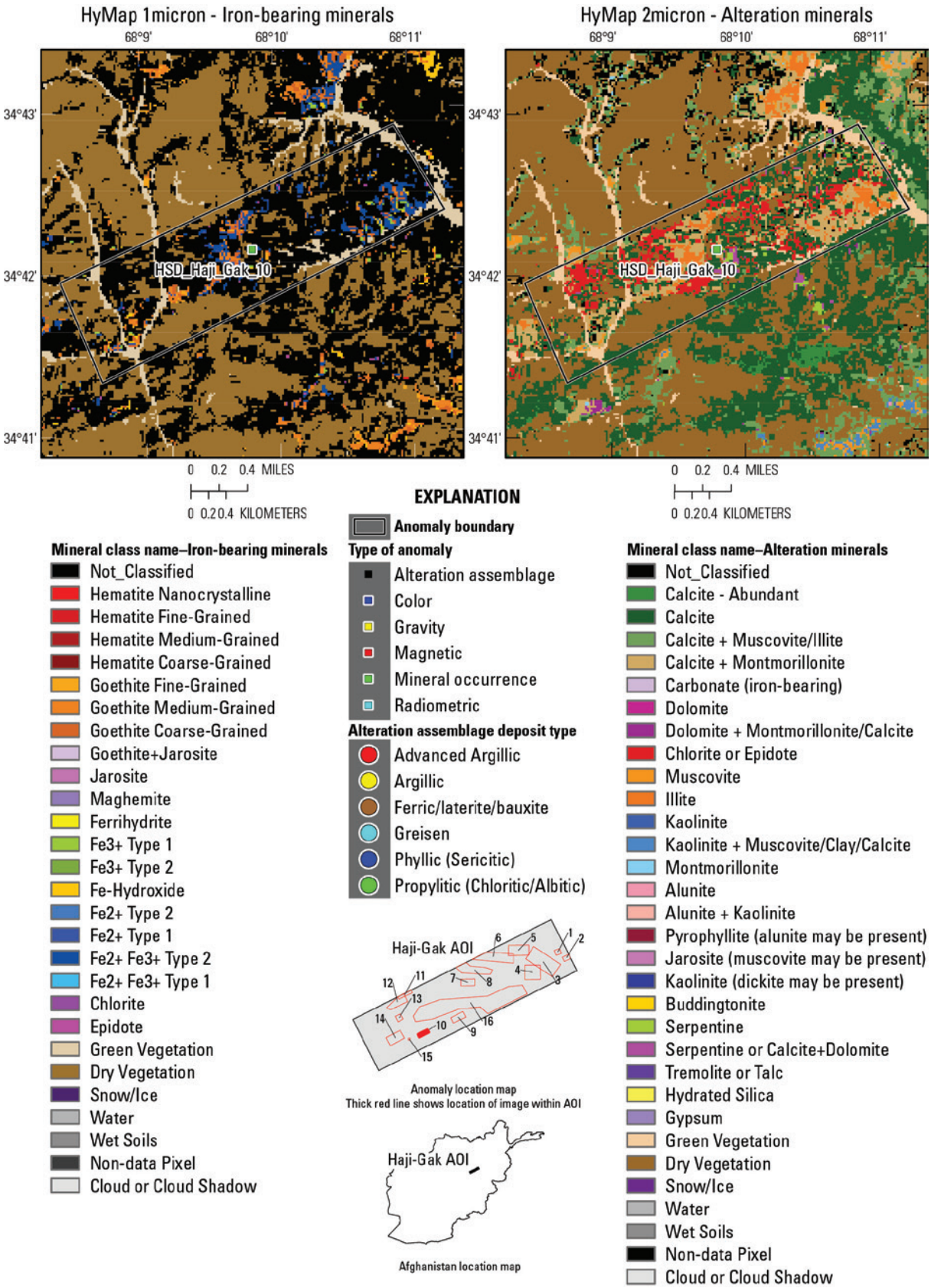

Figure 5.9.10. Hyperspectral anomaly located in the Haji-Gak Area of Interest (AOI) in Afghanistan based on presence of Chlorite or Epidote.

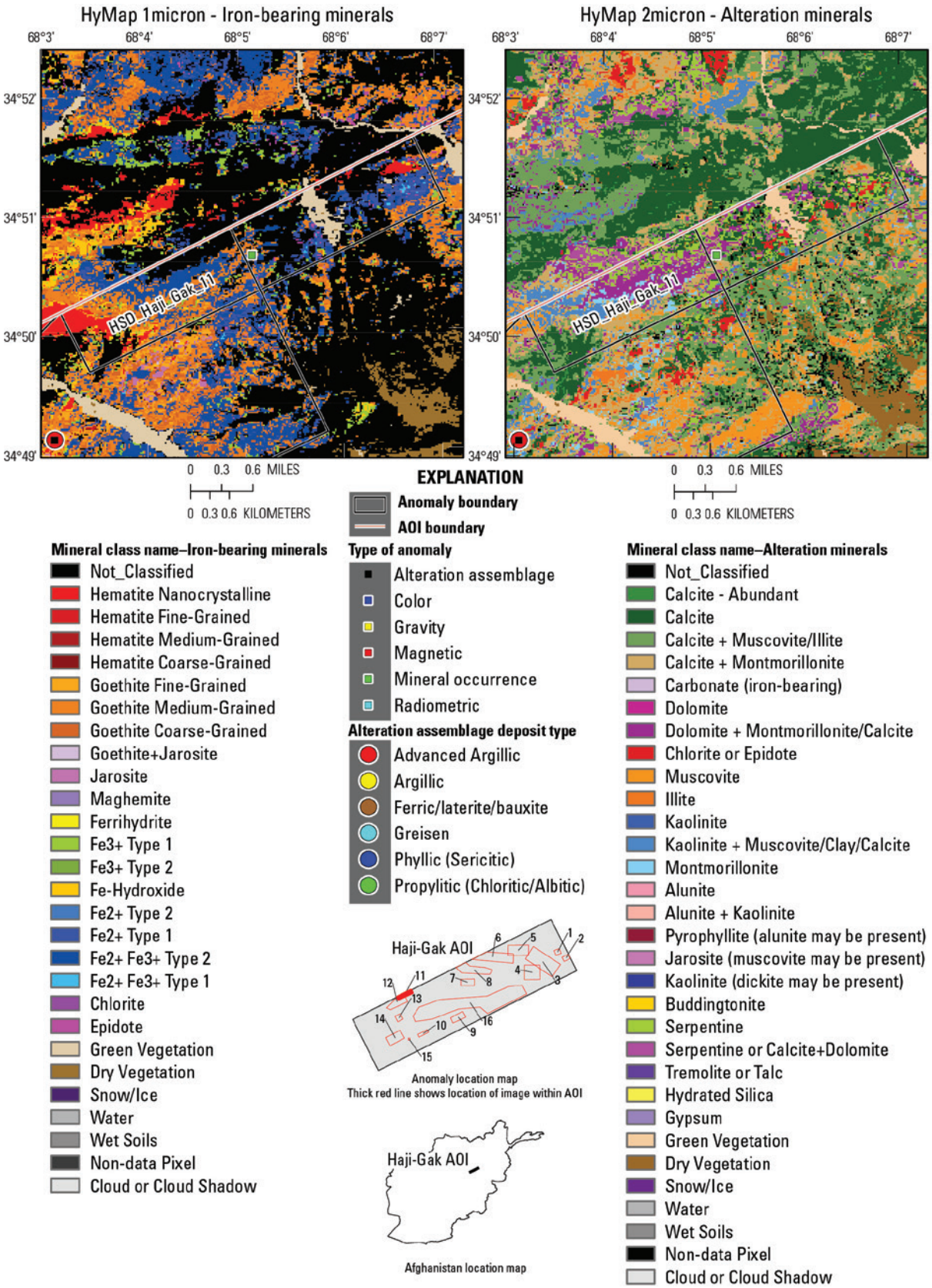

Figure 5.9.11. Hyperspectral anomaly located in the Haji-Gak Area of Interest (AOI) in Afghanistan based on presence of Dolomite minerals, Serpentine minerals, Kaolinite minerals, Chlorite or Epidote, Hematite minerals, Goethite minerals, and Fe-Hydroxide.

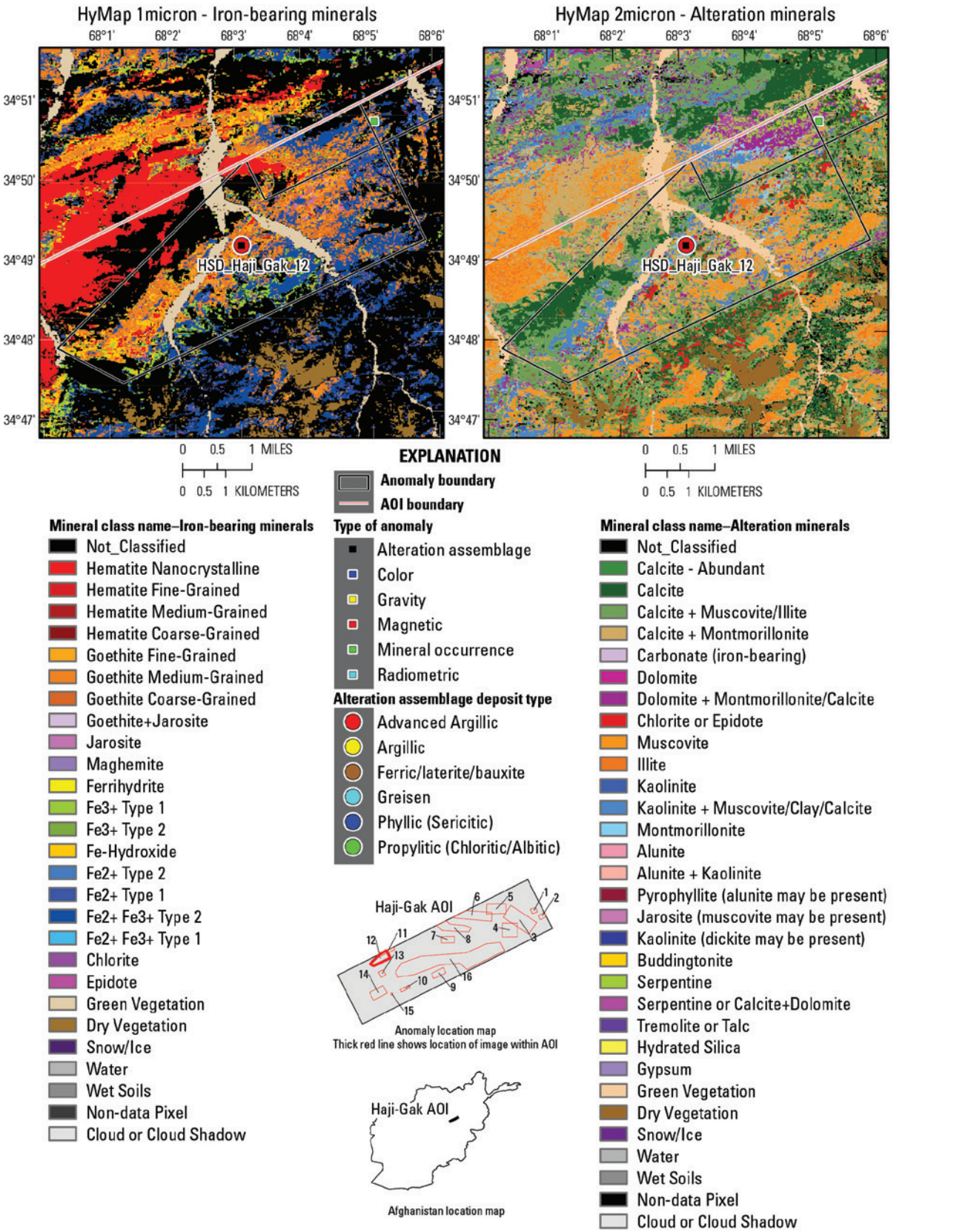

Figure 5.9.12. Hyperspectral anomaly located in the Haji-Gak Area of Interest (AOI) in Afghanistan based on presence of Muscovite, Illite, Kaolinite minerals, Chlorite or Epidote, Serpentine minerals, Montmorillonite, Jarosite, Goethite minerals, Fe-Hydroxide, and Hematite minerals.

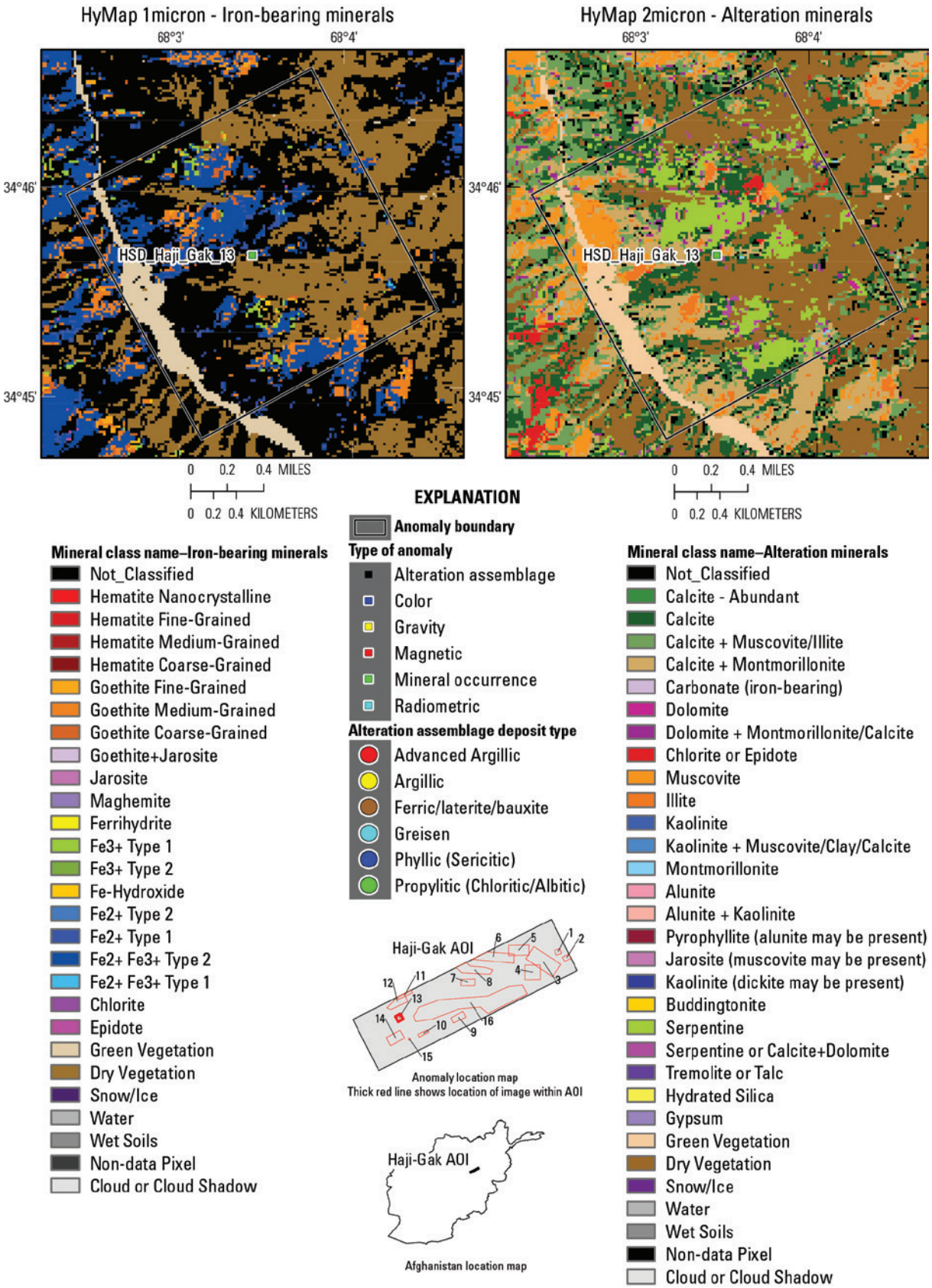

Figure 5.9.13. Hyperspectral anomaly located in the Haji-Gak Area of Interest (AOI) in Afghanistan based on presence of Serpentine minerals, Chlorite or Epidote, and Tremolite or Talc.

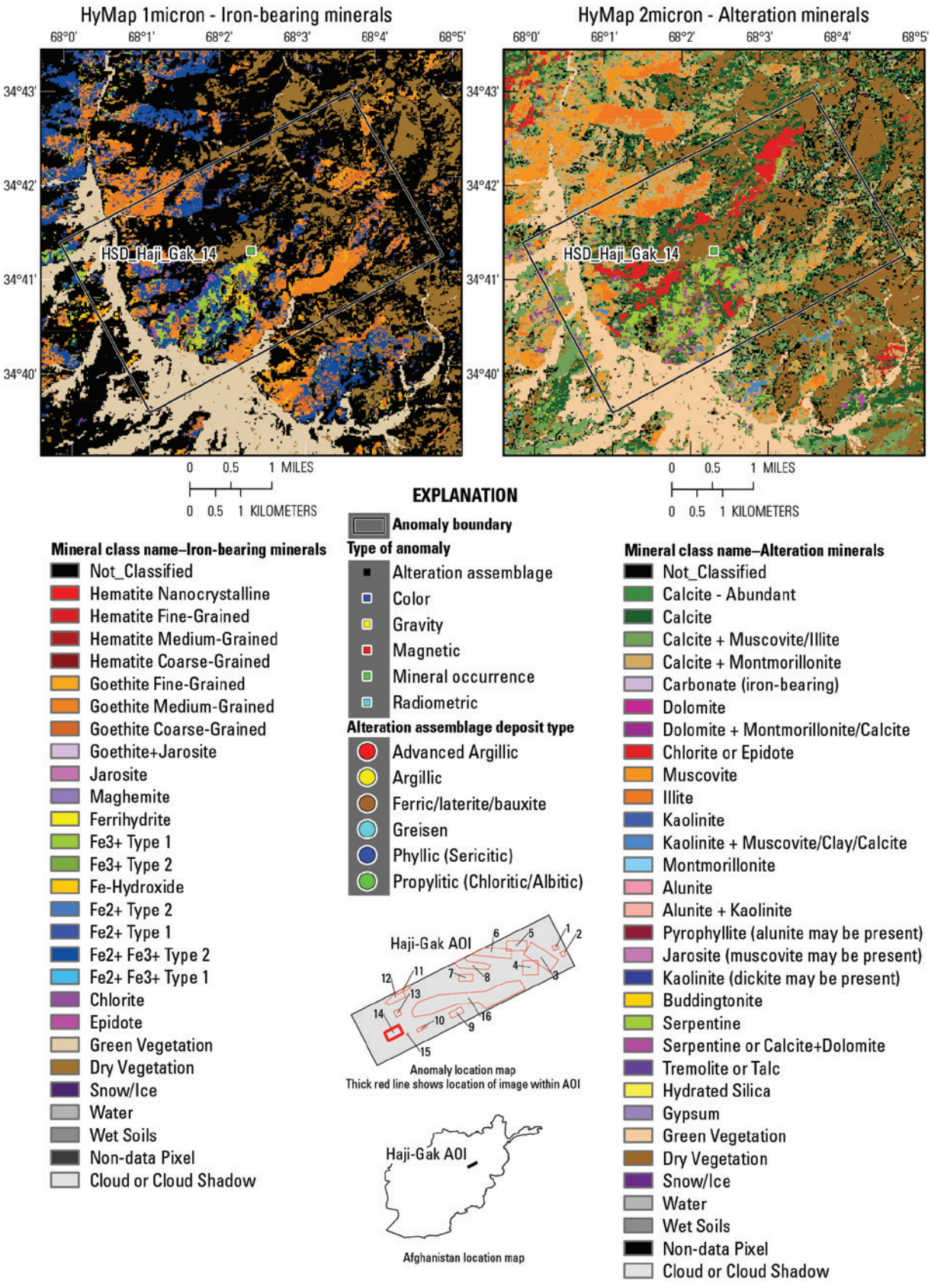

Figure 5.9.14. Hyperspectral anomaly located in the Haji-Gak Area of Interest (AOI) in Afghanistan based on presence of Chlorite or Epidote, Serpentine minerals, Fe^{3+} Type 1, Fe-Hydroxide, and Goethite minerals.

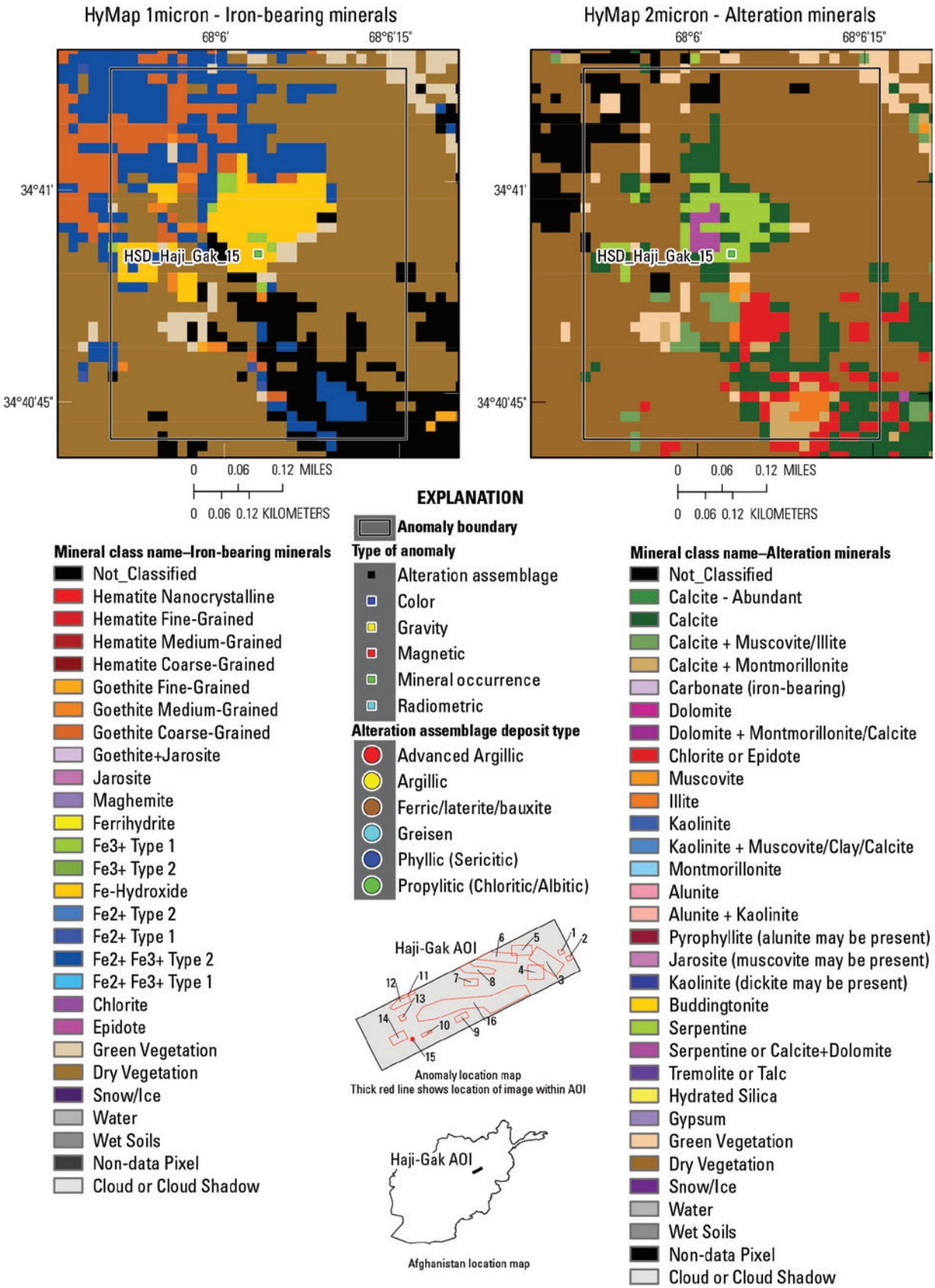

Figure 5.9.15. Hyperspectral anomaly located in the Haji-Gak Area of Interest (AOI) in Afghanistan based on presence of Ferrihydrite and Serpentine.

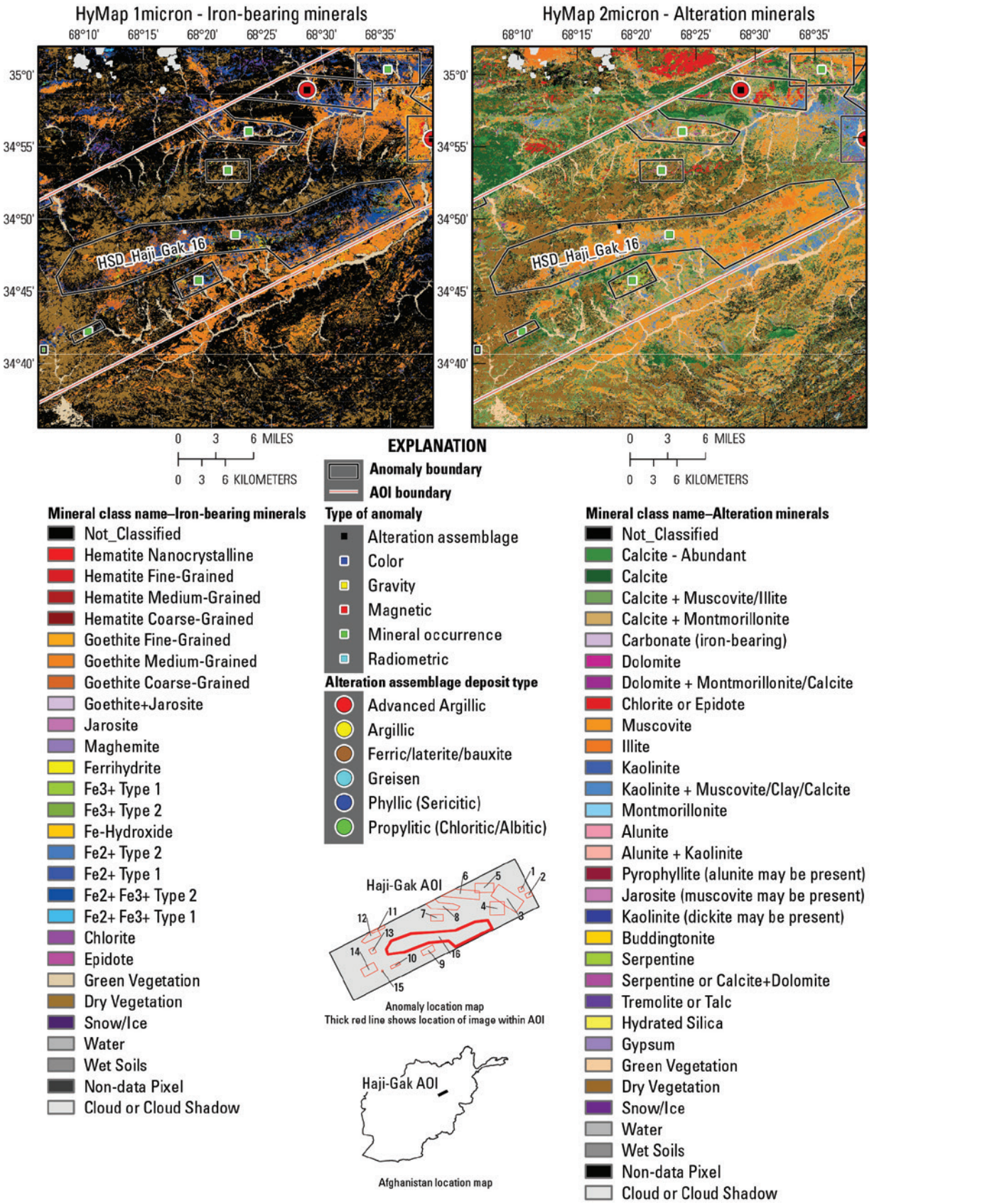

Figure 5.9.16. Hyperspectral anomaly located in the Haji-Gak Area of Interest (AOI) in Afghanistan based on presence of Muscovite, Illite, Goethite minerals, Maghemite, Fe-Hydroxide, and Fe^{3+} Type 1.

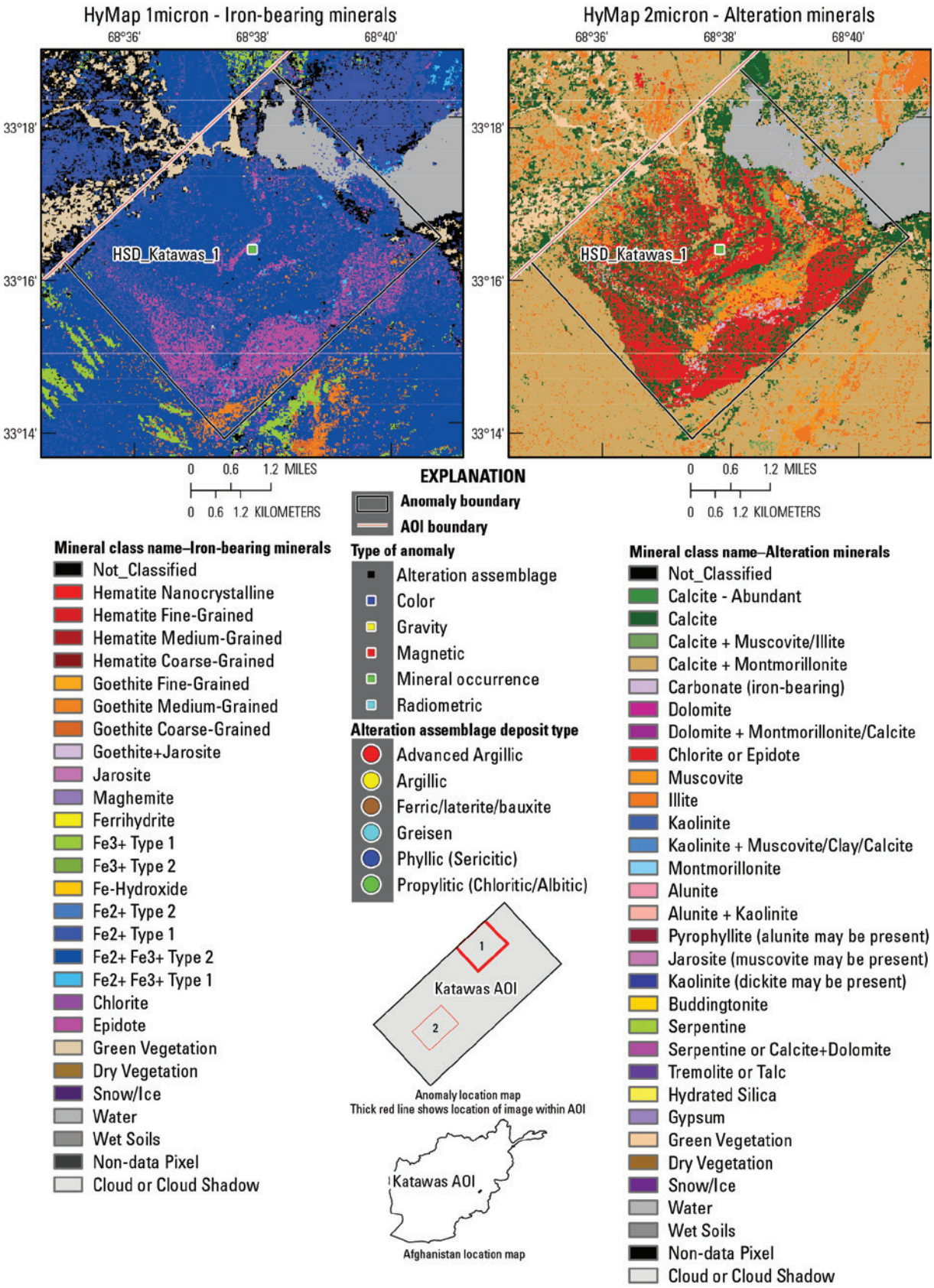

Figure 5.10.1. Hyperspectral anomaly located in the Katawas Area of Interest (AOI) in Afghanistan based on presence of Chlorite or Epidote, Muscovite, Carbonate (iron-bearing), Calcite, and Calcite mixtures. May be geologically controlled.

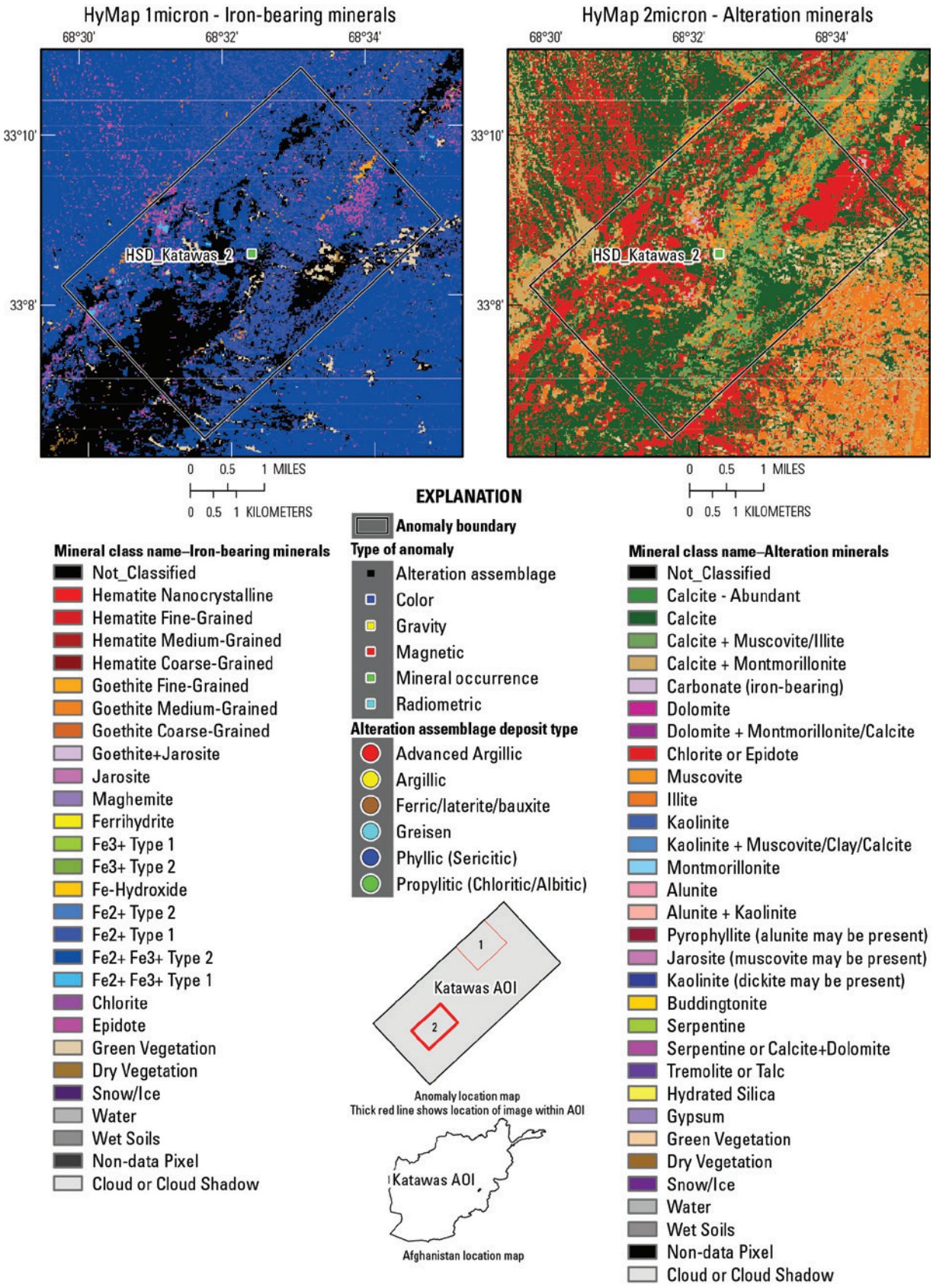

Figure 5.10.2. Hyperspectral anomaly located in the Katawas Area of Interest (AOI) in Afghanistan based on presence of Serpentine, Carbonate (iron-bearing), Chlorite or Epidote, Muscovite, and Goethite minerals.

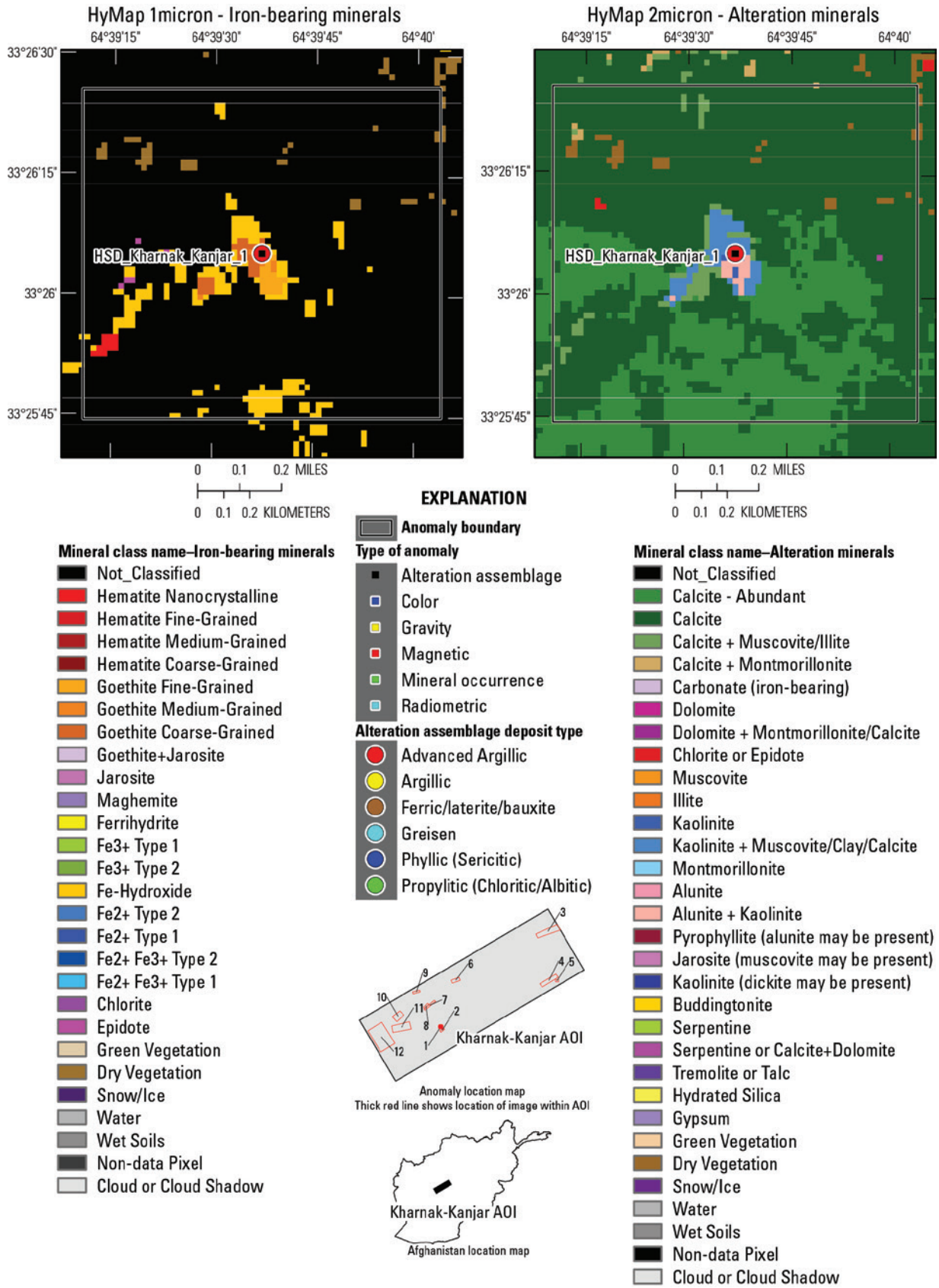

Figure 5.11.1. Hyperspectral anomaly located in the Kharnak-Kanjar Area of Interest (AOI) in Afghanistan based on presence of Kaolinite minerals, Alunite minerals, and Goethite minerals.

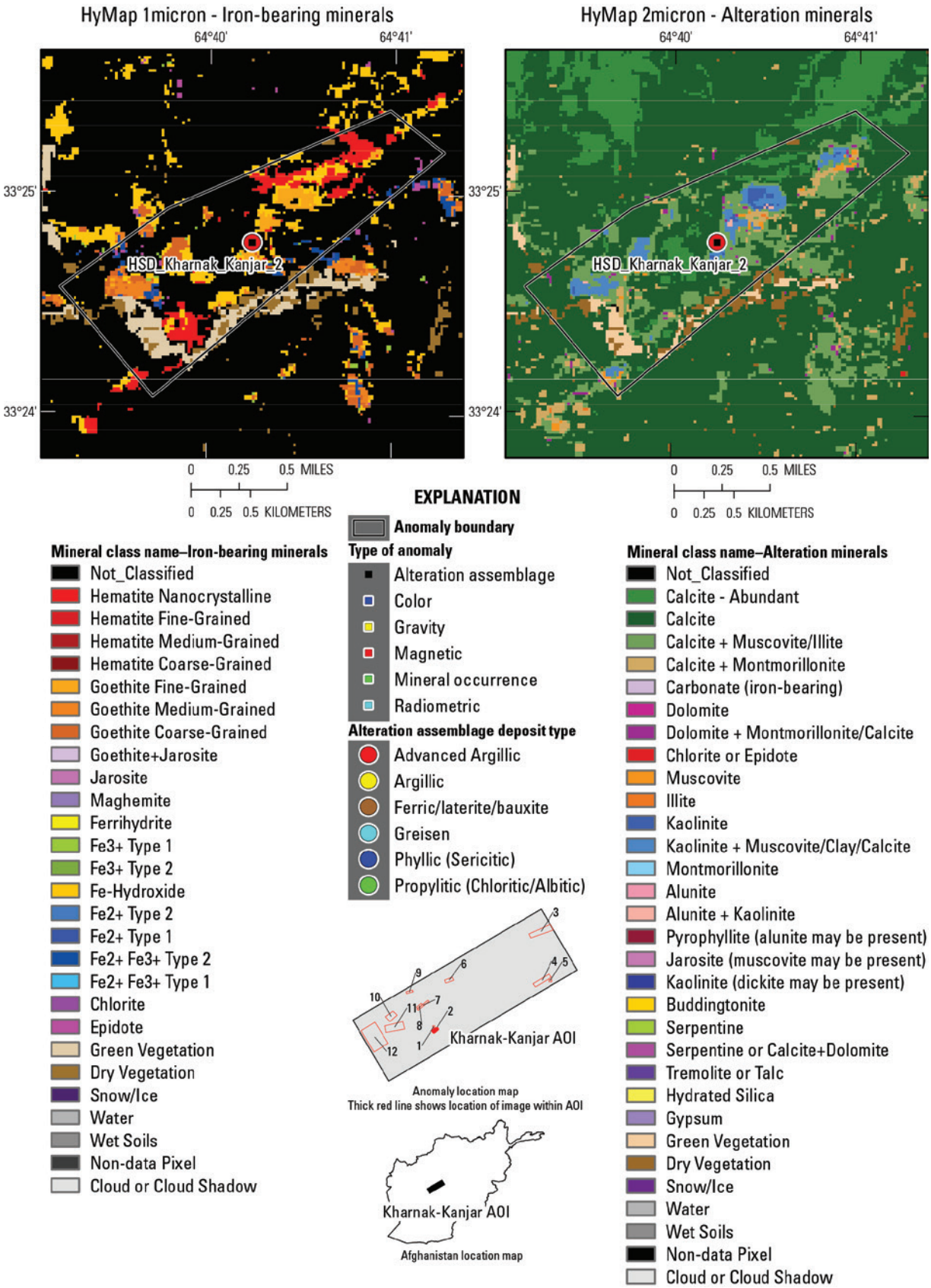

Figure 5.11.2. Hyperspectral anomaly located in the Kharnak-Kanjar Area of Interest (AOI) in Afghanistan based on presence of Kaolinite minerals, Alunite minerals, Geothite minerals, Hematite minerals, and Fe-Hydroxide.

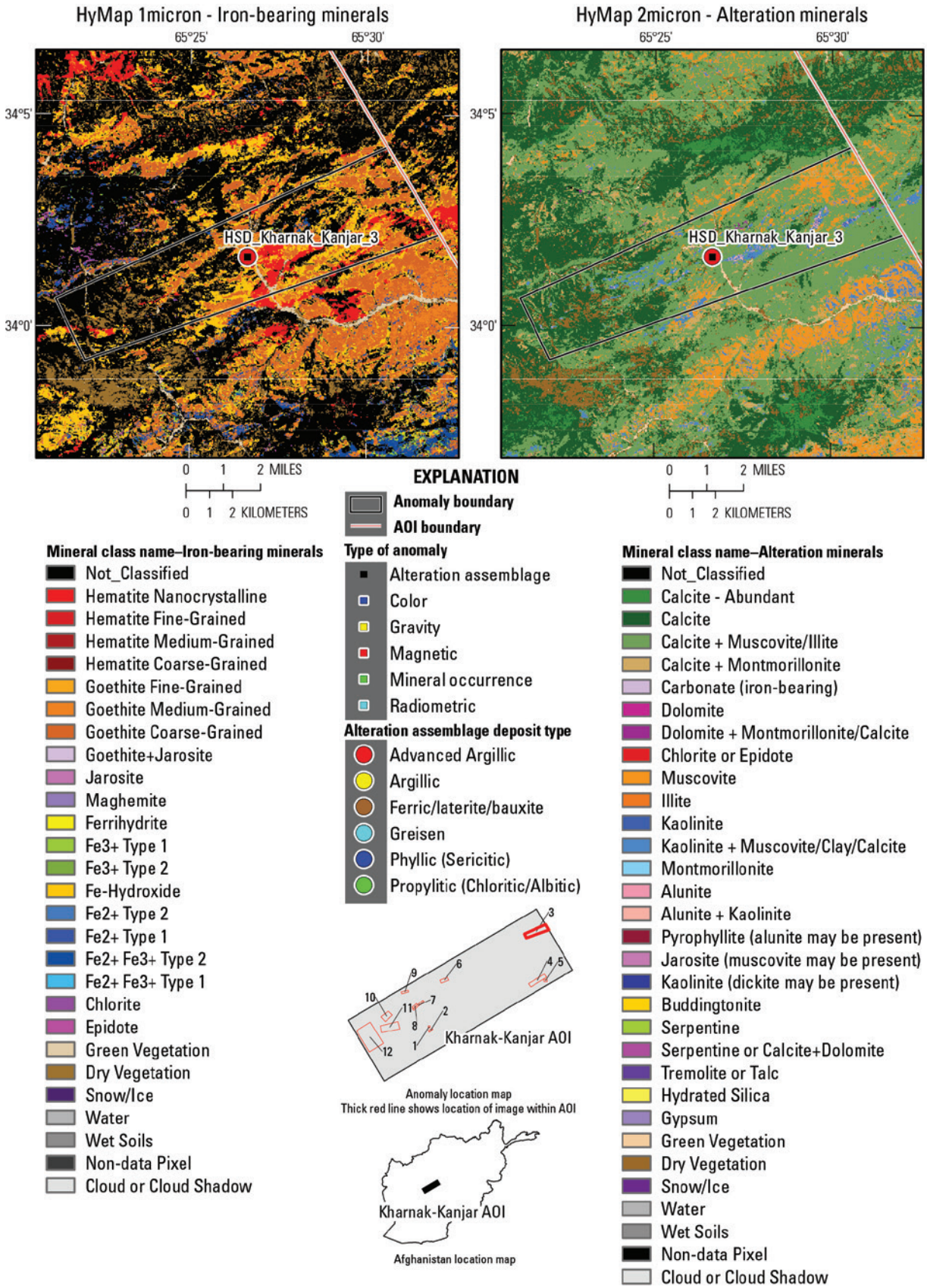

Figure 5.11.3. Hyperspectral anomaly located in the Kharnak-Kanjar Area of Interest (AOI) in Afghanistan based on presence of Kaolinite minerals, Alunite minerals, Geothite minerals, Hematite minerals, and Epidote.

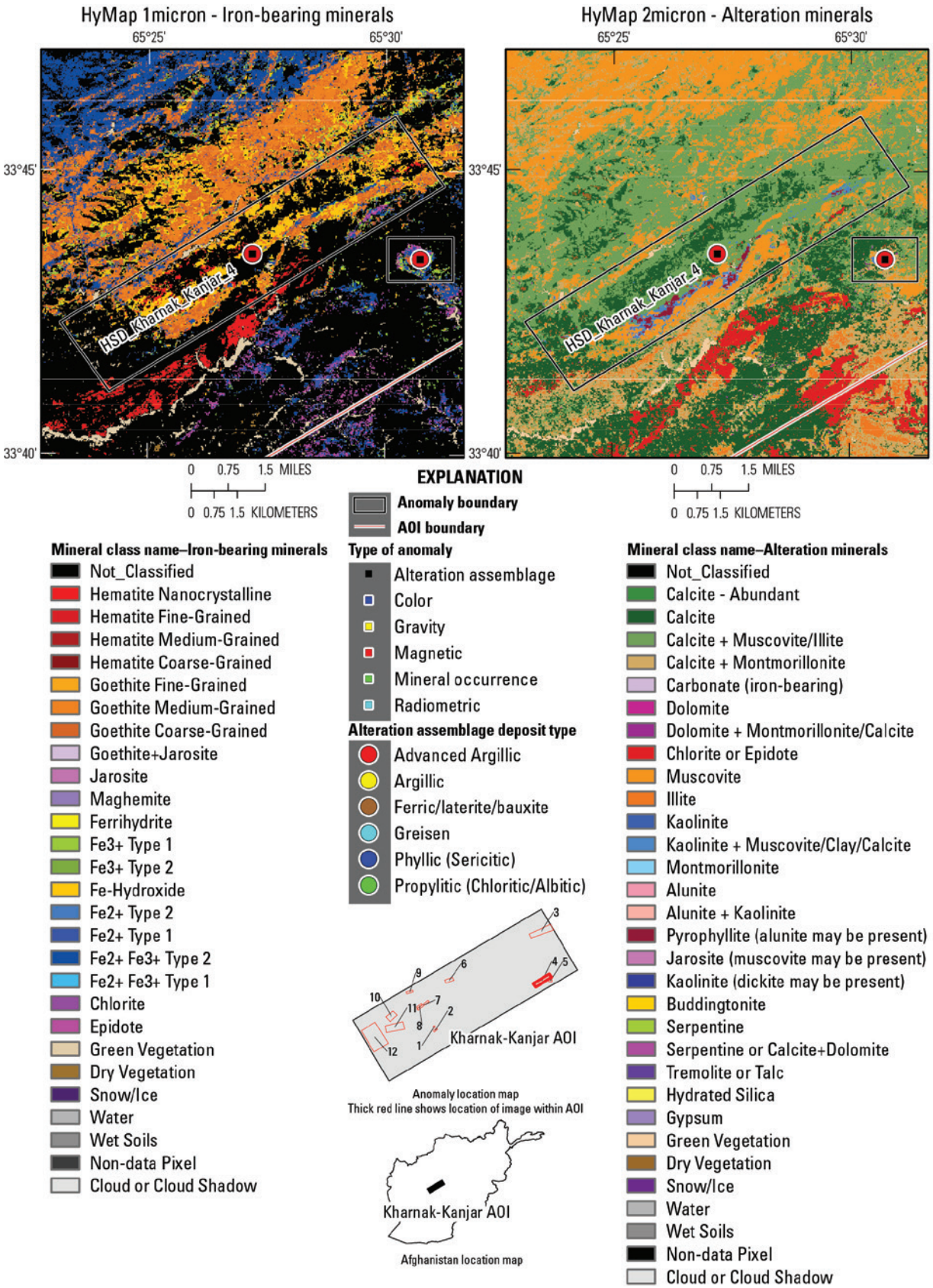

Figure 5.11.4. Hyperspectral anomaly located in the Kharnak-Kanjar Area of Interest (AOI) in Afghanistan based on presence of Pyrophyllite, Kaolinite minerals, Alunite minerals, Dickite, Geothite minerals, and Fe-Hydroxide.

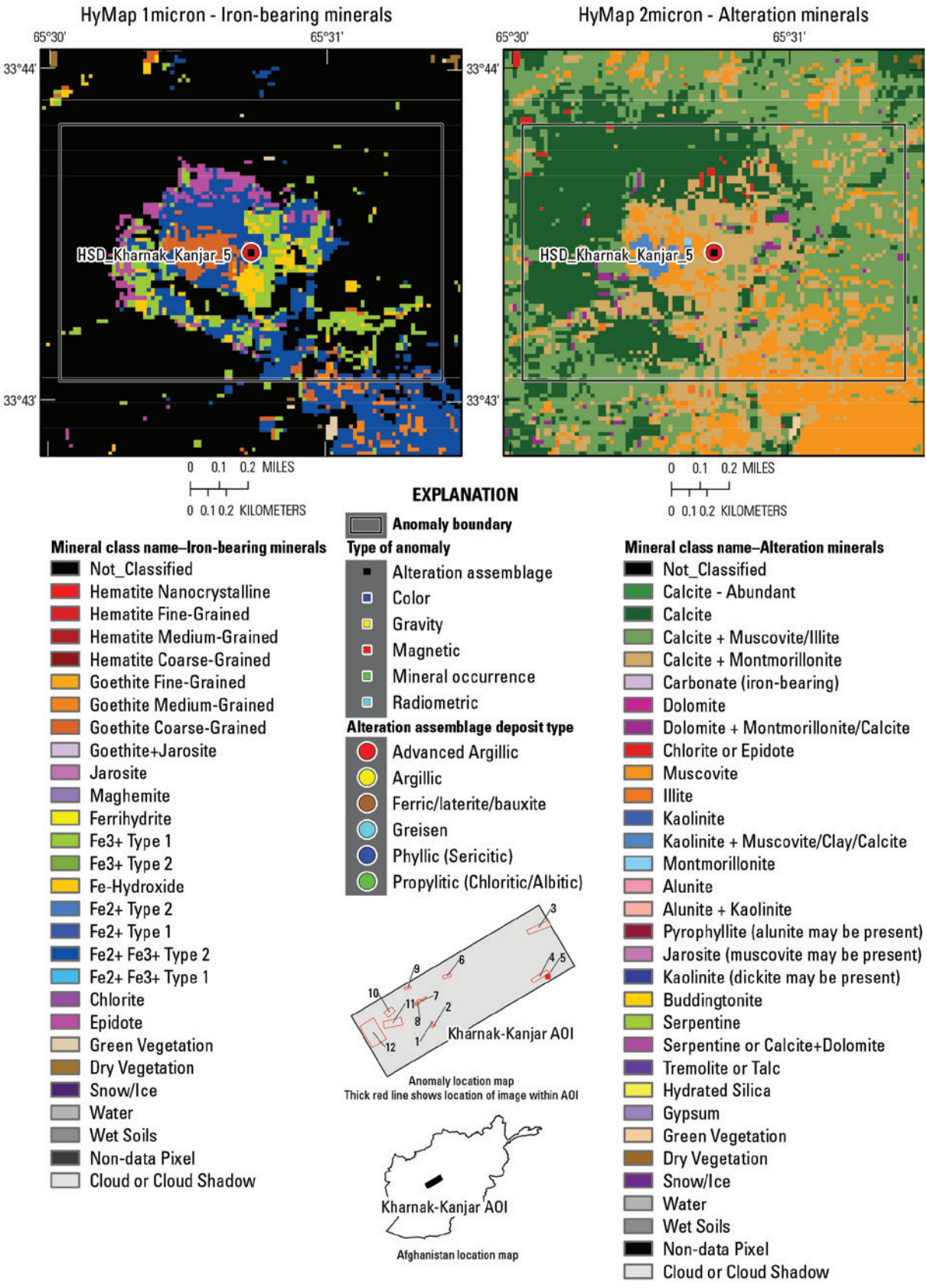

Figure 5.11.5. Hyperspectral anomaly located in the Kharnak-Kanjar Area of Interest (AOI) in Afghanistan based on presence of Kaolinite minerals, Montmorillonite, Dolomite minerals, Goethite minerals, Fe-Hydroxide, Fe^{3+} Type1, Fe^{2+} Fe^{3+} Type2, and Epidote.

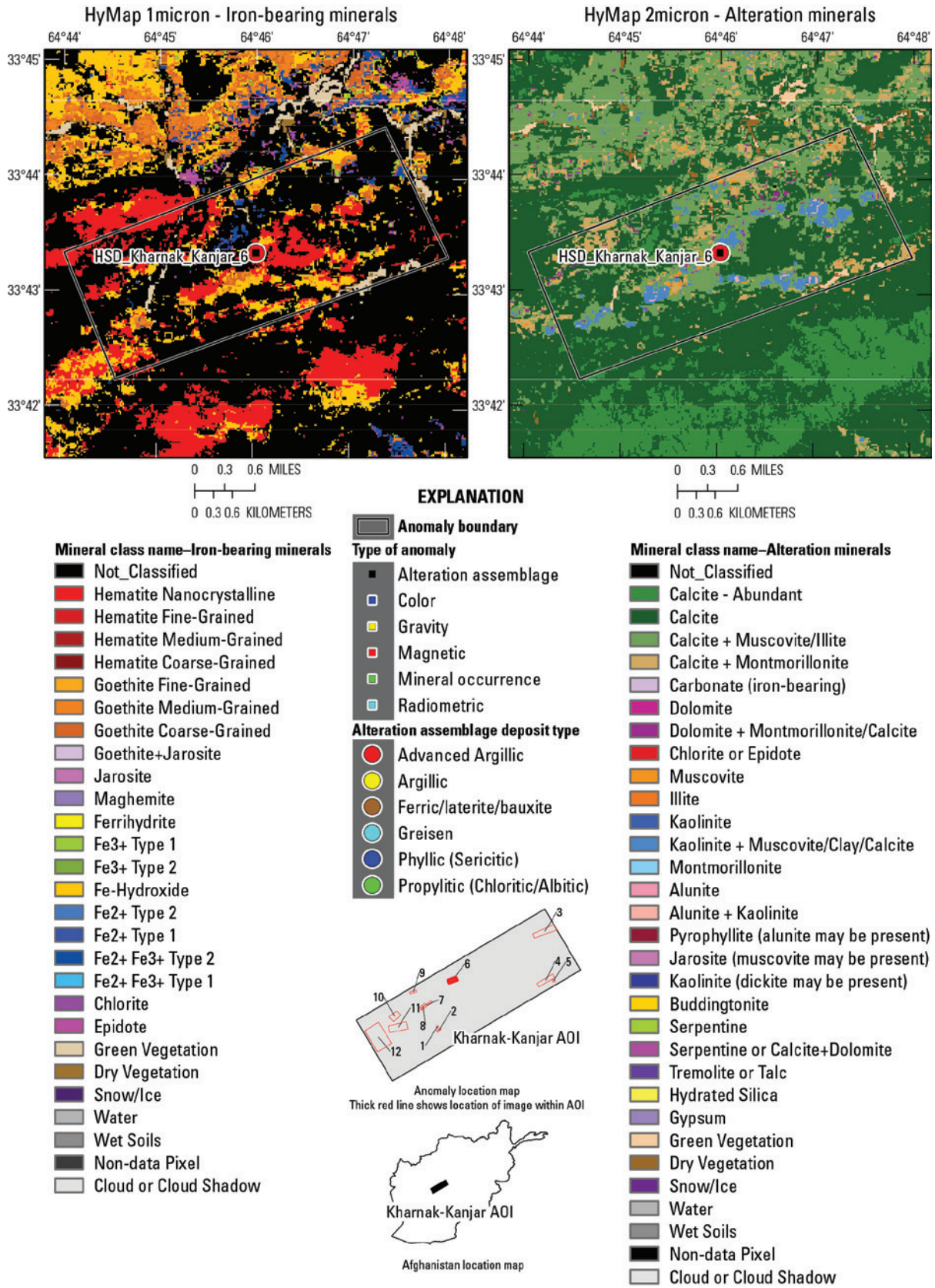

Figure 5.11.6. Hyperspectral anomaly located in the Kharnak-Kanjar Area of Interest (AOI) in Afghanistan based on presence of Kaolinite minerals, Dolomite minerals, Alunite minerals, Hematite minerals, Goethite minerals, Maghemite, Epidote, and Fe-Hydroxide.

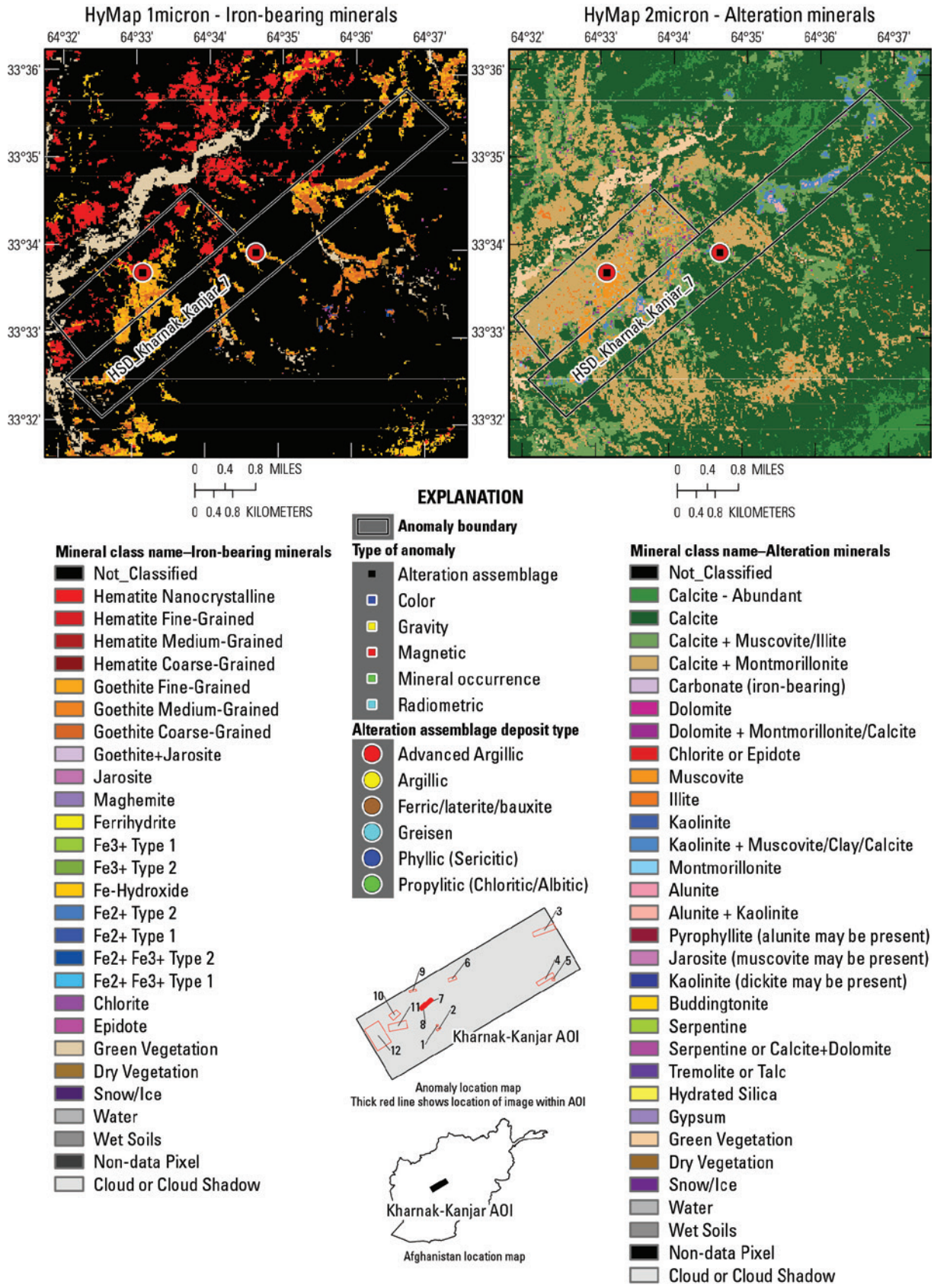

Figure 5.11.7. Hyperspectral anomaly located in the Kharnak-Kanjar Area of Interest (AOI) in Afghanistan based on presence of Kaolinite minerals, Alunite minerals, Goethite minerals, and Hematite minerals.

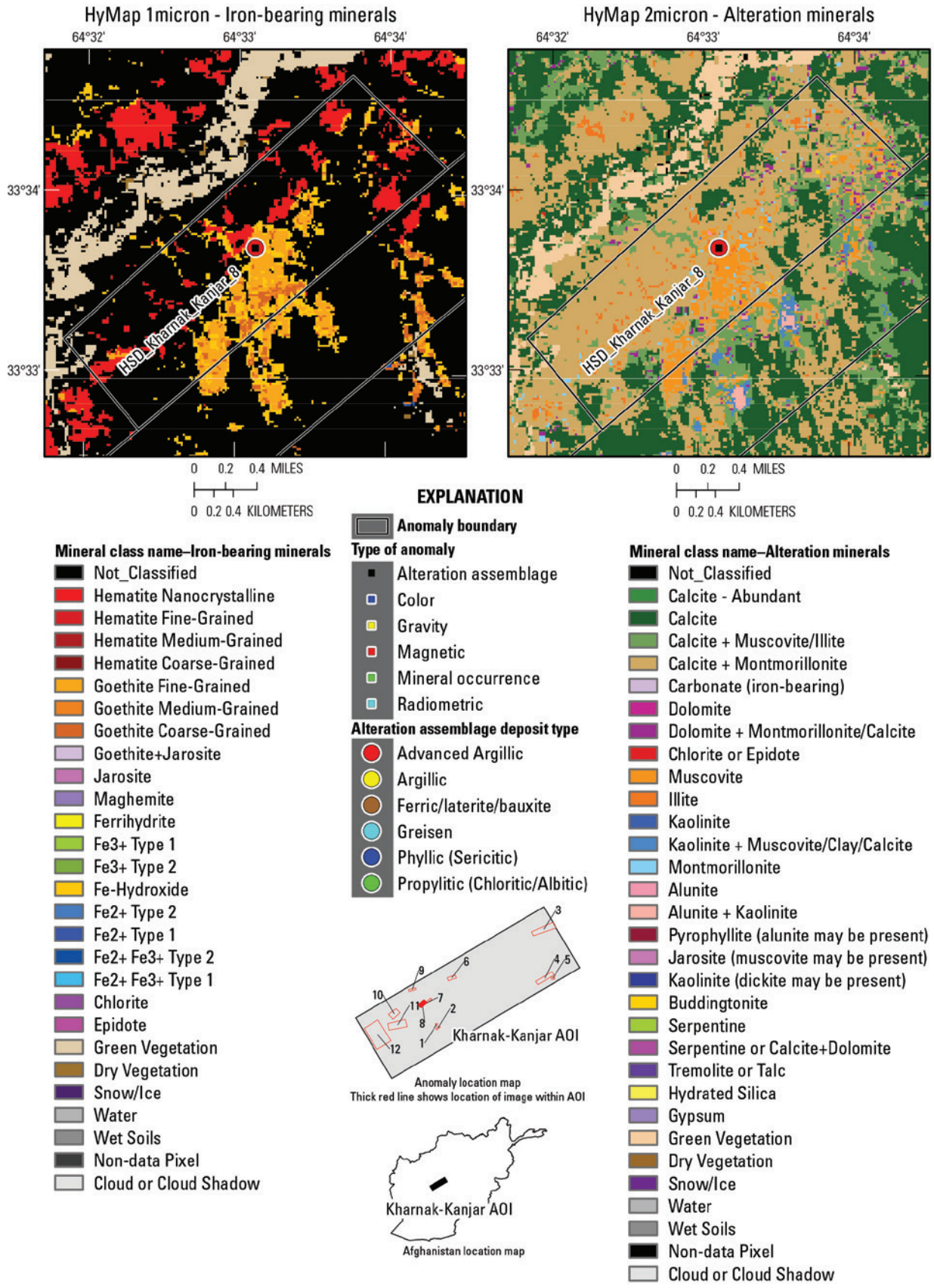

Figure 5.11.8. Hyperspectral anomaly located in the Kharnak-Kanjar Area of Interest (AOI) in Afghanistan based on presence of Muscovite, Montmorillonite, Buddingtonite, Goethite minerals, Fe-Hydroxide, and Hematite minerals.

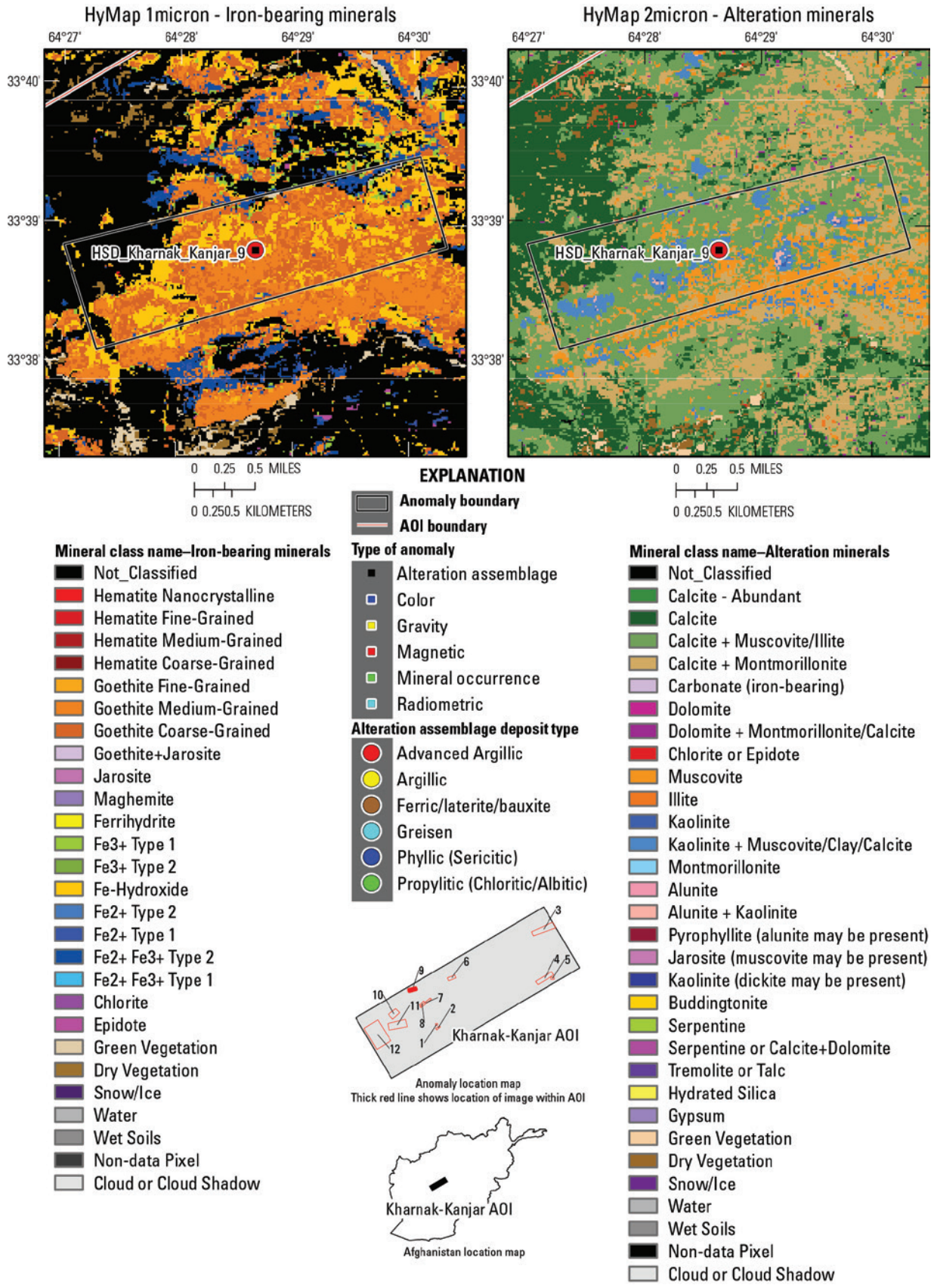

Figure 5.11.9. Hyperspectral anomaly located in the Kharnak-Kanjar Area of Interest (AOI) in Afghanistan based on presence of Kaolinite minerals, Alunite minerals, Geothite minerals, and Fe-Hydroxide.

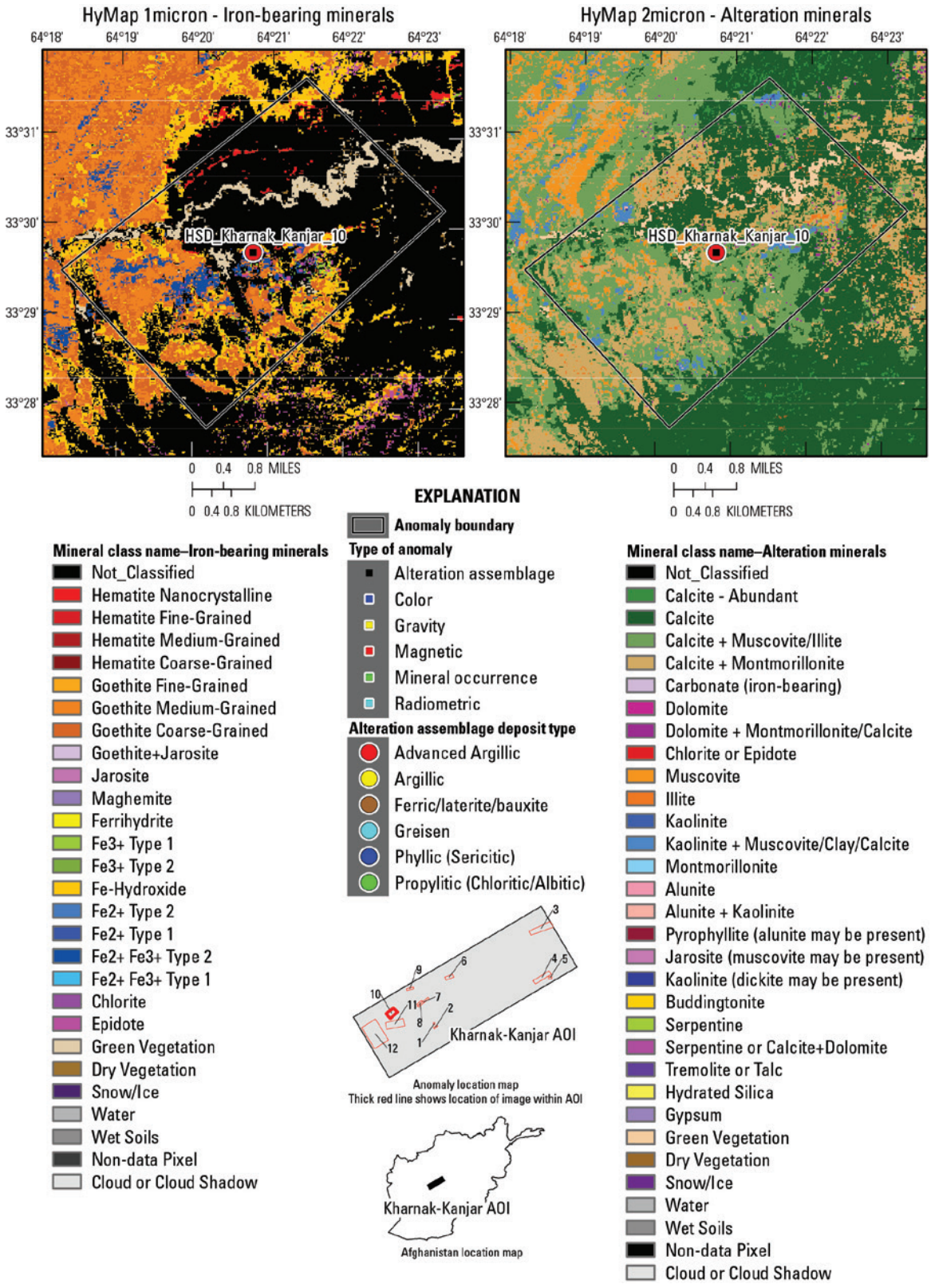

Figure 5.11.10. Hyperspectral anomaly located in the Kharnak-Kanjar Area of Interest (AOI) in Afghanistan based on presence of Kaolinite minerals, Alunite minerals, Geothite minerals, Epidote, Fe^{2+} and Fe^{3+} Type 2, and Fe-Hydroxide.

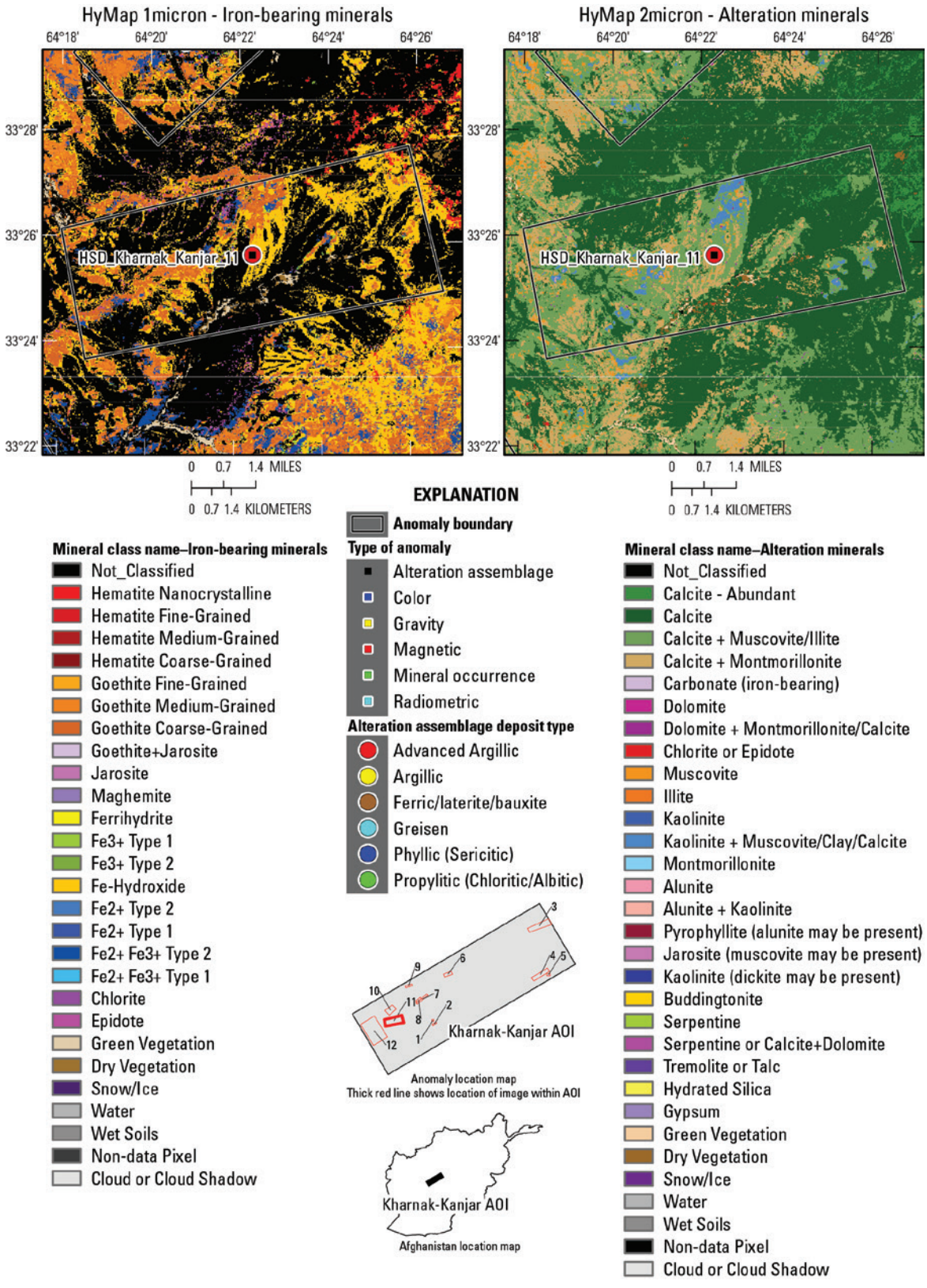

Figure 5.11.11. Hyperspectral anomaly located in the Kharnak-Kanjar Area of Interest (AOI) in Afghanistan based on presence of Kaolinite minerals, Alunite minerals, Muscovite, Geothite minerals, Fe-Hydroxide, Fe^{2+} and Fe^{3+} Type 2, and Epidote.

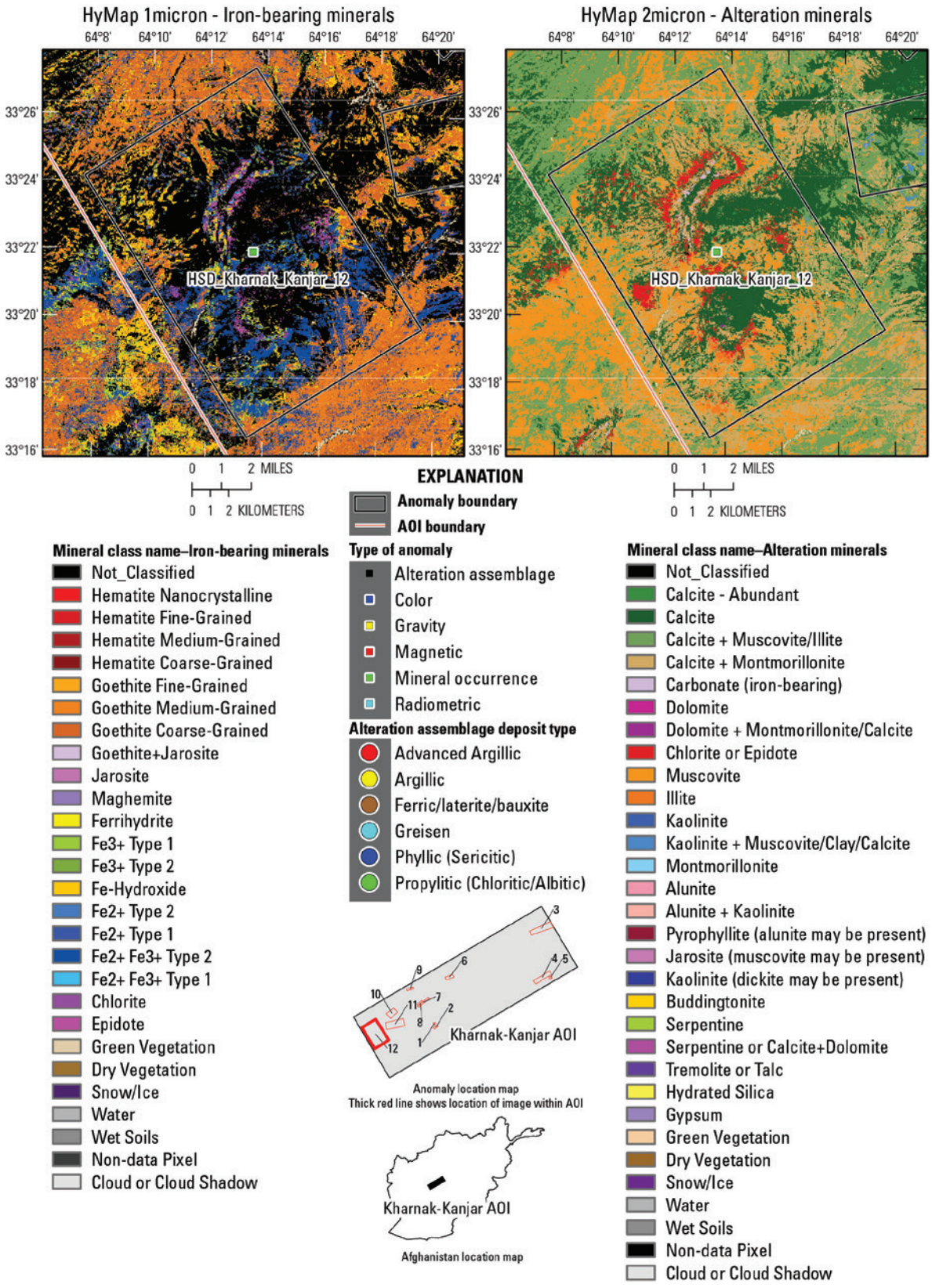

Figure 5.11.12. Hyperspectral anomaly located in the Kharnak-Kanjar Area of Interest (AOI) in Afghanistan based on presence of Carbonate (iron-bearing), Chlorite or Epidote, Muscovite, Goethite minerals, Fe^{3+} Type 1, and Fe-Hydroxide.

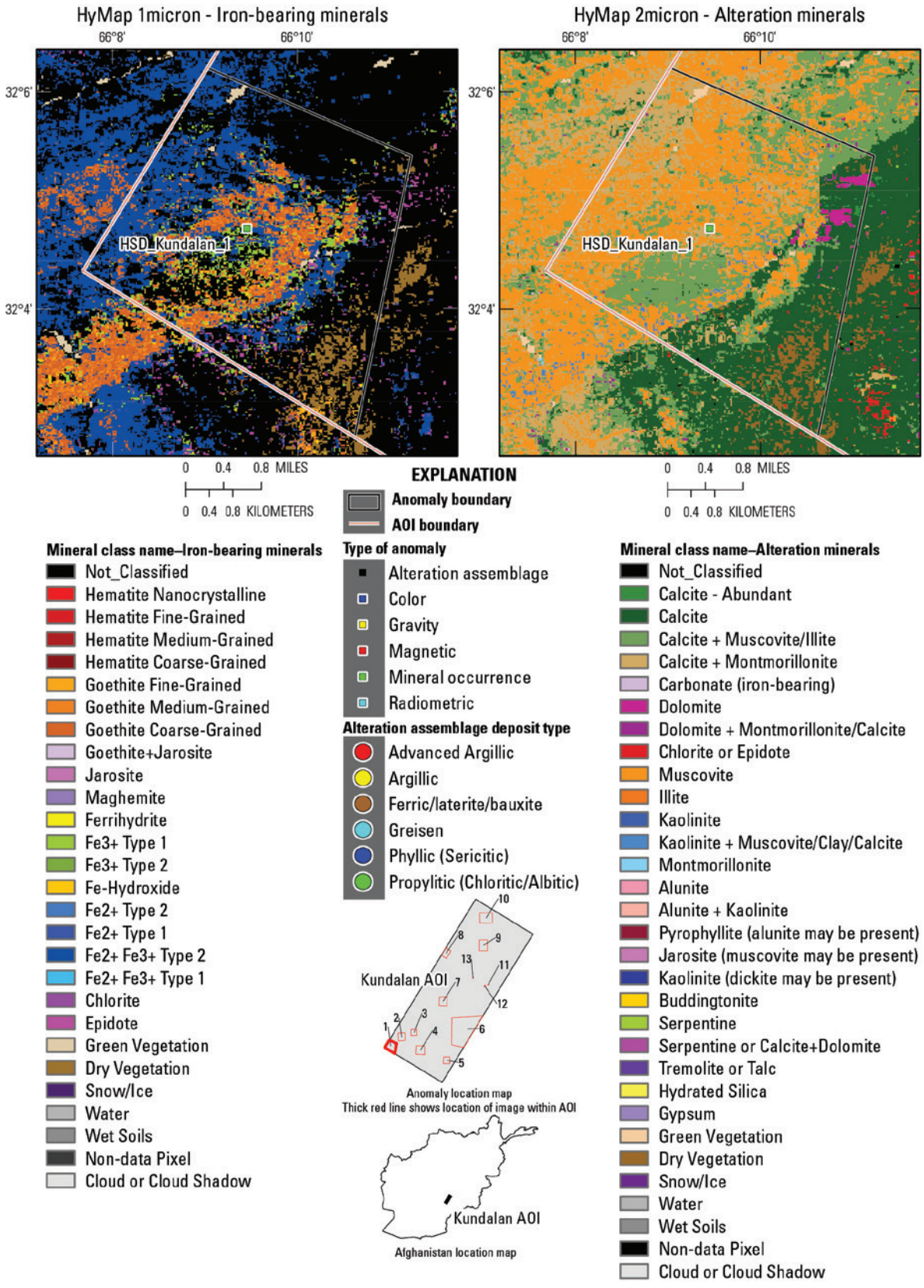

Figure 5.12.1. Hyperspectral anomaly located in the Kundalan Area of Interest (AOI) in Afghanistan based on presence of Goethite minerals, Fe^{3+} Type 1, and Epidote.

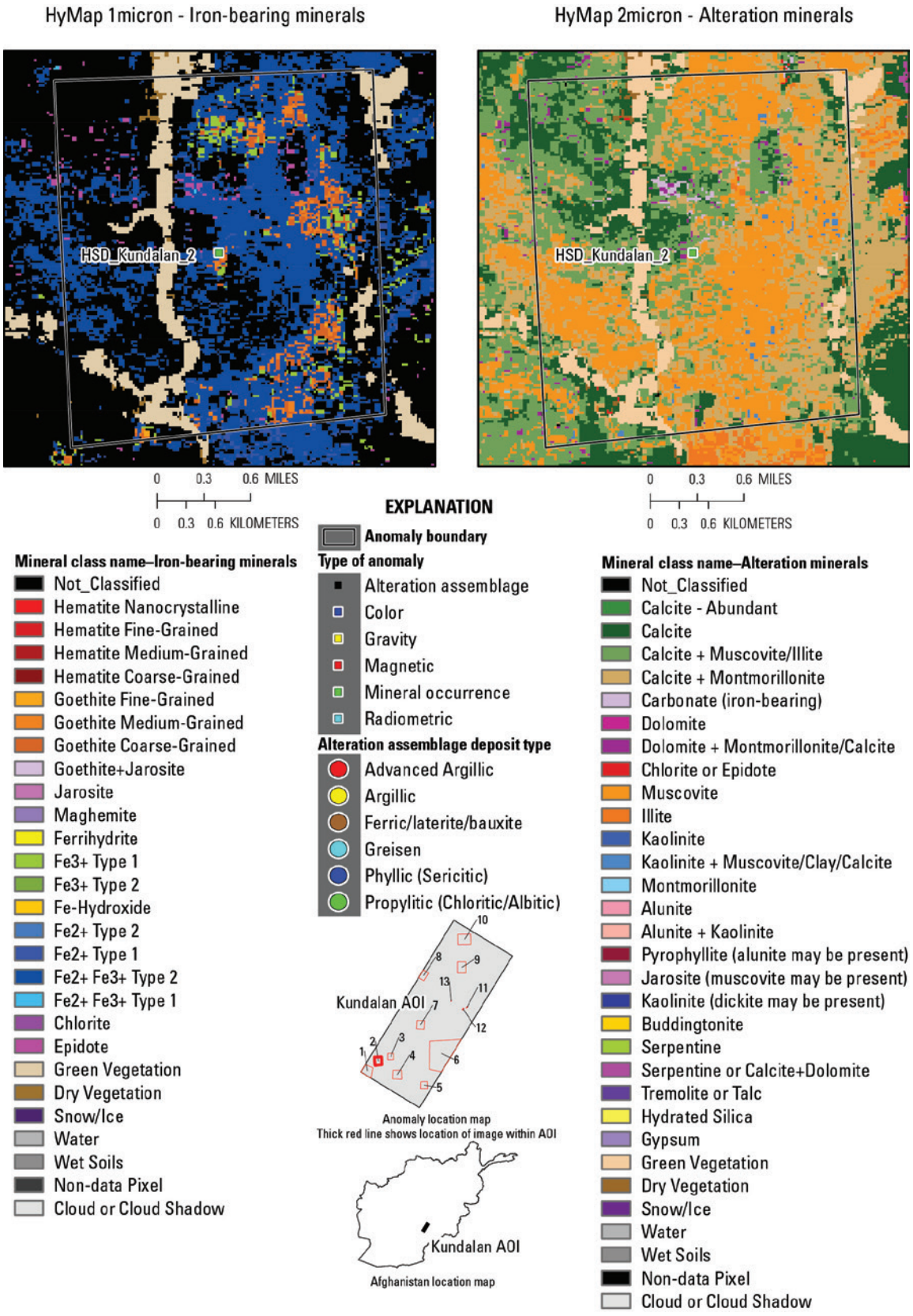

Figure 5.12.2. Hyperspectral anomaly located in the Kundalan Area of Interest (AOI) in Afghanistan based on presence of Muscovite, Illite, Kaolinite minerals, Goethite minerals, Fe^{3+} Type 1, and Epidote.

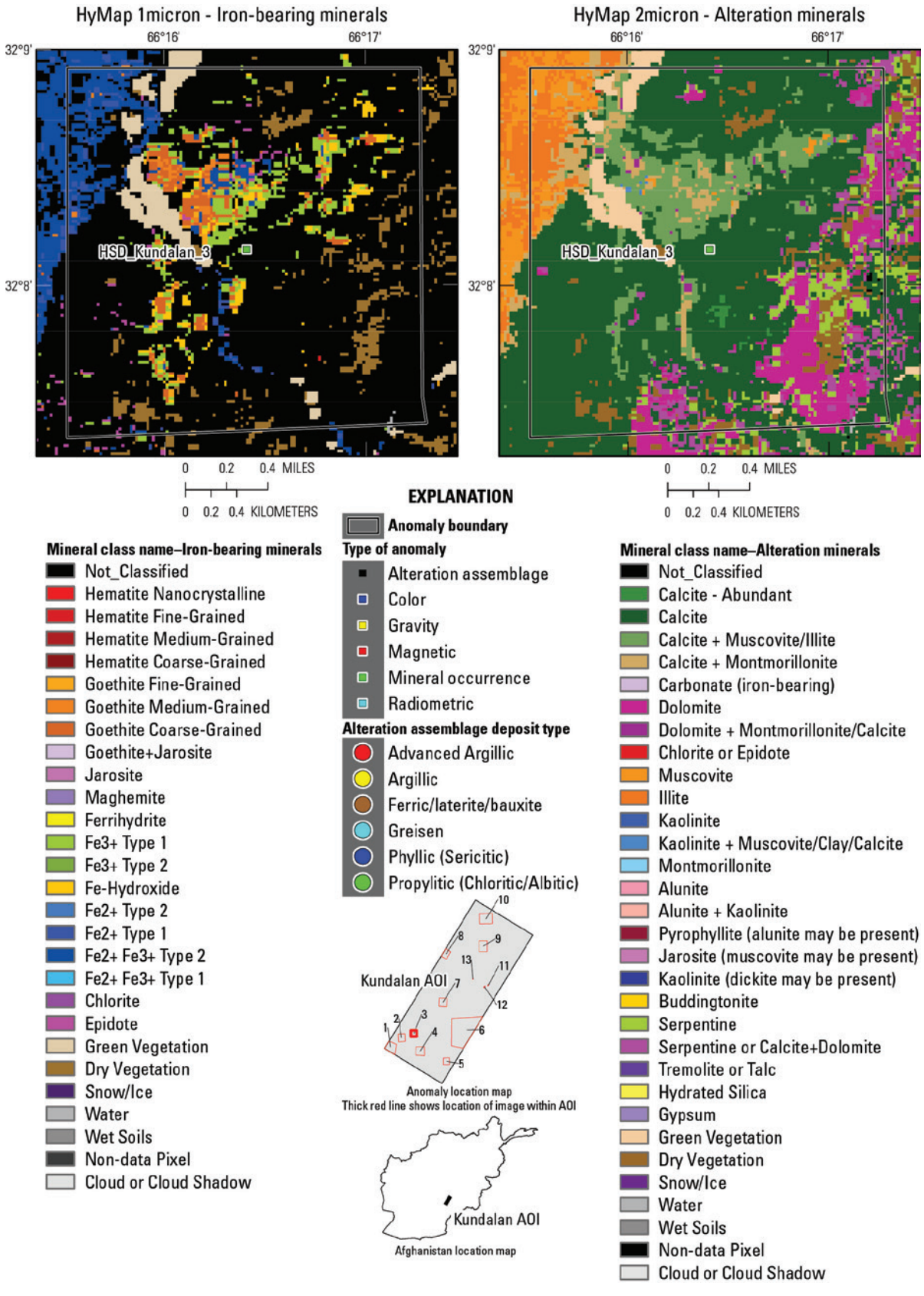

Figure 5.12.3. Hyperspectral anomaly located in the Kundalan Area of Interest (AOI) in Afghanistan based on presence of Goethite minerals, Fe^{3+} Type 1, Fe-Hydroxide, and Epidote.

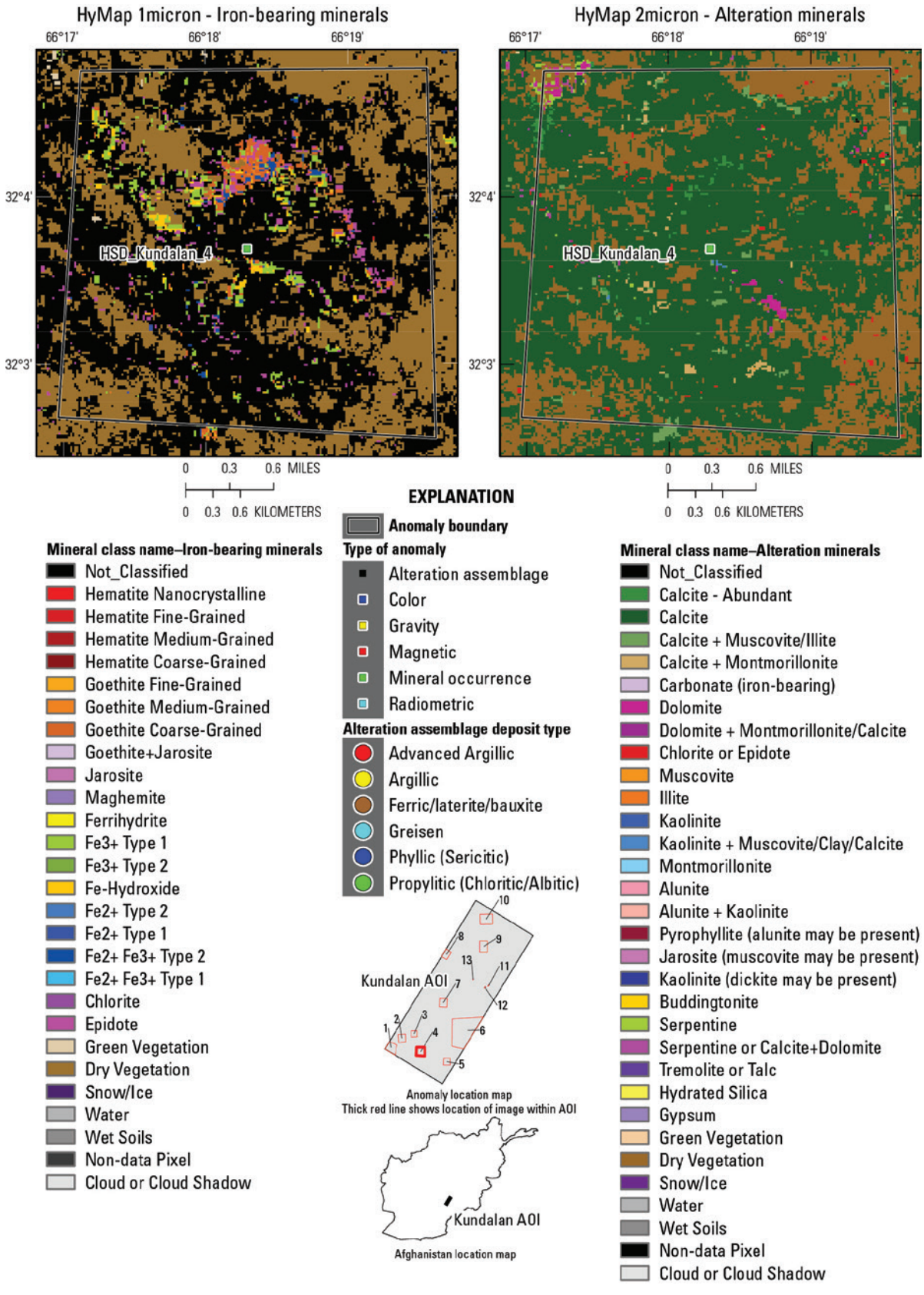

Figure 5.12.4. Hyperspectral anomaly located in the Kundalan Area of Interest (AOI) in Afghanistan based on presence of Goethite minerals, Fe^{3+} Type 1, Fe-Hydroxide, and Epidote.

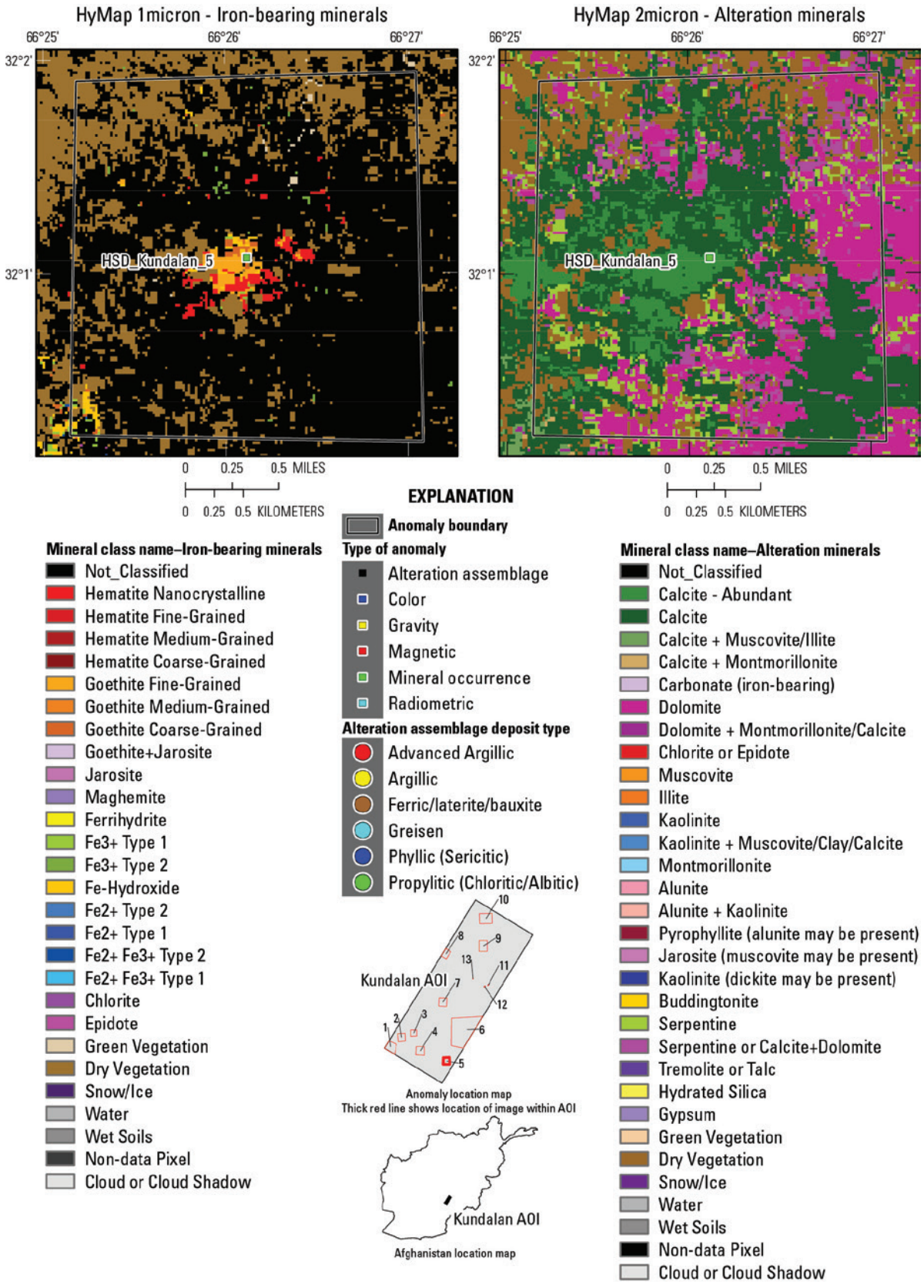

Figure 5.12.5. Hyperspectral anomaly located in the Kundalan Area of Interest (AOI) in Afghanistan based on presence of Calcite, Goethite minerals, and Hematite minerals.

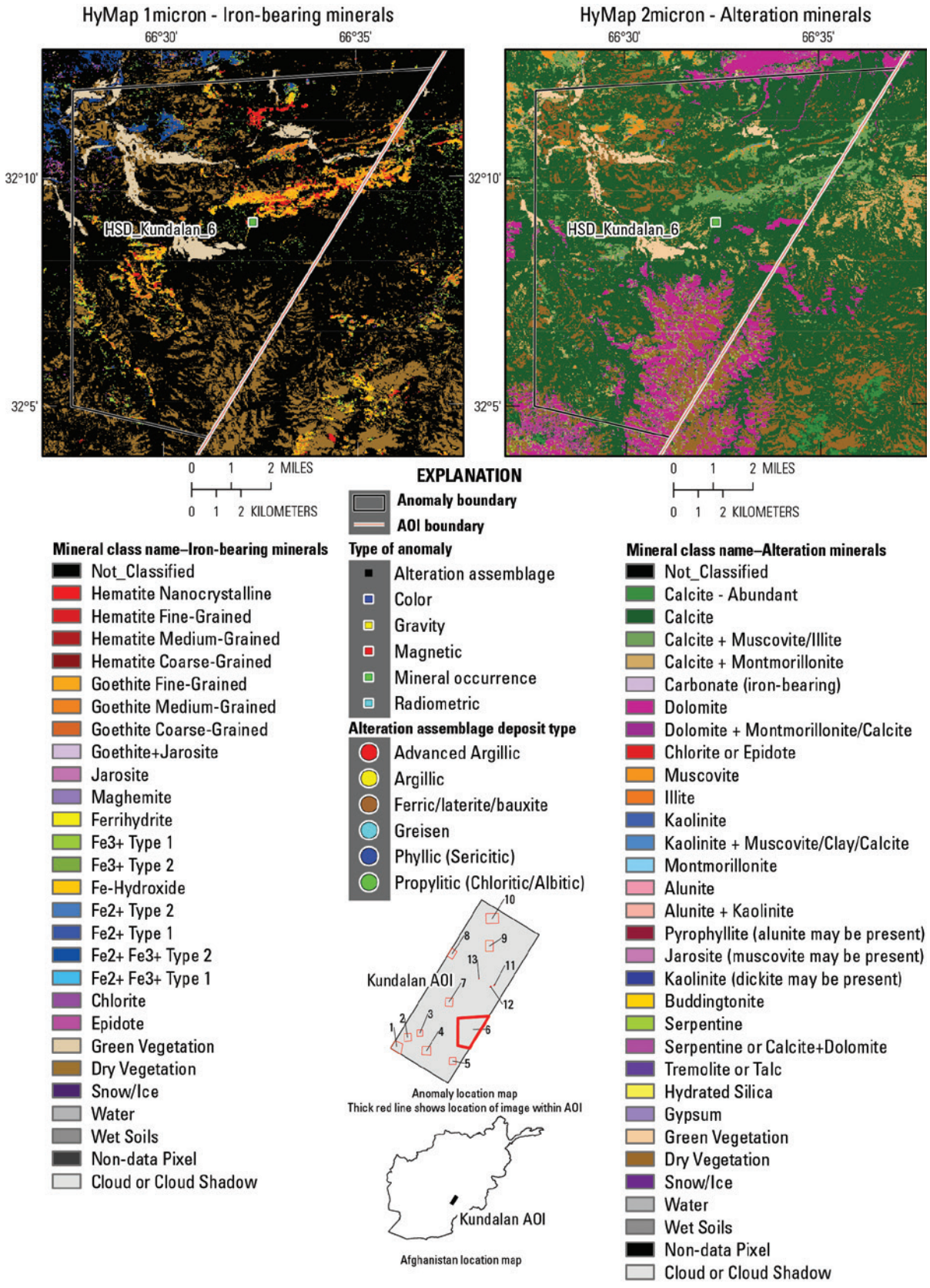

Figure 5.12.6. Hyperspectral anomaly located in the Kundalan Area of Interest (AOI) in Afghanistan based on presence of Muscovite, Hematite minerals, Goethite minerals, and Fe^{3+} Type 1.

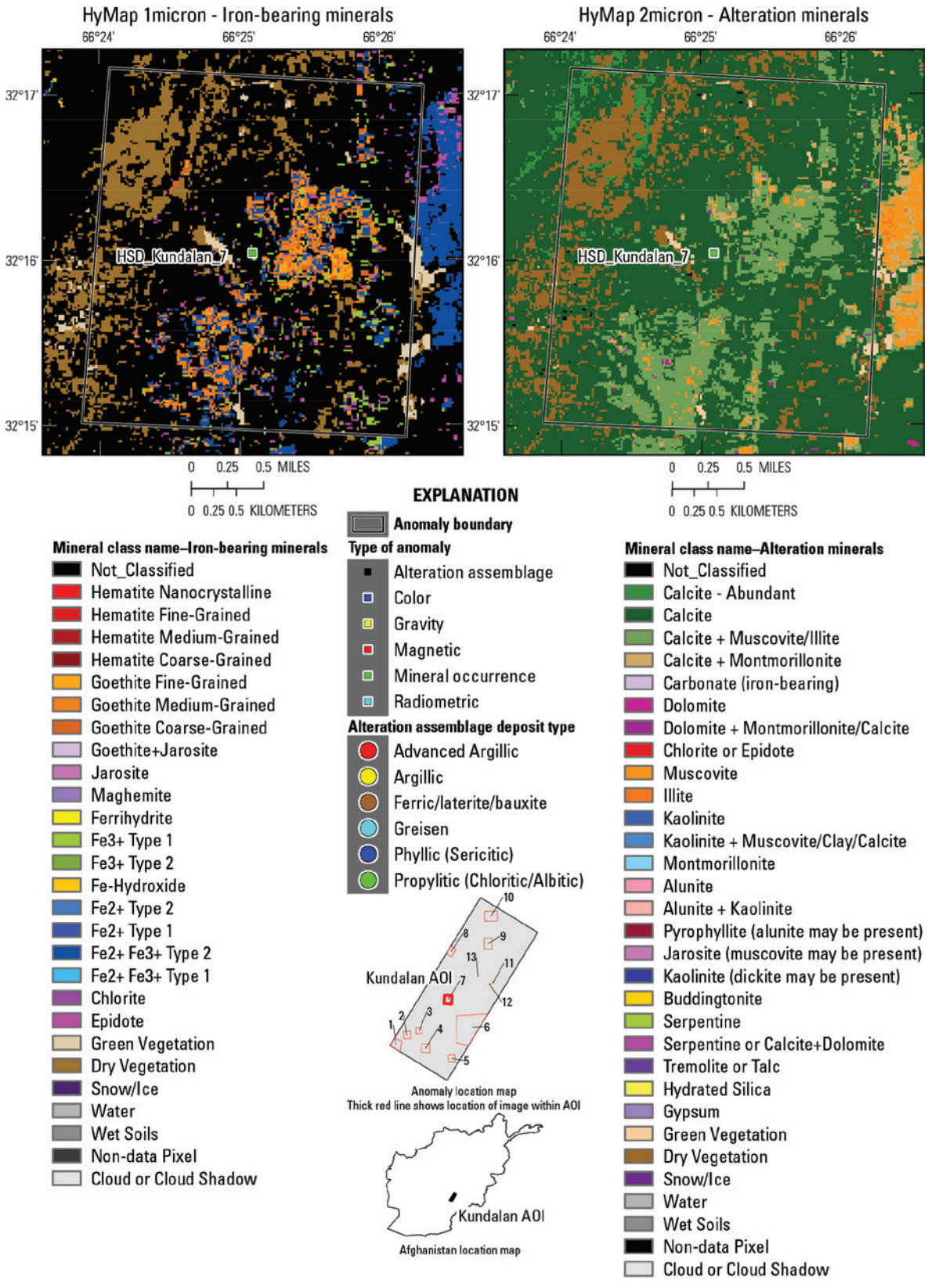

Figure 5.12.7. Hyperspectral anomaly located in the Kundalan Area of Interest (AOI) in Afghanistan based on presence of Goethite minerals, Fe^{3+} Type 1, Fe-Hydroxide, and Epidote.

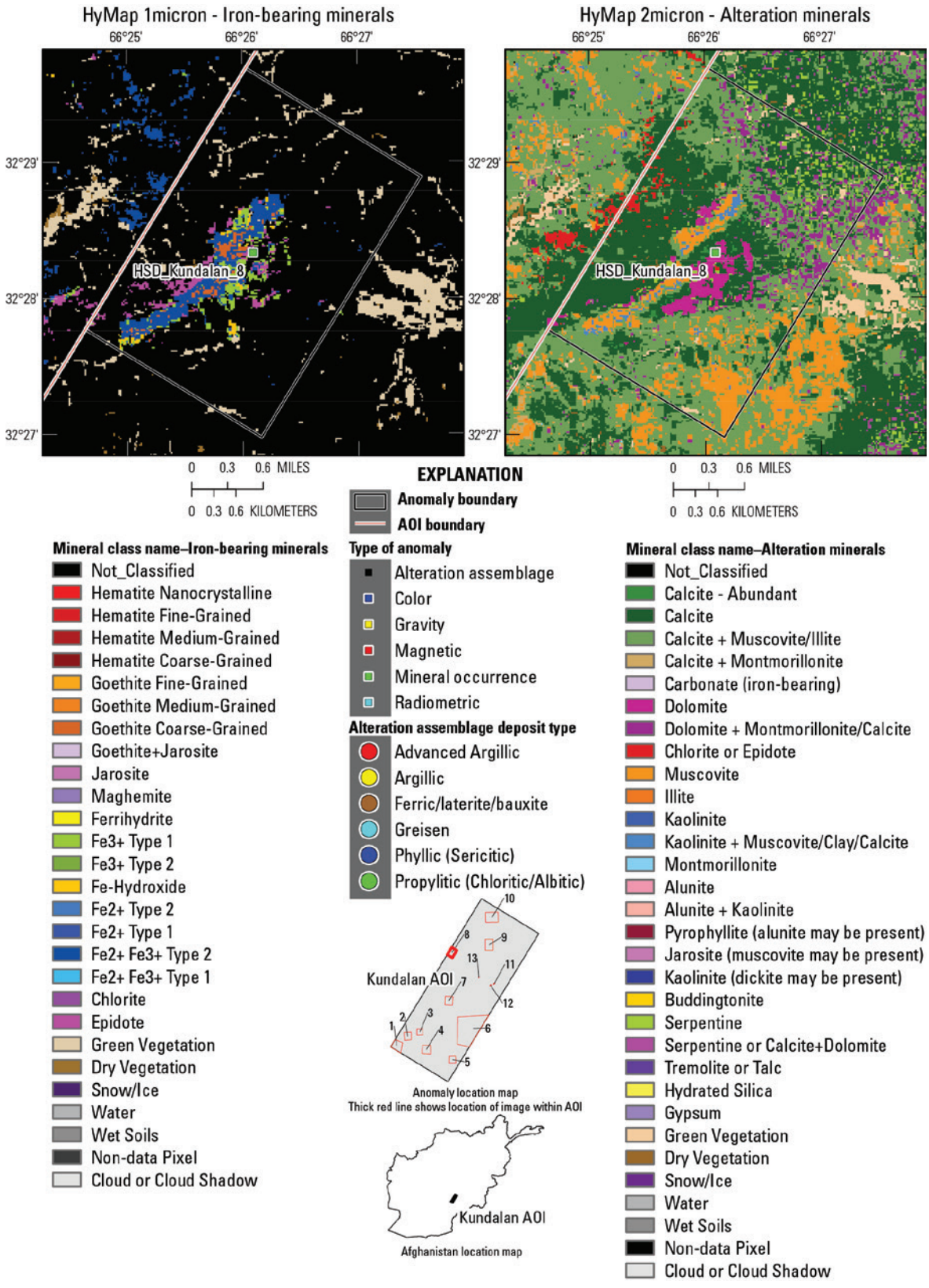

Figure 5.12.8. Hyperspectral anomaly located in the Kundalan Area of Interest (AOI) in Afghanistan based on presence of Chlorite or Epidote, Dolomite minerals, Muscovite, Kaolinite minerals, Goethite minerals, Fe^{3+} Type 1, and Fe-Hydroxide.

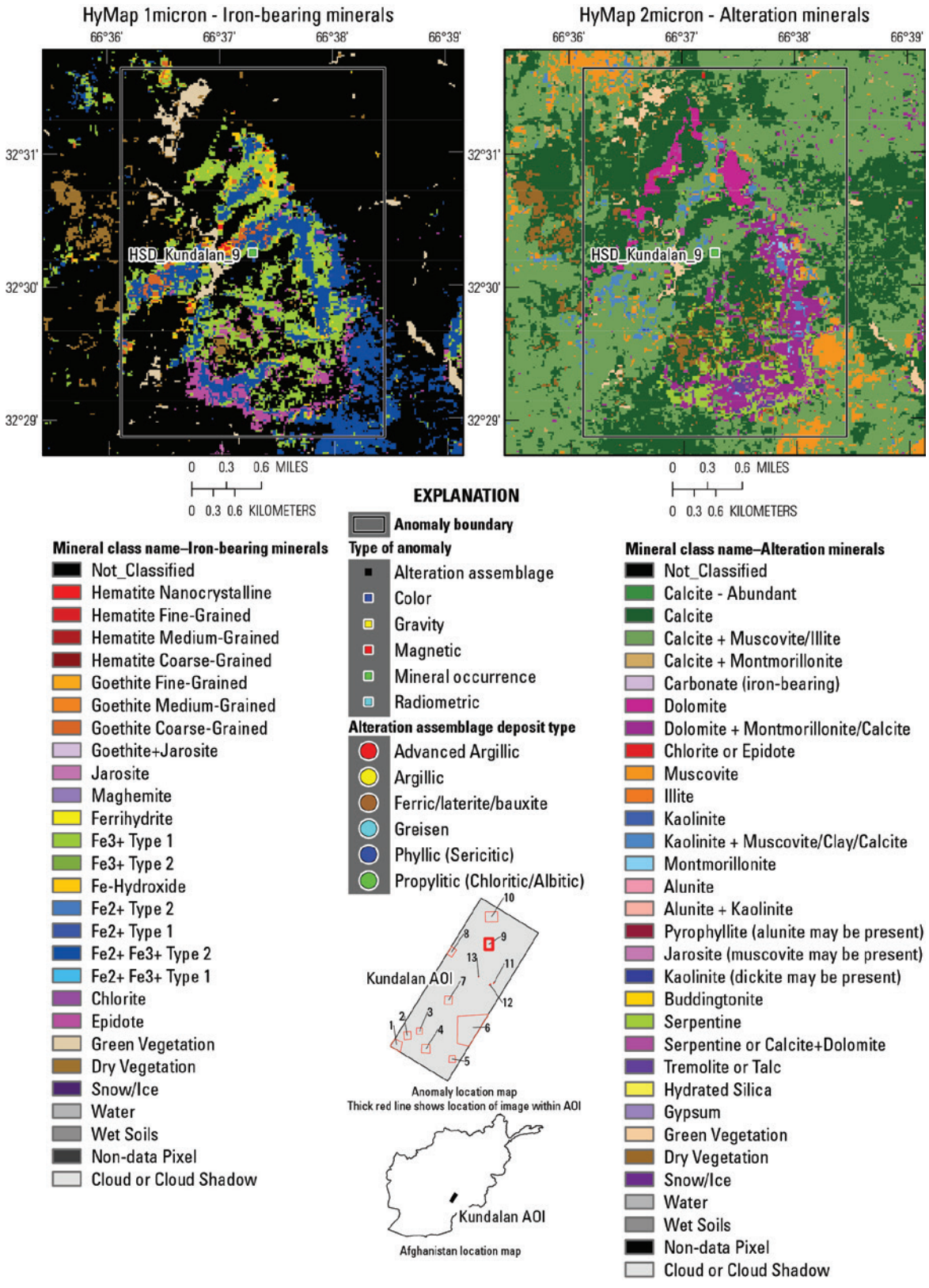

Figure 5.12.9. Hyperspectral anomaly located in the Kundalan Area of Interest (AOI) in Afghanistan based on presence of Dolomite minerals, Serpentine minerals, Tremolite or Talc, Kaolinite minerals, Fe^{3+} Type 1, Epidote, Hematite minerals, Goethite minerals, and Fe-Hydroxide.

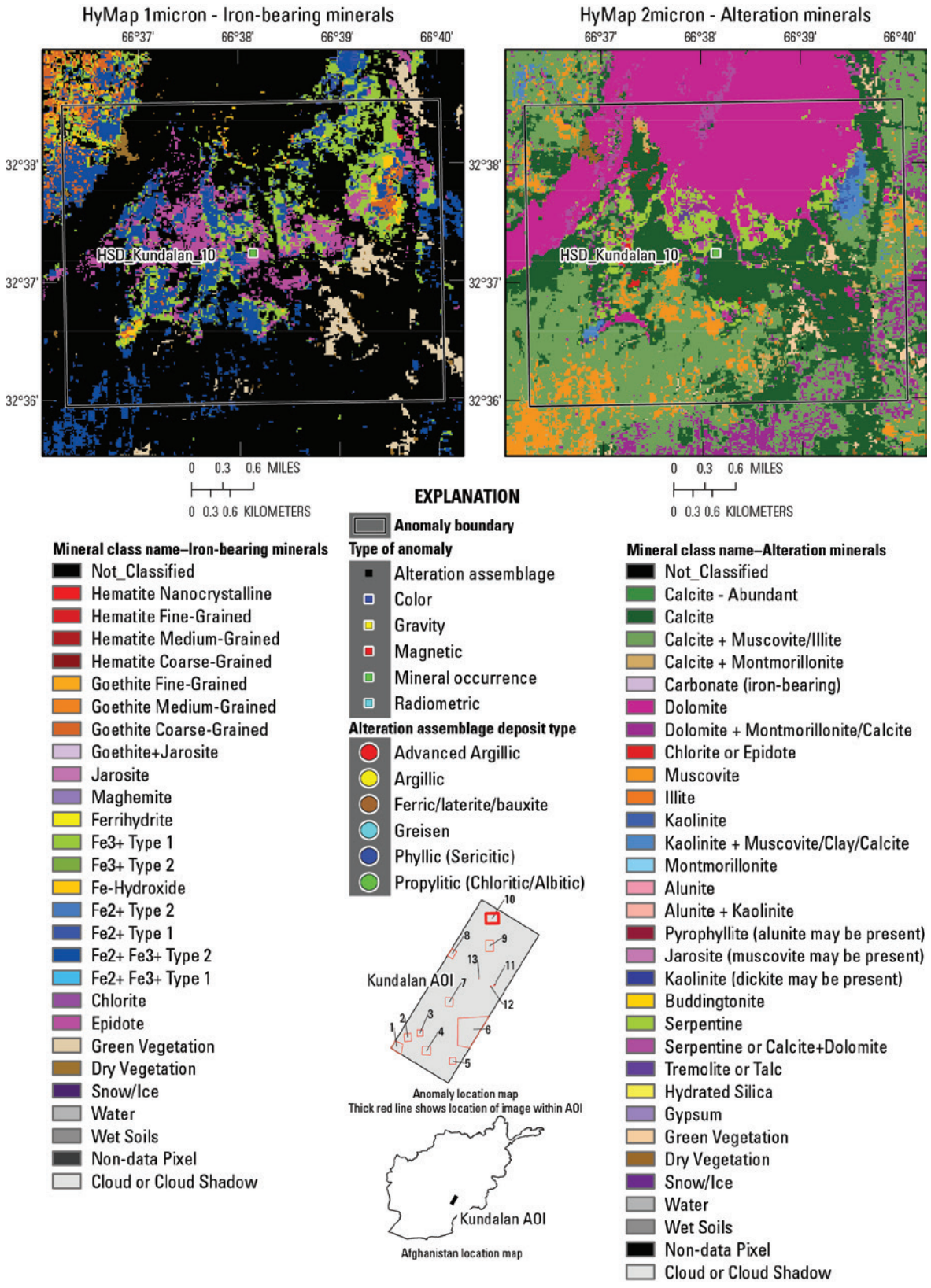

Figure 5.12.10. Hyperspectral anomaly located in the Kundalan Area of Interest (AOI) in Afghanistan based on presence of Serpentine minerals, Dolomite minerals, Kaolinite minerals, Tremolite or Talc, Alunite, Dickite, Chlorite or Epidote, Fe^{3+} Type 1, and Geothite minerals.

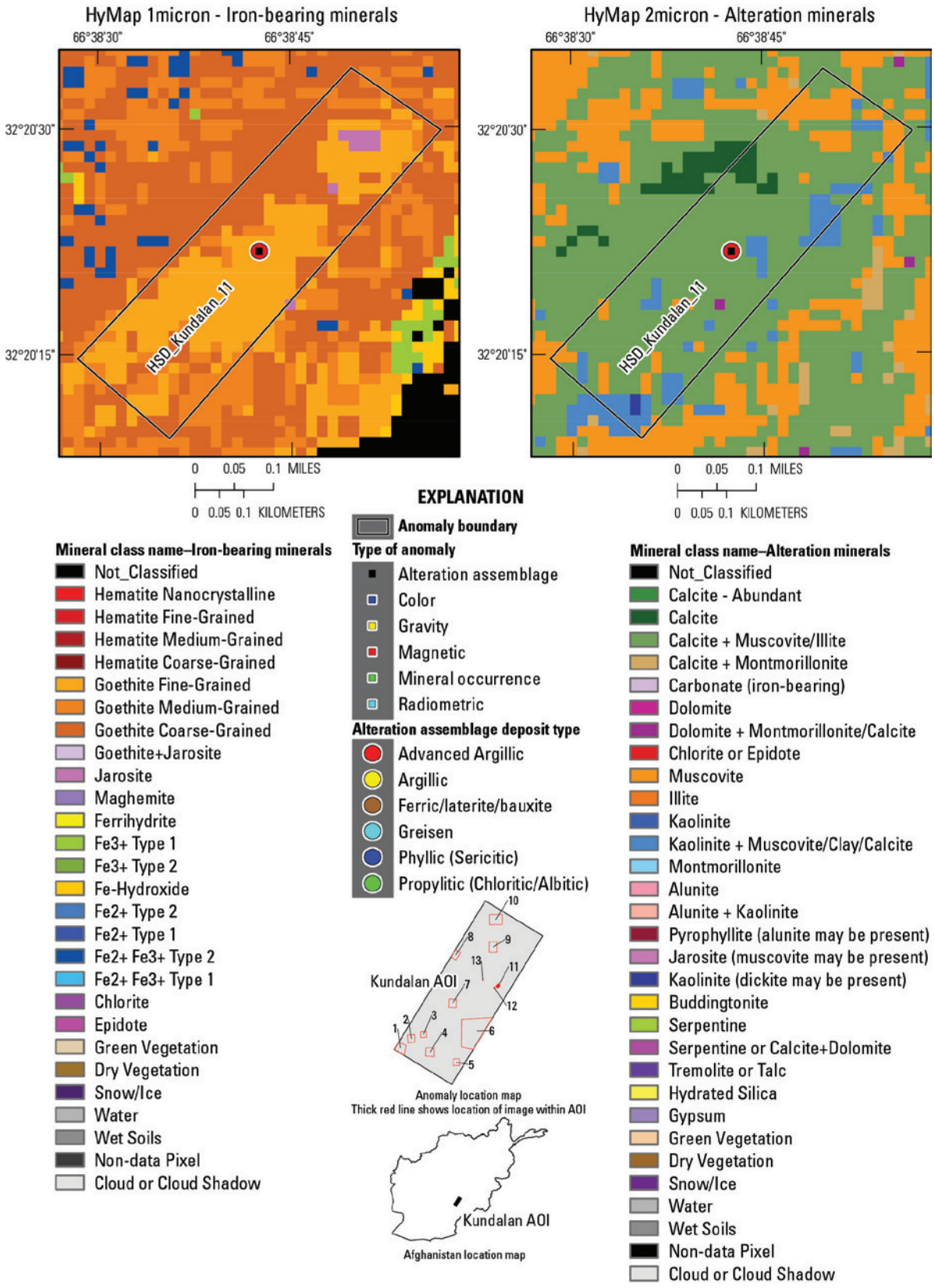

Figure 5.12.11. Hyperspectral anomaly located in the Kundalan Area of Interest (AOI) in Afghanistan based on presence of Kaolinite minerals, Dickite, Jarosite, and Goethite minerals.

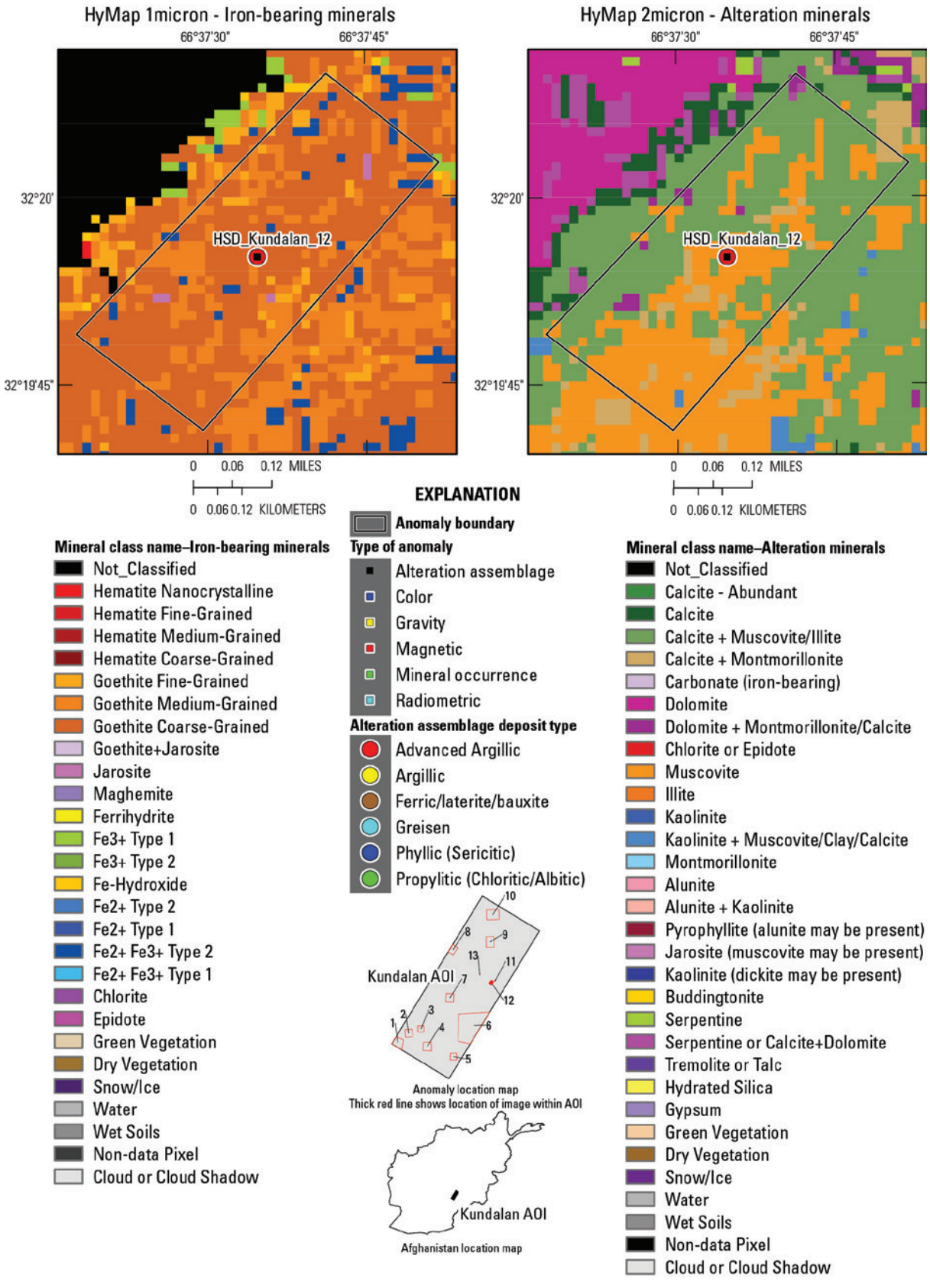

Figure 5.12.12. Hyperspectral anomaly located in the Kundalan Area of Interest (AOI) in Afghanistan based on presence of Kaolinite minerals, Dickite, Jarosite, and Goethite minerals.

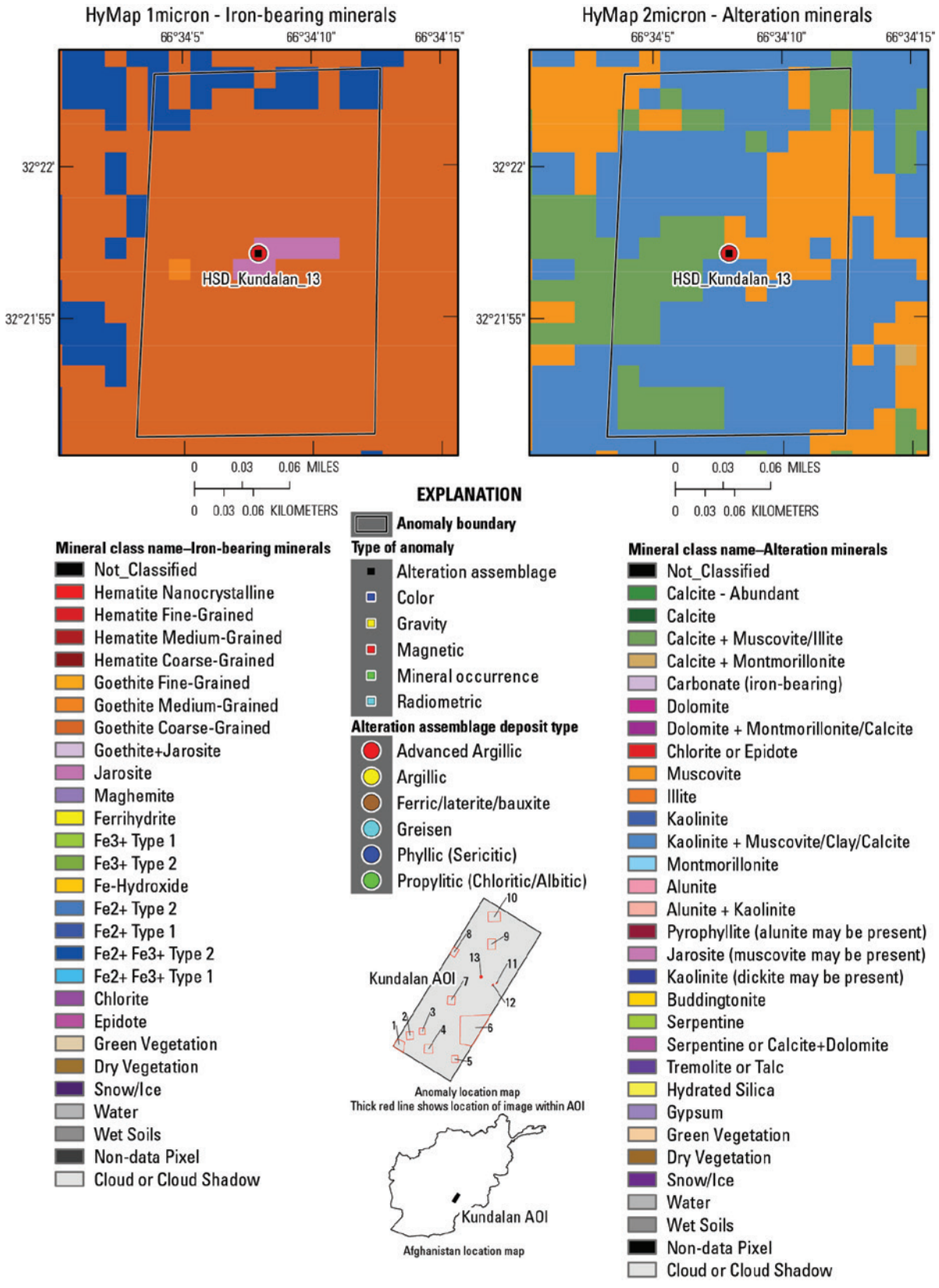

Figure 5.12.13. Hyperspectral anomaly located in the Kundalan Area of Interest (AOI) in Afghanistan based on presence of Kaolinite minerals, Dickite, Jarosite, and Goethite minerals.

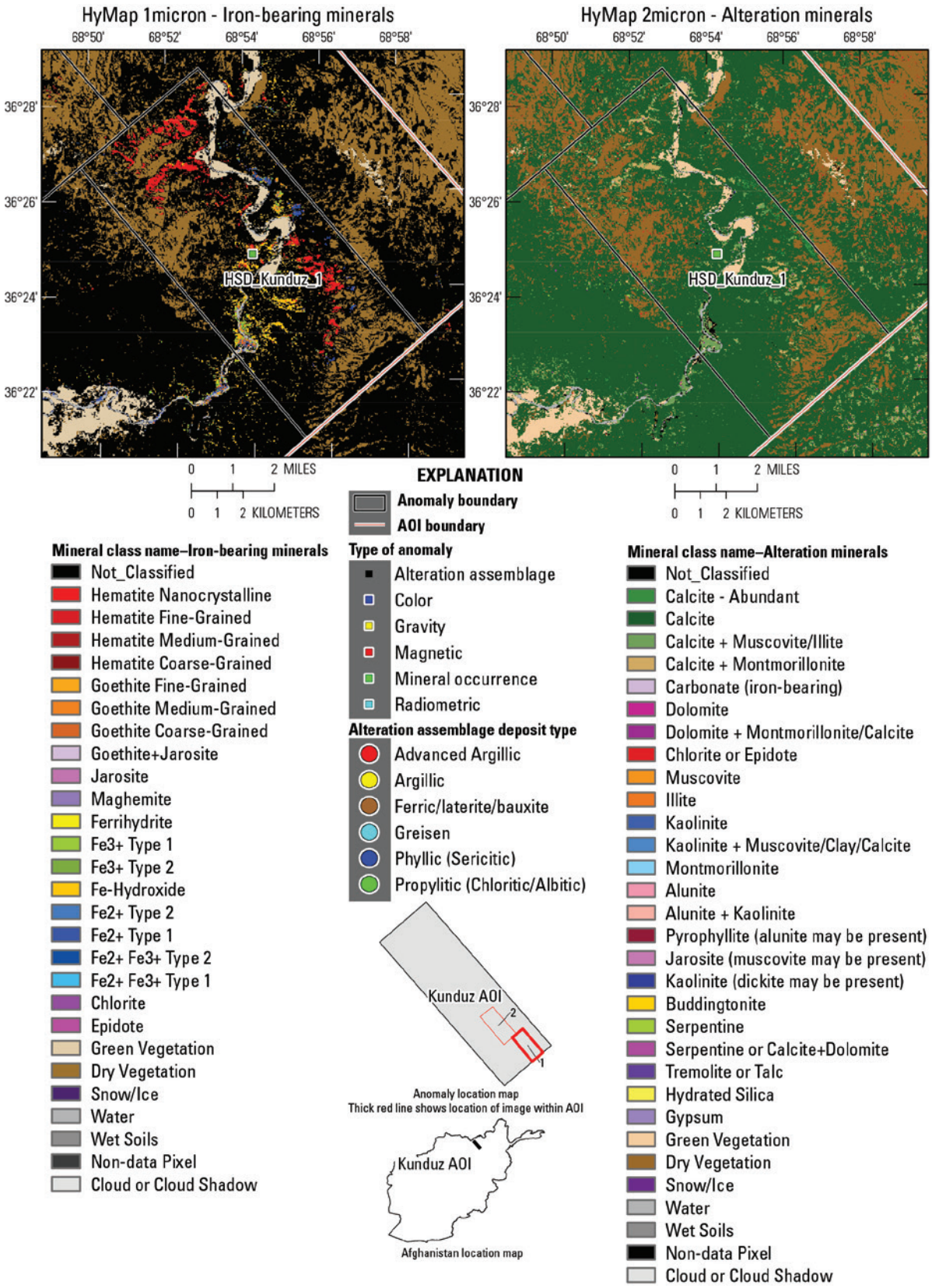

Figure 5.13.1. Hyperspectral anomaly located in the Kunduz Area of Interest (AOI) in Afghanistan based on presence of Hematite minerals, Fe-Hydroxide, and Fe^{2+} Type1.

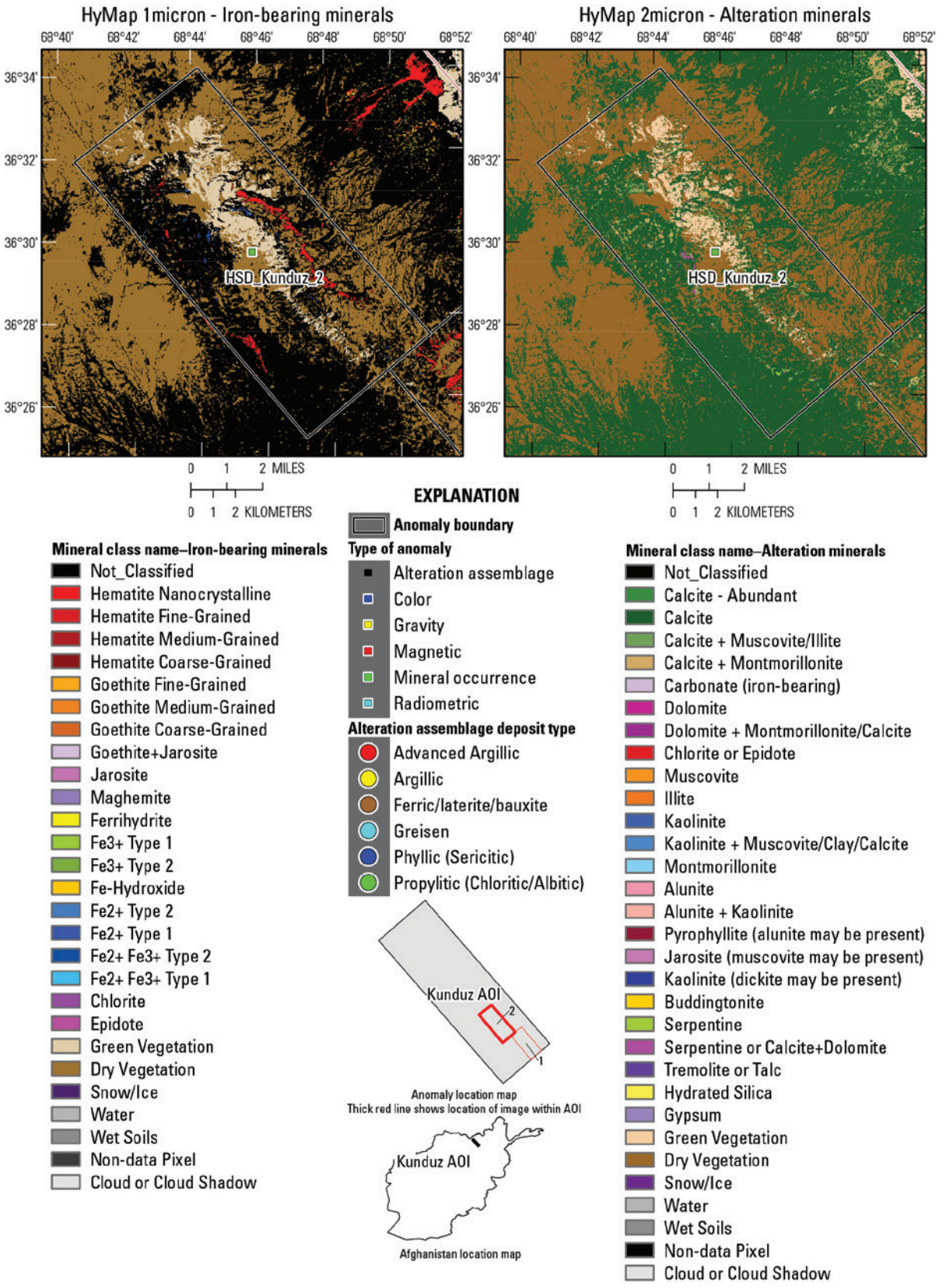

Figure 5.13.2. Hyperspectral anomaly located in the Kunduz Area of Interest (AOI) in Afghanistan based on presence of Hematite minerals and Fe^{2+} Fe^{3+} Type 2.

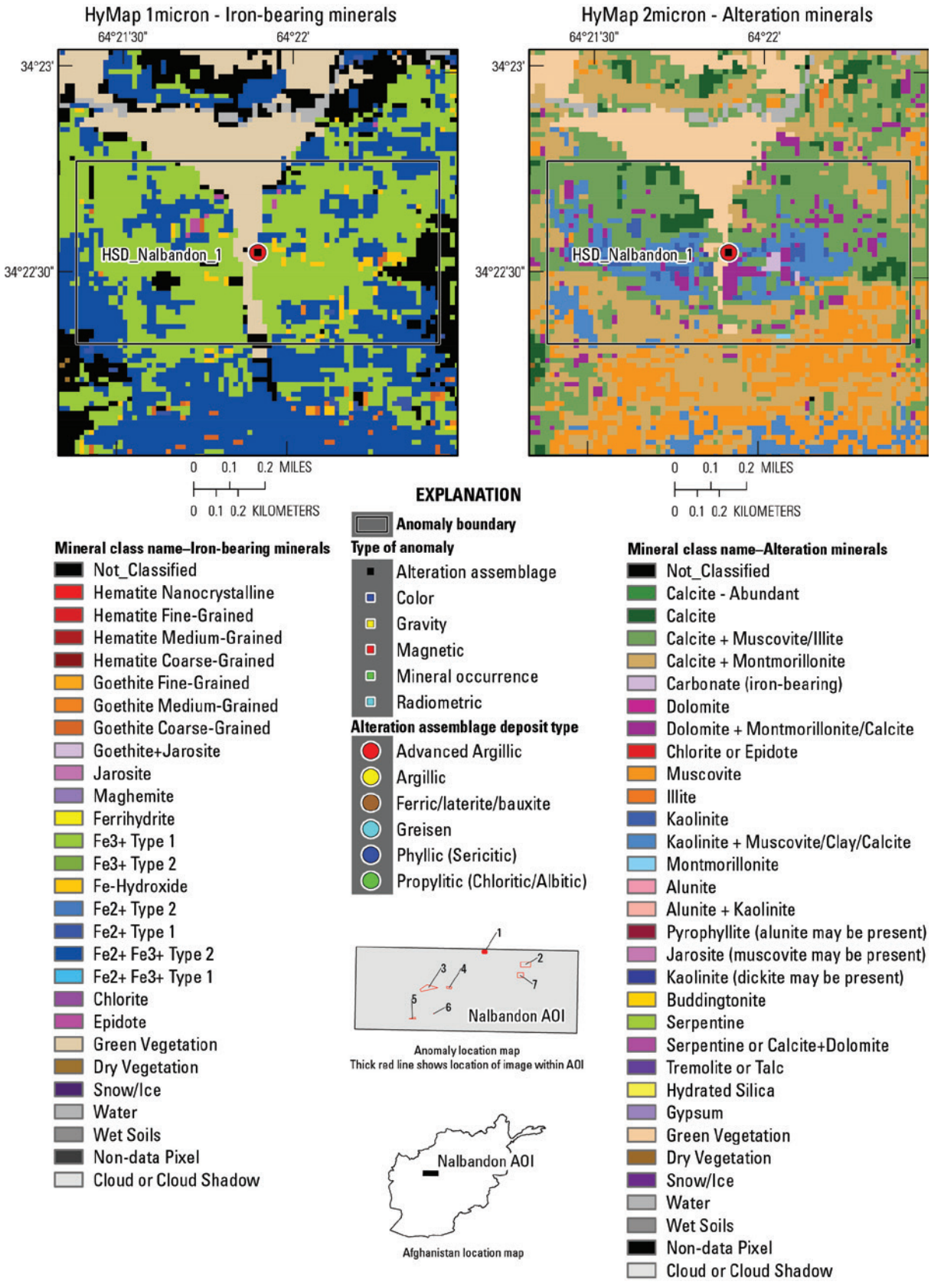

Figure 5.14.1. Hyperspectral anomaly located in the Nalbandon Area of Interest (AOI) in Afghanistan based on presence of Kaolinite minerals, Dolomite minerals, Carbonate (iron-bearing), Dickite, and Fe^{3+} Type1.

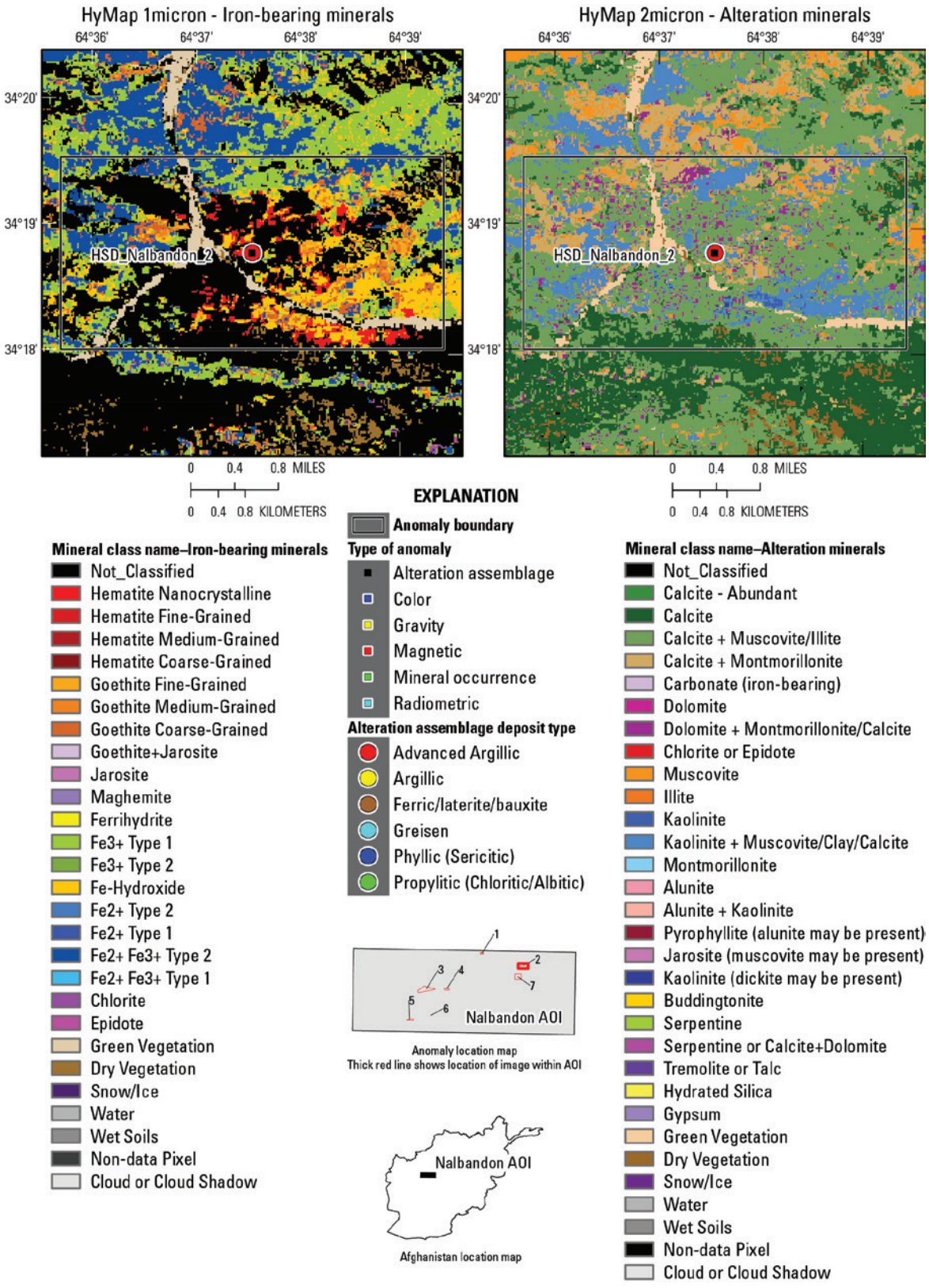

Figure 5.14.2. Hyperspectral anomaly located in the Nalbandon Area of Interest (AOI) in Afghanistan based on presence of Kaolinite minerals, Dolomite minerals, Dickite, Alunite, Fe-Hydroxide, Goethite minerals, and Hematite minerals.

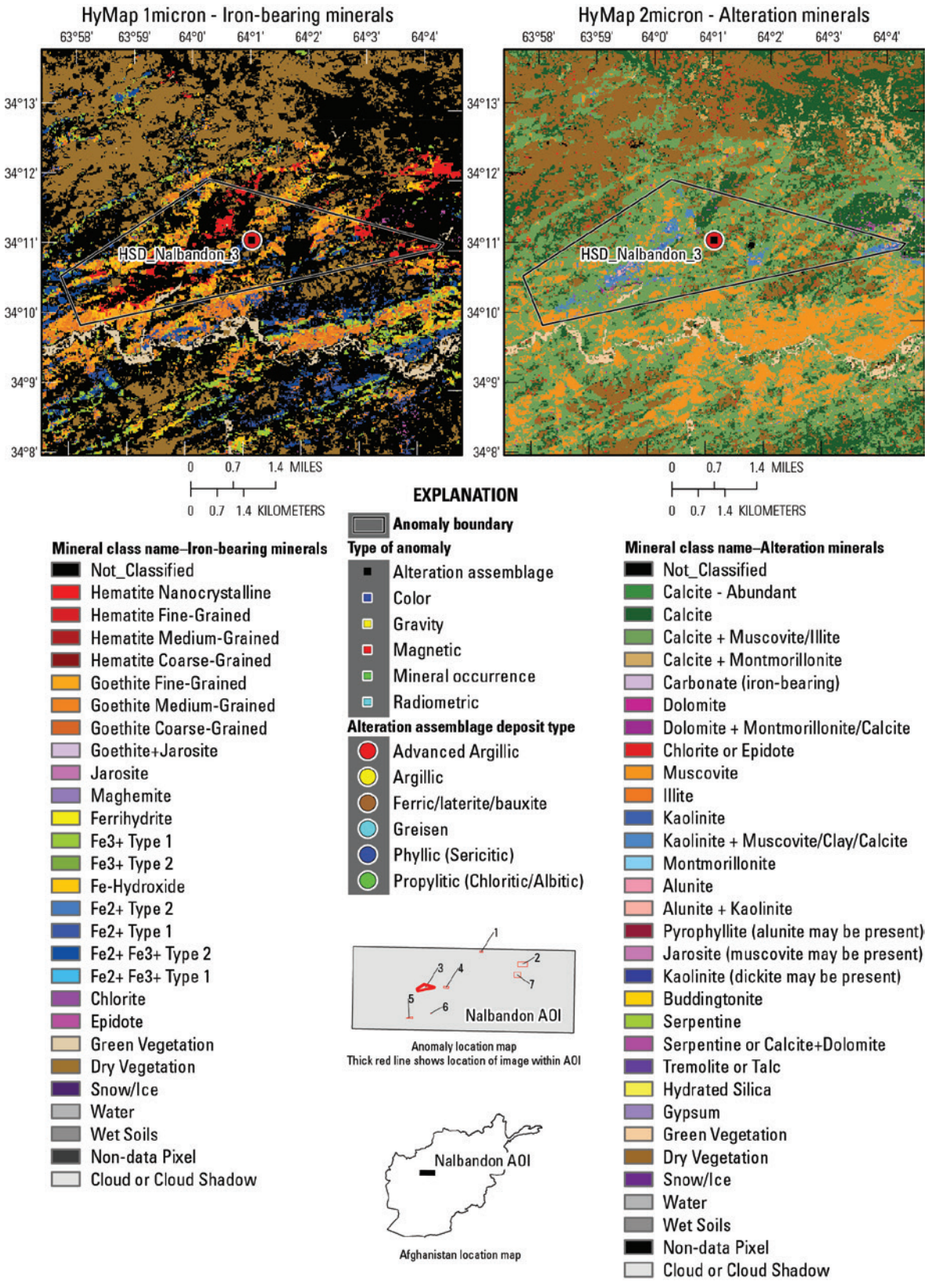

Figure 5.14.3. Hyperspectral anomaly located in the Nalbandon Area of Interest (AOI) in Afghanistan based on presence of Kaolinite minerals, Muscovite, Dolomite minerals, Dickite, Alunite, Fe-Hydroxide, Goethite minerals, and Hematite minerals.

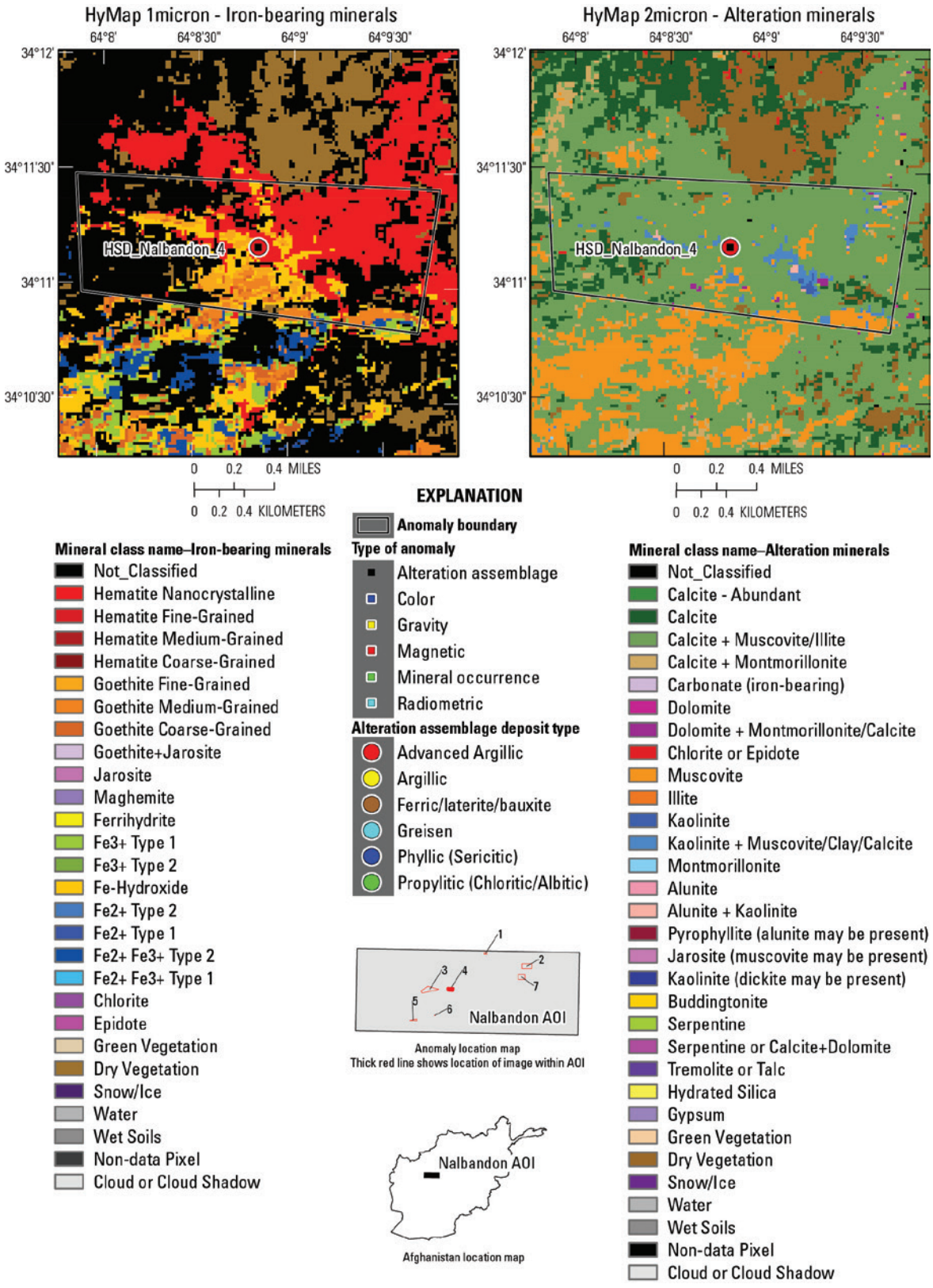

Figure 5.14.4. Hyperspectral anomaly located in the Nalbandon Area of Interest (AOI) in Afghanistan based on presence of Kaolinite minerals, Muscovite, Dolomite minerals, Alunite, Fe-Hydroxide, Goethite minerals, and Hematite minerals.

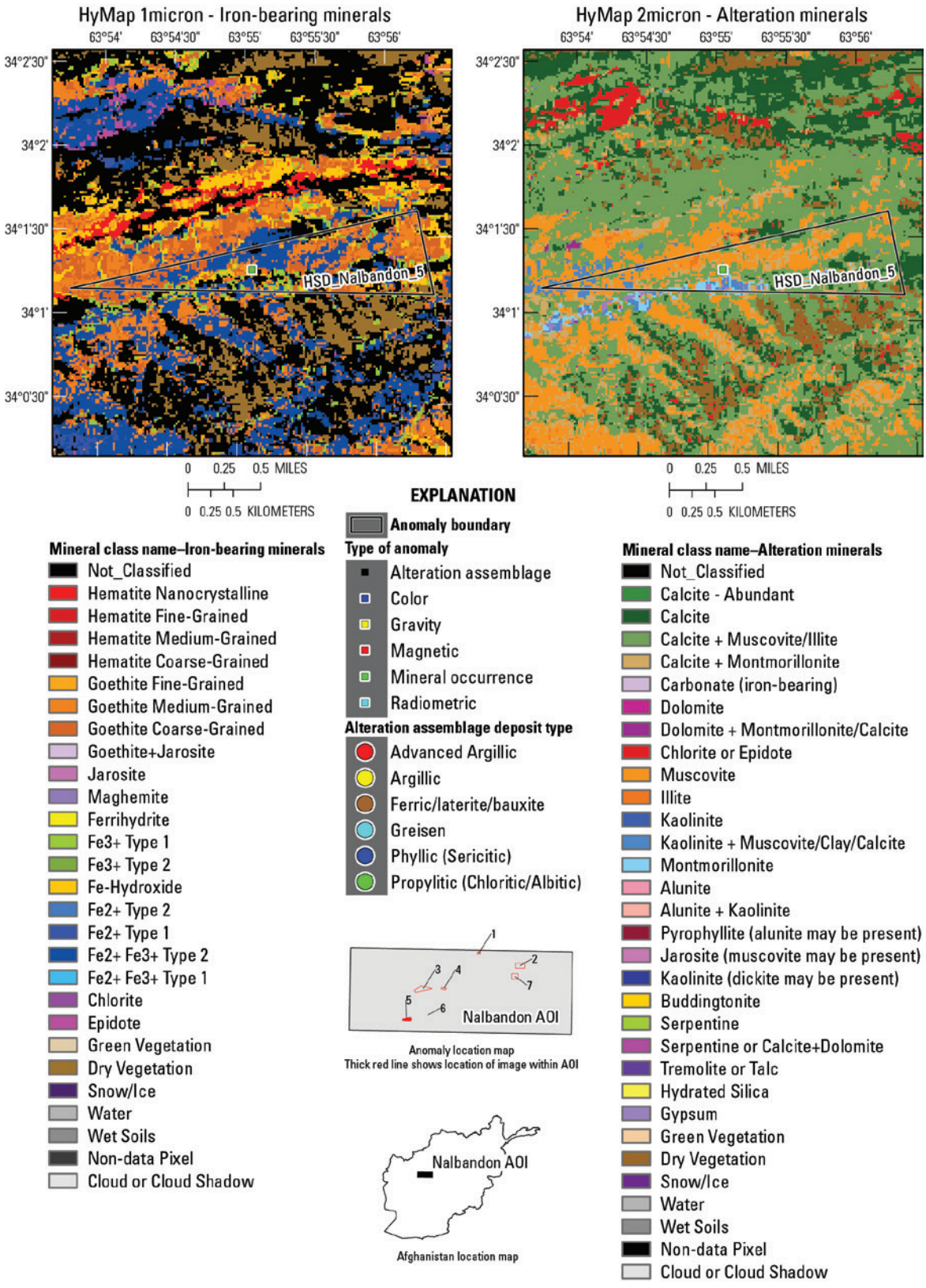

Figure 5.14.5. Hyperspectral anomaly located in the Nalbandon Area of Interest (AOI) in Afghanistan based on presence of Montmorillonite, Kaolinite minerals, Gypsum, Hematite minerals, Goethite minerals, and Fe^{3+} Type1.

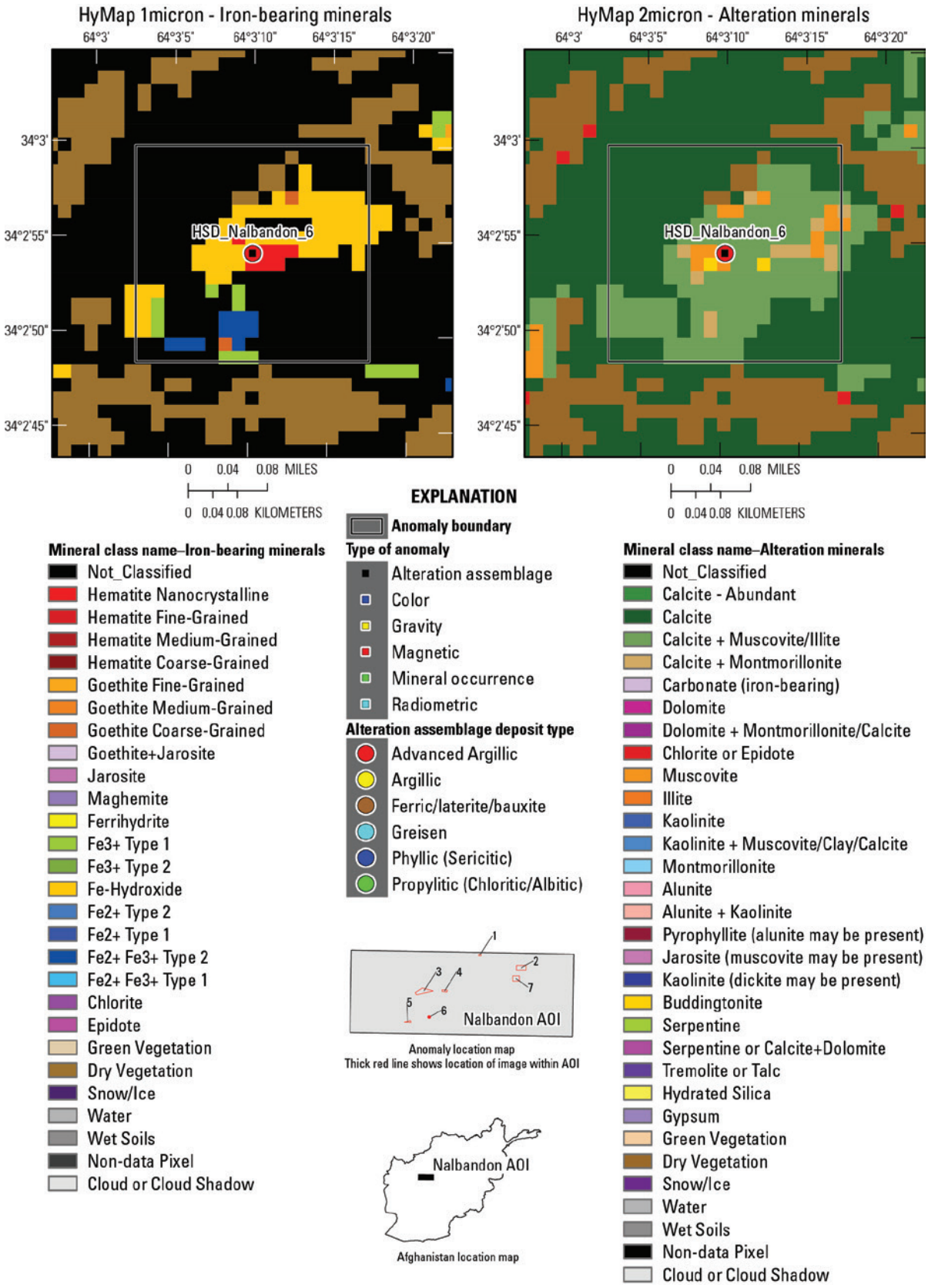

Figure 5.14.6. Hyperspectral anomaly located in the Nalbandon Area of Interest (AOI) in Afghanistan based on presence of Buddingtonite.

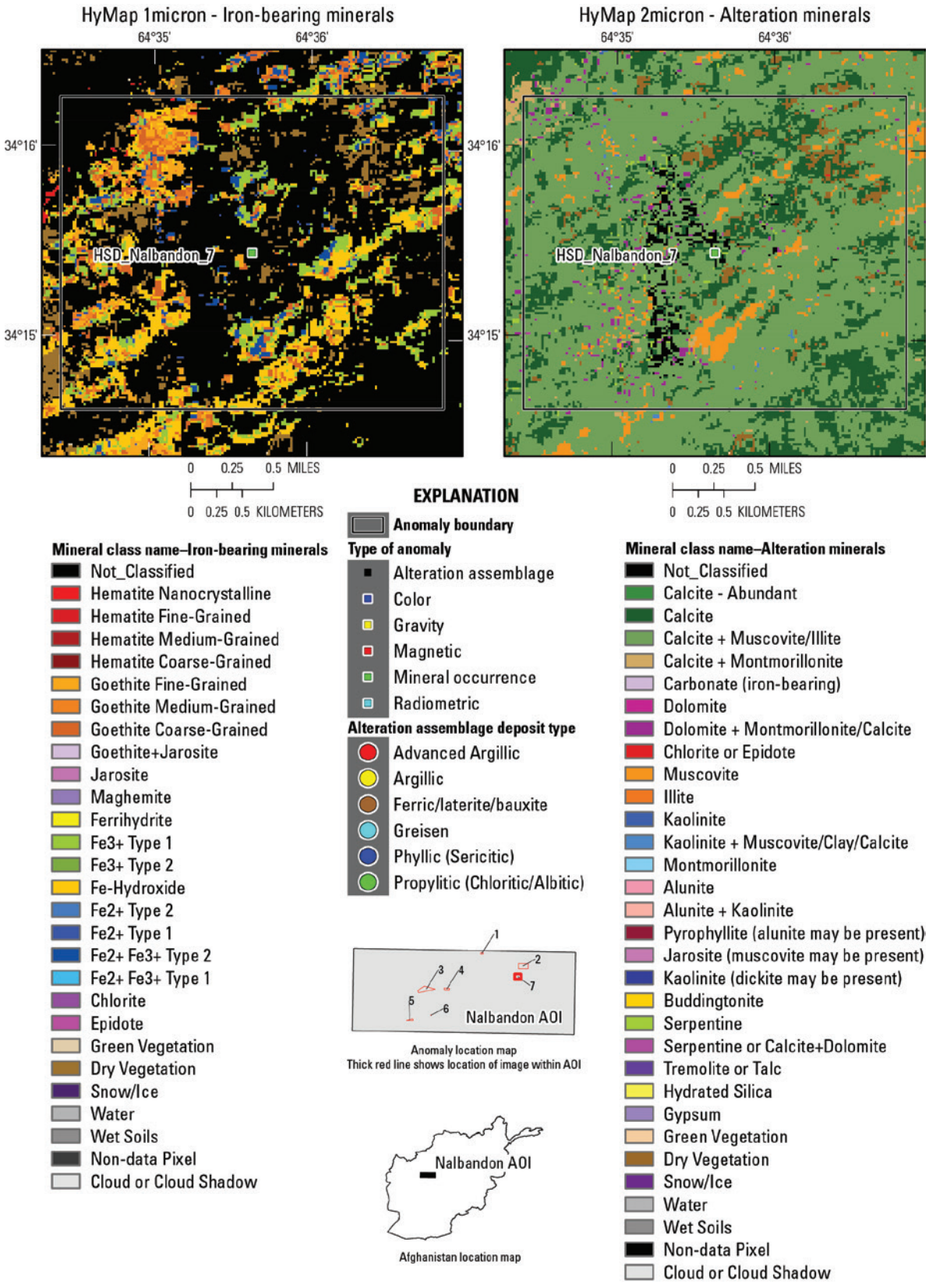

Figure 5.14.7. Hyperspectral anomaly located in the Nalbandon Area of Interest (AOI) in Afghanistan based on presence of Muscovite, Dolomite minerals, Serpentine, and Goethite minerals.

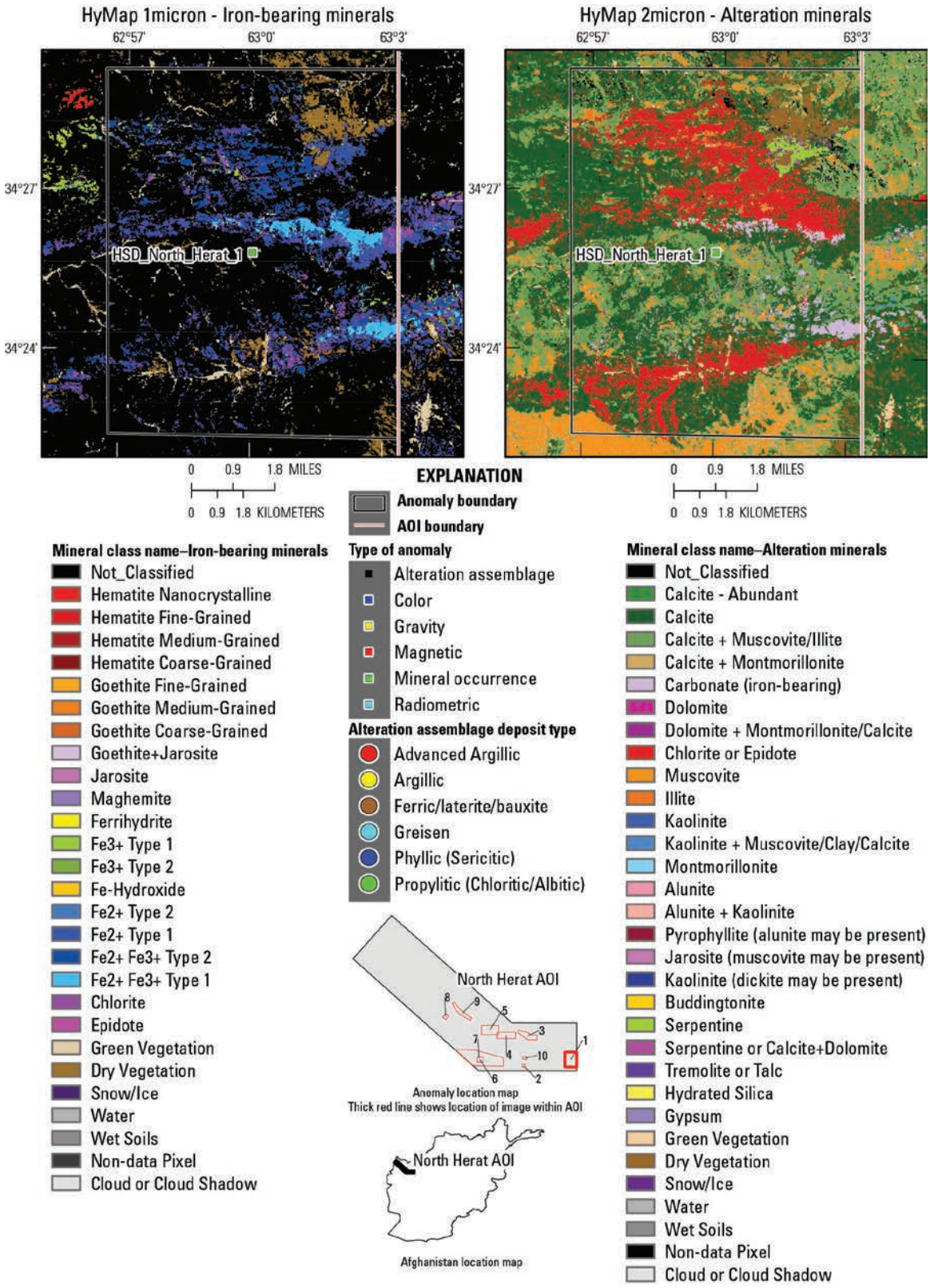

Figure 5.15.1. Hyperspectral anomaly located in the North Herat Area of Interest (AOI) in Afghanistan based on presence of Chlorite or Epidote, Calcite (iron-bearing), Serpentine minerals, Muscovite, Dolomite minerals, Tremolite or Talc, Fe^{2+} Fe^{3+} Type 1, Fe^{2+} Type 1, and Fe^{3+} Type 1.

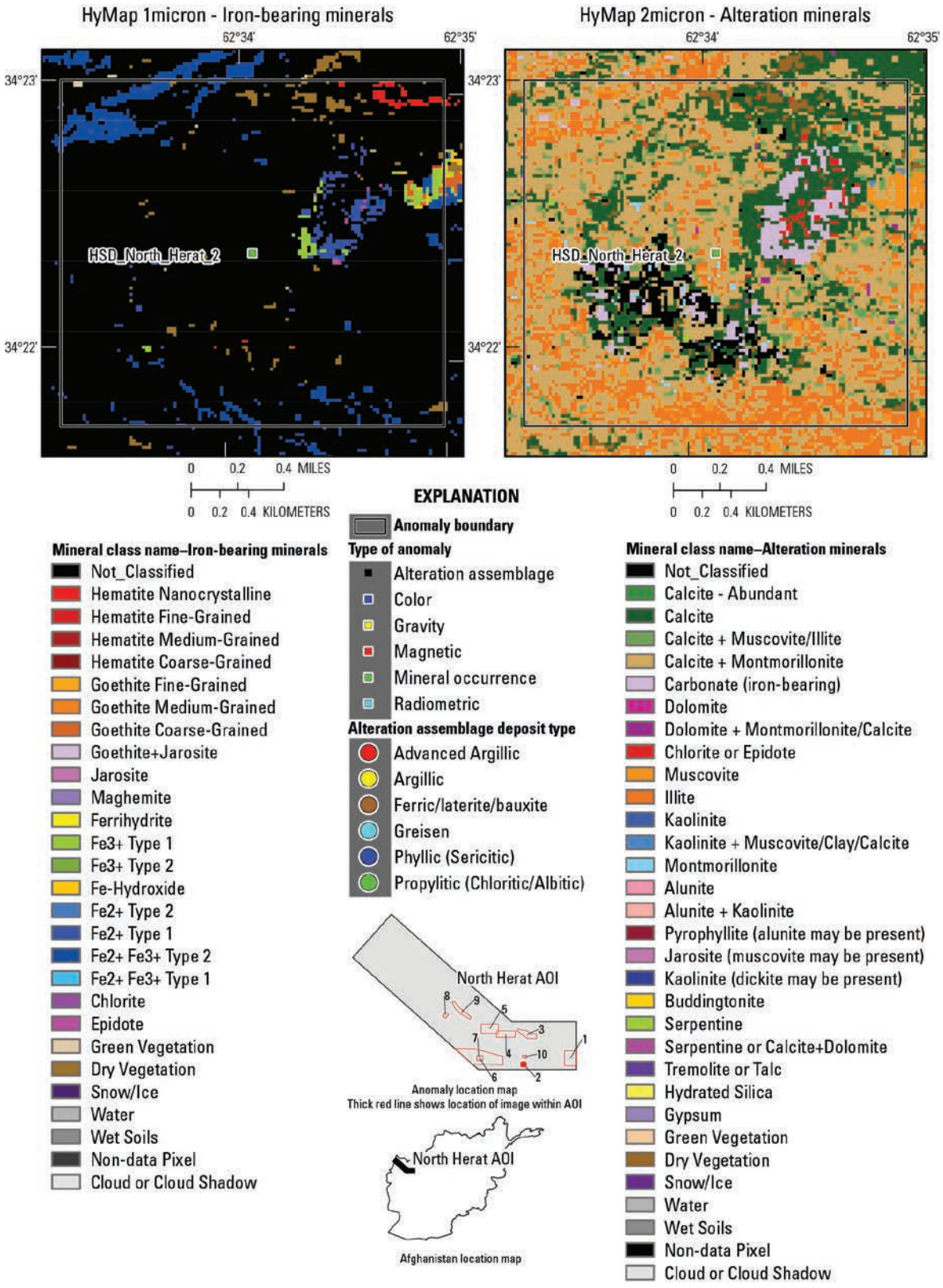

Figure 5.15.2. Hyperspectral anomaly located in the North Herat Area of Interest (AOI) in Afghanistan based on presence of Carbonate (iron-bearing), Chlorite or Epidote, Goethite minerals, Fe^{3+} Type 1, and Fe^{2+} Type 1.

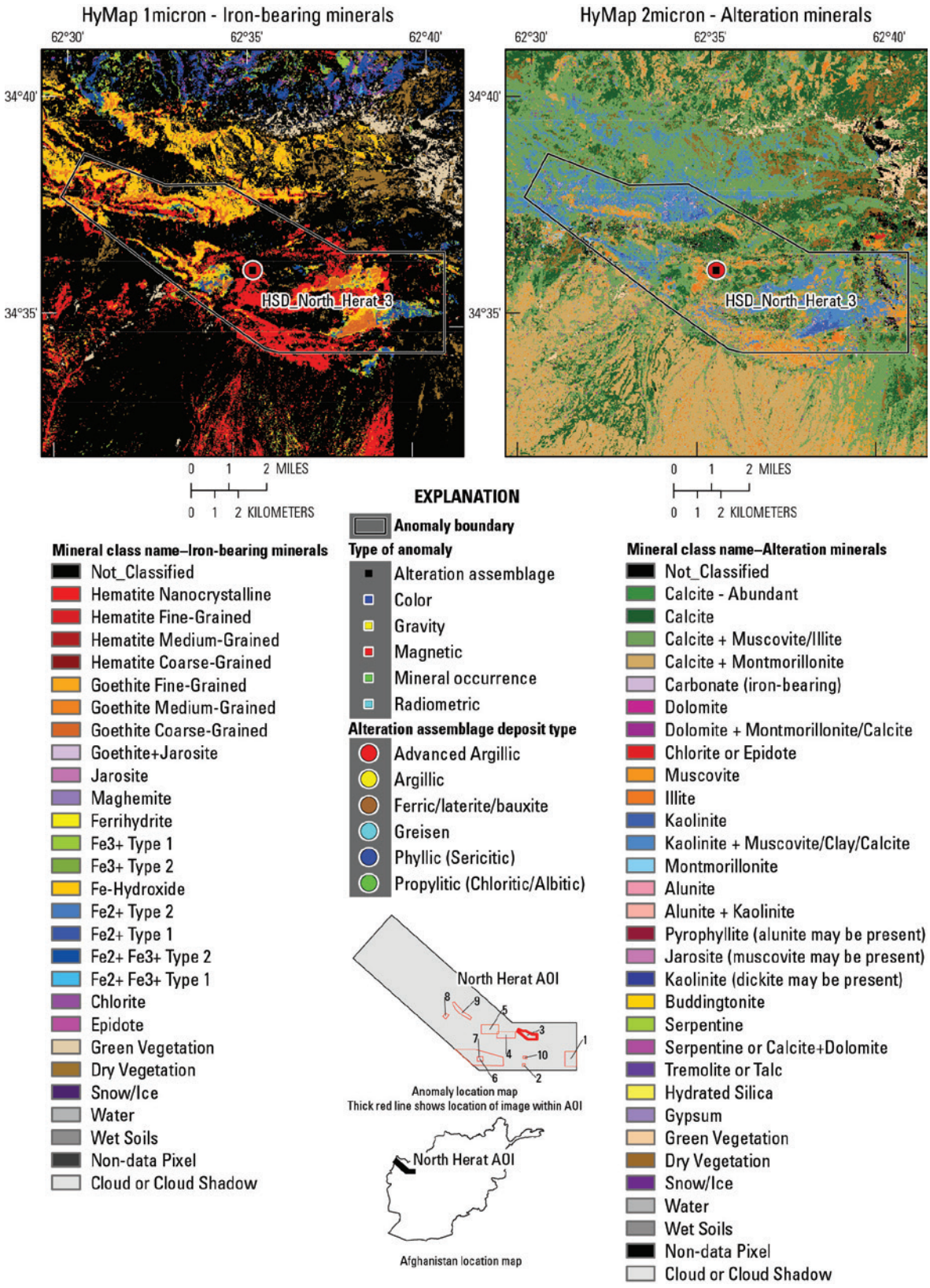

Figure 5.15.3. Hyperspectral anomaly located in the North Herat Area of Interest (AOI) in Afghanistan based on presence of Kaolinite minerals, Alunite minerals, Dickite, Hematite minerals, Goethite minerals, Fe-Hydroxide, and Fe^{3+} Type1.

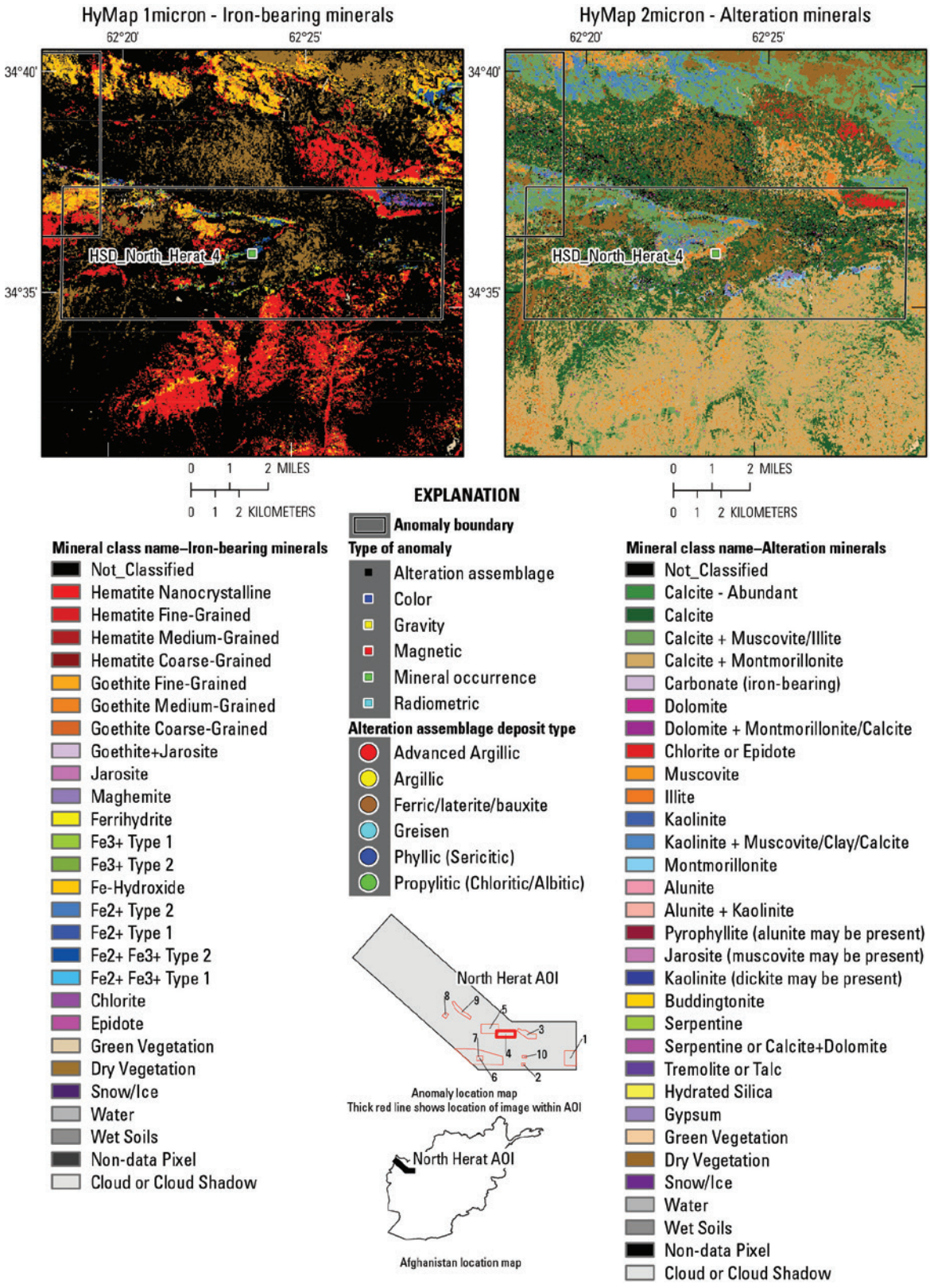

Figure 5.15.4. Hyperspectral anomaly located in the North Herat Area of Interest (AOI) in Afghanistan based on presence of Gypsum, Kaolinite minerals, Montmorillonite, Chlorite or Epidote, Illite, Hematite minerals, Goethite minerals, Fe-Hydroxide, Maghemite, Fe^{3+} Type 1, and Fe^{2+} Fe^{3+} Type 2.

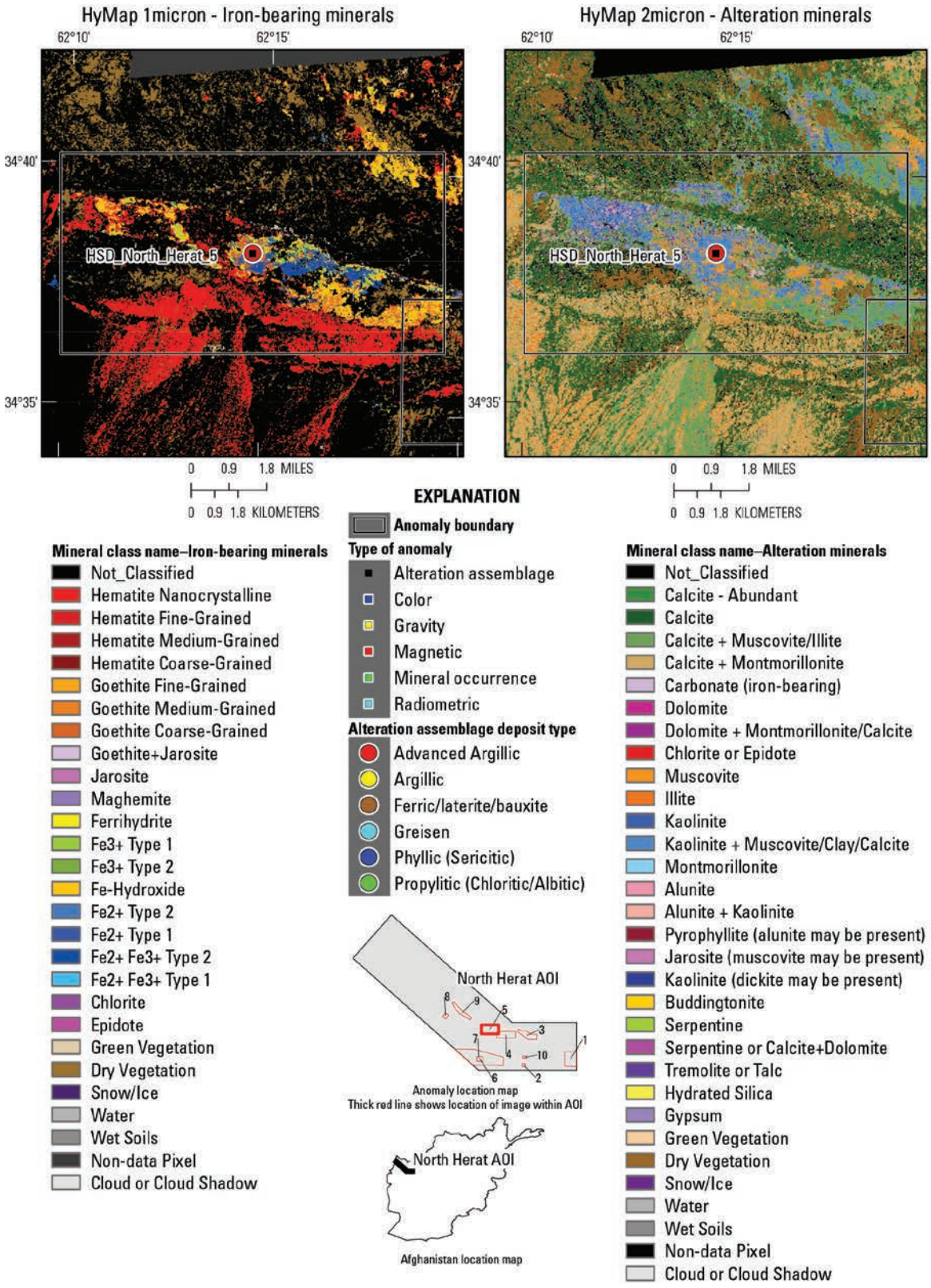

Figure 5.15.5. Hyperspectral anomaly located in the North Herat Area of Interest (AOI) in Afghanistan based on presence of Kaolinite minerals, Muscovite, Carbonite (iron-bearing), Alunite, Dickite, Chlorite or Epidote, Montmorillonite, Fe^{3+} Type 1, Goethite minerals, Hematite minerals, and Maghemite.

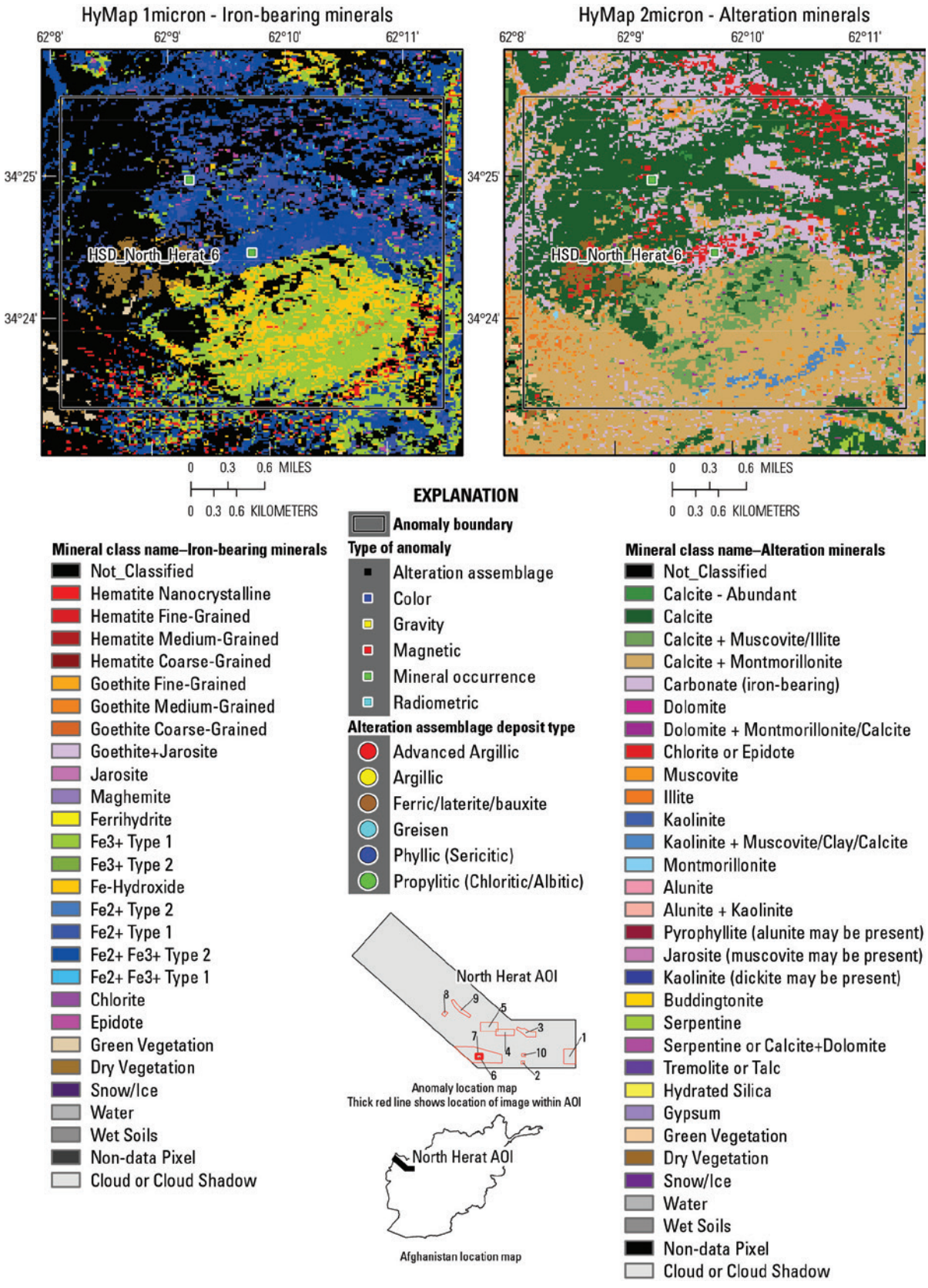

Figure 5.15.6. Hyperspectral anomaly located in the North Herat Area of Interest (AOI) in Afghanistan based on presence of Fe^{3+} Type1 and Fe-Hydroxide.

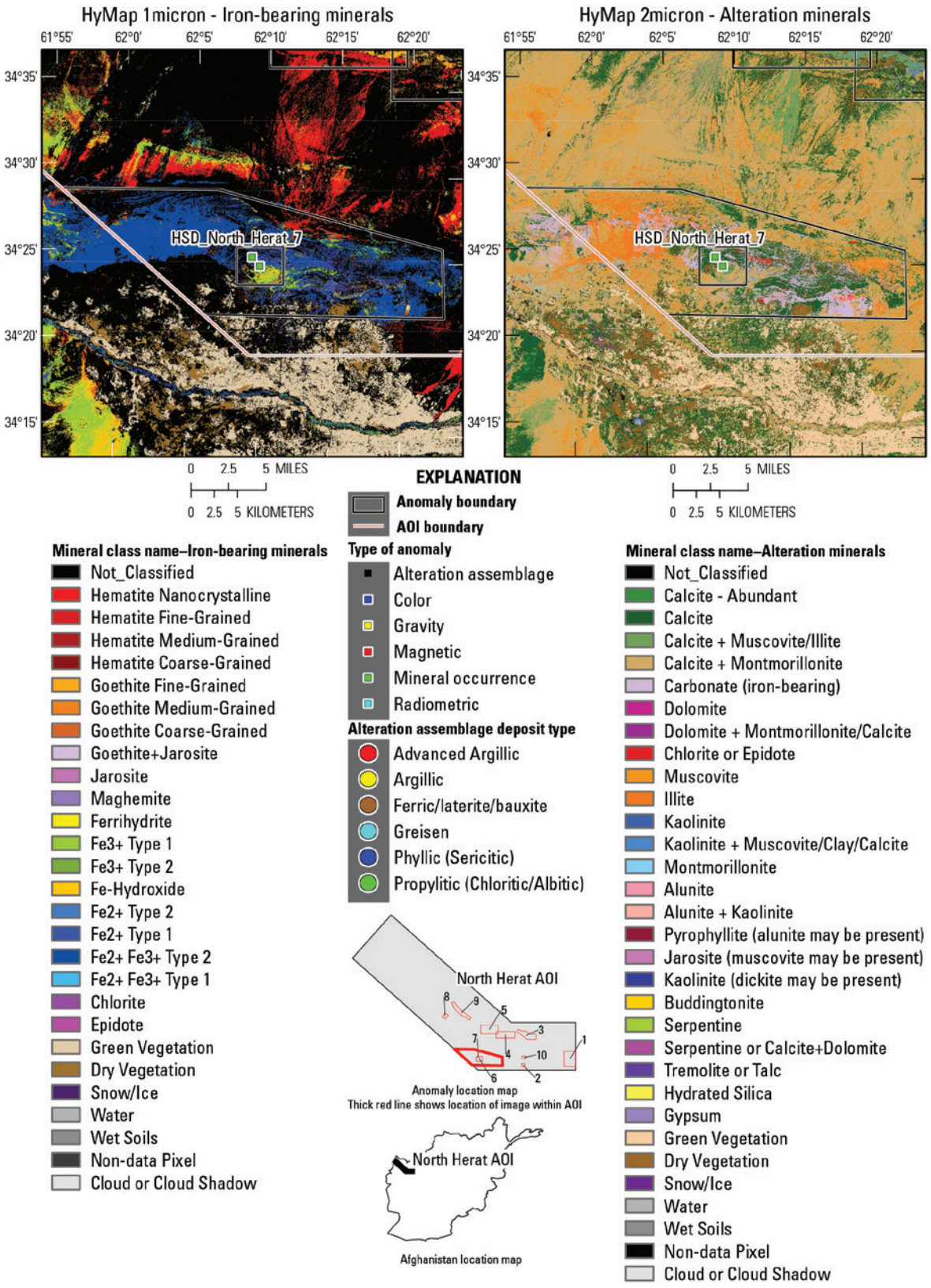

Figure 5.15.7. Hyperspectral anomaly located in the North Herat Area of Interest (AOI) in Afghanistan based on presence of Carbonate (iron-bearing), Chlorite or Epidote, Kaolinite minerals, Fe^{3+} Type 1, Fe-Hydroxide, and Fe^{2+} Fe^{3+} Type2.

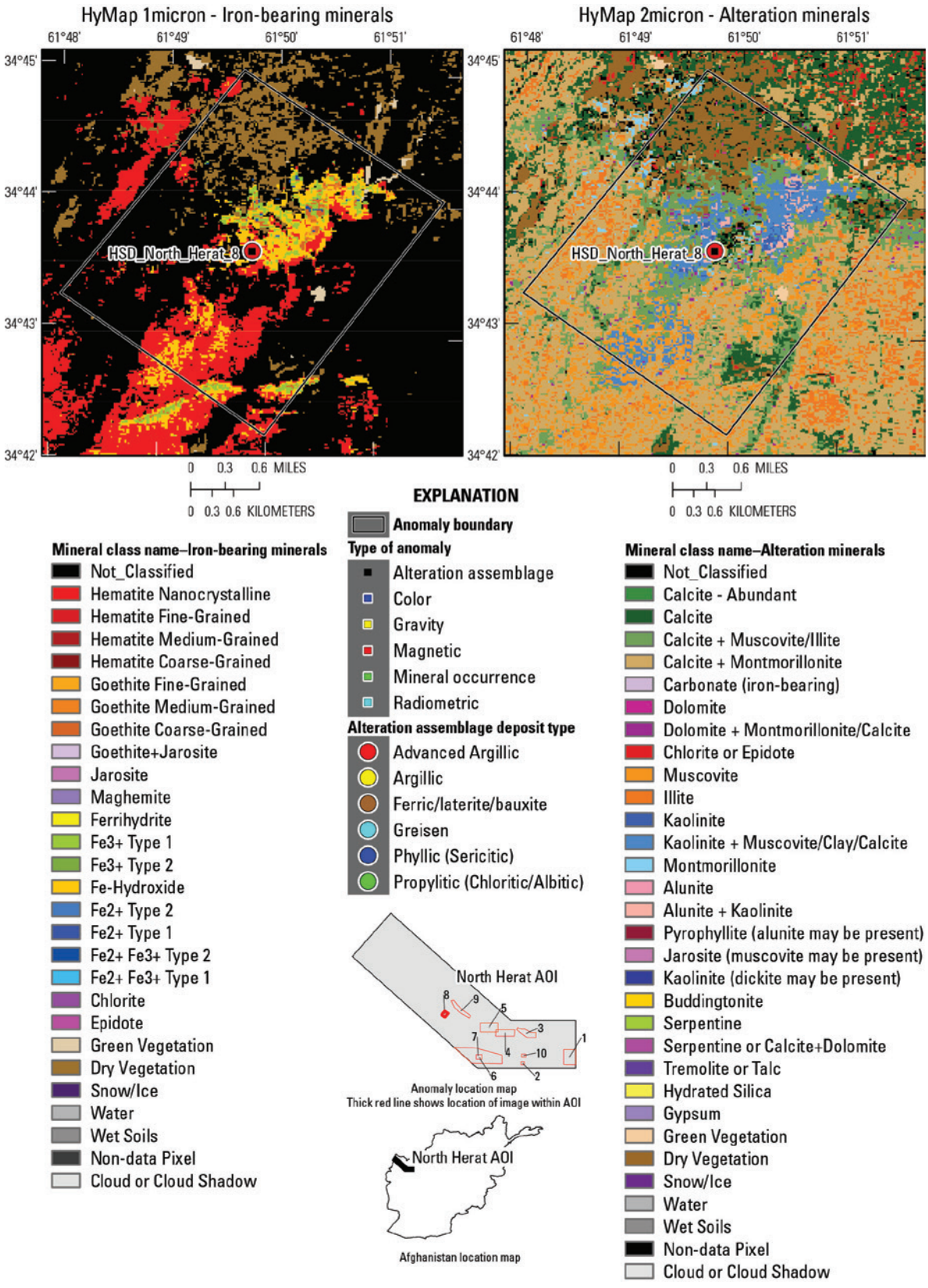

Figure 5.15.8. Hyperspectral anomaly located in the North Herat Area of Interest (AOI) in Afghanistan based on presence of Kaolinite minerals, Alunite minerals, and Chlorite or Epidote.

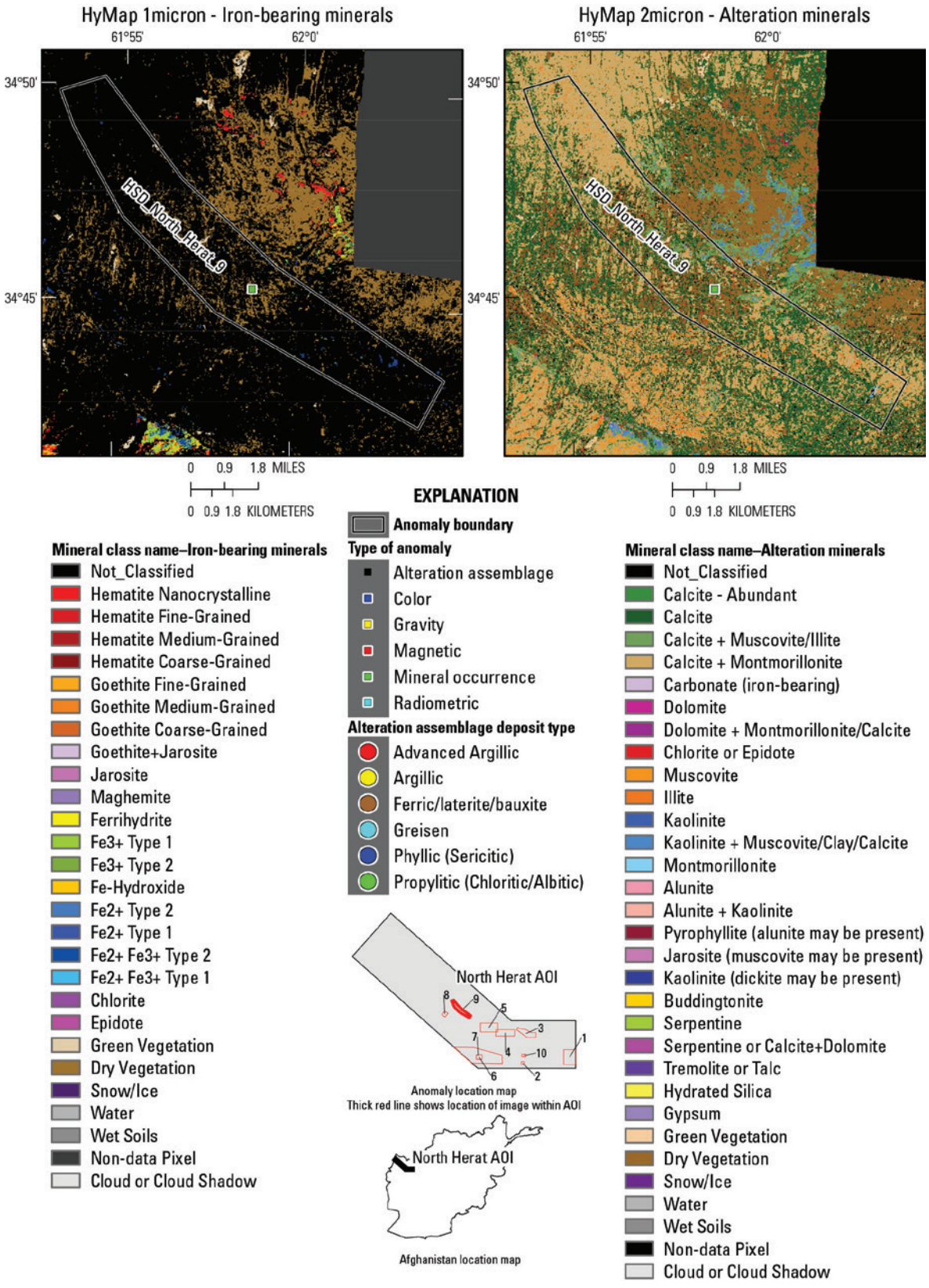

Figure 5.15.9. Hyperspectral anomaly located in the North Herat Area of Interest (AOI) in Afghanistan based on presence of Gypsum.

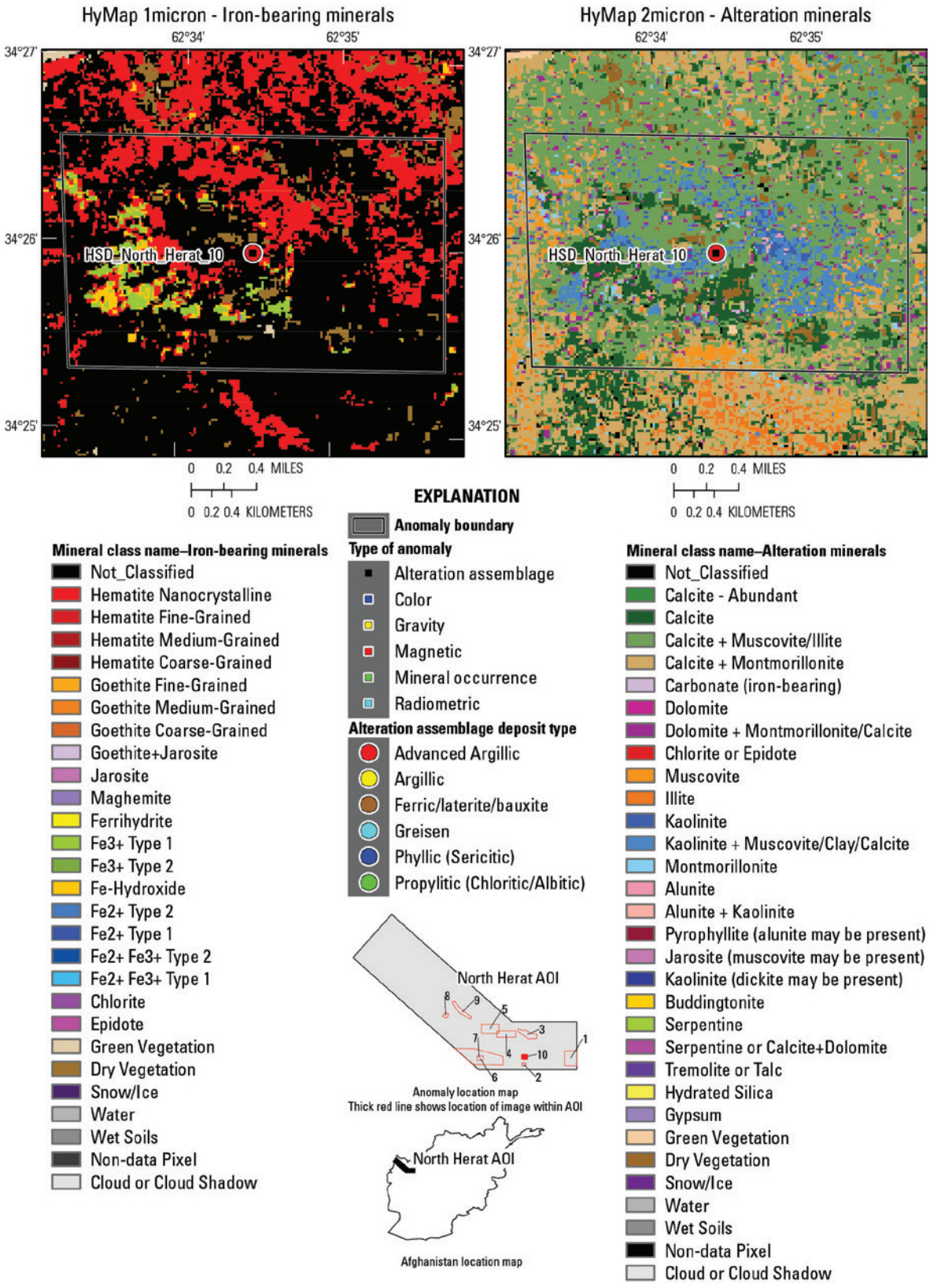

Figure 5.15.10. Hyperspectral anomaly located in the North Herat Area of Interest (AOI) in Afghanistan based on presence of Kaolinite minerals, Alunite minerals, Dickite, Hematite minerals, Maghemite, Fe-Hydroxide, and Fe^{3+} Type1.

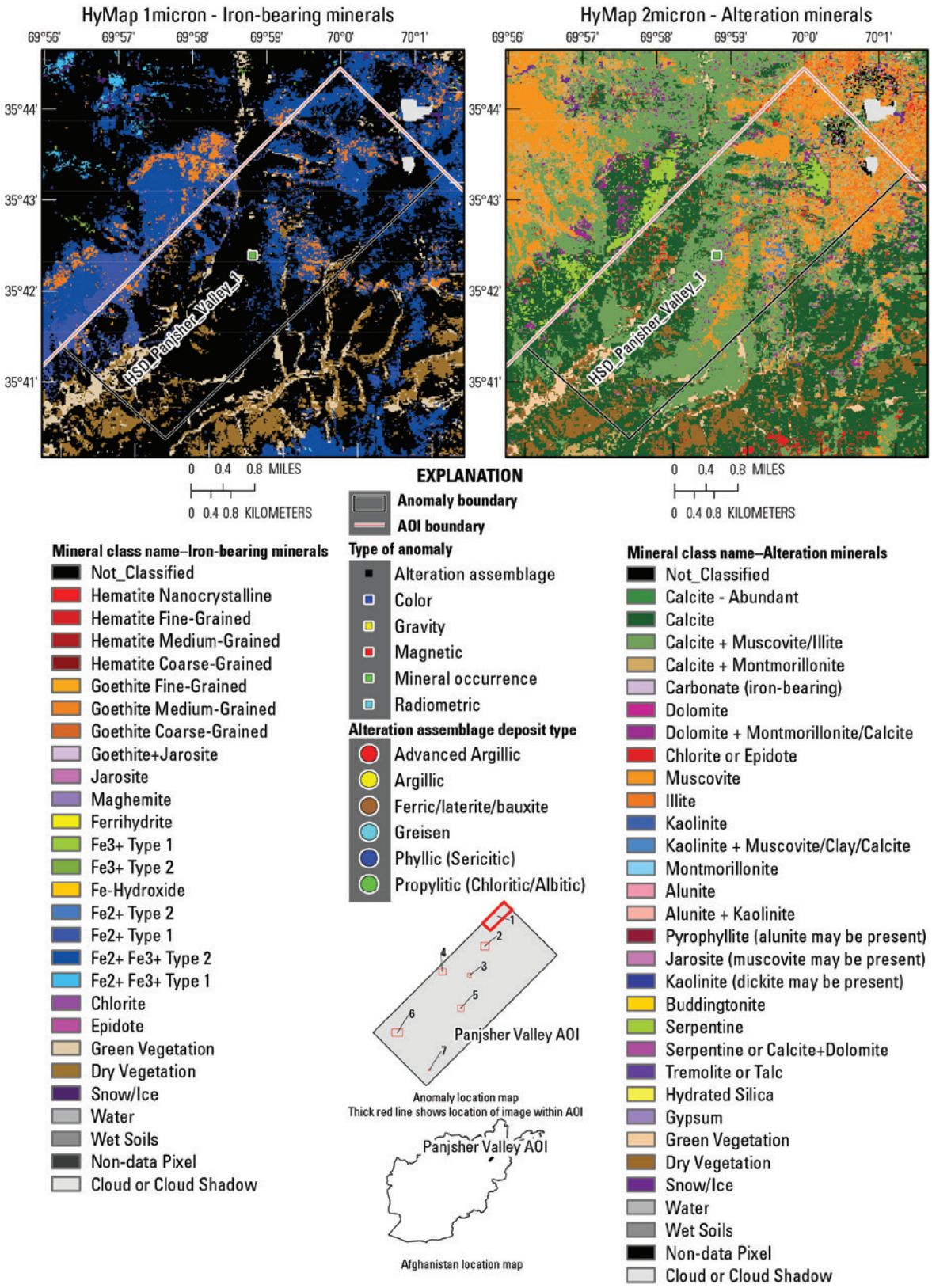

Figure 5.16.1. Hyperspectral anomaly located in the Panjsher Valley Area of Interest (AOI) in Afghanistan based on presence of Serpentine minerals, Dolomite minerals, Muscovite, Illite, and Goethite minerals.

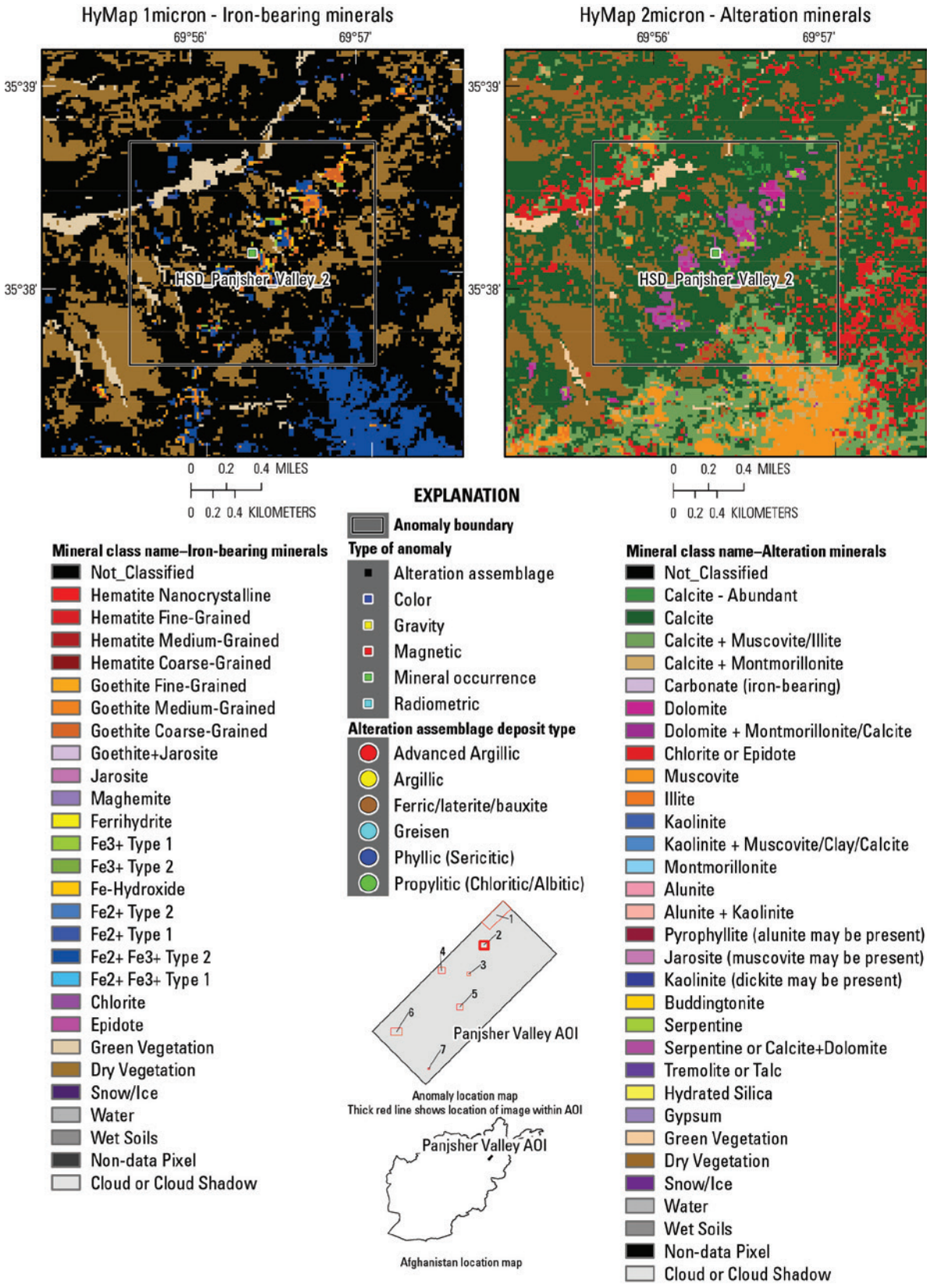

Figure 5.16.2. Hyperspectral anomaly located in the Panjsher Valley Area of Interest (AOI) in Afghanistan based on presence of Serpentine minerals, Dolomite minerals, Goethite minerals, and Fe^{3+} Type1.

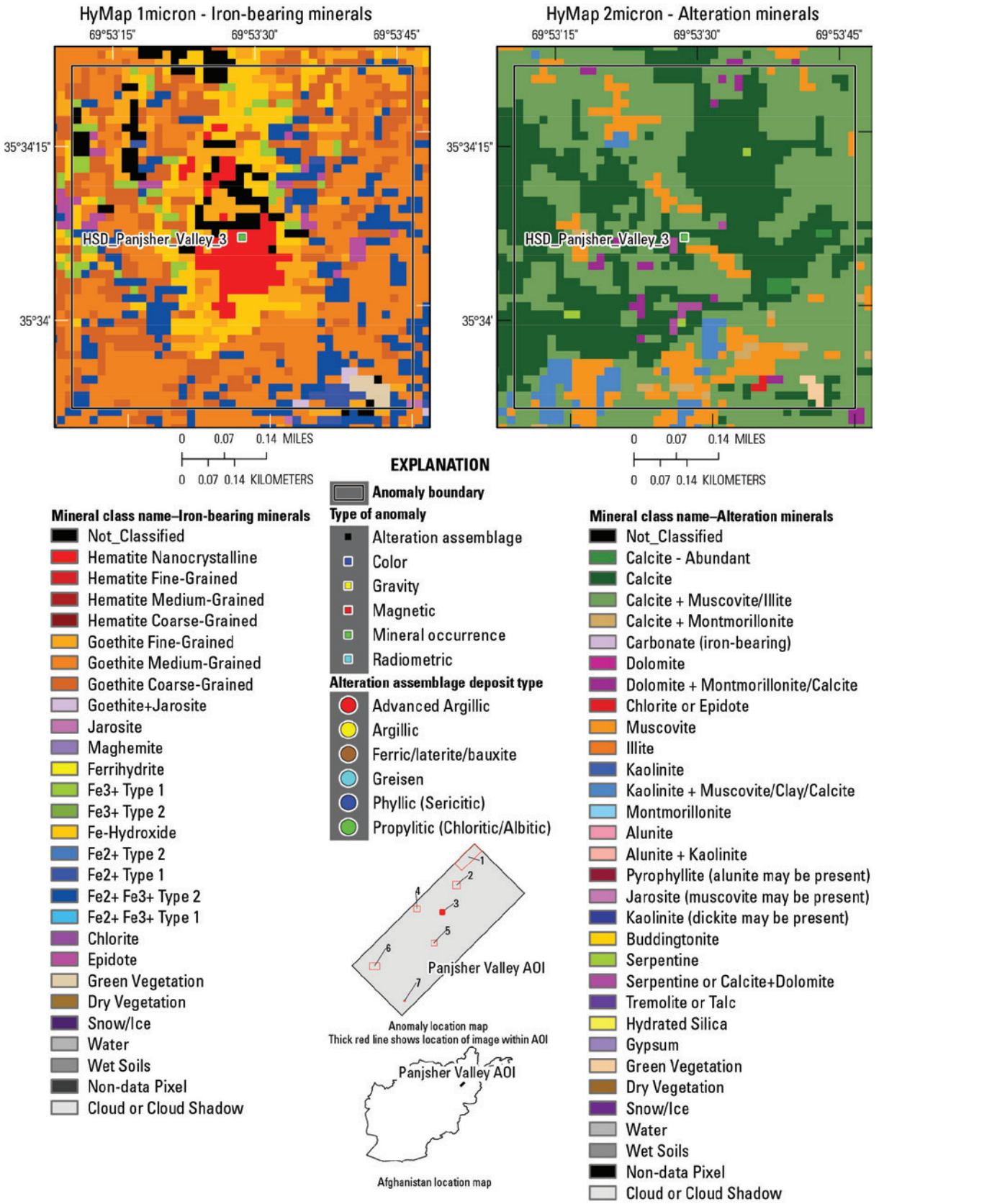

Figure 5.16.3. Hyperspectral anomaly located in the Panjsher Valley Area of Interest (AOI) in Afghanistan based on presence of Hematite minerals, Goethite minerals, Fe^{2+} Fe^{3+} Type2, and Fe^{3+} Type1.

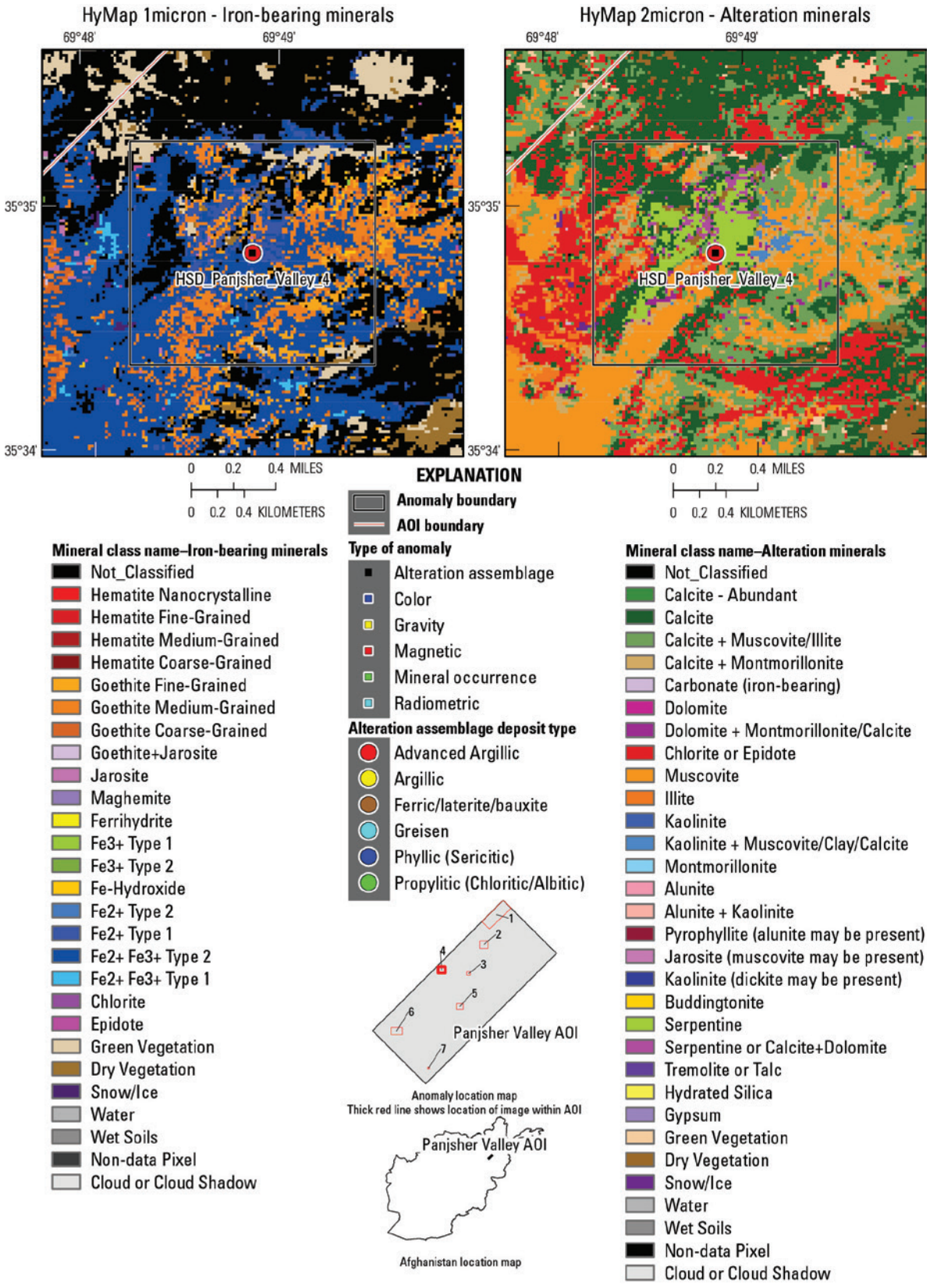

Figure 5.16.4. Hyperspectral anomaly located in the Panjsher Valley Area of Interest (AOI) in Afghanistan based on presence of Serpentine minerals, Dolomite minerals, Goethite minerals, and Fe^{3+} Type1.

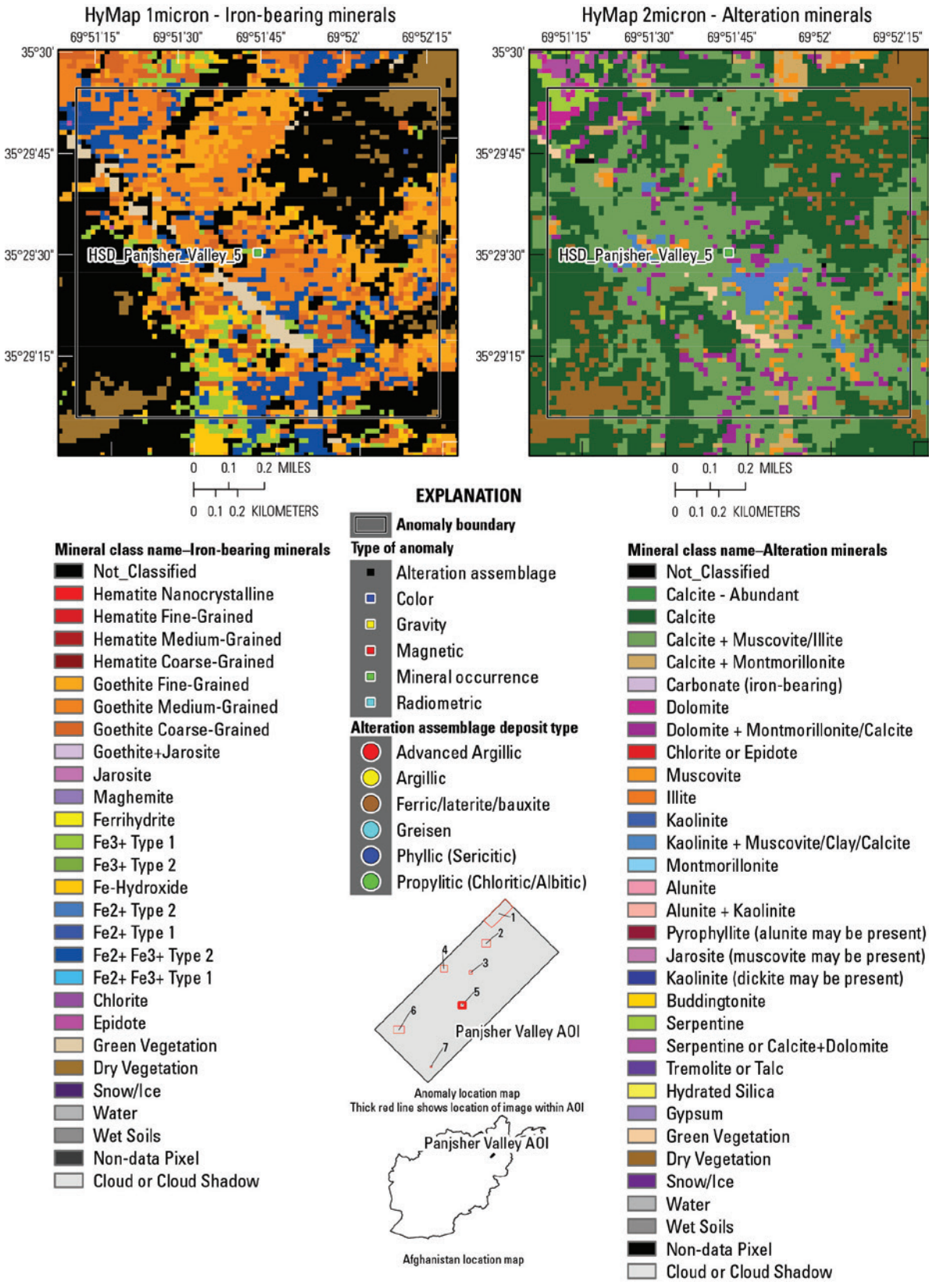

Figure 5.16.5. Hyperspectral anomaly located in the Panjsher Valley Area of Interest (AOI) in Afghanistan based on presence of Kaolinite minerals.

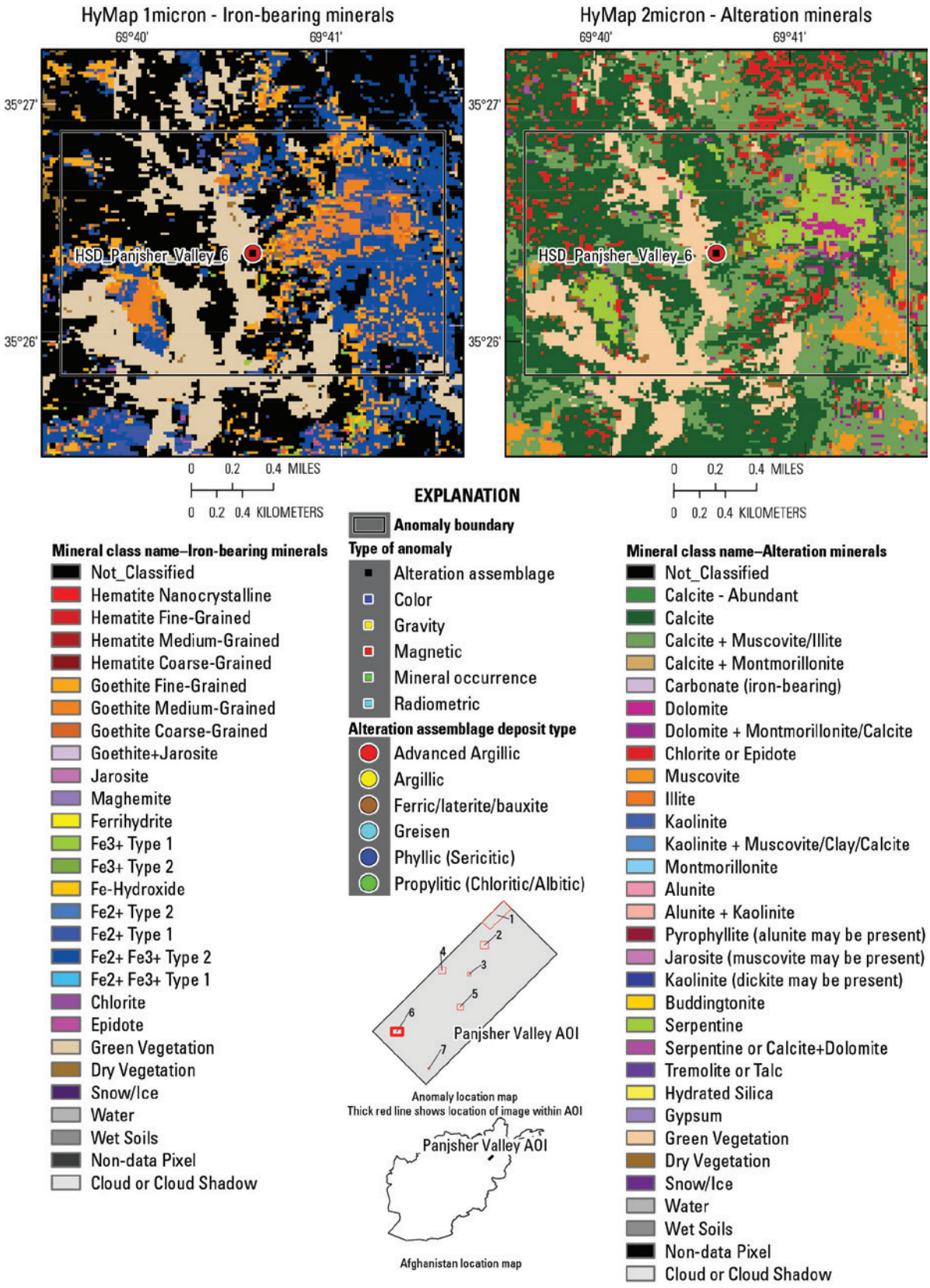

Figure 5.16.6. Hyperspectral anomaly located in the Panjsher Valley Area of Interest (AOI) in Afghanistan based on presence of Serpentine minerals, Dolomite minerals, Goethite minerals, and Jarosite.

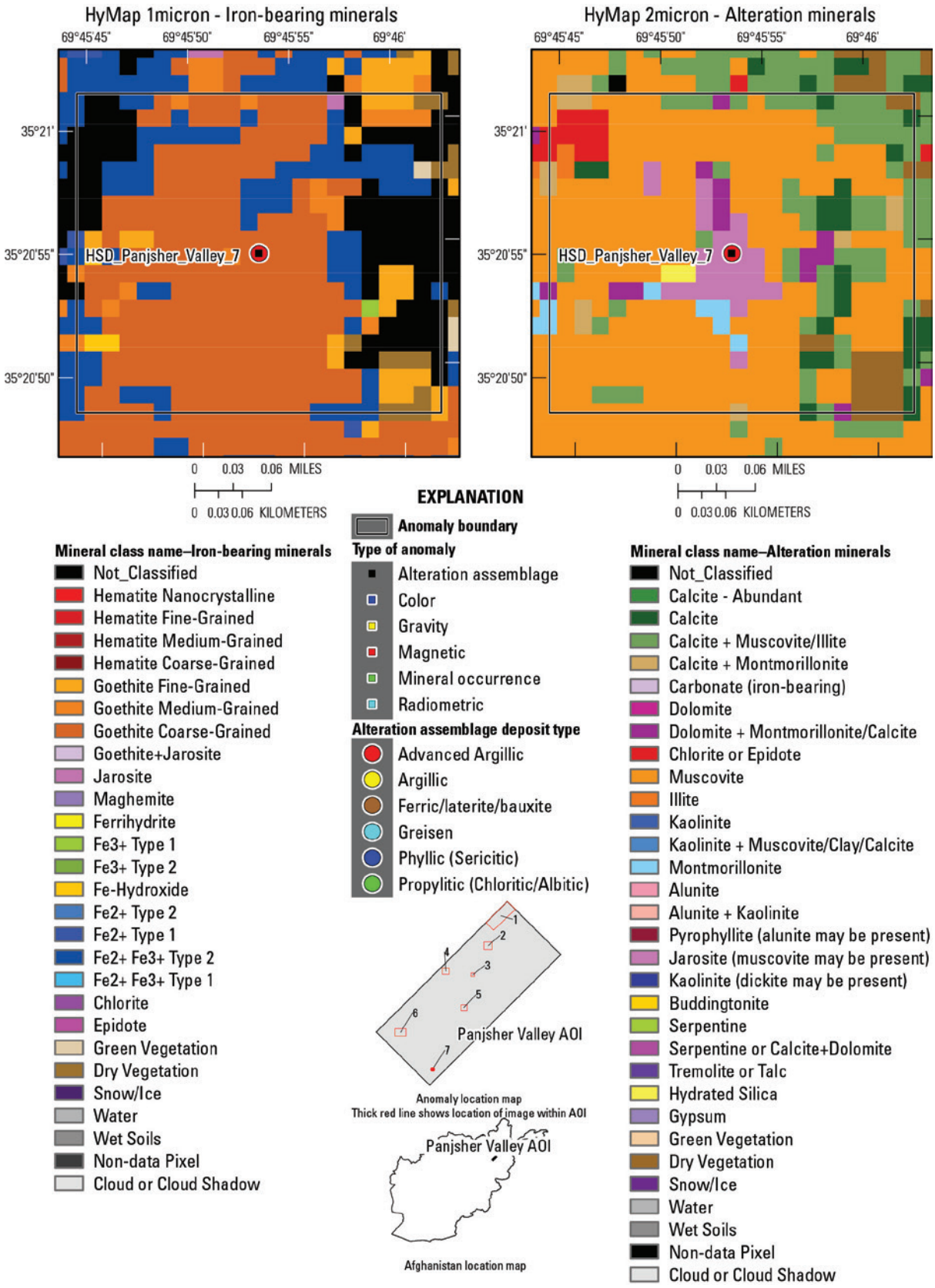

Figure 5.16.7. Hyperspectral anomaly located in the Panjsher Valley Area of Interest (AOI) in Afghanistan based on presence of Jarosite, Hydrated Silica, and Montmorillonite minerals.

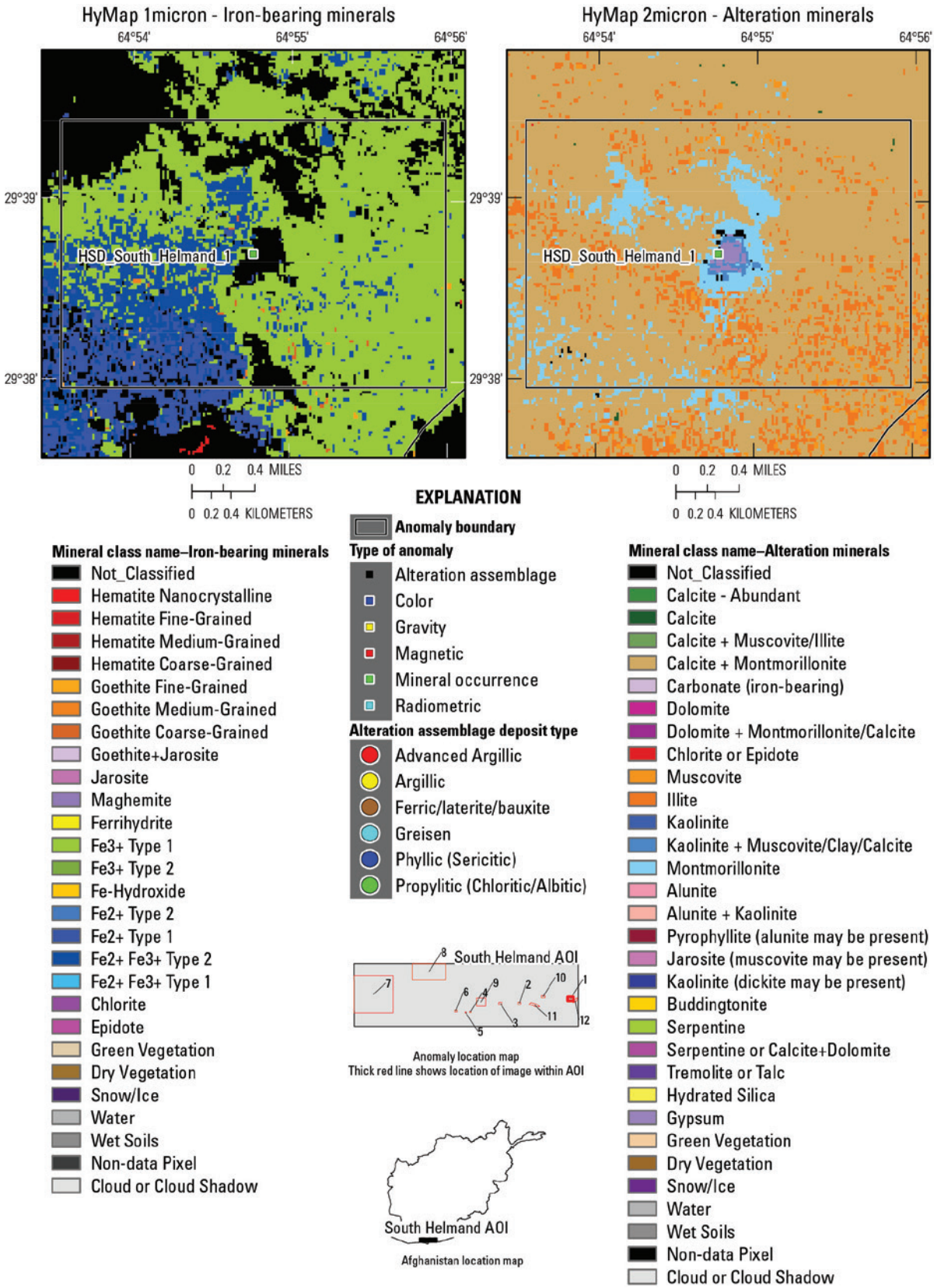

Figure 5.17.1. Hyperspectral anomaly located in the South Helmand Area of Interest (AOI) in Afghanistan based on presence of Gypsum, Kaolinite minerals, and Montmorillonite.

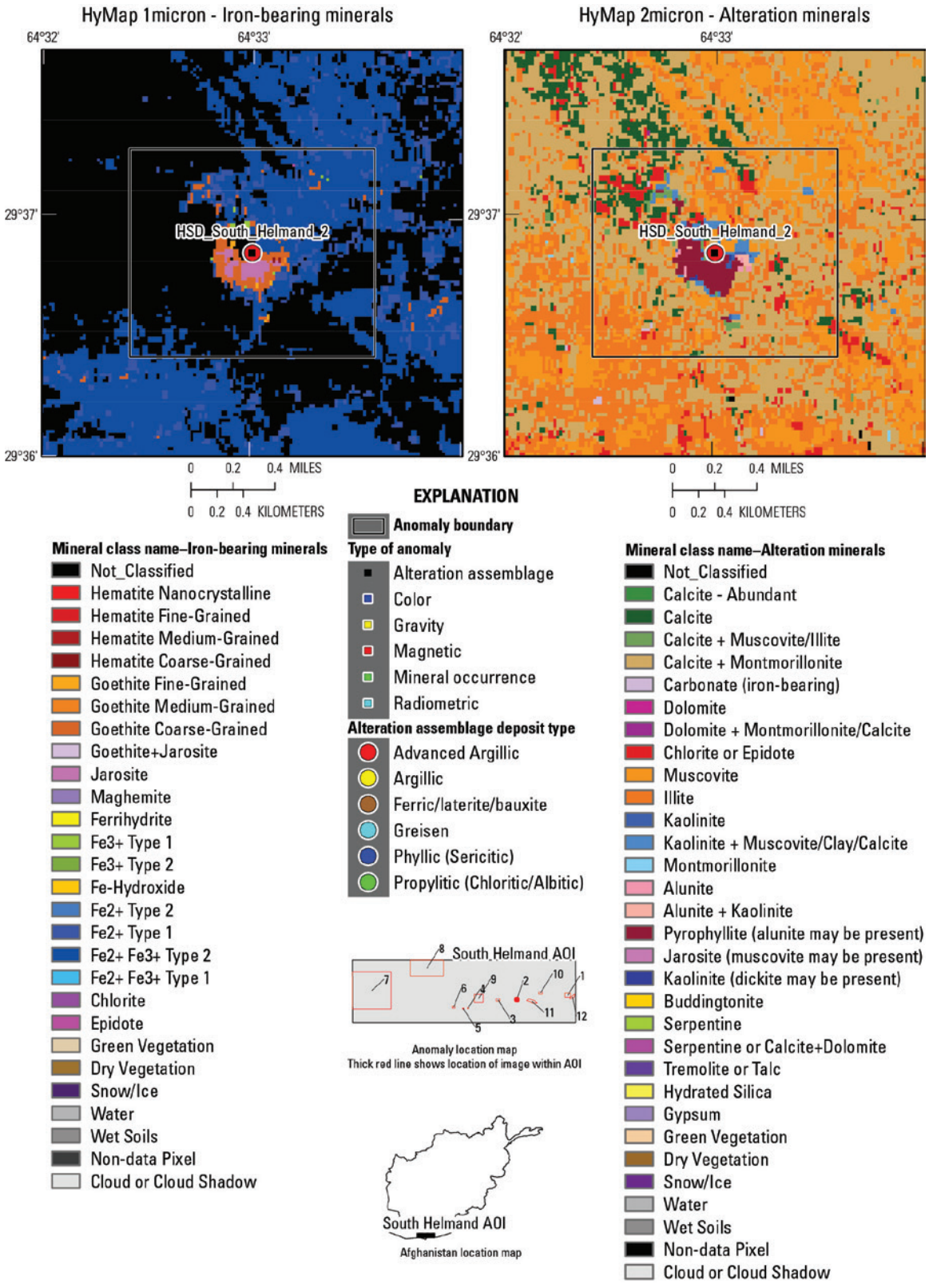

Figure 5.17.2. Hyperspectral anomaly located in the South Helmand Area of Interest (AOI) in Afghanistan based on presence of Pyrophyllite, Alunite minerals, Kaolinite minerals, Dickite, Chlorite or Epidote, Goethite minerals, Jarosite, and Hematite minerals.

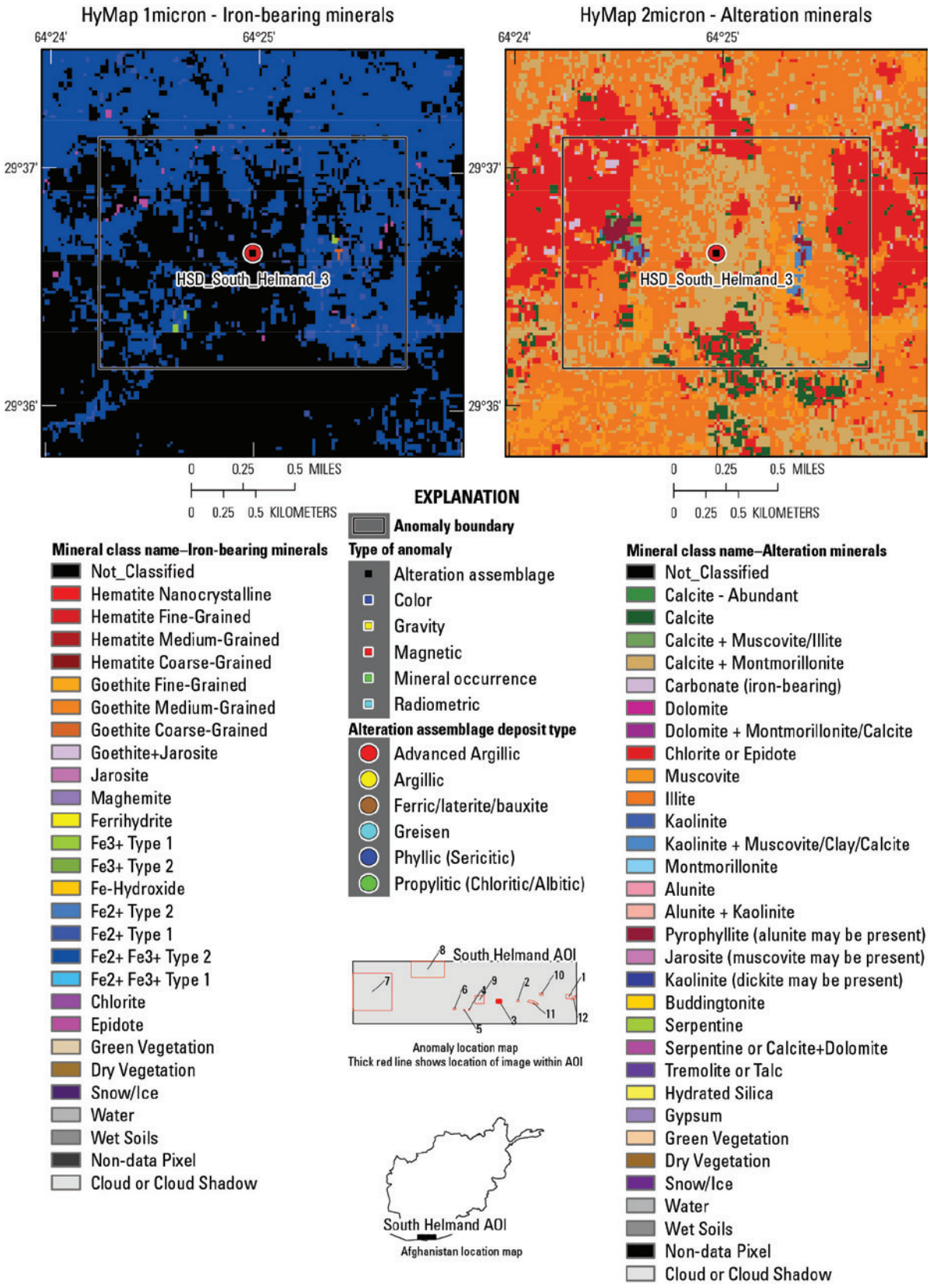

Figure 5.17.3. Hyperspectral anomaly located in the South Helmand Area of Interest (AOI) in Afghanistan based on presence of Pyrophyllite, Alunite minerals, Kaolinite minerals, and Chlorite or Epidote.

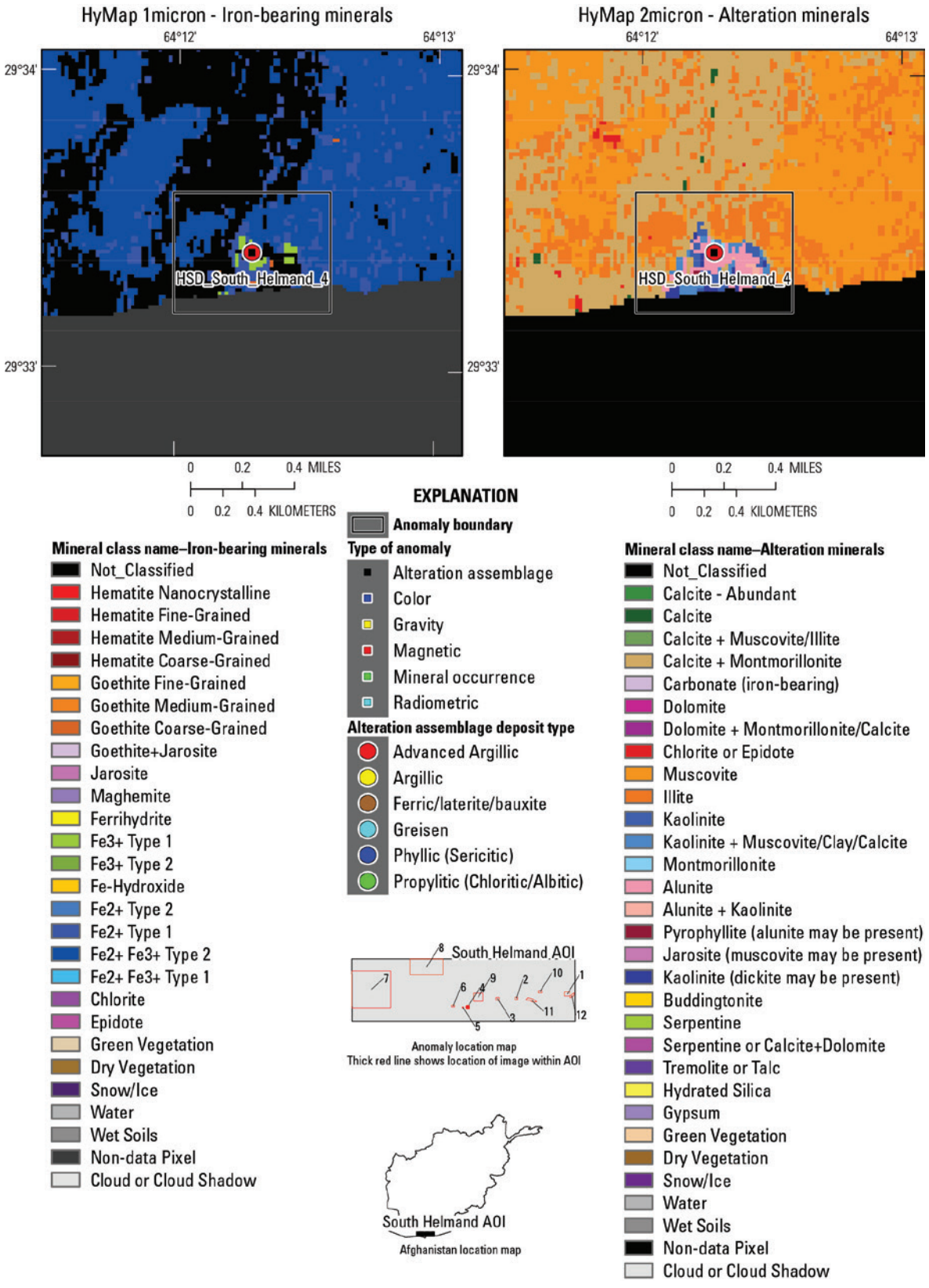

Figure 5.17.4. Hyperspectral anomaly located in the South Helmand Area of Interest (AOI) in Afghanistan based on presence of Pyrophyllite, Alunite minerals, Kaolinite minerals, Dickite, and Chlorite or Epidote.

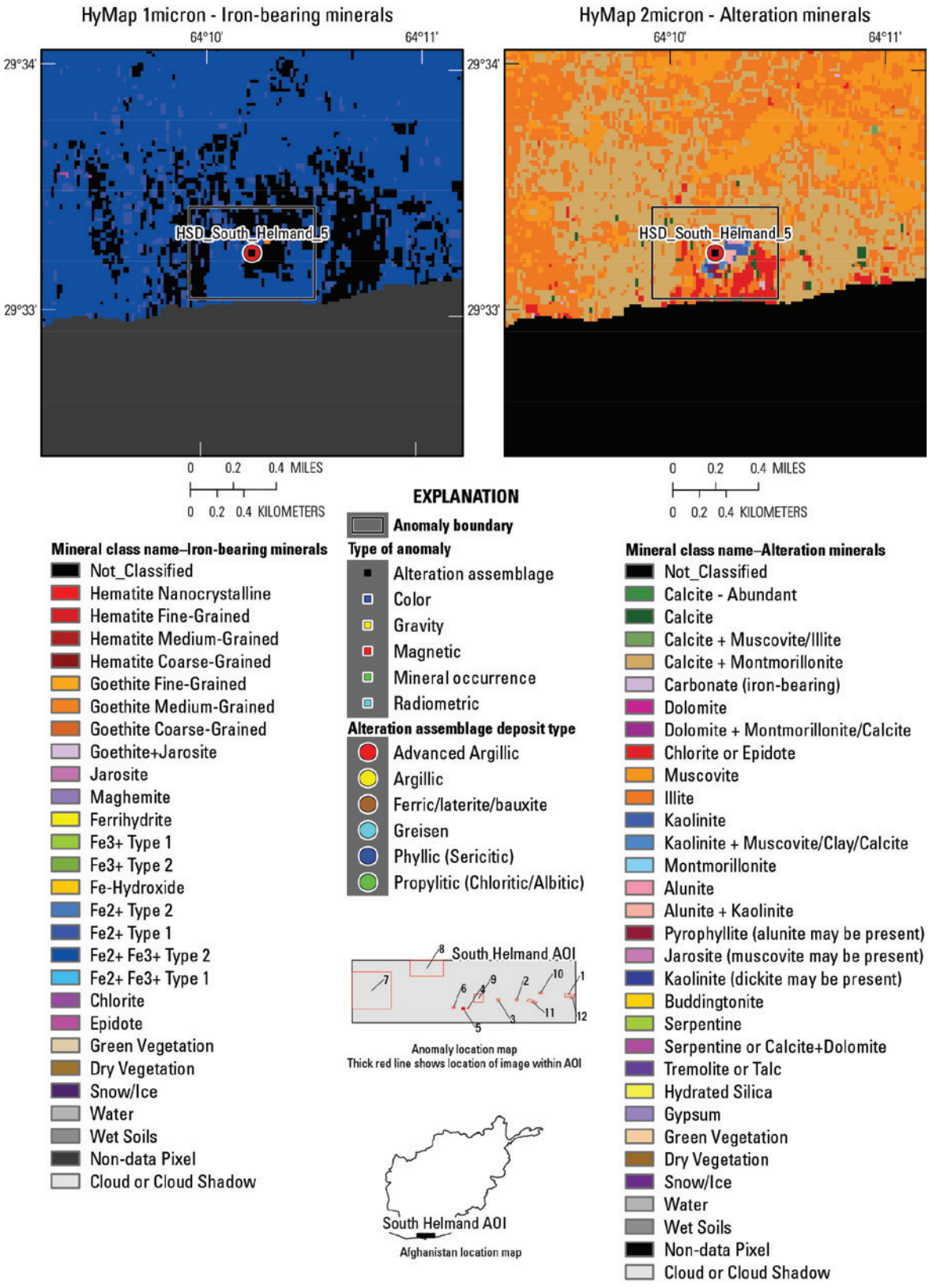

Figure 5.17.5. Hyperspectral anomaly located in the South Helmand Area of Interest (AOI) in Afghanistan based on presence of Pyrophyllite, Alunite minerals, Kaolinite minerals, Dickite, and Chlorite or Epidote.

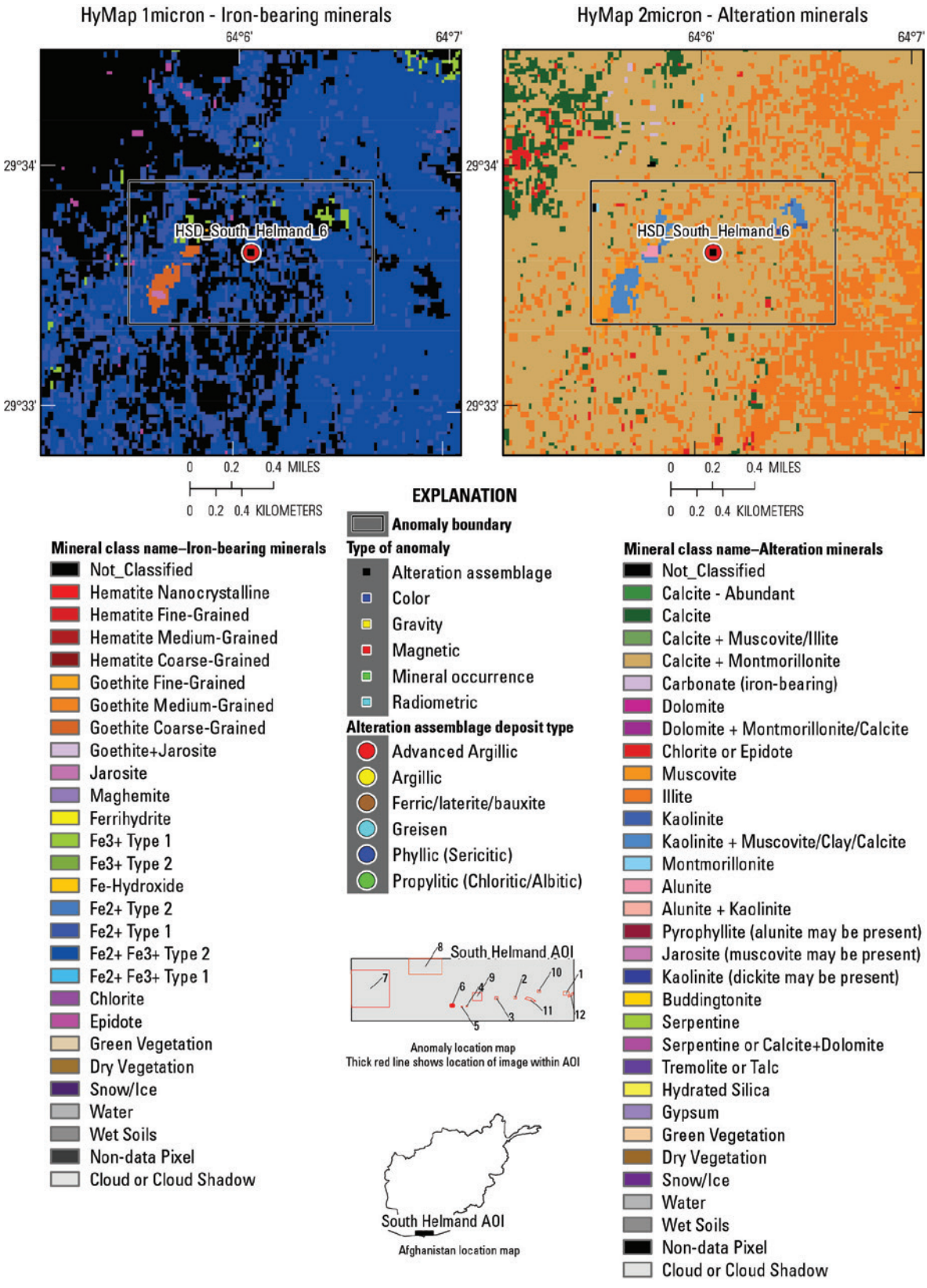

Figure 5.17.6. Hyperspectral anomaly located in the South Helmand Area of Interest (AOI) in Afghanistan based on presence of Alunite minerals, Kaolinite minerals, Dickite, Goethite minerals, Jarosite, and Fe^{3+} Type 1.

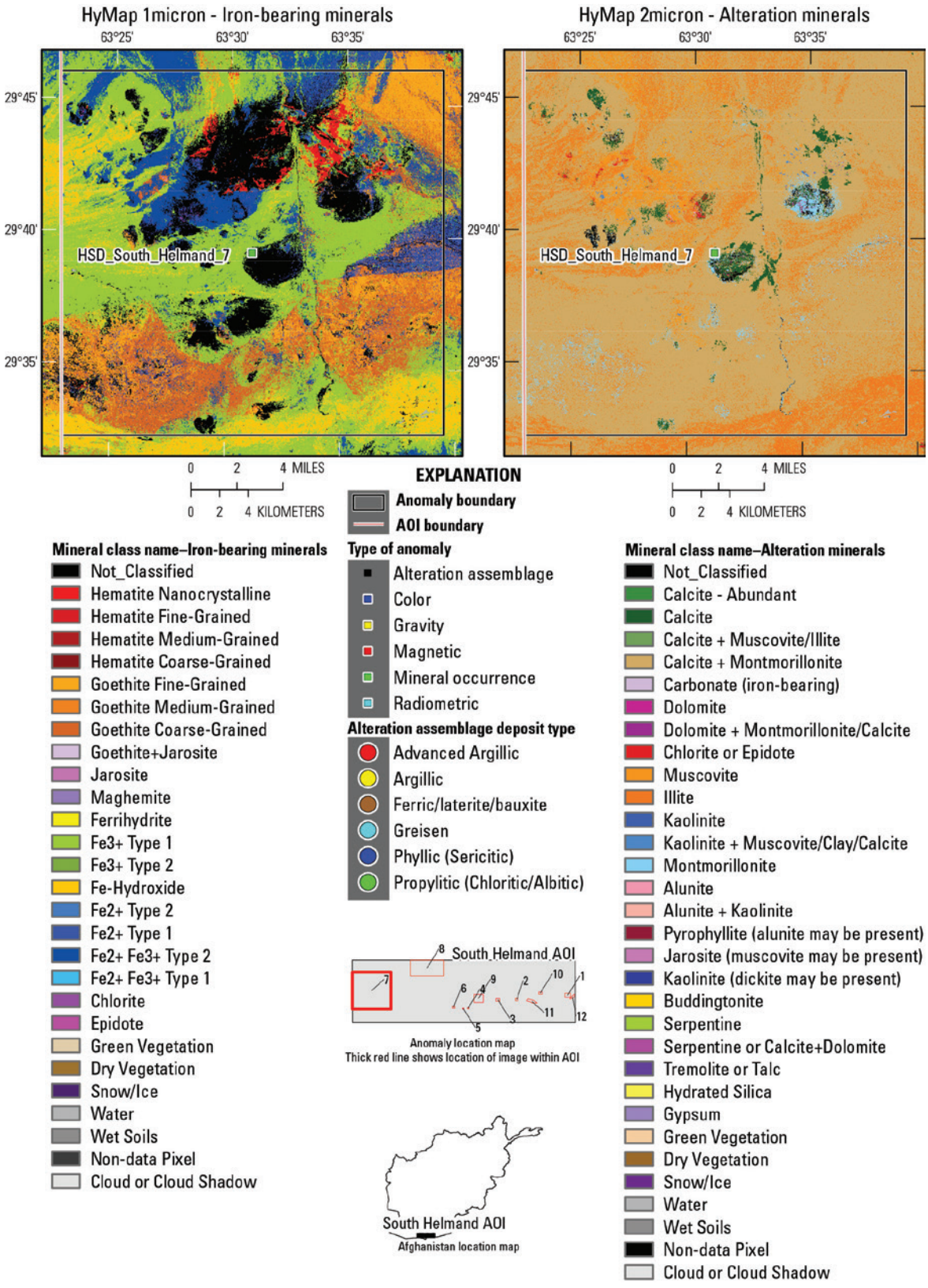

Figure 5.17.7. Hyperspectral anomaly located in the South Helmand Area of Interest (AOI) in Afghanistan based on presence of Montmorillonite, Chlorite or Epidote, Carbonate (iron-bearing), Dolomite minerals, Kaolinite minerals, Hematite minerals, Fe^{3+} Type1, Fe^{2+} Fe^{3+} Type2, Fe-Hydroxide, and Jarosite.

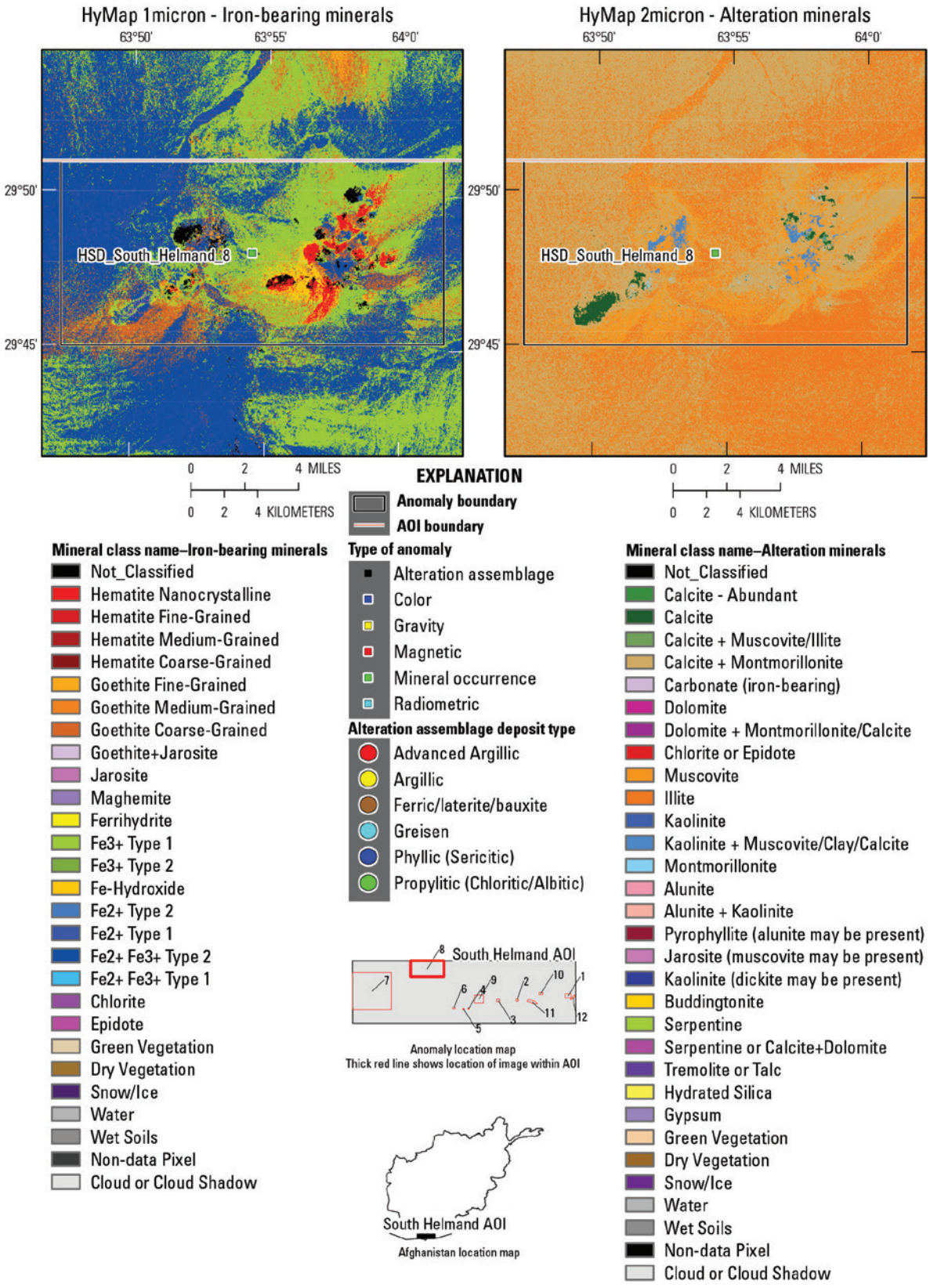

Figure 5.17.8. Hyperspectral anomaly located in the South Helmand Area of Interest (AOI) in Afghanistan based on presence of Calcite, Kaolinite minerals, Montmorillonite, Hematite minerals, Fe-Hydroxide, Goethite minerals, Fe^{3+} Type1, and Fe^{2+} Fe^{3+} Type2.

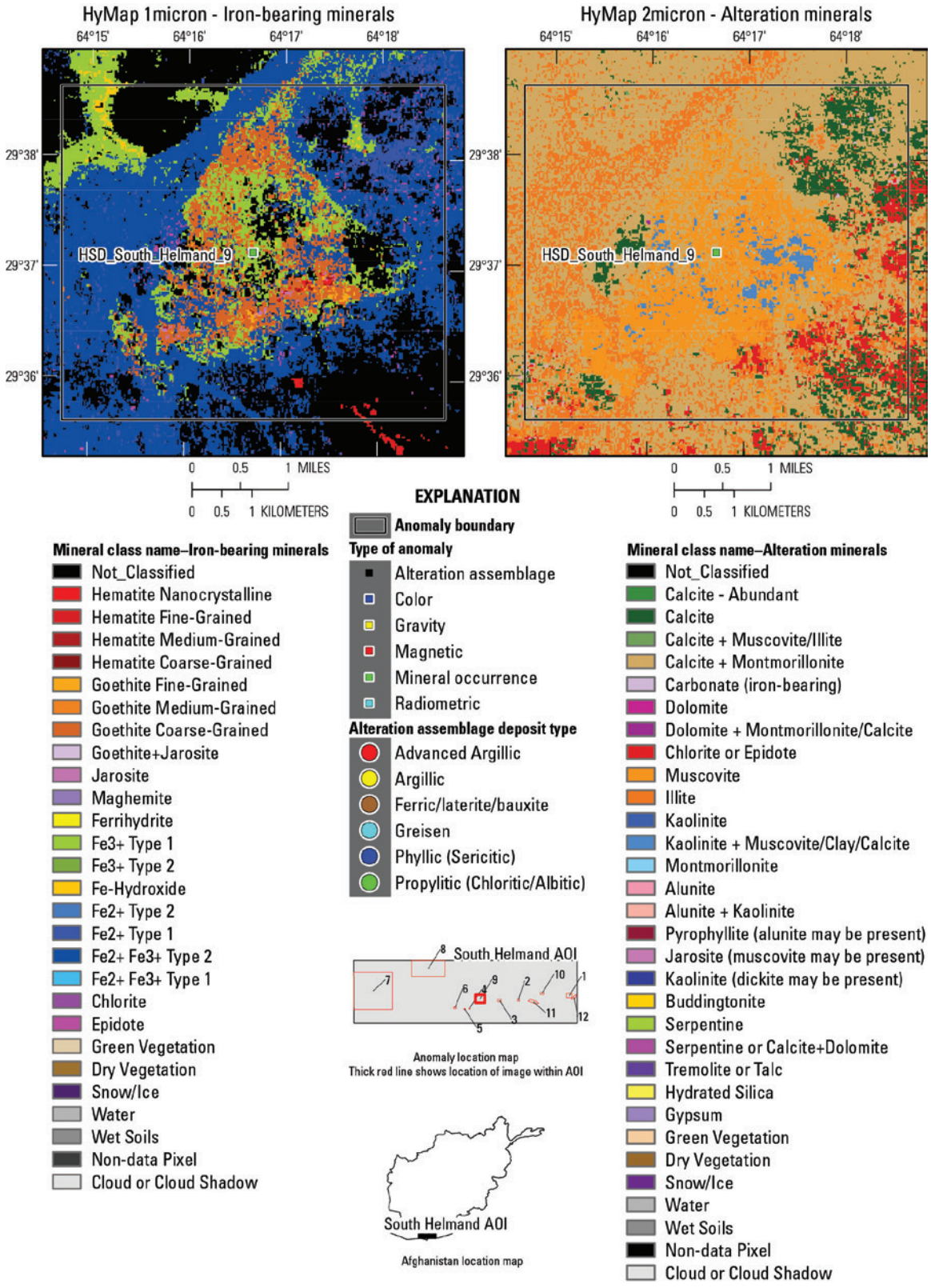

Figure 5.17.9. Hyperspectral anomaly located in the South Helmand Area of Interest (AOI) in Afghanistan based on presence of Kaolinite minerals, Montmorillonite, Goethite minerals, Fe^{3+} Type1, Hematite minerals, and Jarosite.

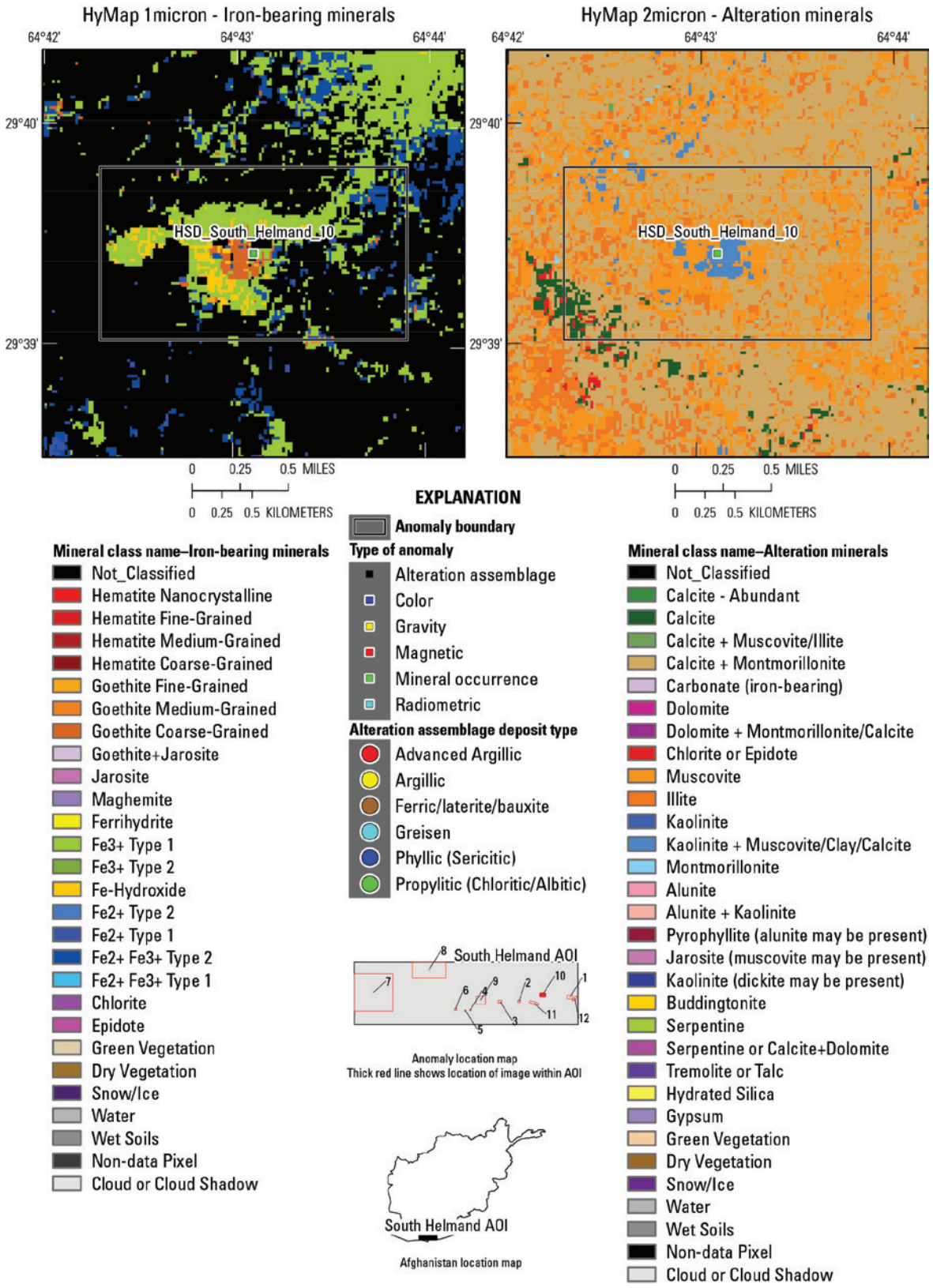

Figure 5.17.10. Hyperspectral anomaly located in the South Helmand Area of Interest (AOI) in Afghanistan based on presence of Muscovite, Illite, Kaolinite minerals, Goethite minerals, Fe^{3+} Type1, Fe-Hydroxide, and Hematite minerals.

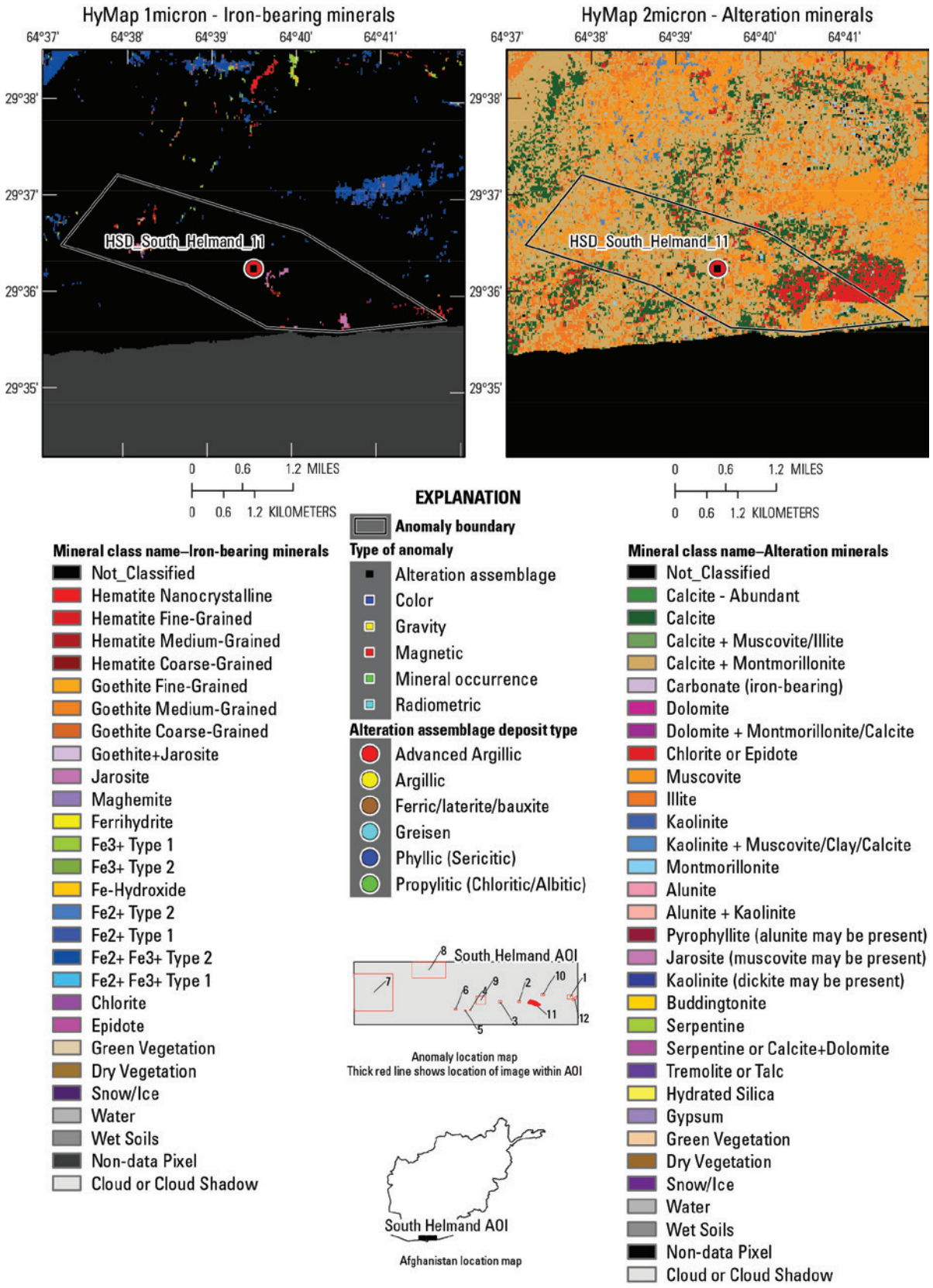

Figure 5.17.11. Hyperspectral anomaly located in the South Helmand Area of Interest (AOI) in Afghanistan based on presence of Jarosite, Hematite minerals, and Goethite minerals.

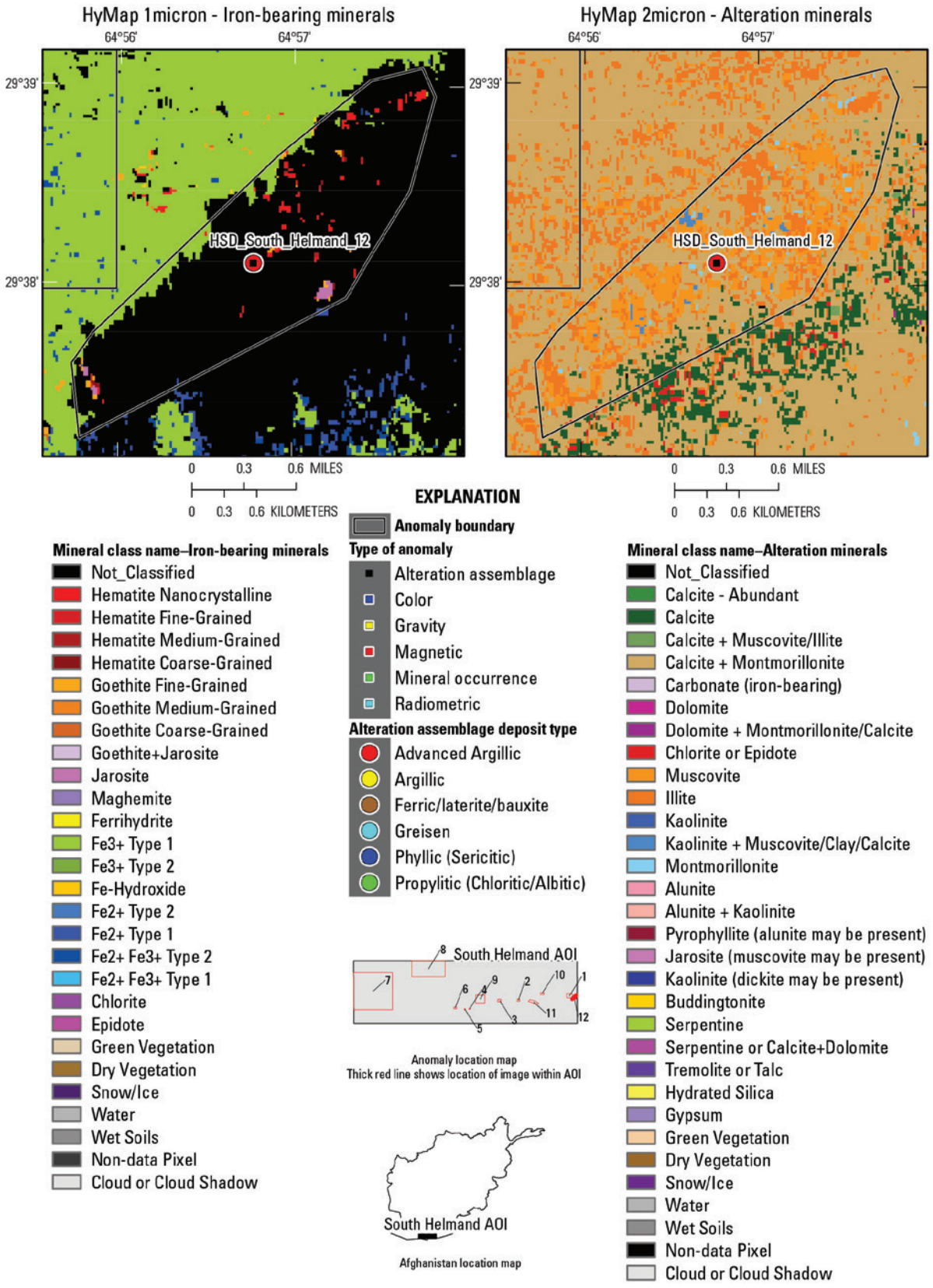

Figure 5.17.12. Hyperspectral anomaly located in the South Helmand Area of Interest (AOI) in Afghanistan based on presence of Jarosite, Hematite minerals, and Goethite minerals.

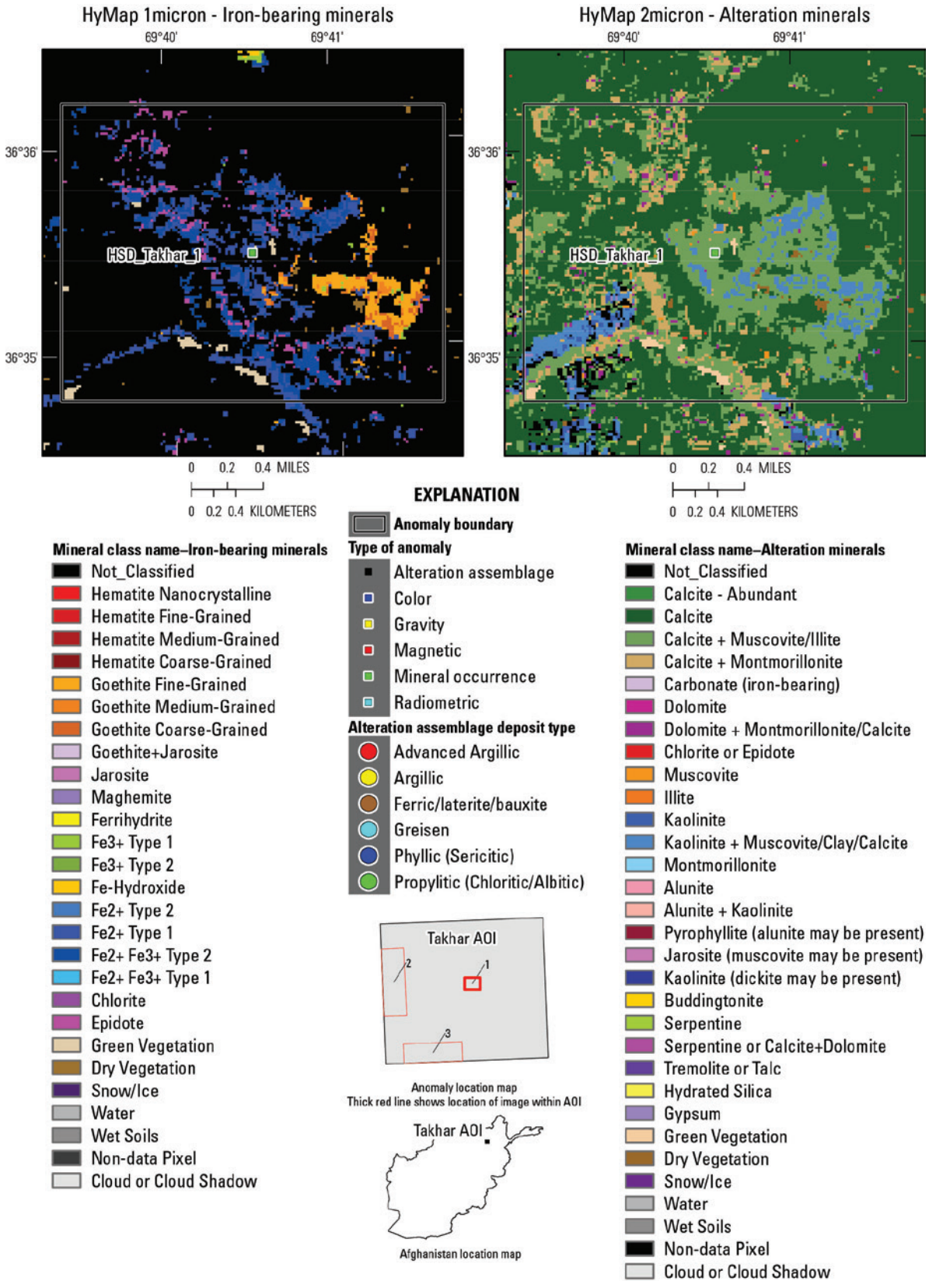

Figure 5.18.1. Hyperspectral anomaly located in the Takhar Area of Interest (AOI) in Afghanistan based on presence of Goethite minerals, Fe^{3+} Type 1, and Epidote.

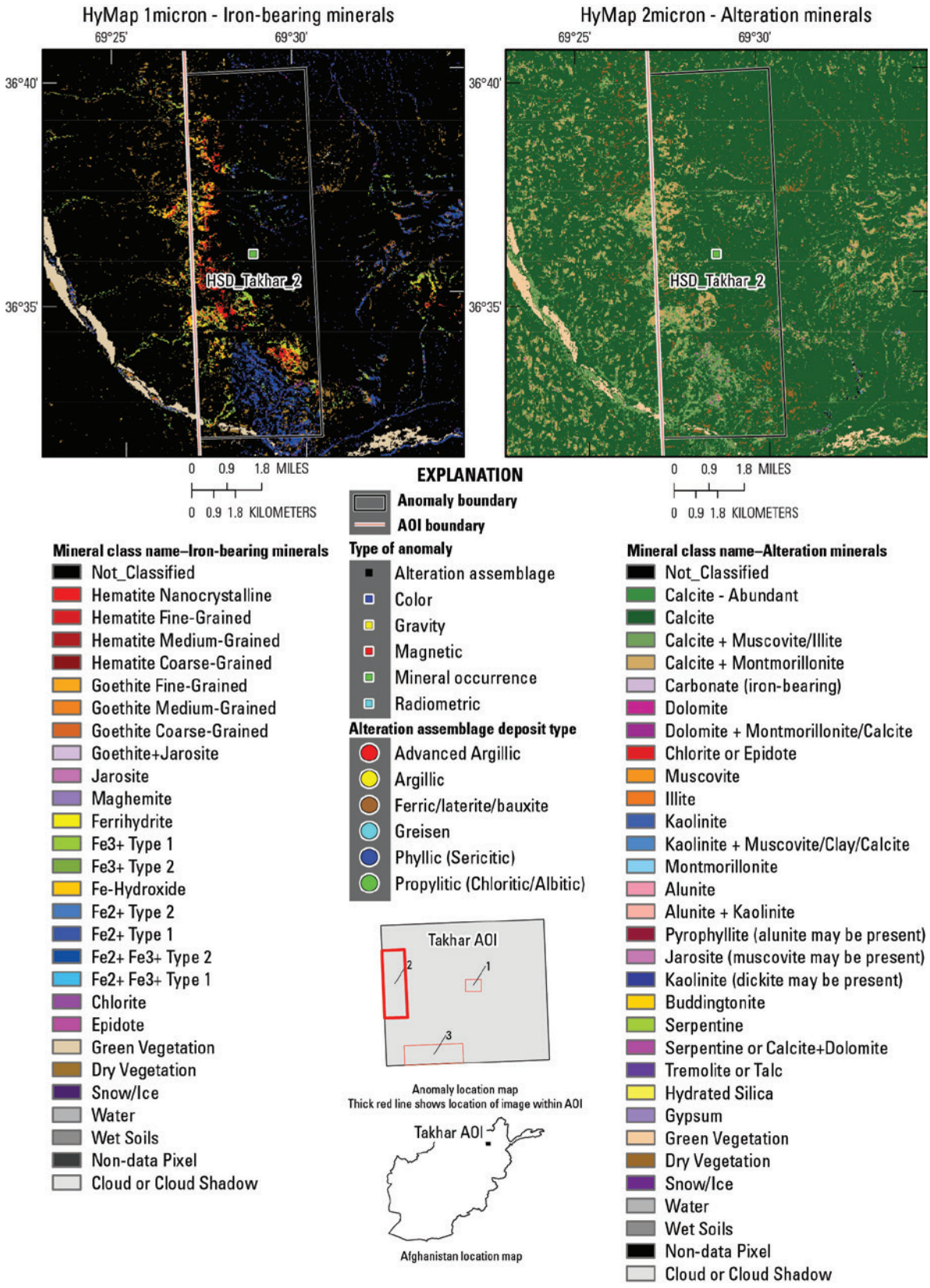

Figure 5.18.2. Hyperspectral anomaly located in the Takhar Area of Interest (AOI) in Afghanistan based on presence of Hematite, Goethite minerals, Fe-Hydroxide, and Fe^{3+} Type 1.

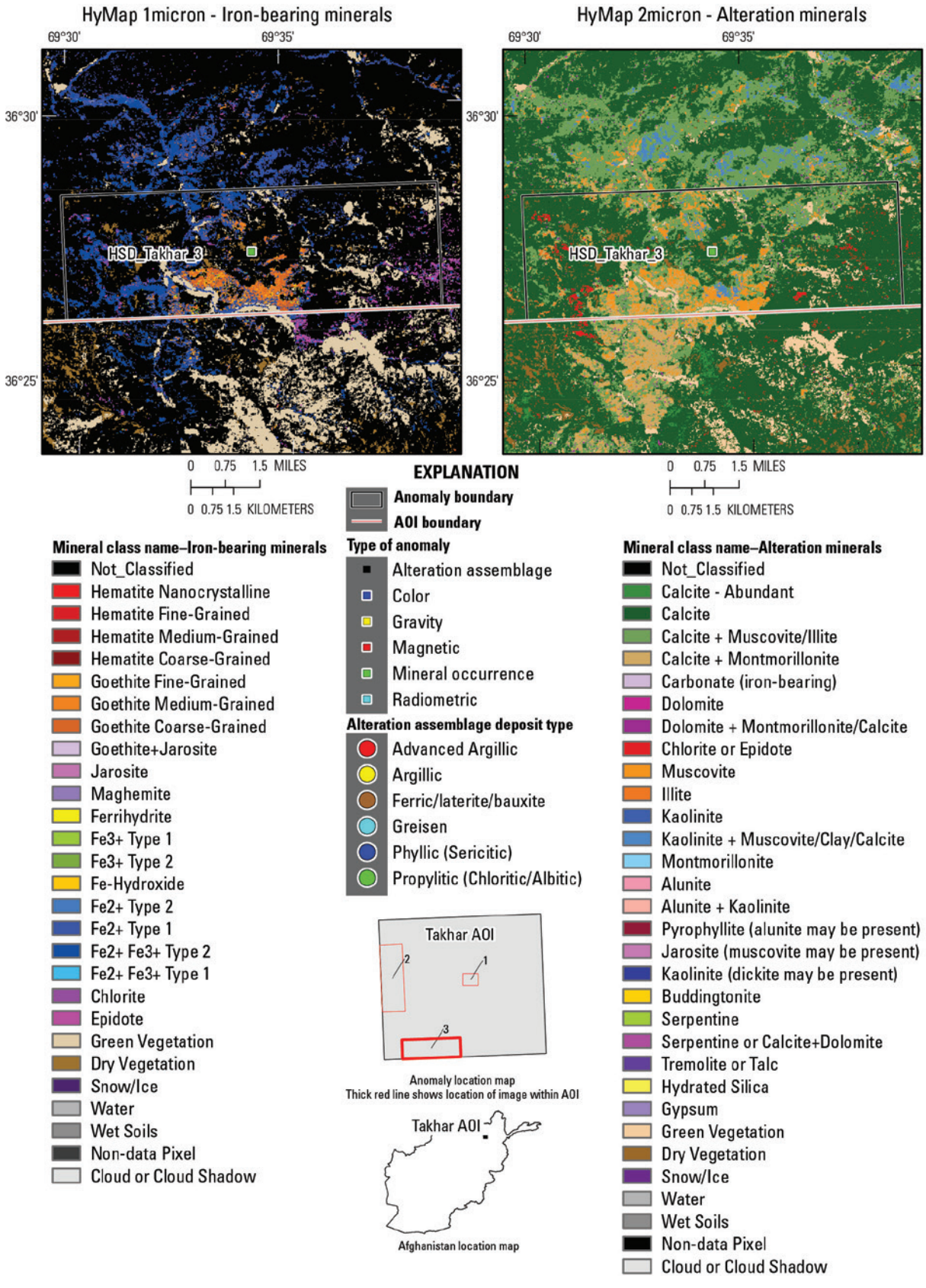

Figure 5.18.3. Hyperspectral anomaly located in the Takhar Area of Interest (AOI) in Afghanistan based on presence of Chlorite or Epidote, Kaolinite minerals, Muscovite, Goethite minerals, and Fe^{3+} Type 1.

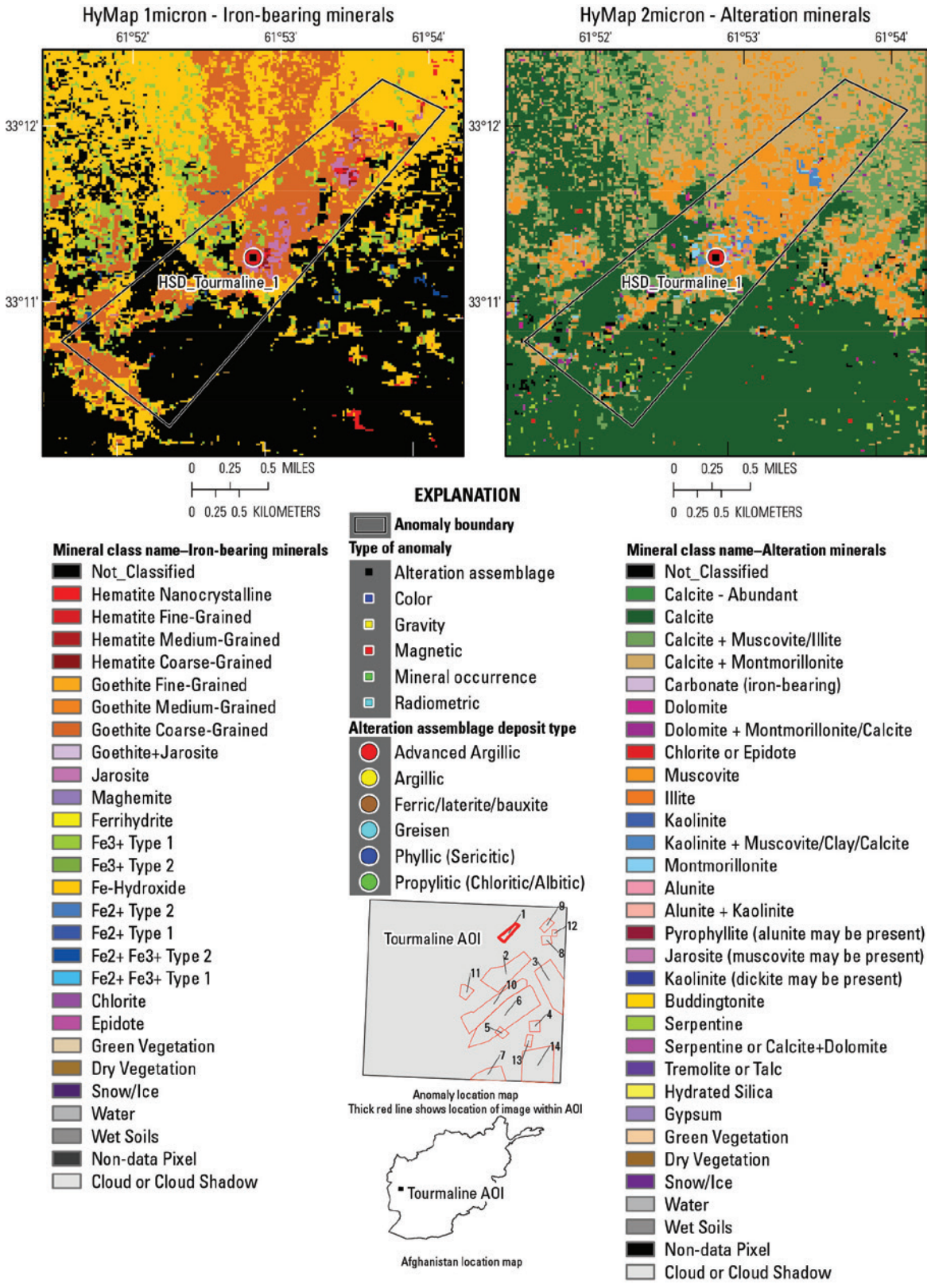

Figure 5.19.1. Hyperspectral anomaly located in the Tourmaline Area of Interest (AOI) in Afghanistan based on presence of Muscovite, Kaolinite minerals, Montmorillonite, Dolomite minerals, Jarosite, Goethite minerals, Fe-Hydroxide, Fe^{3+} Type1, and Hematite minerals.

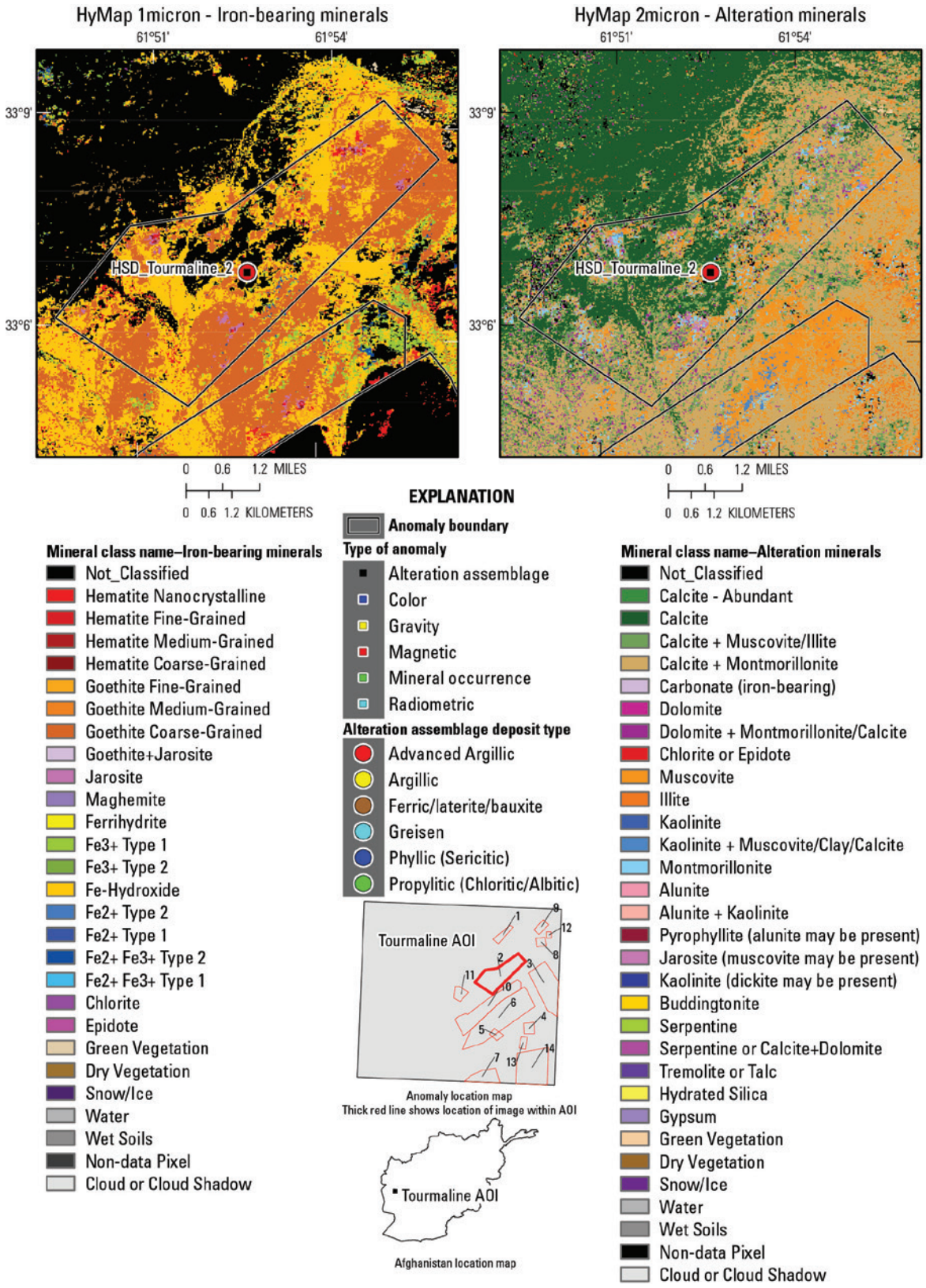

Figure 5.19.2. Hyperspectral anomaly located in the Tourmaline Area of Interest (AOI) in Afghanistan based on presence of Calcite, Montmorillonite, Dolomite minerals, Kaolinite minerals, Muscovite, Jarosite, Hydrated Silica, Goethite minerals, Fe-Hydroxide, and Hematite minerals.

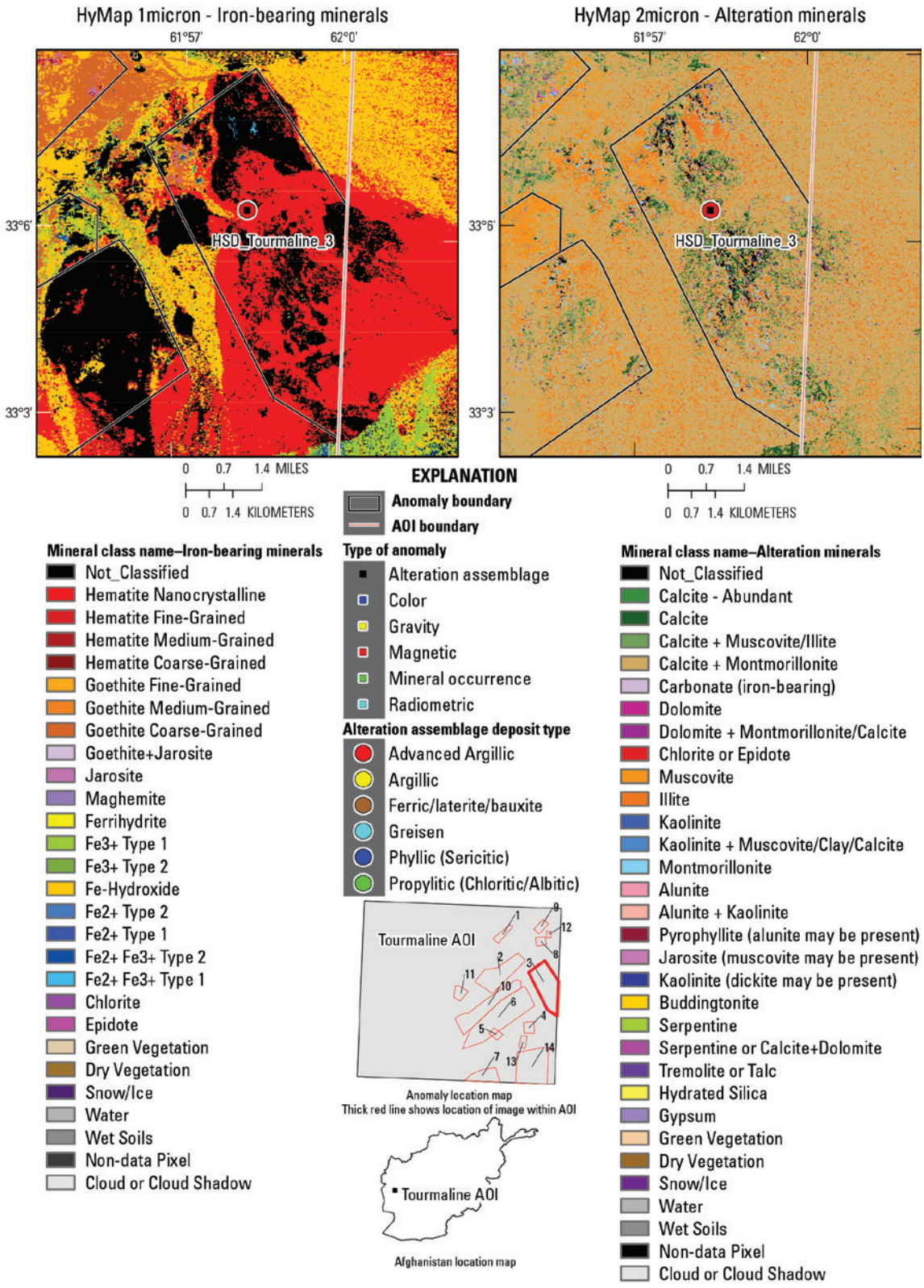

Figure 5.19.3. Hyperspectral anomaly located in the Tourmaline Area of Interest (AOI) in Afghanistan based on presence of Muscovite, Illite, Serpentine minerals, Montmorillonite, Dolomite minerals, Jarosite, Hematite minerals, Goethite minerals, Fe-Hydroxide, and Jarosite.

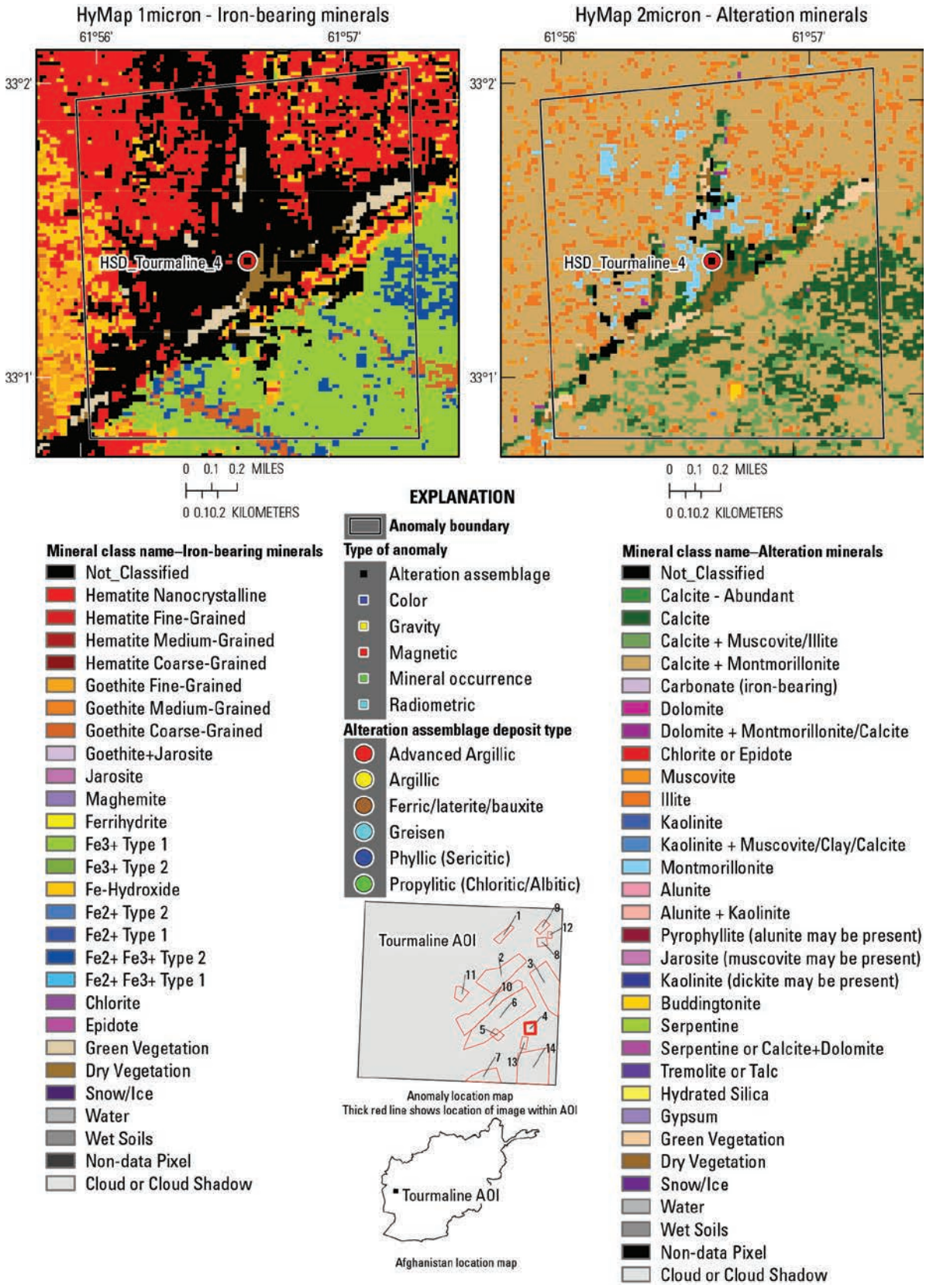

Figure 5.19.4. Hyperspectral anomaly located in the Tourmaline Area of Interest (AOI) in Afghanistan based on presence of Montmorillonite, Serpentine minerals, Buddingtonite, Hematite minerals, and Fe^{3+} Type1.

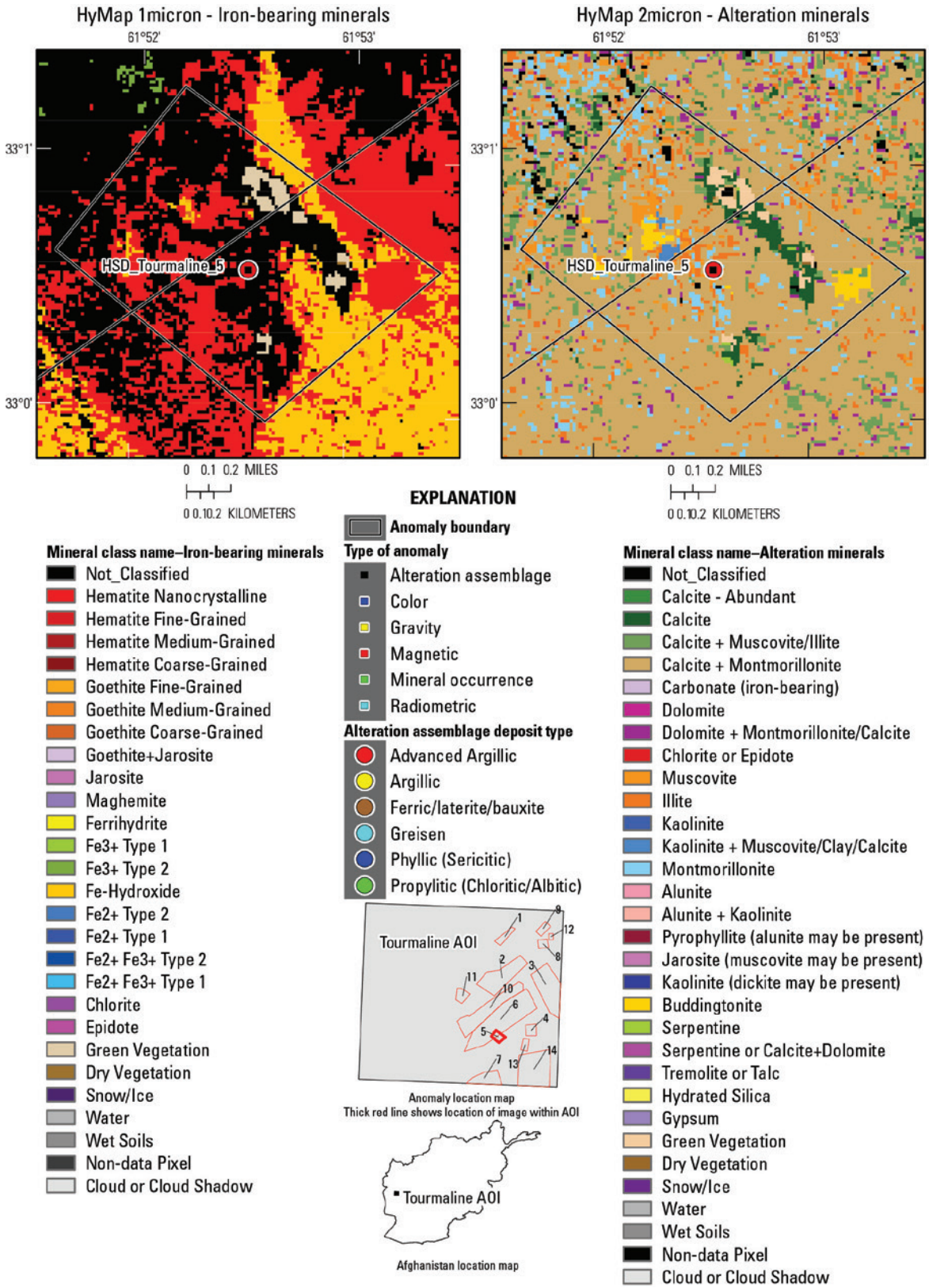

Figure 5.19.5. Hyperspectral anomaly located in the Tourmaline Area of Interest (AOI) in Afghanistan based on presence of Montmorillonite, Kaolinite minerals, Muscovite, Illite, Buddingtonite, Hematite minerals, and Fe-Hydroxide.

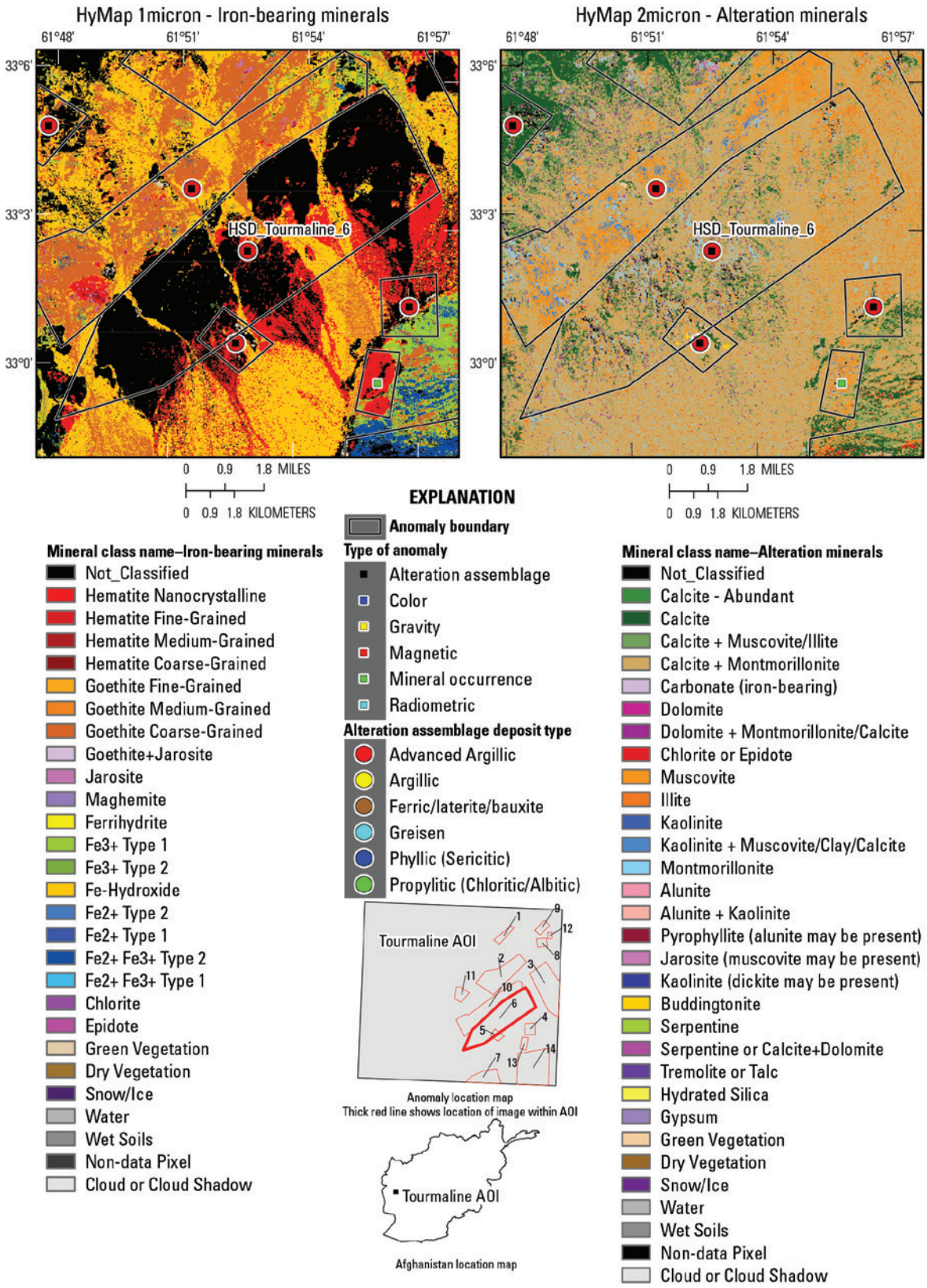

Figure 5.19.6. Hyperspectral anomaly located in the Tourmaline Area of Interest (AOI) in Afghanistan based on presence of Montmorillonite, Dolomite minerals, Kaolinite minerals, Muscovite, and Illite.

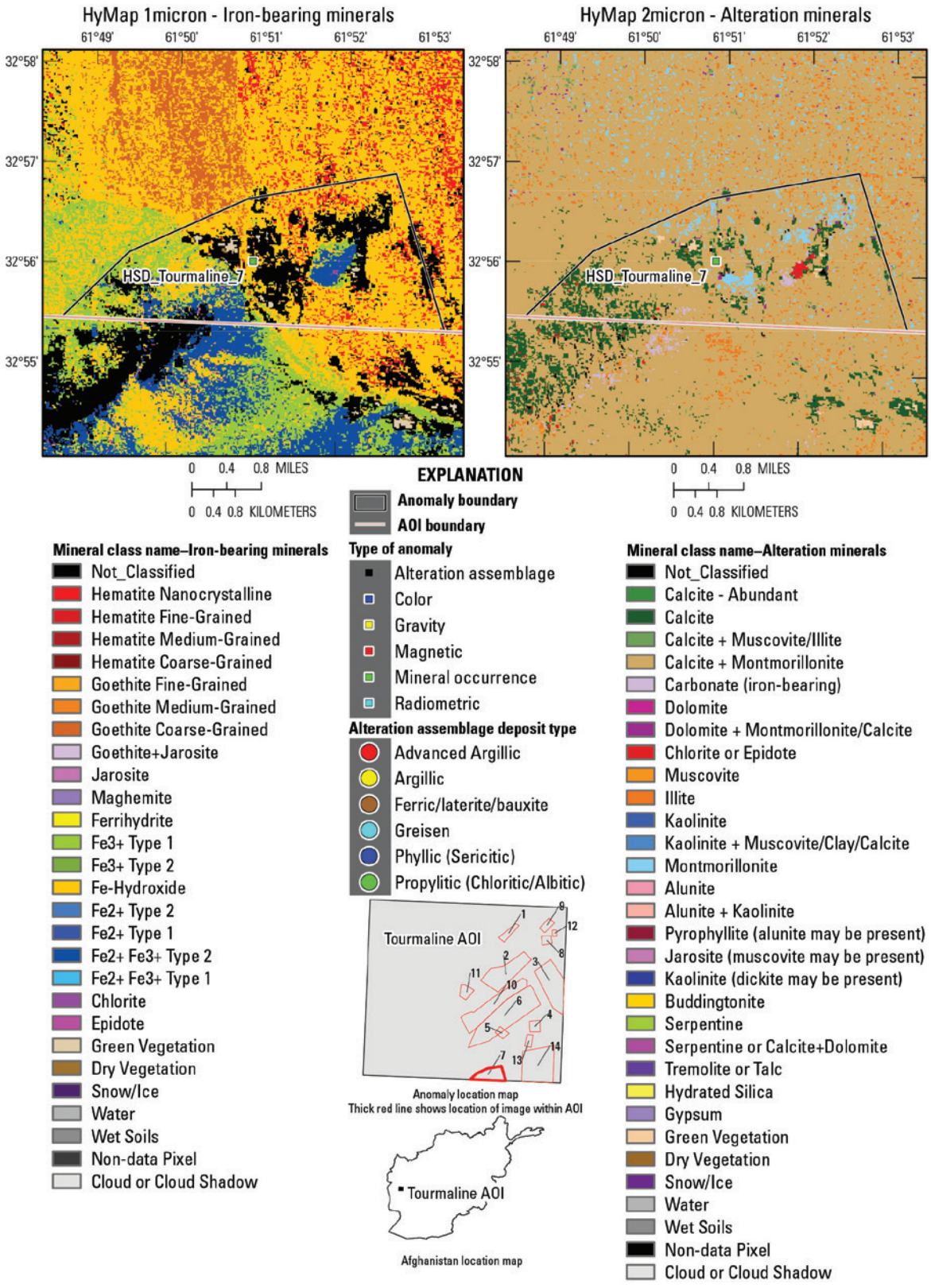

Figure 5.19.7. Hyperspectral anomaly located in the Tourmaline Area of Interest (AOI) in Afghanistan based on presence of Calcite (iron-bearing), Chlorite or Epidote, Montmorillonite, Fe^{2+} Fe^{3+} Type2, Fe^{3+} Type1, and Fe-Hydroxide.

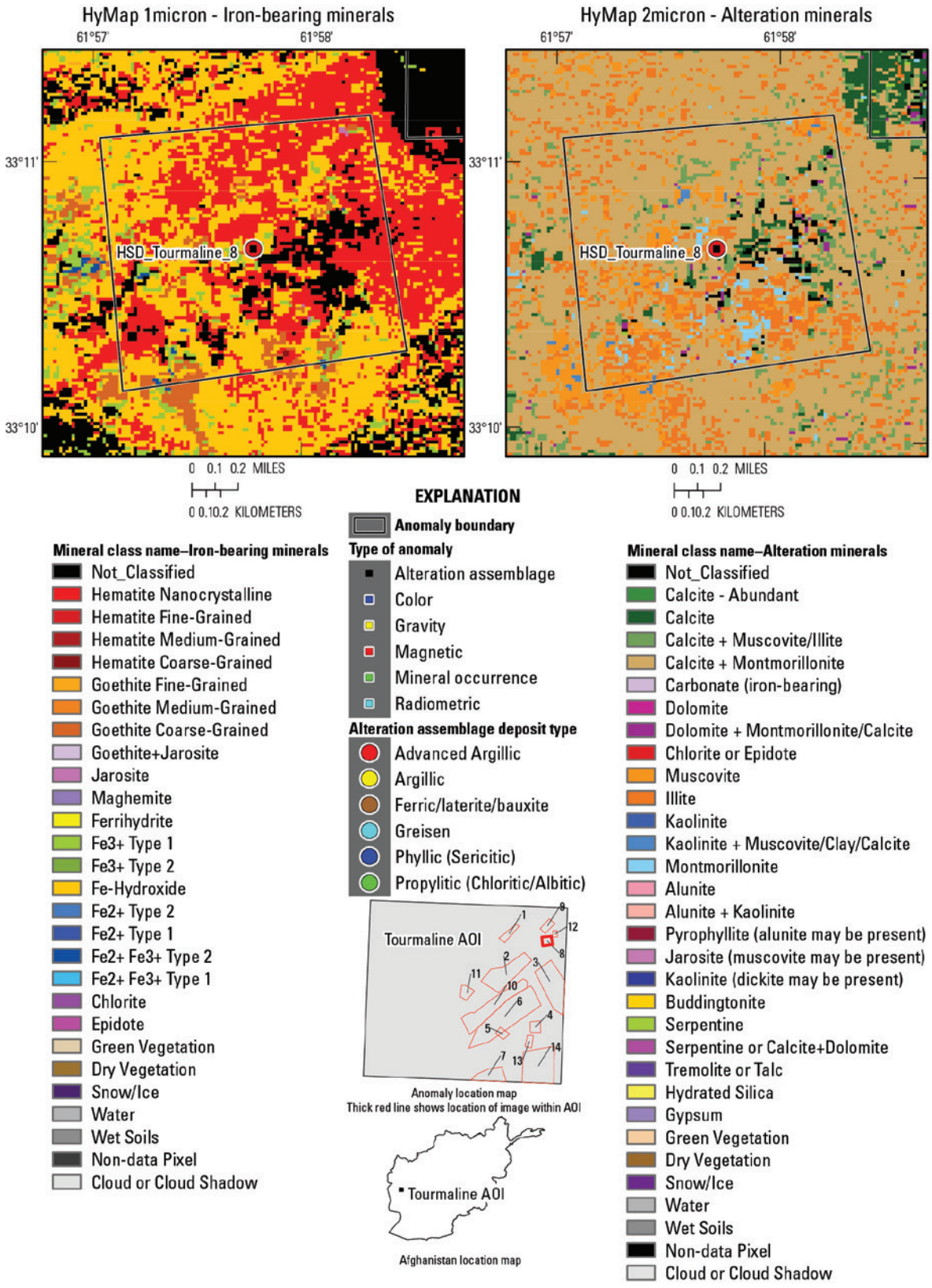

Figure 5.19.8. Hyperspectral anomaly located in the Tourmaline Area of Interest (AOI) in Afghanistan based on presence of Muscovite, Illite, Montmorillonite, Dolomite minerals, Kaolinite minerals, Jarosite, Hematite minerals, and Fe-Hydroxide.

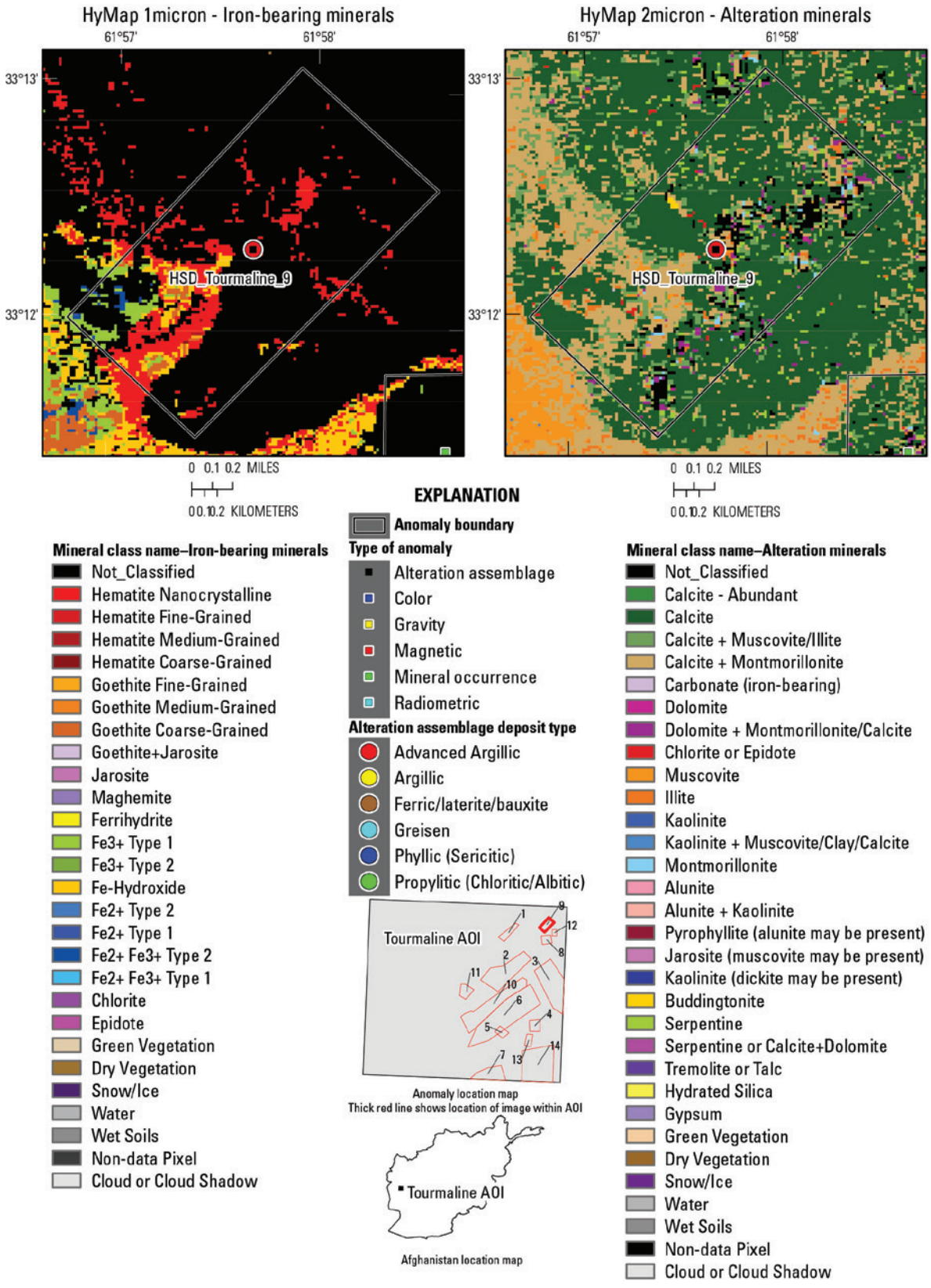

Figure 5.19.9. Hyperspectral anomaly located in the Tourmaline Area of Interest (AOI) in Afghanistan based on presence of Dolomite minerals, Serpentine minerals, Montmorillonite, and Buddingtonite.

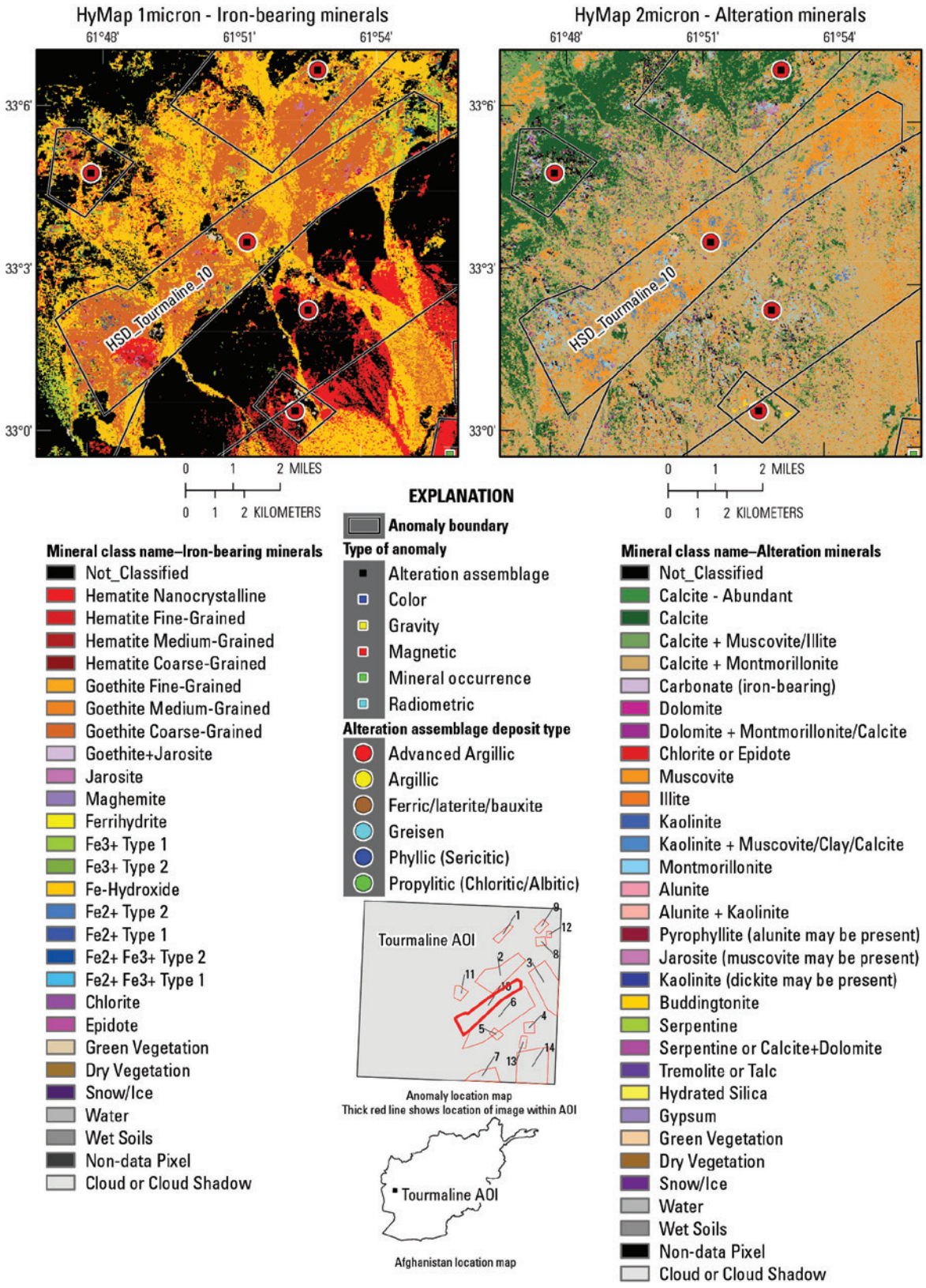

Figure 5.19.10. Hyperspectral anomaly located in the Tourmaline Area of Interest (AOI) in Afghanistan based on presence of Muscovite, Illite, Kaolinite minerals, Montmorillonite, Jarosite, Dolomite minerals, Goethite minerals, Hematite minerals, and Fe^{2+} Type 1.

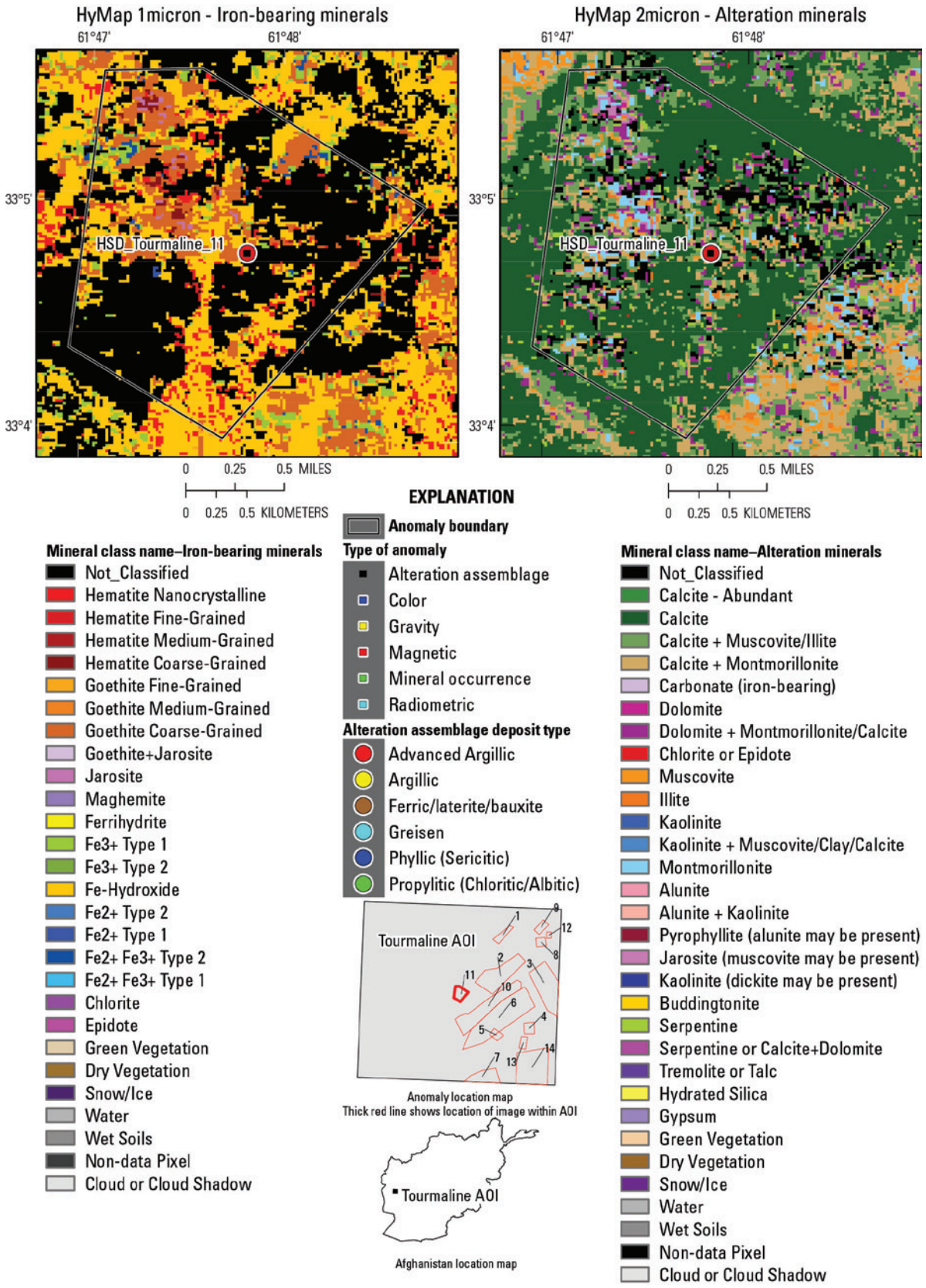

Figure 5.19.11. Hyperspectral anomaly located in the Tourmaline Area of Interest (AOI) in Afghanistan based on presence of Dolomite minerals, Montmorillonite, Jarosite, Goethite minerals, and Hematite minerals.

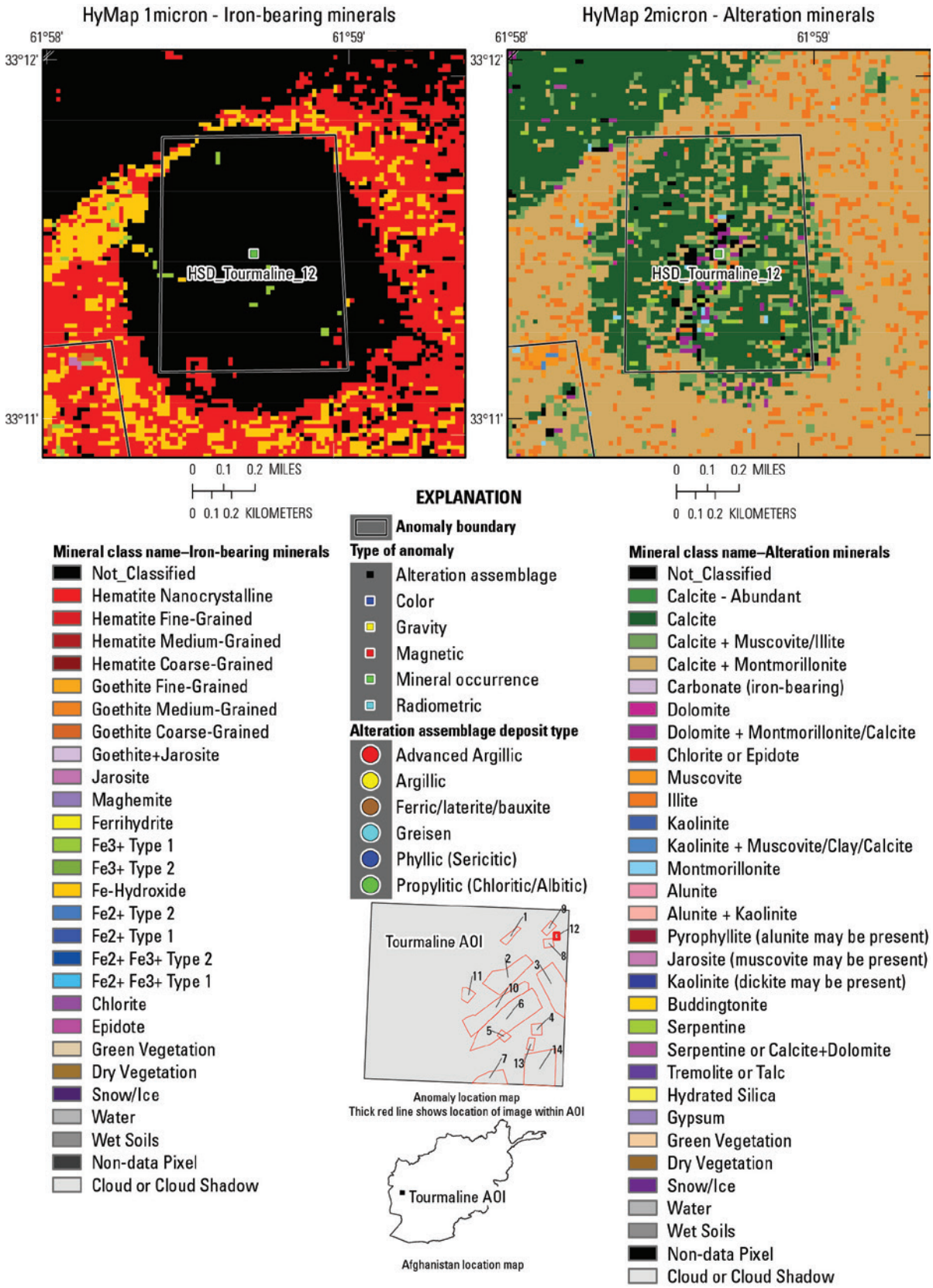

Figure 5.19.12. Hyperspectral anomaly located in the Tourmaline Area of Interest (AOI) in Afghanistan based on presence of Calcite, Dolomite minerals, and Serpentine minerals.

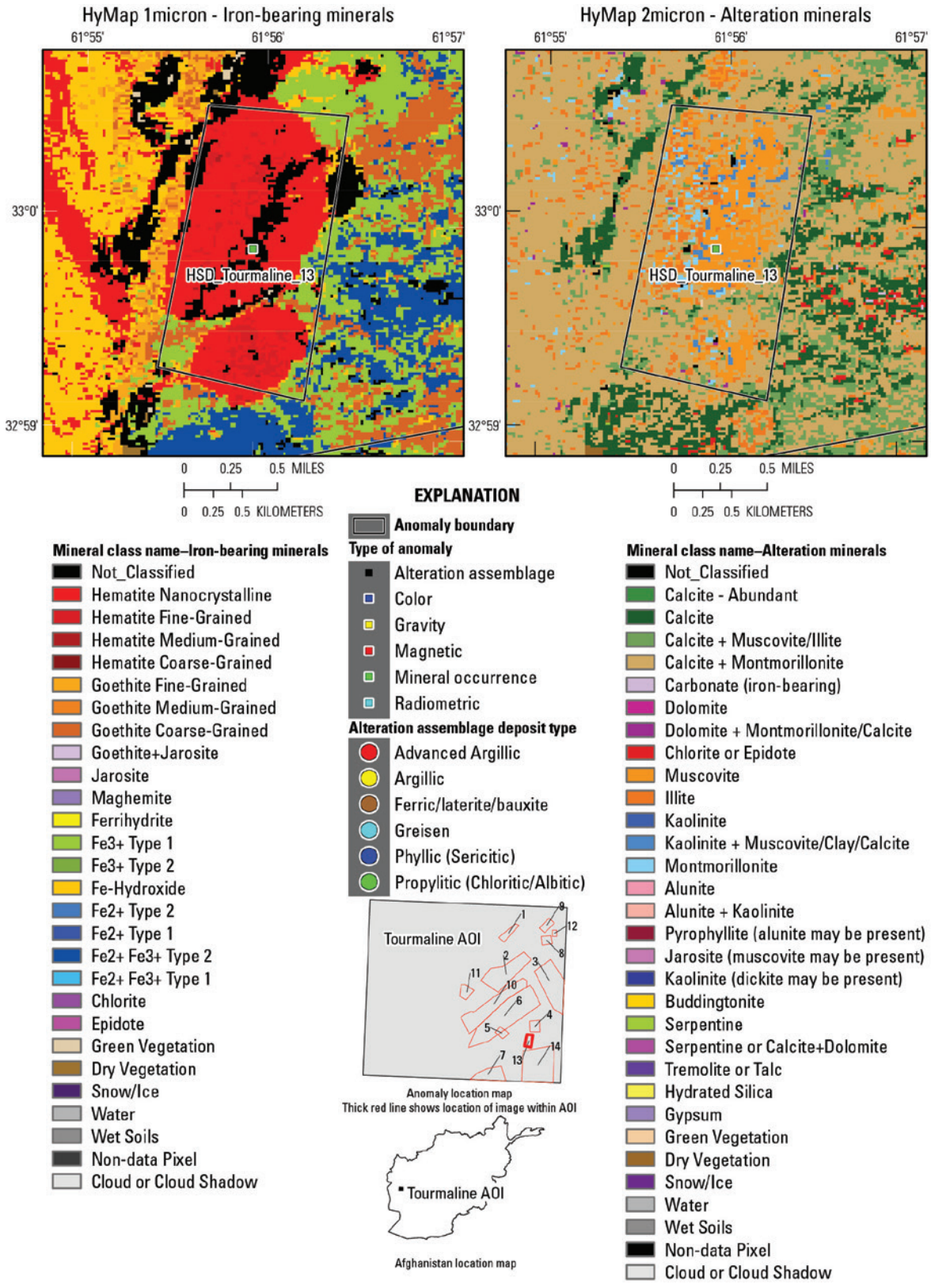

Figure 5.19.13. Hyperspectral anomaly located in the Tourmaline Area of Interest (AOI) in Afghanistan based on presence of Muscovite, Illite, Montmorillonite, Kaolinite minerals, Hematite minerals, Goethite minerals, and Fe3+ Type1.

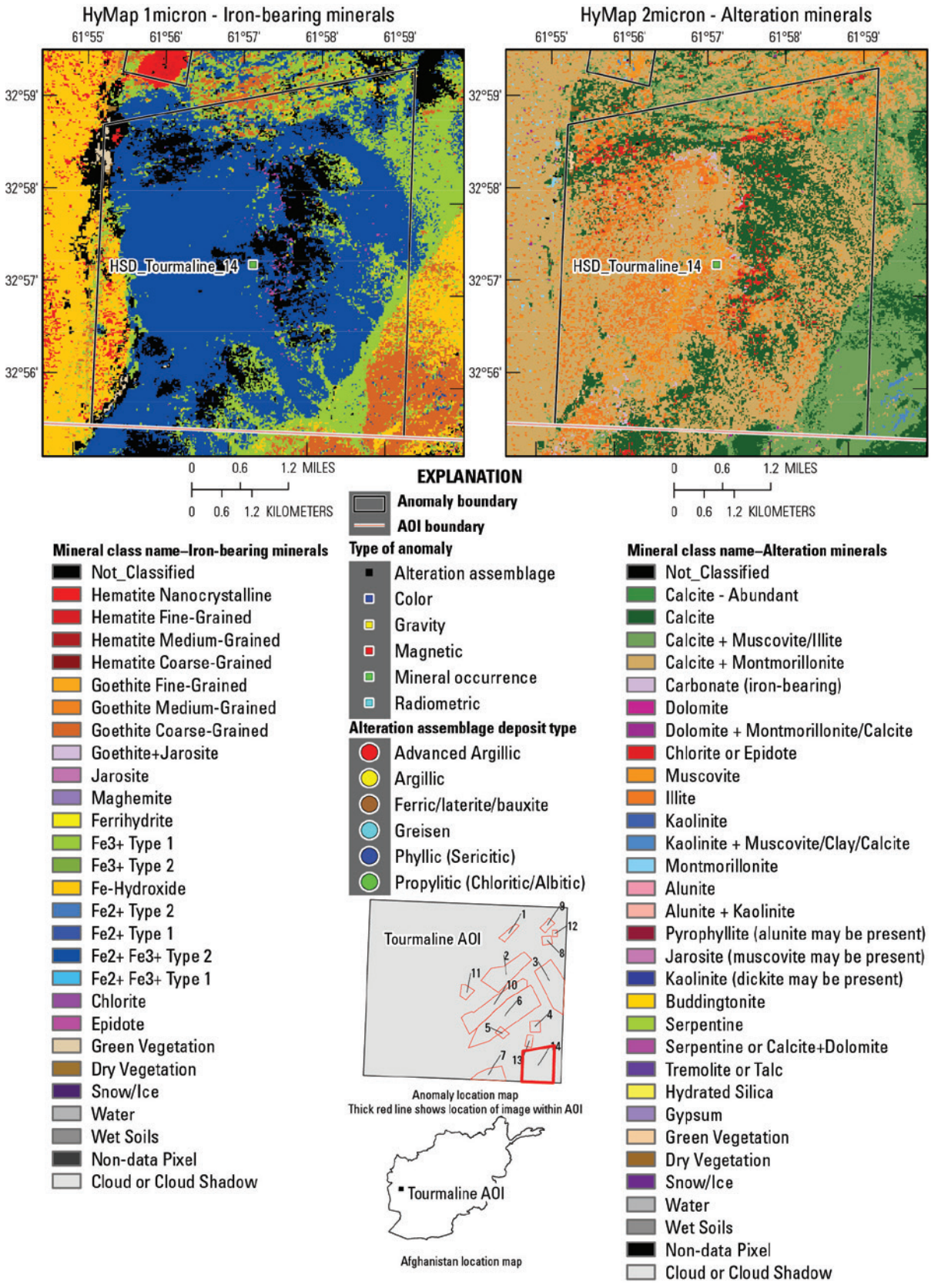

Figure 5.19.14. Hyperspectral anomaly located in the Tourmaline Area of Interest (AOI) in Afghanistan based on presence of Muscovite, Illite, Chlorite or Epidote, Carbonate (iron-bearing), and Fe2+ Fe3+ Type2.

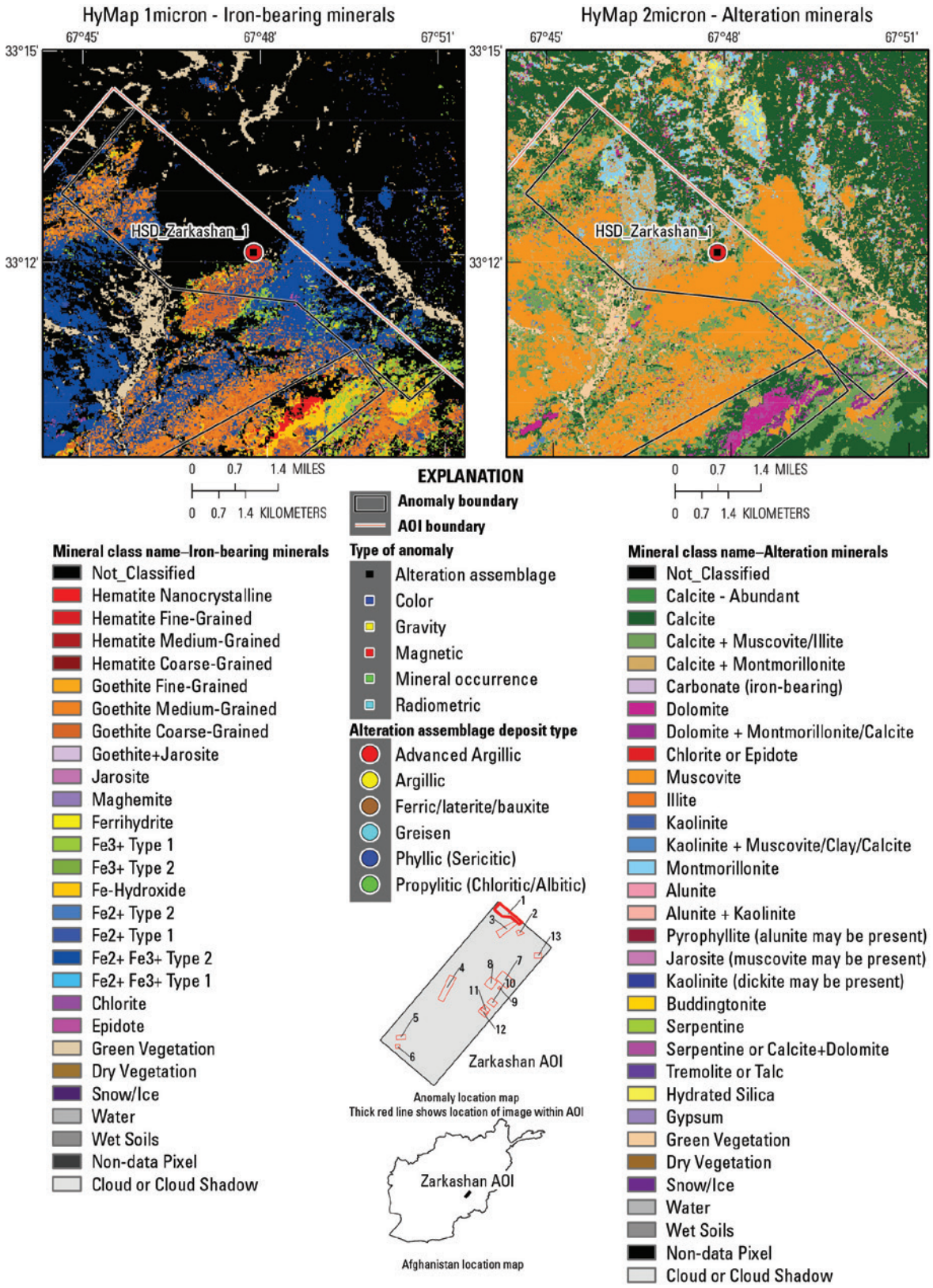

Figure 5.20.1. Hyperspectral anomaly located in the Zarkashan Area of Interest (AOI) in Afghanistan based on presence of Montmorillonite, Hydrated Silica, Dolomite minerals, Goethite minerals, Fe-Hydroxide, and Fe3+ Type 1.

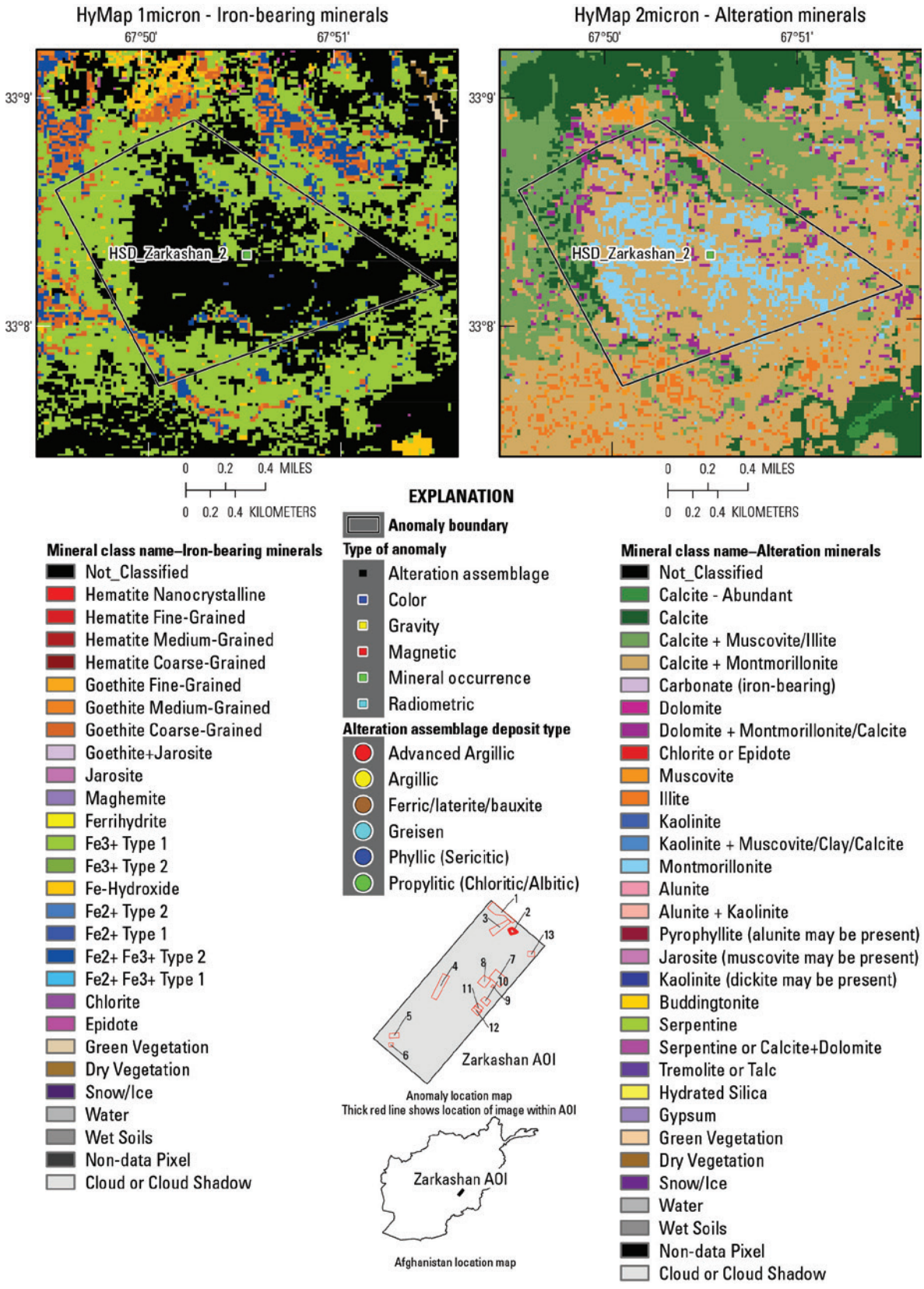

Figure 5.20.2. Hyperspectral anomaly located in the Zarkashan Area of Interest (AOI) in Afghanistan based on presence of Montmorillonite, Dolomite minerals, and Fe^{3+} Type 1.

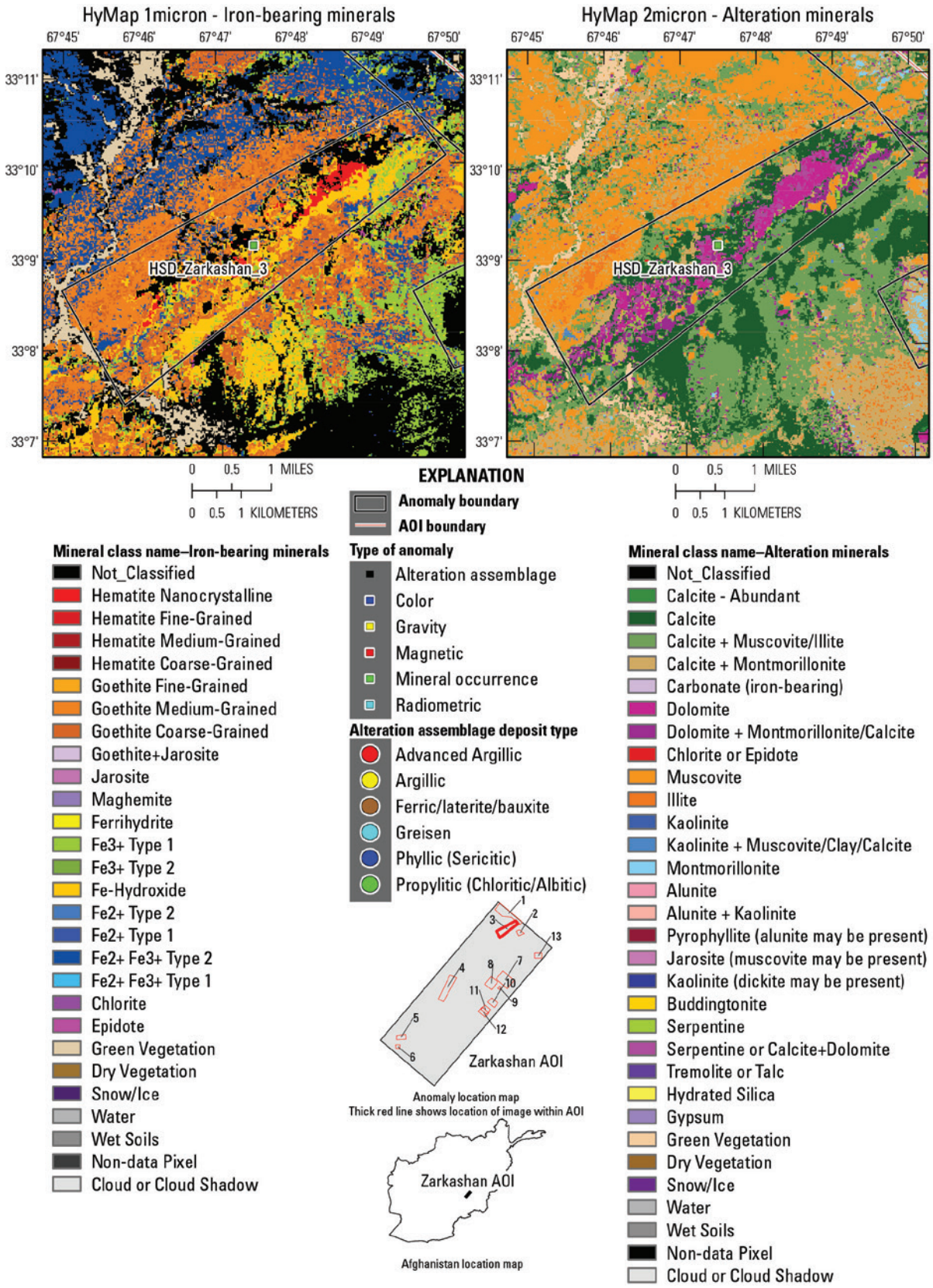

Figure 5.20.3. Hyperspectral anomaly located in the Zarkashan Area of Interest (AOI) in Afghanistan based on presence of Dolomite minerals, Serpentine minerals, Hematite minerals, and Goethite minerals.

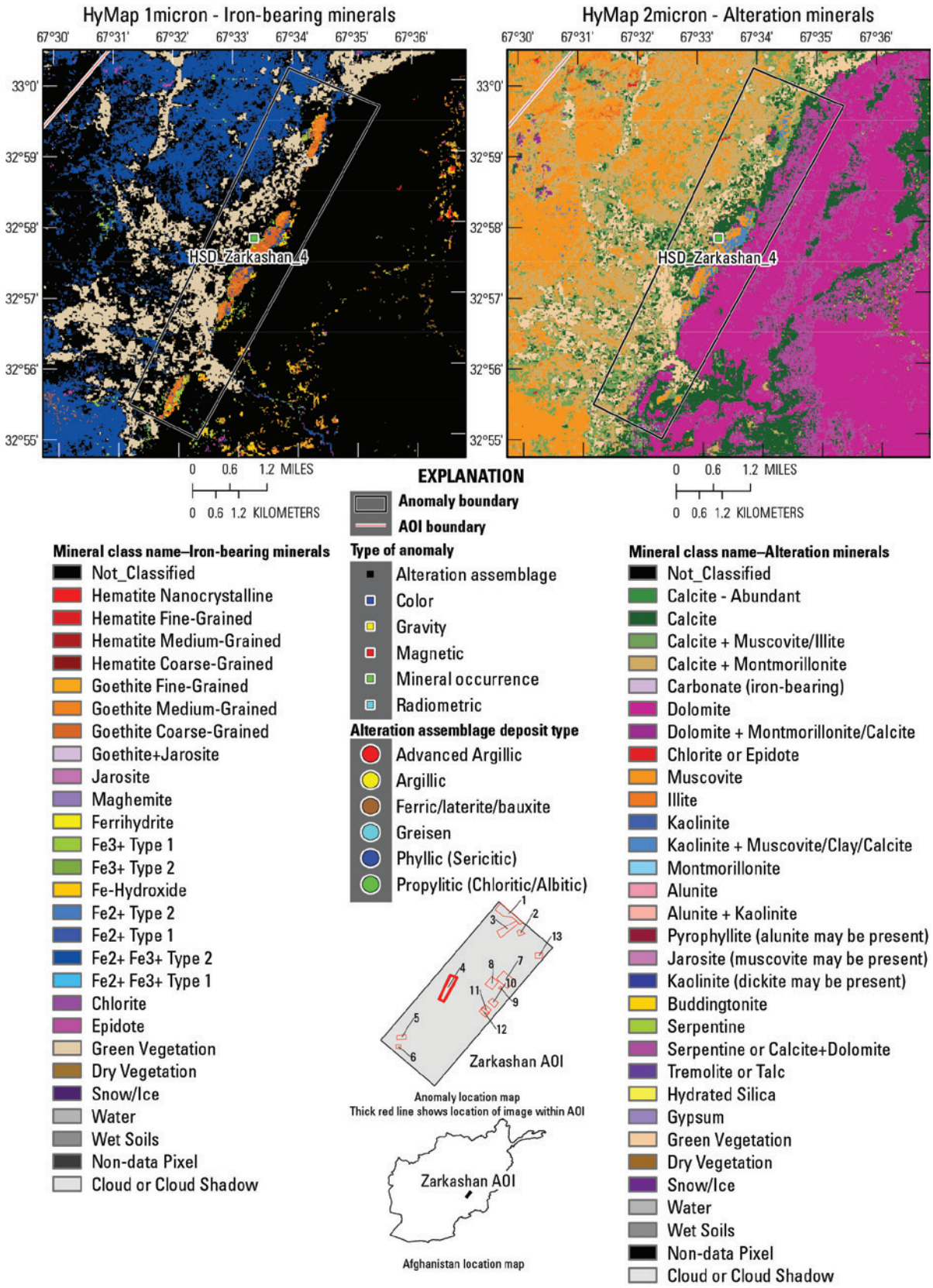

Figure 5.20.4. Hyperspectral anomaly located in the Zarkashan Area of Interest (AOI) in Afghanistan based on presence of Muscovite, Kaolinite minerals, Goethite minerals, Fe^{3+} Type 1, and Fe-Hydroxide.

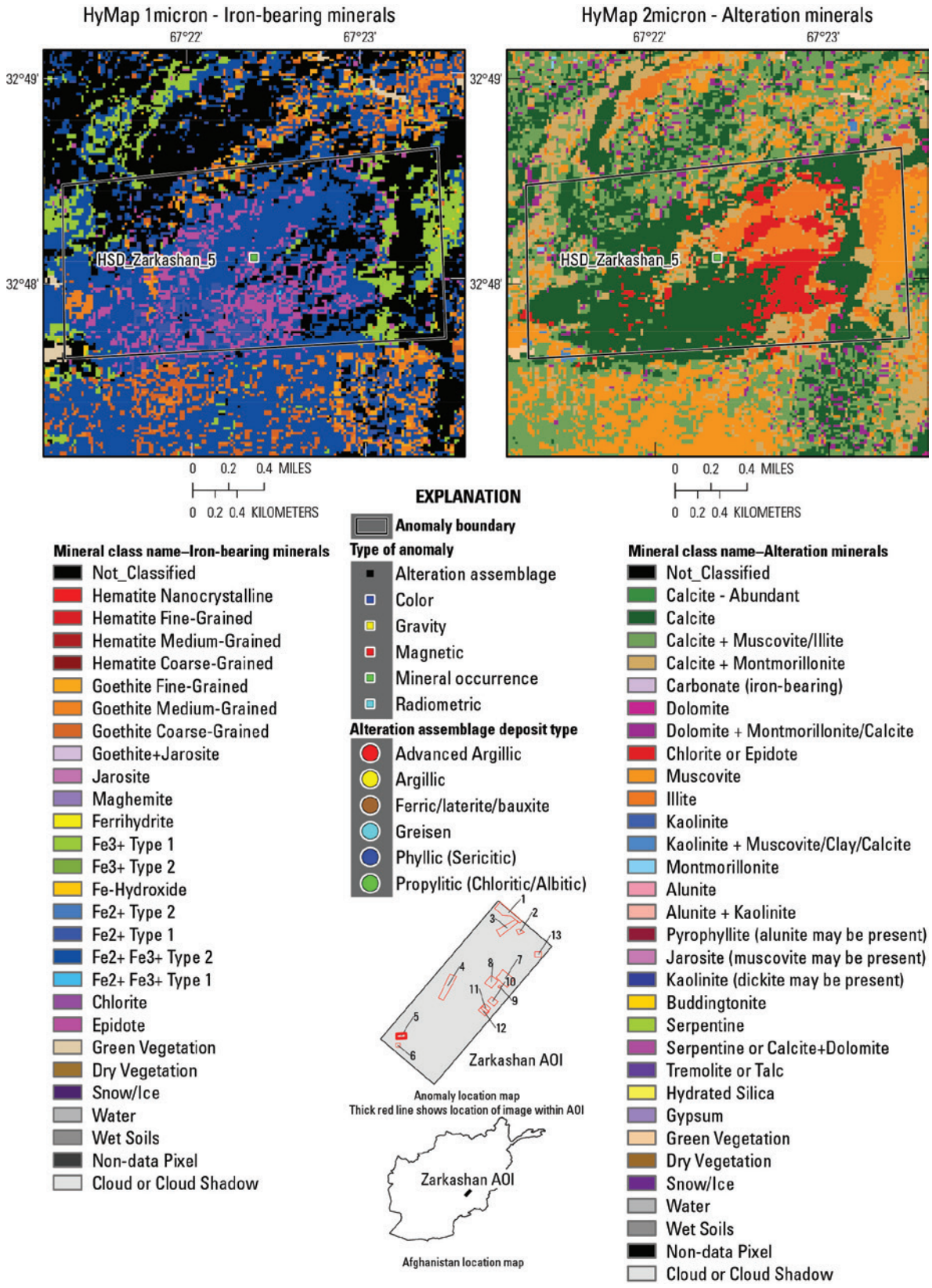

Figure 5.20.5. Hyperspectral anomaly located in the Zarkashan Area of Interest (AOI) in Afghanistan based on presence of Chlorite or Epidote and Fe^{3+} Type 1.

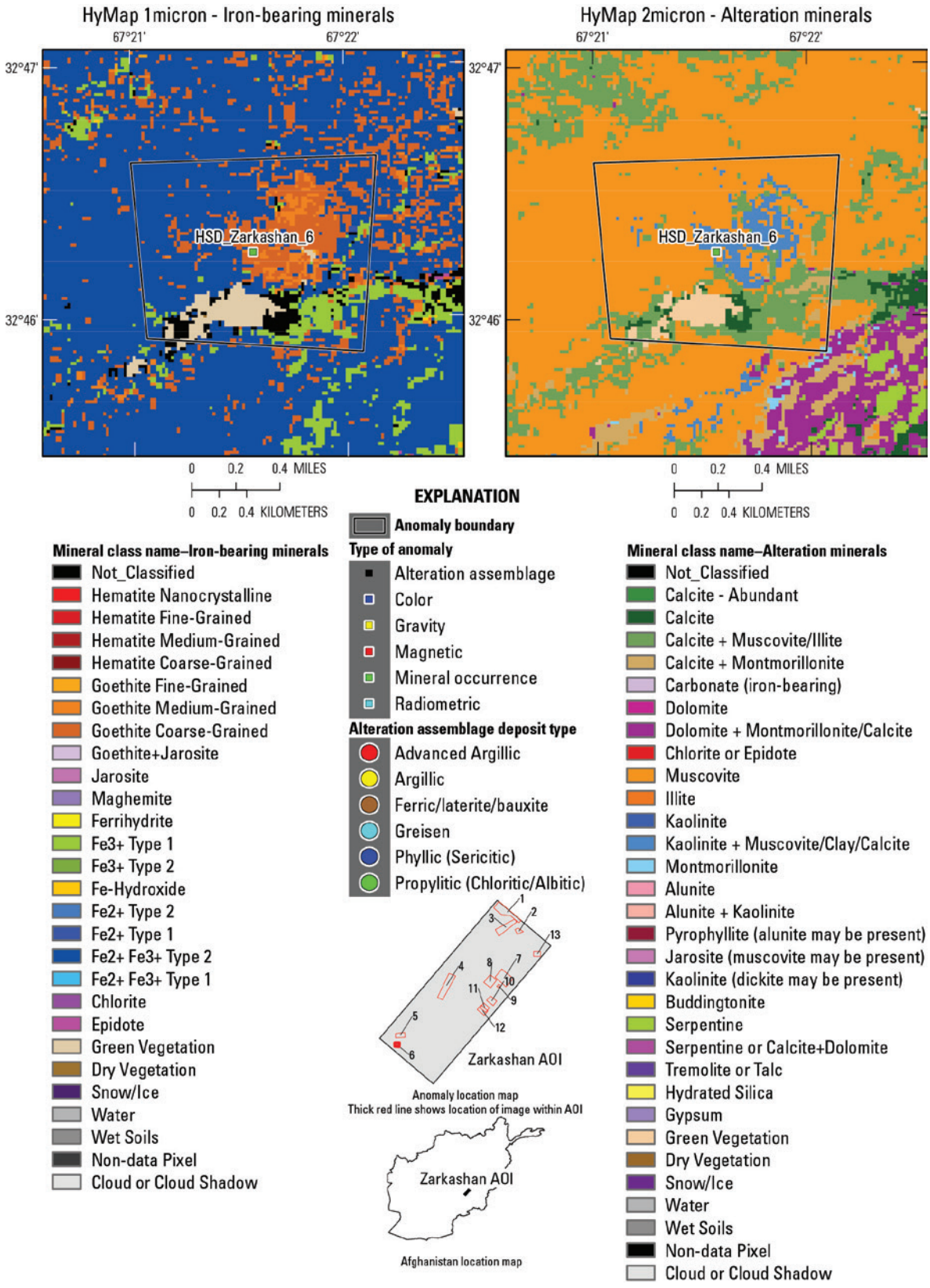

Figure 5.20.6. Hyperspectral anomaly located in the Zarkashan Area of Interest (AOI) in Afghanistan based on presence of Kaolinite minerals, Goethite minerals, and Fe^{3+} Type 1.

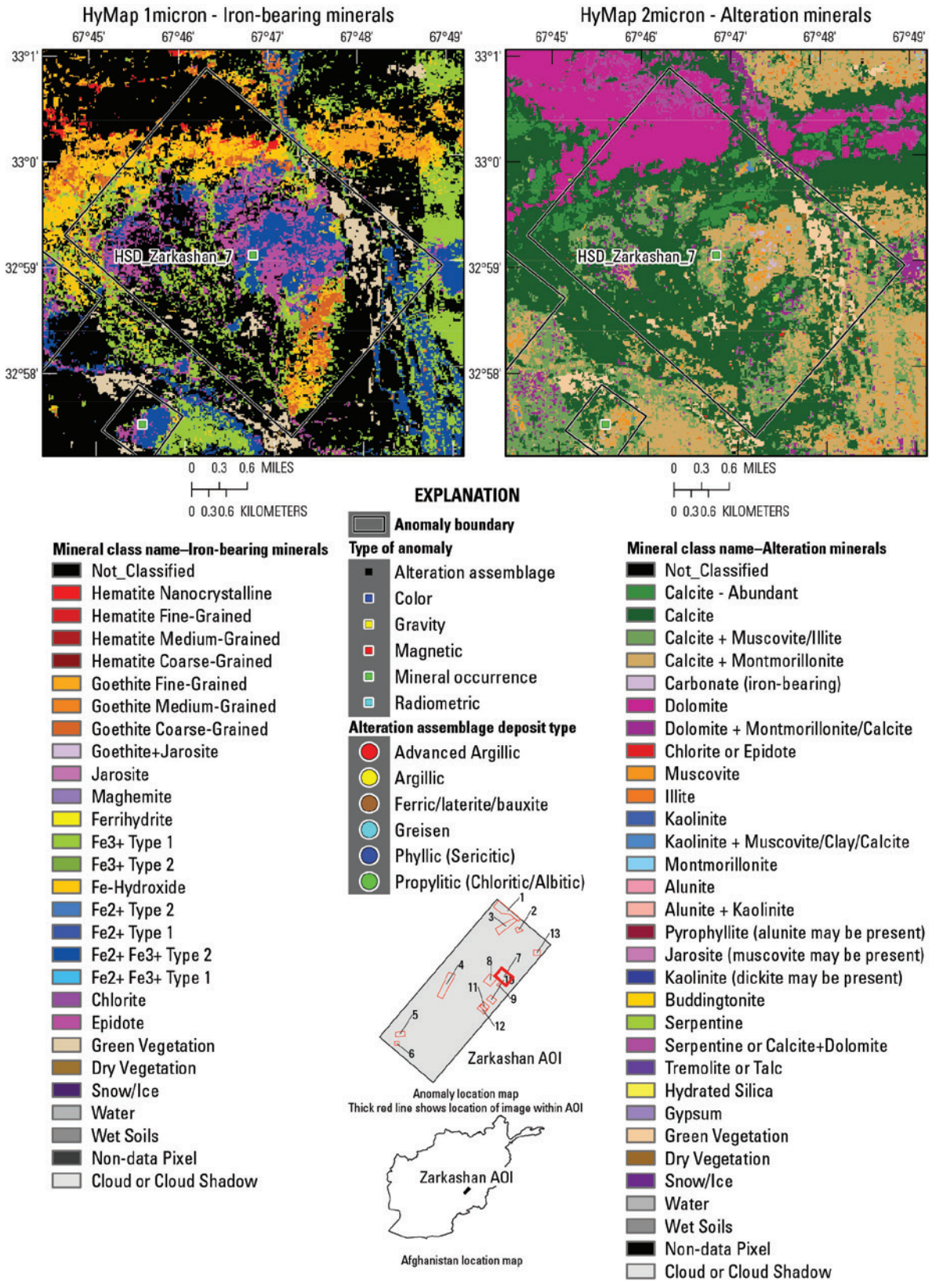

Figure 5.20.7. Hyperspectral anomaly located in the Zarkashan Area of Interest (AOI) in Afghanistan based on presence of Carbonate (iron-bearing), Calcite minerals, Serpentine minerals, Dolomite minerals, Epidote, Fe^{3+} Type 1, Goethite minerals, and Hematite minerals.

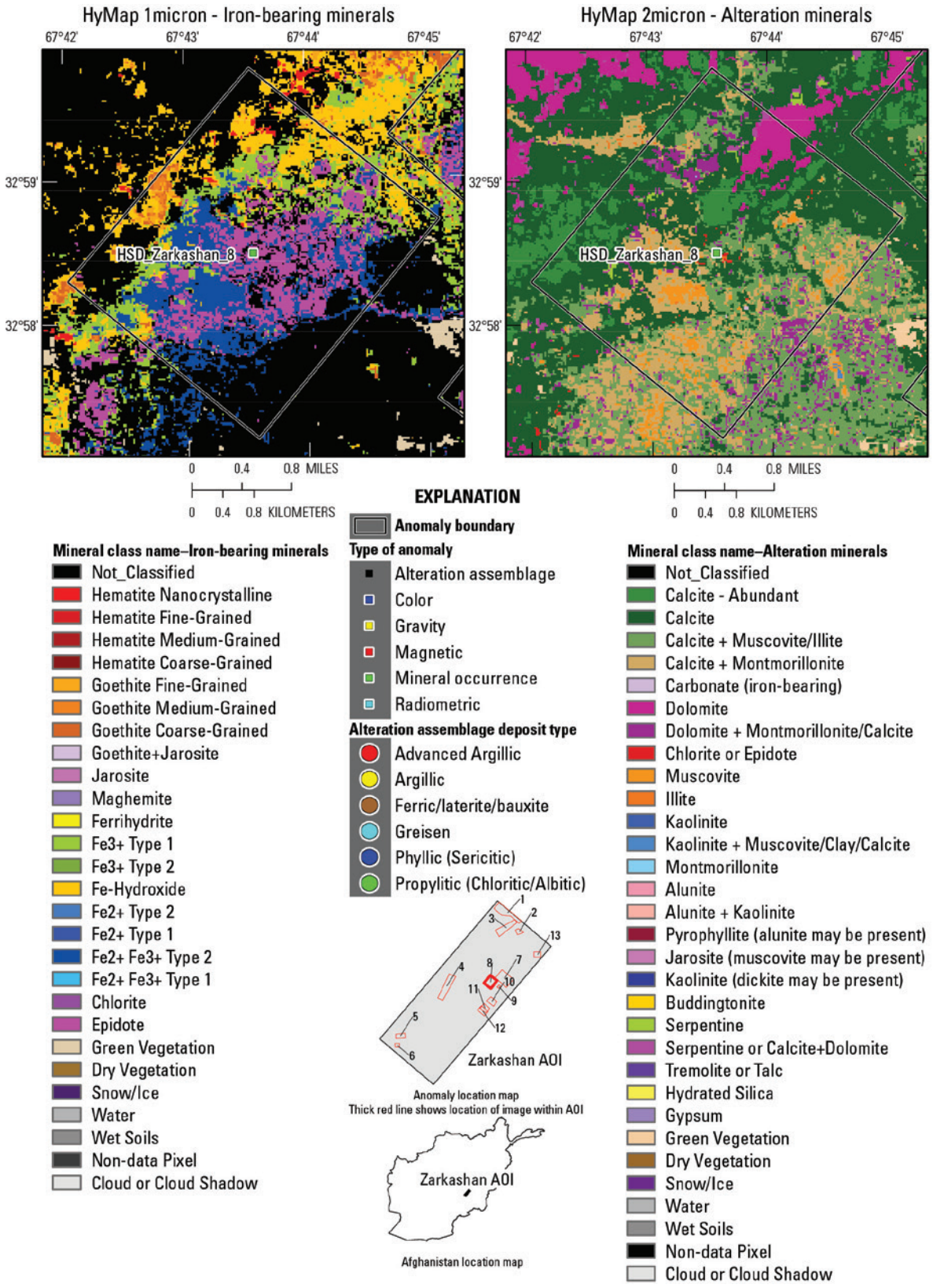

Figure 5.20.8. Hyperspectral anomaly located in the Zarkashan Area of Interest (AOI) in Afghanistan based on presence of Carbonate (iron-bearing), Calcite minerals, Serpentine minerals, Dolomite minerals, Muscovite, Chlorite or Epidote, Fe^{3+} Type 1, Goethite minerals, and Hematite minerals.

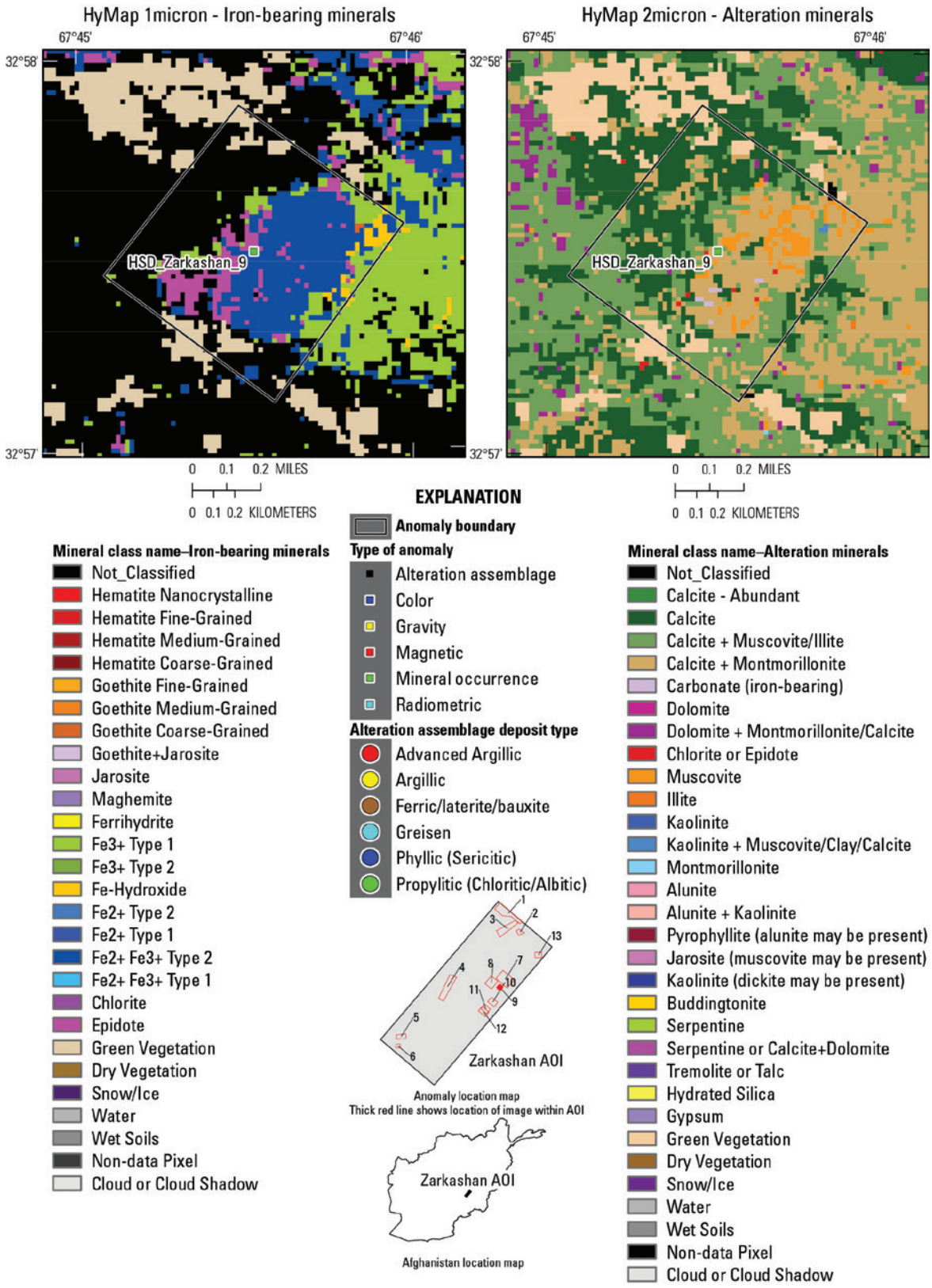

Figure 5.20.9. Hyperspectral anomaly located in the Zarkashan Area of Interest (AOI) in Afghanistan based on presence of Carbonate (iron-bearing), Calcite minerals, Dolomite minerals, Muscovite, Chlorite or Epidote, Fe^{3+} Type 1, and Fe-Hydroxide.

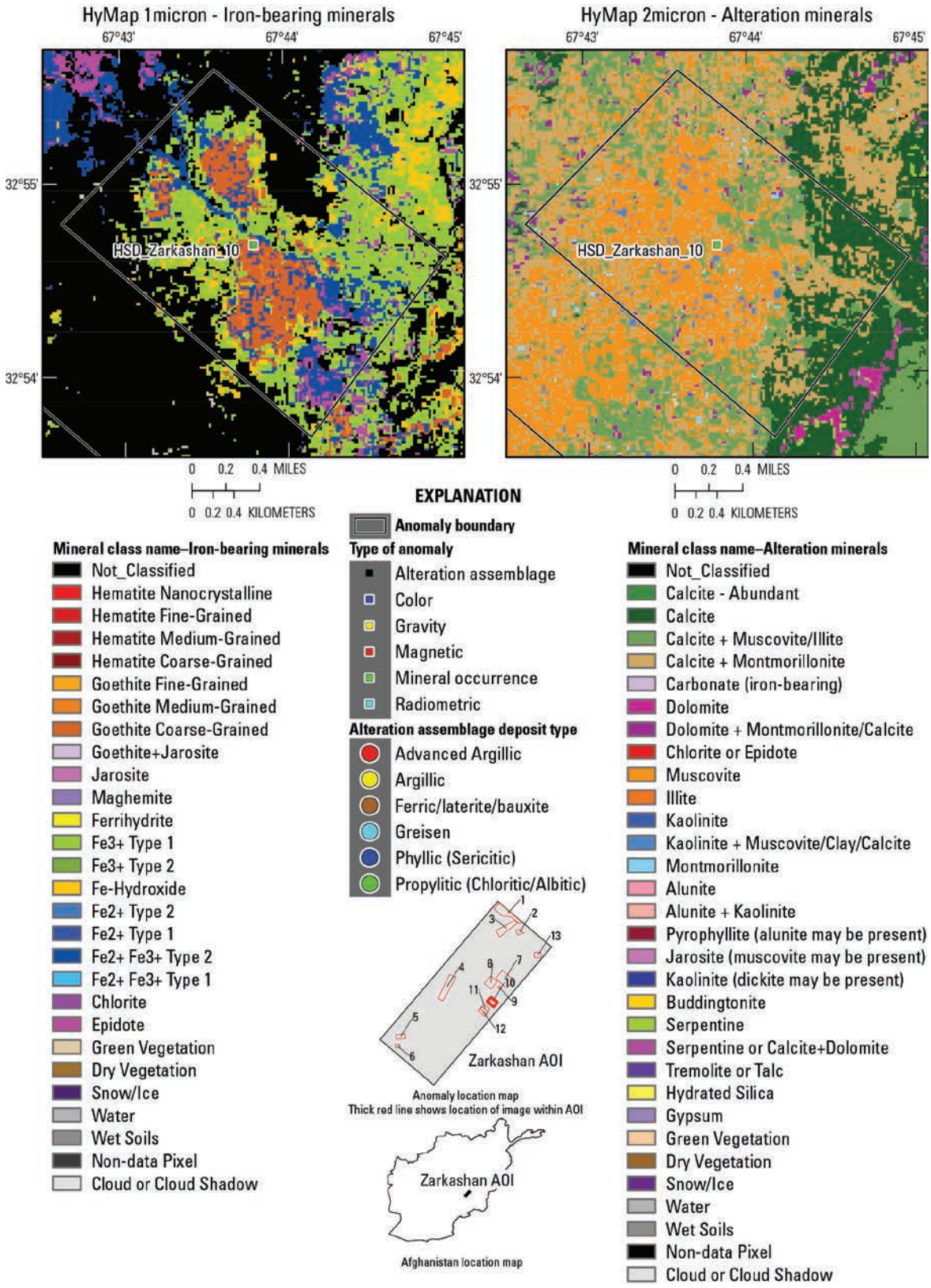

Figure 5.20.10. Hyperspectral anomaly located in the Zarkashan Area of Interest (AOI) in Afghanistan based on presence of Muscovite, Kaolinite minerals, Goethite minerals, Epidote, Fe^{3+} Type 1, and Fe-Hydroxide.

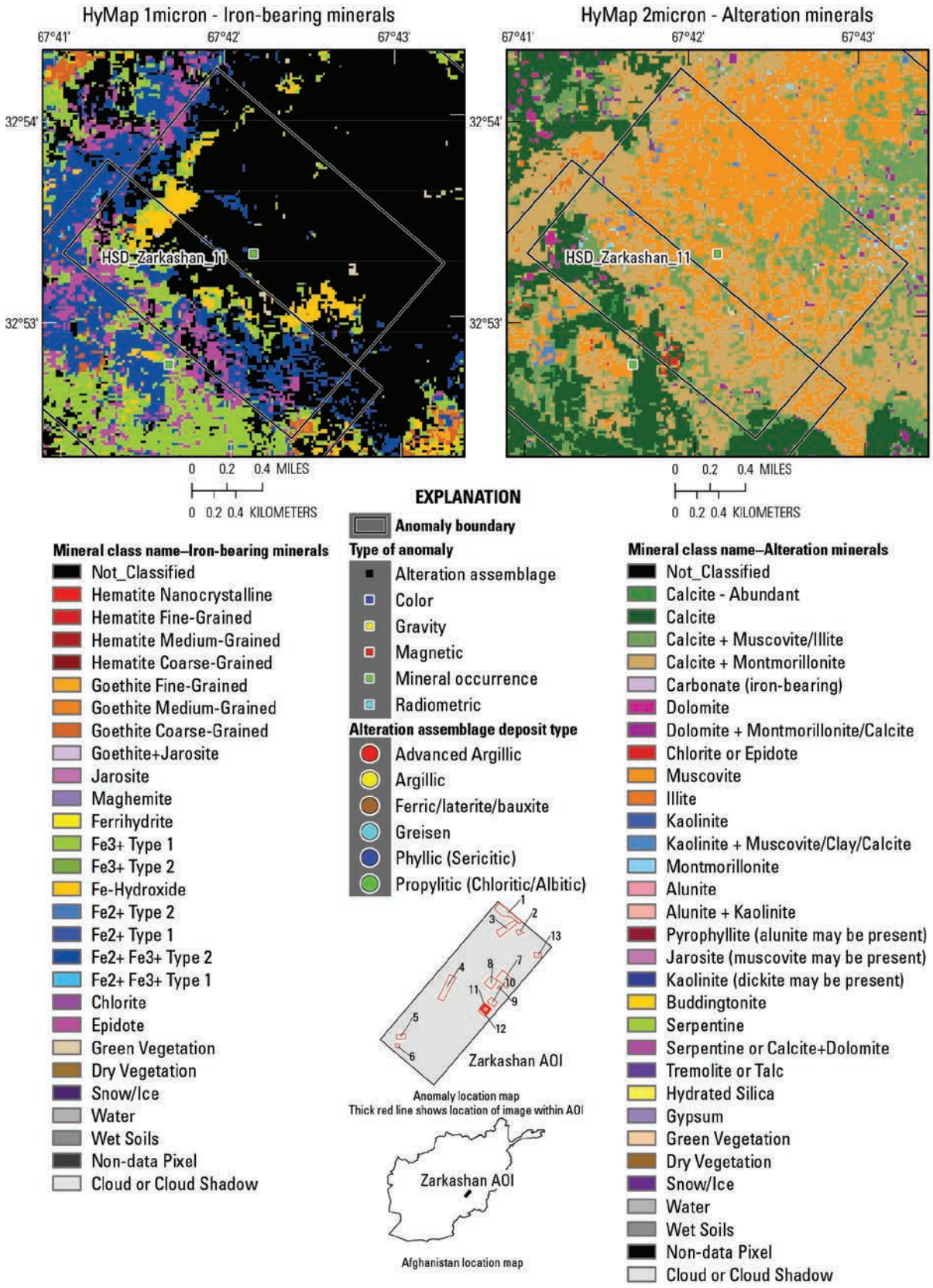

Figure 5.20.11. Hyperspectral anomaly located in the Zarkashan Area of Interest (AOI) in Afghanistan based on presence of Muscovite, Chlorite or Epidote, Dolomite minerals, Fe-Hydroxide, and Fe^{3+} Type 1.

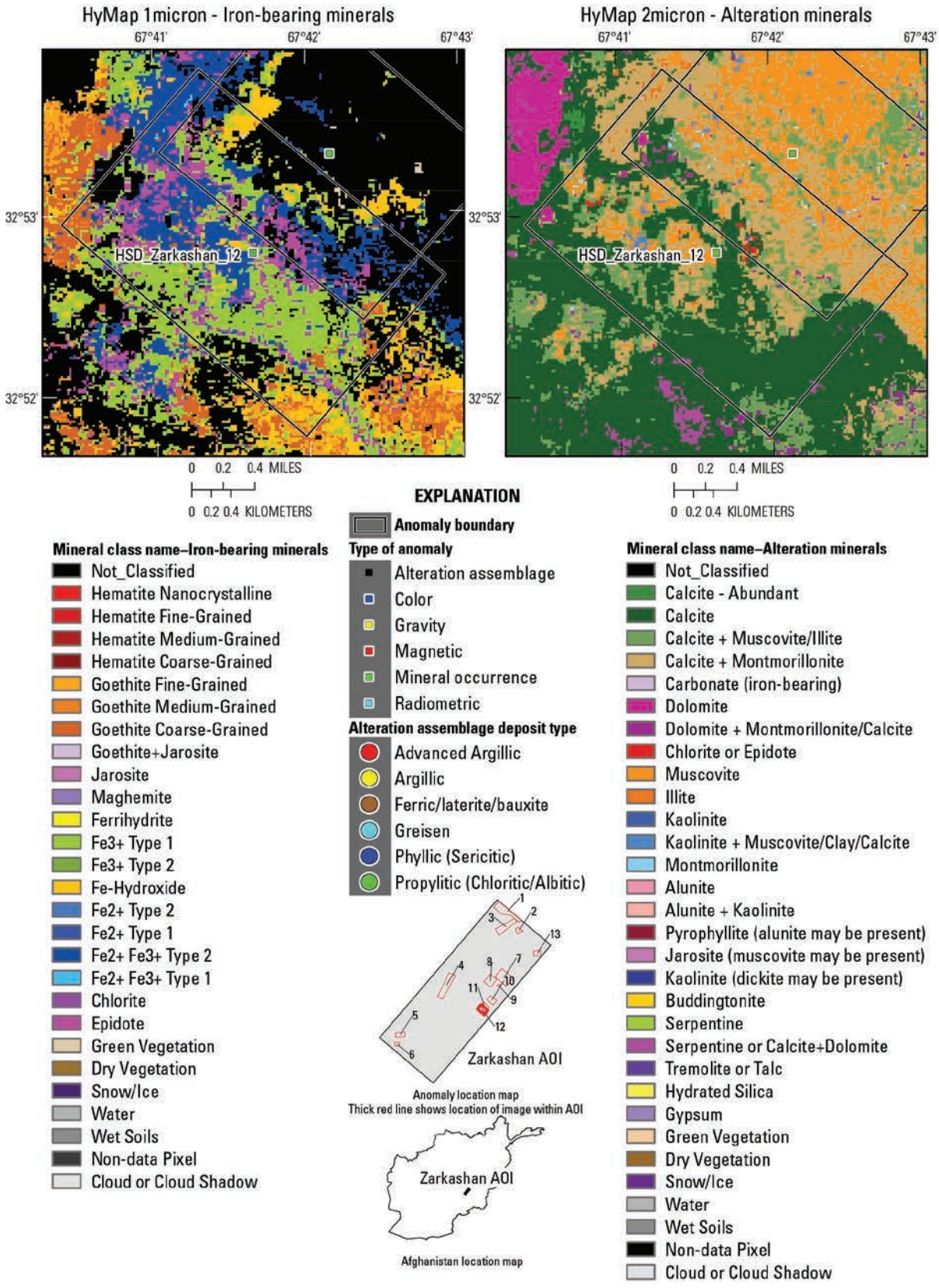

Figure 5.20.12. Hyperspectral anomaly located in the Zarkashan Area of Interest (AOI) in Afghanistan based on presence of Muscovite, Chlorite or Epidote, Kaolinite minerals, Fe^{3+} Type 1, and Fe^{2+} Fe^{3+} Type 2.

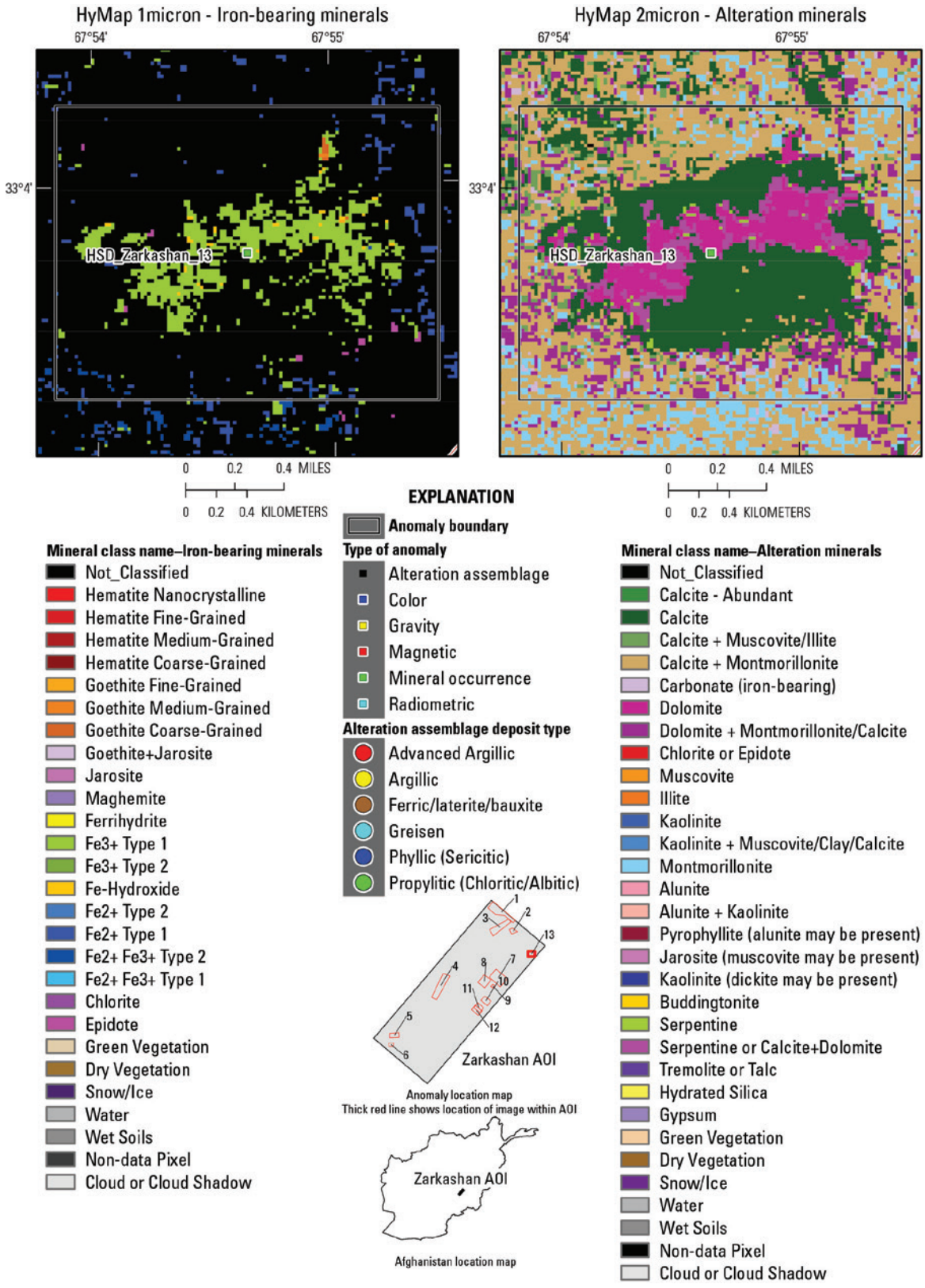

Figure 5.20.13. Hyperspectral anomaly located in the Zarkashan Area of Interest (AOI) in Afghanistan based on presence of Dolomite minerals, Serpentine minerals, Fe^{3+} Type 1, Fe-Hydroxide, and Goethite minerals.

5.5 References Cited

Abdullah, S., Chmiriov, V.M., Stazhilo-Alekseev, K.F., Dronov, V.I., Kofarsky, A.K., and Malyarov, E.P., 1977, Mineral resources of Afghanistan—Republic of Afghanistan: Ministry of Mines and Industries, Afghan Geological and Mines Survey, 419 p., accessed August 19, 2011, at *http://www.bgs.ac.uk/downloads/browse.cfm?sec=7&cat=83.*

Cocks T., Jenssen, R., Stewart, A., Wilson, I., and Shields, T., 1998, The HyMap airborne Hymap sensor: The System, calibration and performance, *in* Schaepman, M., Schlapfer, D., and Itten, K.I., eds., Proceedings of the 1st EARSeL Workshop on Imaging Spectroscopy, 6–8 October 1998, Zurich: Paris, EARSeL, p. 37–43, accessed August 19, 2011, at *http://www.neodc.rl.ac.uk/docs/Hymap_specs.pdf.*

Davis, P.A., 2006, Calibrated Landsat ETM+ nonthermal-band image mosaics of Afghanistan: U.S. Geological Survey Open-File Report 2006–1345, 16 p., accessed August 19, 2011, at *http://pubs.usgs.gov/of/2006/1345/.*

King, T.V.V., Kokaly, R.F., Hoefen, T.M., Dudek, K., and Livo, K.E., in press, Surface materials map of Afghanistan: Iron-bearing minerals and other materials: U.S. Geological Survey Scientific Investigations Map 3152-B.

Kokaly, R.F., 2011, PRISM: Processing routines in IDL for spectroscopic measurements (installation manual and user's guide, version 1.0): U.S. Geological Survey Open-File Report 2011–1155, 512 p., accessed August 19, 2011, at *http://pubs.usgs.gov/of/2011/1155/.*

Kokaly, R.F., King, T.V.V., and Livo, K.E., 2008, Airborne hyperspectral survey of Afghanistan 2007: Flight line planning and HyMap data collection: U.S. Geological Survey Open-File Report 2008–1235, 14 p., accessed August 19, 2011, at *http://pubs.usgs.gov/of/2008/1235/.*

Kokaly, R.F., King, T.V.V., Hoefen, T.M., Dudek, K. and Livo, K.E., in press, Surface materials map of Afghanistan: Carbonates, phyllosilicates, sulfates, altered minerals, and other materials: U.S. Geological Survey Scientific Investigations Map 3152-A.

Peters, S.G., Ludington, S.D., Orris, G.J., Sutphin, D.M., Bliss, J.D., and Rytuba, J.J., eds., and the U.S. Geological Survey-Afghanistan Ministry of Mines Joint Mineral Resource Assessment team, 2007, Preliminary non-fuel mineral resource assessment of Afghanistan: U.S. Geological Survey Open-File Report 2007–1214, 810 p., 1 CD-ROM, accessed August 19, 2011, at *http://pubs.usgs.gov/of/2007/1214/.*

Peters, S.G., King, T.V.V, Mack, T.J., Chornack, M.P., eds., and the U.S. Geological Survey Afghanistan Mineral Assessment Team, 2011, Summaries of important areas for mineral investment and production opportunities of nonfuel minerals in Afghanistan: U.S. Geological Survey Open-File Report 2011–1204, 1,810 p. plus appendixes on DVD. (Also available at *http://pubs.usgs.gov/of/2011/1204/.)*

Shenwary, G.S.; Kohistany, A.H.; Hussain, Sardar; Ashan, Said; Mutty, A.S.; Daud, M.A.; Wussow, M.W.; Sweeney, R.E.; Phillips, J.D.; Lindsay, C.R.; Kucks, R.P.; Finn, C.A.; Drenth, B.A.; Anderson, E.D.; Abraham, J.D.; Liang, R.T.; Jarvis, J.L.; Gardner, J.M.; Childers, V.A.; Ball, D.C.; and Brozena, J.M., 2011, Aeromagnetic surveys in Afghanistan—An updated website for distribution of data: U.S. Geological Survey Open-File Report 2011–1055, 8 p., accessed August 19, 2011, at *http://pubs.usgs.gov/of/2011/1055/.*

Sweeney, R.E., Kucks, R.P, Hill, P.L., and Finn, C.A., 2006, Aeromagnetic and gravity surveys in Afghanistan: A web site for distribution of data: U.S. Geological Survey Open-File Report 2006–1204, accessed August 19, 2011, at *http://pubs.usgs.gov/of/2006/1204/.*

Thompson, A.J.B, Hauff, P.L., and Robitaille, A.J., 2009, Alteration mapping in exploration: Application of Short-Wave Infrared (SWIR) spectroscopy, *in* Bendell, R., Crosta, A.P., and Grunsky, E., eds., Remote sensing and spectral geology: Society of Economic Geologists (SEG) Reviews in Economic Geology, v. 16, p. 12–23.

Chapter 6: Discussion of Anomaly Overlap Areas and Potential for Economic Development

By Bernard E. Hubbard, Trude V.V. King, Michaela R. Johnson, and Benjamin J. Drenth

6.1 Anomaly Overlap—Conclusions and Discussion

A total of 334 mineral anomaly polygon locations were mapped using geophysical data (GEO), ASTER data (AST), and HyMap imaging spectrometer data (also referred to as hyperspectral data, HSD). Although each dataset covers different parts of Afghanistan, they provide overlapping coverage within 16 of 24 mineral areas of interest (AOIs) targeted for economic development (Peters and others, 2011). Because each of the three datasets were processed and interpreted independently of one another, and two in particular (HSD and AST) yield similar spectral information related to various types of hydrothermal alteration products (for example, Thompson and others, 2009), overlapping anomalies between two or three of these datasets represent high-priority targets for future ground-based exploration activities and targeted economic development. As a result, the anomalies have been catalogued totaling 225 overlapping anomalies, of which 55 are between AST and HSD, 107 are between HSD and GEO, 34 are between AST and GEO, and 29 are between AST, HSD, and GEO. These overlapping anomalies were further prioritized based on (1) the number of datasets that provide overlapping agreement; (2) other known and nearby mineral occurrences in the area (for example, Oriss and Bliss, 2002; Doebrich and Wahl, 2006); (3) proximity to roads, infrastructure, and major population centers; and (4) the knowledge base regarding the geology and processes related to mineral formation based on analyses and interpretations (this study) and prior studies (for example, Peters and others, 2007; Peters and others, 2011). Figure 6.1.1 shows the location and distribution of five anomaly overlap areas discussed as follows.

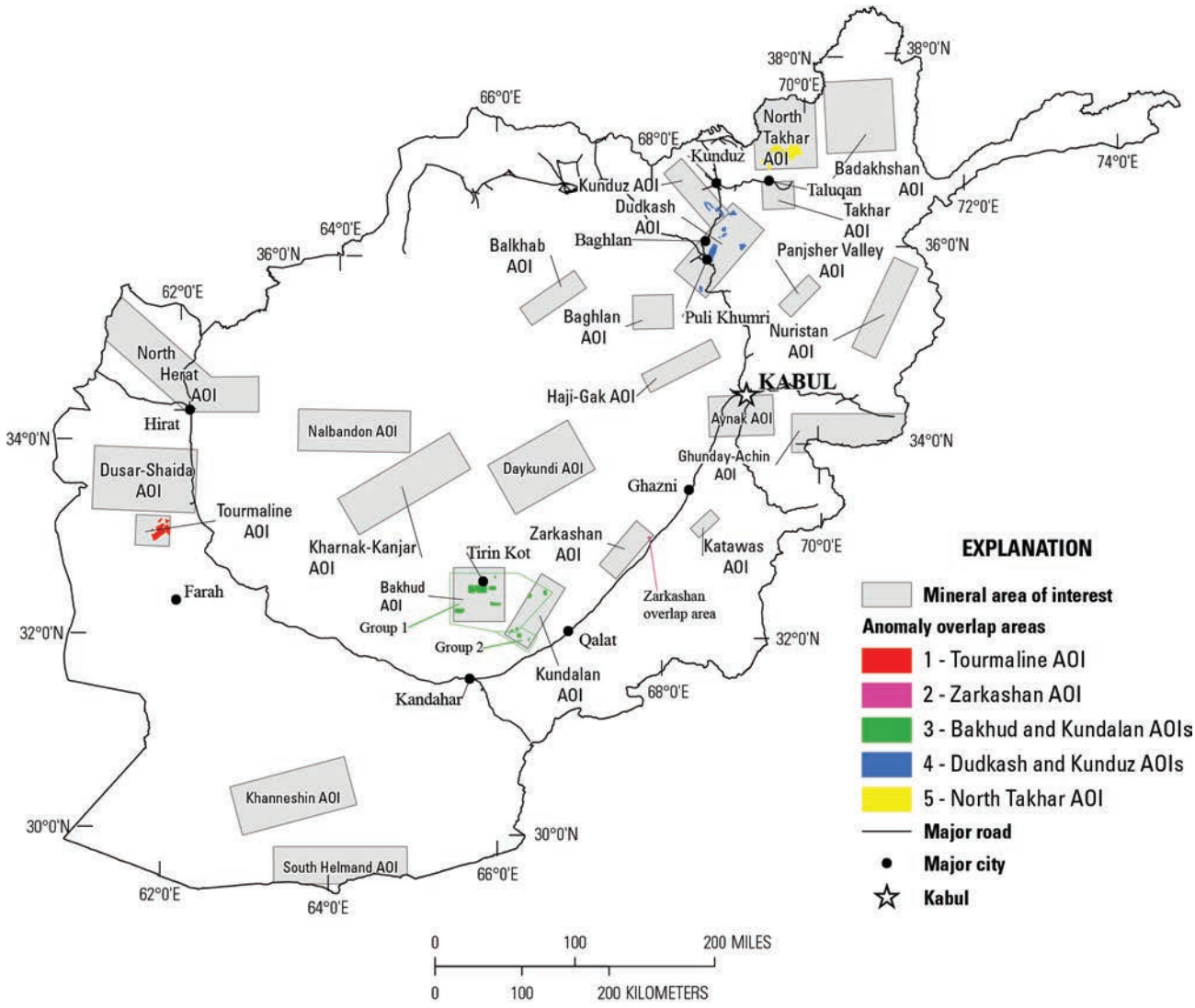

Figure 6.1.1. Location map of selected overlapping anomalies defined by the source data (geophysical [GEO], ASTER [AST], or HyMap hyperspectral [HSD]) within mineral areas of interest (AOI) in Afghanistan. (1) GEO/AST/HSD overlap in the Tourmaline AOI, (2) GEO/AST/HSD overlap in the Zarkashan AOI, (3) GEO/HSD overlap in the Bakhud and Kundalan AOIs, (4) AST/HSD overlap in the Dudkash and Kunduz AOIs, and (5) GEO/AST overlap in the North Takhar AOI.

6.1.1 Anomaly Overlap Priority 1

The highest-priority anomaly-overlap areas occur within the tin-vein Tourmaline AOI (fig. 6.1.1). This is one of two AOIs where all three datasets (HSD, AST and GEO) overlap. Proximal to these anomaly overlap areas are known tin and tungsten greisen deposits associated with Oligocene age granite and granodiorite intrusive rocks (Peters and others, 2007; Peters and others, 2011). Some of the intrusive rocks are characterized by magnetic highs, which suggest shallow plutons or groups of plutons associated with the Cretaceous-Oligocene age Farah Rod plutonic belt (Debon and others, 1987). In the areas of overlap shown in figure 6.1.1, a multitude of magnetic highs (and a few sharp lows) are located over Cenozoic volcanic rocks and intrusions. Radiometric highs are located over mapped Cenozoic

sediments and volcanic rocks (Doebrich and Wahl, 2006). Mapped within the AST and HSD datasets, linearly trending hydrothermal alteration patterns suggest possible structural control (such as a "paleo-graben") of magmatic-hydrothermal fluids that could be driven by a shallow anomaly identified in the airborne geophysical data (GEO).

Both AST and HSD data map corresponding broad areas of advanced argillic alteration containing mixtures of kaolinite with illite and (or) muscovite, as well as smaller localized areas containing jarosite and (or) hydrous silica minerals. In addition, HSD mapping suggests the presence of buddingtonite, which was not detected in AST data. The presence of buddingtonite suggests either exposure of the uppermost portions of the hydrothermal system, or more preferably, that sufficient erosion has occurred within the volcanic rocks to expose the core of a possible porphyry system (Krohn and others, 1993). The latter would contain concentrated amounts of precious- and base-metal sulfide minerals.

6.1.2 Anomaly Overlap Priority 2

The second-highest-priority anomaly overlap occurs within the Zarkashan AOI (fig. 6.1.1). Zarkashan AOI is the second area that represents commonality between mapped anomalies derived from all three—HSD, AST, and GEO—datasets. This area is a single, small (4.3 km^2) polygon representing an unmapped bedrock outcrop surrounded by a large plain of Quaternary basin-fill alluvium (Doebrich and Wahl, 2006). This topographically "higher" bedrock-outcrop feature and the surrounding "lower" alluvial plains are well depicted in shaded relief maps derived from the 90-m-resolution Shuttle Radar Topography Mission (SRTM) DEM.

This anomaly overlap area is characterized by one of three magnetic-high anomalies in the Zarkashan AOI; the area is interpreted to reflect strongly magnetized Late Cretaceous/Paleocene gabbro and monzonite plutons (Kleimenev and others, 1974; Doebrich and Wahl, 2006; Peters and others, 2007). These plutons likely provided the heat source for hydrothermal alteration of the surrounding (predominantly carbonate) bedrock to yield known skarn gold deposit occurrences in three nearby areas (that is, Bolo, Luman Tamaki, and Zarkashan Mine subareas [Peters and others, 2011]).

AST mapping suggests a possible lithologic contact between rocks containing a clay + carbonate mixture, with rocks containing mixtures of ferric iron, smectite clays, and minor amounts of illite and (or) muscovite. The HSD data suggest that much of this carbonate + clay mixture may be dominated more specifically by dolomite + montmorillonite (King and Johnson, 2011). However, imaging spectrometer maps, derived from the 1-µm-wavelength region, suggest the presence of a Fe^{3+} Type 1 mineral (King and Johnson, 2011) that was not mapped in other rocks containing this same dolomite and (or) dolomite + montmorillonite mixture. This anomalous bedrock outcrop is less than 5 km from the main road linking Kabul and Kandahar between the cities of Qalat and Ghazni (fig. 6.1.1). Stream geochemistry data, collected downstream of this bedrock outcrop near the main road, suggest high concentrations of mercury, which is a gold-compatible element.

6.1.3 Anomaly Overlap Priority 3

The third-highest-priority anomaly-overlap areas occur within the fluorite Bakhud AOI and the porphyry Kundalan AOI (fig. 6.1.1). These areas represent overlap between anomalies identified within the HSD and GEO datasets. Within the Bakhud AOI and the northwesternmost four polygons shown as Group 1 (fig. 6.1.1) within the Kundalan AOI, the anomaly overlaps represent either (1) gravity lows interpreted to reflect a relatively thick portion of the Arghandab granitoid batholith (Debon and others, 1987; Doebrich and Wahl, 2006; Peters and others, 2007), or (2) magnetic highs interpreted to reflect strongly magnetized portions of the Arghandab granitoid batholith (Debon and others, 1987; Doebrich and Wahl, 2006; Peters and others, 2007). In the southeast section of the Kundalan AOI, the remaining

three overlap areas shown as Group 2 (fig. 6.1.1) include a gravity high caused by an unknown source and two magnetic highs. The magnetic highs are interpreted to reflect strongly magnetized Late Cretaceous/Paleocene gabbro and monzonite plutons (Kleimenev and others, 1974; Doebrich and Wahl, 2006; Peters and others, 2007) similar to the one characterizing the unmapped bedrock exposure discussed above within the Zarkashan AOI. In particular, the Arghandab batholith could have provided an excellent heat source for the surface alteration detected in the HSD data, which are dominated by dolomite, serpentine, tremolite or talc, muscovite, and kaolinite minerals in the 2-µm-wavelength-derived maps, and hematite, Fe $^{3+}$ Type 1, epidote, goethite, and Fe-hydroxide minerals in the l-µm-wavelength-derived maps.

6.1.4 Anomaly Overlap Priority 4

Although known to host numerous occurrences of gypsum, sulfur, and celestite deposits (Orris and Bliss, 2002), both AST and HSD mapping in the Dudkash and Kunduz AOIs identify overlapping anomalous areas (fig. 6.1.1). These areas contain ferric iron and clay minerals, which may be associated with either coal deposits and karst-hosted laterite and (or) bauxite deposits. Much of these two AOIs were mapped as various carbonate mineral mixtures using both AST and HSD datasets, which would be expected given their locations on the Asian-Afghan carbonate platform north of the Hari Rud accretionary fault zone (Doebrich and Wahl, 2006).

The two southeasternmost anomaly overlap areas within the Dudkash AOI (fig. 6.1.1) may alternatively be phyllic to argillic hydrothermal alteration in origin, and they are possibly related to Mississippian age diorite, granodiorite, and granites and Late Triassic granitic rocks intruding Namurian, Ordovician, and Silurian-Devonian sedimentary rocks (Kokaly and Johnson, 2011). These areas should be further explored as targets for precious- and base-metal sulfide mineralization.

As mapped using the AST dataset, most of the other anomaly overlap areas are dominated by strong abundance of ferric iron, which was mapped more specifically as goethite, other iron oxy-hydroxides, and nano-crystalline forms of hematite in the HSD data. All of these minerals may occur as either cements within mapped sandstone units (Kokaly and Giles, 2011; Kokaly and Johnson , 2011), or the matrix of karst-hosted bauxite and laterite deposits, which are known to occur in the area based on prior field investigations (John Sanfilipo, written commun., December 12, 2004).

Kaolinite mixtures also dominate the largest overlap polygon within the Dudkash AOI, as mapped using both the AST and HSD datasets. These areas may be associated with abundant coal deposits (Kokaly and Johnson, 2011). However, neither sulfur nor celestite were considered during HSD classification using either the 1-µm wavelengths (for sulfur) or the 2-µm wavelengths (for celestite) (Kokaly and Johnson, 2011). Additional understanding of the spectral characteristics of both minerals and their deposits is needed in order to derive methods for differentiating these deposits from host carbonate rocks mapped using either AST or HSD.

6.1.5 Anomaly Overlap Priority 5

The North Takhar AOI is the fifth-highest priority area (fig. 6.1.1) containing anomalies that represent geospatial overlap between those identified using the AST and GEO datasets. In this case, the GEO anomaly characterizes a magnetic high, interpreted to reflect strongly magnetized basement rocks at great depths beyond economic exploitation. In contrast, the surface cover is dominated by strongly ferric-iron-cemented quartz sand and conglomerate deposits (that is, ferricrete), perhaps related to valley-filling placer gold deposits and fluvial terraces eroded from upstream lode sources known to occur in the nearby Badakshan AOI (Chirico and others, 2011). The lack of a relation between AST-mapped alteration patterns on the surface and GEO-identified anomalies at depth demonstrates why caution should be exercised when interpreting the origin and type of mineral anomalies based on

overlapping optical and geophysical remote sensing datasets from various sources. However, thick deposits of both modern floodplain and older terrace-related gold placers (Chirico and others, 2011) still makes the North Takhar AOI the fifth-highest priority area to consider for ground-based exploration and exploitation.

6.2 Potential for Economic Development from Mineral Resources

The potential for undiscovered porphyry-related precious and base metals in hydrothermally altered volcanic rocks, in addition to nearby known greisen occurrences in the neighboring intrusive rocks, makes the tin-vein Tourmaline AOI anomaly overlap areas the highest priority areas for more intensive ground-based exploration and future development. Such development could benefit communities in and around the nearby cities of Hirat and Farah (fig. 6.1.1).

The Zarkashan AOI anomaly overlap area provides the greatest potential for an undiscovered, unmapped bedrock area that may host additional skarn gold deposits, which could provide economic benefits to communities near and within the cities of Qalat and Ghazni.

All of the Bakhud and some of the Kundalan anomaly overlap areas are characterized by strong surface alteration (HSD) and subsurface geophysical (GEO) expression. These areas may be related to the Arghandab batholith, which is known to host several nearby fluorite, gold, and copper porphyry deposits (Peters and others, 2007; Peters and others, 2011). From an economic development vantage point, most of these anomaly overlap areas lay within the triangular-shaped region of the country bounded by the cities of Kandahar, Tirin Kot and Qalat (fig. 6.1.1), each of which could benefit from future ground-based exploration and eventual exploitation of newly discovered mineral deposits.

Overlapping mineral anomalies in the Dudkash and Kunduz AOIs may represent coal and (or) bauxite-related sources of kaolinite for raw materials needed to make both bricks and cement. The only working cement plant in the country is located at Puli Khumri, just south of the provincial capital of Baghlan (fig. 6.1.1). These two cities, as well as Kunduz to the north, could benefit from these newly discovered sources of fuel and raw materials.

The North Takhar AOI overlapping anomalies have no relation to each other; surface anomalies mapped within the AST dataset are unrelated to the deep-seated strongly magnetized basement rocks mapped using the GEO dataset. However, exploitation of placer gold deposits within the North Takhar AOI could economically benefit people living within and near the city of Talaquan (fig. 6.1.1).

6.3 References Cited

Chirico, P.G., Stamm, R.G., Moran, T.W., and Chaihorsky, A., 2011, Information package summary for the North Takhar Placer Gold Area of Interest, chap. 12A *of* Peters and others, Summaries of important areas for mineral investment and production opportunities of nonfuel minerals in Afghanistan: U.S. Geological Survey Open-File Report 2011–1204, 1,810 p. plus appendixes on DVD. (Also available at http://pubs.usgs.gov/of/2011/1204/.)

Debon, F., Afzali, H., Le-Fort, P., and Sonet, J., 1987, Major intrusive stages in Afghanistan; typology, age and geodynamic setting: Geologische Rundschau, vol. 76, no. 1, p. 245–264.

Doebrich, J.L., and Wahl, R.R., 2006, Geologic and mineral resource map of Afghanistan: U.S. Geological Survey Open-File Report 2006–1038, 1 sheet, scale 1:850,000, available at *http://pubs.usgs.gov/of/2006/1038.*

King, T.V.V., and Johnson, M.R., 2011, Analysis of imaging spectrometer data for the Zarkashan Area of Interest, Afghanistan, chap. 15B *of* Peters and others, Summaries of important areas for mineral investment and production opportunities of nonfuel minerals in Afghanistan: U.S. Geological Survey Open-File Report 2011–1204, 1,810 p. plus appendixes on DVD. (Also available at http://pubs.usgs.gov/of/2011/1204/.)

Kleimenev, M.A., Kamaev, S.V., and Kelesnichenke, V.A., 1974, Report on the results of geophysical investigations carried out in 1973–beginning of 1974 for solid minerals: Part 1: Republic of Afghanistan Ministry of Mines and Industries Department of Geology and Mineral Survey, 74 p.

Kokaly, R.F., and Giles, S.A., 2011, Analysis of imaging spectroscopy data for the Kunduz Area of Interest, Afghanistan, chap. 22B *of* Peters and others, Summaries of important areas for mineral investment and production opportunities of nonfuel minerals in Afghanistan: U.S. Geological Survey Open-File Report 2011–1204, 1,810 p. plus appendixes on DVD. (Also available at http://pubs.usgs.gov/of/2011/1204/.)

Kokaly, R.F., and Johnson, M.R., 2011, Analysis of imaging spectroscopy data for the Dudkash Area of Interest, Afghanistan, chap. 19B *of* Peters and others, Summaries of important areas for mineral investment and production opportunities in nonfuel minerals in Afghanistan: U.S. Geological Survey Open-File Report 2011–1204, 1,810 p. plus appendixes on DVD. (Also available at http://pubs.usgs.gov/of/2011/1204/.)

Krohn, M.D., Kendall, C., Evans, J.R., and Fries, T.L., 1993, Relations of ammonium minerals at several hydrothermal systems in the western U.S.: Journal of Volcanology and Geothermal Research, v. 56, p. 401–413.

Orris, G.J., and Bliss, J.D., 2002, Mines and mineral occurrences of Afghanistan: U.S. Geological Survey Open-File Report 2002–110, 95 p., accessed August 19, 2011, at *http://pubs.usgs.gov/of/2002/110/.*

Peters, S.G., Ludington, S.D., Orris, G.J., Sutphin, D.M., Bliss, J.D., and Rytuba, J.J., eds., and the U.S. Geological Survey-Afghanistan Ministry of Mines Joint Mineral Resource Assessment team, 2007, Preliminary non-fuel mineral resource assessment of Afghanistan: U.S. Geological Survey Open-File Report 2007–1214, 810 p., 1 CD-ROM, accessed August 19, 2011 at *http://pubs.usgs.gov/of/2007/1214/.*

Peters, S.G., King, T.V.V, Mack, T.J., Chornack, M.P., eds., and the U.S. Geological Survey Afghanistan Mineral Assessment Team, 2011, Summaries of important areas for mineral investment and production opportunities of nonfuel minerals in Afghanistan: U.S. Geological Survey Open-File Report 2011–1204, 1,810 p. plus appendixes on DVD. (Also available at *http://pubs.usgs.gov/of/2011/1204/.)*

Thompson, A.J.B, Hauff, P.L., and Robitaille, A.J., 2009, Alteration mapping in exploration: Application of Short-Wave Infrared (SWIR) spectroscopy: Society of Economic Geologists (SEG) Reviews in Economic Geology, v. 16, p. 12–23.